Synthesis and Properties of Glycoazobenzene Macrocycles

Dissertation

zur Erlangung des Doktorgrades

der Mathematisch-Naturwissenschaftlichen Fakultät

der Christian-Albrechts-Universität zu Kiel

vorgelegt von

Julia Hain

Otto Diels-Institut für Organische Chemie

Kiel 2020

I am among those who think that science has great beauty.

- Marie Curie

Referentin: Prof. Dr. Thisbe K. Lindhorst

Koreferentin: Prof. Dr. Anna McConnell

Tag der mündlichen Prüfung: 16.04.20

Zum Druck genehmigt:

Die vorliegende Arbeit wurde unter Anleitung von

Prof. Dr. Thisbe K. Lindhorst

am Otto Diels-Institut für Organische Chemie

der Christian-Albrechts-Universität zu Kiel

im Zeitraum von

März 2015 bis Dezember 2019 angefertigt.

Hiermit erkläre ich, Julia Hain, dass ich die vorliegende Arbeit selbstständig und nur unter Verwendung der angegebenen Quellen und Hilfsmittel angefertigt habe. Inhalt und Form dieser Arbeit sind eigenständig erarbeitet und verfasst worden. Die Arbeit ist unter Einhaltung der Regeln guter wissenschaftlicher Praxis der Deutschen Forschungsgemeinschaft entstanden. Weder die gesamte Arbeit noch Teile davon sind an anderer Stelle im Rahmen eines Prüfungsverfahrens eingereicht worden. Dies ist mein erster Promotionsversuch. Mir wurde kein akademischer Grad entzogen.

Kiel, den

_____

Julia Hain

Abstract

Since their discovery more than 100 years ago, macrocycles have attracted much attention in chemistry. They define a distinct chemical space where molecular structures are located between small substances and macromolecules and applications at the junction between physics, chemistry and biology. Macrocycles have a wide range of applications in molecular recognition and self-organization, in catalysis and in drug discovery.

Carbohydrate-containing macrocycles are found in nature in a large variety of forms, such as cyclodextrins and various antibiotically active substances. Carbohydrates are of great interest for the synthesis of macrocycles not only because of their biological activity, but also because of their good availability from natural sources and because of their complex but defined stereochemistry and multifunctionality, which allows a great structural diversity and broad modulation of the properties of the macrocycles derived from them.

The main interest of this work was the synthesis and properties of photoswitchable glycoazobenzene macrocycles. Here, the azobenzene units serve as photoswitches, which can be reversibly converted from their thermodynamically more stable planar *trans*-isomer to the bent *cis*-isomer by irradiation with light. In the macrocycle, the energy of the light can thus be transformed into molecular motion. The temporal and spatial control of form and function by irradiation makes azobenzene conjugates ideal building blocks for incorporation into macrocyclic structures.

While azobenzene glycoconjugates, in which the properties of carbohydrates are combined with those of the photoisomerizable azobenzene units, have been successfully developed in the past, the combination of azobenzene derivatives with carbohydrates in macrocyclic systems was unknown until now. The present work explores new territory in this field.

The synthesis and photochromic properties of the first glycoazobenzene macrocycles are described in this thesis. The syntheses were designed in such a way that the different glycoazobenzene macrocycles could be obtained easily and as modular as possible from readily available building blocks in a few steps. Four different reactions were successfully used as key steps for macrocyclization in the synthesis, the thiourea bridging, the click reaction, the Sonogashira coupling and the Glaser coupling.

The detailed investigation of the photochromic properties of the new macrocycles showed that the isomerization of the azobenzene units significantly and in a defined way changes the macrocycle structure and is associated with the switching of molecular properties such as solubility and chiroptic and physicochemical properties.

Kurzzusammenfassung

Seit ihrer Entdeckung vor über 100 Jahren haben Makrozyklen in der Chemie viel Aufmerksamkeit auf sich gezogen. Sie definieren einen besonderen chemischen Raum, wo sich die Molekülstrukturen zwischen kleinen Substanzen und Makromolekülen und Anwendungen an der Schnittstelle zwischen Physik, Chemie und Biologie befinden. Makrozyklen finden in der molekularen Erkennung und Selbstorganisation, in Katalyse bis zur Wirkstoffforschung ein breites Anwendungsspektrum.

Kohlenhydrathaltige Makrozyklen finden sich in der Natur in verschiedensten Formen, wie Cyclodextrine und verschiedene antibiotisch aktive Substanzen. Kohlenhydrate sind nicht nur wegen ihrer biologischen Aktivität von großem Interesse für die Synthese von Makrozyklen, sondern auch durch ihre gute Verfügbarkeit aus natürlichen Quellen und wegen ihrer komplexen, aber definierten Stereochemie und Multifunktionalität, die eine große strukturelle Vielfalt und breite Modulation der Eigenschaften der davon abgeleiteten Makrozyklen ermöglicht.

Das Interesse dieser Arbeit galt insbesondere der Synthese und den Eigenschaften von photoschaltbaren Glykoazobenzolmakrozyklen. Dabei dienen die Azobenzoleinheiten als Photoschalter, welche durch die Bestrahlung mit Licht von ihrem thermodynamisch stabileren planaren *trans*-Isomer in das verdrehte *cis*-Isomer reversibel überführt werden können. Im Makrozyklus kann dadurch die Energie der Lichteinwirkung in molekulare Bewegung transformiert werden. Die zeitliche und räumliche Kontrolle von Form und Funktion durch Bestrahlung macht Azobenzolkonjugate zu idealen Bausteinen für den Einbau in makrozyklische Strukturen.

Während Azobenzol-Glykokonjugate, in denen die Eigenschaften von Kohlenhydraten mit denen der photoisomerisierbaren Azobenzoleinheiten verbunden sind, bereits früher erfolgreich entwickelt wurden, war die Kombination von Azobenzolderivaten mit Kohlenhydraten in makrozyklischen Systemen bisher unbekannt. Mit der vorliegenden Arbeit wurde hier Neuland betreten.

Es werden hier die Synthese und die photochromen Eigenschaften der ersten Glykoazobenzol Makrozyklen beschrieben. Die Synthesen wurden so konzipiert, dass die verschiedenen Glykoazobenzolmakrozyklen einfach und möglichst modular aus leicht verfügbaren Bausteinen in wenigen Schritten erhalten werden konnten. Vier verschiedene Reaktionen wurden erfolgreich als Schlüsselschritt für die Makrozyklisierung in der Synthese eingesetzt, die Thiourea-Verbrückung, die Click-Reaktion, die Sonogashira-Kupplung und die Glaser-Kupplung.

Die ausführliche Untersuchung der photochromen Eigenschaften der neuen Makrozyklen zeigte, dass die Isomerisierung der Azobenzoleinheiten die Makrozyklenstruktur signifikant und definiert verändern und mit der Schaltbarkeit von Moleküleigenschaften einhergeht, wie der Löslichkeit und den chiroptischen und physikochemischen Eigenschaften.

Table of Contents

List of Abbreviations

Ac	acetyl
ADDP	azodicarbonyldipiperidine
aq.	aqueous
Boc	*tert*-butyloxycarbonyl
calc.	calculated
CD	circular dichroism
conc.	concentrated
CuAAC	copper catalyzed alkyne azide cycloaddition
d	day
d (NMR)	doublet
DBU	1,8-Diazabicyclo[5.4.0]undec-7-en
DCM	dichloromethane
DFT	density functional theory
DIAD	diisopropyl azodicarboxylate
DMF	*N,N*-dimethylformamide
DMSO	dimethyl sulfoxide
ESI	electrospray ionization
FWHM	full width at half maximum
g	gram
h	hour
Hz	Hertz
IR	infrared
J	coupling constant
L	liter
LED	light emitting diode
lit.	literature
m	meta
m (NMR)	multiplett
M	molarity
MeOH	methanol

min	minute
m.p.	melting point
MS	mass spectrometry
NCS	*N*-chlorosuccinimide
NMR	nuclear magnetic resonance
o	ortho
p	para
PIDA	phenyliodine(III) diacetate
PMDTA	*N*,*N*,*N*',*N*'',*N*''-pentamethyldiethylenetriamine
PSS	photostationary state
quant.	quantitative
R	residue
RPA	random-phase approximation
rt	room temperature
RuAAC	ruthenium catalyzed alkyne azide cycloaddition
s	second
s (NMR)	singlet
sat.	saturated
t (NMR)	triplet
TDDFT	time-dependent density functional theory
TFA	trifluoroacetic acid
THF	tetrahydrofuran
TLC	thin layer chromatography
Ts	tosyl
UV	ultraviolet

1. Introduction

1.1 Macrocycles - from nature to design

The most well-known carbohydrate macrocycles found in nature are cyclodextrins. They were first described by VILLIERS in 1891[1] as non-reducing products derived from the digestion of starch by bacteria. It took 60 years until the three major components, respectively α-, β- and γ-cyclodextrin had been isolated and fully characterized as cyclic structures containing only α-1,4 linked glucose units.[2] By this time it was already established that cyclodextrins are able to form inclusion complexes with various organic and inorganic substances, a feature that could be exploited for several applications like solubility enhancement of drugs, reduction of volatility and protection of oxidation-sensitive compounds such as vitamin A.[2, 3]

Their ability to include guest molecules stems from the macrocyclic structure of the cyclodextrins. The α-1,4 linked glucose units (six units for α-, seven for β- and eight for γ-cyclodextrin) form a truncated cone-like structure with a small and a large rim. The primary alcohols are located at the smaller rim, the primary face, while the secondary alcohols of the glucose units are located at the secondary face. This leads to a hydrophilic exterior of the macrocycle and a slightly more hydrophobic cavity, from which polar solvent molecules can be readily displaced by a hydrophobic guest to form a host-guest complex (Figure 1.1).[3]

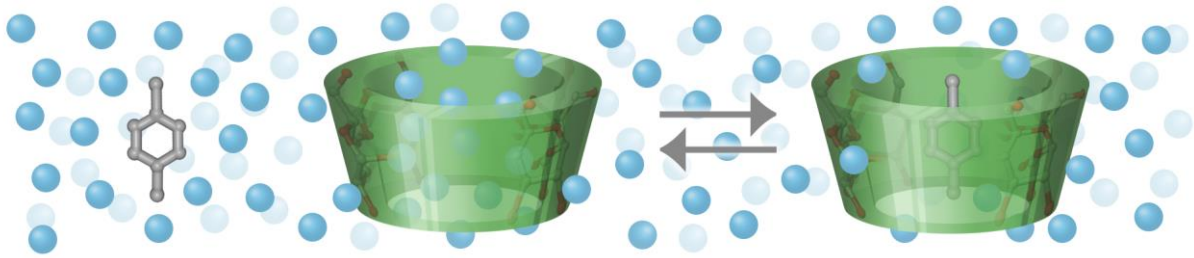

Figure 1.1: Illustration of an inclusion complex formed between β-cyclodextrin and *p*-xylene in water. Based on a depiction by SZEJTLI.[3]

The ease of their enzymatic preparation led to widespread industrial use of cyclodextrins, including pharmaceutical, cosmetical as well as food and flavor applications.[4]

Before the structure of cyclodextrins was fully elucidated, RUZICKA was able to correctly characterize the structure of 17-membered ring civetone[5] and 15-membered ring muscone in 1926,[6] two strongly odorous substances used in the perfume industry (Figure 1.2). However, he did not only characterize the structures of these cyclic ketones, but also developed a synthetic route towards 15- to 18-membered cyclic ketones.[7] With this work, he pioneered the synthesis of macrocycles in a time where it was still generally believed that the construction of larger rings was impossible.[8]

Figure 1.2: Structure of civetone (left) and muscone (right).

Forty years later, PEDERSEN discovered dibenzo[18]crown-6, whose synthesis he published together with thirty-two other cyclic polyethers, a class of compounds he named crown ethers in 1967.[9, 10] This marked the beginning of fully synthetic macrocycles in the context of the field of host-guest and supramolecular chemistry, and in 1987 he was awarded with a Nobel Prize together with CRAM and LEHN "for their development and use of molecules with structure-specific interactions of high selectivity."[11-13]

Since then, the field of macrocyclic chemistry has grown tremendously including the context of pharmaceutical applications. A vast amount of naturally occurring macrocycles display biological activities, making them and their synthetic analogues relevant for drug design.[14-18] Their conformational preorganization allows target binding without a large entropic loss, while their flexibility permits selective positioning of functional groups in different chemical environments. By changing their spatial structure in this manner, membrane permeability can be improved.[19-21] In addition, macrocycles are effective ligands for low-druggability targets, such as protein-protein interactions, due to their ability to bind several hot spots in shallow binding sites, which are too far apart for conventional (linear) drug design.[22]

1.2 Azobenzene photoswitches

The ability of natural macrocycles to reversibly change their spatial structure and conformational preorganization is a property whose emulation is desirable for synthetic analogues as well. This makes azobenzene with its well-known ability to isomerize between a *trans*- and *cis*-form an ideal building block for the incorporation into the macrocyclic backbone.[23-25]

Although the first azo dyes were discovered and synthesized already some 70 years prior,[26] the photochemical *trans* → *cis* isomerization of azobenzene was first described by HARTLEY in 1937.[27] He observed a change in the polarity and absorption of azobenzene solutions in bright sunlight, which was thermally reversible with no change in pressure. Hence, he concluded that the different properties observed were due to a *trans/cis* isomerization of the azobenzene (Scheme 1.1).

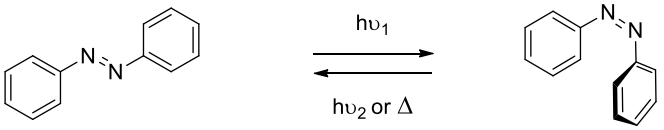

Scheme 1.1: Photoisomerization between *trans*- and *cis*-azobenzene.

The thermodynamically favored *trans*-isomer adopts a planar structure and shows absorption bands corresponding to a strong π → π* transition and a not fully resolved, weak and symmetry-forbidden n → π* transition at higher wavelengths in UV/Vis absorption spectra. Irradiation with light of an appropriate wavelength to excite either transition leads to the corresponding non-planar *cis*-isomer. The isomerization goes hand in hand with a decrease in absorption for the blue-shifted π → π* transition and a stronger band for the n → π* transition due to the torsional twist between the two phenyl rings. Back-isomerization to *trans*-azobenzene can be achieved either by excitation of any transition or through thermal relaxation.[28, 29] The isomerization in either direction is possible over four different mechanisms, rotation, inversion, concerted inversion and inversion-assisted rotation with four different transition states. Which mechanism is favored strongly depends on various factors, like the solvent, substituents or irradiation wavelength.[30]

The wavelengths needed for isomerization are usually in the range between UV-A and blue light. However, the appropriate wavelengths needed for switching can be fine-tuned with shifting of the π → π* or n → π* transition through introduction of different substituents.[23, 31, 32] Electron-rich groups in *ortho* position of the azo bond shift the n → π* transition to higher wavelengths, allowing for switching with lower energy red light, which is favorable in a biological context.[31, 33] A red shift of the n → π* transition leads to more stable *cis*-isomers resulting in longer half-lives, meanwhile red shifting of the π → π* transitions leads to considerably shorter half-lives.[34] Ultra short half-lives for *cis*-azobenzene compounds, which can be relevant for the mimicry of biological processes, can be obtained by implementing push-pull substituents into the molecule.[35]

Increasing the strain upon the azobenzene unit through constriction in a small cyclic system leads to stabilization of the bent *cis*-isomer, until it is more thermodynamically stable than the *trans*-isomer, like in the highly strained diazocine.[36] This is due to the shape change upon isomerization between the elongated *trans*-form and the compact, bent *cis*-form with a decreased distance from 9 Å to 5.5 Å for the carbon atoms in *para* position to the azo bond.[37]

This change in end to end distance is a driving-force of photoinduced molecular motion, converting non-invasive electromagnetic radiation in the form of light with a high spatial and temporal resolution into mechanical work through the change of conformation. This makes azobenzene the ideal moiety for the implementation in molecular machines,[37, 38] a topic which has been awarded with the Nobel Prize for SAUVAGE, STODDART and FERINGA in 2016.[39-41]

1.3 Examples for the interaction between form and function in azobenzene-containing systems

In his essay *The Chemist and the Architect* (*Der Chemiker und der Architekt*)[42] TRAUNER draws ostensive parallels between the creative processes of constructing buildings and molecules. He reasons that one of the architectural guiding principles "form follows function" is also true for chemists, as the simplification of biologically active structures to their active components proved to be very successful. However, conformational switching between two distinct shapes might prove the opposite: function follows form. The interactions between form and function are manifold, but the shape switching ability of azobenzene moieties makes them uniquely qualified to illustrate these interactions, in small molecules as well as supramolecular structures.[43]

The combination of azobenzene and cyclodextrin in a supramolecular context has already attracted great interest.[44] The inclusion of *trans*-azobenzene into the cyclodextrin cavity as a guest is thermodynamically more favored and isomerization to the corresponding *cis*-isomer leads to a

dissociation of the host-guest complex.[45, 46] This behavior is utilized in the design of (pseudo-) rotaxanes and catenanes for molecular machines, [47, 48] where the *trans*→*cis* isomerization upon irradiation with light is the driving force for molecular shuttles, where the cyclodextrin moves along the axis containing the azobenzene unit (Scheme 1.2).[49]

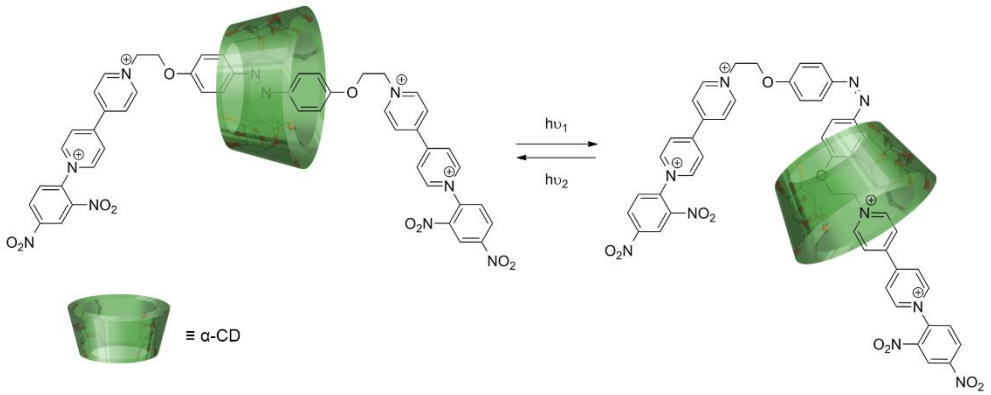

Scheme 1.2: A photoswitchable shuttle using an azobenzene-containing axle and α-cyclodextrin ring.[49]

Another application of the reversible complexation of azobenzene is a photoinduced release mechanism. It was shown that supramolecular vesicles formed through self-assembly of an amphiphilic cyclodextrin could be assembled with an azobenzene glycoconjugate to form highly dense multivalent structures which are able to cross-link lectins.[50] Upon isomerization with light, the azobenzene glycoconjugates depart from the cyclodextrin cavity and are released from the supramolecular structure. The lectin shows high affinity (avidity, respectively) towards the multivalently presented carbohydrate ligands assembled on the high-density surface of the cross-linkers but has no affinity towards the monovalent carbohydrate ligands which are displayed after their photoinduced release. This process of lectin binding and release is fully reversible.

Covalently bound azobenzene cyclodextrin conjugates are also known for the reversible formation of pseudo-rotaxanes in intermolecular or intramolecular self-assemblies. The supramolecular structures dissociated upon isomerization with light from *trans*- to *cis*-isomer and were formed anew through thermal relaxation.[51] The reversible inclusion and dissociation of an azobenzene moiety into the cyclodextrin cavity can also be utilized for the synthesis of synthetic ion channels.[52] Here, the included *trans*-azobenzene blocks the cavity, so that only small cations can pass whereas larger ions are excluded. The isomerized *cis*-azobenzene dissociates from the cavity and allows for the passage of the larger ions, such as anions. Meanwhile, azobenzene-bridged bis-cyclodextrins displayed an increased complex formation of bidentate ligands through cooperative binding only in the *cis*-form of the azobenzene moiety, owing to the closer proximity of the two cyclodextrin units. [53]

MANABE et al. extensively investigated photoresponsive crown ethers in the 1980s, predominantly by incorporating azobenzene moieties into the backbone of crown ethers.[54] They could show that it was possible to selectively extract potassium ions from an aqueous phase with isomerization of an azobenzene-bridged bis-crown ether.[53, 55] The larger potassium ions form 1:2 complexes with [15]crown-5, as they are slightly too large in diameter for the crown ether. This leads to the inability of the *trans*-isomerized bis-crown ether to complex potassium ions. However, upon isomerization, the bis-crown ether can again form a 1:2 complex with a potassium ion (Scheme 1.3, left), thus enabling the extraction of the cations from the aqueous phase. For azobenzophane-type crown ethers, where the azobenzene moiety is fully incorporated into the crown ether backbone, only the *cis*-isomer

displays the ability to complex metal ions while the *trans*-isomer is not showing affinity towards any of the tested metal ions (Scheme 1.3, right).[56] Presumably, the polyoxyethylene chains are linearly extended in the *trans*-isomer and thus unable to form the crown-like structure needed for the ion complexation.

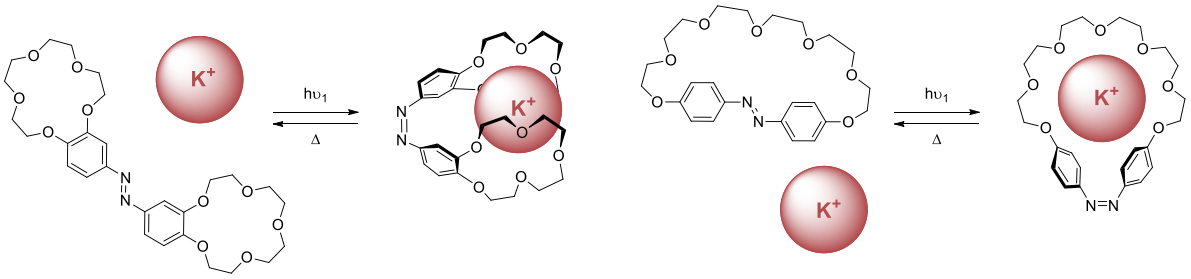

Scheme 1.3: Depiction of photoresponsive complexation of potassium ions by azobenzene-modified crown-ethers in aqueous solution.

Photoresponsive polymer films and threads, simulating muscle behavior, can be created with implementing azobenzene units into the side chains of a polymer[57] or directly into the polymer backbone.[58] Combined with a passive substrate to form bi- or unimorph actuators, they show reversible bending and stretching upon isomerization with light, which can be easily inspected by the naked eye.

Azobenzene derivatives, especially those which are switchable with red light, are exceptionally suitable as semisynthetic biomaterials for applications in photopharmacology.[23, 59-62] Similar to the photoswitchable cyclodextrin ion channel, the potassium transporting Shaker channels, modified with an azobenzene ligand terminated with a quaternary ammonium group, block the passage of potassium ions through insertion into the protein pore, where the quaternary ammonium binds to a site in the pore-lining domain.[63] The *cis*-isomerized tether is too short for binding to the site and dissociates from the cavity to restore potassium migration.

Moreover, it could be shown that the cross-linking of short peptide chains with azobenzene moieties enables the reversible switching of their secondary structure. The stretching and bending of iodoacetamide azobenzene linked to two cysteines in an α-helix structure would either increase helix content or distort the structure leading to a random coil secondary structure, depending on the distance between the two cysteine moieties (Scheme 1.4).[64]

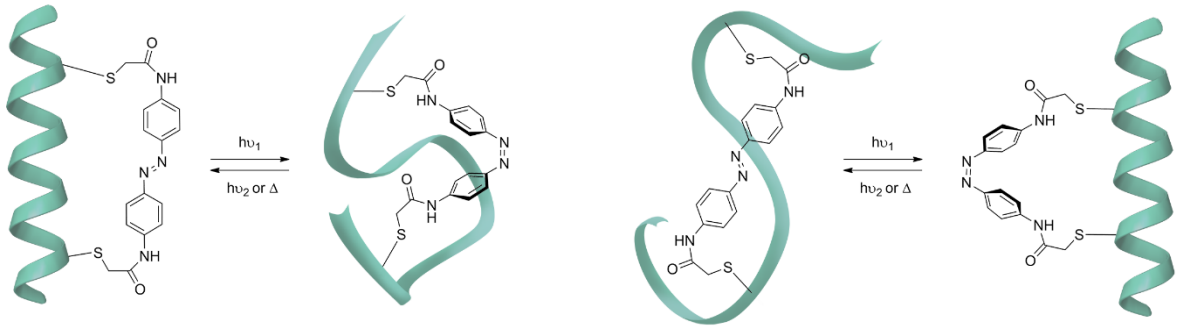

Scheme 1.4: Schematic representation of short peptide chains cross-linked by azobenzene units. Isomerization of the azobenzene moiety from *trans* to *cis* leads to either destruction (left) or formation (right) of a helical secondary structure.

1.4 Approaches to macrocyclization

Often, the most challenging step in the synthesis of macrocycles is the ring-closing reaction. So much so that in the beginning of the 20th century the synthesis of larger carbocycles was still deemed an impossible task.[8] There are two possible ways for the creation of macrocycles, the end-to-end cyclization of a chain and the assembly of two or more building blocks into a cyclic structure. Both synthetic routes come with their own set of challenges and can often be improved with the assistance of pre-organization or use of templates.

The starting point for the synthesis of artificial macrocycles was RUZICKA's preparation of cyclic ketones after his elucidation of the structures of civetone and muscone (see chapter 1.1). He prepared 10- to 18-membered cyclic ketones in an end-to-end cyclization of the corresponding dicarboxylic acid metal salts. Harsh reaction conditions of vacuum distillation with temperatures up to 500 °C were needed to generate the macrocycles in yields lower than 1.5 %.[7]

By then it was already known that for intramolecular end-to-end cyclization to take place, appropriate dilution must be applied to prevent intermolecular side reactions. From a kinetic standpoint, the first order process of the intramolecular reaction is in competition with the formation of intermolecular reaction side products. As these latter pathway follows second order kinetics, they are dependent on the concentration,[65] which leads to a favorable cyclization under high dilution or pseudo-high-dilution conditions. However, high dilution does not always lead to satisfying yields in end-to-end cyclization of linear precursors. In molecules with higher degrees of freedom the reaction facilitating proximity of the end groups becomes statistically unlikely, leading to slow reaction rates and low turnover numbers. Therefore, pre-organization is an important tool to improve the yields of macrocyclizations.[66, 67]

Pre-organization can be favorably used for the cyclization of peptides, where certain turn motifs can be exploited for the cyclization of longer peptide chains. For this, N- and C-terminus of the desired macrocyclic peptide are chosen via retrosynthetic disconnection so that intermolecular hydrogen bonding pre-organizes the linear precursor in an appropriate secondary structure where the distance between the two end groups of the chain becomes minimal, thus facilitating peptide coupling and hence macrolactamization.[66, 68]

The application of templates in macrocycle synthesis can be advantageous not only for intramolecular reactions but especially for multicomponent macrocyclization. The pre-organization around a template structure leads to binary or tertiary complexes with an energetically favored conformation that facilitates the macrocyclization towards a well-defined product, which is often tunable according to the used template.[69] Various positively or negatively charged ions, as well as neutral organic guest molecules can act as template structures.[70] For example, the synthesis of crown ethers is facilitated by the very same cations that are able to form complexes with them.[9] However, the identification of a suitable template molecule is a challenging task and has to be optimized for every envisioned macrocyclic structure.

Without the assistance of templates, the synthesis of macrocycles from multiple components in a one-pot-type synthesis is demanding. A reaction proven to be useful in this regard is the Ugi multi component reaction. Here, simple, bifunctionalized building blocks generate diverse macrocyclic structures rapidly and with great ease.[71-73]

Macrocyclizations with only two components require the synthesis of less building blocks, while still allowing for the preparation of diverse cycles through the substitution of components, unlike linear

precursors for end-to-end cyclization. Facile macrocyclization of two components is favored when the interatomic distance between the functional groups of the building blocks is similar, ensuing optimal contact of the two components for synthesis with minimum strain.[74, 75] Changing the distance between functional groups of one building block can lead to the preference for a different cyclization pattern, as seen in the light-controlled macrocyclization of bis-bromomethylazobenzene with tetrathiafulvalene (Scheme 1.5).[76] While the reaction with the *cis*-configured azobenzene leads to the formation of the [1:1] macrocycle, the *trans*-azobenzene facilitates the formation of the [2:2] macrocycle, as the distance between the reaction partners of both building blocks is too large to allow the formation of a smaller cycle.

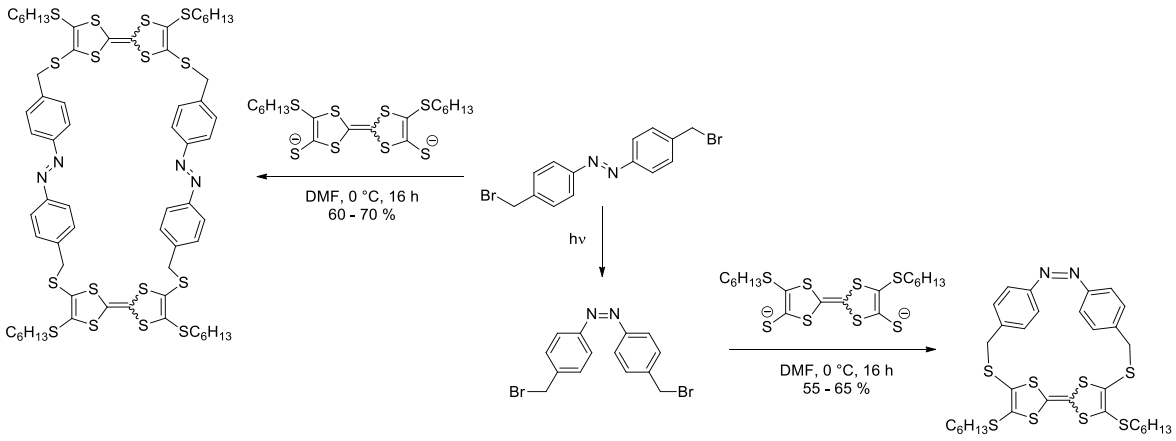

Scheme 1.5: Photochemically controlled macrocyclization leading to either [1:1] or [2:2] cycle.

2. Project Idea

We envisioned a design that unites photoisomerizable azobenzene moieties and carbohydrates in the backbone of a single macrocyclic structure. In these glycoazobenzene macrocycles, switching between two well defined conformational states upon irradiation with light or thermal relaxation leads to switching between two distinct forms (Figure 1.2). This should in turn influence the function of the molecule, its chirality, biological activity and ability to form self-assembled supramolecular structures.

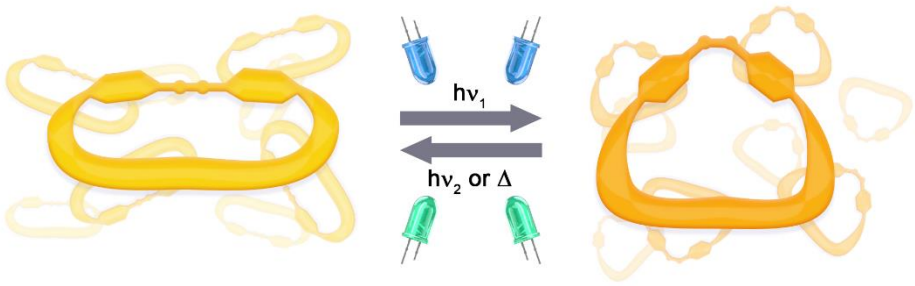

Figure 1.2: Schematic representation of photoresponsive, shape-switchable glycoazobenzene macrocycles.

With an increasing number of applications of macrocyclic structures in various areas, carbohydrate-containing macrocycles attract interest far beyond the context of cyclodextrin.[77] Carbohydrates are stereochemically defined, natural building blocks with conformational restriction. They can be exchanged in an almost modular fashion to give an assortment of stereochemical diverse, chiral products, while being biocompatible, water soluble and multifunctional, with well-established methods for site-selective derivatization.[78]

Photoresponsive glycoconjugates, where their molecular geometry could be controlled in a spatially and temporally resolved manner, have already been successfully synthesized through the introduction of azobenzene moieties.[79, 80] However, even though azobenzene-containing macrocycles are quite common,[43] glycoazobenzene macrocycles, where carbohydrate and azobenzene moieties are implemented into the backbone of the same macrocycle, constitute a new research field and were not yet devised at the start of this project.

Concomitantly with our work, XIE et al. reported their research on related structures where one carbohydrate and one azobenzene were cyclized via O-arylation to 16- and 17-membered rings (Scheme 1.6).[81, 82] They could show that the synthesized glycomacrocycles could be reversibly photoisomerized between two distinct states and displayed multistimuli-responsive self-assembly properties. Similar to other azobenzene-containing macrocycles with chiral elements,[83-86] the glycomacrolactones displayed a distinct helical chirality with a preferred orientation.

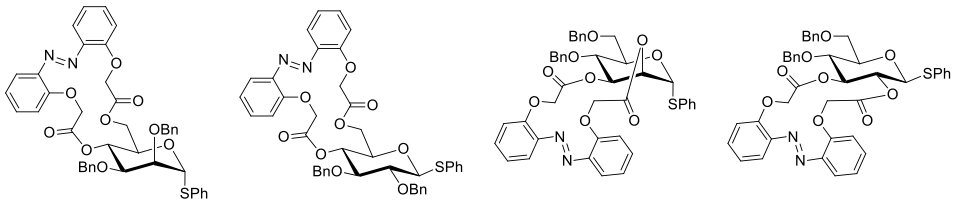

Scheme 1.6: Glycoazobenzene macrocycles prepared in the group of XIE.[81, 82]

As there are many possible synthetic glycomacrocyclic structures, the focus of this work lays on a modular approach for the preparation of the macrocycles. For this, several criteria were chosen: The macrocycles were built up in a symmetrical manner with readily accessible building blocks, while the implementation into the macrocyclic backbones was limited to the *para*-position for the azobenzene moieties and to the anomeric position and primary hydroxyls of the carbohydrates (Figure 1.3).

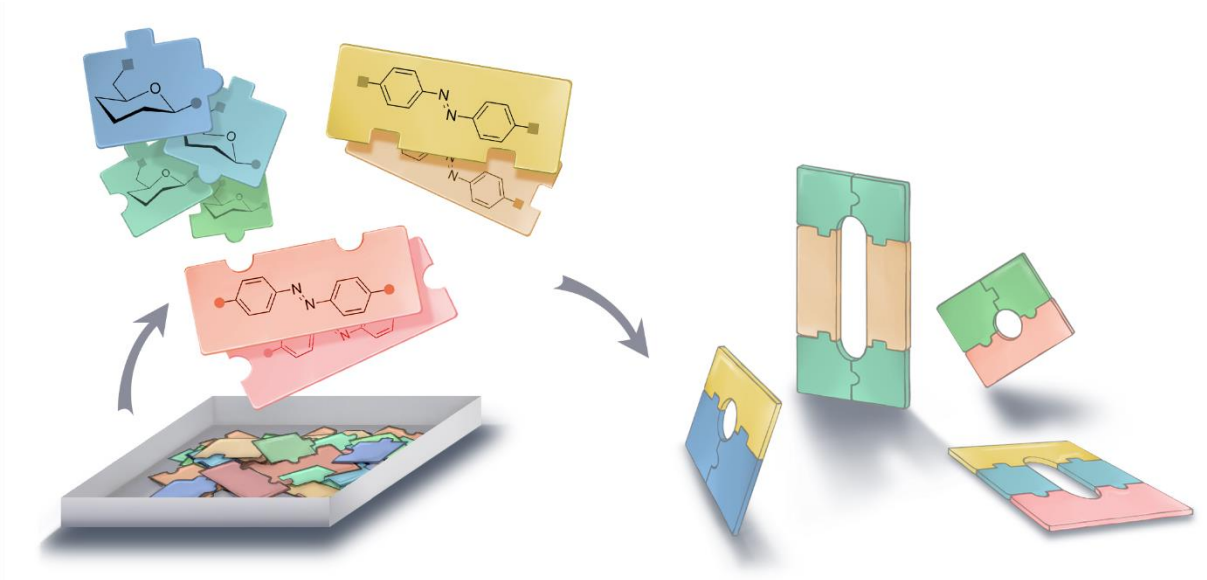

Figure 1.3: Formation of symmetrical macrocycles through combination of building blocks.

In the following, the results are reported in an order that is built on the cyclization reaction. Hence, chapters 3 to 6 describe the synthetic work based on macrocyclization by thiourea bridging, CuAAC click reaction, Sonogashira coupling and Glaser coupling. Each chapter is preceded by a short introduction which is specific for the employed cyclization chemistry.

Published manuscripts are included in the respective chapters together with experimental procedures and analytical data and spectra, while all literature references are compiled in chapter 9.

Chapter 7 summarizes the successful work towards photoswitchable azobenzene macrocycles, whereas in chapter 8, other collaborative works are added.

3. Thiourea Bridging

3.1 Introduction

Isothiocyanates readily react with amines to thiourea bridged ligation products. OSSIAN ASCHAN described the reaction of phenyl isothiocyanate with amino acids to yield the corresponding thiourea derivatives under heating.[87] Based on this work, in 1950 EDMAN further developed the reaction conditions to require less heating under weak basic conditions[88] and subsequently used it for sequence analysis of peptides starting at the N-terminus, the so-called Edman degradation.[89]

Thiourea bridging tolerates many functional groups and reacts mostly quantitively and without the formation of byproducts, hence this ligation method belongs to a set of reactions regarded as "Click Chemistry" by SHARPLESS in 2001.[90] The reaction has a high potential as ligating method in organic and biological chemistry.

Thiourea bridging is also an ideal reaction for macrocyclization and hence has been successfully applied in the synthesis of *m*-xylene macrocycles,[91] cyclic peptides[92] and glycomacrocycles, notably in the preparation of the trehalose-based cyclodextrin analogues by the group of GARCÍA-FERNÁNDEZ.[93-95]

Here, two target macrocycles **1** and **2** were envisioned, which both rely on thiourea bridging for macrocyclization (Figure 3.1). They comprise an azobenzene moiety as photoswitchable hinge, which is glycosidically linked to an NCS-functionalized glucose or maltose derivative, respectively. Ring closure would be facilitated with piperazine (**3**) as a small but rigid cyclic diamine spacer.[96]

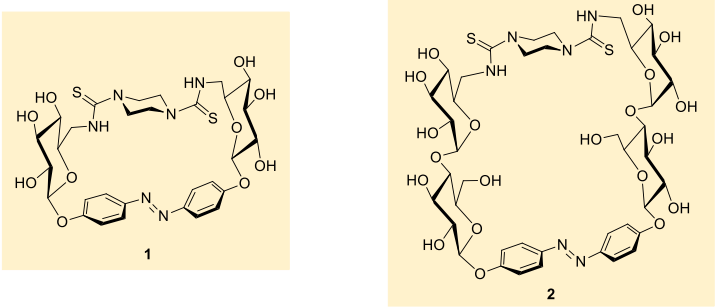

Figure 3.1: The two target thiourea-bridged macrocycles glucoside **1** and maltoside **2**.

3.2 Synthesis

For the synthesis of macrocycle **1**, the glucoside donor **4** was required and prepared from D-glucose in 6 steps according to the literature.[97] The azido-functionalized glucosyl donor was subsequently used with 4,4'-dihydroxyazobenzene (**5**)[98] to yield the bis-glucosylated azobenzene derivative **6** in 52 % yield (Scheme 3.1). Then, the reaction with carbon disulfide and triphenylphosphine converted **6** into the isothiocyanate **7** in an aza-Wittig reaction in a good yield of 79 %.[99]

In the next step, **7** and piperazine (**3**) were reacted to yield **8**.[94] However, the simple addition of both reactants in pyridine gave only traces of the desired cycle **8**, presumably because the interatomic distance between the functional groups of the precursor **7** is too large for the cyclization with piperazine (**3**). Instead, a mixture of different oligomers is formed. However, when *trans*-**7** was isomerized to *cis*-**7** prior to the cyclization reaction, using a 365 nm LED for 20 min, the reaction with **3** led to the desired macrocycle **8** in a good yield of 48 % (Scheme 3.2). Then, deprotection under Zemplén conditions using catalytic sodium methoxide in methanol[100] gave the target macrocycle **1** in quantitative yield.

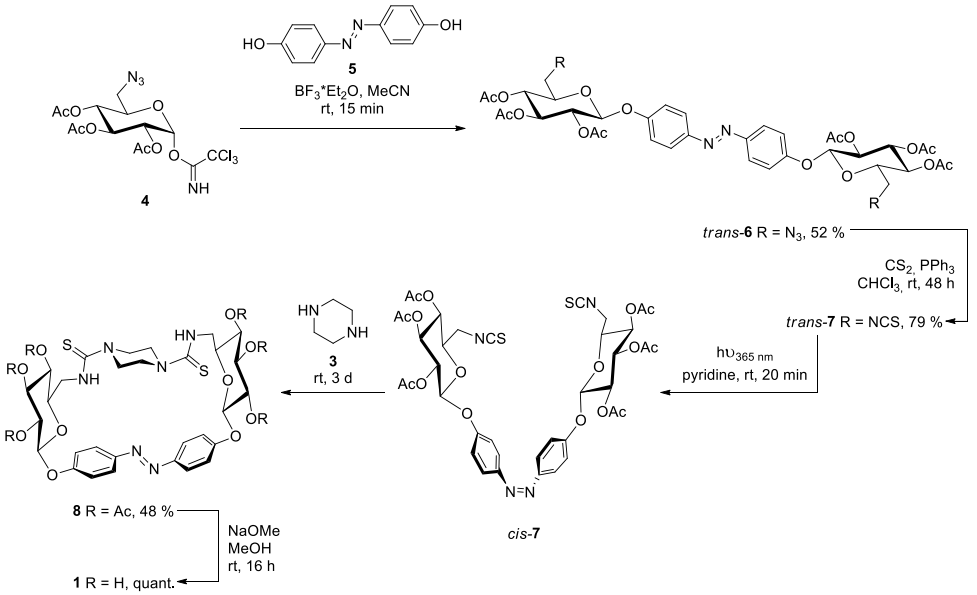

Scheme 3.1: Synthesis of the macrocycle **1**, starting from **4** and **5**.

In analogy to the synthesis of **1**, the reaction of the *cis*-bis-maltosylated azobenzene derivative with piperazine and subsequent deprotection led to the azobenzene maltoside macrocycle **2**, which was synthesized by JAESCHKE and DESPRAS, cf. chapter 3.5. Both macrocycles were investigated for their photochromic properties and the consequences of the *trans/cis* isomerization of the azobenzene hinge on form and function of the macrocycles.

3.3 Photochromic properties of 1

The photochromic properties of the two target macrocycles **1** and **2** were investigated by NMR, UV/Vis and circular dichroism (CD) spectroscopy. The results for **2** were collected by DESPRAS and are shown in chapter 3.5.

Force field-minimized structures (OPLS3 force field in implicit water)[101] show a great change in shape upon isomerization for both macrocycles, *trans*-**1** isomerizes from a flattened out structure to a triangle shape for *cis*-**1** with a perpendicular bisector as the C_2 symmetry axis (Figure 3.2). These changes can also be seen in the ^{1}H NMR, where especially the H-6 and the piperazine protons of both **1** and **2** undergo a significant change in their chemical shift, for macrocycle **1** from 3.8 ppm and 3.3 ppm to 4.2 ppm and 3.1 ppm for both H-6 protons and from 3.4 ppm to 3.8 ppm for the piperazine protons

(see Figure 7 in chapter 3.5). The other carbohydrate protons are, as suggested by the minimized structures, located outside of the macrocyclic ring and are thus less affected by the change of the ring shape.

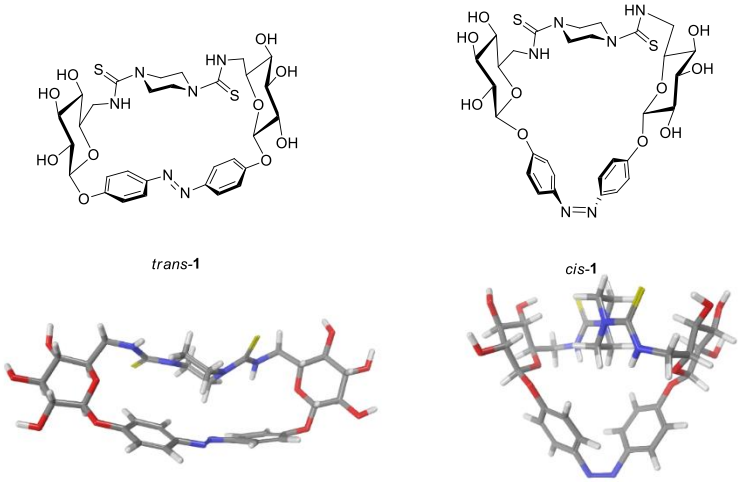

Figure 3.2: Force field-minimized structures of macrocycle **1** in *trans*- and *cis*-form (left).

The UV/Vis absorption spectrum of *trans*-**1** in DMSO shows a large band corresponding to the π → π* transition (λ_{max} = 360 nm) (Figure 3.3a). The forbidden n → π* transition is considerably weaker and not well separated from the π → π* transition, with a λ_{max} of 450 nm. The photostationary state (PSS) was reached after irradiation with a 365 nm LED for 10 min, giving a *trans:cis* ratio of 2:98 (see Figure 5 in chapter 3.5) and leading to the typical decrease in intensity and a hypsochromic shift of the π → π* transition to 310 nm, while the n → π* transition only slightly increased in absorbance. Due to the overlapping of the respective n → π* transitions of *trans*- and *cis*-**1**, complete back switching was only possible through thermal relaxation with a half-life for *cis*-**1** of 6 h (at 300 K in DMSO-d_6, chapter 3.5). Irradiation with a 435 nm LED for 5 min led to a PSS with a *trans:cis* ratio of 53:47. The PSS for macrocycle **2** was similar for the *trans* → *cis* isomerization, but back switching with a 435 nm LED led to a higher amount of *trans*-**2** with a *trans*:*cis* ratio of 37:63 (Figure 5, chapter 3.5). The absorption spectra in water with 0.5 % DMSO (Figure 3.3b) show similar bands but with slightly decreased absorbance. Both macrocycles are stable for at least 10 switching cycles without any photobleaching (Figure 6, chapter 3.5).

CD spectra of the linear precursor **7** show weak bands for the transitions corresponding to the UV/Vis bands of the azobenzene unit, which shows that there is a chirality transfer from the carbohydrate moieties to the otherwise planar and thus optically inactive *trans*-azobenzene. But upon macrocyclization, the bands of **1** show a significant increase in the ellipticity of the π → π* and n → π* transition of the azobenzene hinge (Figure 3.3 c and d) and high values for the specific optical rotation of +439 ° for *trans*-**1** and +683 ° for *cis*-**1** (9:1 water/DMSO). This indicates a twist of the π-electron system,[102] leading to helical chirality in the macrocycle, which azobenzene moieties are known to cause upon clamping in a strained system.[84, 86, 103-105] In DMSO and water (0.5 % DMSO), the CD spectra of *trans*-**1** show a very weak negative band for the π → π* transition and a strong positive one for the n → π* transition, which is even more pronounced in water. After isomerization with 365 nm light, the signals for both transitions do not change their sign but get stronger in intensity in DMSO, while the intensity increases to a minor extent in water. The changes between the measured spectra in DMSO

or water indicate a solvent dependent change in the twisting of the azobenzene moiety, which may influence the overall shape of the molecule.

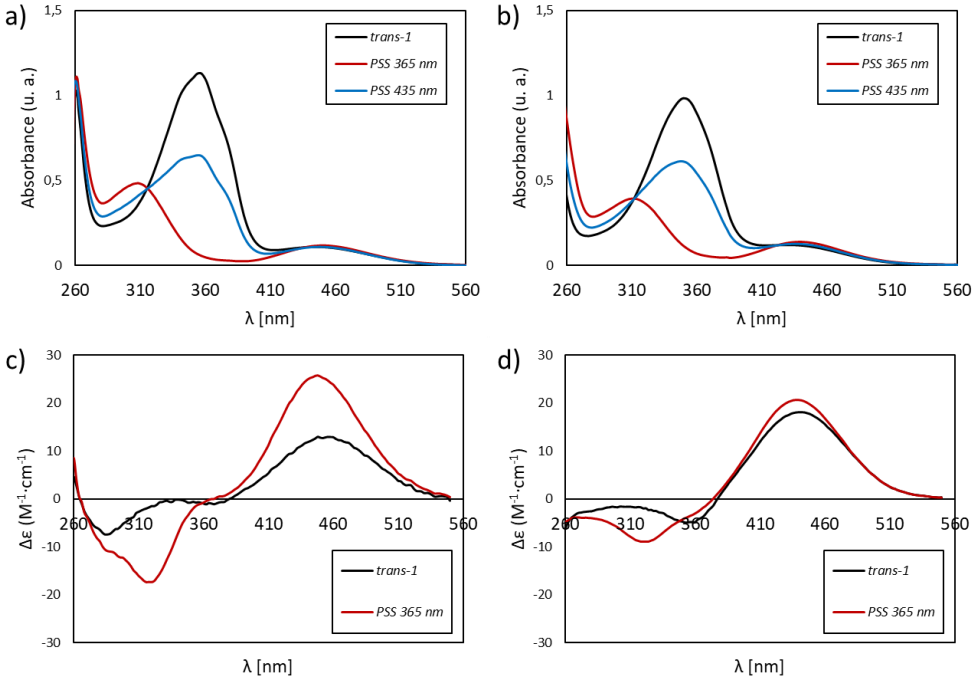

Figure 3.3: UV/Vis and CD spectra of **1** at 298 K at a concentration of 50 µM (a) UV/Vis spectra in DMSO; (b) UV/Vis spectra in water with 0.5 % DMSO; (c) CD spectra in DMSO; (d) CD spectra in water with 0.5 % DMSO; black line: *trans*-**1**, red line: PSS after irradiation with 365 nm for 5 min, blue line: PSS after irradiation with 435 nm for 5 min.

Theoretical CD spectra were calculated by RAEKER in the HARTKE group[106] for *trans*-**1** and each possible helical conformers of *cis*-**1** in implicit DMSO (Figure 3.4). The computational setup used was force field optimizations, followed by DFT and RPA-TDDFT calculations.

The experimental spectra of **1** are in good agreement with the calculated spectra for *trans*-**1** and *cis-(M)*-**1**, supporting that *trans*-**1** switches in a unidirectional motion to the *cis-(M)* conformer. This findings are in agreement with the literature, where comparisons between experimental and theoretical spectra showed that the helical conformation can be directly deduced from the region around 450 nm of CD spectra: *(M)*-helices give exclusively a positive Cotton effect in this region, while *(P)*-helices give a negative one.[86, 103-105]

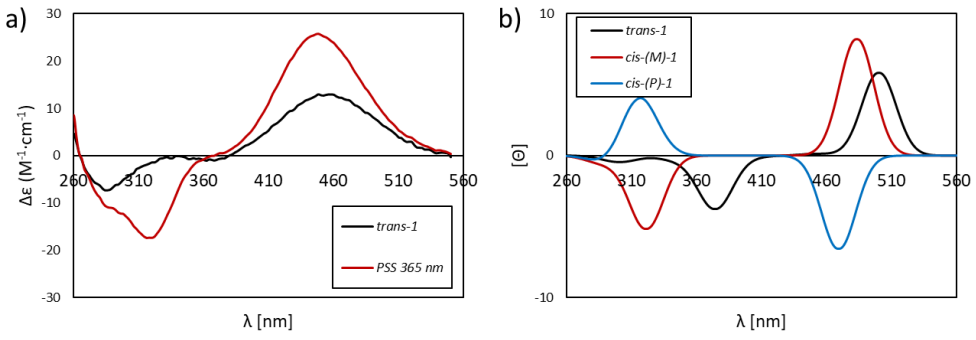

Figure 3.4: Comparison of experimental (a) and theoretical (b) CD spectra of **1** in DMSO.

3.4 Conclusion

In summary, the macrocycle **1** was synthesized using thiourea bridging for the key macrocyclization step in a good yield of 48 %. The linear isothiocyanate precursor **7** was synthesized via glycosylation of literature-known substances and followed by an aza-Wittig reaction, in a yield of 41 % over two steps. Most importantly, the intermolecular macrocyclization with piperazine (**3**) could only be realized with pre-orientation of the linear precursor **7** through isomerization to the *cis*-form, which led to a bent structure where the electrophilic sites were close enough to each other to facilitate the reaction. This signifies the importance of the azobenzene moiety, not only for changing the shape of the macrocycle, but also for the construction of the macrocyclic structure. As shown with the synthesis of macrocycle **2** by JAESCHKE and DESPRAS, the synthesis route allows for the implementation of different carbohydrates, leading to a variety of macrocyclic structures.

The photochemical properties of **1** were tested and together with obtained theoretical CD spectra indicate that *cis*-**1** adopts a helically twisted structure through a chirality transfer from the carbohydrate moieties, with a unidirectional switching to the *cis-(M)*-conformation.

3.5 Publication: Photocontrol over Molecular Shape: Synthesis and Photochemical Evaluation of Glycoazobenzene Macrocycles

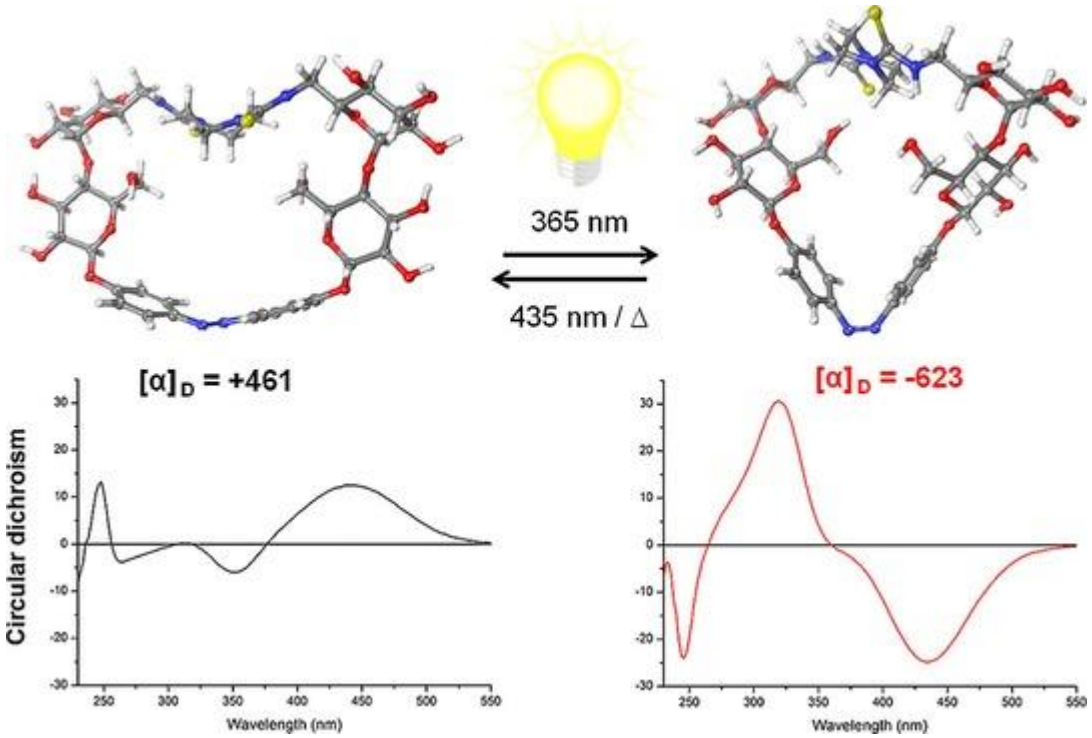

G. Despras, J. Hain, S.-O. Jaeschke, *Chem. Eur. J.* **2017**, *23*, 10838 – 10847.

DOI: 10.1002/chem.201701232

ChemPubSoc Europe
DOI: 10.1002/chem.201701232
CHEMISTRY A European Journal Full Paper

Macrocycles

Photocontrol over Molecular Shape: Synthesis and Photochemical Evaluation of Glycoazobenzene Macrocycles

Guillaume Despras,* Julia Hain, and Sven Ole Jaeschke[a]

Abstract: Reversible shape switching due to external stimuli is an attractive property for the control of molecular features. Hence, we aimed at macrocycles to investigate photoswitching of molecular shape. We prepared the first carbohydrate-based macrocycles comprising a photoresponsive azobenzene hinge. These macrocycles were readily obtained by cyclization of isothiocyanate-armed bis-azobenzene glycosides with piperazine. The unprotected macrocycles exhibit favorable photochromic properties in water and DMSO. Notably, the efficient *trans*→*cis* isomerization results in a remarkable shape transformation of the molecule. Additionally, the structure is characterized by restricted conformational freedom of the backbone, resulting in a single main conformer in each geometrical state (*trans* or *cis*). Measurement of optical rotation values and circular dichroism spectra revealed a tremendous change in chirality upon photoisomerization, with a strong helical induction in the *cis* state. These findings highlight the applicability of the new macrocycles as chiroptical molecular switches.

Introduction

Among bioactive natural products, macrocycles have often captivated chemists as they display unique physicochemical properties and also because their synthesis remains a challenging task.[1] Besides naturally occurring macrocycles, unnatural counterparts have aroused great interest since their functional features can be tuned by organic chemistry.[1] In this regard, carbohydrates are valuable building blocks[2] as they are readily available, chiral and biocompatible, and they offer broad synthetic possibilities due to their polyfunctional nature, defined stereochemistry, and structural diversity. Such versatility enables the fine-tuning of the physicochemical properties (polarity and solubility, size and shape, ligand properties, etc.) of macrocycles derived thereof. Importantly, the cyclic nature of sugar units (pyranose or furanose) imparts conformational restriction to a carbohydrate-based macrocyclic backbone. Hence, numerous cyclic glycoarchitectures have been designed with various shapes and functionalities, such as cyclic neoglycoconjugates,[3] cyclo-glycopeptides,[4] cyclic oligomers of sugar amino acids,[5] cyclodextrin surrogates,[6] glycophanes,[7] or sugar-derived crown ethers.[8] These compounds have been used as bioactive analogues of natural oligosaccharides,[4d,9] artificial receptors (for chiral recognition,[6c,7d,8f,10] hydrophobic guest molecules,[5c,6d–f,7c,11] as well as ions[8d,12] and sugars[7d,13]), asymmetric catalysts[8a,b,14] or multivalent scaffolds.[6i,15]

We envisioned the design of carbohydrate-based macrocycles that can be reversibly switched between two defined structural shapes by external stimuli. As the shape of a functional molecule can be correlated with its properties,[16] switching the molecular shape of a carbohydrate-based macrocycle is expected to induce a change of its physicochemical properties, chirality, supramolecular features, and of the spatial arrangement of attached functionalities. To achieve such shape switching we planned to incorporate a photoresponsive hinge into the cycle, like an azobenzene derivative (Figure 1).

Indeed, light is a bioorthogonal noninvasive stimulus which can be employed with high spatiotemporal resolution. Azobenzene is the most attractive photoswitch for our purpose, as it displays excellent photochemical properties (robust, reversible and efficient photoswitching) and mediates a significant alteration of geometry and polarity upon *trans*/*cis* isomerization by light of the appropriate wavelength.[17] Azobenzene glycosides, in particular, exhibit efficient *trans*→*cis* photoisomerization and good thermostability of the *cis* form.[18] Several stud-

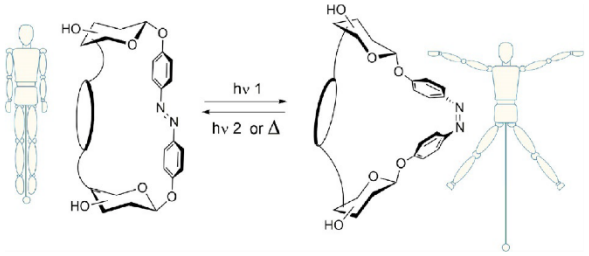

Figure 1. Reversible shape switching of glycoazobenzene macrocycles upon photoirradiation or heating.

[a] *Dr. G. Despras, J. Hain, S. O. Jaeschke*
Otto Diels Institute of Organic Chemistry
Christiana Albertina University of Kiel
Otto-Hahn-Platz 3/4, 24118 Kiel (Germany)
E-mail: gdespras@oc.uni-kiel.de

Supporting information and the ORCID identification number(s) for the author(s) of this article can be found under https://doi.org/10.1002/chem.201701232.

ChemPubSoc Europe

CHEMISTRY A European Journal Full Paper

ies reported in the literature describe the use of azobenzene derivatives for the design of functional macrocycles.[19] These structures found applications in supramolecular chemistry (inclusion complexes,[20] self-assembly,[21] interlocked systems[22]) or were used as chiroptical switches[23] and for the construction of molecular machines.[24]

Two types of glycoazobenzene macrocycles were targeted, both consisting of symmetrical azobenzene bis-glycoside units which are cyclized with piperazine through thiourea bridges (**1** and **2**, Figure 2). We report the synthesis of this new type of

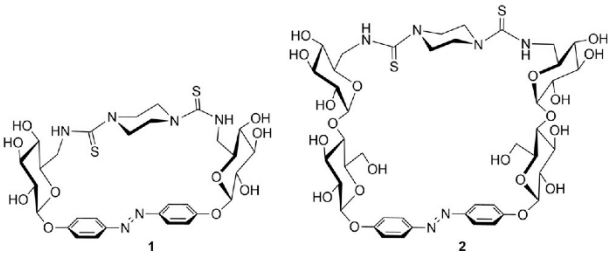

Figure 2. Structures of the targeted glycoazobenzene macrocycles.

photoswitchable macrocycles, their photochromic properties and the investigation of the overall conformational change resulting from irradiation. Moreover, we report on a remarkable photoswitching of the chiroptical properties of **1** and **2**, underpinning the potential of glycoazobenzene macrocycles to modulate molecular function by controlled shape changes.

Results and Discussion

Synthesis of the glycoazobenzene macrocycles

Retrosynthetic analysis of the target glycoazobenzene macrocycles leads both molecules back to piperazine, 4,4′-dihydroxyazobenzene, and glycosyl donors **3** and **4**, bearing azido groups at the 6- and 6′-position, respectively, which can be transformed into isothiocyanates at a later stage of the synthesis (Scheme 1).

The photoswitchable azobenzene moiety is directly attached to the anomeric position of the sugar units because the glycosidic linkage was assumed to confer stiffness to the macrocycle skeleton. On the other hand, the cyclization was accomplished through the primary positions of the carbohydrate rings, in order to achieve a good balance between rigidity and flexibility. The size and properties of the macrocycles were modulated by using different carbohydrate building blocks according to the same structural design, D-glucose in the case of **1** and the disaccharide D-maltose for **2**.

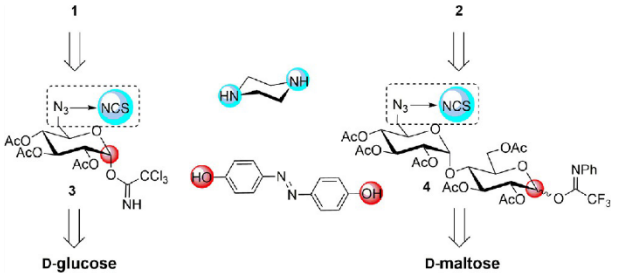

Scheme 1. Retrosynthesis of the glycoazobenzene macrocycles **1** and **2**. The positions used for building the glycosidic linkages are highlighted in red, the ones used for cyclizing are highlighted in blue.

Whereas the glucosyl donor **3** was prepared following a procedure reported by Müller et al.,[18c] the synthesis of the maltosyl donor **4** required discrimination of the 6′-position. For this, D-maltose was first protected by forming the 1,6-anhydro derivative **5**[6i,25] (Scheme 2). The primary alcohol at the non-reducing end was then regioselectively silylated and the remaining free secondary alcohol groups were acetylated in a one-pot fashion to afford **6** in 68% yield. After a silyl cleavage step, the free 6′-alcohol on compound **7** was converted into a primary azide by a Mitsunobu reaction using diphenylphosphoryl azide[26] to give **8** in 80% yield. The 1,6-anhydro ring was cleanly opened by acetolysis,[27] then the resulting anomeric acetyl group was selectively cleaved in the presence of hydrazine acetate.[28] Finally, the reducing sugar was treated with 2,2,2-trifluro-*N*-phenylacetimidoyl chloride, in the presence of caesium carbonate, to obtain the glycosyl trifluoroacetimidate[29] **4** in a good overall yield (74% over three steps).

The imidate derivatives **3** and **4** were reacted with 4,4′-dihydroxyazobenzene,[30] in the presence of boron trifluoride etherate, to afford the bis-glycosyl azobenzene derivatives **9**[18c] and

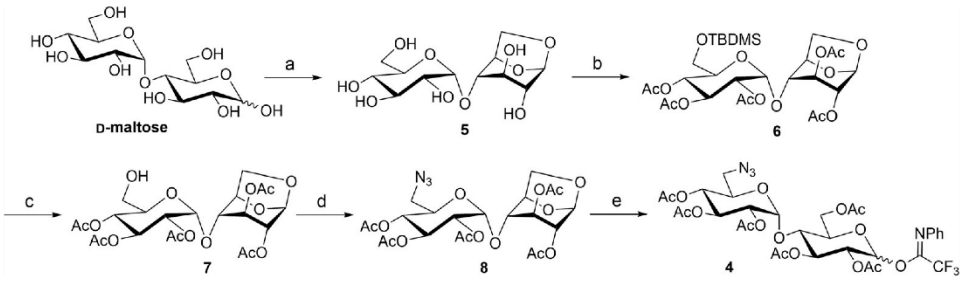

Scheme 2. Preparation of the 6′-azido-6′-deoxy-maltosyl donor **4**. Reagents and conditions: a) (i) dimethyl imidazolium chloride (3 equiv), triethylamine (9 equiv), water, 0 °C to RT; (ii) Ac_2O (13 equiv), pyridine, RT; (iii) NaOMe, MeOH, RT; 94% over three steps; b) TBDMSCl (2 equiv), pyridine, RT, 5 h, then Ac_2O (12 equiv), DMAP (0.2 equiv), RT, 15 h, 68% over two steps; c) TBAF (3 equiv), AcOH (15 equiv), THF, 0°, 3 h, 83%; d) PPh_3 (1.5 equiv), DIAD (2.5 equiv), diphenylphosphoryl azide (1.5 equiv), THF, −5 °C to RT, 22 h, 80%; e) (i) Ac_2O/AcOH (7:3), conc. H_2SO_4 (cat.), RT, 3 h 30; (ii) N_2H_4.AcOH (1.1 equiv), DMF, 55 °C, 1 h; (iii) ClC(NPh)CF_3 (1.5 equiv), Cs_2CO_3 (1.5 equiv), CH_2Cl_2, RT, 1 h 30, 74% over three steps.

ChemPubSoc Europe
CHEMISTRY A European Journal Full Paper

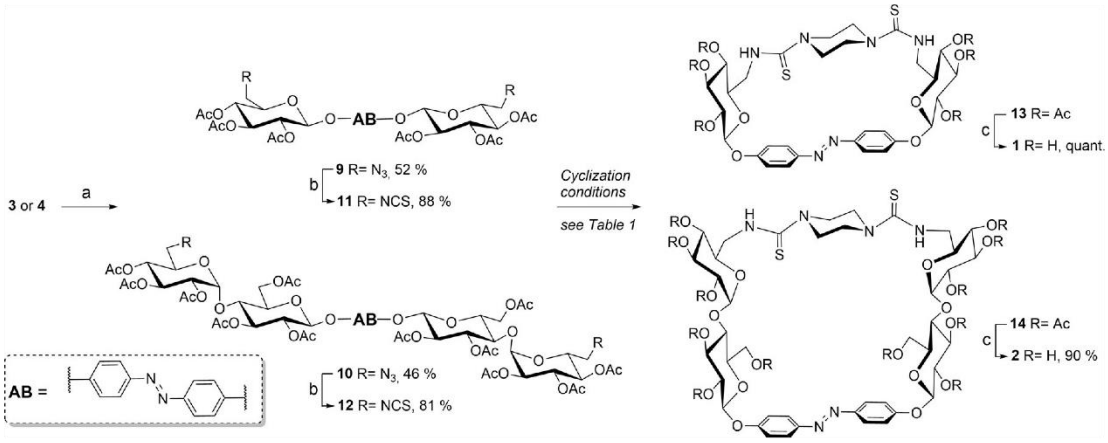

Scheme 3. Synthesis of photoswitchable macrocycles **1** and **2**. Reagents and conditions: a) 4,4′-dihydroxyazobenzene (1 equiv), **3** or **4** (2.2 equiv), $BF_3{\cdot}Et_2O$ (1.1 equiv), 3 Å MS, acetonitrile, RT, 15–45 min; b) PPh_3 (8-8.5 equiv), CS_2 (85–100 equiv), chloroform, RT, 2 d; c) NaOMe, MeOH, RT, 16 h.

10 in moderate yields (Scheme 3). The primary azido functions were further converted into isothiocyanates (NCS) by an efficient aza-Wittig reaction[31] that provided **11** and **12** in 88 and 81 % yield, respectively. The isothiocyanate group was selected because it readily and cleanly reacts with amines under mild conditions. For instance, it has been successfully used by García-Fernández et al. for cyclizing trehalan building blocks.[6d,11a,b] Piperazine was chosen as the ring-closing moiety because it is a reactive diamine and also known as a rigid spacer molecule.[32] The key macrocyclization step was carried out in pyridine under dilution conditions,[11a] using a slight excess of piperazine and shielding the glassware from ambient light during the course of the reaction. Modulations of the experimental conditions are summarized in Table 1. We reasoned that the rigidity of the linear azobenzene glycoside precursor would prevent macrocyclization. Therefore, the linear *trans*-configured glycoazobenzene precursor molecules **11** and **12** were first irradiated to give the bent *cis* isomers, in order to bring the two distal NCS functions in closer proximity, before adding the piperazine spacer. Such pre-organization of functionalities[33] led to the desired macrocyclic products in fair yields. The cyclic structure of **13** and **14** was confirmed by analytical data. The measured molecular masses and the integrals of the ^{1}H NMR signals corresponding to the piperazine cycle are consistent with the presence of a single piperazine unit. Infrared spectroscopy showed the disappearance of the band at around 2100 cm^{-1}, which is characteristic of isothiocyanato groups,[34] and the appearance of new bands corresponding to the thiourea moiety (Supporting Information Figure S33).[35] ^{1}H NMR (Figures S15 and S19) spectra[36] indicate that the isolated products are symmetrical and HSQC spectra (Figure 3 a,b, Figures S17 and S21) clearly show only two resonances corresponding to the four H-6 protons involved in the thiourea bridges. This is supported by the observation, on the ^{1}H NMR spectra, of a single signal matching with the two thiourea NH protons. Importantly, these NH protons strongly correlate through space with the piperazine protons, as it can be seen

Table 1. Conditions for macrocyclization.[a]

Entry	Substrate	Temp.	Time	Product, yield[b]
1	**11**[c]	RT	3 d	**13**, 48 %
2	**11**[d]	RT	3 d	**13**, trace
3	**12**[c]	RT	3 d	**14**, 61 %
4	**12**[d]	RT	3 d	**14**, trace
5	**12**[c]	RT	16 h	**14**, 65 %
6	**12**[c]	0 °C to RT	20 h	**14**, 70 %

[a] Macrocyclizations were carried out in the dark with 1.05 equiv of piperazine in pyridine (c = 0.015 mol L^{-1}). [b] Isolated yields. [c] The substrate was irradiated at 365 nm for 20 min before adding piperazine. [d] Without pre-irradiation.

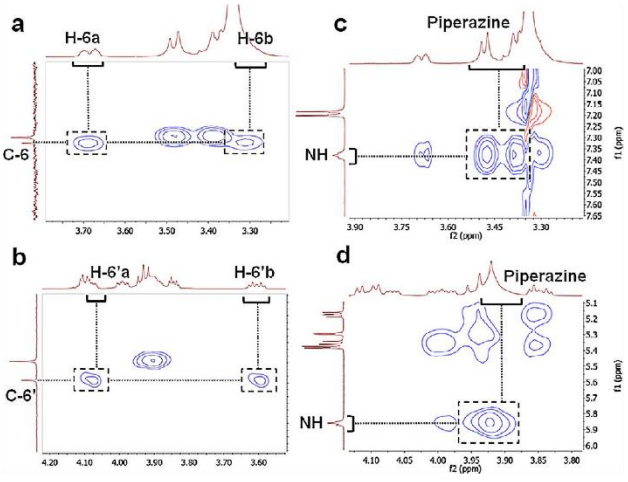

Figure 3. NMR proofs of the macrocyclization. (a) Expansion of the HSQC spectrum of **13** ([D_6]DMSO, 300 K) showing a single set of resonances for the H-6 protons; (b) expansion of the HSQC spectrum of **14** ($CDCl_3$, 300 K) showing a single set of resonances for the H-6′ protons; (c) expansion of the NOESY spectrum of **13** ([D_6]DMSO, 300 K, mixing time = 300 ms) showing a crosspeak between the thiourea protons and the protons of the piperazine; (d) expansion of the NOESY spectrum of **14** ($CDCl_3$, 300 K, mixing time = 700 ms) showing a crosspeak between the thiourea protons and the protons of the piperazine.

ChemPubSoc Europe
CHEMISTRY A European Journal Full Paper

on the NOESY spectra of **13** and **14** (Figure 3c,d, Figures S18 and S22).

In sharp contrast, when the reaction was performed under identical conditions but with no preliminary photoisomerization, only traces of the targeted macrocycles were detected by TLC analysis. As shown in Table 1 (entry 5), decreasing the reaction time did not affect the yield. In addition, we checked whether increasing the life-time of the *cis* linear scaffold, by cooling the mixture after irradiation, would improve the cyclization yield (entry 6, Table 1). Although the yield increased to 70%, this improvement was not really significant, suggesting that the percentage of conversion to **14** rather depends on the *cis*/*trans* ratio in the photostationary state (PSS) after irradiation.

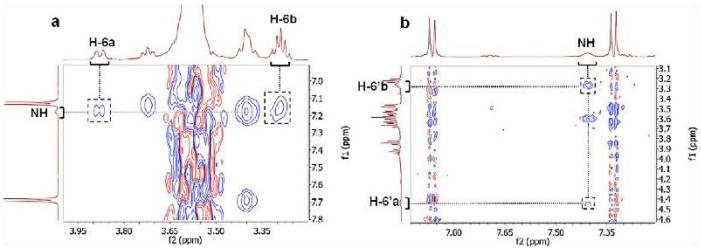

Figure 4. Expansion of the NOESY spectra showing the cross peaks between the NH of the thiourea and the H-6 forming the bridging moiety. (a) *trans*-**1** ([D_6]DMSO, 300 K, mixing time = 500 ms): the intensity ratio between the two cross peaks is 0.41. (b) *trans*-**2** (H_2O/D_2O, 300 K, mixing time = 500 ms, water suppression): the intensity ratio between the two crosspeaks is 0.39.

In a final step, compounds **13** and **14** were deacetylated under Zemplén conditions[37] to yield macrocycles **1** and **2** cleanly. As expected, the two compounds have different solubility in water: **1** is poorly soluble while **2** is fairly soluble. However, it is possible to prepare dilute aqueous solutions (ca. 10^{-4}–10^{-5} mol L^{-1}) of macrocycle **1** by using a concentrated stock solution in DMSO. The *trans* isomers of **1** and **2** were easily characterized by NMR spectroscopy. Each compound displays a single set of resonances for the two glucosides and the two maltosides units, respectively (Supporting Information Figures S23 and S26). Several data suggest that the *trans* form of **1** and **2** exhibit conformational restriction. First, the ^{1}H NMR spectra of **1** (in [D_6]DMSO) and **2** (in D_2O) show a large difference of the chemical shifts of the two H-6 involved in the thiourea bridges, with a $\Delta\delta$ of 0.58 ppm for **1** and of 1.17 ppm for **2** (Supporting Information Figures S37 and S43). Second, NOE cross peaks of the NH portion of the thiourea bridge, correlating with each of those H-6, have strongly different intensities, thereby indicating that the rotational freedom around the (C-6)–N or the N–C(S) bond is restricted (Figure 4).

Photoswitching properties and investigation of the conformational change

We next investigated the photoswitching ability of the unprotected macrocycles **1** and **2** by UV/visible absorption and NMR spectroscopy (Figure 5, Table 2). The absorption curves of the *trans* isomers show a large band with a maximum at around 350 nm, corresponding to the $\pi \rightarrow \pi^*$ transition of the azoben-

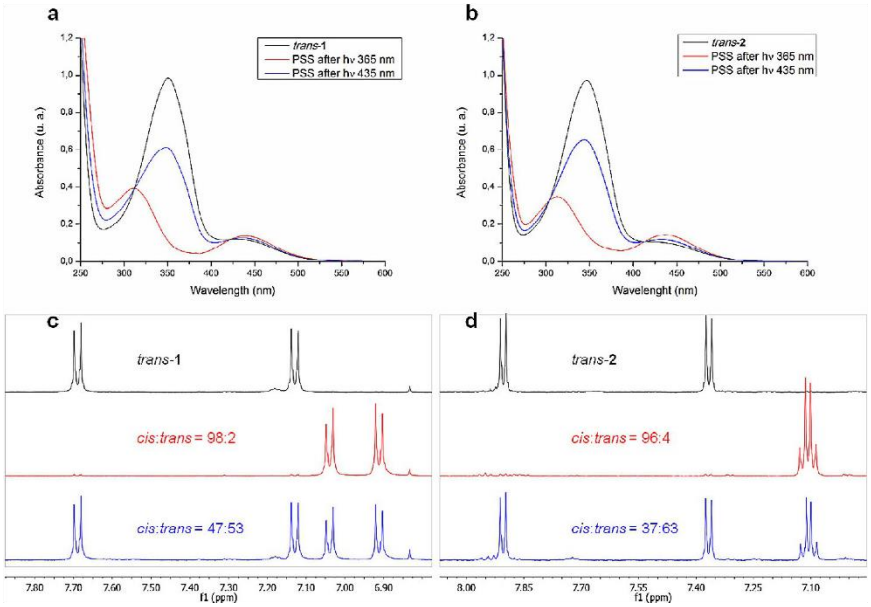

Figure 5. (a) Absorption spectra of **1** (5.10^{-5} mol L^{-1} in water (0.5% DMSO)) at 298 K. Black line: *trans* isomers; red lines: PSS after irradiating the *trans* form for 2 min at 365 nm; blue line: PSS after irradiating the *cis* form for 2 min at 435 nm; b) Absorption spectra of **2** (5.10^{-5} mol L^{-1} in water) at 298 K. Black line: *trans* isomers; red line: PSS after irradiating the *trans* form for 2 min at 365 nm; blue line: PSS after irradiating the *cis* form for 2 min at 435 nm; (c) Partial ^{1}H NMR spectra of **1** ([D_6]DMSO, 300 K). Black line: *trans* isomers; red line: PSS after irradiating the *trans* form for 5 min at 365 nm; blue line: PSS after irradiating the *cis* form for 5 min at 435 nm; (d) Partial ^{1}H NMR spectra of **2** (D_2O, 300 K). Black line: *trans* isomers; red line: PSS after irradiating the *trans* form for 5 min at 365 nm; blue line: PSS after irradiating the *cis* form for 5 min at 435 nm.

ChemPubSoc Europe

CHEMISTRY A European Journal Full Paper

Table 2. Photochromic parameters of the photoswitchable macrocycles **1** and **2**.

Compound	λ_{max} (*trans*) [nm]	λ_{max} (PSS 365 nm) [nm]		ε (*trans*)[a] [L mol^{-1} cm^{-1}]	ε (PSS 365 nm)[b] [L mol^{-1} cm^{-1}]	PSS 365 nm *trans*:*cis* ratio[c]	PSS 435 nm *trans*:*cis* ratio[c]	$\tau_{1/2}$[d] [h]
1	350	310	439	20256	2105	2:98	53:47	6.2
2	347	313	437	16764	2491	4:96	63:37	17.2

[a] Molar extinction coefficient at 350 nm for **1**, 347 nm for **2**. [b] Molar extinction coefficient at 439 nm for **1**, 437 nm for **2**. [c] Ratio measured by integrating the signals of *trans* and *cis* azobenzene moieties in the ^{1}H NMR spectra, PSS = photostationary state. [d] Half-life of the *cis* isomer determined by ^{1}H NMR at 300 K; the *trans*/*cis* ratio was measured as described in [c].

zene moiety. It is noteworthy that this band also exhibits a shoulder, from 400 to 500 nm, corresponding to an overlap between the $\pi\rightarrow\pi^*$ and $n\rightarrow\pi^*$ bands. Upon irradiation at 365 nm for a few minutes, the *trans* isomers of **1** and **2** readily switch to their *cis* form with respective *cis*:*trans* ratio of 98:2 and 96:4 in the PSS. Also, the absorption spectra in the *cis* state show a hypsochromic shift of the $\pi\rightarrow\pi^*$ band at around 310 nm and the $n\rightarrow\pi^*$ was observed at around 440 nm. As shown in Table 2, the absorption wavelength and the molar extinction coefficients are in agreement with those previously reported for azobenzene glycosides.[18b] In contrast, the back photoisomerization, by irradiating the *cis* forms at 435 nm, leads to a PSS with, respectively 53 and 63% of recovered *trans*-**1** and *trans*-**2**. This can be explained by the fact that the respective $n\rightarrow\pi^*$ transitions of the *trans* and *cis* isomers overlap and the intensity of the $n\rightarrow\pi^*$ band of the *trans* form is high enough for allowing *trans*$\rightarrow$*cis* isomerization by irradiation with blue light.

However, it is possible to fully relax the *cis* isomer by heating the sample in the dark (ca. 16 h at 45 °C). We also examined the robustness of **1** and **2** towards alternating photoirradiation at 365 and 435 nm where no photobleaching was observed within ten irradiation cycles (Figure 6).

The thermal relaxation of *cis*-**1** and *cis*-**2** was monitored by ^{1}H NMR (Table 2). At 300 K, the half-life of *cis*-**1** (in [D$_6$]DMSO) is about 6 h compared to 17 h for *cis*-**2** (in D$_2$O). Such a difference is not surprising, given that **1** is probably more strained due to its smaller size, hence leading to a less thermally stable *cis* macrocycle. As expected, the shape of our macrocycles greatly changes upon photoswitching, as confirmed by the significant shift of some characteristic signals in the sugar region (Figure 7). In the case of **1**, the resonances of H-1, H-6a and the protons of the piperazine spacer are shifted downfield whereas the H-6b signal is shifted upfield. The shape switching of macrocycle **2** is evident as shown by the swapping of the two anomeric protons resonances, and the two H-6′ and the piperazine protons are shifted in a similar fashion as described for *cis*-**1**. It is also notable that the free primary C-6 alcohol un-

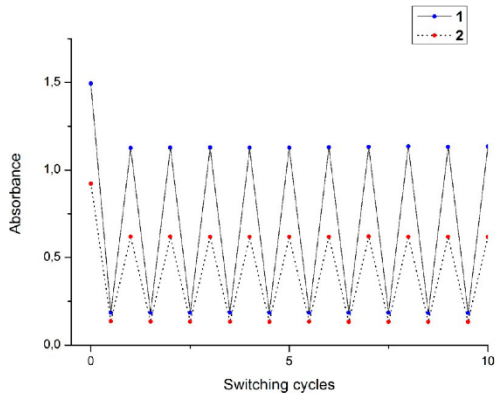

Figure 6. Measured absorbance after alternating photoirradiation at 365 nm for 2 min and at 435 nm for 2 min, over 10 cycles. Solid lines, blue points: absorbance at 350 nm for **1** (1.10^{-4} mol L^{-1} in water (0.5% DMSO)); dotted lines, red points: absorbance at 347 nm for **2** (5.10^{-5} mol L^{-1} in water).

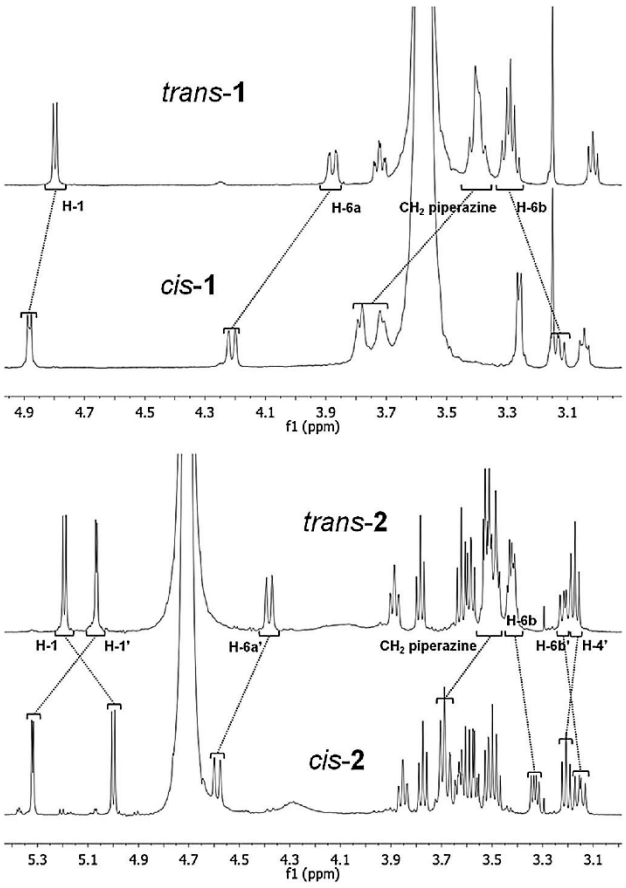

Figure 7. Evidence for large amplitude shape switching of **1** and **2** upon photoisomerization. ^{1}H NMR spectra of macrocycles **1** (5.10^{-3} mol L^{-1} in [D$_6$]DMSO, 600 MHz, 300 K) and **2** (5.10^{-3} mol L^{-1} in D$_2$O, 600 MHz, 300 K) before and after photoirradiation at 365 nm for 5 min.

ChemPubSoc Europe
CHEMISTRY A European Journal Full Paper

dergoes a significant environmental modification, according to the upfield shift of the signal of H-6b. As observed for *trans*-**1** and *trans*-**2**, their *cis* counterparts are also conformationally restricted. In this case, the two H-6 of the closing bridge have even larger difference of chemical shift ($\Delta\delta$ of 1.08 and 1.44 ppm for *cis*-**1** and *cis*-**2**, respectively, see Supporting Information, Figure S37 and S43) and the NOESY spectra also showed different intensities of the cross-peaks between the NH moieties and those H-6 (Figures S40 and S46).

We performed stochastic dynamics with MacroModel[38] (OPLS3 force field in implicit water at 300 K, see Supporting Information), in order to generate plausible structures of the *trans* and *cis* isomers of each macrocycle (Figure 8). The calculations yielded difference in energy between *trans* and *cis* isomers of 91.59 and 39.83 kJ mol^{-1}, respectively for **1** and **2**. In comparison with **2**, the larger energy gap between *trans*- and *cis*-**1** is consistent with a stronger ring strain due to the smaller size of macrocycle **1**. Also, the interglycosidic linkage of the maltoside units composing **2** may allow for more rotational freedom, thereby lowering the energy difference between the *trans* and *cis* isomers. The low-energy conformers depict the large amplitude shape change occuring by isomerization of the azobenzene hinge with each macrocycle exhibiting cavities that strongly vary in size and shape upon light-irradiation or heating.

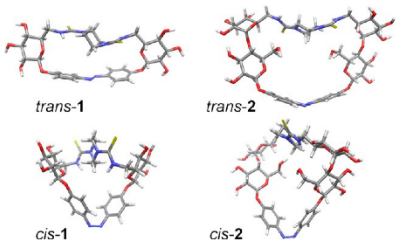

Figure 8. Low-energy conformers of *trans* and *cis* forms of **1** and **2** calculated with Macromodel 11.1 (OPLS3 force field in implicit water).

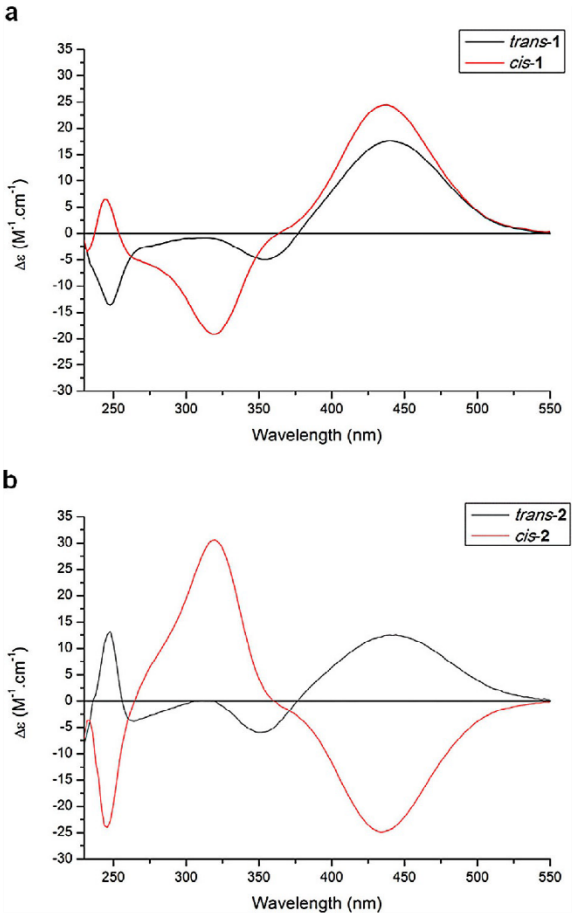

Figure 9. Chiroptical properties of **1** and **2**. (a) Circular dichroism spectra of **1** (5.10^{-5} mol L^{-1} in water (0.5% DMSO), light path length = 10 mm, 293 K) before (black line, *trans*) and after (red line, PSS) 10 min irradiation at 365 nm; specific rotation of **1** (c 0.044, 9:1 water/DMSO, light path length = 10 cm, 293 K) before (*trans*) and after 10 min irradiation at 365 nm; (b) Circular dichroism spectra of **2** (5.10^{-5} mol L^{-1} in water, light path length = 10 mm, 293 K) before (black line, *trans*) and after (red line, PSS) 10 min irradiation at 365 nm; specific rotation of **2** (c 0.054, water, light path length = 10 cm, 293 K) before (*trans*) and after 10 min irradiation at 365 nm.

Chiroptical properties

The influence of shape switching on the chirality of macrocycles **1** and **2** was also investigated. We first measured the specific rotation of the *trans* isomers and observed high values, +439° and +461° for **1** and **2**, respectively. These values dramatically change after irradiation at 365 nm to +683° for *cis*-**1** and −623° for *cis*-**2**. We also measured circular dichroism (CD) spectra before and after irradiation (Figure 9).

Both *trans* and *cis* macrocycles show two bands, at around 350 and 440 nm, matching with the azobenzene moiety (see Figure 5 and Table 2) and a third one at around 245 nm, that can be attributed to the thiourea function.[39] The CD spectra of *trans*-**1** and *trans*-**2** show comparable patterns, with significant positive and negative Cotton effects at around 440 nm (n→π* transition) and 350 nm (π→π* transition), respectively. As observed in specific rotation measurements, photoswitching induces a drastic alteration of the CD signals, producing strong bands at around 435 nm (n→π* transition) and 320 nm (π→π* transition). Interestingly, a negative band at 319 nm ($\Delta\varepsilon = -19\ M^{-1}cm^{-1}$) and a positive band at 437 nm ($\Delta\varepsilon = +24\ M^{-1}cm^{-1}$) were observed for *cis*-**1** whereas the opposite pattern was seen in the spectrum of *cis*-**2** ($\Delta\varepsilon = +30\ M^{-1}cm^{-1}$ at 320 nm, $-25\ M^{-1}cm^{-1}$ at 434 nm).

These data provide valuable clues about the structure and the chiroptical properties of our macrocycles. First, the specific rotation values show that the chirality is strongly influenced by the *trans*→*cis* isomerization, especially in the case of **2**, where the sign of the optical rotation switches from plus to minus. In addition, the CD spectra prove that a transfer of chirality occurs from the optically active carbohydrate units to the achiral azobenzene part.[23b,c,e] On the one hand NMR data (Figure 4, Supporting Information Figures S23 and S26) prove that each *trans* isomer exists in the form of one predominant

ChemPubSoc Europe

CHEMISTRY A European Journal Full Paper

conformer; on the other hand, the corresponding CD spectra (Figure 9) indicate that the *trans* macrocycles exhibit a well-defined chirality. More strikingly, the CD signature of the azobenzene moiety after photoswitching is typical of a helical twist, for which a left-handed (*M*) or right-handed (*P*) conformations are possible.[23b,e] The observed strong Cotton effect indicates that only one of these single conformers of the *cis*-macrocycle predominates in solution. Moreover, a comparison of the spectra of *cis*-**1** and *cis*-**2** reveals that they display opposite handedness. This result is important because it also suggests that the *trans*→*cis* isomerization of the photoresponsive hinge may occur following an unidirectional motion, as it has been demonstrated by Haberhauer et al. in the case of azobenzenes clamped with small cyclo-peptide scaffolds.[23b,f]

Conclusion

In this report, we have described the synthesis and characterization of the first photoswitchable macrocycles based on carbohydrate units. These compounds were prepared from inexpensive naturally occurring sugars by an efficient photo-assisted macrocyclization reaction. The stable *trans* macrocycles readily isomerize into their *cis* form upon irradiation with UV-light, and yield a high *cis*:*trans* ratio in the photostationary state. The isomerization process is fully reversible by thermal relaxation, whereas the *trans* derivative is only partially recovered by irradiation with blue light. NMR spectroscopy proved that photoswitching induces a significant structural change, with a restricted conformational freedom in both *trans* and *cis* states. Significantly, the measurements of specific rotation and circular dichroism spectra revealed intriguing chiroptical properties. Indeed, the important shape modification triggered by photoirradiation results in a remarkable chiroptical switching, notably with the induction of a single helical conformer in the *cis* state. Based on this last observation, we postulated that the *trans*→*cis* isomerization of the azobenzene hinge may take place following an unidirectional motion.

The data reported in this paper demonstrate that macrocycles **1** and **2** fulfill the essential criteria initially defined: a reversible shape switching between two well-defined structural forms. This allows for the photocontrol of functional features such as the uptake of guest molecules into the cavity, for instance. Efforts will be made for installing functional groups on the carbohydrate units, thereby making the macrocycles amenable for the preparation of photoswitchable catalysts or multivalent scaffolds. Further NMR and modeling investigations are under way in our group in order to accurately solve the structure of **1** and **2**. Also, we need to calculate the theoretical CD spectra for supporting the assumption that a sole *cis*-helical conformation exists in solution and to determine the handedness of each respective helix. Overall, this study demonstrates the great potential of these new functional macrocycles for a range of applications, including the design of water-soluble chiroptical switches.

Experimental Section

General methods

Moisture-sensitive reactions were carried out in flame-dried glassware and under a positive pressure of nitrogen. Analytical thin layer chromatography (TLC) was performed on silica gel plates (GF 254, Merck). Visualization was achieved by UV light and/or with 10% sulfuric acid in ethanol, vanillin (3.0 g vanillin and 0.5 mL H_2SO_4 in 100 mL EtOH) or ninhydrin, followed by heat treatment at ca. 200 °C. The products were purified by flash chromatography on silica gel columns (Merck, 230–400 mesh, particle size 0.040–0.063 mm) or by automated flash chromatography using a puriFlash 450 device from the Interchim company. Acetonitrile was dried over calcium hydride and methanol was dried over magnesium under a nitrogen atmosphere. Melting points (mp) were determined on a Büchi M-56 apparatus. Optical rotations were measured with a PerkinElmer 241 polarimeter with a sodium D-line (589 nm) and a cuvette of 10 cm path length, in the solvents indicated. Circular dichroism spectroscopy was performed on a Jasco J-720 CD spectrometer (Jasco, Tokyo, Japan) with a bandwidth of 1 nm and a cuvette of 10 mm path length. Proton (^{1}H) nuclear magnetic resonance spectra and carbon (^{13}C) nuclear magnetic resonance spectra were recorded on a Bruker DRX-500 and AV-600 spectrometer. Chemical shifts are referenced to internal tetramethylsilane (TMS) or 4,4-dimethyl-4-silapentane-1-sulfonic acid (DSS), or to the residual proton of the NMR solvent. Data are presented as follows: chemical shift, multiplicity (s = singlet, d = doublet, t = triplet, q = quartet, m = multiplet, and br = broad signal), coupling constant in hertz (Hz) and, integration. Full assignment of the signals was achieved by using 2D NMR techniques (^{1}H–^{1}H COSY and ^{1}H–^{13}C HSQC. All NMR spectra of the *E*-isomers of the azobenzene derivatives were recorded after they were kept for 20 h in the dark at 45 °C. Infrared (IR) spectra were measured with a PerkinElmer FT-IR Paragon 1000 (ATR) spectrometer and were reported in cm^{-1}. ESI mass spectra were recorded on a LCQ Classic from Thermo Finnigan and HRMS MALDI-TOF spectra on a ThermoScientific LTQ Orbitrap XL. *Trans*→*cis* photoisomerization experiments were performed using a LED emitting a 365 nm light from Nichia Corporation with a FWHW of 10 nm and an optical power output of 1100 mW. *Cis*→*trans* photoisomerization experiments were performed using a LED emitting a 435 nm light from Roithner Corporation with a FWHW of 14 nm and an optical power output of 350 mW. UV/Vis absorption spectra were measured on PerkinElmer Lambda-241.

Synthetic procedures for the preparation of compounds **4**, **6**–**8**, **9** and **10** are given in the Supporting information, as well as detailed description of the photoswitching experiments (UV/Vis, NMR, CD, optical rotation), the determination of the photochromic properties and the molecular modeling.

(*E*)-*p*,*p*′-Di-(2,3,4-tri-*O*-acetyl-6-deoxy-6-isothiocyanato-β-D-glucopyranosyloxy)azobenzene (11). To a solution of **9** (0.300 g, 0.357 mmol) in chloroform (6.00 mL) were sequentially added carbon disulfide (1.82 mL, 30.3 mmol, 85 equiv) then triphenylphosphine (0.787 g, 3.00 mmol, 8.5 equiv). The mixture was stirred at room temperature for 2 d then concentrated to dryness. The residue was purified by flash chromatography (cyclohexane/ethyl acetate 1:1) to give **11** (0.274 g, 88%) as a pale-orange foam. $[\alpha]^{20}_D$ −30.8 (c = 0.25 in $CHCl_3$); ^{1}H NMR (500 MHz, $CDCl_3$) δ = 7.91 (d, $J_{ortho\text{-}meta}$ = 8.6 Hz, 4H, 4Ar-H_{ortho}), 7.14 (d, $J_{meta\text{-}ortho}$ = 8.6 Hz, 4H, 4Ar-H_{meta}), 5.35–5.28 (m, 4H, H-2, H-3), 5.22 (d, $J_{1,2}$ = 7.2 Hz, 2H, H-1), 5.04 (dd, $J_{4,3}$ = $J_{4,5}$ = 9.3 Hz, 2H, H-4), 3.96–3.87 (m, 2H, H-5), 3.73 (dd, $J_{6a,6b}$ = 15.0 Hz, $J_{6a,5}$ = 7.0 Hz, 2H, H-6a), 3.67 (dd, $J_{6b,6a}$ = 14.8 Hz, $J_{6b,5}$ = 3.1 Hz, 2H, H-6a), 2.09 (s, 6H, 2CH_3C=O), 2.08 (s, 6H, 2CH_3C=

ChemPubSoc Europe

CHEMISTRY A European Journal Full Paper

O), 2.05 (s, 6H, $2CH_3C{=}O$); ^{13}C NMR (126 MHz, $CDCl_3$) $\delta = 170.2$ ($CH_3C{=}O$), 169.7 ($CH_3C{=}O$), 169.4 ($CH_3C{=}O$), 158.6 (Ar-C_{para}), 148.8 (Ar-C_{ipso}), 135.0 (NCS), 124.8 (Ar-C_{ortho}), 117.4 (Ar-C_{meta}), 98.9 (C-1), 73.0 (C-5), 72.3 (C-3), 71.2 (C-2), 69.7 (C-4), 46.3 (C-6), 20.8 ($CH_3C{=}O$), 20.7 ($CH_3C{=}O$); IR (ATR): $\tilde{\nu} = 2937$, 2100, 1748, 1597, 1497, 1435, 1369, 1211, 1153, 1063, 1035, 909, 853, 732, 695 cm^{-1}; MALDI-TOF HRMS: *m/z*: calcd for $C_{38}H_{40}N_4O_{16}S_2{+}K^+$: 911.1512 [$M+K^+$]; found: 911.1515.

(*E*)-*p*,*p*′-Di-((2,3,4-tri-*O*-acetyl-6-deoxy-6-isothiocyanato-α-D-glucopyranosyl)-(1→4)-2,3,6-tri-*O*-acetyl-β-D-glucopyranosyloxy)azobenzene (12): To a solution of 10 (0.583 g, 0.411 mmol) in chloroform (2.50 mL) were sequentially added carbon disulfide (2.50 mL, 41.1 mmol, 100 equiv) then triphenylphosphine (0.916 g, 3.29 mmol, 8 equiv). The mixture was stirred at room temperature for 2 d then concentrated to dryness. The residue was purified by flash chromatography (cyclohexane/ethyl acetate 9:1 to 2:3 within 15 min) to give 12 (0.480 g, 81%) as a pale-orange foam. $[\alpha]^{20}_D$ +88.4 ($c = 0.5$ in $CHCl_3$); ^1H NMR (500 MHz, $CDCl_3$) $\delta = 7.92$–7.84 (m, 4H, 4Ar-H_{ortho}), 7.15–7.05 (m, 4H, 4Ar-H_{meta}), 5.46 (d, $J_{1',2'} = 3.9$ Hz, 2H, H-1′), 5.39 (dd, $J_{3',2'} = 10.4$ Hz, $J_{3',4'} = 9.5$ Hz, 2H, H-3′), 5.34 (dd, $J_{3,2} = J_{3,4} = 8.7$ Hz, 2H, H-3), 5.24 (d, $J_{1,2} = 7.4$ Hz, 2H, H-1), 5.14 (dd, $J_{2,3} = 8.7$ Hz, $J_{2,1} = 7.4$ Hz, 2H, H-2), 4.97 (dd, $J_{4',3'} = J_{4',5'} = 9.8$ Hz, 2H, H-4′), 4.85 (dd, $J_{2',3'} = 10.5$ Hz, $J_{2',1'} = 3.9$ Hz, 2H, H-2′), 4.54 (dd, $J_{6a,6b} = 12.0$ Hz, $J_{6a,5} = 2.7$ Hz, 2H, H-6a), 4.28 (dd, $J_{6b,6a} = 12.1$ Hz, $J_{6b,5} = 5.3$ Hz, 2H, H-6b), 4.12 (dd, $J_{4,5} = 9.4$ Hz, $J_{4,3} = 8.8$ Hz, 2H, H-4), 4.01–3.96 (m, 2H, H-5′), 3.93 (ddd, $J_{5,4} = 9.4$ Hz, $J_{5,6b} = 5.2$ Hz, $J_{5,6a} = 2.8$ Hz, 2H, H-5), 3.63 (d, $J = 4.2$ Hz, 4H, H-6′a, H-6′b), 2.11 (s, 6H, $2CH_3C{=}O$), 2.08 (s, 6H, $2CH_3C{=}O$), 2.07 (s, 6H, $2CH_3C{=}O$), 2.06 (s, 12H, $4CH_3C{=}O$), 2.02 (s, 6H, $2CH_3C{=}O$); ^{13}C NMR (126 MHz, $CDCl_3$) $\delta = 170.7$ ($CH_3C{=}O$), 170.6 ($CH_3C{=}O$), 170.4 ($CH_3C{=}O$), 170.0 ($CH_3C{=}O$), 169.7 ($CH_3C{=}O$), 169.6 ($CH_3C{=}O$), 158.7 (Ar-C_{para}), 148.7 (Ar-C_{ipso}), 135.7 (NCS), 124.6 (Ar-C_{ortho}), 117.2 (Ar-C_{meta}), 98.2 (C-1), 95.8 (C-1′), 75.2 (C-3), 73.3 (C-4), 72.3 (C-5), 72.0 (C-2), 70.2 (C-2′), 69.5 (C-4′), 69.0 (2C, C-3′, C-5′), 62.9 (C-6), 46.0 (C-6′), 21.1 ($CH_3C{=}O$), 20.93 ($CH_3C{=}O$), 20.8 ($CH_3C{=}O$), 20.7 ($CH_3C{=}O$); IR (ATR): $\tilde{\nu} = 2944$, 2072, 1743, 1598, 1497, 1367, 1208, 1031, 938, 900, 846, 751 cm^{-1}; MALDI-TOF HRMS: *m/z*: calcd for $C_{62}H_{72}N_4O_{32}S_2{+}K^+$: 1487.3203 [$M+K^+$]; found: 1487.3240.

Macrocycle 13. A solution of **11** (0.050 g, 0.057 mmol) in dry pyridine (1.90 mL) was irradiated at 365 nm for 20 min then shielded from light. A solution of piperazine (5.2 mg, 0.060 mmol, 1.05 equiv) in dry pyridine (1.90 mL) was added then the mixture was stirred in the dark at room temperature for 3 days then concentrated to dryness. The residue was dissolved in ethyl acetate then washed three times with 1 M aqueous HCl. The aqueous layer was extracted with ethyl acetate then the combined organic layers were washed with brine, dried over magnesium sulfate, filtered and concentrated under reduced pressure. The residue was purified by flash chromatography (CH_2Cl_2/ethyl acetate 2:3). The isolated compound was filtered through Sephadex LH20 permeation gel (elution with 1:1 CH_2Cl_2/methanol) to give **13** (0.026 g, 48%) as an amorphous yellow solid. $[\alpha]^{20}_D$ +996 ($c = 0.25$ in $CHCl_3$); ^1H NMR (500 MHz, [D_6]DMSO) $\delta = 7.82$–7.68 (m, 4H, 4Ar-H_{ortho}), 7.38 (t, $J = 5.2$ Hz, 2H, HN-C=S), 7.27–7.14 (m, 4H, 4Ar-H_{meta}), 5.52 (d, $J_{1,2} = 8.1$ Hz, 2H, H-1), 5.42 (dd, $J_{3,2} = J_{3,4} = 9.3$ Hz, 2H, H-3), 5.11 (dd, $J_{2,3} = 9.4$ Hz, $J_{2,1} = 8.2$ Hz, 2H, H-2), 4.83 (dd, $J_{4,3} = J_{4,5} = 9.6$ Hz, 2H, H-4), 4.30–4.26 (m, 2H, H-5), 3.76–3.62 (m, 2H, H-6a), 3.48 (d, $J = 9.7$ Hz, 4H, 4H-piperazine), 3.45–3.25 (m, 6H, H-6b, 4H-piperazine), 2.09 (s, 6H, $2CH_3C{=}O$), 2.02 (s, 6H, $2CH_3C{=}O$), 1.99 (s, 6H, $2CH_3C{=}O$); ^{13}C NMR (126 MHz, [D_6]DMSO) $\delta = 181.0$ (C=S), 169.6 ($CH_3C{=}O$), 169.3 ($CH_3C{=}O$), 157.3 (Ar-C_{para}), 148.0 (Ar-C_{ipso}), 123.5 (Ar-C_{ortho}), 120.0 (Ar-C_{meta}), 97.3 (C-1), 72.5 (C-3), 71.4 (C-4), 70.8 (C-2), 70.1 (C-5), 46.1 (C-6), 45.7 (C-piperazine), 20.5 ($CH_3C{=}O$), 20.4 ($CH_3C{=}O$), 20.3 ($CH_3C{=}O$); IR (ATR): $\tilde{\nu} = 3305$, 2934, 1748, 1597,1529, 1499, 1364, 1319, 1204, 1032, 1002, 894, 837, 694 cm^{-1}; MALDI-TOF HRMS: *m/z*: calcd for $C_{42}H_{51}N_6O_{16}S_2$: 959.2798 [$M+H^+$]; found: 959.2799.

Macrocycle 14. A solution of **12** (0.108 g, 0.075 mmol) in dry pyridine (2.50 mL) was irradiated at 365 nm for 20 min then shielded from light. A solution of piperazine (6.8 mg, 0.079 mmol, 1.05 equiv) in dry pyridine (2.50 mL) was added then the mixture was stirred in the dark at room temperature for 3 days then concentrated to dryness. The residue was dissolved in ethyl acetate then washed three times with 1 M aqueous HCl. The aqueous layer was extracted with ethyl acetate then the combined organic layers were washed with brine, dried over magnesium sulfate, filtered and concentrated under reduced pressure. The residue was purified by automated flash chromatography (CH_2Cl_2/ethyl acetate 9:1 to 1:1 within 10 min) to give **14** (0.070 g, 61%) as an amorphous pale orange solid. $[\alpha]^{20}_D$ +45.0 ($c = 0.25$ in $CHCl_3$); ^1H NMR (600 MHz, $CDCl_3$) $\delta = 7.89$–7.82 (m, 4H, 4Ar-H_{ortho}), 7.17–7.09 (m, 4H, 4Ar-H_{meta}), 5.85 (t, $J = 5.6$ Hz, 2H, *H*N–C=S), 5.40–5.33 (m, 4H, H-1, H-3′), 5.29 (d, $J_{1',2'} = 3.9$ Hz, 2H, H-1′), 5.17 (dd, $J_{3,4} = 8.3$ Hz, $J_{3,2} = 6.3$ Hz, 2H, H-3), 5.00 (dd, $J_{2,3} = J_{2,1} = 6.1$ Hz, 2H, H-2), 4.81 (dd, $J_{4',3'} = J_{4',5'} = 9.8$ Hz, 2H, H-4′), 4.74 (dd, $J_{2',3'} = 10.5$ Hz, $J_{2',1'} = 3.9$ Hz, 2H, H-2′), 4.32 (dd, $J_{6a,6b} = 12.0$ Hz, $J_{6a,5} = 3.2$ Hz, 2H, H-6a), 4.15–4.05 (m, 4H, H-6b, H-6′a), 4.03–3.96 (m, 2H, H-5′), 3.97–3.87 (m, 10H, H-4, 8H-piperazine), 3.86–3.83 (m, 2H, H-5), 3.63–3.58 (m, 2H, H-6′b), 2.16 (s, 6H, $2CH_3C{=}O$), 2.09 (s, 6H, $2CH_3C{=}O$), 2.06 (s, 6H, $2CH_3C{=}O$), 2.05 (s, 6H, $2CH_3C{=}O$), 1.99 (s, 6H, $2CH_3C{=}O$), 1.98 (s, 6H, $2CH_3C{=}O$); ^{13}C NMR (151 MHz, $CDCl_3$) $\delta = 182.5$ (C=S), 170.8 ($CH_3C{=}O$), 170.6 ($CH_3C{=}O$), 170.2 ($CH_3C{=}O$), 170.1 ($CH_3C{=}O$), 169.9 ($CH_3C{=}O$), 169.7 ($CH_3C{=}O$), 156.2 (Ar-C_{para}), 149.3 (Ar-C_{ipso}), 124.2 (Ar-C_{ortho}), 121.0 (Ar-C_{meta}), 97.7 (C-1), 96.5 (C-1′), 75.3 (C-3), 73.6 (C-4), 72.5 (C-5), 71.6 (C-2), 70.8 (C-2′), 69.7 (C-5′), 69.5 (C-4′), 69.1 (C-3′), 62.5 (C-6), 46.8 (C-6′), 45.4 (C-piperazine), 21.1 ($CH_3C{=}O$), 20.9 ($CH_3C{=}O$), 20.7 ($CH_3C{=}O$); IR (ATR): $\tilde{\nu} = 3380$, 2942, 1742, 1597, 1527, 1497, 1367, 1209, 1144, 1029, 940, 899, 847, 748 cm^{-1}; MALDI-TOF HRMS: *m/z*: calcd for $C_{66}H_{83}N_6O_{32}S_2$: 1535.4488 [$M+H^+$]; found: 1535.4471.

Macrocycle 1. To a solution of **13** (0.016 g, 0.017 mmol) in dry methanol (1.00 mL) was added 5.4 M sodium methoxide in methanol (2 drops) then the mixture was stirred at room temperature for 16 h. After neutralization with IR-120 H^+ amberlite resin, the solution was diluted with methanol then filtered and the filtrate was concentrated to dryness to furnish **1** (12 mg, quant.) as an amorphous yellow solid.

***Trans* isomer:** $[\alpha]^{20}_D$ +439 ($c = 0.044$ in 9:1 water/DMSO); ^1H NMR (600 MHz, [D_6]DMSO + εD_2O) $\delta = 7.69$ (d, $J_{ortho\text{-}meta} = 8.9$ Hz, 4H, 4Ar-H_{ortho}), 7.18 (t, $J = 5.0$ Hz, 2H, 2*H*N-C=S), 7.13 (d, $J_{meta\text{-}ortho} = 8.6$ Hz, 4H, 4Ar-H_{meta}), 5.56 (d, $J = 4.1$ Hz, 2H, OH-2 or OH-3), 5.33–5.19 (m, 4H, OH-2 or OH-3, OH-4), 4.80 (d, $J_{1,2} = 7.4$ Hz, 2H, H-1), 3.88 (dd, $J_{6a,6b} = 13.5$ Hz, $J_{6a,5} = 2.4$ Hz, 2H, H-6a), 3.74–3.70 (m, 2H, H-5), 3.42–3.37 (m, 8H, 8H-piperazine), 3.33–3.26 (m, 6H, H-2, H-3, H-6b), 3.02 (dd, $J_{4,3} = J_{4,5} = 8.9$ Hz, 2H, H-4); ^{13}C NMR (151 MHz, [D_6]DMSO + εD_2O) $\delta = 181.07$ (C=S), 158.4 (Ar-C_{para}), 147.9 (Ar-C_{ipso}), 123.6 (Ar-C_{ortho}), 120.0 (Ar-C_{meta}), 100.8 (C-1), 77.1 (C-2 or C-3), 73.8 (C-4), 73.3 (C-2 or C-3), 72.6 (C-5), 47.3 (C-6), 45.9 (C-piperazine); IR (ATR): $\tilde{\nu} = 3387$, 2918, 1600, 1587, 1524, 1501, 1436, 1380, 1333, 1310, 1279, 1242, 1214, 1074, 1057, 1036, 882, 850, 834, 822, 763, 718, 655 cm^{-1}; MALDI-TOF HRMS: *m/z*: calcd for $C_{30}H_{39}N_6O_{10}S_2$: 707.2164 [$M+H^+$]; found: 707.2165.

***Cis* isomer:** $[\alpha]^{20}_D$ +683 ($c = 0.044$ in 9:1 water/DMSO); ^1H NMR (600 MHz, [D_6]DMSO) $\delta = 7.04$ (d, $J_{ortho\text{-}meta} = 8.8$ Hz, 4H, 4Ar-H_{ortho}), 6.92–6.90 (m, 6H, 4Ar-H_{meta}, 2*H*N–C=S), 5.48 (s, 1H, 2H, OH-2 or OH-3), 5.37 (d, $J = 4.9$ Hz, 2H, OH-4), 5.25 (s, 2H, OH-2 or OH-3),

ChemPubSoc Europe

CHEMISTRY A European Journal Full Paper

4.88 (d, $J_{1,2}=7.2$ Hz, 2H, H-1), 4.21 (d, $J_{6a,6b}=12.2$ Hz, 2H, H-6a), 3.84–3.67 (m, 8H, 8H-piperazine), 3.33–3.22 (m, 4H, H-2, H-3), 3.13 (dd, $J_{6b,6a}=13.5$ Hz, $J_{6b,5}=10.3$ Hz, 2H, H-6b), 3.06–3.03 (m, 2H, H-4); ^{13}C NMR (151 MHz, [D$_6$]DMSO) $\delta=181.7$ (C=S), 156.3 (Ar-C$_{para}$), 147.3 (Ar-C$_{ipso}$), 122.5 (Ar-C$_{ortho}$), 116.4 (Ar-C$_{meta}$), 99.7 (C-1), 76.4 (C-2 or C-3), 74.0 (C-5), 73.2 (C-2 or C-3), 72.2 (C-4), 47.7 (C-6), 45.6 (C-piperazine).

Macrocycle 2. To a solution of **14** (0.060 g, 0.039 mmol) in dry methanol (2.00 mL) was added 5.4 M sodium methoxide in methanol (3 drops) then the mixture was stirred at room temperature for 5 h. After neutralization with IR-120 H$^+$ amberlite resin, the solution was diluted with methanol and water then filtered and the filtrate was concentrated then lyophilized to afford **2** (0.036 g, 90%) as an amorphous pale-orange solid.

***Trans* isomer:** $[\alpha]^{20}_D$ +461 ($c=0.054$ in water); ^{1}H NMR (600 MHz, D$_2$O) $\delta=7.89$ (d, $J_{ortho\text{-}meta}=8.9$ Hz, 4H, 4Ar-H$_{ortho}$), 7.35 (d, $J_{meta\text{-}ortho}=9.0$ Hz, 4H, 4Ar-H$_{meta}$), 5.28 (d, $J_{1,2}=7.6$ Hz, 2H, H-1), 5.15 (d, $J_{1',2'}=3.9$ Hz, 2H, H-1′), 4.47 (d, $J_{6'a\text{-}6'b}=12.7$ Hz, 2H, H-6′a), 3.99–3.95 (m, 2H, H-5′), 3.87 (dd, $J_{3,4}=J_{3,2}=8.9$ Hz, 2H, H-3), 3.70 (dd, $J_{3',4'}=J_{3',2'}=9.5$ Hz, 2H, H-3′), 3.68–3.53 (m, 16H, H-2, H-4, H-6a, H-2′, 8H-piperazine), 3.52–3.49 (m, 4H, H-5, H-6b), 3.30 (dd, $J_{6'b,6'a}=14.5$ Hz, $J_{6'b,5'}=9.2$ Hz, 2H, H-6′b), 3.26 (dd, $J_{4',3'}=J_{4',5'}=9.6$ Hz, 2H, H-4′); ^{13}C NMR (151 MHz, D$_2$O, DSS) $\delta=181.6$ (C=S), 160.0 (Ar-C$_{para}$), 151.5 (Ar-C$_{ipso}$), 126.8 (Ar-C$_{ortho}$), 123.6 (Ar-C$_{meta}$), 104.2 (C-1′), 103.1 (C-1), 82.7 (C-4), 78.7 (C-3), 77.8 (C-5), 75.4 (C-3′), 75.3 (C-2), 74.7 (C-2′), 74.5 (C-4′), 74.0 (C-5′), 62.7 (C-6), 49.9 (C-piperazine); IR (ATR): $\tilde{\nu}=$ 3326, 2925, 1597, 1537, 1496, 1347, 1276, 1231, 1144, 1042, 1004, 896, 843, 764, 751 cm^{-1}; MALDI-TOF HRMS: *m/z*: calcd for $C_{42}H_{58}N_6O_{20}S_2$: 1031.3220 [$M+H^+$]; found: 1031.3222.

***Cis* isomer:** $[\alpha]^{20}_D$ −623 ($c=0.054$ in water); ^{1}H NMR (600 MHz, D$_2$O) $\delta=7.16$–7.04 (m, 8H, 4Ar-H$_{ortho}$, 4Ar-H$_{meta}$), 5.39 (d, $J_{1',2'}=3.8$ Hz, 2H, H-1′), 5.07 (d, $J_{1,2}=7.9$ Hz, 2H, H-1), 4.66 (d, $J_{6'a\text{-}6'b}=12.9$ Hz, 2H, H-6′a), 3.94–3.90 (m, 2H, H-5′), 3.84 (dd, $J_{3,4}=J_{3,2}=9.2$ Hz, 2H, H-3), 3.80–3.65 (m, 14H, H-5, H-6a, H-2′, H-3′, 8H-piperazine), 3.64 (dd, $J_{2',3'}=9.9$ Hz, $J_{2',1'}=3.9$ Hz, 2H, H-2′), 3.61–3.53 (m, 4H, H-2, H-4), 3.40 (dd, $J_{6b,6a}=12.3$ Hz, $J_{6b,5}=6.7$ Hz, 2H, H-6b), 3.28 (dd, $J_{4',5'}=J_{4',3'}=9.4$ Hz, 2H, H-4′), 3.22 (dd, $J_{6'b,6'a}=14.3$ Hz, $J_{6'b,5'}=10.2$ Hz, 2H, H-6′b); ^{13}C NMR (151 MHz, D$_2$O, DSS) $\delta=181.21$ (C=S), 159.3 (Ar-C$_{para}$), 149.4 (Ar-C$_{ipso}$), 125.7 (Ar-C$_{ortho}$), 119.0 (Ar-C$_{meta}$), 102.8 (C-1′), 102.4 (C-1), 80.6 (C-4), 78.8 (C-3), 77.6 (C-5), 75.3 (C-3′), 75.1 (C-2), 74.7 (C-4′), 74.3 (C-2′), 73.5 (C-5′), 63.9 (C-6), 49.5 (C-6′), 48.1 (C-piperazine).

Acknowledgements

The authors warmly thank Prof. Dr. T. K. Lindhorst for fundamental support, Prof. F. D. Sönnichsen for fruitful discussion and Prof. Dr. J. Grötzinger for CD measurements. G. D. also thanks Dr. J.-P. Montserrat and Dr. V. Poonthiyil for relevant advice.

Conflict of interest

The authors declare no conflict of interest.

Keywords: chirality · glycoconjugate · macrocycles · molecular shape · photoswitch

[1] a) S. E. Gibson, C. Lecci, *Angew. Chem. Int. Ed.* **2006**, *45*, 1364–1377; *Angew. Chem.* **2006**, *118*, 1392–1405; b) L. A. Wessjohann, D. G. Rivera, O. E. Vercillo, *Chem. Rev.* **2009**, *109*, 796–814; c) C. M. Madsen, M. H. Clausen, *Eur. J. Org. Chem.* **2011**, 3107–3115; d) E. Marsault, M. L. Peterson, *J. Med. Chem.* **2011**, *54*, 1961–2004; e) K. Yamato, M. Kline, B. Gong, *Chem. Commun.* **2012**, *48*, 12142–12158; f) J. A. Wisner, *Nat. Chem.* **2013**, *5*, 646–647; g) Z. Qi, C. A. Schalley, *Acc. Chem. Res.* **2014**, *47*, 2222–2233.

[2] a) D. V. Jarikote, P. V. Murphy, *Eur. J. Org. Chem.* **2010**, 4959–4970; b) J. C. López, J. Plumet, *Eur. J. Org. Chem.* **2011**, 1803–1825; c) J. Xie, N. Bogliotti, *Chem. Rev.* **2014**, *114*, 7678–7739.

[3] a) N. Navarre, A. H. van Oijen, G. J. Boons, *Tetrahedron Lett.* **1997**, *38*, 2023–2026; b) D. R. Bundle, R. Alibés, S. Nilar, A. Otter, M. Warwas, P. Zhang, *J. Am. Chem. Soc.* **1998**, *120*, 5317–5318; c) K. S. Bisht, R. A. Gross, D. L. Kaplan, *J. Org. Chem.* **1999**, *64*, 780–789; d) G.-w. Chen, A. Kirschning, *Chem. Eur. J.* **2002**, *8*, 2717–2729; e) V. K. Tiwari, A. Kumar, R. R. Schmidt, *Eur. J. Org. Chem.* **2012**, 2945–2956.

[4] a) C.-Y. Tsai, X. Huang, C.-H. Wong, *Tetrahedron Lett.* **2000**, *41*, 9499–9503; b) J. F. Billing, U. J. Nilsson, *J. Org. Chem.* **2005**, *70*, 4847–4850; c) R. S. McGavin, R. A. Gagne, M. C. Chervenak, D. R. Bundle, *Org. Biomol. Chem.* **2005**, *3*, 2723–2732; d) M. Kaiser, A. De Cian, M. Sainlos, C. Renner, J.-L. Mergny, M.-P. Teulade-Fichou, *Org. Biomol. Chem.* **2006**, *4*, 1049–1057; e) T. Haag, R. A. Hughes, G. Ritter, R. R. Schmidt, *Eur. J. Org. Chem.* **2007**, 6016–6033.

[5] a) R. M. van Well, H. S. Overkleeft, M. Overhand, E. Vang Carstenen, G. A. van der Marel, J. H. van Boom, *Tetrahedron Lett.* **2000**, *41*, 9331–9335; b) E. Locardi, M. Stöckle, S. Gruner, H. Kessler, *J. Am. Chem. Soc.* **2001**, *123*, 8189–8196; c) J. F. Billing, U. J. Nilsson, *Tetrahedron* **2005**, *61*, 863–874; d) M. Ménand, J.-C. Blais, L. Hamon, J.-M. Valéry, J. Xie, *J. Org. Chem.* **2005**, *70*, 4423–4430; e) F. Fujimura, T. Hirata, T. Morita, S. Kimura, Y. Horikawa, J. Sugiyama, *Biomacromolecules* **2006**, *7*, 2394–2400.

[6] a) M. Mori, Y. Ito, T. Ogawa, *Carbohydr. Res.* **1989**, *192*, 131–146; b) S. A. Nepogodiev, G. Gattuso, J. F. Stoddart, *J. Inclusion Phenom. Mol. Recognit. Chem.* **1996**, *25*, 47–52; c) R. Bürli, A. Vasella, *Angew. Chem. Int. Ed. Engl.* **1997**, *36*, 1852–1853; d) J. M. Benito, J. L. Jiménez Blanco, C. Ortiz Mellet, J. M. García Fernández, *Angew. Chem. Int. Ed.* **2002**, *41*, 3674–3676; *Angew. Chem.* **2002**, *114*, 3826–3828; e) K. D. Bodine, D. Y. Gin, M. S. Gin, *J. Am. Chem. Soc.* **2004**, *126*, 1638–1639; f) S. Muthana, H. Yu, H. Cao, J. Cheng, X. Chen, *J. Org. Chem.* **2009**, *74*, 2928–2936; g) M. L. Gening, D. V. Titov, A. A. Grachev, A. G. Gerbst, O. N. Yudina, A. S. Shashkov, A. O. Chizhov, Y. E. Tsvetkov, N. E. Nifantiev, *Eur. J. Org. Chem.* **2010**, 2465–2475; h) M. L. Conte, D. Grotto, A. Chambery, A. Dondoni, A. Marra, *Chem. Commun.* **2011**, *47*, 1240–1242; i) M. L. Lepage, J. P. Schneider, A. Bodlenner, P. Compain, *J. Org. Chem.* **2015**, *80*, 10719–10733; j) K. Maiti, N. Jayaraman, *J. Org. Chem.* **2016**, *81*, 4616–4622.

[7] a) A. G. M. Barrett, N. S. Mani, *Tetrahedron Lett.* **1987**, *28*, 6133–6136; b) R. R. Bukownik, C. S. Wilcox, *J. Org. Chem.* **1988**, *53*, 463–471; c) S. Penadés, J. M. Coteron, *J. Chem. Soc. Chem. Commun.* **1992**, 683–684; d) J. M. Coteron, C. Vicent, C. Bosso, S. Penades, *J. Am. Chem. Soc.* **1993**, *115*, 10066–10076; e) R. Leyden, P. V. Murphy, *Synlett* **2009**, *2009*, 1949–1950; f) Y. Li, J. Sun, Y. Gong, B. Yu, *J. Org. Chem.* **2011**, *76*, 3654–3663; g) M. A. Potopnyk, P. Cmoch, S. Jarosz, *Org. Lett.* **2012**, *14*, 4258–4261.

[8] a) P. Bakó, Z. Bajor, L. Toke, *J. Chem. Soc. Perkin Trans. 1* **1999**, 3651–3655; b) P. Bakó, A. Makó, G. Keglevich, M. Kubinyi, K. Pál, *Tetrahedron: Asymmetry* **2005**, *16*, 1861–1871; c) M. Ménand, J.-C. Blais, J.-M. Valéry, J. Xie, *J. Org. Chem.* **2006**, *71*, 3295–3298; d) J. Xie, M. Ménand, S. Maisonneuve, R. Métivier, *J. Org. Chem.* **2007**, *72*, 5980–5985; e) S. Jarosz, B. Lewandowski, *Carbohydr. Res.* **2008**, *343*, 965–969; f) B. Lewandowski, S. Jarosz, *Chem. Commun.* **2008**, 6399–6401; g) A. Rathjens, J. Thiem, *C. R. Chim.* **2011**, *14*, 286–300.

[9] a) N. Navarre, N. Amiot, A. van Oijem, A. Imberty, A. Poveda, J. Jiménez-Barbero, A. Cooper, M. A. Nutley, G.-J. Boons, *Chem. Eur. J.* **1999**, *5*, 2281–2294; b) M. C. Galan, A. P. Venot, J. Glushka, A. Imberty, G.-J. Boons, *J. Am. Chem. Soc.* **2002**, *124*, 5964–5973; c) R. M. van Well, H. S. Overkleeft, G. A. van der Marel, D. Bruss, G. Thibault, P. G. de Groot, J. H. van Boom, M. Overhand, *Bioorg. Med. Chem. Lett.* **2003**, *13*, 331–334.

[10] a) M. Shizuma, Y. Kadoya, Y. Takai, H. Imamura, H. Yamada, T. Takeda, R. Arakawa, S. Takahashi, M. Sawada, *J. Org. Chem.* **2002**, *67*, 4795–4807; b) B. Lewandowski, S. Jarosz, *Org. Lett.* **2010**, *12*, 2532–2535.

[11] a) D. Rodríguez-Lucena, J. M. Benito, E. Álvarez, C. Jaime, J. Perez-Miron, C. Ortiz Mellet, J. M. García Fernández, *J. Org. Chem.* **2008**, *73*, 2967–2979; b) D. Rodríguez-Lucena, C. Ortiz Mellet, C. Jaime, K. K. Burusco,

ChemPubSoc Europe

CHEMISTRY A European Journal Full Paper

J. M. García Fernández, J. M. Benito, *J. Org. Chem.* **2009**, *74*, 2997 – 3008; c) A. Pathigoolla, K. M. Sureshan, *Chem. Commun.* **2014**, *50*, 317 – 319.

[12] a) C. Coppola, L. Simeone, R. Trotta, L. De Napoli, A. Randazzo, D. Montesarchio, *Tetrahedron* **2010**, *66*, 6769 – 6774; b) S.-T. Yang, D.-J. Liao, S.-J. Chen, C.-H. Hu, A.-T. Wu, *Analyst* **2012**, *137*, 1553 – 1555; c) T. Saha, A. Roy, M. L. Gening, D. V. Titov, A. G. Gerbst, Y. E. Tsvetkov, N. E. Nifantiev, P. Talukdar, *Chem. Commun.* **2014**, *50*, 5514 – 5516.

[13] a) J. Jimenez-Barbero, E. Junquera, M. Martin-Pastor, S. Sharma, C. Vicent, S. Penades, *J. Am. Chem. Soc.* **1995**, *117*, 11198 – 11204; b) J. C. Morales, S. Penadés, *Angew. Chem. Int. Ed.* **1998**, *37*, 654 – 657; *Angew. Chem.* **1998**, *110*, 673 – 676; c) J. C. Morales, D. Zurita, S. Penadés, *J. Org. Chem.* **1998**, *63*, 9212 – 9222.

[14] a) A. Makó, Á. Szöllősy, G. Keglevich, D. K. Menyhárd, P. Bakó, L. Tőke, *Monatsh. Chem.* **2008**, *139*, 525 – 535; b) A. Makó, Z. Rapi, G. Keglevich, Á. Szöllősy, L. Drahos, L. Hegedűs, P. Bakó, *Tetrahedron: Asymmetry* **2010**, *21*, 919 – 925; c) Z. Rapi, T. Szabó, G. Keglevich, Á. Szöllősy, L. Drahos, P. Bakó, *Tetrahedron: Asymmetry* **2011**, *22*, 1189 – 1196; d) Z. Rapi, P. Bakó, G. Keglevich, Á. Szöllősy, L. Drahos, A. Botyánszki, T. Holczbauer, *Tetrahedron: Asymmetry* **2012**, *23*, 489 – 496.

[15] a) R. Leyden, T. Velasco-Torrijos, S. André, S. Gouin, H.-J. Gabius, P. V. Murphy, *J. Org. Chem.* **2009**, *74*, 9010 – 9026; b) V. L. Campo, I. Carvalho, C. H. T. P. Da Silva, S. Schenkman, L. Hill, S. A. Nepogodiev, R. A. Field, *Chem. Sci.* **2010**, *1*, 507 – 514.

[16] A. N. Magpusao, K. Rutledge, T. A. Hamlin, J.-M. Lawrence, B. Q. Mercado, N. E. Leadbeater, M. W. Peczuh, *Chem. Eur. J.* **2016**, *22*, 6001 – 6011.

[17] a) F. Hamon, F. Djedaini-Pilard, F. Barbot, C. Len, *Tetrahedron* **2009**, *65*, 10105 – 10123; b) A. A. Beharry, G. A. Woolley, *Chem. Soc. Rev.* **2011**, *40*, 4422 – 4437; c) H. M. D. Bandara, S. C. Burdette, *Chem. Soc. Rev.* **2012**, *41*, 1809 – 1825; d) M. Baroncini, G. Ragazzon, S. Silvi, M. Venturi, A. Credi, *Pure Appl. Chem.* **2015**, *87*, 537 – 546.

[18] a) V. Chandrasekaran, T. K. Lindhorst, *Chem. Commun.* **2012**, *48*, 7519 – 7521; b) V. Chandrasekaran, E. Johannes, H. Kobarg, F. D. Sönnichsen, T. K. Lindhorst, *ChemistryOpen* **2014**, *3*, 99 – 108; c) A. Müller, H. Kobarg, V. Chandrasekaran, J. Gronow, F. D. Sönnichsen, T. K. Lindhorst, *Chem. Eur. J.* **2015**, *21*, 13723 – 13731; d) A. Müller, T. K. Lindhorst, *Eur. J. Org. Chem.* **2016**, 1669 – 1672.

[19] a) R. Reuter, H. A. Wegner, *Chem. Commun.* **2011**, *47*, 12267 – 12276; b) Z. Li, J. Liang, W. Xue, G. Liu, S. H. Liu, J. Yin, *Supramol. Chem.* **2014**, *26*, 54 – 65.

[20] a) Y. Norikane, K. Kitamoto, N. Tamaoki, *J. Org. Chem.* **2003**, *68*, 8291 – 8304; b) E. Luboch, E. Wagner-Wysiecka, T. Rzymowski, *Tetrahedron* **2009**, *65*, 10671 – 10678; c) Y.-T. Shen, L. Guan, X.-Y. Zhu, Q.-D. Zeng, C. Wang, *J. Am. Chem. Soc.* **2009**, *131*, 6174 – 6180; d) M. Liu, X. Yan, M. Hu, X. Chen, M. Zhang, B. Zheng, X. Hu, S. Shao, F. Huang, *Org. Lett.* **2010**, *12*, 2558 – 2561; e) S. T. J. Ryan, J. del Barrio, R. Suardíaz, D. F. Ryan, E. Rosta, O. A. Scherman, *Angew. Chem. Int. Ed.* **2016**, *55*, 16096 – 16100; *Angew. Chem.* **2016**, *128*, 16330 – 16334.

[21] a) E. Karp, C. S. Pecinovsky, M. J. McNevin, D. L. Gin, D. K. Schwartz, *Langmuir* **2007**, *23*, 7923 – 7927; b) K. Tanaka, S. Fukuoka, H. Miyanishi, H. Takahashi, *Tetrahedron Lett.* **2010**, *51*, 2693 – 2696; c) Y. Norikane, Y. Hirai, M. Yoshida, *Chem. Commun.* **2011**, *47*, 1770 – 1772; d) R. Reuter, H. A. Wegner, *Chem. Commun.* **2013**, *49*, 146 – 148.

[22] a) F. Vögtle, W. M. Müller, U. Müller, M. Bauer, K. Rissanen, *Angew. Chem. Int. Ed. Engl.* **1993**, *32*, 1295 – 1297; b) M. Bauer, W. Manfred Müller, U. Müller, K. Rissanen, F. Vögtle, *Liebigs Ann.* **1995**, *4*, 649 – 656; c) M. Asakawa, P. R. Ashton, V. Balzani, C. L. Brown, A. Credi, O. A. Matthews, S. P. Newton, F. M. Raymo, A. N. Shipway, N. Spencer, A. Quick, J. F. Stoddart, A. J. P. White, D. J. Williams, *Chem. Eur. J.* **1999**, *5*, 860 – 875.

[23] a) K. Takaishi, M. Kawamoto, K. Tsubaki, T. Wada, *J. Org. Chem.* **2009**, *74*, 5723 – 5726; b) G. Haberhauer, C. Kallweit, *Angew. Chem. Int. Ed.* **2010**, *49*, 2418 – 2421; *Angew. Chem.* **2010**, *122*, 2468 – 2471; c) K. Takaishi, A. Muranaka, M. Kawamoto, M. Uchiyama, *J. Org. Chem.* **2011**, *76*, 7623 – 7628; d) R. Reuter, H. A. Wegner, *Org. Lett.* **2011**, *13*, 5908 – 5911; e) K. Takaishi, M. Kawamoto, K. Tsubaki, T. Furuyama, A. Muranaka, M. Uchiyama, *Chem. Eur. J.* **2011**, *17*, 1778 – 1782; f) G. Haberhauer, C. Kallweit, C. Wölper, D. Bläser, *Angew. Chem. Int. Ed.* **2013**, *52*, 7879 – 7882; *Angew. Chem.* **2013**, *125*, 8033 – 8036; g) J. Lu, A. Xia, N. Zhou, W. Zhang, Z. Zhang, X. Pan, Y. Yang, Y. Wang, X. Zhu, *Chem. Eur. J.* **2015**, *21*, 2324 – 2329.

[24] a) Y. Norikane, N. Tamaoki, *Org. Lett.* **2004**, *6*, 2595 – 2598; b) T. Muraoka, K. Kinbara, T. Aida, *Nature* **2006**, *440*, 512 – 515; c) T. Muraoka, K. Kinbara, T. Aida, *Chem. Commun.* **2007**, 1441 – 1443; d) M. C. Basheer, Y. Oka, M. Mathews, N. Tamaoki, *Chem. Eur. J.* **2010**, *16*, 3489 – 3496; e) P. Commins, M. A. Garcia-Garibay, *J. Org. Chem.* **2014**, *79*, 1611 – 1619.

[25] T. Tanaka, W. C. Huang, M. Noguchi, A. Kobayashi, S.-i. Shoda, *Tetrahedron Lett.* **2009**, *50*, 2154 – 2157.

[26] P.-O. Johansson, Y. Chen, A. K. Belfrage, M. J. Blackman, I. Kvarnström, K. Jansson, L. Vrang, E. Hamelink, A. Hallberg, Å. Rosenquist, B. Samuelsson, *J. Med. Chem.* **2004**, *47*, 3353 – 3366.

[27] T. Takamura, T. Chiba, S. Tejima, *Chem. Pharm. Bull.* **1979**, *27*, 721 – 725.

[28] G. Excoffier, D. Gagnaire, J.-P. Utille, *Carbohydr. Res.* **1975**, *39*, 368 – 373.

[29] B. Yu, H. Tao, *Tetrahedron Lett.* **2001**, *42*, 2405 – 2407.

[30] W.-h. Wei, T. Tomohiro, M. Kodaka, H. Okuno, *J. Org. Chem.* **2000**, *65*, 8979 – 8987.

[31] M. I. García-Moreno, P. Díaz-Pérez, J. M. Benito, C. Ortiz Mellet, J. Defaye, J. M. García Fernández, *Carbohydr. Res.* **2002**, *337*, 2329 – 2334.

[32] Y. S. Lee, J. Nyberg, S. Moye, R. S. Agnes, P. Davis, S.-w. Ma, J. Lai, F. Porreca, R. Vardanyan, V. J. Hruby, *Bioorg. Med. Chem. Lett.* **2007**, *17*, 2161 – 2165.

[33] a) K. Takaishi, M. Kawamoto, A. Muranaka, M. Uchiyama, *Org. Lett.* **2012**, *14*, 3252 – 3255; b) V. A. Azov, J. Cordes, D. Schlüter, T. Dülcks, M. Böckmann, N. L. Doltsinis, *J. Org. Chem.* **2014**, *79*, 11714 – 11721.

[34] E. Lieber, C. N. R. Rao, J. Ramachandran, *Spectrochim. Acta* **1959**, *13*, 296 – 299.

[35] a) R. K. Gosavi, U. Agarwala, C. N. R. Rao, *J. Am. Chem. Soc.* **1967**, *89*, 235 – 239; b) G. Vassilev, V. Koleva, M. Ilieva, B. Galabov, *J. Mol. Struct.* **1982**, *82*, 35 – 41.

[36] In order to observe only the *trans* isomer, each sample was preliminary heated at 45 °C for 16 h.

[37] G. Zemplén, E. Pacsu, *Ber. Dtsch. Chem. Ges. A and B* **1929**, *62*, 1613 – 1614.

[38] Schrödinger Release 2016 – 1: MacroModel, version 11.2, Schrödinger, LLC, New York, NY, **2016**.

[39] a) J. Barrett, F. S. Deghaidy, *Spectrochim. Acta Part A* **1975**, *31*, 707 – 713; b) J. Gawronski, M. Kwit, P. Skowronek, *Org. Biomol. Chem.* **2009**, *7*, 1562 – 1572.

Manuscript received: March 19, 2017

Accepted manuscript online: June 14, 2017

Version of record online: July 24, 2017

CHEMISTRY
A European Journal

Supporting Information

Photocontrol over Molecular Shape: Synthesis and Photochemical Evaluation of Glycoazobenzene Macrocycles

Guillaume Despras,* Julia Hain, and Sven Ole Jaeschke[a]

chem_201701232_sm_miscellaneous_information.pdf

Supporting Information

Table of contents

Synthesis

(2,3,4-tri-*O*-acetyl-6-*O*-*tert*-butylidemethylsilyl-α-D-glucopyranosyl)-(1→4)-1,6-anhydro-2,3-di-*O*-acetyl-β-D-glucopyranose (6). To a solution of maltosan **5**[1] (1.44 g, 4.45 mmol) in dry pyridine (9.00 mL) was added *tert*-butyldimethylsilyl chloride (1.00 g, 6.68 mmol, 1.5 equiv). After stirring at room temperature for 2 h, additional *tert*-butyldimethylsilyl chloride (0.335 g, 2.23 mmol, 0.5 equiv) was added. The solution was stirred for a further 3 h then acetic anhydride (4.85 mL, 53.4 mmol, 12 equiv) and *N,N*-dimethylaminopyridine (0.109 g, 0.890 mmol, 0.2 equiv) were added. After stirring at room temperature for 15 h, methanol (10 mL) was added and the solution stirred for 30 min then concentrated to dryness. The residue was dissolved in ethyl acetate then washed three times with 1M aqueous HCl. The aqueous layer was extracted with ethyl acetate then the combined organic layers were washed with brine, dried over magnesium sulfate, filtered and concentrated under reduced pressure. The residue was purified by flash chromatography (cyclohexane/ethyl acetate 65:35 to 55:45) to give **6** (1.97 g, 68 %) as a white foam. $[\alpha]^{20}_{D}$ +56.3 (c= 1 in $CHCl_3$); ^{1}H NMR (600 MHz, $CDCl_3$) δ = 5.53 (dd, $J_{3',2'}$ = 10.1 Hz, $J_{3',4'}$ = 9.7 Hz, 1H, H-3'), 5.47 (s, 1H, H-1), 5.26 (d, $J_{1',2'}$ =3.7 Hz, 1H, H-1'), 4.99 (dd, $J_{4',5'}$ = 10.1 Hz, $J_{4',3'}$ = 9.6 Hz, 1H, H-4'), 4.81 (dd, $J_{2',3'}$ = 10.3 Hz, $J_{2',1'}$ = 3.7 Hz, 1H, H-2'), 4.79 – 4.78 (m, 1H, H-3), 4.77 (d, $J_{5,6b}$ = 5.4 Hz, 1H, H-5), 4.56 (s, 1H, H-2), 4.21 – 4.18 (m, 1H, H-5'), 3.94 (d, $J_{6a,6b}$ = 7.7 Hz, 1H, H-6a), 3.75 (dd, $J_{6b,6a}$ = 7.6 Hz, $J_{6b,5}$ = 5.8 Hz, 1H, H-6b), 3.69 – 3.65 (m, 2H, H-6'a, H-6'b), 3.44 (s, 1H, H-4), 2.19 (s, 3H,

$CH_3C=O$), 2.09 (s, 3H, $CH_3C=O$), 2.07 (s, 3H, $CH_3C=O$), 2.02 (s, 3H, $CH_3C=O$), 2.00 (s, 3H, $CH_3C=O$), 0.87 (s, 9H, $SiC(CH_3)_3$), 0.03 (s, 3H, $SiCH_3$), 0.02 (s, 3H, $SiCH_3$); ^{13}C NMR (151 MHz, $CDCl_3$) δ = 170.5, 170.3, 169.7, 169.5 (5C, $5CH_3\underline{C}=O$), 99.2 (C-1), 97.6 (C-1'), 74.7 (C-5), 71.0 (C-2' or C-5'), 70.9 (C-2' or C-5'), 70.7 (C-3), 70.3 (C-3'), 69.2 (2C, C-4, C-4'), 65.3 (C-6), 62.5 (C-6'), 26.0 (3C, $SiC(\underline{C}H_3)_3$), 21.1, 21.0, 20.9, 20.8, 20.7 (5C, $5\underline{C}H_3C=O$), 18.5 ($Si\underline{C}(CH_3)_3$), -5.3 (2C, $2Si\underline{C}H_3$); MALDI-TOF HRMS: m/z: calcd for $C_{28}H_{44}O_{15}Si + Na^+$: 671.2342 [M+$Na^+$]; found: 671.2343.

(2,3,4-tri-*O*-acetyl-α-D-glucopyranosyl)-(1→4)-1,6-anhydro-2,3-di-*O*-acetyl-β-D-glucopyranose (7). A solution of **6** (1.97 g, 3.04 mmol) in dry THF (2.80 mL) was cooled to 0°C and glacial acetic acid (2.60 mL, 45.7 mmol, 15 equiv) was added then 1M *n*-tetrabutylammonium fluoride in THF (9.10 mL, 9.12 mmol, 3 equiv) was added dropwise. The mixture was stirred at 0°C for 3 h then diluted with CH_2Cl_2 and the solution was poured into satd. aq. $NaHCO_3$ (200 mL). After vigorously stirring until complete neutralization, the layers were separated and the aqueous phase was extracted with CH_2Cl_2. The combined organic layers were washed with brine, dried over magnesium sulfate, filtered and concentrated under reduced pressure. The residue was purified by flash chromatography (cyclohexane/ethyl acetate 1:4 to 15:85) to give **7** (1.35 g, 83 %) as a white foam. **$[\alpha]^{20}_D$** +51.7 (c= 1 in $CHCl_3$); ^1H NMR (500 MHz, $CDCl_3$) δ = 5.54 (dd, $J_{3',2'}$ = $J_{3',4'}$ = 9.9 Hz, 1H, H-3'), 5.47 (s, 1H, H-1), 5.31 (d, $J_{1',2'}$ =3.7 Hz, 1H, H-1'), 5.01 (dd, $J_{4',5'}$ = $J_{4',3'}$ = 9.9 Hz, 1H, H-4'), 4.85 – 4.78 (m, 2H, H-4, H-2'), 4.74 (d, $J_{5,6b}$ = 5.2 Hz, 1H, H-5), 4.58 (d, J = 0.8 Hz, 1H, H-2), 4.20 (ddd, $J_{5',4'}$ = 10.3 Hz, J = 4.4 Hz, 2.2 Hz, 1H, H-5'), 3.97 (d, $J_{6a,6b}$ = 7.8 Hz, 1H, H-6a), 3.79 (dd, $J_{6b,6a}$ = 7.7 Hz, $J_{6b,5}$ = 5.8 Hz, 1H, H-6b), 3.75 – 3.67 (m, 1H, H-6'a), 3.65 – 3.56 (m, 1H, H-6'b), 3.47 (s, 1H, H-4), 2.31 (t, J = 6.3 Hz, 1H, OH), 2.20 (s, 3H, $CH_3C=O$), 2.10 (s, 3H, $CH_3C=O$), 2.08 (s, 3H, $CH_3C=O$), 2.06 (s, 3H, $CH_3C=O$), 2.02 (s, 3H, $CH_3C=O$); ^{13}C NMR (126 MHz, $CDCl_3$) δ = 170.7, 170.6, 170.2, 170.1, 169.5 (5C, $5CH_3\underline{C}=O$), 99.3 (C-1), 97.4 (C-1'), 77.4 (C-1), 74.5 (C-5), 71.0 (C-2'), 70.5 (2C, C-3, C-5'), 69.6 (C-3'), 69.0 (C-4'), 68.9 (C-4), 65.1 (C-6), 61.3 (C-6'), 21.1, 20.9, 20.8, 20.8, 20.7 (5C, $5\underline{C}H_3C=O$); MALDI-TOF HRMS: m/z: calcd for $C_{22}H_{30}O_{15} + Na^+$: 557.1477 [M+$Na^+$]; found: 557.1465.

(2,3,4-tri-*O*-acetyl-6-azido-6-deoxy-α-D-glucopyranosyl)-(1→4)-1,6-anhydro-2,3-di-*O*-acetyl-β-D-glucopyranose (8). To a solution of **7** (1.45 g, 2.71 mmol) in dry THF (11.0 mL) was added triphenylphosphine (1.07 g, 4.07 mmol, 1.5 equiv). The mixture was cooled to -15 °C then diisopropyl azidocarboxylate (1.35 mL, 6.78 mmol, 2.5 equiv) was added dropwise. After stirring at -15 °C for 15 min, the temperature was raised to -5°C then diphenylphosphoryl azide (0.900 mL, 4.07 mmol, 1.5 equiv) was added dropwise. The mixture was allowed to warm to room temperature and stirred for 22 h then concentrated under reduced pressure. The crude residue was purified by automated flash chromatography (cyclohexane/ethyl acetate 9:1 to 3:2 within 20 min) to give **8** (1.21 g, 80 %) as a white foam. **$[\alpha]^{20}_D$** +45.3 (c= 1 in $CHCl_3$); ^1H NMR (500 MHz, $CDCl_3$) δ = 5.52 (dd, $J_{3',2'}$ = 10.3 Hz, $J_{3',4'}$ = 9.4 Hz, 1H, H-3'), 5.48 (s, 1H, H-1), 5.30 (d, $J_{1',2'}$ =3.7 Hz, 1H, H-1'), 4.99 (dd, $J_{4',5'}$ = 10.1 Hz, $J_{4',3'}$ = 9.4 Hz, 1H, H-4'), 4.83 (dd, $J_{2',3'}$ = 10.3 Hz, $J_{2',1'}$ = 3.7 Hz, 1H, H-2'), 4.81 – 4.78 (m, 1H, H-3), 4.74 (d, $J_{5,6b}$ = 5.2 Hz, 1H, H-5), 4.58 (d, J=1.1 Hz, 1H, H-2), 4.38 – 4.29 (m, 1H, H-5'), 3.98 (dd, $J_{6a,6b}$ = 7.7 Hz, $J_{6a,5}$ = 0.8 Hz, 1H, H-6a), 3.81 (dd, $J_{6b,6a}$ = 7.7 Hz, $J_{6b,5}$ = 5.8 Hz, 1H, H-6b), 3.48 (s, 1H, H-4), 3.39 – 3.29 (m, 2H, H-6'a, H-6'b), 2.19 (s, 3H, $CH_3C=O$), 2.09 (s, 3H, $CH_3C=O$), 2.07 (s, 3H, $CH_3C=O$), 2.03 (s, 3H, $CH_3C=O$), 2.01 (s, 3H, $CH_3C=O$).

^{13}C NMR (126 MHz, $CDCl_3$) δ = 170.5, 170.2, 170.1, 169.8, 169.6 (5C, $5CH_3\underline{C}$=O), 99.3 (C-1), 97.3 (C-1'), 77.1 (C-4), 74.6 (C-5), 70.7 (C-2'), 70.5 (C-3), 69.8 (C-4'), 69.7 (C-3'), 69.5 (C-5'), 69.0 (C-2), 65.2 (C-6), 51.3 (C-6'), 21.0 ($\underline{C}H_3C$=O), 20.9 ($\underline{C}H_3C$=O), 20.8 ($\underline{C}H_3C$=O), 20.7 ($\underline{C}H_3C$=O); MALDI-TOF HRMS: m/z: calcd for $C_{22}H_{29}N_3O_{14}$ + K^+: 598.1281 [M+K^+]; found: 598.1272.

(2,3,4-tri-*O*-acetyl-6-azido-6-deoxy-α-D-glucopyranosyl)-(1→4)- 2,3,6-tri-*O*-acetyl- D-glucopyranosyl 1-(*N*-phenyl)-2,2,2-trifluoroacetimidate (4). To a solution of **8** (1.21 g, 2.16 mmol) in acetic anhydride/glacial acetic acid (7:3, 20 mL) was added conc. sulfuric acid (0.220 mL). The mixture was stirred at room temperature for 3 h 30 then diluted with ethyl acetate and poured into cold satd. aq. $NaHCO_3$ (250 mL). After stirring for 16 h at room temperature, the layers were separated then the aqueous phase was extracted with ethyl acetate. The combined organic layers were washed with brine, dried over magnesium sulfate, filtered and concentrated to dryness. The resulting white foam was dried under vacuum for 3 h then dissolved in *N*,*N*-dimethylformamide (6.00 mL). The solution was heated to 55 °C then hydrazine acetate (0.216 g, 2.38 mmol, 1.1 equiv) was added and the mixture was stirred at 55 °C for 1 h then cooled to room temperature and diluted with ethyl acetate. The solution was washed three times with brine then the aqueous layer was extracted with ethyl acetate. The combined organic layers were dried over magnesium sulfate, filtered and concentrated to dryness then the residue was dried under vacuum for 2 h to give a white solid. To a solution of the crude hemiacetal in CH_2Cl_2 (20.0 mL) were added caesium carbonate (1.03 g, 3.24 mmol, 1.5 equiv) then 2,2,2-trifluoro-*N*-phenylacetimidoyl chloride (0.500 mL, 3.24 mmol, 1.5 equiv). After stirring at room temperature for 1 h 30, the mixture was diluted with CH_2Cl_2 and filtered through a celite pad. The filtrate was concentrated under reduced pressure then purified by flash chromatography (cyclohexane/ethyl acetate 100:0 to 65:35 within 20 min) to give **4** (1.26 g, 74 % yield over three steps, α/β mixture) as a white foam. ^{1}H NMR (500 MHz, $CDCl_3$) δ = 7.36 – 7.28 (m, 2H, 2Ar-H), 7.19 – 7.10 (m, 1H, Ar-H), 6.91 – 6.75 (m, 2H, 2Ar-H), 5.84 (br s, 1H), 5.54 (t, *J*=9.1 Hz, 1H), 5.46 – 5.30 (m, 4H, H-1', H-3'), 5.29 – 5.17 (m, 1H), 5.09 (t, *J*=8.0 Hz, 1H), 5.03 – 4.96 (m, 2H, H-4'), 4.89 – 4.80 (m, 2H, H-2'), 4.51 (d, $J_{6a,6b}$ = 10.3 Hz, 1H, H-6a), 4.23 – 4.18 (m, 1H, H-6b), 4.16 – 4.03 (m, 2H, H-4), 3.97 – 3.86 (m, 2H, H-5'), 3.34 – 3.29 (m, 2H, H-6'a, H-6'b), 2.16 (s, 3H, CH_3C=O), 2.14 (s, 3H, CH_3C=O), 2.08 (s, 3H, CH_3C=O), 2.07 (s, 3H, CH_3C=O), 2.05 (s, 3H, CH_3C=O), 2.05 (s, 3H, CH_3C=O), 2.04 (s, 3H, CH_3C=O), 2.03 (s, 3H, CH_3C=O), 2.01 (s, 3H, CH_3C=O), 2.00 (s, 3H, CH_3C=O); ^{13}C NMR (126 MHz, $CDCl_3$) δ = 170.7, 170.6, 170.3, 170.1, 170.0, 169.9, 169.7, 169.6, 169.5 ($CH_3\underline{C}$=O), 129.0 (Ar-C), 124.9 (Ar-C), 119.4 (Ar-C), 95.8 (C-1'), 94.2 (C-1), 75.0, 73.1, 72.6 (C-4), 72.4, 72.1, 71.0, 70.6, 70.2 (2C, C-2'), 70.0 (C-5'), 69.9, 69.3 (C-4'), 69.2 (C-3'), 62.5, 62.4 (C-6), 51.1 (C-6'), 21.1 ($\underline{C}H_3C$=O), 21.0 ($\underline{C}H_3C$=O), 20.9 ($\underline{C}H_3C$=O), 20.7 ($\underline{C}H_3C$=O), 20.6 ($\underline{C}H_3C$=O); ESI MS: m/z: calcd for $C_{32}H_{37}F_3N_4O_{16}$ + Na^+: 813.2 [M+Na^+]; found: 813.1.

(*E*)-*p*,*p*'-Di-(2,3,4-tri-*O*-acetyl-6-azido-6-deoxy-β-D-glucopyranosyloxy)azobenzene (9). To a solution of 4,4'-dihydroxyazobenzene (0.152 g, 0.706 mmol) and donor **3**[2] (0.750 g, 1.58 mmol, 2.2 equiv) in dry acetonitrile (16.0 mL) was added 3 Å molecular sieves (0.900 g). The mixture was stirred at room temperature for 15 min then boron trifluoride diethyl etherate (0.100 mL, 0.810 mmol, 1.1 equiv) was added. The solution was stirred at room temperature for 15 min then diluted with CH_2Cl_2 and filtered through a celite pad. The filtrate was washed with satd. aq. $NaHCO_3$ then the aqueous layer was extracted with CH_2Cl_2. The combined

organic layers were dried over magnesium sulfate, filtered and concentrated under reduced pressure. The residue was purified by flash chromatography (cyclohexane/ethyl acetate 3:2) to give **9** (0.311 g, 52 %) as a pale orange foam. Analytical and spectroscopic data were found to be in agreement with reported literature.[2]

(*E*)-*p*,*p*'-Di-((2,3,4-tri-*O*-acetyl-6-azido-6-deoxy-α-D-glucopyranosyl)-(1→4)-2,3,6-tri-*O*-acetyl-β-D-glucopyranosyloxy)azobenzene (10). To a solution of 4,4'-dihydroxyazobenzene (0.204 g, 0.960 mmol) and donor **4** (1.65 g, 2.09 mmol, 2.2 equiv) in dry acetonitrile (21.0 mL) was added 3 Å molecular sieves (1.90 g). The mixture was stirred at room temperature for 15 min then boron trifluoride diethyl etherate (0.130 mL, 1.06 mmol, 1.1 equiv) was added. The solution was stirred at room temperature for 45 min then diluted with CH_2Cl_2 and filtered through a celite pad. The filtrate was washed with satd. aq. $NaHCO_3$ then the aqueous layer was extracted with CH_2Cl_2. The combined organic layers were dried over magnesium sulfate, filtered and concentrated under reduced pressure. The residue was purified by flash chromatography (cyclohexane/ethyl acetate 85:15 to 44:56 within 20 min). The isolated compound was recrystallized from methanol to afford **10** (0.617 g, 46 %) as a pale orange solid. $[\alpha]^{20}_D$ +81.5 (c= 1 in $CHCl_3$); ^{1}H NMR (500 MHz, $CDCl_3$) δ = 7.91 – 7.84 (m, 4H, 4Ar-H_{ortho}), 7.12 – 7.06 (m, 4H, 4Ar-H_{meta}), 5.45 (d, $J_{1',2'}$ =4.0 Hz, 2H, H-1'), 5.40 – 5.32 (m, 4H, H-3, H-3'), 5.24 (d, $J_{1,2}$ =7.4 Hz, 2H, H-1), 5.14 (dd, $J_{2,3}$ = 8.7 Hz, $J_{2,1}$ = 7.4 Hz, 2H, H-2), 5.00 (dd, $J_{4',3'}$ = $J_{4',5'}$ = 9.8 Hz, 2H, H-4'), 4.85 (dd, $J_{2',3'}$ = 10.5 Hz, $J_{2',1'}$ = 4.0 Hz, 2H, H-2'), 4.54 (dd, $J_{6a,6b}$ = 12.1 Hz, $J_{6a,5}$ = 2.8 Hz, 2H, H-6a), 4.27 (dd, $J_{6b,6a}$ = 12.1 Hz, $J_{6b,5}$ = 5.0 Hz, 2H, H-6b), 4.14 (dd, *J*=9.4 Hz, 8.8 Hz, 2H, H-4), 3.97 – 3.91 (m, 4H, H-5, H-5'), 3.33 (d, *J* = 4.2 Hz, 4H, H-6'a, H-6'b), 2.10 (s, 6H, 2CH_3C=O), 2.06 (s, 6H, 2CH_3C=O), 2.06 (s, 6H, 2CH_3C=O), 2.05 (s, 6H, 2CH_3C=O), 2.04 (s, 6H, 2CH_3C=O), 2.01 (s, 6H, 2CH_3C=O); ^{13}C NMR (126 MHz, $CDCl_3$) δ = 170.7 ($CH_3\underline{C}$=O), 170.6 ($CH_3\underline{C}$=O), 170.4 ($CH_3\underline{C}$=O), 170.1 ($CH_3\underline{C}$=O), 169.7 ($CH_3\underline{C}$=O), 169.6 ($CH_3\underline{C}$=O), 158.7 (Ar-C_{para}), 148.7 (Ar-C_{ipso}), 124.6 (Ar-C_{ortho}), 117.2 (Ar-C_{meta}), 98.2 (C-1), 95.7 (C-1'), 75.4 (C-3), 72.9 (C-4), 72.6 (C-5 or C-5'), 72.1 (C-2), 70.2 (C-2'), 70.0 (C-5 or C-5'), 69.3 (C-4'), 69.2 (C-3'), 62.9 (C-6), 51.1 (C-6'), 21.1 ($\underline{C}H_3$C=O), 20.9 ($\underline{C}H_3$C=O), 20.8 ($\underline{C}H_3$C=O), 20.7 ($\underline{C}H_3$C=O); IR (ATR): ũ = 2943, 2105, 1744, 1598, 1496, 1433, 1367, 1209, 1147, 1030, 938, 899, 845, 788 cm^{-1}; MALDI-TOF HRMS: m/z: calcd for $C_{28}H_{44}O_{15}Si$ + K^+: 1455.3884 [M+K^+]; found: 1455.3916.

NMR spectra of the synthesized compounds

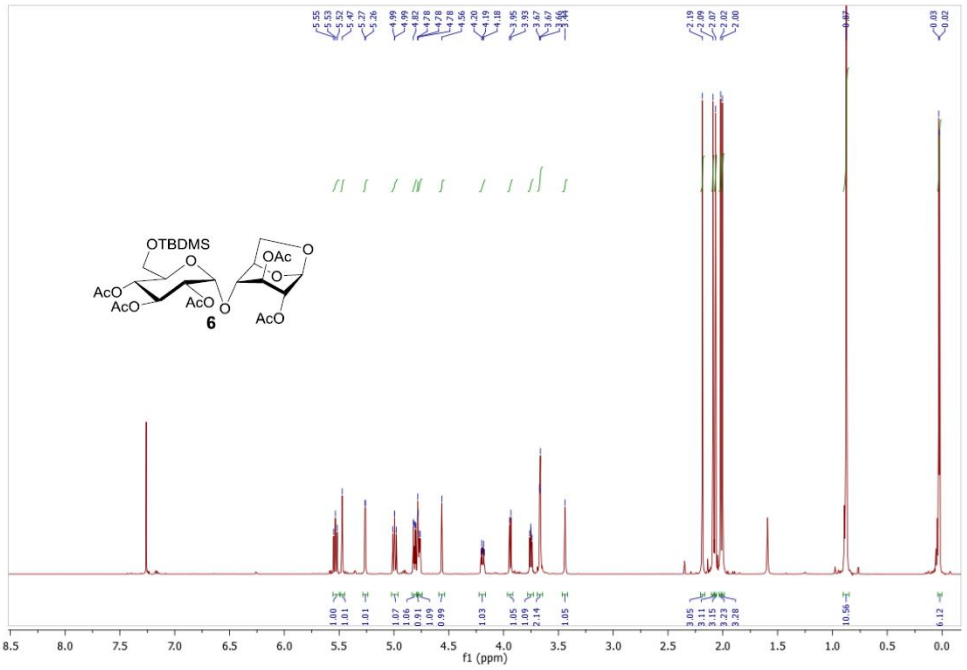

Figure S1. ^{1}H NMR spectrum of **6** (600 MHz, $CDCl_3$, 300 K).

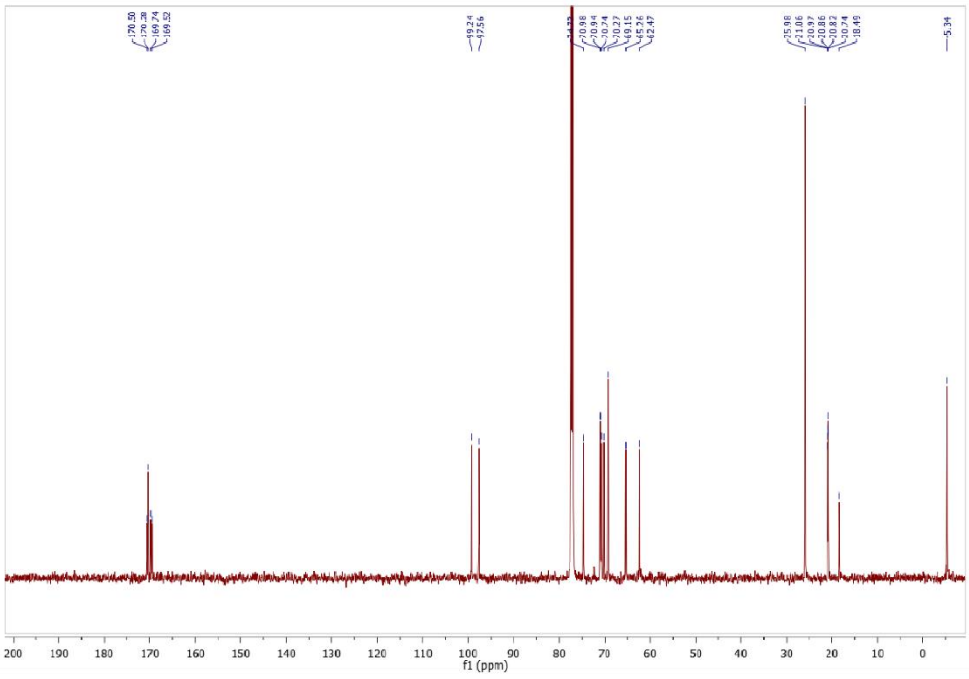

Figure S2. ^{13}C NMR spectrum of **6** (151 MHz, $CDCl_3$, 300 K).

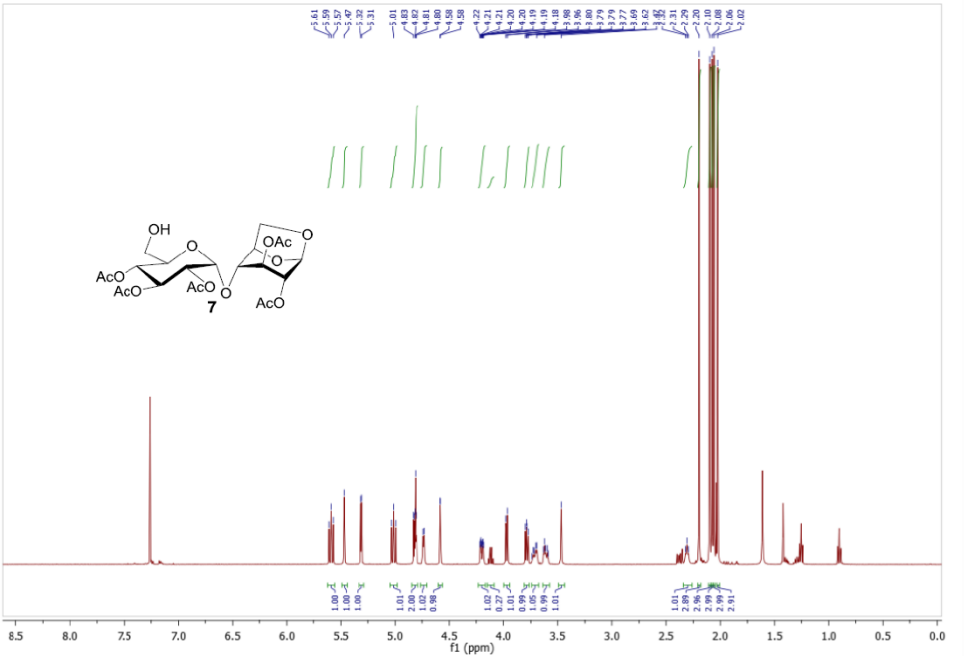

Figure S3. ^{1}H NMR spectrum of **7** (500 MHz, $CDCl_3$, 300 K).

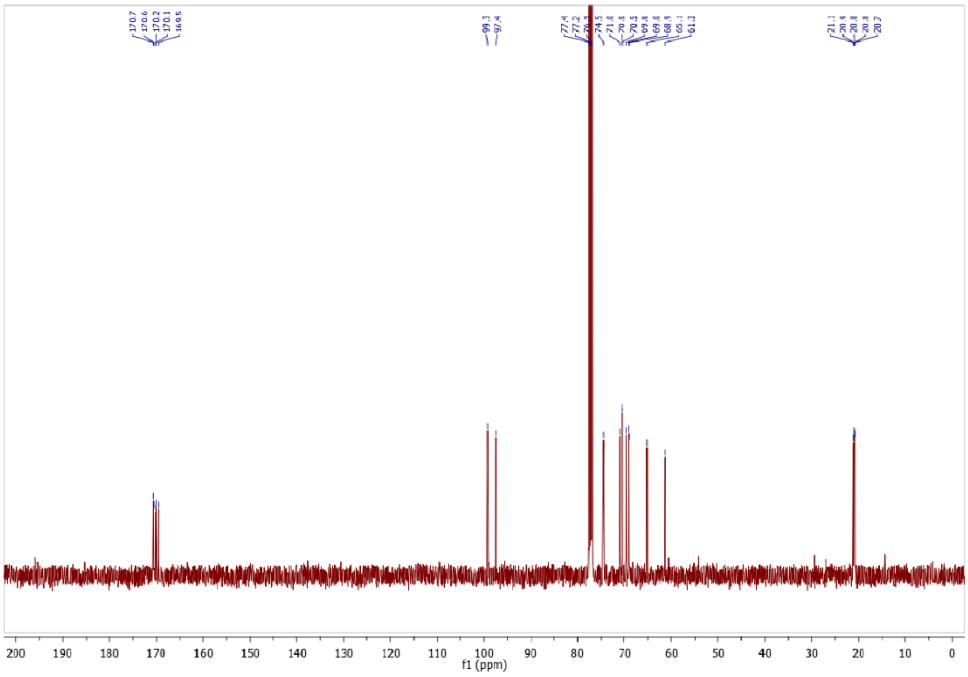

Figure S4. ^{13}C NMR spectrum of **7** (126 MHz, $CDCl_3$, 300 K).

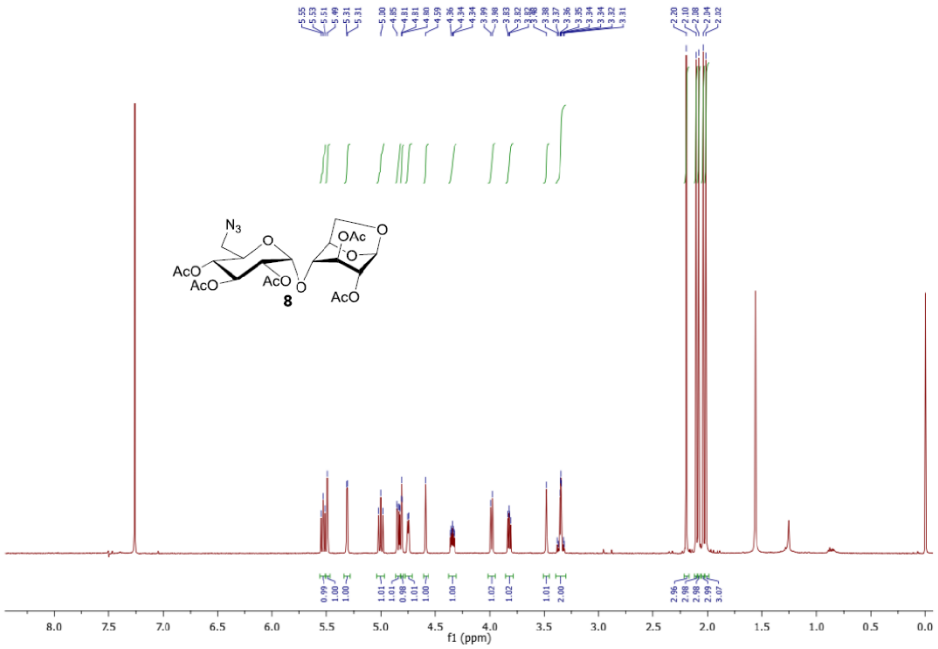

Figure S5. ^{1}H NMR spectrum of **8** (500 MHz, $CDCl_3$, 300 K).

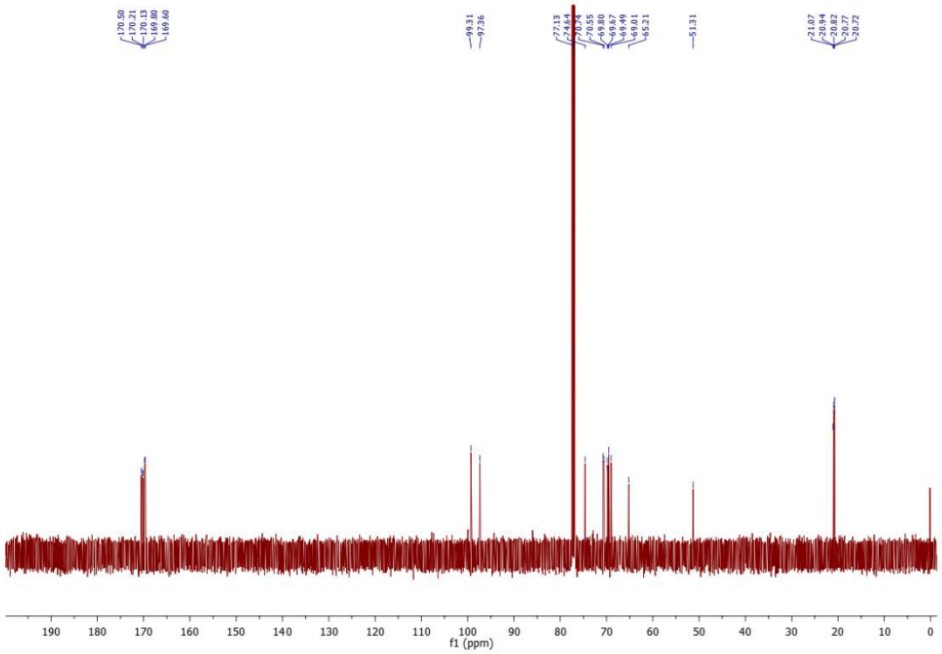

Figure S6. ^{13}C NMR spectrum of **8** (126 MHz, $CDCl_3$, 300 K).

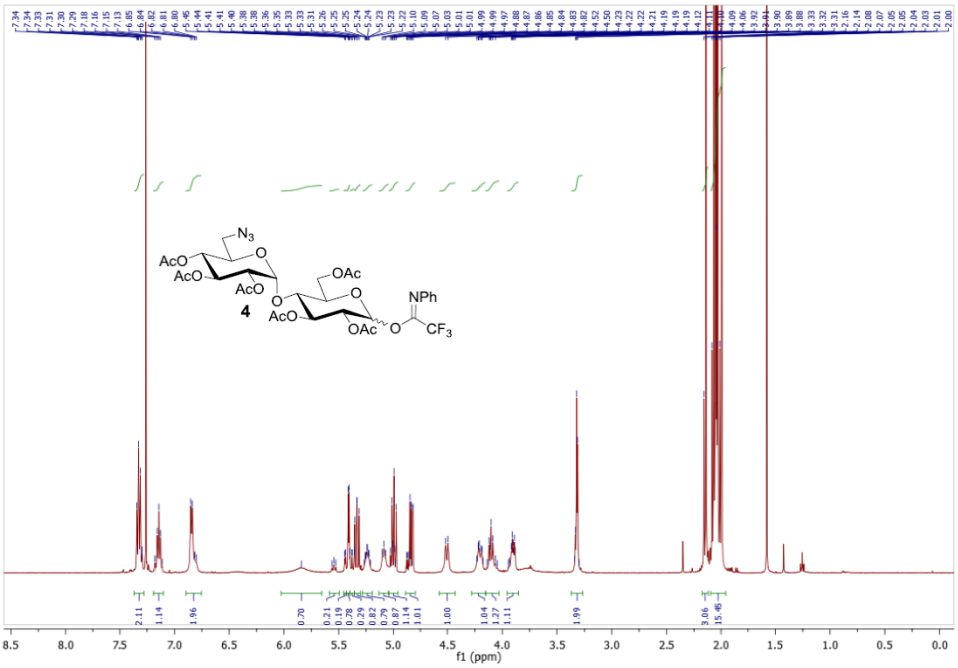

Figure S7. ^{1}H NMR spectrum of **4** (500 MHz, $CDCl_3$, 300 K).

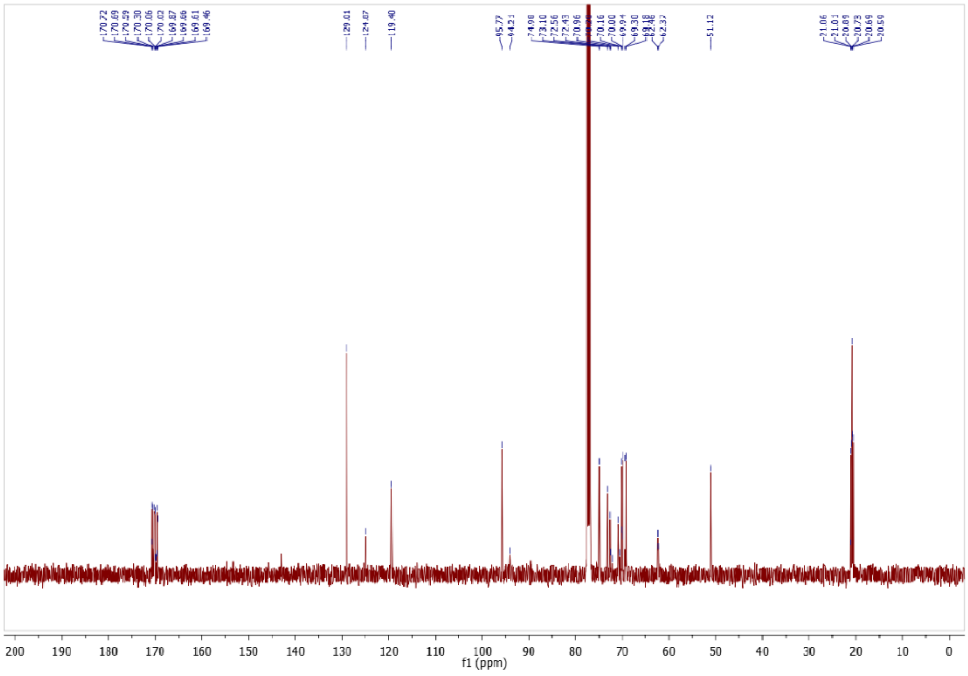

Figure S8. ^{13}C NMR spectrum of **4** (126 MHz, $CDCl_3$, 300 K).

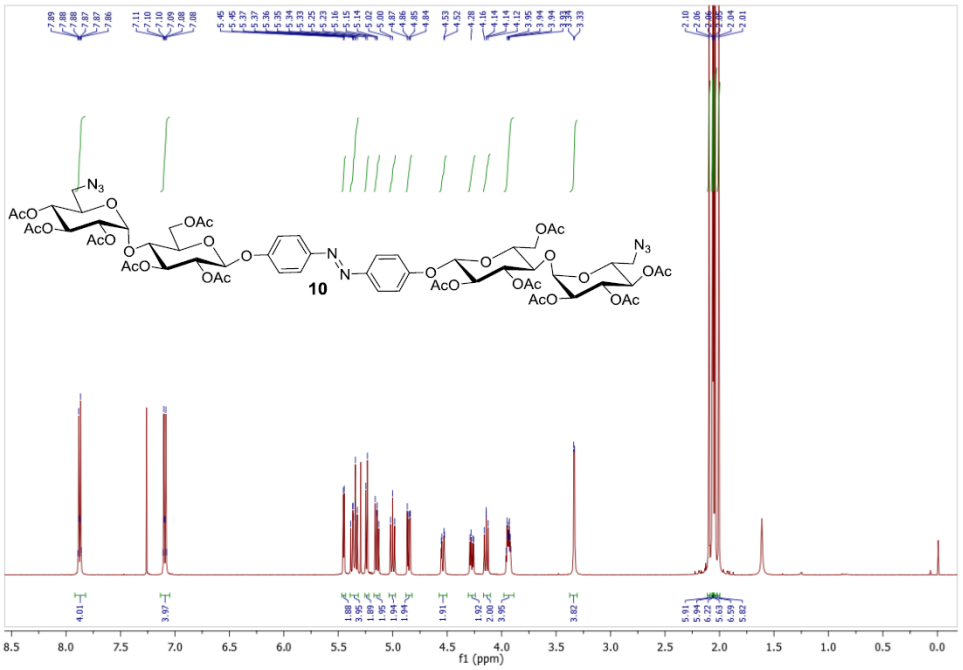

Figure S9. ^{1}H NMR spectrum of **10** (500 MHz, $CDCl_3$, 300 K).

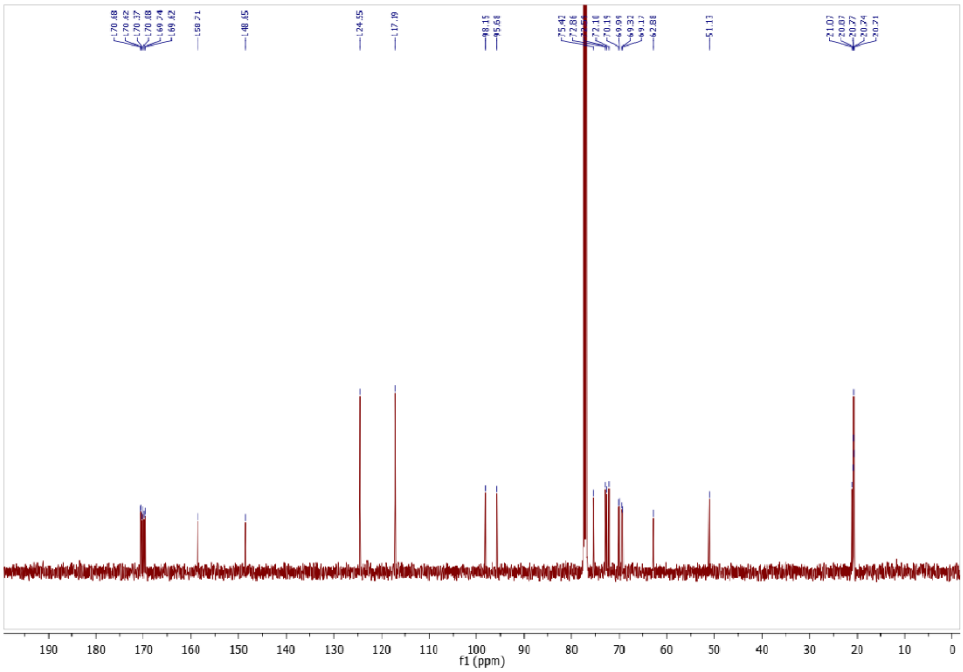

Figure S10. ^{13}C NMR spectrum of **10** (126 MHz, $CDCl_3$, 300 K).

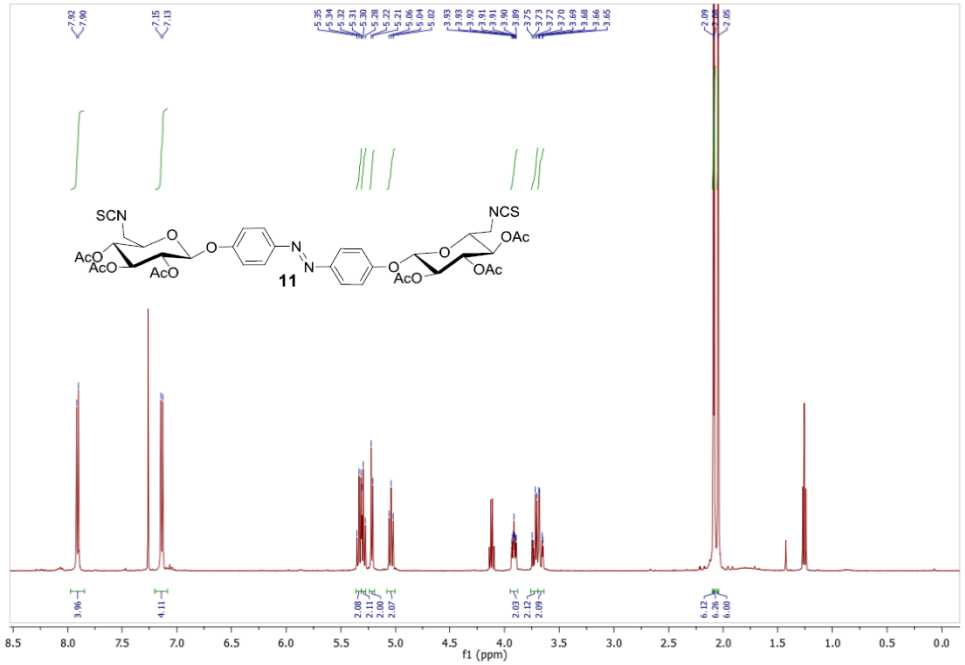

Figure S11. ^{1}H NMR spectrum of **11** (500 MHz, $CDCl_3$, 300 K).

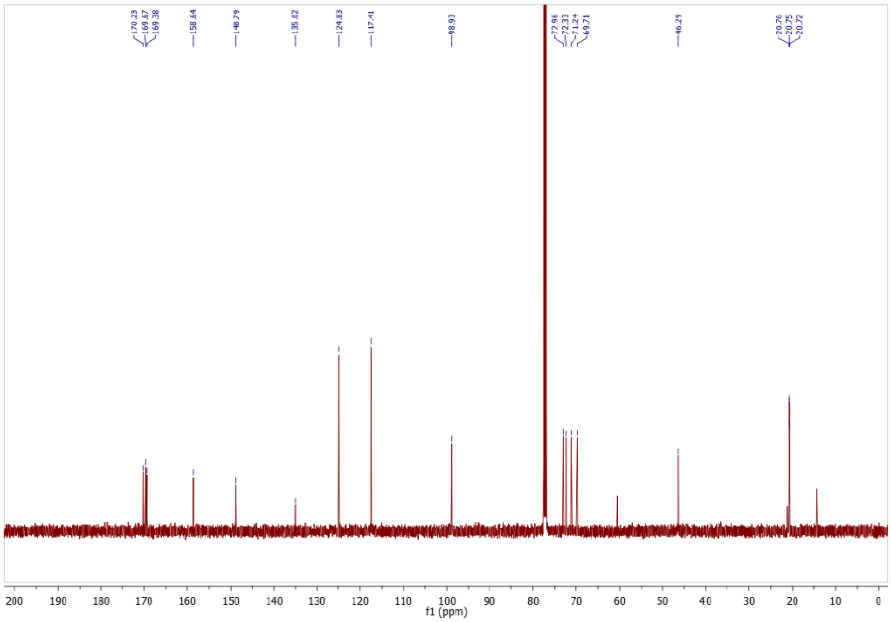

Figure S12. ^{13}C NMR spectrum of **11** (126 MHz, $CDCl_3$, 300 K).

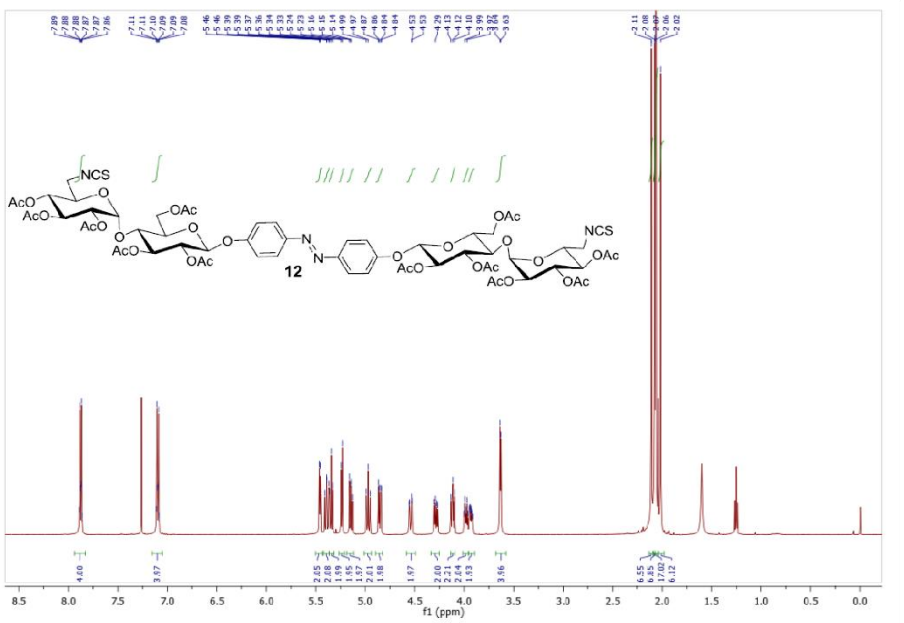

Figure S13. ^{1}H NMR spectrum of **12** (500 MHz, $CDCl_3$, 300 K).

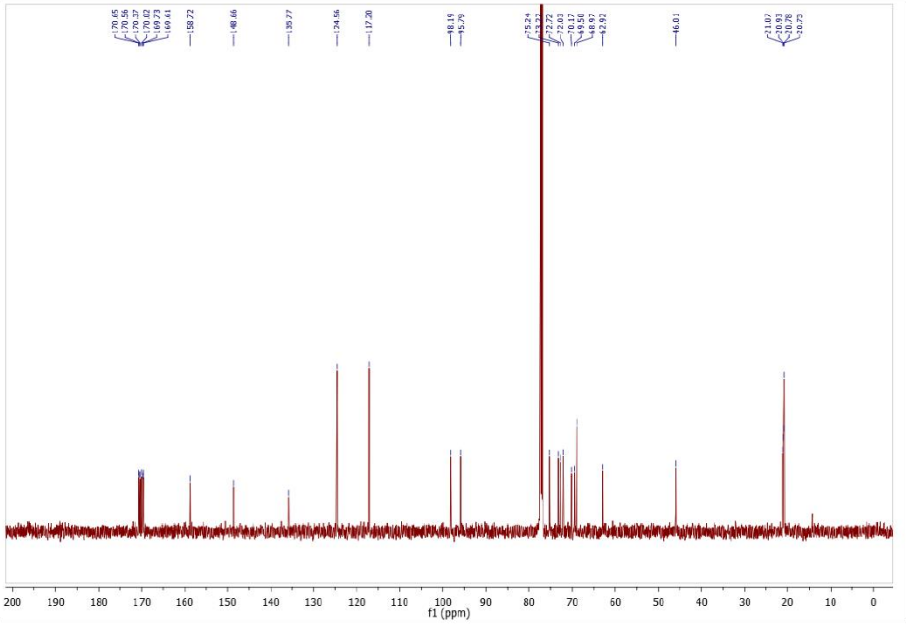

Figure S14. ^{13}C NMR spectrum of **12** (126 MHz, $CDCl_3$, 300 K).

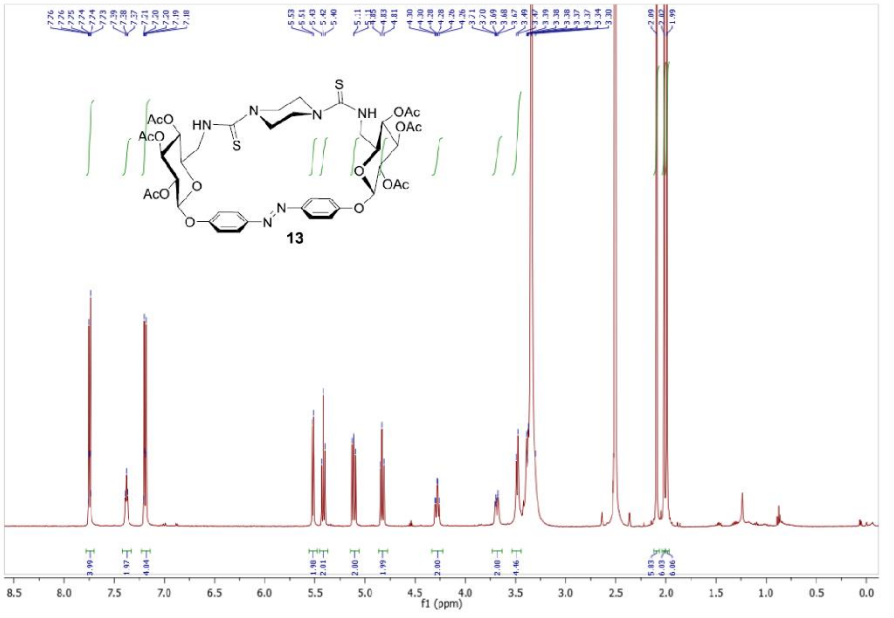

Figure S15. ^{1}H NMR spectrum of **13** (500 MHz, DMSO-d_6, 300 K).

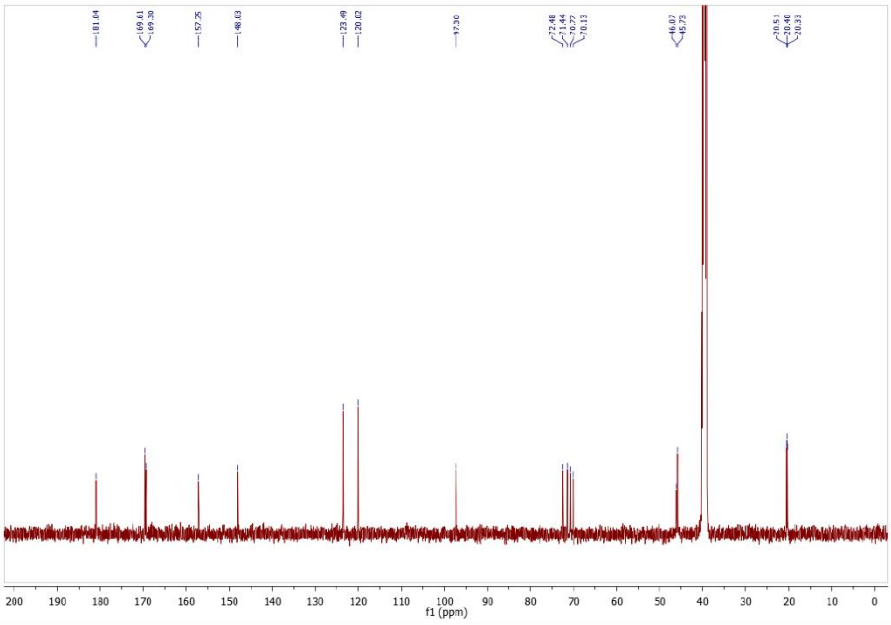

Figure S16. ^{13}C NMR spectrum of **13** (126 MHz, DMSO-d_6, 300 K).

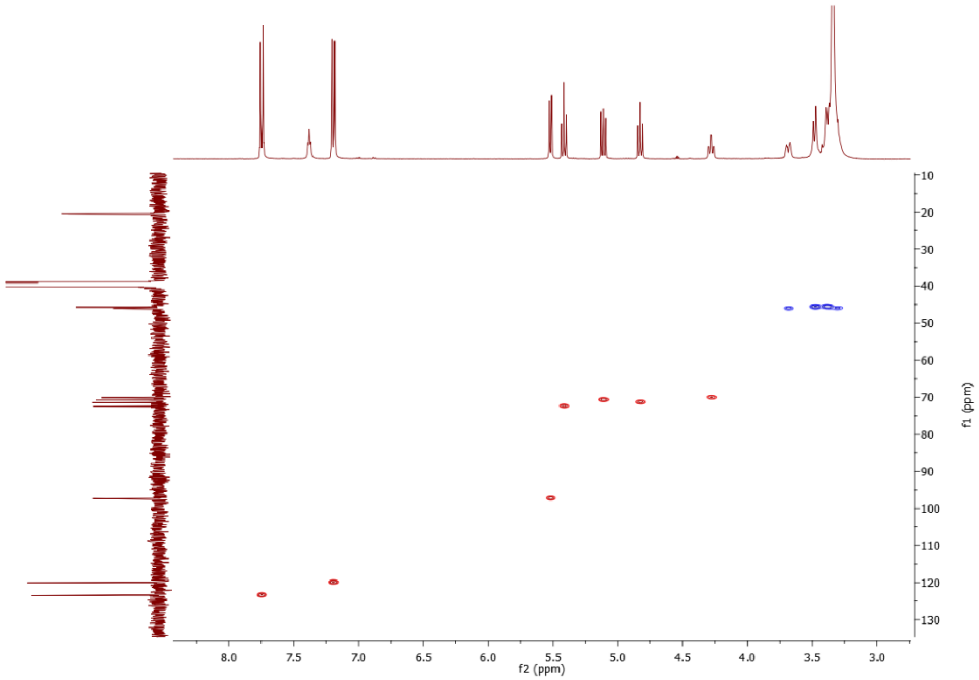

Figure S17. HSQC spectrum of **13** (DMSO-d_6, 300 K).

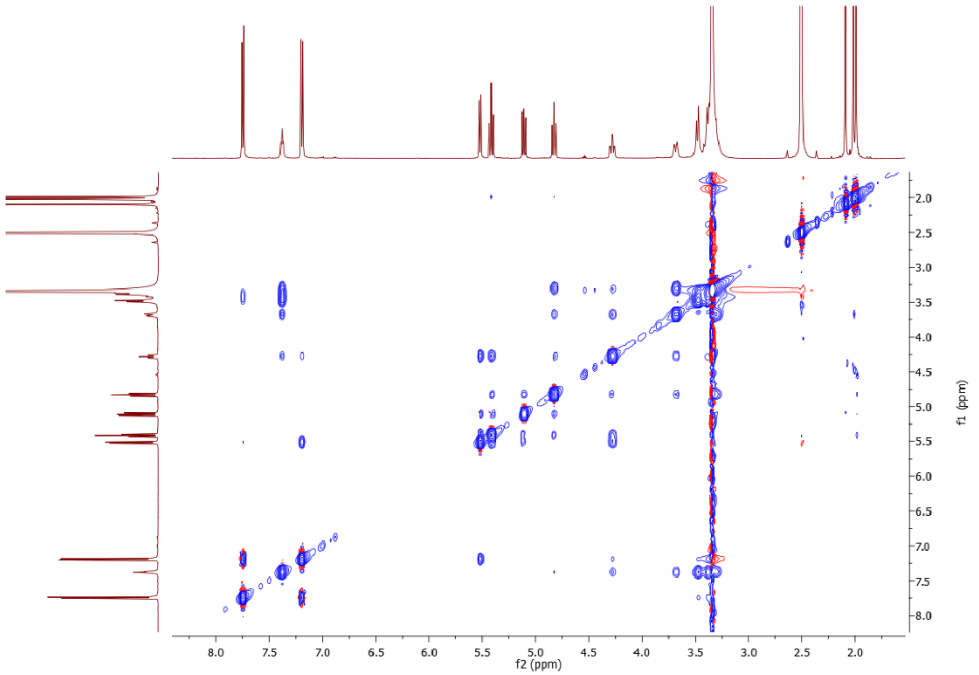

Figure S18. NOESY spectrum of **13** (DMSO-d_6, 300 K, mixing time = 300 ms).

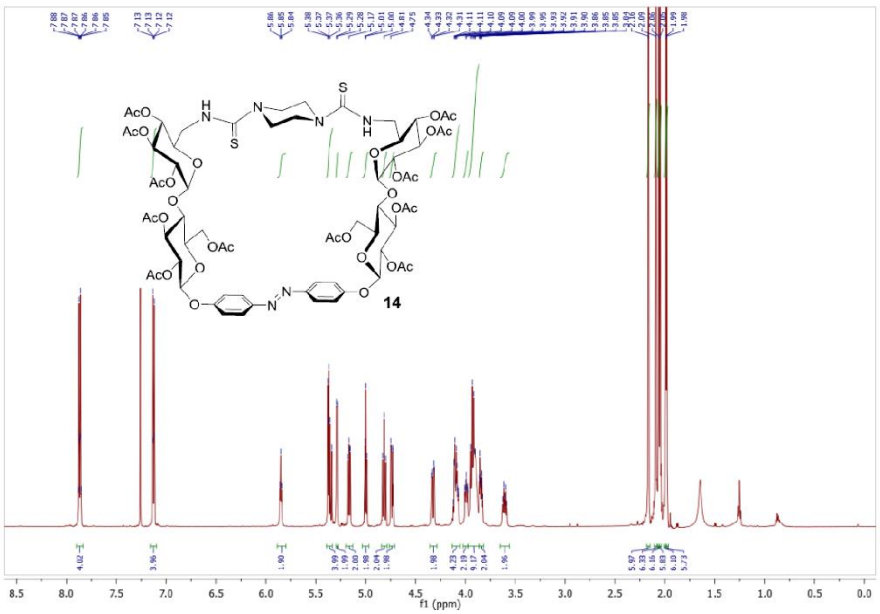

Figure S19. ^{1}H NMR spectrum of **14** (600 MHz, $CDCl_3$, 300 K).

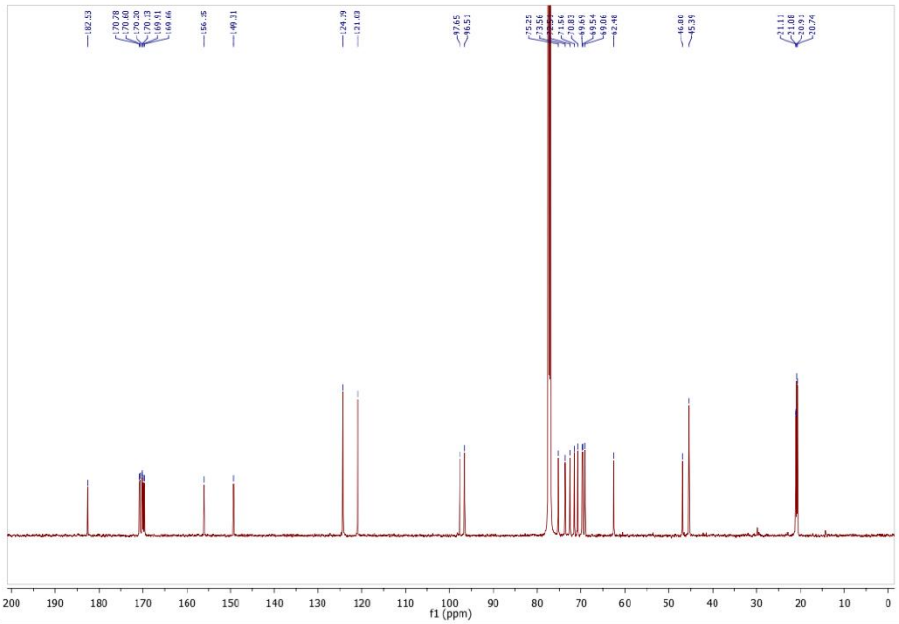

Figure S20. ^{13}C NMR spectrum of **14** (151 MHz, $CDCl_3$, 300 K).

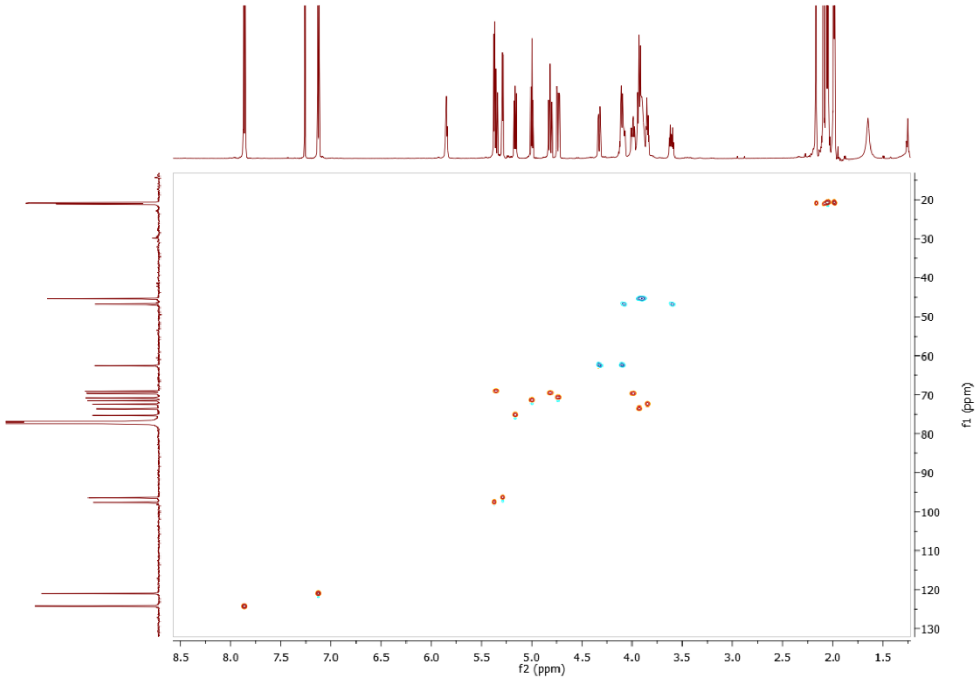

Figure S21. HSQC spectrum of **14** ($CDCl_3$, 300 K).

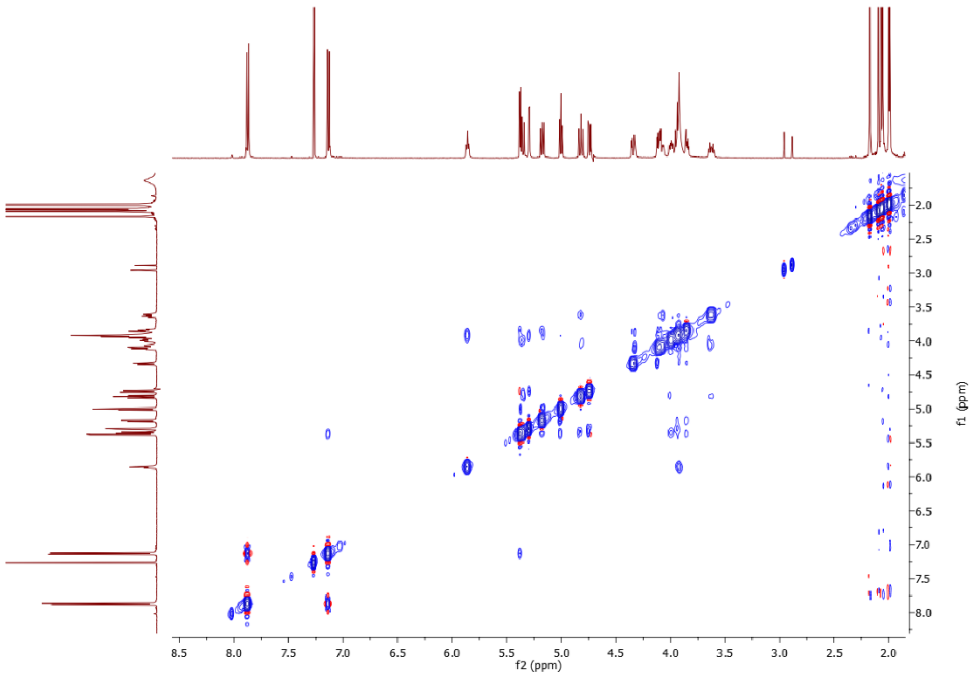

Figure S22. NOESY spectrum of **14** ($CDCl_3$, 300 K, mixing time = 700 ms).

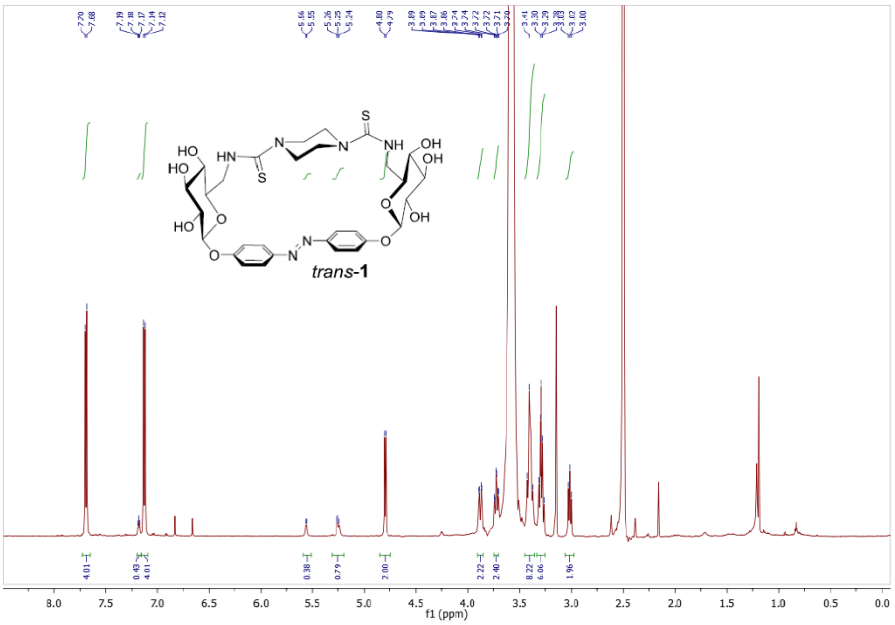

Figure S23. ^{1}H NMR spectrum of *trans*-**1** (600 MHz, DMSO-d_6 + εD_2O, 300 K).

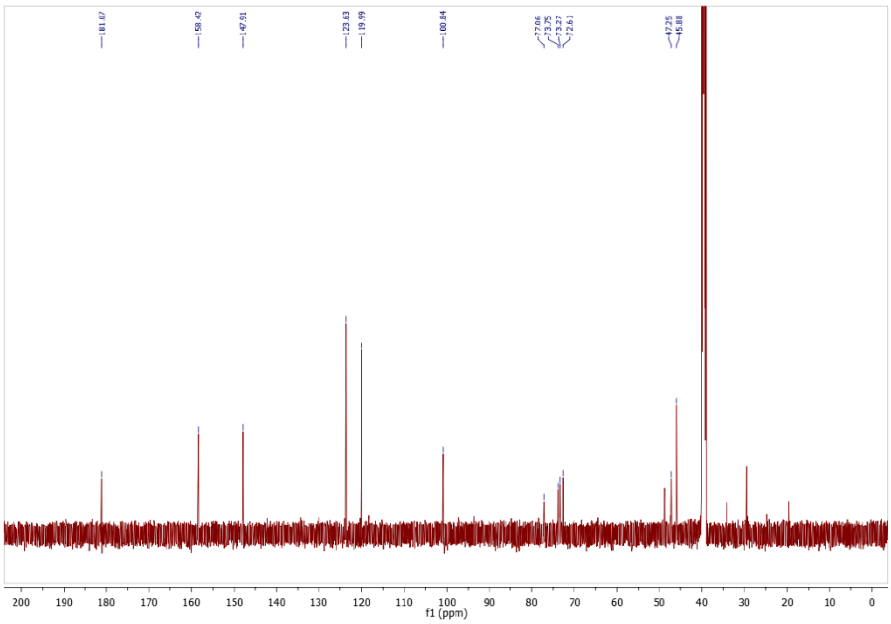

Figure S24. ^{13}C NMR spectrum of *trans*-**1** (151 MHz, DMSO-d_6 + εD_2O, 300 K).

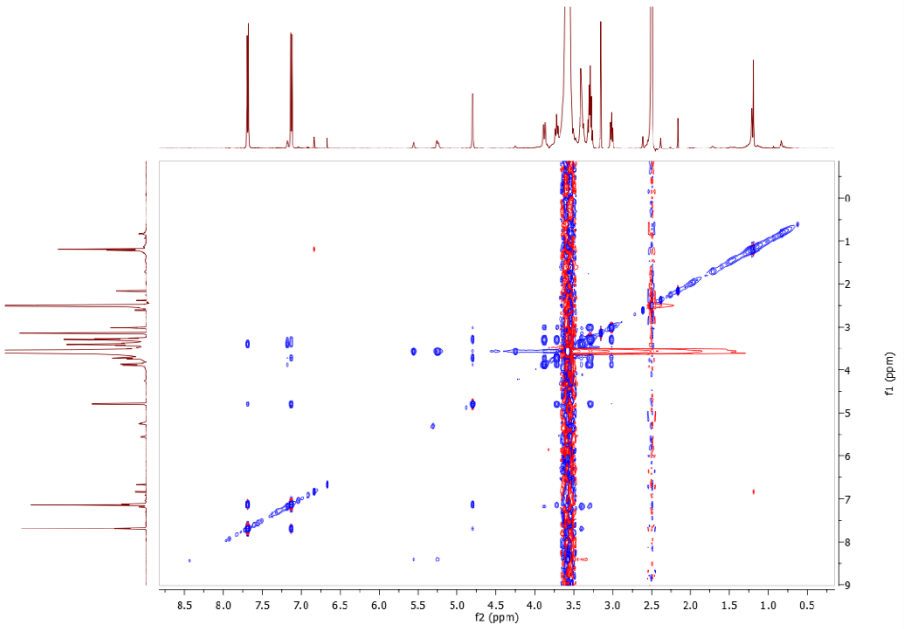

Figure S25. NOESY spectrum of *trans*-**1** (DMSO-d_6 + εD_2O, 300 K, mixing time = 500 ms).

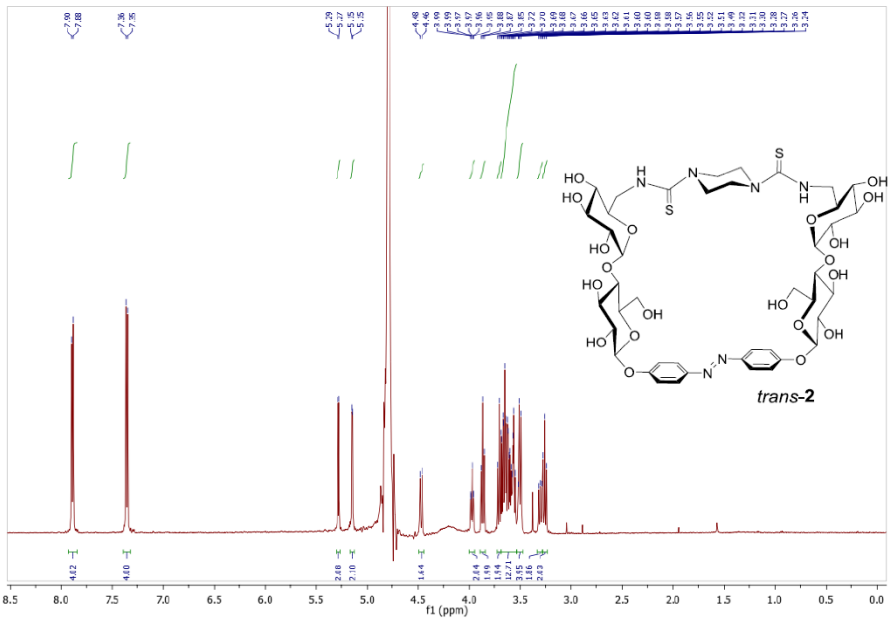

Figure S26. ^{1}H NMR spectrum of *trans*-**2** (600 MHz, D_2O, 300 K).

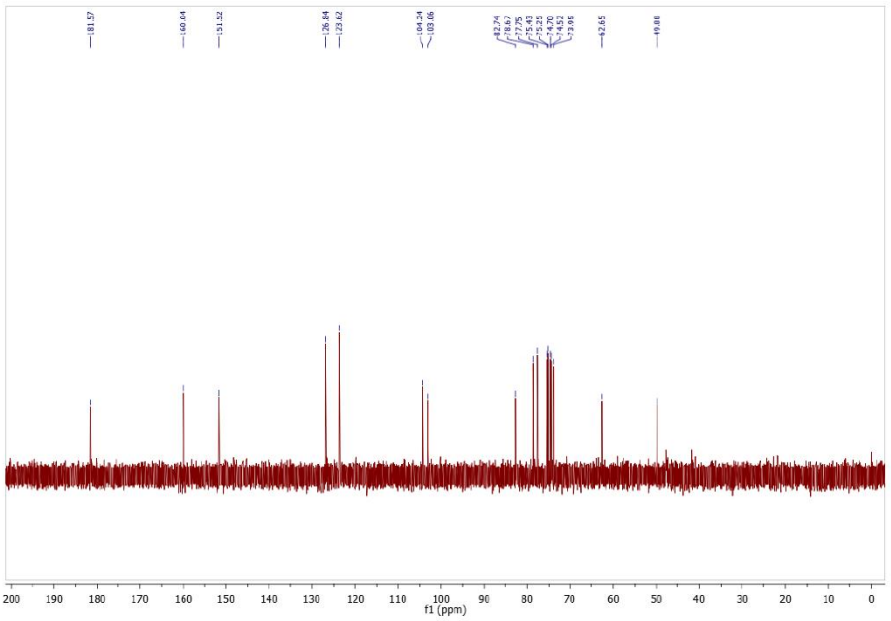

Figure S27. ^{13}C NMR spectrum of *trans*-**2** (151 MHz, D_2O, 300 K).

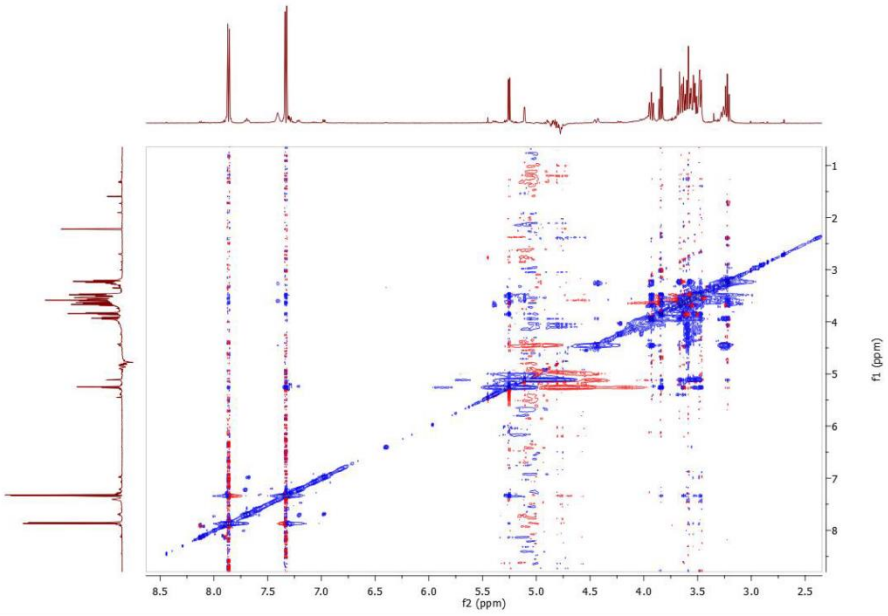

Figure S28. NOESY spectrum of *trans*-**2** (H_2O/D_2O, 300 K, mixing time = 500 ms, water suppression).

MALDI-TOF spectra of macrocycles 13, 14, 1 and 2

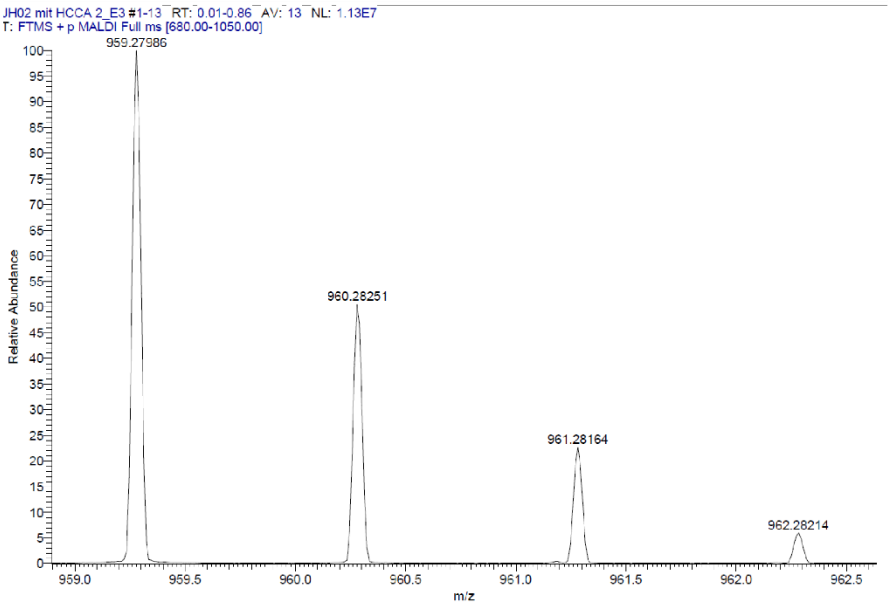

Figure S29. HRMS MALDI-TOF spectrum of macrocycle **13** (HCCA matrix).

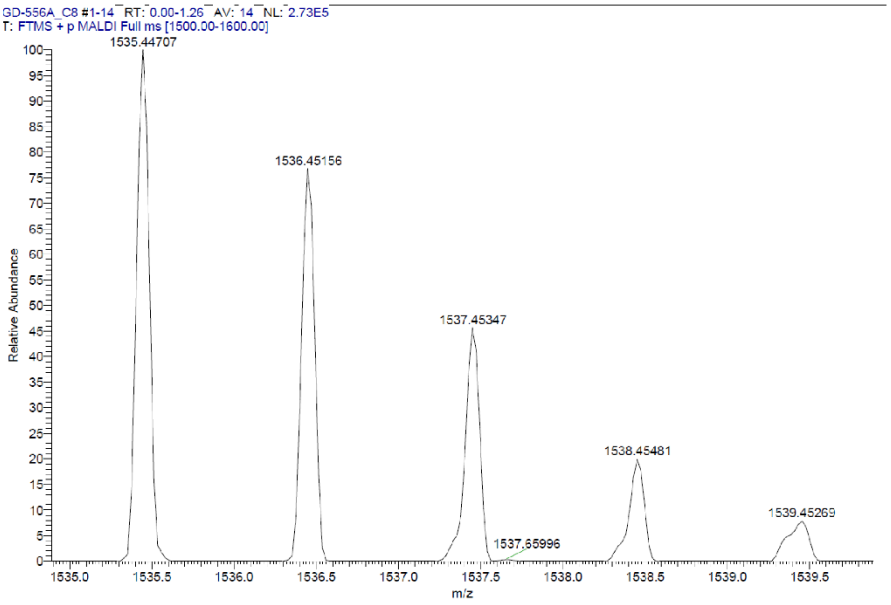

Figure S30. HRMS MALDI-TOF spectrum of macrocycle **14** (HCCA matrix).

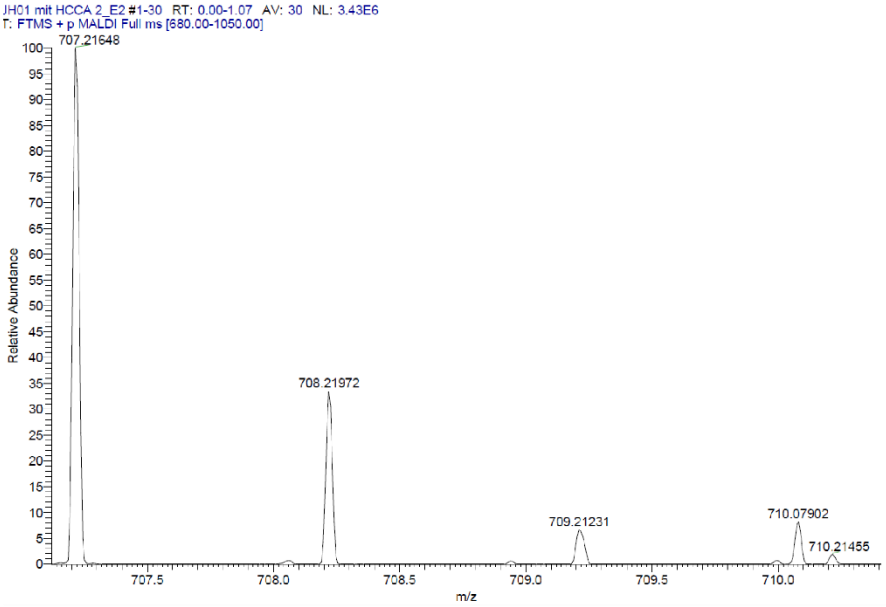

Figure S31. HRMS MALDI-TOF spectrum of macrocycle **1** (HCCA matrix).

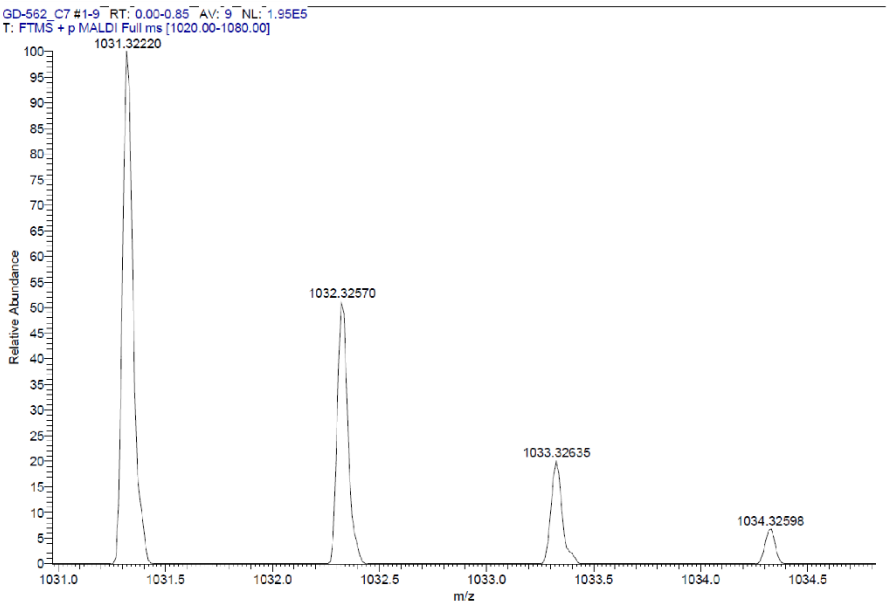

Figure S32. HRMS MALDI-TOF spectrum of macrocycle **1** (HCCA matrix).

Infrared spectra before and after macrocyclization

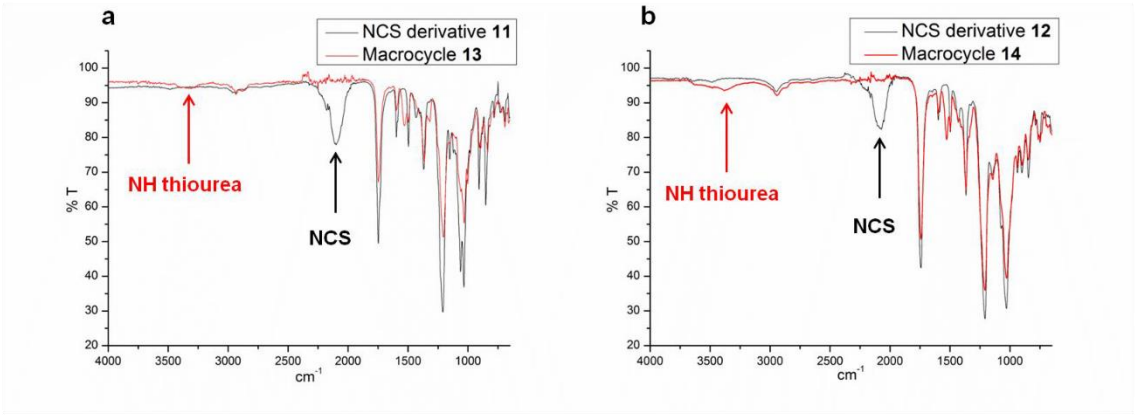

Figure S33. (a) superimposed IR spectra of the linear NCS-functionalized derivative **11** and the cyclized product **13**; (b) superimposed IR spectra of the linear NCS-functionalized derivative **12** and the cyclized product **14.**

Irradiation experiments

Each sample was heated at 45 °C in the dark for 20 h prior to the beginning of each experiment in order to fully relax the azobenzene to its *trans* form. The respective sample was irradiated in the dark, the distance between the lamp and the sample being about 5 cm, then the respective measurement was performed immediately afterwards.

Absorption spectroscopy

Photostationary states (PSS) were reached after irradiating the respective sample for 2 min at 365 nm or 435 nm. Extinction coefficients (ε) were calculated using the Beer-Lambert law (see equation below), plotting the absorbance at the respective λ_{max} versus the concentration (6 - 8 different concentrations in a range of 2.10^{-5} to 10^{-4} mol.L^{-1}). In the case of PSS 365 nm, the λ_{max} of the n-π* band was used. A linear fitting gave the value of ε as the slope of the linear plot.

$A = \varepsilon * c * l$

A = absorbance

ε = extinction coefficient = slope of the plot

c = molar concentration in mol.L^{-1}

l = optical path length in cm

Switching cycles experiments were performed by irradiating the respective sample alternatively for 2 min at 365 nm and 435 nm, within ten cycles. The value of the absorbance at $\lambda_{max(E)}$ was plotted against the number of times the sample was irradiated.

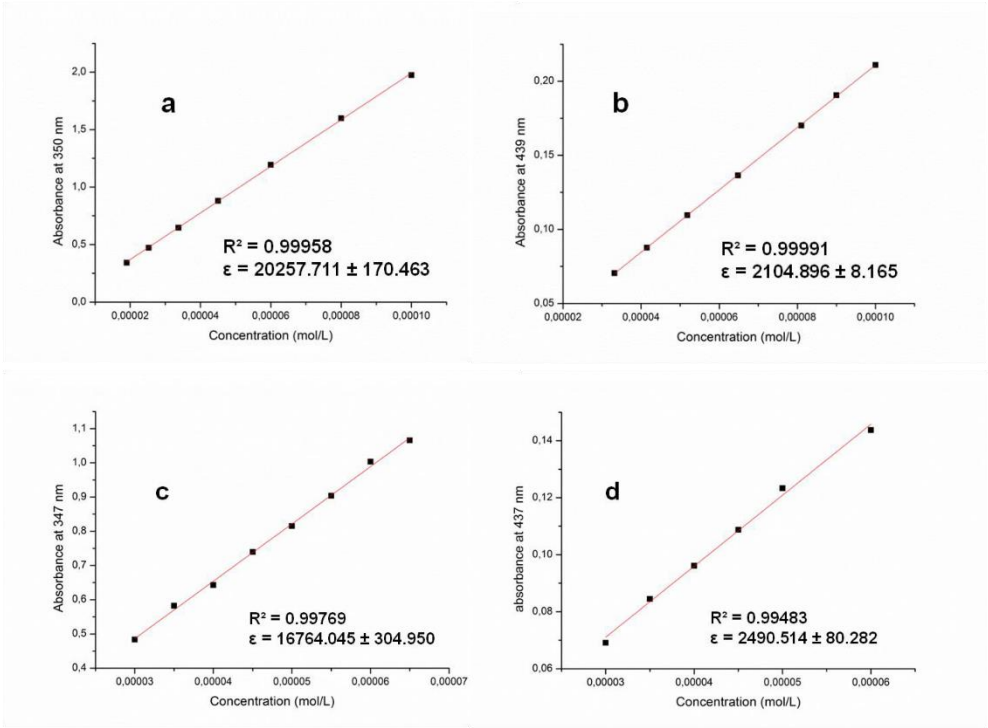

Figure S34. Plot of the absorbance at the λ_{max} versus the concentration; the slope of the linear curve gives the value of the molar extinction coefficient (ε). (a) *trans*-**1** (298 K in water (0.5 % DMSO)); concentration varied from $1.9.10^{-5}$ mol.L^{-1} to 10^{-4} mol.L^{-1}; (b) PSS 365 nm for **1** (298 K in water (0.5 % DMSO)); concentration varied from $3.3.10^{-5}$ mol.L^{-1} to 10^{-4} mol.L$_{-1}$; (c) *trans*-**2** (298 K in water); concentration varied from 3.10^{-5} mol.L^{-1} to $6.5.10^{-5}$ mol.L^{-1}; (d) PSS 365 nm for **2** (298 K in water); concentration varied from 3.10^{-5} mol.L^{-1} to 6.10^{-5} mol.L^{-1}.

NMR spectroscopy

PSS was reached after irradiating the respective sample for 5 min and the *cis*:*trans* ratios were measured by ^{1}H NMR spectroscopy. The PSS were determined by integration of one aromatic signal of each isomer.

The kinetics of thermal *cis*→*trans* relaxation process was determined by ^{1}H NMR. After irradiation, the spectra of the samples were recorded in regular intervals, keeping the sample inside the magnet at a constant temperature of 300 K, over a period of 2 to 4 days.

The decay of the integral of the *cis* form was plotted versus the time, and an exponential decay of first order fitted to the data, according to the following equation:

$I = I_{inf} + A*\exp^{-k*t}$

I = integral of the *cis* isomer

I_{inf} = integral of the *cis* isomer at infinite time

A = pre-exponential factor proportional to the initial integral of the *cis* isomer

k = rate of thermal isomerization

t = time

A linear fitting gave the value of *k* as the slope of the following plot:

$\ln(I - I_{inf}) = \ln(A) - kt$

The half-life of the *cis* isomer ($\tau_{1/2}$) was determined as $\tau_{1/2} = \ln 2/k$.

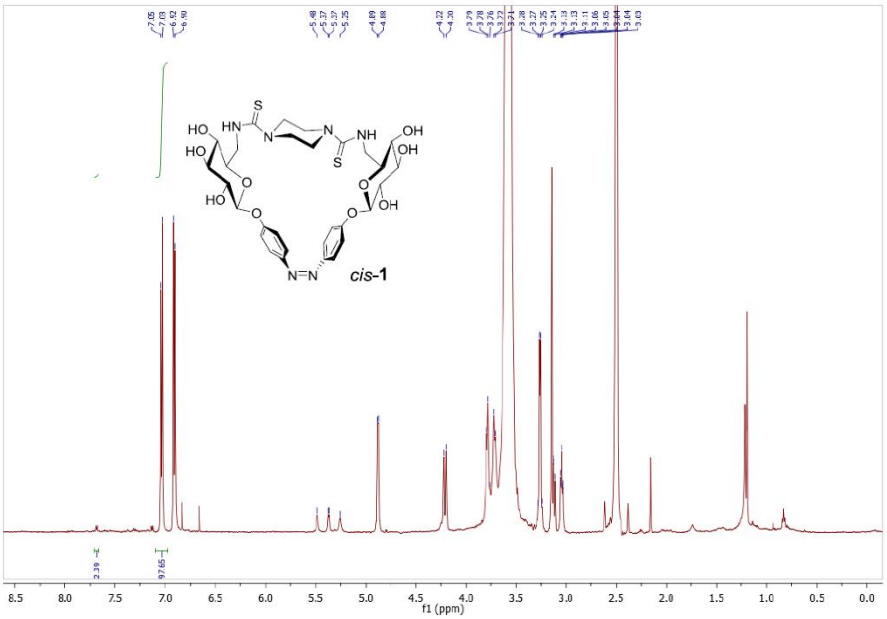

Figure S35. ^{1}H NMR spectrum of *cis*-**1** (600 MHz, DMSO-d_6 + εD_2O, 300 K).

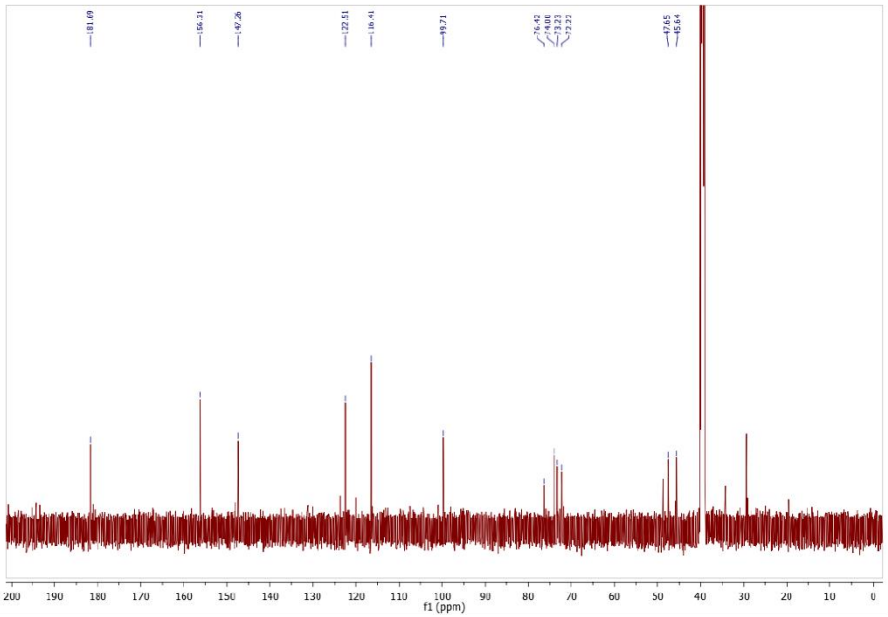

Figure S36. ^{13}C NMR spectrum of *cis*-**1** (151 MHz, DMSO-d_6 + εD_2O, 300 K).

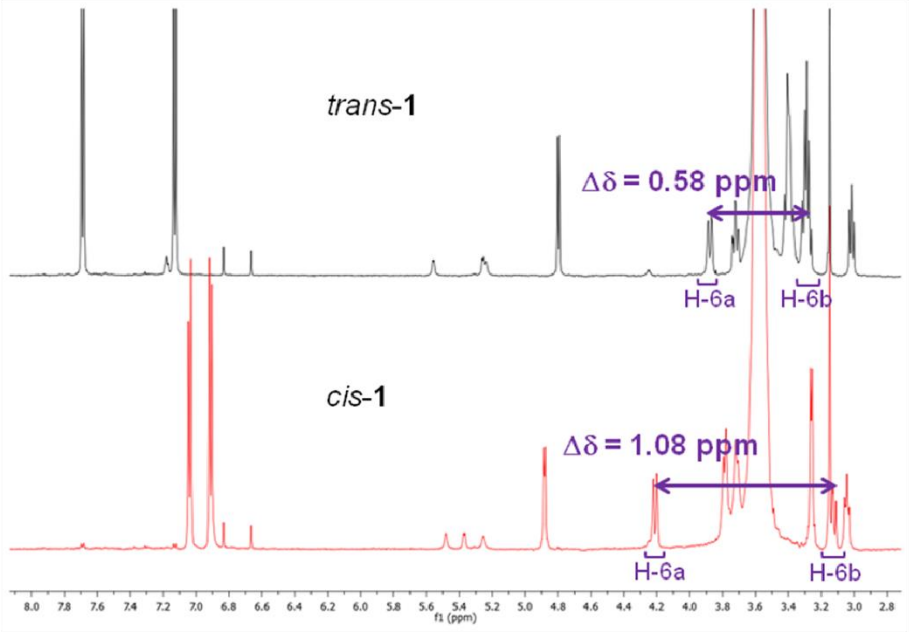

Figure S37. Stacked ^{1}H spectra of *trans*-**1** and *cis*-**1** (600 MHz, DMSO-d_6 + εD_2O, 300 K), showing the difference in chemical shift between H-6a and H-6b.

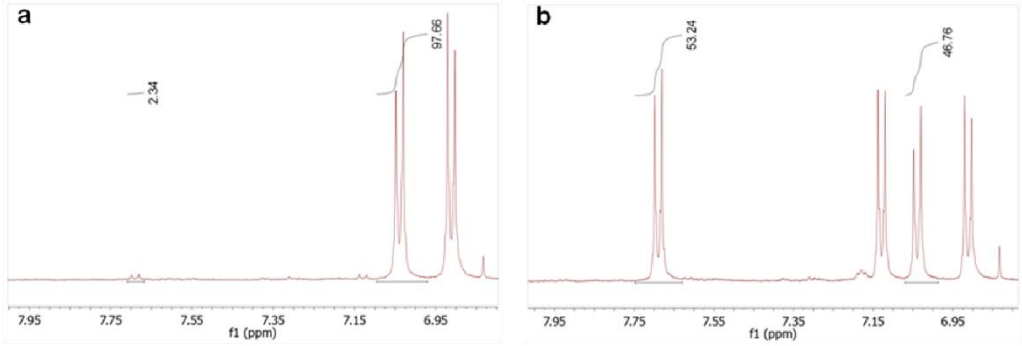

Figure S38. Expansion of the ^{1}H NMR spectra of **1** at the photostationary states (600 MHz, DMSO-d_6 + εD_2O, 300 K). (a) After irradiating *trans*-**1** for 5 min at 365 nm; (b) after irradiating *cis*-**1** for 5 min at 435 nm.

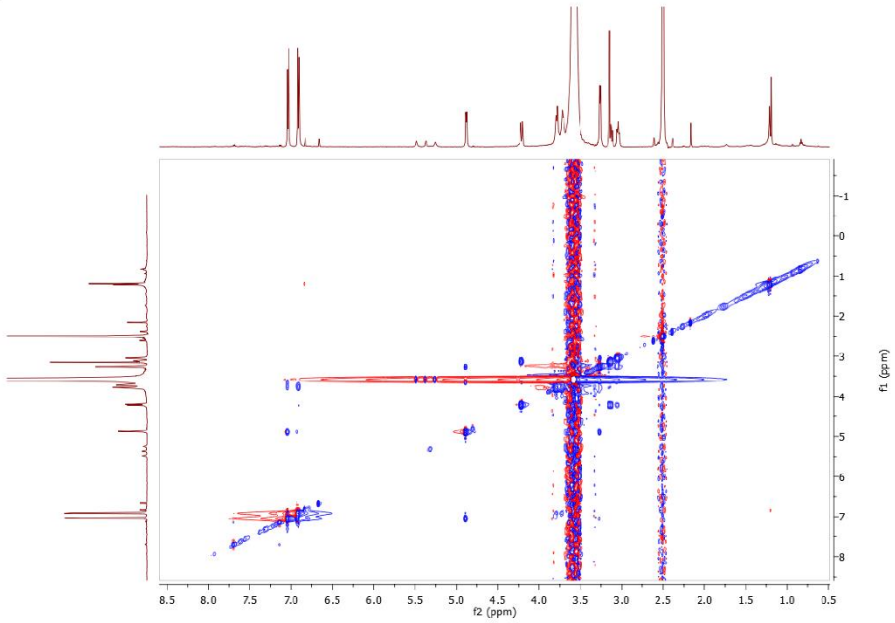

Figure S39. NOESY spectrum of *cis*-**1** (600 MHz, DMSO-d_6, 300 K, mixing time = 300 ms).

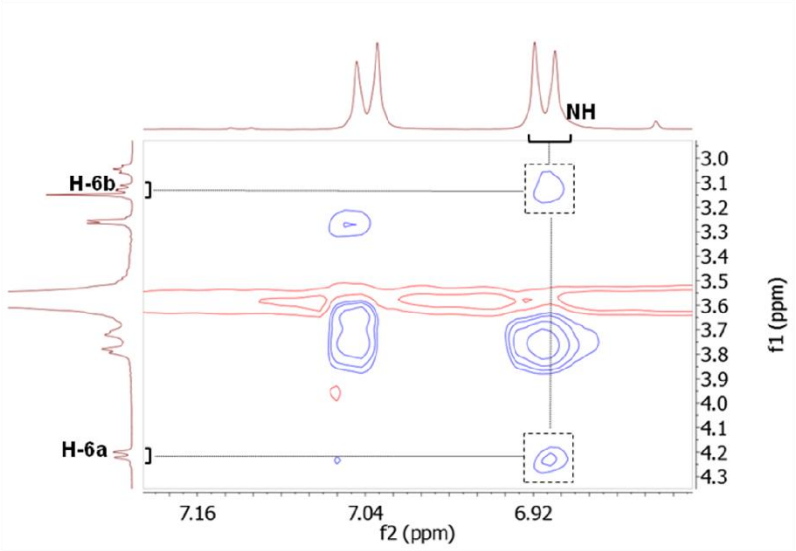

Figure S40. Expansion of the NOESY spectrum of *cis*-**1** showing the crosspeaks between the NH moiety forming the thiourea bridge and the H-6; the intensity ratio between the two crosspeaks is 0.82.

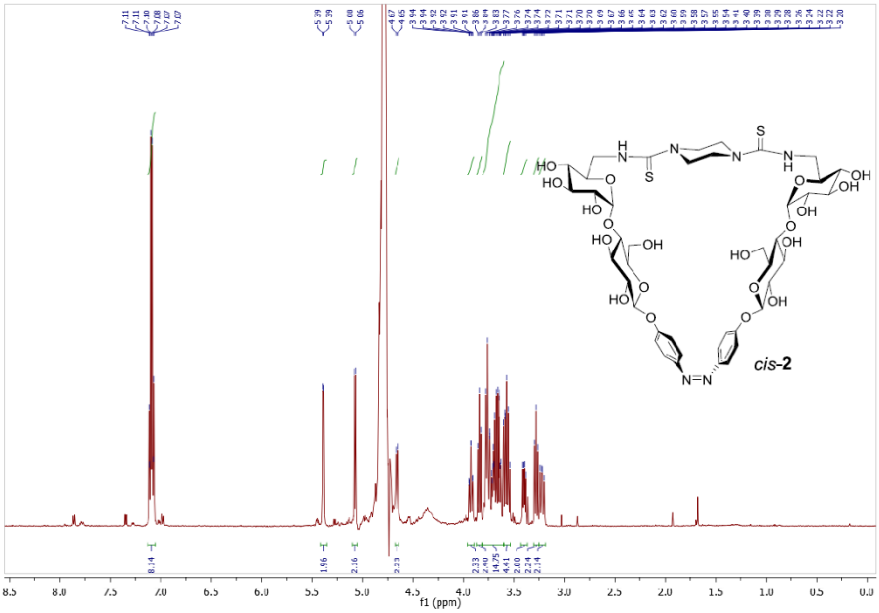

Figure S41. ^{1}H NMR spectrum of *cis*-**2** (600 MHz, D_2O, 300 K).

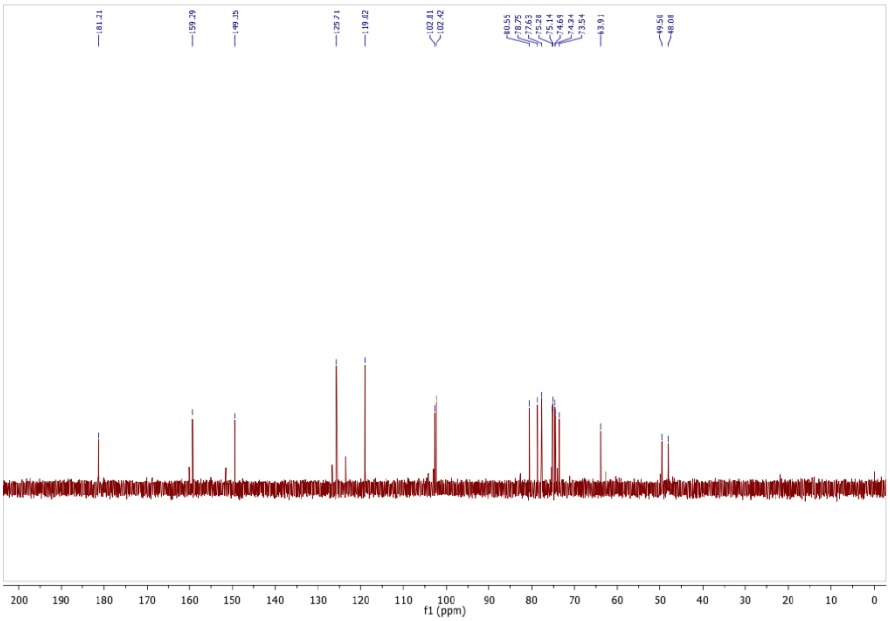

Figure S42. ^{13}C NMR spectrum of *cis*-**2** (151 MHz, D_2O, 300 K).

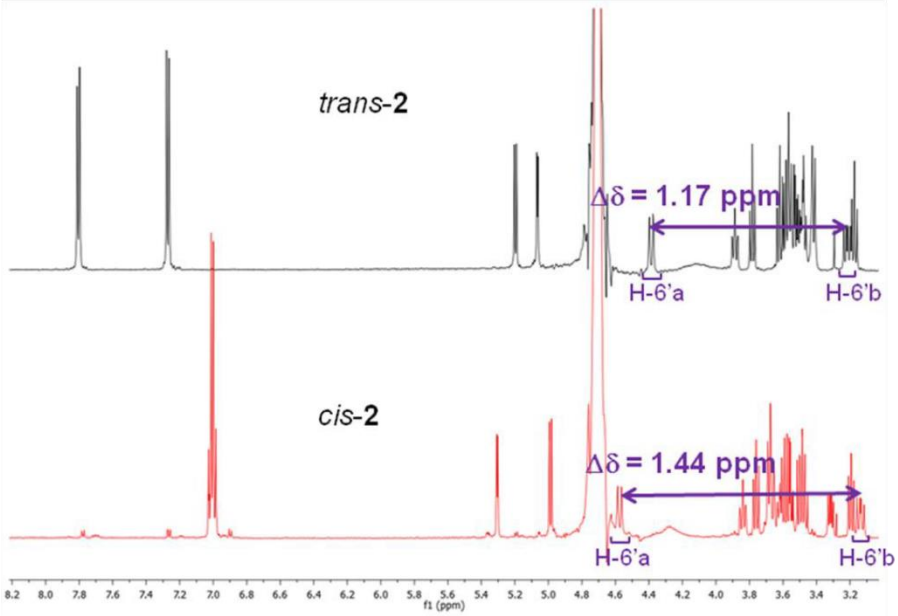

Figure S43. Stacked ^{1}H spectra of *trans*-**2** and *cis*-**2** (600 MHz, D_2O, 300 K) showing the difference in chemical shift between H-6'a and H-6'b.

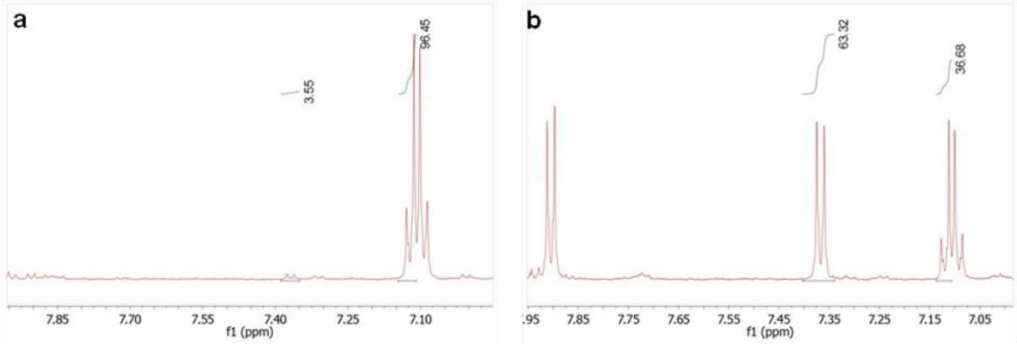

Figure S44. Expansion of the ^{1}H NMR spectra of **2** at the photostationary states (600 MHz, D_2O, 300 K). (a) After irradiating *trans*-**2** for 5 min at 365 nm; (b) after irradiating *cis*-**2** for 5 min at 435 nm.

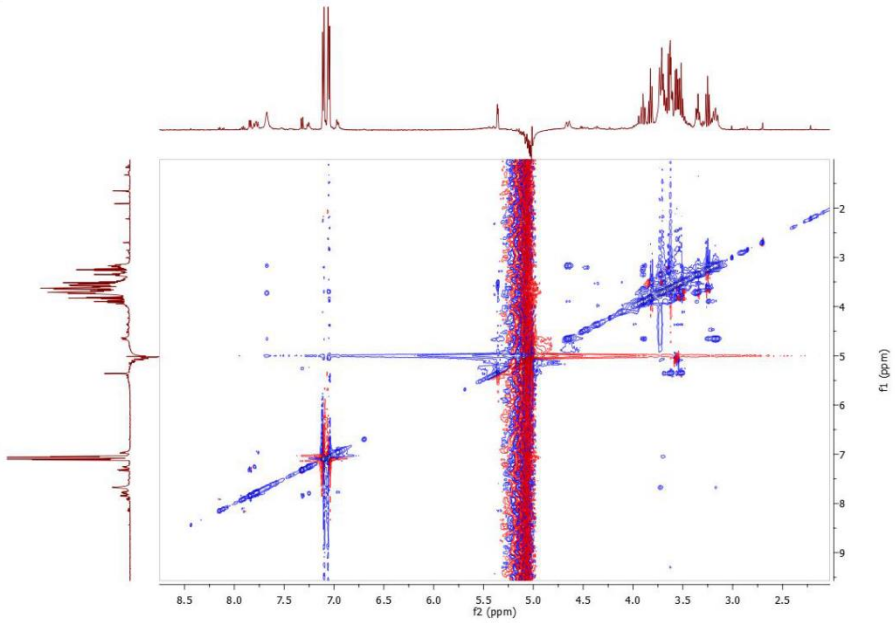

Figure S45. NOESY spectrum of *cis*-**2** (600 MHz, 9:1 H_2O/D_2O, 300 K, water suppression, mixing time = 200 ms).

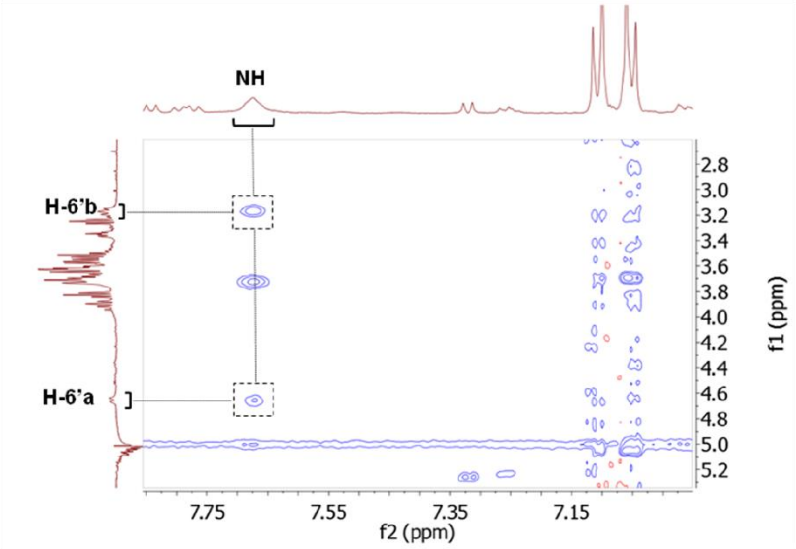

Figure S46. Expansion of the NOESY spectrum of *cis*-**2** showing the crosspeaks between the NH moiety forming the thiourea bridge and the H-6' ; the intensity ratio between the two crosspeaks is 0.59.

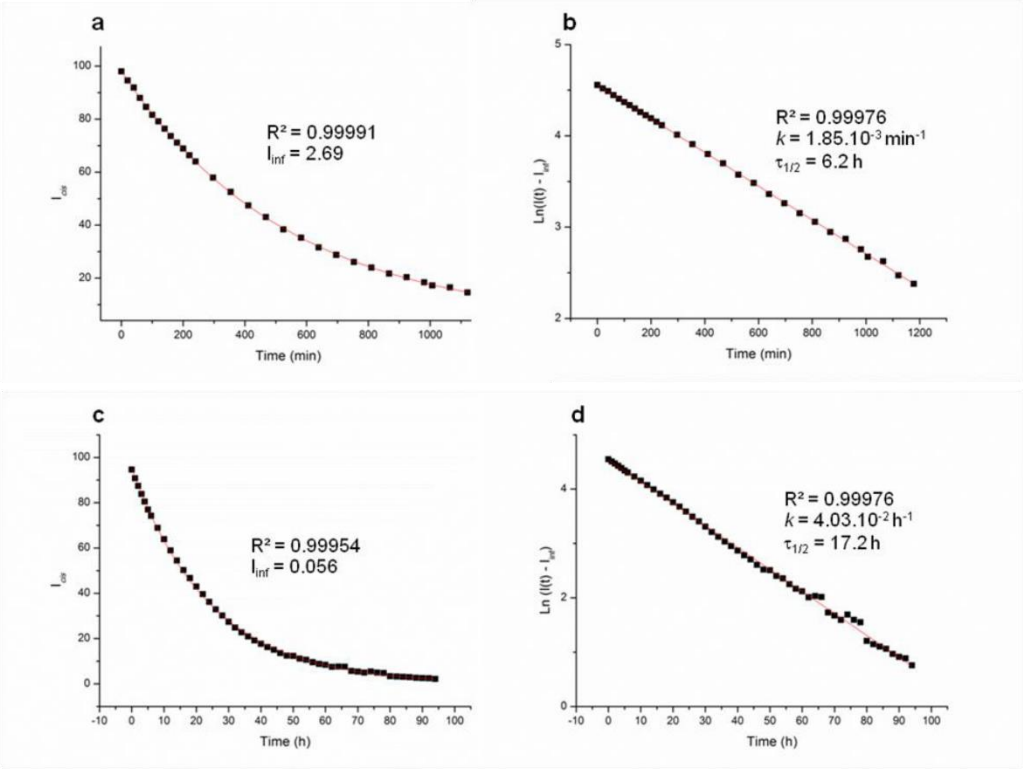

Figure S47. Kinetics of the *cis*→*trans* thermal relaxation process at 300 K investigated by ^{1}H NMR spectroscopy. (a) Exponential decay of the integral of an aromatic signal of *cis*-**1**(600 MHz, DMSO-d_6); (b) Linearization of the exponential decay of cis-**1**; (c) Exponential decay of the integral of an aromatic signal of *cis*-**2** (600 MHz, D_2O); (d) Linearization of the exponential decay of cis-**2**.

Specific rotation and circular dichroism

The optical rotation and the circular dichroism spectra were measured at 293 K after irradiating the respective sample at 365 nm for 10 min. The CD signal was recorded as ellipticity (θ), expressed in units of millidegrees (mdeg). The ellipticity was converted into difference in molar absorption coefficient ($\Delta\varepsilon$), expressed in $M^{-1}.cm^{-1}$, by using the following equation:

$\Delta\varepsilon = \theta$ /(32980*c*l)

$\Delta\varepsilon$ = difference in molar absorption coefficient

θ = ellipticity

c = molar concentration in $mol.L^{-1}$

l = optical path length in cm

Molecular modeling

Structures were built using Schrödinger Maestro,[3] and calculations were performed using MacroModel,[4] with the OPLS3 force field in implicit water (GB/SA continuum solvation model).
The respective starting geometry was minimized (PRCG method, maximum iterations = 2500, converge on gradient, convergence treshold = 0.05) without any constraint then the minimized structure was sampled by stochastic dynamics (simulation temperature = 300 K, time step = 1.5 fs, equilibration time = 1.5 ps, simulation time = 10000 ps, number of saved structures = 100) and the resulting structures were minimized. The most stable structure was chosen, according to a reasonable planarity of the *trans*-azobenzene unit, then minimized to the *cis*-isomer by constraining the azo bond (force constant 100).[5] The minimized *cis* form was then sampled by stochastic dynamics, inputting the parameters afore given, and keeping the azo bond constrained (force constant 100).

Literature references

[1] M. L. Lepage, J. P. Schneider, A. Bodlenner, P. Compain, *J. Org. Chem.* **2015**, *80*, 10719-10733.
[2] A. Müller, H. Kobarg, V. Chandrasekaran, J. Gronow, F. D. Sönnichsen, T. K. Lindhorst, *Chem. Eur. J.* **2015**, *21*, 13723-13731.
[3] Schrödinger Release 2016-1: Maestro, version 10.5, Schrödinger, LLC, New York, NY, 2016.
[4] Schrödinger Release 2016-1: MacroModel, version 11.1, Schrödinger, LLC, New York, NY, 2016.
[5] P. Cattaneo, M. Persico, *Phys. Chem. Chem. Phys.* **1999**, *1*, 4739-4743.

4. CuAAC Click Reaction

4.1 Introduction

A powerful ligation reaction, frequently used today, leads to triazole-bridged ligation products from alkynes and alkyl azides. The thermal cycloaddition of an azide with an alkyne was first described by MICHAEL in 1893.[107] 60 years later, this 1,3-dipolar cycloaddition reaction was studied extensively by HUISGEN.[108] The great drawback of this pericyclic reaction according to Huisgen are harsh reaction conditions and slow reaction rates. In addition, an unwanted regioisomeric mixture of 1,4- and 1,5-triazoles is obtained with asymmetric alkynes (Scheme 4.1a).

In 2002, a copper(I)-catalyzed variation of this reaction was concomitantly introduced by the groups of MELDAL[109] and SHARPLESS,[110] where terminal alkynes and azides yield 1,4-triazoles regioselectively and under mild reaction conditions (Scheme 4.1b). This reaction is a prime example for a "click reaction" as suggested by SHARPLESS. According to Sharpless a click reaction is a reaction which is high in yield, with broad scopes and applications and only generates minimal or no byproducts.[90] This Cu(I)-catalyzed azide-alkyne cycloaddition (CuAAC) today serves as the most commonly known click-type reaction.

The suggested mechanism of CuAAC is based on DFT calculations and involves a stable dinuclear Cu(I)-acetylide complex and subsequent binding of the distal nitrogen atom of the azide to the acetylene C-2, leading to the regioselectivity of the reaction.[111]

Other variants of the reaction include the ruthenium-catalyzed process (RuAAC),[112] which leads to 1,5-tirazole isomers regioselectively, and the strain-promoted copper-free reaction using cyclooctynes, which was first observed by WITTIG and KREBS in 1961[113] and utilized by BERTOZZI et al. in 2004 as a bioorthogonal ligation reaction.[114]

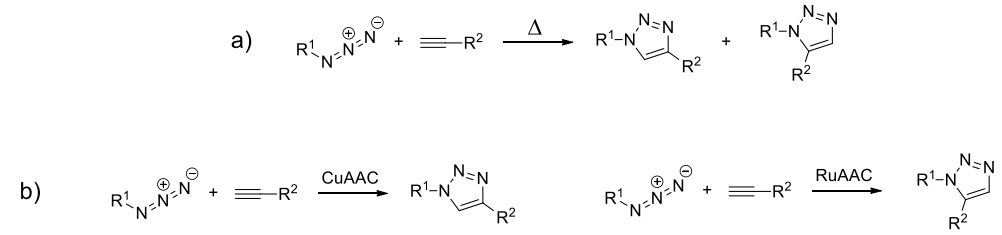

Scheme 4.1: Overview of the different 1,3-dipolar cycloadditions with an alkyne and azide. (a) Huisgen reaction; (b) copper catalyzed reaction; (c) ruthenium catalyzed reaction.[115]

The efficient and rapid click reaction soon became a popular tool in the synthesis of macrocycles, including glycomacrocycles,[116] where the isosterism of the 1,2,3 triazole with peptide bond makes it especially interesting for the synthesis of macrocyclic peptide mimetics.[68]

Here, the synthesis of a glycoazobenzene macrocycle **9** through Cu(I)-catalyzed click macrocyclization was targeted, comprising two azobenzene and two disaccharide moieties. As carbohydrate building blocks the symmetric trehalose diazide, 6,6'-diazido-6,6'-dideoxy-trehalose **10**[117] was chosen for macrocyclization. Retrosynthesis of **9** suggests two possible synthetic routes, first a one-pot condensation of two molecules **10** with two equivalents 4,4'-dipropargyloxy azobenzene (**11**),[118] and

second the sequential construction from azido trehalose **10** with monopropargyl azobenzene **12**[118] followed by conversion of the product **13** with propargyl bromide (**14**) and a subsequent second click reaction of **15** with the second equivalent of **10** as the cyclization step (Scheme 4.2).

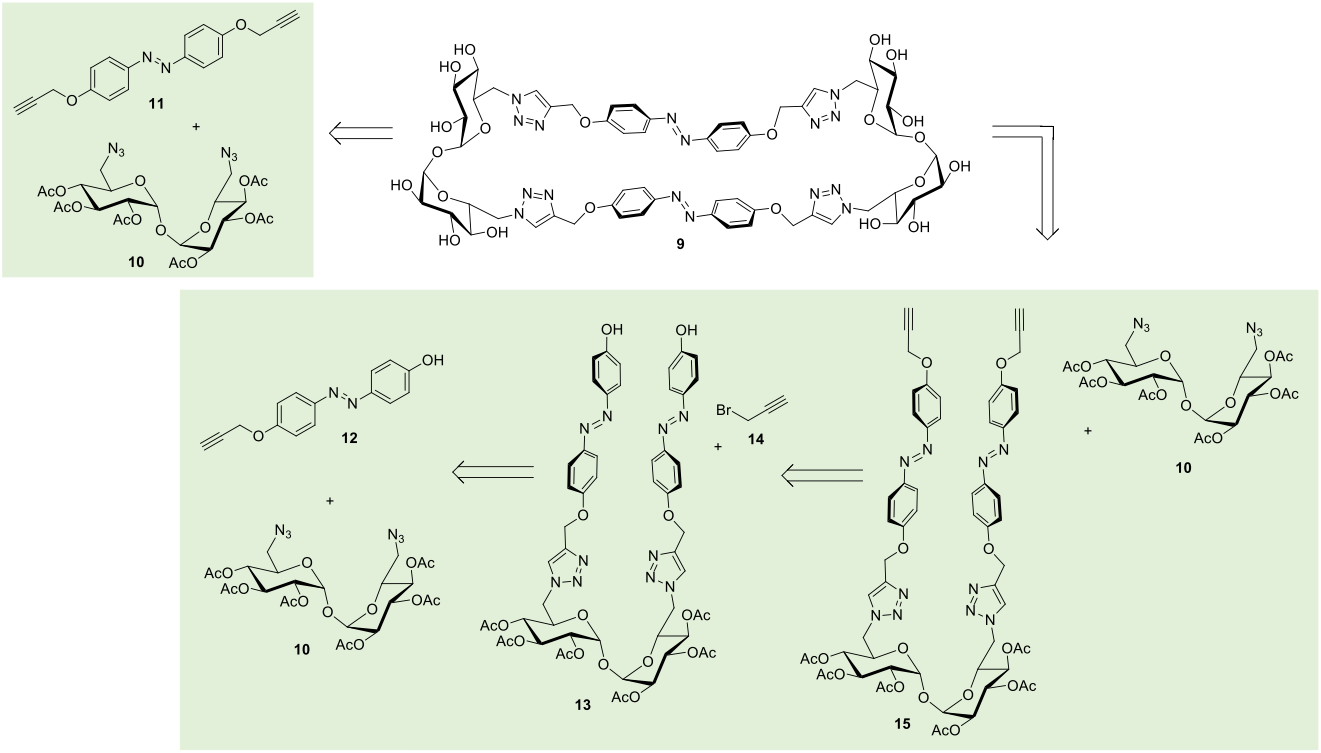

Scheme 4.2: Two retrosynthetic pathways for macrocycle **9** and their corresponding building blocks.

4.2 Synthesis

Not completely unexpectedly, the one-pot macrocyclization, reacting **10** and **11** under Cu(I) catalysis, did not yield the desired macrocycle but instead an inseparable mixture of different products.

Reaction of **10** with the unsymmetrical propargyl azobenzene **12** afforded the difunctionalized trehalose derivative **13** in 73 % yield using Cu(I)Br and *N,N,N′,N″,N‴*-pentamethyldiethylenetriamine (PMDETA) in DMF (Scheme 4.3).[119] Subsequent Williamson etherification with propargyl bromide **14** gave the precursor **15** in 78 % yield, which was then reacted to **16** via a second click reaction in an intermolecular macrocyclization with **10** in a yield of 28 %. For the subsequent intramolecular click reaction, the dilution of the reaction was increased significantly from 100 mM to 5 mM and **10** and **15** were added equimolarly to the reaction, to prevent oligomer formation.

Nevertheless, the yield of the click reaction (28 %) was clearly poorer than for the first intermolecular click ligation (73 %) in the sequence but satisfying for a non-templated macrocyclization reaction. Pre-organization of the precursor **15** was not necessary to facilitate the reaction, despite the considerably higher degree of freedom in its structure compared to the reaction partner **10**. Presumably, π-π stacking aligns the azobenzene moieties parallelly, leading to a similar distance in the functional groups for the click reaction of **10** and **15**. Finally, **16** was deprotected under ZEMPLÉN conditions[100] to give the target macrocycle **9** in quantitative yield.

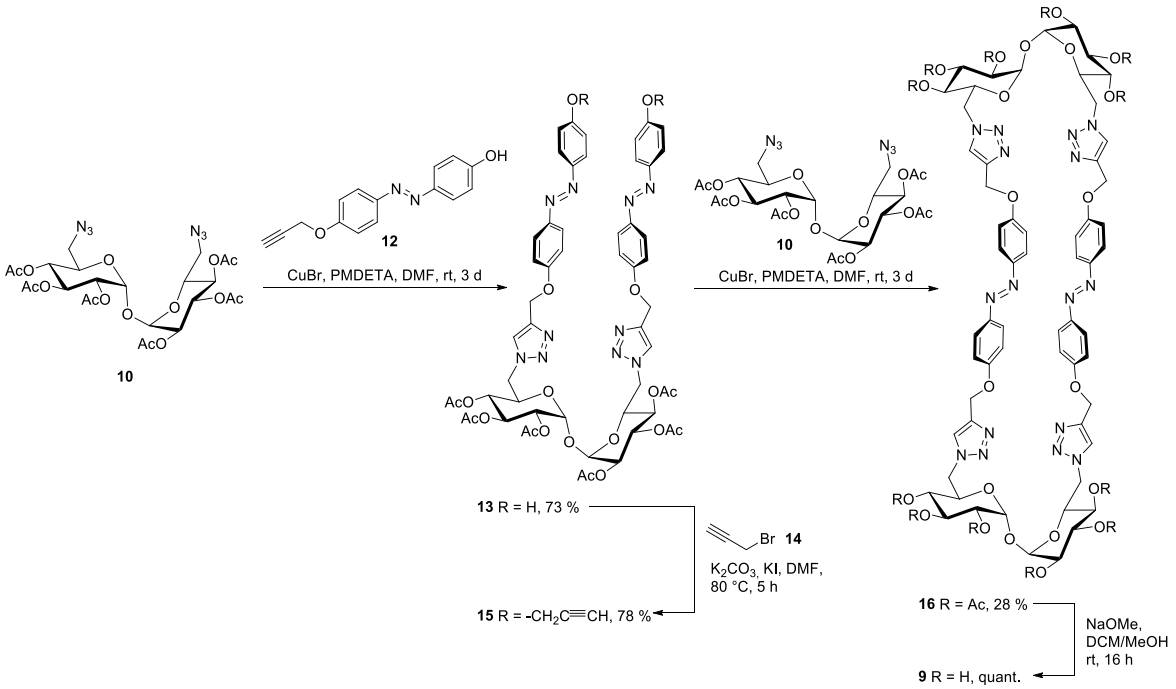

Scheme 4.3: Synthesis of macrocycle **9** with a yield of 16 % over four steps. PMDETA: *N,N,N′,N″,N‴*-pentamethyldiethylenetriamine.

4.3 Photochromic properties

The macrocycle **9** was investigated by NMR, UV/Vis and CD spectroscopy. In NMR measurements the molecule is highly symmetric, showing only a single set of signals representing one fourth of the cycle. Change in the chemical shifts of the carbohydrate protons upon *trans* → *cis* isomerization is minimal, with only H-1 and H-6 being affected by the switching, which shows that *trans*/*cis* isomerization does not lead to a significant change in their chemical environment while the high symmetry of the molecule persists (Figure 4.1). The signal for the CH_2 protons between the triazole and azobenzene moiety is shifted downfield by 0.2 ppm and collapses from two doublets with ^2J = 12 Hz to a singlet, indicating fewer rotational freedom at this position in the *trans*-form compared to the *cis*-form. However, the structures which were determined by force field-minimization (OPL3 in water, Figure 4.2)[101] reveal a twisted structure for *trans*-**9** and a bent shape for *cis*-**9** where this high degree of symmetry cannot be observed.

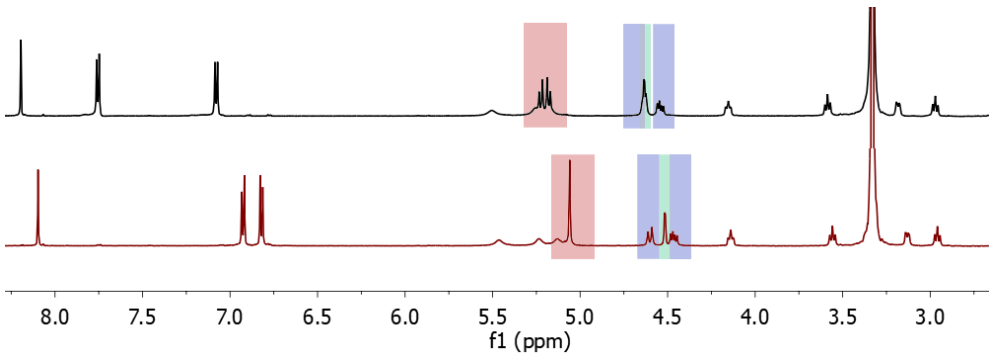

Figure 4.1: Cutout of the ^{1}H NMR spectra of **9** (600 MHz, DMSO-d_6, 298 K): black line: all *trans*-macrocycle, red line: PSS after irradiation with 365 nm for 5 min; red highlight: diyne CH_2a and CH_2b, blue highlight: H-6a and H-6b, green highlight: H-1.

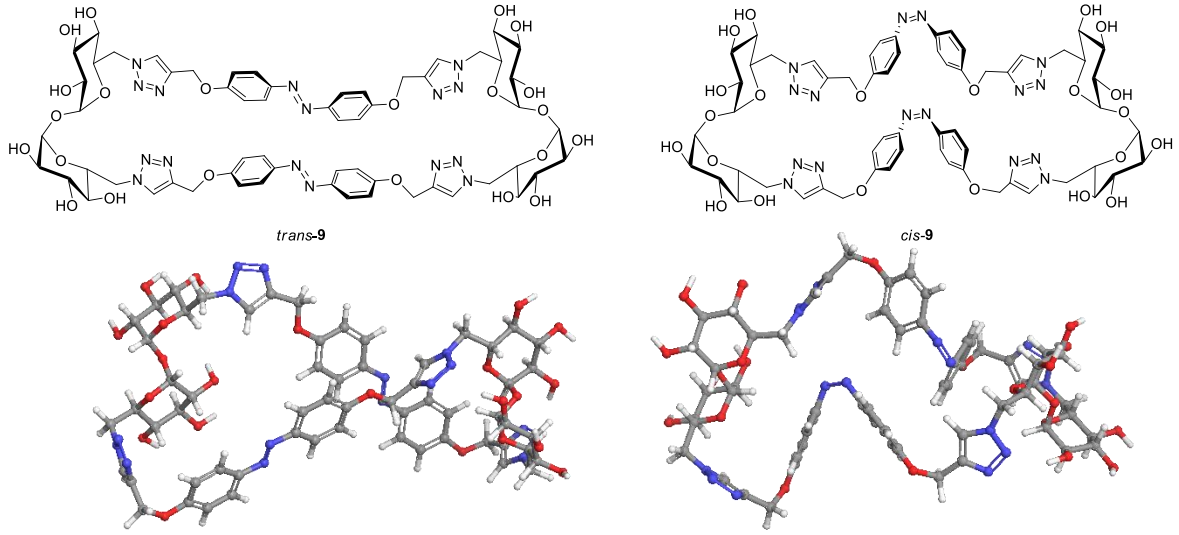

Figure 4.2: Force field-minimized structures (OPLS3 in water) of the different *all trans*- and *all cis*-isomers of **9**.[101]

UV/Vis absorption spectra in DMSO show a strong π → π* transition (λ_{max} = 360 nm) and a weak n → π* transition in the region of 450 nm (Figure 4.3a). Upon isomerization at 365 nm, the weakened π → π* transition undergoes a blue shift towards a λ_{max} of 310 nm, while in the n → π* transition the absorption is slightly increased. The switching efficiency was quantified using ^{1}H NMR, after 5 min of irradiation at 365 nm the PSS with a *trans:cis* ratio of 2:98 was reached. Even though both *trans* and *cis* n → π* transitions overlap, they are resolved in the green range and through irradiation with a 520 nm LED the initial relaxed state could be almost recovered with a PSS with a *trans:cis* ratio of 90:10. Thermal relaxation was determined by UV/Vis measurements, to give the half-life of *cis*-**9** at 298 K in DMSO as $\tau_{1/2}$ = 16 h.

Absorption measurements in water (0.5 % DMSO) shows a broader band for *trans*-**9**, with a reduced absorbance and a λ_{max} blue-shifted to 340 nm (Figure 4.3b). In contrast, the spectrum corresponding to the PSS after irradiation at 365 nm is very similar to the one measured in DMSO. The reduced absorbance in addition to the higher baseline indicate that the macrocycle is not fully dissolved in the water/DMSO mixture, while the solubility improves upon irradiation with 365 nm light. This is a known effect for *cis*-azobenzene-containing compounds, as their bent shape weakens intermolecular stacking, thus improving solvation in polar solvents.[120]

The CD spectrum for *trans*-**9** in DMSO shows a weak negative Cotton effect for the n → π* transition at 450 nm and an exciton coupling around the π → π* transition from the interaction of one azobenzene unit with the other (Figure 4.3 c).[121] Upon isomerization the exciton coupling disappears and the spectrum corresponding to the PSS at 365 nm shows a negative Cotton effect for the π → π* transition and a positive one for the n → π* transition. In water (0.5 % DMSO) the amplitude for the exciton coupling in *trans*-**9** is severely increased in intensity (Figure 4.3 d), while the Cotton effect for the n → π* transition changes its sign to positive. The spectrum corresponding to the PSS at 365 nm has the same pattern in water and in DMSO, but with an increased intensity as well.

An increase of the ellipticity of the Cotton effect generally implies a more strongly twisted conjugated π-electron system, while the increase in the amplitude of an exciton couplet is influenced by a change in the angle between the two interacting chromophores or their distance.[102, 121] The amplitude reaches a maximum at a projection angle of 70°, while being inversely proportional to the square of

the distance between the two chromophores. The increased intensities in water for the Cotton effects of the n → π* transition in *trans*-**9** and the n → π* and π → π* transition in *cis*-**9** indicate that the azo bond of the azobenzene moieties is more twisted than in DMSO. The strong increase in the amplitude of the exciton coupling for the π → π* transition in *trans*-**9** shows that either the angle between the two azobenzene units or their distance differs in water as the solvent. This shows that the solvent has a profound effect on the shape and chirality of the macrocycle. Presumably, the increased polarity in water increases the π-π stacking of the azobenzene moieties, leading to the twist in the *trans*-configured molecule as seen in the force field-minimized structure.

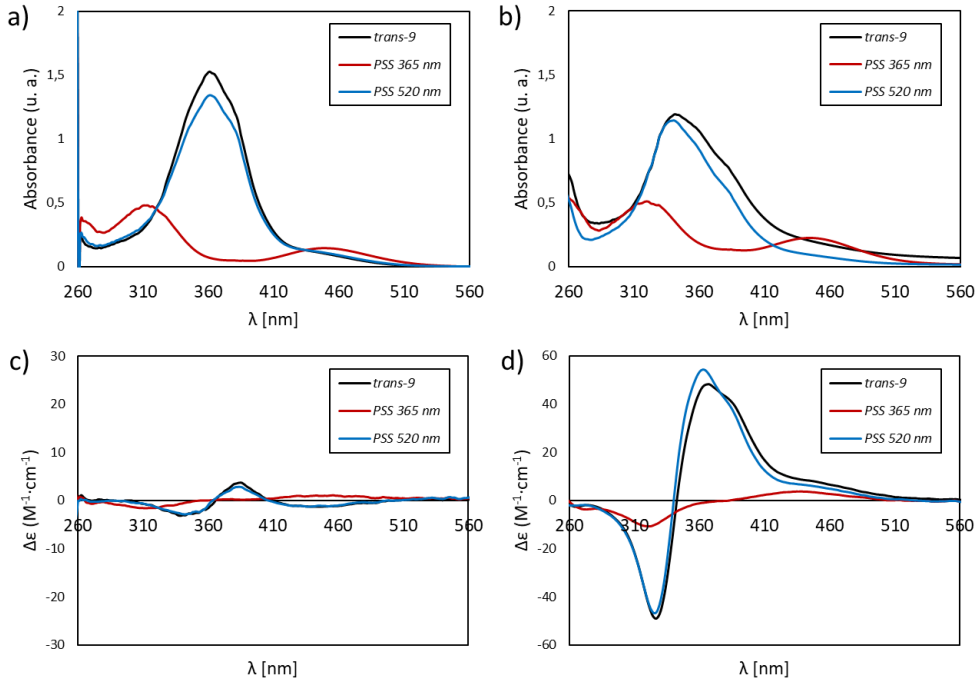

Figure 4.3: UV/Vis and CD spectra of **9** at 298 K in a concentration of 50 µM (a) UV/Vis spectra in DMSO; (b) UV/Vis spectra in water with 0.5 % DMSO; (c) CD spectra in DMSO; (d) UV/Vis spectra in water with 0.5 % DMSO; black line: *trans*-**9**, red line: PSS after irradiation with 365 nm for 5 min, blue line: PSS after irradiation with 520 nm for 5 min.

4.4 Conclusion

After constructing macrocycles through thiourea bridging, the CuAAC click reaction was also successfully applied to the synthesis of glycoazobenzene macrocycles. The target macrocycle **9** could be obtained after an attempt at a one-pot macrocyclization of four building blocks was unsuccessful.

The change in the shape of the macrocycle upon *trans* → *cis* isomerization leads to a better solvation in polar solvents. Additionally, changing the solvents affects the shape of the macrocycle as well, as CD spectroscopy revealed that the angle between the two di-triazole-azobenzene linkers differs largely in different solvents. This indicated that solvation has a strong influence on the shape of the macrocycle and vice versa. It might be possible that the *trans*-macrocycle has a straight structure in DMSO and a twisted one in water. However, DFT calculations are needed to study this effect further.

4.5 Experimental section

General methods and instrumentation

Moisture-sensitive reactions were carried out in flame-dried glassware and under a positive pressure of nitrogen. Analytical thin layer chromatography (TLC) was performed on silica gel plates (GF 254, Merck). Visualization was achieved by UV light and/or with 10 % sulfuric acid in ethanol or vanillin (3.0 g vanillin and 0.5 mL H_2SO_4 in 100 mL EtOH), followed by heat treatment at ca. 200 °C. The products were purified by flash chromatography on silica gel columns (Merck, 230–400 mesh, particle size 0.040–0.063 mm). Pyridine was dried over KOH, tetrahydrofuran and *N,N*-dimethylformamide were stored over 3Å molecular sieves under a nitrogen atmosphere.

Melting points were determined on a Büchi M-560 apparatus. Optical rotations were measured with a PerkinElmer 241 polarimeter with a sodium D-line (589 nm) and a cuvette of 10 cm path length, in the solvents indicated. Circular dichroism spectroscopy was performed on a Jasco J-720 CD spectrometer (Jasco, Tokyo, Japan) with a bandwidth of 1 nm and a cuvette of 10 mm path length. Infrared (IR) spectra were measured with a PerkinElmer FTIR Paragon 1000 (ATR) spectrometer and were reported in cm^{-1}. ESI mass spectra were recorded on a Thermo Scientific™ Q Exactive™. *Trans* → *cis* photoisomerization experiments were performed using a LED emitting a 365 nm light from Nichia Corporation with a FWHM of 10 nm and intensity of 25 mW/cm^2. *Cis* → *trans* photoisomerization experiments were performed using a LED emitting a 520 nm light from Nichia Corporation with a FWHM of 45 nm and intensity of 1 mW/cm^2. UV/Vis absorption spectra were measured on a PerkinElmer Lambda-241. Proton (^1H) nuclear magnetic resonance spectra and carbon (^{13}C) nuclear magnetic resonance spectra were recorded on a Bruker DRX-500 and AV-600 spectrometer. Chemical shifts are referenced to internal tetramethylsilane (TMS) or 4,4-dimethyl-4-silapentane-1-sulfonic acid (DSS), or to the residual proton of the NMR solvent. Data are presented as follows: chemical shift, multiplicity (s=singlet, d=doublet, t=triplet, q=quartet, m=multiplet, and br=broad signal), coupling constant in hertz (Hz) and, integration. Full assignment of the signals was achieved by using 2D NMR techniques (^1H - ^1H COSY and ^1H - ^{13}C HSQC and HMBC). To differentiate the aromatic signals of the unsymmetrically substituted azobenzene moieties, the signals of the aromatic ring furthest from the carbohydrate center are labeled with an apostrophe.

Specific rotation and circular dichroism

The optical rotation and the circular dichroism spectra were measured at 293 K. The CD signal was recorded as ellipticity (θ), expressed in units of millidegrees (mdeg). The ellipticity was converted into difference in molar absorption coefficient (Δε), expressed in $M^{-1}\cdot cm^{-1}$, by using the following equation:

$\Delta\varepsilon = \theta / (32980 \cdot c \cdot l)$
Δε = difference in molar absorption coefficient
θ = ellipticity
c = molar concentration in $mol\cdot L^{-1}$
l = optical path length in cm

Irradiation experiments

Each sample was heated at 45 °C in the dark for 20 h prior to the beginning of each experiment in order to fully relax the azobenzene to its *trans*-form. The respective sample was irradiated in the dark, the distance between the lamp and the sample being about 5 cm. Photostationary states (PSS) were reached after irradiating the respective sample with a LED emitting light with the wavelength of 365 nm or 520 nm. Then the respective measurement was performed immediately afterwards.

The *cis*:*trans* ratios were determined by ^{1}H NMR spectroscopy. The photostationary states (PSS)were determined by integration of one aromatic signal of each isomer.

Extinction coefficients (ε) were calculated using the Beer-Lambert law (see equation below), plotting the absorbance at the respective λ_{max} versus different concentrations. In the case of PSS 365 nm, the λ_{max} of the n-π* band was used. A linear fitting gave the value of ε as the slope of the linear plot.

$$A = \varepsilon \cdot c \cdot l$$

A = absorbance
ε = extinction coefficient = slope of the plot
c = molar concentration in $mol \cdot L^{-1}$
l = optical path length in cm

Switching cycle experiments were performed by irradiating the respective sample alternatively for 1 min with the different LEDs within 20 cycles. The value of the absorbance at $\lambda_{max(E)}$ was plotted against the number of times the sample was irradiated to showcase the switching stability.

The kinetics of the thermal *cis*→*trans* relaxation process was determined by the decay of the λ_{max} of the n-π* band of the *cis*-form. After irradiation the spectra of the samples were recorded in regular intervals, keeping the sample inside the probe at a constant temperature of 298 K, until the relaxation was almost complete. The absorbance at was plotted versus the time, and an exponential decay of first order fitted to the data, according to the following equation:

$$A_{\lambda max} = A_{inf} + A \cdot \exp^{-k \cdot t}$$

$A_{\lambda max}$ = absorbance at the n-π* band of the *cis*-form
A_{inf} = absorbance at infinite time
A = pre-exponential factor proportional to the initial integral of the *cis*-isomer
k = rate of thermal isomerization
t = time

A linear fitting gave the value of *k* as the slope of the following plot:

$$\ln(A_{\lambda max} - A_{inf}) = \ln(A) - kt$$

The half-life of the *cis*-isomer ($\tau_{1/2}$) was determined as $\tau_{1/2} = \ln 2/k$.

Synthesis

2,3,4,2′,3′,4′-Hexa-*O*-acetyl-6,6′-dideoxy-6,6′-[5-[[4-[(1*E*)-2-(4-(hydroxy)phenyl)diazenyl]phenoxy]methyl]-1H-1,2,3-triazol-1-yl]-α,α-D-trehalose (**13**):

2,3,4,2′,3′,4′-Hexa-*O*-acetyl-6,6′-diazido-6,6′-dideoxy-α,α-D-trehalose (**10**)[117] (65.0 mg, 100 µmol), 4-hydroxy-4′-propargyloxy azobenzene (**12**)[118] (76.0 mg, 300 µmol) and CuBr (6.00 mg, 47.0 µmol) were dissolved in dry DMF (1.00 mL) under nitrogen and PMDETA (10.0 µL, 47.0 µmol) was added. The mixture was stirred at room temperature for 3 d and then concentrated under reduced pressure. The crude residue was dissolved in ethyl acetate, washed with water (3 x 100 mL) and dried over $MgSO_4$. After filtration and concentration under reduced pressure, the residue was purified by flash chromatography (cyclohexane/ethyl acetate/methanol 3:2:0 → 0:99:1) to give **13** (83.9 mg, 73.0 µmol, 73 %) as an orange foam.

$[\alpha]^{20}_D$= +56.5 (c= 0.68 in CH_2Cl_2); ^{1}H NMR (600 MHz, $CDCl_3$) δ = 7.88 – 7.84 (m, 4 H, Ar-H_{ortho}), 7.81 – 7.76 (m, 4 H, Ar-$H_{ortho'}$), 7.43 (s, 2 H, triazole-H), 7.04 – 6.99 (m, 4 H, Ar-H_{meta}), 6.91 – 6.86 (m, 4 H, Ar-$H_{meta'}$), 6.14 (s, 2 H, O*H*), 5.35 – 5.23 (m, 6 H, H-3, CH_2), 4.85 (dd, $^3J_{2,3}$ = 10.3 Hz, $^3J_{2,1}$ = 3.7 Hz, 2 H, H-2), 4.75 (dd~t, $^3J_{4,3}$ = $^3J_{4,5}$ = 9.7 Hz, 2 H, H-4), 4.34 (d, $^2J_{6a,6b}$ = 12.4 Hz, 2 H, H-6a), 4.03 (d, $^3J_{1,2}$ = 3.7 Hz, 2 H, H-1), 3.95 (ddd~td, $^3J_{5,4}$ = $^3J_{5,6b}$ = 10.0 Hz, $^3J_{5,6a}$ = 1.8 Hz, 2 H, H-5), 3.82 (dd, $^2J_{6b,6a}$ = 14.2 Hz, $^3J_{6b,5}$ = 9.8 Hz, 2 H, H-6b), 2.07 (s, 6 H, 2 CH_3C=O), 2.04 (s, 6 H, 2 CH_3C=O), 2.00 (s, 6 H, 2 CH_3C=O) ppm; ^{13}C NMR (151 MHz, $CDCl_3$) δ = 169.8 (CH_3*C*=O), 169.7 (CH_3*C*=O), 169.4 (CH_3*C*=O), 159.6 (Ar-C_{para}), 158.5 (Ar-$C_{para'}$), 147.1 (Ar-C_{ipso}), 146.7 (Ar-$C_{ipso'}$), 144.2 (triazole-*C*q), 124.7 (Ar-$C_{ortho'}$), 124.4 (Ar-C_{ortho}), 124.1 (triazole-*C*H), 116.0 (Ar-$C_{meta'}$), 115.1 (Ar-C_{meta}), 91.6 (C-1), 69.9 (C-4), 69.5 (C-3), 68.9 (C-5), 68.4 (C-2), 61.7 (CH_2), 50.4 (C-6), 20.6 (6 C, *C*H_3C=O) ppm; IR (ATR): ũ = 3148, 2948, 1751, 1585, 1499, 1213, 1147, 1040, 845 cm^{-1}; ESI-MS m/z: calc. 1149.37960 for $[C_{54}H_{56}O_{19}N_{10}+H]^+$; found 1149.37874 for $[C_{54}H_{56}O_{19}N_{10}+H]^+$.

2,3,4,2′,3′,4′-Hexa-*O*-acetyl-6,6′-dideoxy-6,6′-[5-[[4-[(1*E*)-2-(4-(prop-2-yn-1-yloxy)phenyl)diazenyl]phenoxy]methyl]-1H-1,2,3-triazol-1-yl]-α,α-D-trehalose (**15**):

Azobenzene trehalose conjugate **13** (77.4 mg, 67.0 µmol), K_2CO_3 (69.0 mg, 500 µmol) and KI (cat. amount) were suspended in dry DMF (1.00 mL) under nitrogen and propargyl bromide (80 % in toluene, 20.0 µL, 200 µmol) was added. Stirred at 80 °C for 5 h and at room temperature for 16 h. Dichloromethane was added, and the org. phase was washed twice with water and brine (50 mL each), dried over $MgSO_4$, filtrated and concentrated to dryness. The crude residue was purified by column chromatography (dichloromethane/ethyl acetate/methanol 8:2:0 → 59:40:1) to give **15** (64.1 mg, 52.3 µmol, 78 %) as an orange foam.

$[\alpha]^{20}_D$= +72.9 (c= 1.02 in CH_2Cl_2); ^{1}H NMR (500 MHz, $CDCl_3$) δ = 7.93 – 7.83 (m, 8 H, Ar-H_{ortho}, $H_{ortho'}$), 7.42 (s, 2 H, triazole-H), 7.09 – 7.00 (m, 8 H, Ar-H_{meta}, Ar-$H_{meta'}$), 5.30 (m, 6 H, H-3, CH_2), 4.86 (dd, $^3J_{2,3}$ = 10.3 Hz, $^3J_{2,1}$ = 3.8 Hz, 2 H, H-2), 4.78 – 4.73 (m, 6 H, H-4, CH_2CCH), 4.34 (dd, $^2J_{6a,6b}$ = 14.2 Hz, $^3J_{6b,5}$ = 2.1 Hz, 2 H, H-6a), 4.02 (d, $^3J_{1,2}$ = 3.8 Hz, 2 H, H-1), 3.95 (ddd~td, $^3J_{5,4}$ = $^3J_{5,6b}$ = 10.0 Hz, $^3J_{5,6a}$ = 2.0 Hz, 2 H, H-5), 3.80 (dd, $^2J_{6b,6a}$ = 14.2 Hz, $^3J_{6b,5}$ = 9.8 Hz, 2 H, H-6b), 2.54 (t, $^4J_{CH,CH2}$ = 2.4 Hz, 2 H, CH_2CCH), 2.06 (s, 6 H, 2 CH_3C=O), 2.04 (s, 6 H, 2 CH_3C=O), 2.00 (s, 6 H, 2 CH_3C=O) ppm; ^{13}C NMR (126 MHz, $CDCl_3$) δ = 169.7 (CH_3*C*=O), 169.6 (CH_3*C*=O), 169.2 (CH_3*C*=O), 159.8, 159.6 (Ar-C_{para}, Ar-$C_{para'}$), 147.2, 147.1 (Ar-C_{ipso}, Ar-$C_{ipso'}$), 144.2 (triazole-*C*q), 124.4, 124.3 (Ar-C_{ortho}, Ar-$C_{ortho'}$), 124.0 (triazole-*C*H), 115.3, 115.1 (Ar-C_{meta}, Ar-$C_{meta'}$), 91.5 (C-1), 78.0 (CH_2*C*CH), 75.9 (CH_2C*C*H), 69.9 (C-4), 69.5 (C-3), 68.9 (C-5), 68.4 (C-2), 61.9 (CH_2), 56.0 (*C*H_2CCH), 50.3 (C-6), 20.6 (6 C, *C*H_3C=O) ppm; IR (ATR): ũ = 3282, 1751, 1497, 1368, 1208, 1149, 1018, 838 cm^{-1}; ESI-MS m/z: calc. 1225.41090 for $[C_{60}H_{60}O_{19}N_{10}+H]^+$; found 1225.40862 for $[C_{60}H_{60}O_{19}N_{10}+H]^+$.

Macrocycle **16**:

Precursor **15** (62.0 mg, 50.0 µmol), 2,3,4,2′,3′,4′-hexa-*O*-acetyl-6,6′-diazido-6,6′-dideoxy-α,α-D-trehalose (**10**)[117] (33.0 mg, 50.0 µmol) and CuBr (5.00 mg, 34.9 µmol) were dissolved in dry DMF (10.0 mL) under nitrogen and PMDETA (10.00 µL, 47.0 µmol) was added. The mixture was stirred at room temperature for 3 d and then concentrated under reduced pressure. The crude residue was dissolved in ethyl acetate, washed with water (3 x 50 mL) and dried over $MgSO_4$. After filtration and concentration under reduced pressure, the residue was purified by flash chromatography (dichloromethane/ethyl acetate/methanol 250:250:15) to give **16** (26.6 mg, 14.2 µmol, 28 %) as an orange foam.

$[\alpha]^{20}_D$= +97.8 (c= 0.50 in CH_2Cl_2); ^{1}H NMR (500 MHz, $CDCl_3$) δ = 7.88 – 7.80 (m, 8 H, Ar-H_{ortho}), 7.42 (s, 4 H, triazole-H), 7.04 – 6.91 (m, 8 H, Ar-H_{meta}), 5.39 (dd, $^3J_{3,2}$= 10.1 Hz, $^3J_{3,4}$=9.4 Hz, 4 H, H-3), 5.26 (s, 8 H, CH_2), 4.95 (dd, $^3J_{2,3}$ = 10.3 Hz, $^3J_{2,1}$ = 3.8 Hz, 4 H, H-2), 4.85 (dd~t, $^3J_{4,3}$ = $^3J_{4,5}$ = 9.6 Hz, 4 H, H-4), 4.48 (d, $^3J_{1,2}$ = 3.8 Hz, 4 H, H-1), 4.42 (dd, $^2J_{6a,6b}$ = 13.7 Hz, $^3J_{6a,5}$ = 1.7 Hz, 4 H, H-6a), 4.18 – 4.00 (m, 8 H, H-5, H-6b), 2.09 (s, 12 H, 4 CH_3C=O), 2.09 (s, 12 H, 4 CH_3C=O), 2.01 (s, 12 H, 4 CH_3C=O) ppm; ^{13}C NMR (126 MHz, $CDCl_3$) δ = 169.7 (CH_3*C*=O), 169.7 (8 C, CH_3*C*=O), 169.4 (CH_3*C*=O), 160.0 (Ar-C_{para}), 147.0 (Ar-C_{ipso}), 144.1 (triazole-*C*q), 124.5 (Ar-C_{ortho}), 124.0 (triazole-*C*H), 115.2 (Ar-C_{meta}), 91.6 (C-1), 69.9 (C-4), 69.5 (C-3), 68.9 (C-5), 68.6 (C-2), 62.1 (*C*H_2), 50.6 (C-6), 20.6 (12 C, *C*H_3C=O) ppm; IR (ATR): ũ = 3470, 2946, 1752, 1598, 1498, 1370, 1215, 1040 cm^{-1}; ESI-MS m/z: calc. 1869.603346 for $[C_{84}H_{92}O_{34}N_{16}+H]^+$; found 1869.60727 for $[C_{84}H_{92}O_{34}N_{16}+H]^+$.

Deprotected target macrocycle **9**:

To a solution of the macrocycle **16** (20.1 mg, 10.8 µmol) in a mixture of dichloromethane and methanol (1:4, 5.00 mL) NaOMe (5.4 M in methanol, 40.0 µL) was added and stirred at room temperature for 16 h. The mixture was neutralized with Amberlite® IR120 H^+, filtered and concentrated to dryness to give the corresponding macrocycles as a yellow amorphous solid (14.6 mg, 10.7 µmol, quant.).

trans-**9**:

$[\alpha]^{20}_D$= -11.5 (c= 0.09 in DMSO); ^{1}H NMR (500 MHz, DMSO- d_6) δ = 8.20 (s, 4 H, triazole-H), 7.78 – 7.71 (m, 8 H, Ar-H_{ortho}), 7.13 – 7.02 (m, 8 H, Ar-H_{meta}), 5.51 (s, 4 H, O*H*), 5.35 – 5.20 (s, 8 H, O*H*) 5.22 (d, $^2J_{CH2,CH2}$ = 11.5 Hz, 4 H, CH_2a), 5.17 (d, $^2J_{CH2,CH2}$ = 11.5 Hz, 4 H, CH_2b), 4.67 – 4.59 (m, 8 H, H-1, H-6a), 4.54 (dd, $^2J_{6b,6a}$ = 14.2 Hz, $^3J_{6b,5}$ = 6.9 Hz, 4 H, H-6b), 4.20 – 4.11 (m, 4 H, H-5), 3.60 (dd~t, $^3J_{3,2}$ = $^3J_{3,4}$= 9.2 Hz, 4 H, H-3), 3.18 (dd, $^3J_{2,3}$ = 9.5 Hz, $^3J_{2,1}$ = 3.4 Hz, 4 H, H-2), 2.96 (dd~t, $^3J_{4,3}$ = $^3J_{4,5}$ = 9.3 Hz, 4 H, H-4) ppm; ^{13}C NMR (151 MHz, DMSO-d_6) δ = 160.4 (Ar-C_{para}), 146.4 (Ar-C_{ipso}), 142.2 (triazole-*C*q), 125.4 (triazole-*C*H), 124.2 (Ar-C_{ortho}), 115.1 (Ar-C_{meta}), 93.3 (C-1), 72.7 (C-3), 71.2 (C-2), 71.1 (C-4), 69.6 (C-5), 61.7 (*C*H_2), 50.6 (C-6) ppm; IR (ATR): ũ = 3302, 2921, 1562, 1408, 1243, 1150, 1039, 993 cm^{-1}; ESI-MS m/z: calc. 1365.47668 for $[C_{60}H_{68}O_{22}N_{16}+H]^+$; found 1365.47764 for $[C_{60}H_{68}O_{22}N_{16}+H]^+$.

cis-**9**:

$[\alpha]^{20}_D$= +68.3 (c= 0.09 in DMSO); ^{1}H NMR (500 MHz, DMSO- d_6) δ = 8.10 (s, 4 H, triazole-H), 6.94 – 6.90 (m, 8 H, Ar-H_{meta}), 6.87 – 6.72 (m, 8 H, Ar-H_{ortho}), 5.59 (s, 4 H, O*H*), 5.44 (s, 4 H, O*H*), 5.24 (s, 4 H, O*H*), 5.06 (s, 8 H, CH_2), 4.60 (d, $^2J_{6a,6b}$ = 12.1 Hz, 4 H, H-6a), 4.51 (d, $^3J_{1,2}$ = 3.5 Hz, 4 H, H-1), 4.46 (dd, $^2J_{6b,6a}$ = 14.1 Hz, $^3J_{6b,5}$ = 7.7 Hz, 4 H, H-6b), 4.19 – 4.11 (m, 4 H, H-5), 3.57 (dd~t, $^3J_{3,2}$ = $^3J_{3,4}$= 9.1 Hz, 4 H, H-3), 3.13 (dd, $^3J_{2,3}$ = 9.6 Hz, $^3J_{2,1}$ = 3.4 Hz, 4 H, H-2), 2.95 (dd~t, $^3J_{4,3}$ = $^3J_{4,5}$ = 9.3 Hz, 4 H, H-4) ppm; ^{13}C NMR (126 MHz, DMSO- d_6) δ = 156.9 (Ar-C_{para}), 146.7 (Ar-C_{ipso}), 141.9 (triazole-*C*q), 125.0 (triazole-*C*H), 122.0 (Ar-C_{ortho}), 114.6 (Ar-C_{meta}), 93.6 (C-1), 72.4 (C-3), 71.6 (C-4), 71.0 (C-2), 69.6 (C-5), 61.0 (*C*H_2), 50.6 (C-6) ppm.

NMR spectra of synthesized compounds

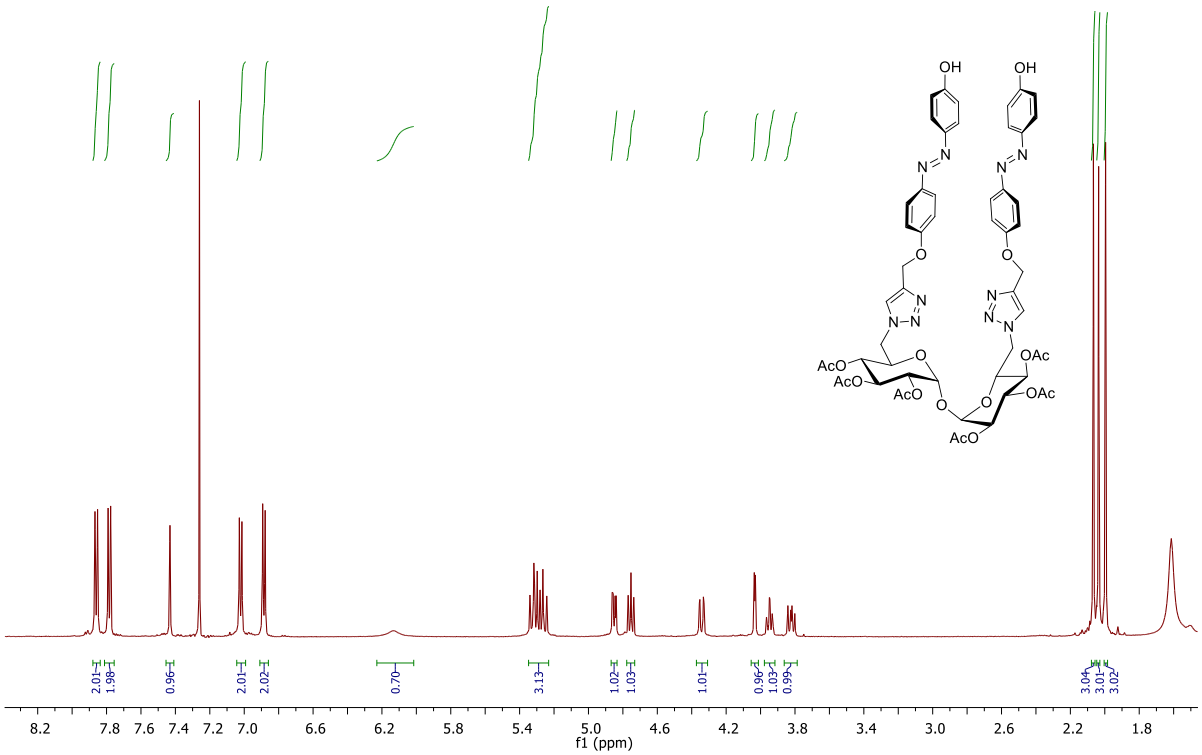

Figure 4.5: ^{1}H NMR spectrum of **13** (600 MHz, $CDCl_3$, 298 K).

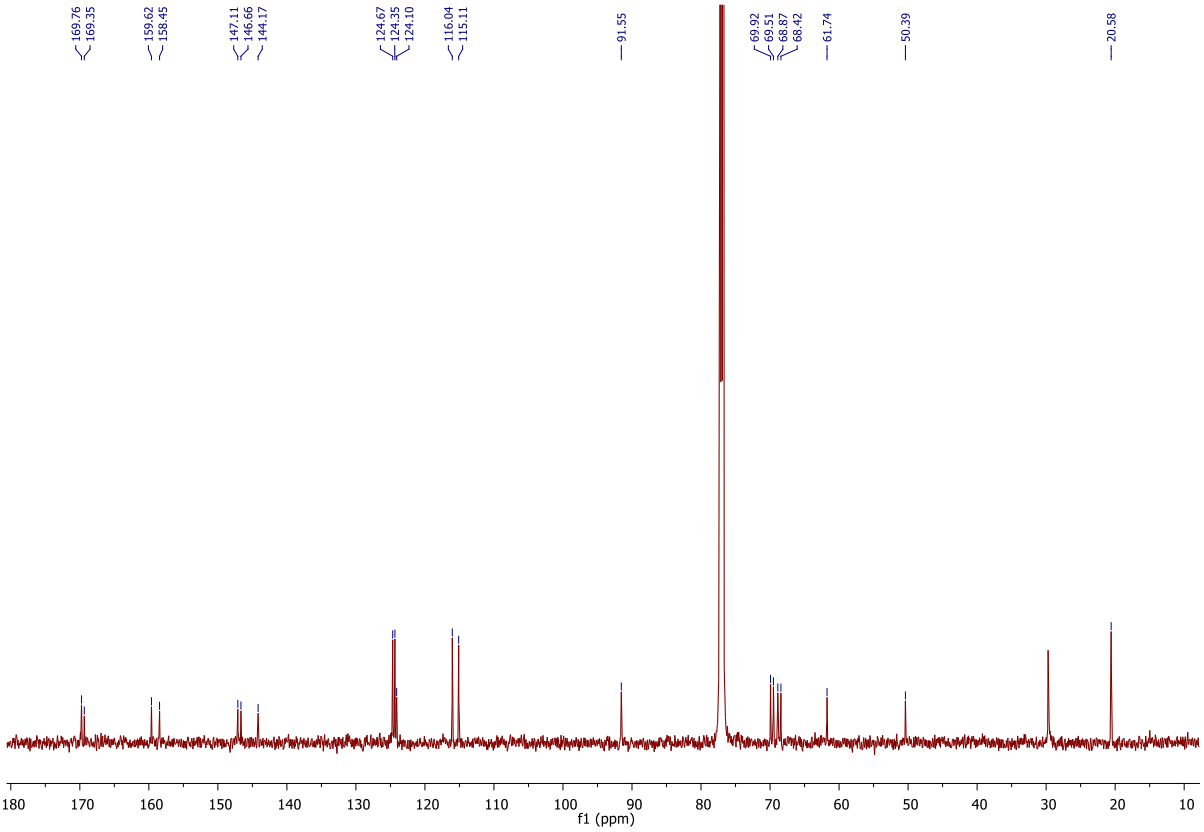

Figure 4.6: ^{13}C NMR spectrum of **13** (151 MHz, $CDCl_3$, 298 K).

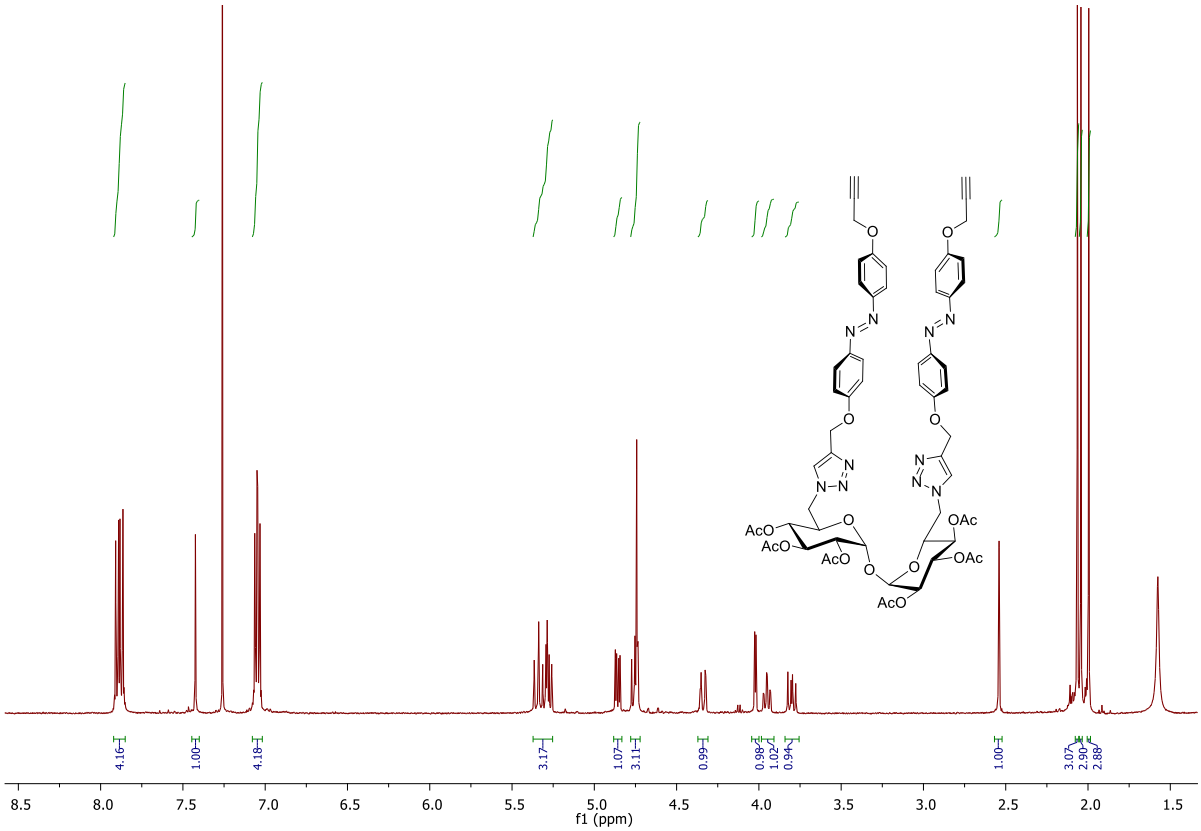

Figure 4.7: ^{1}H NMR spectrum of **15** (500 MHz, $CDCl_3$, 298 K).

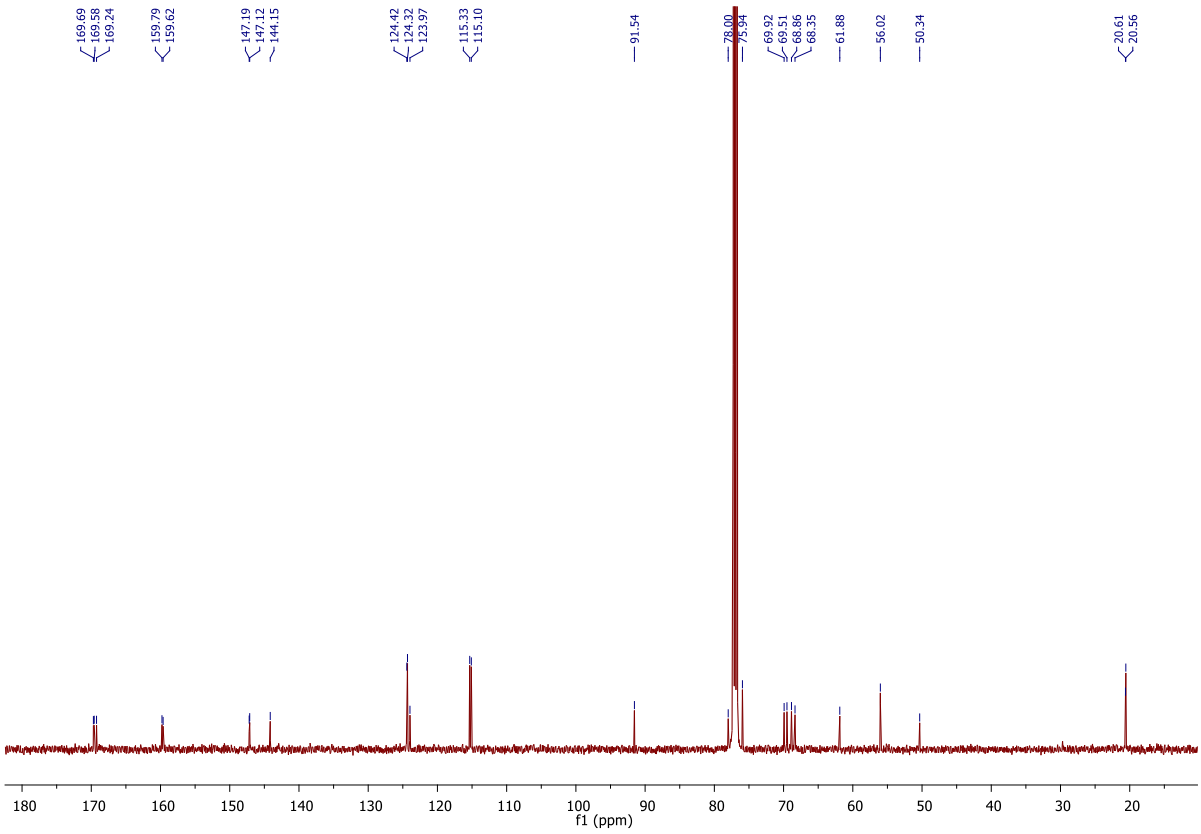

Figure 4.8: ^{13}C NMR spectrum of **15** (126 MHz, $CDCl_3$, 298 K).

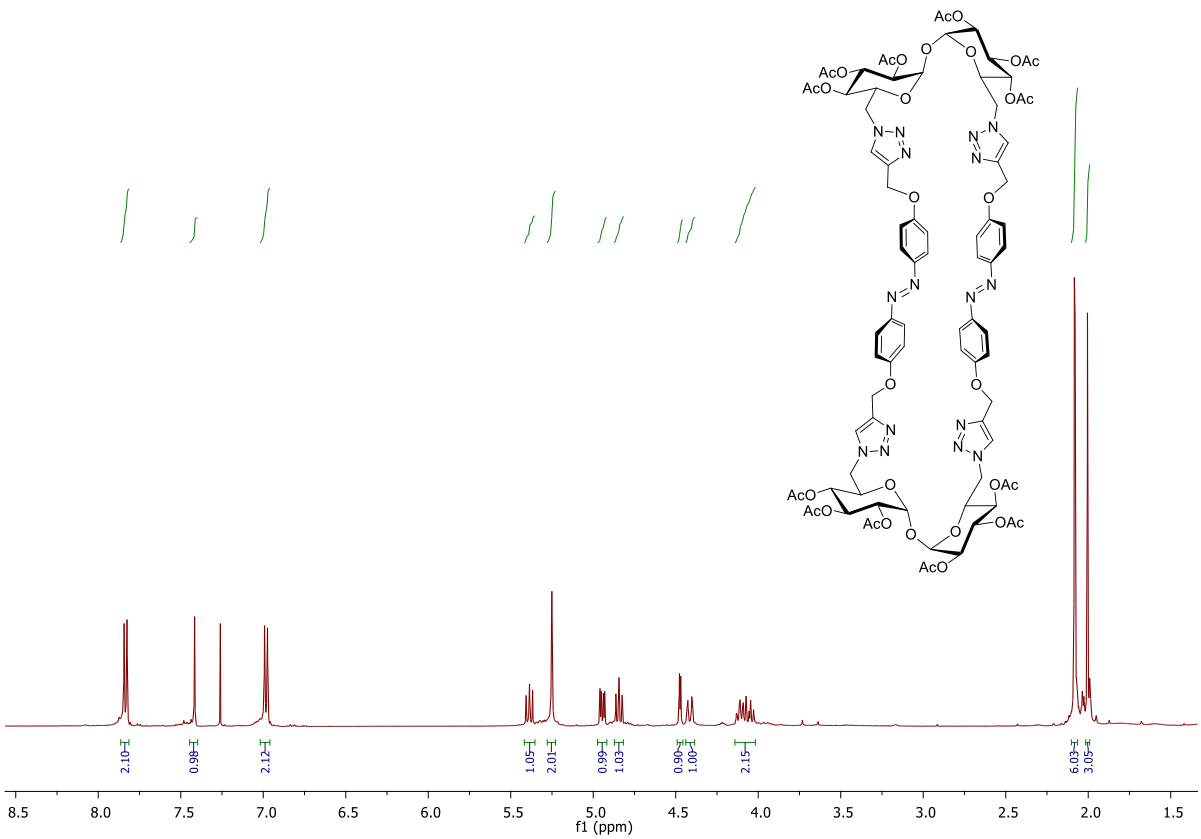

Figure 4.9: ^{1}H NMR spectrum of **16** (500 MHz, $CDCl_3$, 298 K).

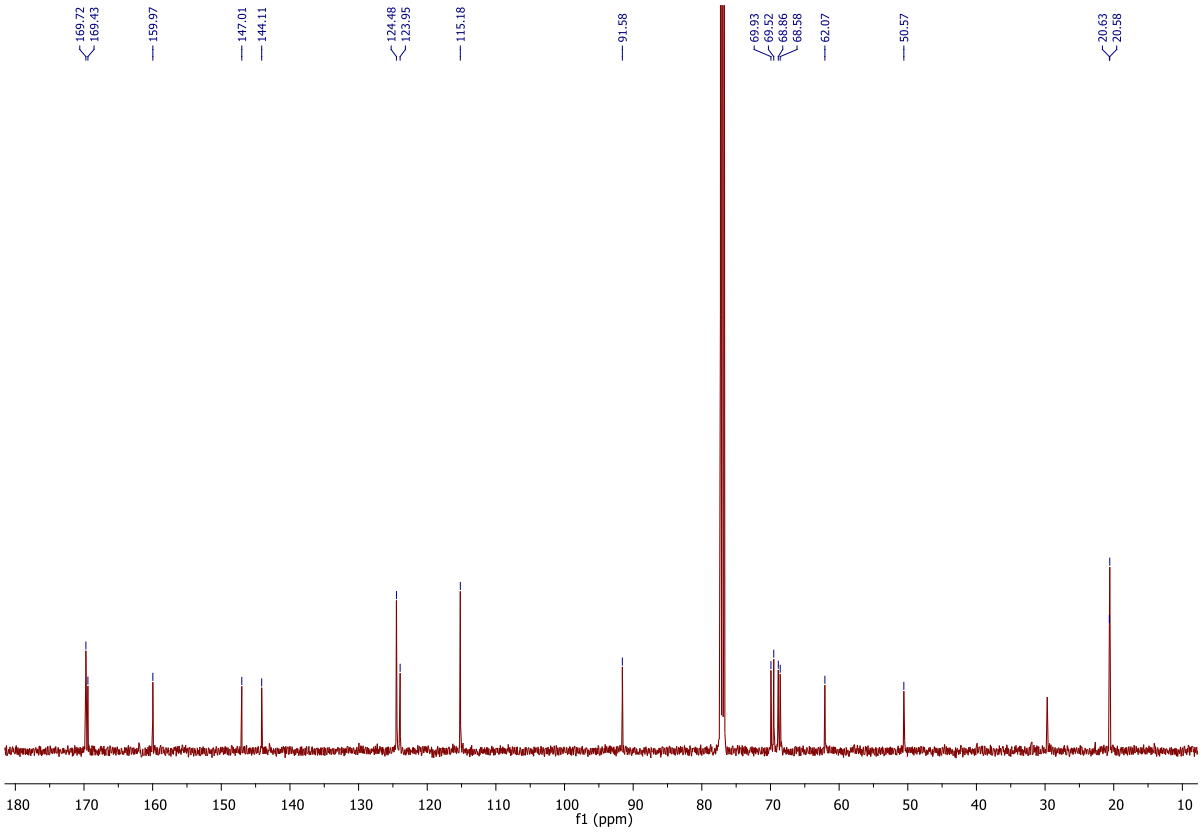

Figure 4.10: ^{13}C NMR spectrum of **16** (126 MHz, $CDCl_3$, 298 K).

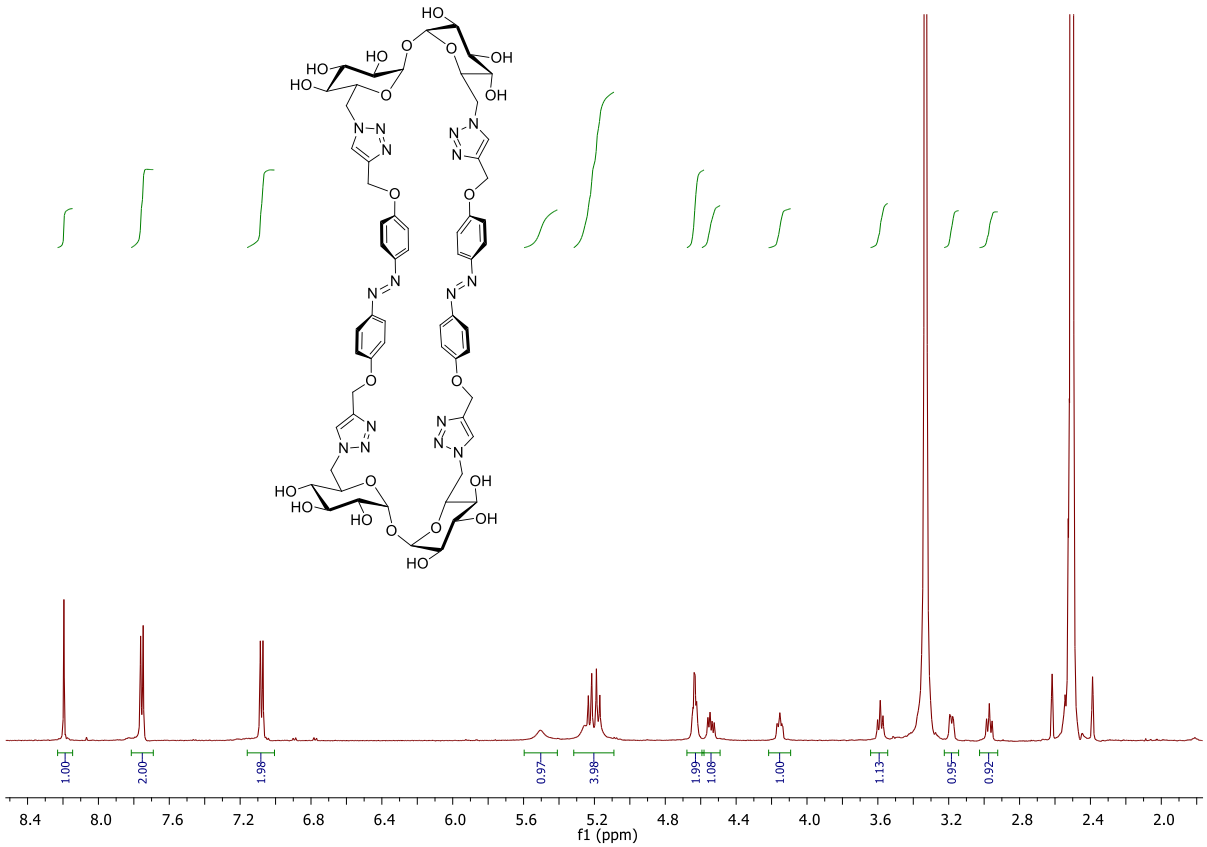

Figure 4.11: ^{1}H NMR spectrum of *trans*-**9** (500 MHz, DMSO-d_6, 298 K).

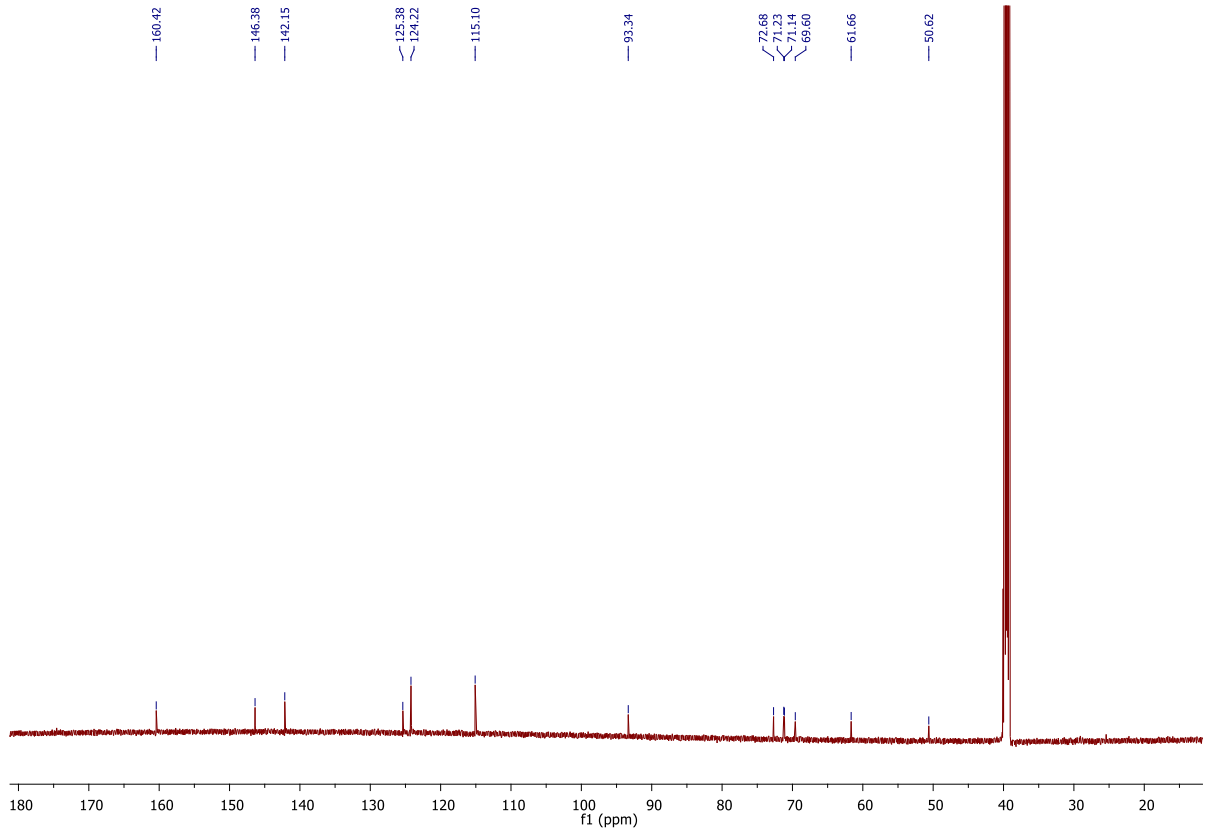

Figure 4.12: ^{13}C NMR spectrum of *trans*-**9** (151 MHz, DMSO-d_6, 298 K).

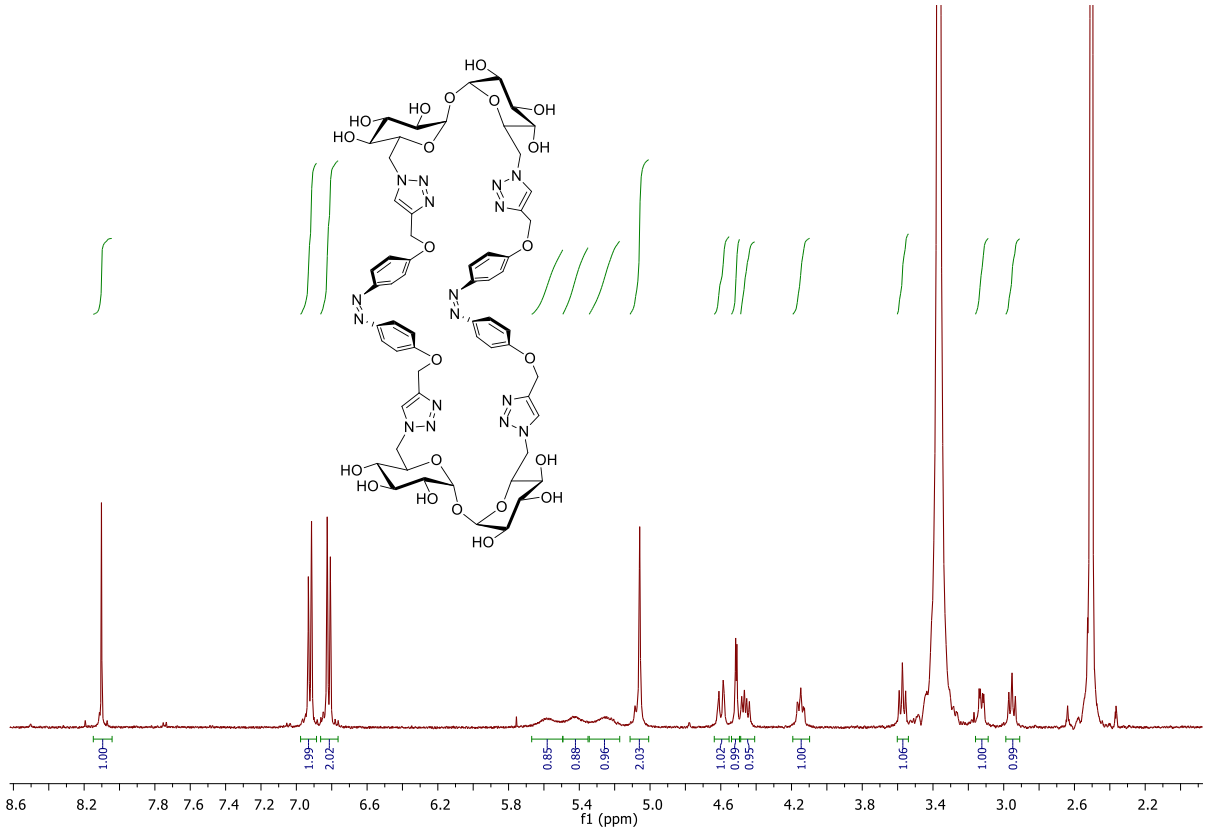

Figure 4.13: ^{1}H NMR spectrum of *cis*-**9** (500 MHz, DMSO-d_6, 298 K).

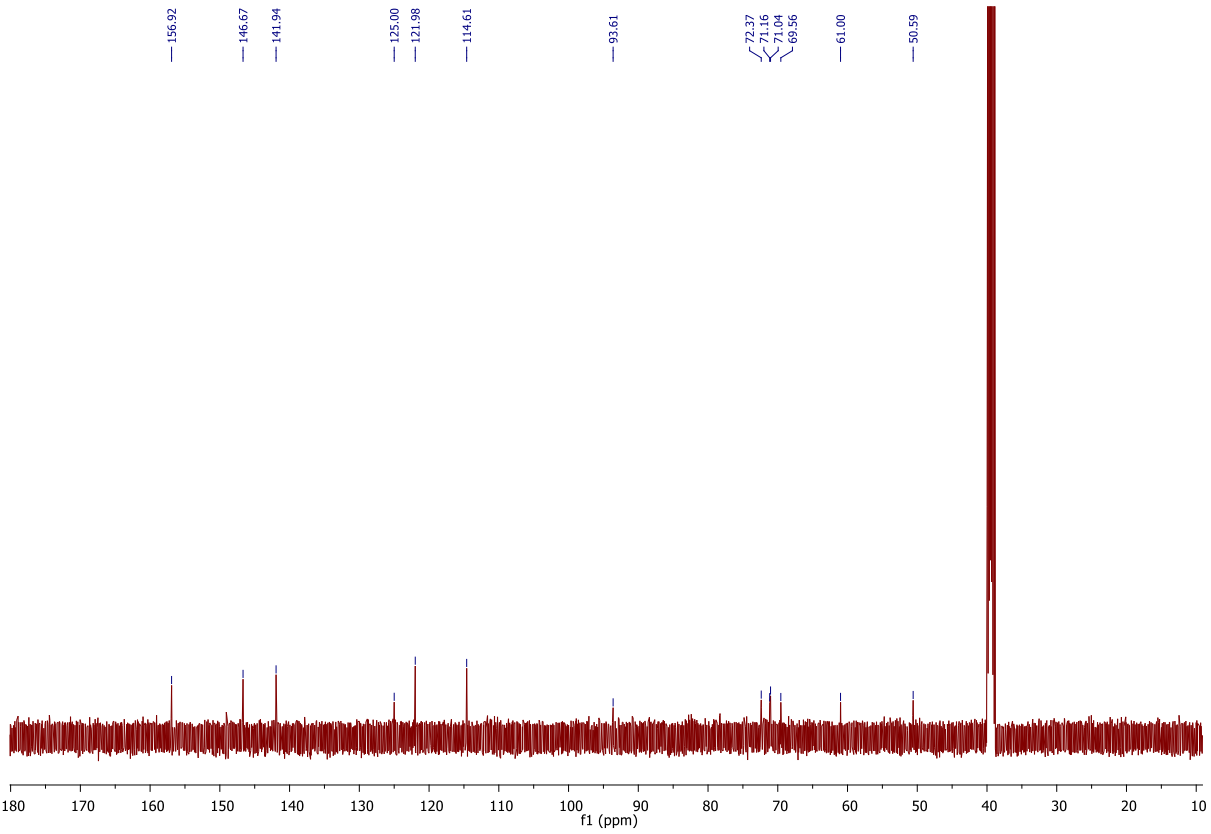

Figure 4.14: ^{13}C NMR spectrum of *cis*-**9** (126 MHz, DMSO-d_6, 298 K).

Irradiation experiments

The photostationary states (PSS) were reached after irradiating the respective sample for 5 min with 365 nm or 5 min with 520 nm and the respective *trans:cis* ratios of are shown in Figure 4.15.

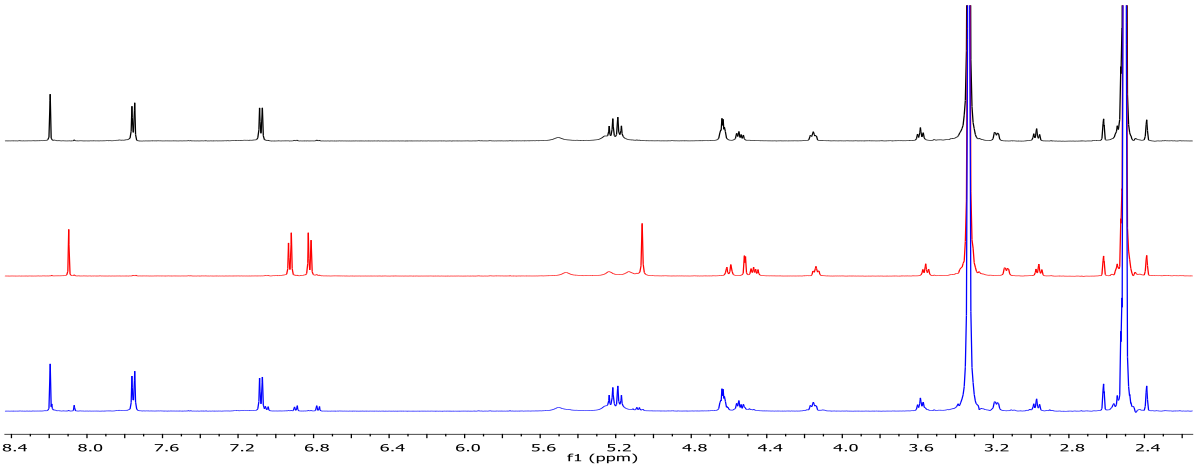

Figure 4.15: NMR spectra of *trans*-**9** after heating at 45 °C in the dark for 20 h (black), after irradiation with 365 nm for 5 min with a PSS of *trans:cis* 2:98 (red)and after irradiation with 520 nm (blue) for 5 min with a PSS of *trans:cis* 90:10.

The extinction coefficient ε and the coefficient of determination of the linear fitting for *trans*- and *cis*-**9** are shown along the plot of the absorbance at 365 nm or 450 nm against the concentration in Figure 4.16.

The switching cycle experiment for **9** is shown in Figure 4.17 with the plot of the value of the absorbance at $\lambda_{max(E)}$ against the number of times the sample was irradiated.

The decay of the absorbance of the n-π* band λ_{max} of *cis*-**9** is shown alongside the coefficient of determination of the exponential fitting and the absorbance at infinite time in Figure 4.18. The linearization of the absorbance is shown with the coefficient of determination of the linear fitting, the rate constant and the ensuing half-life.

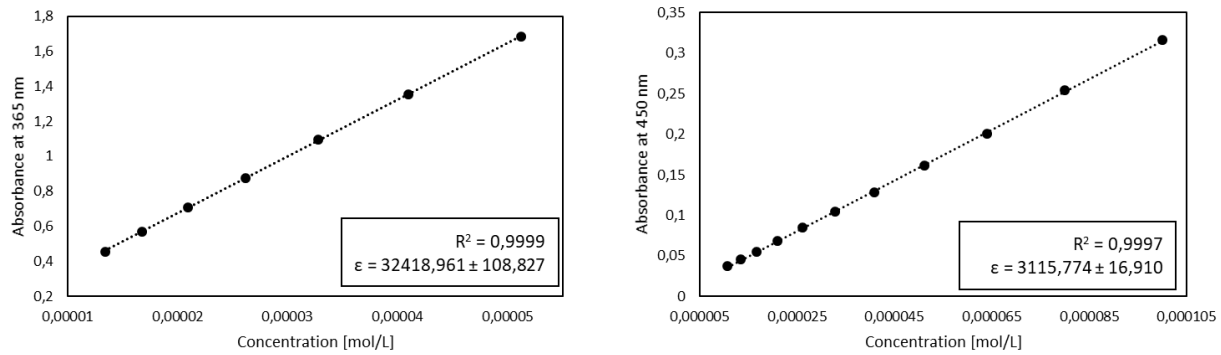

Figure 4.16: Plot of the absorbance of **9** at λ_{max} versus the concentration; the slope of the linear curve gives the value of the extinction coefficient ε. Measured at 298 K in DMSO in concentrations from $8 \cdot 10^{-6}$ to 10^{-4} mol·L^{-1}.

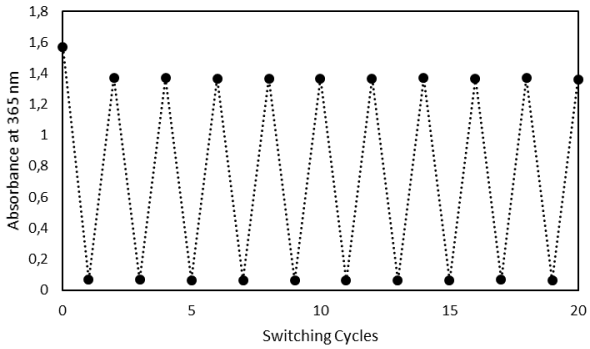

Figure 4.17: Measured absorbance of **9** at 365 nm after alternating photoirradiation with 365 nm and 520 nm. Measured at 298 K in DMSO in a concentration of 50 µM.

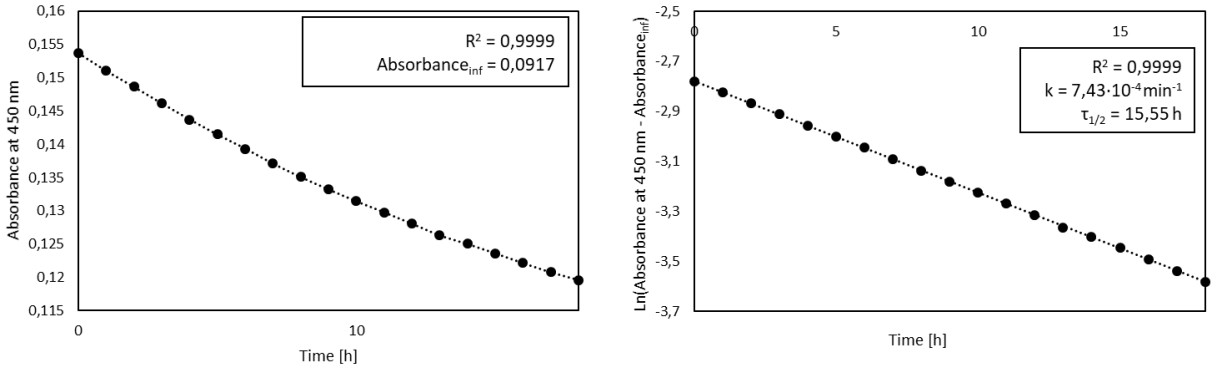

Figure 4.18: Kinetics of the *cis*→*trans* thermal relaxation process, measured at 298 K in DMSO at a concentration of 50 µM, showing the exponential decay of the absorbance at 450 nm and the linearization with the corresponding coefficient of determination and the half-life for the *cis*-form of **9**.

5. Sonogashira Coupling

5.1 Introduction

An advancement from the Castro-Stephens coupling,[122] where C-C bonds are formed using easily combustible copper(I) acetylene[123] and an aromatic halide was the reaction SONOGASHIRA et al. reported in 1975, the cross-coupling of iodobenzene with acetylene gas, using copper(I) iodine and a palladium(II) complex in catalytic amounts.[124]

Similar reactions towards the synthesis of aromatic acetylenes were developed by CASSAR[125] and HECK[126] in the same year. But these syntheses require a larger amount of palladium species and high heating for the reaction to give satisfactory results, while the Sonogashira coupling proceeded at room temperature.

One disadvantage of the copper-cocatalyzed Sonogashira coupling is the formation of homocoupled dialkyne as an unwanted side reaction in the presence of oxygen,[127] (known as Glaser coupling, cf. chapter 6), thus making strict oxygen exclusion necessary. To circumvent this problem, the copper-free approach of CASSAR and HECK has been optimized over the years to develop a copper-free cross-coupling reaction (Scheme 5.1), which is called the copper-free Sonogashira reaction despite the denomination as Heck-Cassar coupling being better suited.[128, 129]

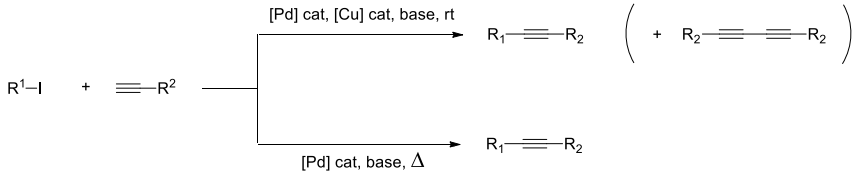

Scheme 5.1: Differences between the copper-cocatalyzed and copper-free Sonogashira reaction.

The mechanism of the copper-cocatalyzed Sonogashira coupling is not fully elucidated yet, while the palladium cycle, consisting of oxidative addition, transmetallation and reductive elimination operates like other palladium-catalyzed cross-couplings, the copper cycle is not well understood.[128, 129] Meanwhile, the mechanism of the copper-free Sonogashira reaction has been proven only recently to operate through a tandem catalytic cycle of palladium-palladium transmetallation.[129]

The Sonogashira coupling has found a wide application in macrocyclization reactions[130] for natural product synthesis and medical applications,[46, 131] and the synthesis of rigid shape-persistent macrocycles.[132, 133]

Here, Sonogashira coupling was envisioned for the synthesis of glycomacrocycles comprising two different azobenzene moieties. The target macrocycles **17** and **18** were designed as symmetric structures with a two-fold rotation axis which can be achieved in only two steps, consisting of a Mitsunobu reaction and Sonogashira coupling for the cyclization step (Figure 5.1). The envisioned design with acetylene-linked azobenzene units promises interesting changes in molecular shape upon *trans* → *cis* isomerization of the azobenzene units due to an increased end-to-end distance change between both isomers.[134] In combination with an *O*-functionalized azobenzene, the contraction upon switching the macrocycle from *all trans* to *all cis* should be different for the two azobenzene moieties.

Different macrocycles can be achieved easily through variation of the diiodo azobenzene moiety for the ring closure. To test this, two different variations should be synthesized using the same synthetic protocol with 4,4'-diiodoazobenzene (**19**)[135] and 2,2',6,6'-tetrafluoro-4,4'-diiodoazobenzene (**20**)[136] for the macrocyclization. *Ortho*-fluorination causes a bathochromic shift in the absorption spectrum,[136] which could be used to selectively switch the obtained macrocycle between three states with the appropriate wavelengths, *all trans* as the thermodynamically stable conformation, *all cis* through irradiation with UV light and *trans,cis* through irradiation with green light.

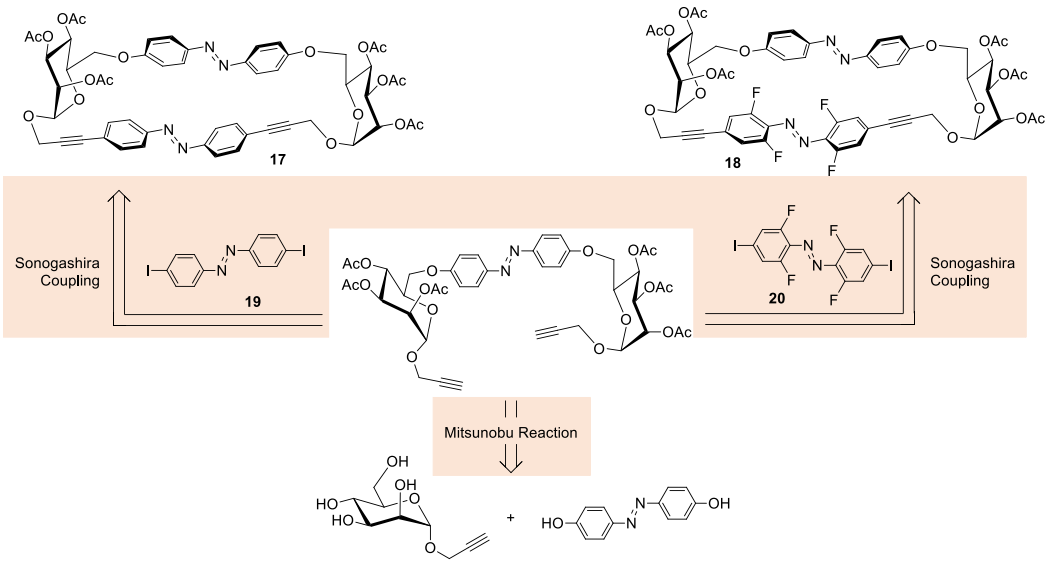

Figure 5.1: Retrosynthesis of the targeted macrocycles obtainable in two steps.

5.2 Synthesis

In a first reaction with propargyl mannoside **21**[137] and 4,4'-diiodoazobenzene (**19**), the efficiency of the Sonogashira coupling[138] was tested and the bifunctionalized azobenzene glycoconjugate **22** could be isolated in a satisfying yield of 66 % (Scheme 5.2). A copper-free reaction procedure was chosen in order to prevent Glaser coupling as an unwanted side reaction.[139]

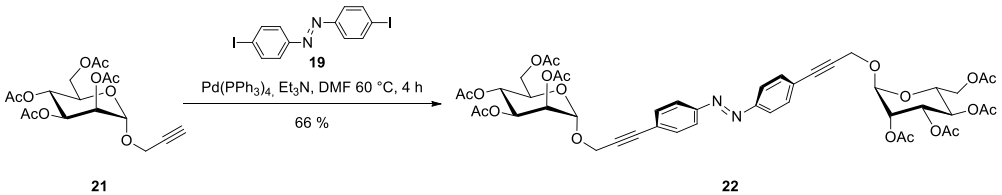

Scheme 5.2: Synthesis of **22** in a Sonogashira cross-coupling reaction.

On the other hand, the azobenzene glycoconjugate **23** was synthesized via Mitsunobu reaction and subsequent acetylation of propargyl mannoside **24**[137] and 4,4'-dihydroxyazobenzene (**5**)[98] in a yield of 50 % over two steps. This reaction is discussed in greater detail in chapter 6.2. Both 4,4'-diiodoazobenzene (**19**) and 2,2',6,6'-tetrafluoro-4,4'-diiodoazobenzene (**20**) were applied in the intermolecular Sonogashira coupling macrocyclization with **23** (Scheme 5.3). The reaction conditions

were optimized for the macrocyclization step. Hence, both reactants were added in equimolar amounts and the concentration was lowered from 25 mM to 5 mM to prevent oligomerization.

In chapter 3.2, the macrocyclization of two building blocks could only be realized after isomerization of the precursor **7** from *trans* to *cis*, as the difference in distance between the active sites of *trans*-**7** and piperazine (**3**) was too large for the reaction to take place. As the Sonogashira coupling required heating, prior isomerization of one reaction component to their thermodynamically less stable *cis*-isomer would be futile. Fortunately, pre-organization of the reactants was not necessary in this case, as the reaction proceeded smoothly with the *trans*-configured glycoazobenzene **23** to give the macrocycles **17** and **18** in yields of 39 % and 28 % respectively.

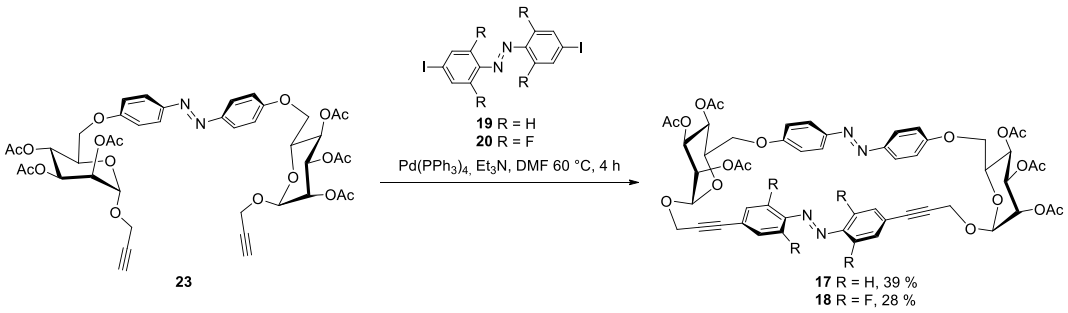

Scheme 5.3: Macrocyclization of **23** with **19** and **20** to give **17** and **18**.

5.3 Photochromic properties

With the two target macrocycles **17** and **18** in hand, their photochromic properties were investigated. UV/Vis absorption spectra show a large band at around 360 nm corresponding to the π → π* transition for both macrocycles (Figure 5.2). The n → π* transition is not well separated from this band and is seen as a weak shoulder with λ_{max} = 450 nm, that is red shifted for the fluorinated **18**. PSS was reached after isomerization with a 365 nm LED for 5 min and led to considerable weakening and hypsochromic shifts of the π → π* transition to λ_{max} = 310 nm. The increased n → π* transitions at around 440 nm is slightly blue shifted as well. For **17**, back switching could be realized with a 520 nm LED lamp as the n → π* transition was well enough resolved in this region to lead back to a spectrum similar to the initial *trans*-**17**. Because of the bathochromic shift of the n → π* band in *trans*-**18**, the best back-switching ratio could be achieved through irradiation with a 450 nm LED.

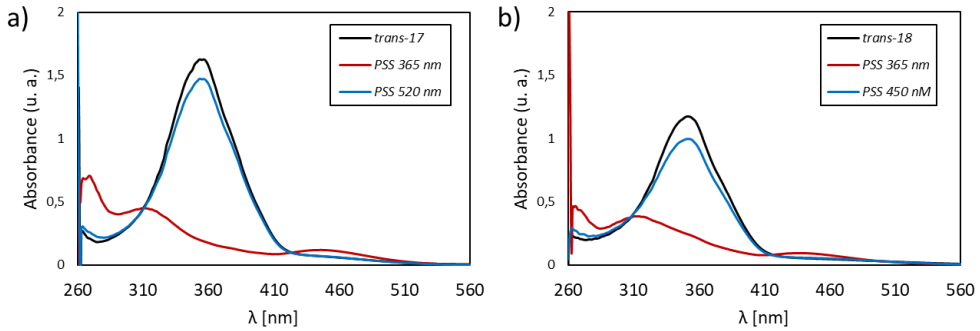

Figure 5.2: Absorption of the macrocycles in DMSO at 298 K in a concentration of 25 µM (a) **17**; (b) **18**; black line: *trans*-macrocycle, red line: PSS after irradiation with 365 nm for 5 min, blue line: PSS after irradiation with 520 nm (a) or 450 nm (b) for 5 min.

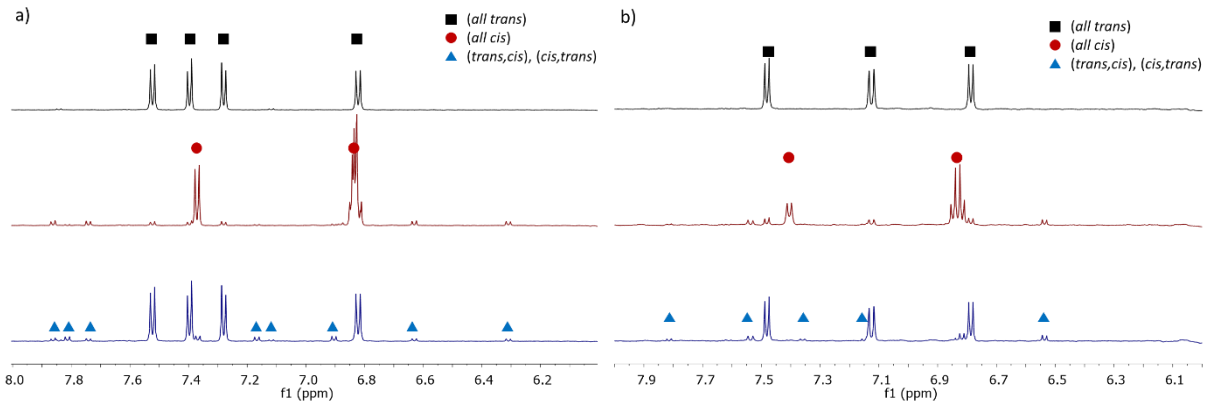

Figure 5.3: Aromatic region of the ^{1}H NMR spectra of the different macrocycles (600 MHz, DMSO-d_6, 298 K): (a) **17**; (b) **18**; black line: *trans*-macrocycle, red line: PSS after irradiation with 365 nm for 5 min; blue line: PSS after irradiation with 520 nm (a) or 450 nm (b) for 5 min.

The *trans*:*cis* ratio for the different PSS were quantified by ^{1}H NMR to be more than 98 % *all trans* after 16 h at 40 °C (Figure 5.3). The PSS at 365 nm contained 7 % *all trans*, 85 % *all cis* and 8 % of a mixture of *trans,cis* and *cis,trans* for macrocycle **17**. Back switching to the PSS at 520 nm led to 87 % *all trans*, 6 % *all cis* and 7 % *trans,cis* mixture. Due to overlapping signals and the need for low concentrations in the NMR in order to facilitate the isomerization, a distinction between *trans,cis* and *cis,trans* was not possible for both macrocycles. For the fluorinated **18**, the PSS at 365 nm led to a ratio of 13 % all *trans*, 73 % *all cis* and 14 % *trans,cis* mixture. The PSS at 450 nm gave a ratio of 79 % *all trans*, 5 % *all cis* and 16 % *trans,cis* mixture. Thermal isomerization after reaching the PSS at 365 nm was monitored by ^{1}H NMR for the different species of both macrocycles (Figure 5.4). It could be shown that the concentration of the *trans,cis*- and *cis,trans*-isomers remained at the same low level after an initial short increase for **17**. For the fluorinated **18**, the *trans,cis*- and *cis,trans*-isomers increased slowly over the relaxation period before decreasing again. This indicates that the intermediate containing one azobenzene in *trans*- and one in *cis*-conformation is not very stable. Possibly, isomerization of one azobenzene unit in the cycle elicits the isomerization of the other, either due to the azobenzene moieties not being electronically decoupled or due to high ring strain in the mixed species.

Half-life of the PSS at 365 nm was calculated using UV/Vis absorption measurement (see Figure 5.18 in chapter 5.5) and with 18 h for **17** and 33 h for **18** accurately display the interception of *all trans* and *all cis* in the corresponding ^{1}H NMR measurements. The longer half-life of *all cis*-**18** is in agreement with the slower relaxation process associated with *ortho*-fluorinated azobenzene moieties.[136]

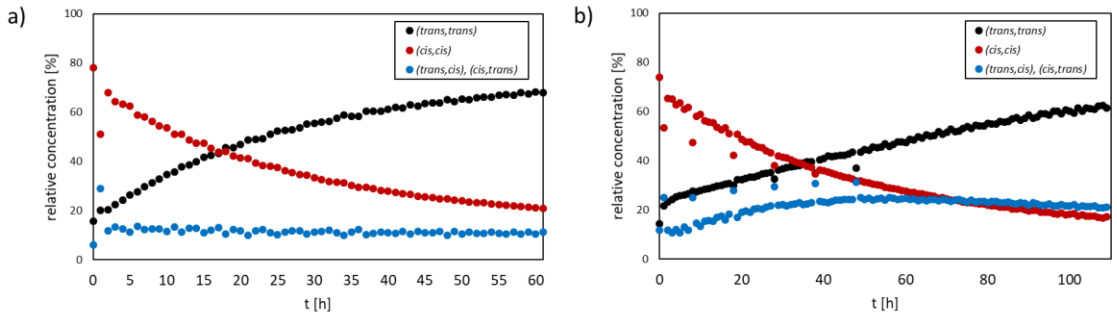

Figure 5.4: Thermal relaxation after irradiation with 365 nm (600 MHz, DMSO-d_6, 298 K), (a) **17**; (b) **18**; black: *all trans*-macrocycle, red: *all cis*, blue: *trans,cis*- and *cis,trans*-macrocycle.

CD measurements provided spectra which bands correspond to the π → π* and n → π* transitions of azobenzene in the UV/Vis spectra, showing that the azobenzene moieties exhibit chirality (Figure 5.5). For both macrocycles the π → π* transition (360 nm) gives an exciton couplet, while the n → π* transition gives a weak negative Cotton effect. Upon isomerization with 365 nm, the exciton coupling disappears and π → π* transition gives a positive Cotton effect while the n → π* transition gives a stronger negative Cotton effect. Back switching with 520 nm or 450 nm result in a near full restoration of the original *all trans*-spectra.

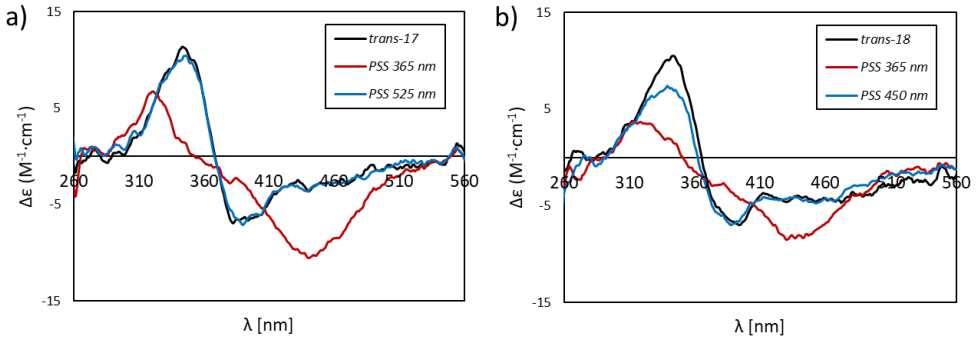

Figure 5.5: CD spectra of the different macrocycles in DMSO at 298 K (a) **17**; (b) **18**; black line: *trans*-macrocycle, red line: PSS after irradiation with 365 nm for 5 min, blue line: PSS after irradiation with 520 nm for 5 min.

The exciton coupling at the π → π* transition is only present in the spectra of the *all trans*-macrocycles, as the angle of the *cis*-isomers towards each other doesn't permit the interaction. This can also be seen in the force field-minimized structures of **17**,[101] where the azobenzene moieties are aligned parallelly in the all *trans*-structure, while turning away from each other in *all cis*, resembling a closed and open gate form (Figure 5.6). The strong Cotton effects in the range of 450 nm for both *cis*-isomers indicates helical chirality, which is expected for *cis*-azobenzene in cyclic structures.[86, 103, 140-142] Comparisons of calculations and experiments showed that the handedness of the helical chirality can be directly deduced form the CD spectra in that region, *(P)*-chirality shows a negative Cotton effect while *(M)*-chirality shows a positive Cotton effect.[82, 86, 104] This suggests that both macrocycles **17** and **18** isomerize in a unidirectional manner, giving only the *(P)*-chirality for both *all cis*-isomers.

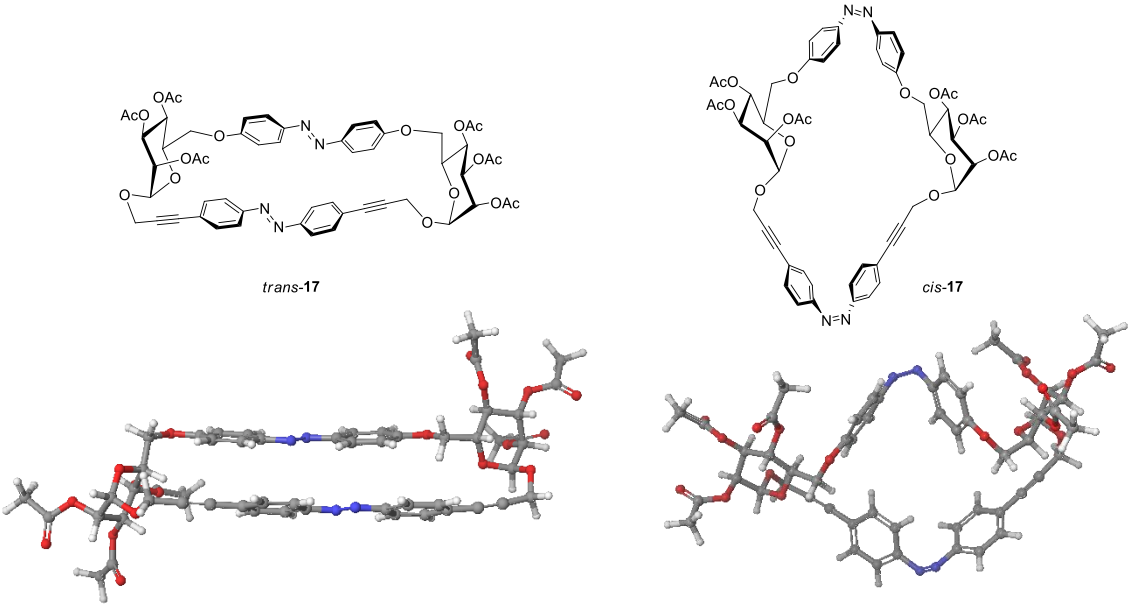

Figure 5.6: Force field-minimized structures (OPLS3 in chloroform) of *trans*- (left) and *cis*- (right) **17**.[101]

5.4 Conclusion

In summary two different macrocycles, **17** and the tetra-*ortho*-fluoro **18** (Figure 5.7), were synthesized. Two different diiodo-azobenzene compounds could be utilized for the intermolecular Sonogashira coupling with a pre-existing dialkyne building block without the need for an alteration of the reaction conditions. Through this, selective modifications of one or both azobenzene moieties can be implemented easily to influence the trans/cis isomerization behavior of the created macrocycle, like required wavelengths or stability in the excited state. The carbohydrate moieties of the dialkyne building block can be easily exchanged (cf. chapter 6.3), creating the possibility of a great variation of macrocyclic structures.

It could be shown from the investigation of the photochromic properties that the fluorination leads to a longer half-life and more stable mixed (*trans,cis* or *cis,trans*) species. As expected, the substitution has little to no effect on the shape of the macrocycle.

5.5 Experimental section

General methods and instrumentation

For general methods and instrumentation and performance of the irradiation experiments refer to **4.5**.

Deviating from the this, *cis* → *trans* photoisomerization experiments were performed using either a LED emitting a 450 nm light from Nichia Corporation with a FWHM of 45 nm and intensity of 1 mW/cm^2 or a LED emitting a 520 nm light as stated above.

To differentiate the two different azobenzene moieties, NMR signals of the azobenzene connected to the primary position of the carbohydrates are labeled with an apostrophe.

Synthesis

(*E*)-1,2-Bis(4-(3-(2,3,4,6-tetra-*O*-acetyl-β-D-mannopyranoside)prop-1-yn-1-yl)phenyl)diazene (**22**):

2-Propynyl 2,3,4,6-tetra-*O*-acetyl-β-D-mannopyranoside[137] (**21**) (150 mg, 388 µmol), 4,4'-diiodoazobenzene[135] (**19**) (82.0 mg, 189 µmol) were dissolved in dry DMF (3.75 mL) and triethylamine (3.75 mL) under a nitrogen atmosphere and nitrogen gas was bubbled through the solution for 30 min. Tetrakis(triphenylphosphine)palladium(0) (tip of spatula, 0.05 eq) was added and the mixture was stirred at room temperature for 5 min before heating to 60 °C for 4 h and then continuing with stirring at room temperature for 16 hours. Ethyl acetate was added, and the mixture was washed twice with 2 N HCl, sat. $NaHCO_3$ solution and water (each 50 mL) and dried over $MgSO_4$. After filtration and concentration under reduced pressure, the residue was purified by flash chromatography (cyclohexane/ethyl acetate 1:1) to give **22** (118 mg, 124 µmol, 66 %) as a dark orange foam.

$[\alpha]^{20}_D$= +90.0 (c= 0.90 in CH_2Cl_2); ^{1}H NMR (600 MHz, DMSO-d_6) δ = 7.96 – 7.90 (m, 4 H, Ar-H_{ortho}), 7.75 – 7.69 (m, 4 H, Ar-H_{meta}), 5.21 – 5.13 (m, 8 H, H-1, H-2, H-3, H-4), 4.68 (d, $^2J_{CH2a,CH2b}$ = 16.3 Hz, 2 H, CH_2a), 4.61 (d, $^2J_{CH2a,CH2b}$ = 16.3 Hz, 2 H, CH_2b), 4.18 (dd, $^2J_{6a,6b}$ = 12.3 Hz, $^3J_{6a,5}$ = 4.6 Hz, 2 H, H-6a), 4.10 (dd, $^2J_{6a,6b}$ = 12.3 Hz, $^3J_{6b,5}$ = 2.4 Hz, 2 H, H-6b), 4.06 – 4.01 (m, 2 H, H-5), 2.14 (s, 6 H, 2 CH_3C=O), 2.03 (s, 6

H, 2 C*H*$_3$C=O), 2.02 (s, 6 H, 2 C*H*$_3$C=O), 1.96 (s, 6 H, 2 C*H*$_3$C=O) ppm; ^{13}C NMR (151 MHz, DMSO-*d*$_6$) δ = 170.1 (CH$_3$*C*=O), 169.7 (4 C, CH$_3$*C*=O), 169.4 (CH$_3$*C*=O), 151.4 (Ar-C$_{ipso}$), 132.8 (Ar-C$_{meta}$), 124.8 (Ar-C$_{para}$), 123.0 (Ar-C$_{ortho}$), 95.8 (C-1), 87.6 (CH$_2$*C*≡C), 85.8 (CH$_2$C≡*C*), 68.6 (4 C, C-2 or C-3 or C-4), 68.4 (C-5), 65.2 (C-2 or C-3 or C-4), 61.7 (C-6), 55.2 (*C*H$_2$), 20.6 (*C*H$_3$C=O), 20.5 (*C*H$_3$C=O), 20.44 (s), 20.4 (*C*H$_3$C=O) ppm; IR (ATR): ũ = 2958, 1742, 1367, 1213, 1044, 852 cm^{-1}; ESI-MS m/z: calc. 973.28491 for [C$_{46}$H$_{50}$O$_{20}$N$_2$+Na]$^+$; found 973.28425 for [C$_{46}$H$_{50}$O$_{20}$N$_2$+Na]$^+$.

Macrocycle **17**:

Precursor **23** (43.3 mg, 50.0 µmol), 4,4'-diiodoazobenzene[135] (**5**) (21.7 mg, 50.0 µmol) were dissolved in dry DMF (5.00 mL) and triethylamine (5.00 mL) under a nitrogen atmosphere and nitrogen gas was bubbled through the solution for 30 min. Tetrakis(triphenylphosphine)palladium(0) (tip of spatula, 0.05 eq) was added and the mixture was stirred at room temperature for 5 min before heating to 60 °C for 4 h. Ethyl acetate was added, and the mixture was washed twice with 2 N HCl, sat. NaHCO$_3$ solution and water (each 125 mL) and dried over MgSO$_4$. After filtration and concentration under reduced pressure, the residue was purified by flash chromatography (cyclohexane/ethyl acetate 1:1) to give **17** (20.6 mg, 19.7 µmol, 39 %) as a dark orange foam.

trans-**17**:

[α]$^{20}_D$= -133 (c= 0.37 in CH$_2$Cl$_2$); ^{1}H NMR (500 MHz, DMSO-*d*$_6$) δ = 7.58 – 7.48 (m, 4 H, Ar-H$_{ortho'}$), 7.47 – 7.35 (m, 4 H, Ar-H$_{ortho}$), 7.35 – 7.24 (m, 4 H, Ar-H$_{meta}$), 6.89 – 6.77 (m, 4 H, Ar-H$_{meta'}$), 5.27 – 5.17 (m, 8 H, H-1, H-2, H-3, H-4), 4.87 (d, $^2J_{CH2a,CH2b}$ = 16.8 Hz, 2 H, C*H*$_2$a), 4.59 (d, $^2J_{CH2a,CH2b}$ = 16.9 Hz, 2 H, C*H*$_2$b), 4.42 – 4.32 (m, 2 H, H-5), 4.18 (dd, $^2J_{6a,6b}$ = 10.8 Hz, $^3J_{6a,5}$ = 6.0 Hz, 2 H, H-6a), 4.08 (dd, $^2J_{6a,6b}$ = 10.8 Hz, $^3J_{6b,5}$ = 4.8 Hz, 2 H, H-6b), 2.16 (s, 6 H, 2 C*H*$_3$C=O), 2.09 (s, 6 H, 2 C*H*$_3$C=O), 2.00 (s, 6 H, 2 C*H*$_3$C=O) ppm; ^{13}C NMR (151 MHz, DMSO-*d*$_6$) δ = 169.8 (CH$_3$*C*=O), 169.7 (CH$_3$*C*=O), 169.6 (CH$_3$*C*=O), 159.9 (Ar-C$_{para'}$), 150.8 (Ar-C$_{ipso}$), 146.1 (Ar-C$_{ipso'}$), 132.1 (Ar-C$_{meta}$), 124.2 (Ar-C$_{para}$), 124.0 (Ar-C$_{ortho'}$), 122.6 (Ar-C$_{ortho}$), 114.4 (Ar-C$_{meta'}$), 98.5 (1), 88.5 (CH$_2$*C*≡C), 85.1 (CH$_2$C≡*C*), 68.8 (5), 68.6 (C-2 or C-3 or C-4), 68.3 (6), 68.2 (C-2 or C-3 or C-4), 67.7 (C-2 or C-3 or C-4), 57.5 (*C*H$_2$), 20.6 (*C*H$_3$C=O), 20.5 (*C*H$_3$C=O), 20.4 (*C*H$_3$C=O) ppm; IR (ATR): ũ = 2922, 1747, 1368, 1218, 1067, 1044, 839 cm^{-1}; ESI-MS m/z: calc. 1045.33494 for [C$_{54}$H$_{52}$O$_{18}$N$_4$+H]$^+$; found 1045.33393 for [C$_{54}$H$_{52}$O$_{18}$N$_4$+H]$^+$.

cis-**17**:

[α]$^{20}_D$= -303 (c= 0.37 in CH$_2$Cl$_2$).

Macrocycle **18**:

Precursor **23** (39.0 mg, 45.0 µmol), 2,2',6,6'-tetrafluoro-4,4'-diiodoazobenzene[136] (**5**) (23.0 mg, 45.0 µmol) were dissolved in dry DMF (4.50 mL) and triethylamine (4.50 mL) under a nitrogen atmosphere and nitrogen gas was bubbled through the solution for 30 min. Tetrakis(triphenylphosphine)palladium(0) (tip of spatula, 0.05 eq) was added and the mixture was stirred at room temperature for 5 min before heating to 60 °C for 4 h. Ethyl acetate was added, and the mixture was washed twice with 2 N HCl, sat. NaHCO$_3$ solution and water (each 100 mL) and dried over MgSO$_4$. After filtration and concentration under reduced pressure, the residue was purified by flash chromatography (cyclohexane/ethyl acetate 1:1) to give **18** (13.9 mg, 12.4 µmol, 28 %) as a dark red foam.

trans-**18**:

$[\alpha]^{20}_{D}$= -270 (c= 0.05 in CH_2Cl_2); ^{1}H NMR (600 MHz, DMSO-d_6) δ = 7.51 – 7.46 (m, 4 H, Ar-$H_{ortho'}$), 7.16 – 7.10 (m, 4 H, Ar-H_{meta}), 6.83 – 6.76 (m, 4 H, Ar-$H_{meta'}$), 5.24 (dd, $^{3}J_{3,4}$ = 10.2 Hz, $^{3}J_{3,2}$ = 3.3 Hz, 2 H, H-3), 5.21 – 5.14 (m, 6 H, H-1, H-2, H-4), 4.88 (d, $^{2}J_{CH2a,CH2b}$ = 16.9 Hz, 2 H, CH_2a), 4.56 (d, $^{2}J_{CH2a,CH2b}$ = 16.9 Hz, 2 H, CH_2b), 4.39 – 4.33 (m, 2 H, H-5), 4.16 (dd, $^{2}J_{6a,6b}$ = 10.8 Hz, $^{3}J_{6a,5}$ = 5.7 Hz, 2 H, H-6a), 4.05 (dd, $^{2}J_{6a,6b}$ = 11.0 Hz, $^{3}J_{6b,5}$ = 5.2 Hz, 2 H, H-6b), 2.15 (s, 6 H, 2 CH_3C=O), 2.08 (s, 6 H, 2 CH_3C=O), 1.99 (s, 6 H, 2 CH_3C=O) ppm; ^{13}C NMR (151 MHz, DMSO-d_6) δ = 170.0 (CH_3*C*=O), 169.9 (CH_3*C*=O), 169.8 (CH_3*C*=O), 159.7 (Ar-$C_{para'}$), 154.6 (d, Ar-C_{ortho}), 146.0 (Ar-$C_{ipso'}$), 130.4 – 130.0 (m, Ar-C_{ipso}), 125.6 (Ar-C_{para}), 123.9 (Ar-$C_{ortho'}$), 116.6 – 115.7 (m, Ar-C_{meta}), 114.2 (Ar-$C_{meta'}$), 98.8 (C-1), 90.7 (CH_2*C*≡C), 83.2 (CH_2C≡*C*), 69.0 (C-5), 68.6 (C-2), 68.4 (C-6), 68.3 (C-3), 67.9 (C-4), 57.4 (*C*H_2), 20.7 (*C*H_3C=O), 20.6 (*C*H_3C=O), 20.5 (*C*H_3C=O) ppm; ^{19}F NMR (471 MHz, DMSO-d_6) δ = -118.8 (s) ppm; IR (ATR): ũ = 2925, 1748, 1369, 1217, 1045, 842 cm^{-1}; ESI-MS m/z: calc. 1117.29725 for $[C_{54}H_{48}O_{18}N_4F_4+H]^+$; found 1117.29533 for $[C_{54}H_{48}O_{18}N_4+H]^+$.

cis-**18**:

$[\alpha]^{20}_{D}$= -130 (c= 0.05 in CH_2Cl_2).

NMR spectra of synthesized compounds

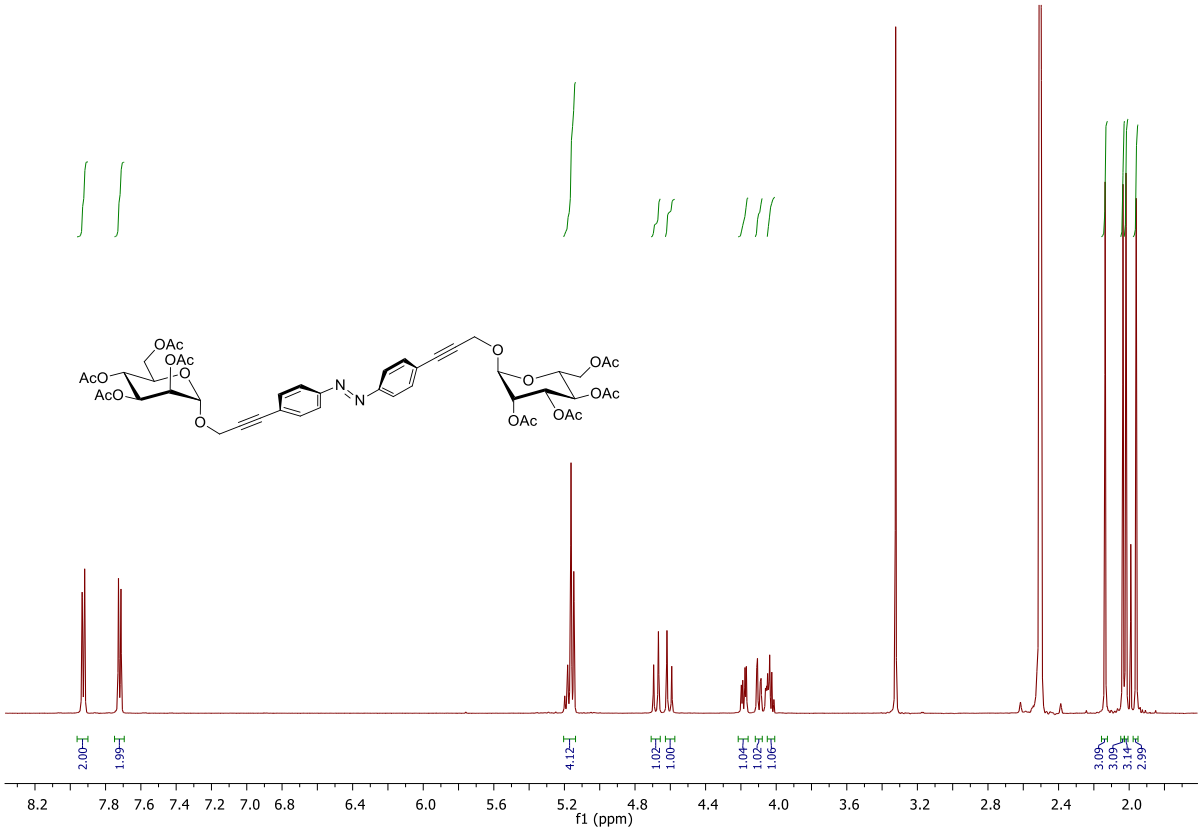

Figure 5.8: ^{1}H NMR spectrum of *trans*-**22** (600 MHz, DMSO-d_6, 298 K).

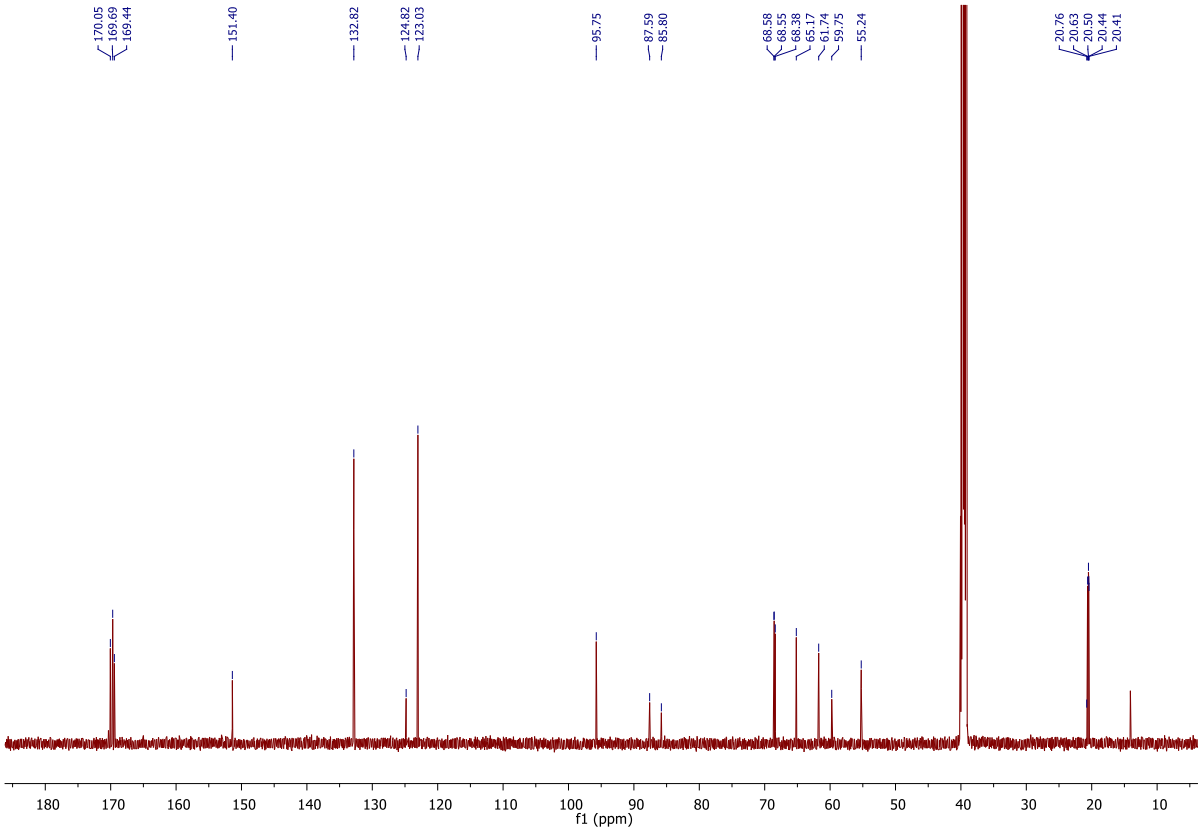

Figure 5.9: ^{13}C NMR spectrum of *trans*-**22** (151 MHz, DMSO-d_6, 298 K).

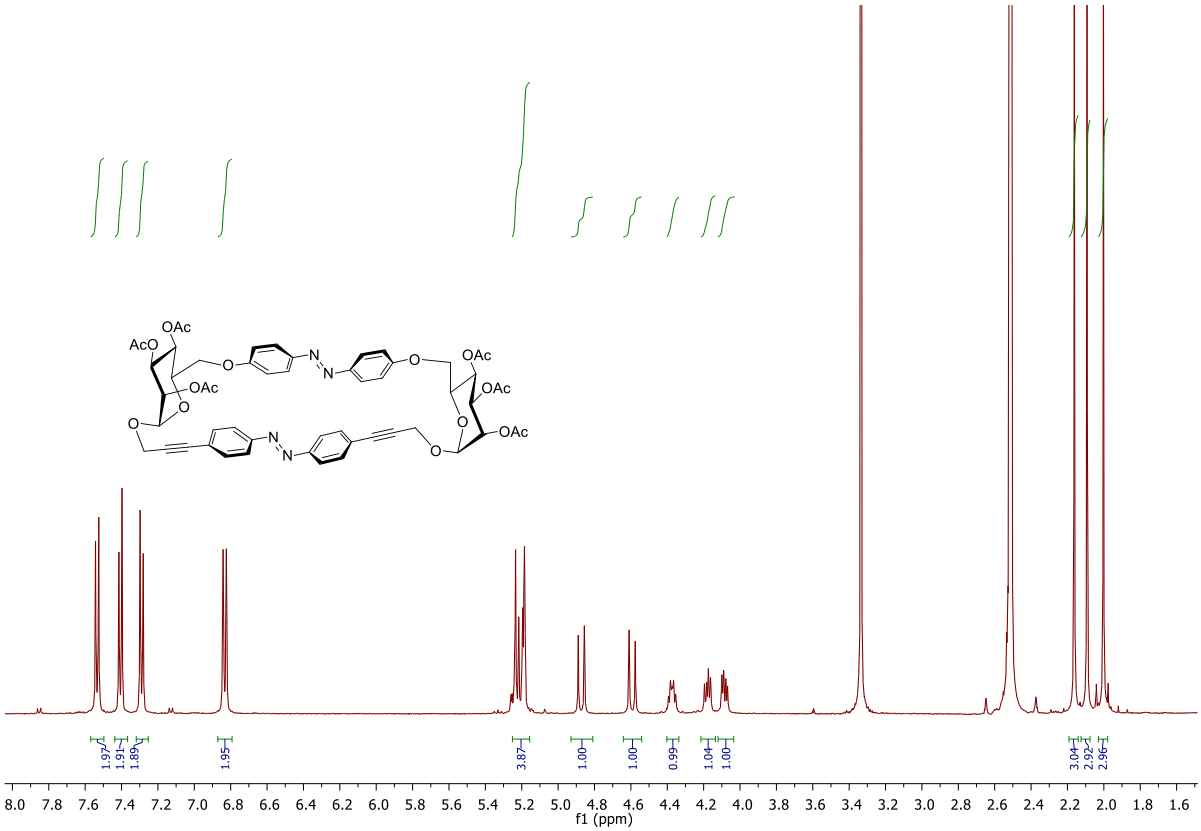

Figure 5.10: ^{1}H NMR spectrum of *trans*-**17** (500 MHz, DMSO-d_6, 298 K).

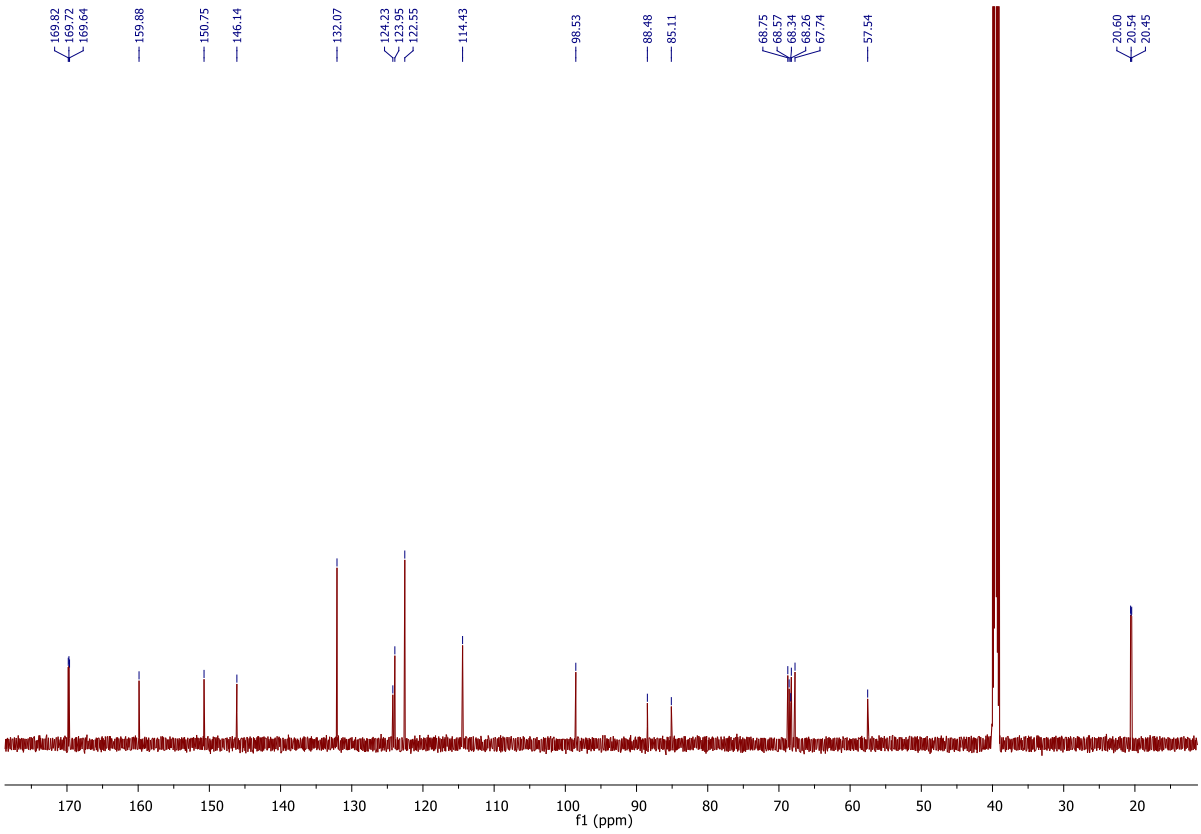

Figure 5.11: ^{13}C NMR spectrum of *trans*-**17** (151 MHz, DMSO-d_6, 298 K).

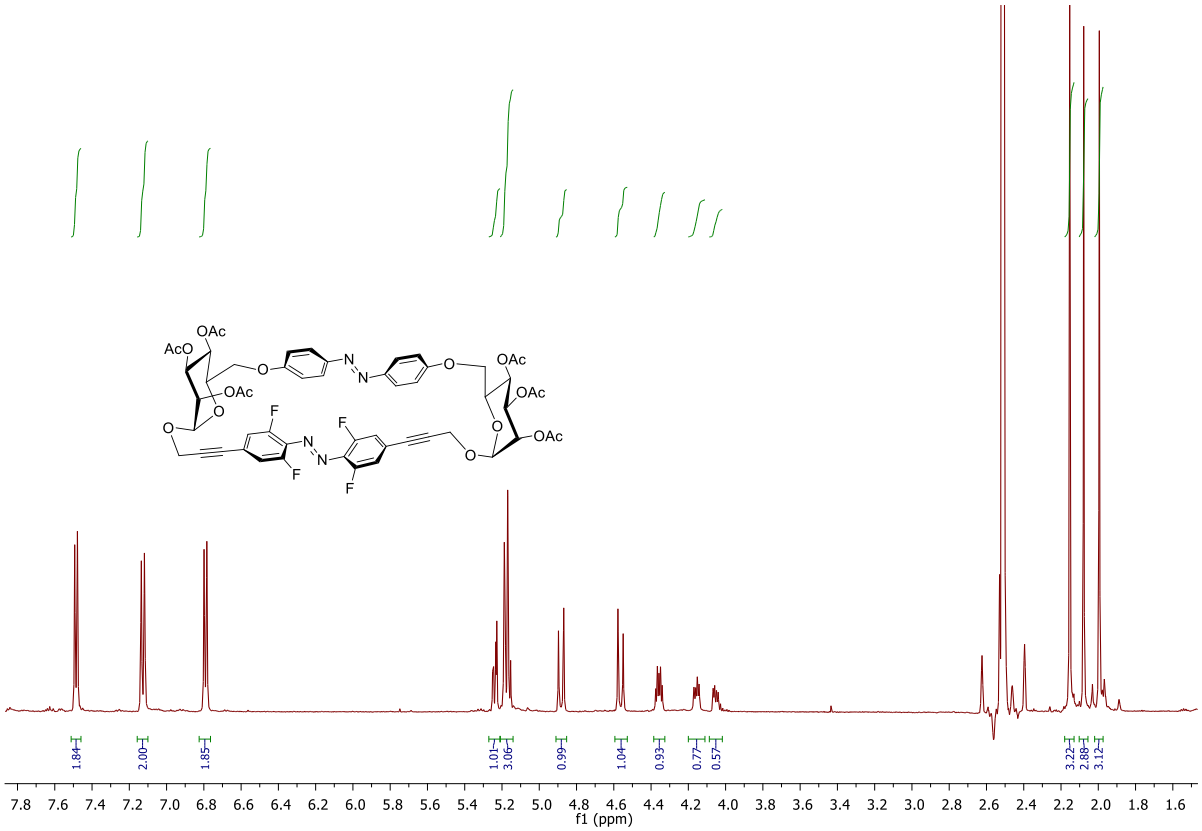

Figure 5.12: ^{1}H NMR spectrum of *trans*-**18** (600 MHz, DMSO-d_6, 298 K).

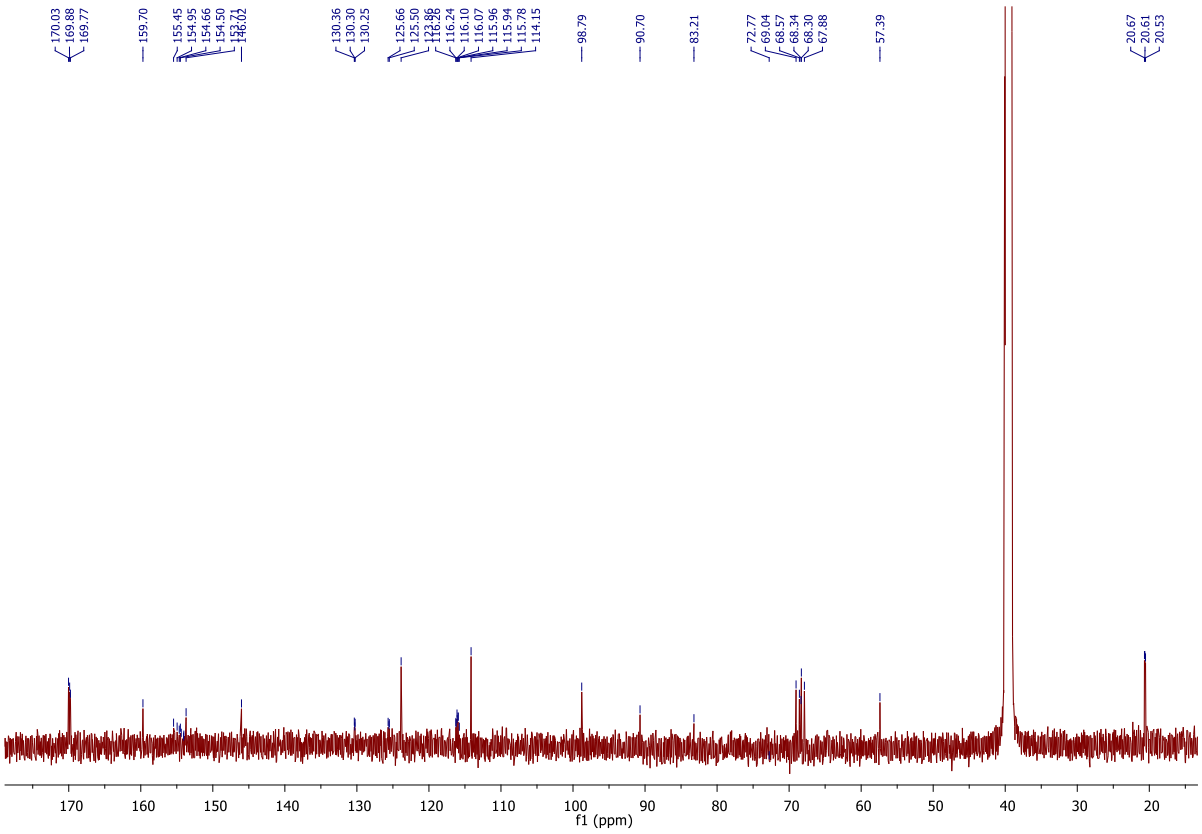

Figure 5.13: ^{13}C NMR spectrum of *trans*-**18** (151 MHz, DMSO-d_6, 298 K).

Irradiation experiments

PSS was reached after irradiating the respective sample for 5 min with 365 nm or 5 min with 450 nm or 520 nm and the respective spectra are shown in Figure 5.14 and 5.15.

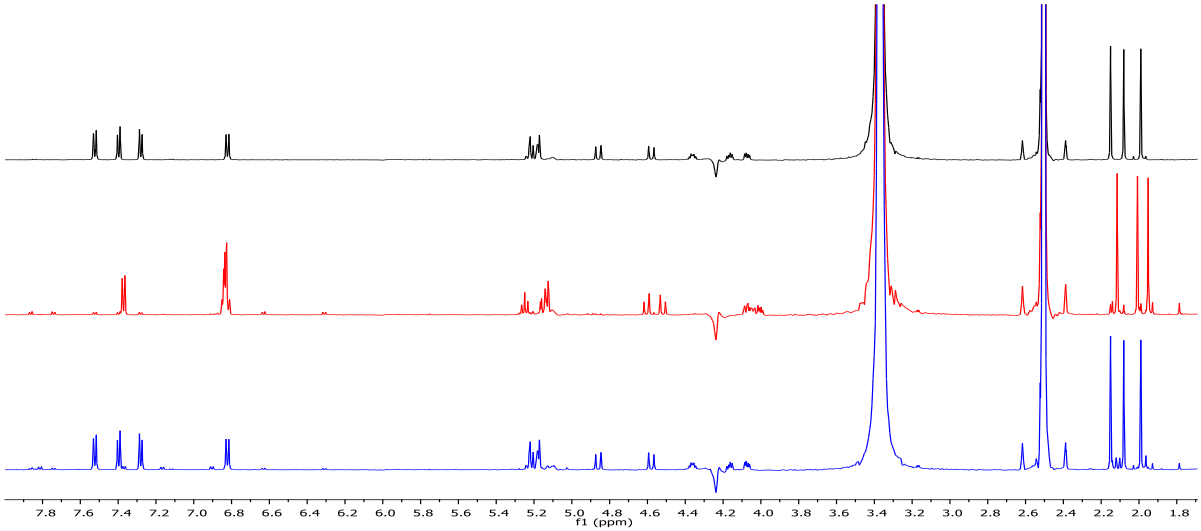

Figure 5.14: NMR spectra of *trans*-**17** after heating at 45 °C in the dark for 20 h (black), after irradiation with 365 nm for 6 min (red)and after irradiation with 520 nm (blue) for 5 min.

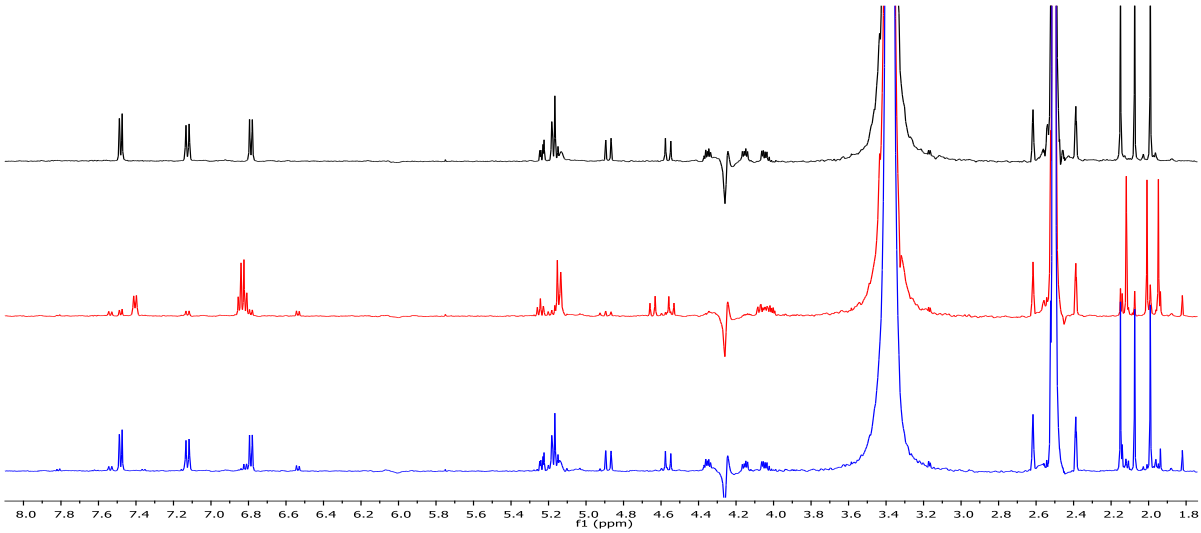

Figure 5.15: NMR spectra of *trans*-**18** after heating at 45 °C in the dark for 20 h (black), after irradiation with 365 nm for 5 min (red) and after irradiation with 450 nm (blue) for 5 min.

The extinction coefficient ε and the coefficient of determination of the linear fitting for *trans*- and *cis*-**17** and **18** are shown along the plot of the absorbance against the concentration in Figure 5.16.

The switching cycle experiments for **17** and **18** are shown in Figure 5.17 with the plot of the value of the absorbance at $\lambda_{max(E)}$ against the number of times the sample was irradiated.

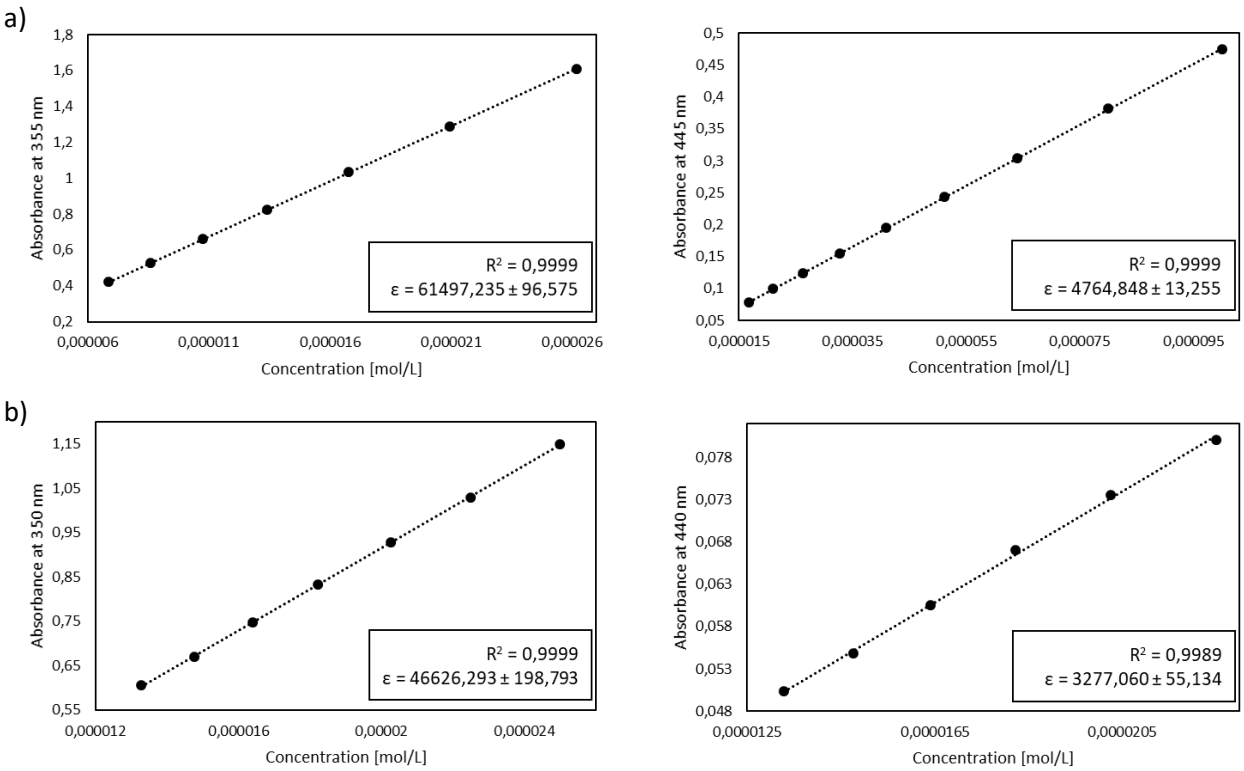

Figure 5.16: Plot of the absorbance at the λ_{max} versus the concentration; the slope of the linear curve gives the value of the molar extinction coefficient ε. Measured at 298 K in DMSO in concentrations from $8 \cdot 10^{-6}$ to 10^{-4} mol·L^{-1}. (a) *trans*-**17** at 355 nm and PSS 365 nm at 445 nm; (b) *trans*-**18** at 350 nm and PSS 365 nm at 440 nm.

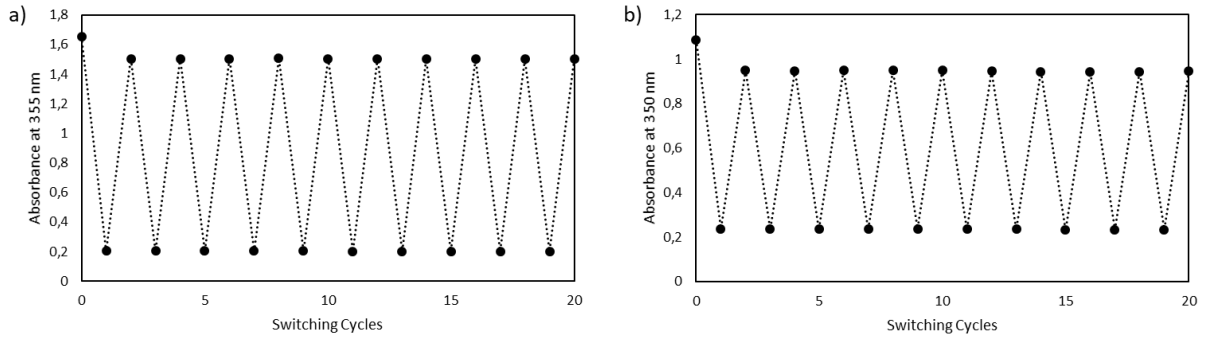

Figure 5.17: Measured absorbance after alternating photoirradiation with 365 nm and 450 or 520 nm. Measured at 298 K in DMSO in a concentration of 25 µM. (a) **17**; (b) **18**.

The decay of the absorbance of the n-π* band λ_{max} of *cis*-**17** and **18** are shown alongside the coefficient of determination of the exponential fitting and the absorbance at infinite time in Figure 5.18. The linearization of the absorbance is shown with the coefficient of determination of the linear fitting, the rate constant and the ensuing half-life time

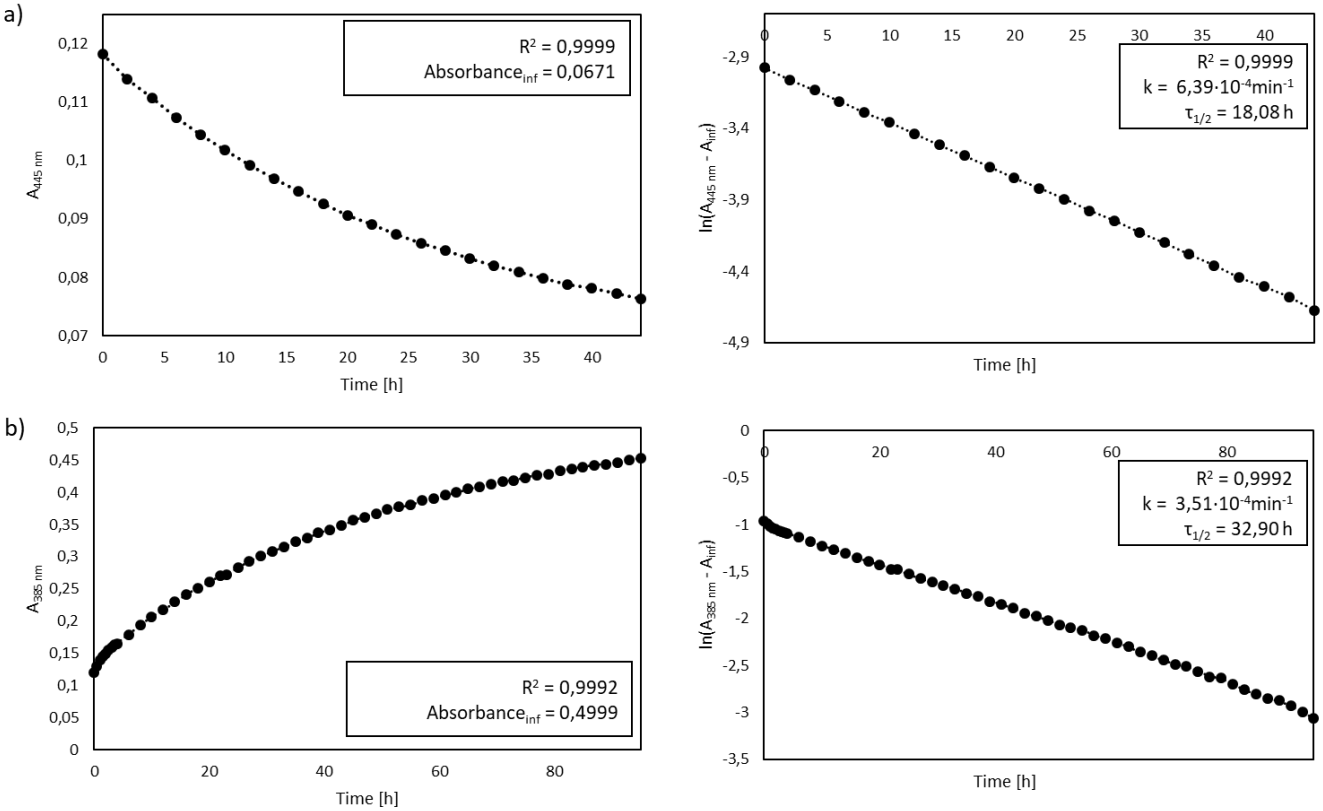

Figure 5.18: Kinetics of the *cis*→*trans* thermal relaxation process, measured at 298 K in DMSO at a concentration of 25 µM, showing the exponential decay of the absorbance, the linearization with the corresponding coefficient of determination and the half-life time for the *cis*-form of the respective compounds. (a) **17**; (b) **18**.

6. Glaser Coupling

6.1 Introduction

GLASER first observed the oxidative homocoupling of copper(I) phenylacetylide in 1896 in the presence of air and a base.[143] However, the application of this reaction was limited as copper(I) acetylenes are hard to isolate and potentially explosive.[123] 60 years later, EGLINTON and GALBRAITH showed that the reaction could be modified to proceed with an excess of copper(II) acetate in methanol and pyridine without the need for preliminary isolation of the copper acetylene salt and they immediately applied their protocol to the synthesis of the first diyne macrocycles under high dilution.[144, 145]

In 1962 HAY showed that the reaction could be performed with catalytic amounts of copper(I) salts if a bidentate nitrogen ligand is used in the presence of dioxygen.[146] The so formed complexes remain soluble in organic solvents and prevent the precipitation of the mostly insoluble copper(I) acetylides.

The mechanism of the reaction was first believed to involve radical intermediates, but this was disproved by BOHLMANN et al. in 1962, who instead suggested the formation of a π complex between the copper ion and the coordinating alkyne.[147] Today, DFT calculations support an inner sphere mechanism for the reaction of dioxygen with copper(II) dimers as intermediates and the deprotonation of the Cu-coordinated alkyne as the rate-limiting step.[148]

Until today, the so-called Glaser coupling finds applications in the synthesis of diyne macrocycles. The rigidity of the conjugated 1,3-diyne bond allows for the formation of so-called shape persistent macrocycles, preventing the collapse of the macrocyclic structure. Shape persistency means, that the lumen of a macrocycle is equal to the length of the molecular backbone divided by π.[133, 149] We wanted to take advantage of features associated with 1,3-diyne linking unit and hence have targeted macrocycles with an increased rigidity to promote the formation of cyclic molecules with a defined shape.

On the other hand, our attempts to apply the Cadiot-Chodkiewicz coupling to macrocyclization, an advancement of the Glaser coupling permitting heterocoupling of bromo acetylenes with terminal alkynes,[150, 151] were unsuccessful.

6.2 First macrocycle based on propargyl mannoside

In order to employ the Glaser reaction for macrocyclization of photoswitchable glycomacrocycles, the precursor must contain terminal alkyne groups to form the 1,3-diyne linkage in addition to the azobenzene hinge. Our preliminary experiments on a protecting group-free *O*-arylation of the primary 6-OH group of the carbohydrate ring led to the decision to introduce the azobenzene moiety at the carbohydrate 6-OH via a Mitsunobu reaction.

It could be shown that using the Mitsunobu reaction on unprotected sugars leads to the exclusive formation of the glycosylated product as the anomeric OH is the most reactive nucleophile. However, if glycosylated, but otherwise unprotected carbohydrates are employed in the reaction, the 6-*O* aryl

derivative is formed as the sole product.[152] Even if the nucleophile is added in excess, the more hindered secondary alcohols were not substituted, making the use of protecting groups unnecessary. Therefore, propargyl mannoside **24** was chosen as an easily available building block, which was obtained in a simple three-step synthesis starting from D-mannose.[137]

The application of the Mitsunobu reaction to **24** and 4,4'-dihydroxyazobenzene (**5**),[98] in the presence of triphenylphosphine and DIAD, leading to the disubstitution of the azobenzene, as expected. The crude material was then acetylated to facilitate the separation of the excess of unreacted mannoside **24** from the product, leading to the macrocycle precursor **23** in 50 % yield over two steps (Scheme 6.1). In an alternative route, the corresponding tosylate **25,** synthesized from **24** according to the literature,[137] reacted with the azobenzene **5** in a Williamson etherification. In this case, **23** could be obtained in a higher yield of 70 %, but the overall yield starting from **24** is lower at 43 %. Hence, as the Mitsunobu reaction requires only one step, it is the more favorable approach to **23**.

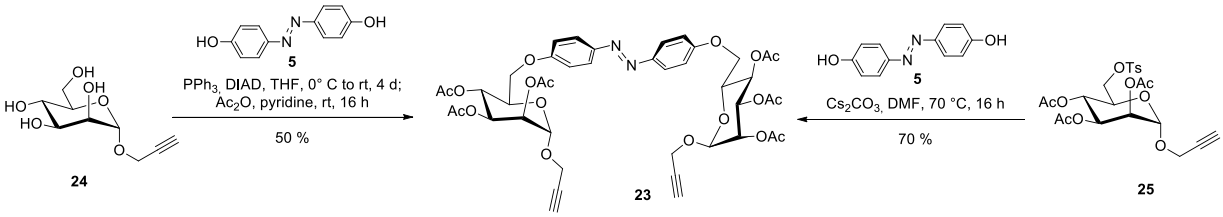

Scheme 6.1: Synthesis of precursor **23** via two alternative methods for 6-*O*-arylation.

In the next step, the Glaser coupling was employed for the intramolecular macrocyclization reaction of **23**. After testing copper(II) acetate under nitrogen without success, a system consisting of copper(I) bromide and PMDETA in pyridine in ambient conditions gave the best results for the macrocyclization of **23** to yield **26** (Table 6.1). Like for the intermolecular macrocyclization of thiourea-bridged macrocycle **8**, the crucial precondition for the reaction to occur was the *trans* → *cis* isomerization of **23** before adding the reagents for the Glaser coupling. The isomerization led to a closer proximity of the terminal alkyne groups, enabling the macrocyclization, as reactions without pre-orientation of **23** led only to traces of the desired macrocycle **26**. The macrocyclization was carried out at different concentrations to determine whether higher dilution would prevent intermolecular side reactions. A maximum yield was reached at a concentration of 2 mM (Entry 3). As the final step, **26** was deprotected under Zemplén conditions[100] in quantitative yield to obtain the target macrocycle **27**.

Table 6.1: Synthesis of macrocycle **27** with conditions and resulting yields for the macrocyclization.

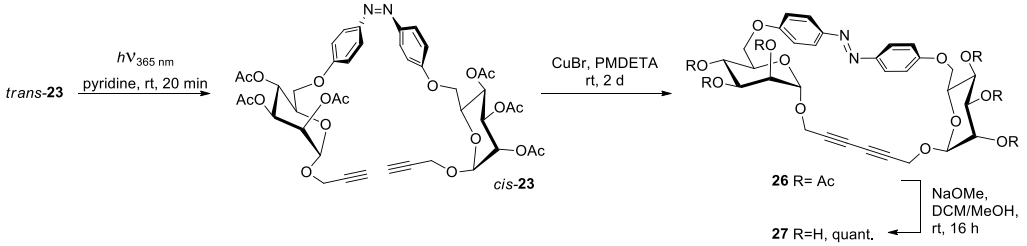

Entry	Concentration (mM)	Pre-irradiation (nm)	Yield of 26 (%)
1	5	-	5[a]
2	1	365	26
3	2	365	50
4	5	365	42
5	7	365	39

[a] Yield determined by ^{1}H NMR.

6.3 Further propargyl glycosides: towards a library of macrocycles

After the successful two-step synthesis of the α-mannoside-based macrocycle **27**, the preparation of a small library of macrocycles differing in their carbohydrate moiety was envisioned, in order to investigate the effect of alcohol epimerization and anomeric configurations on the properties of the respective macrocycles.

Four further macrocycles were targeted by Glaser coupling: α- and β-glucoside-derived macrocycles **28** and **29**, the β-galactoside-based macrocycle **30** and macrocycle **31**, derived from propargyl 2-amino-2-deoxy-β-glucoside (Figure 6.1).

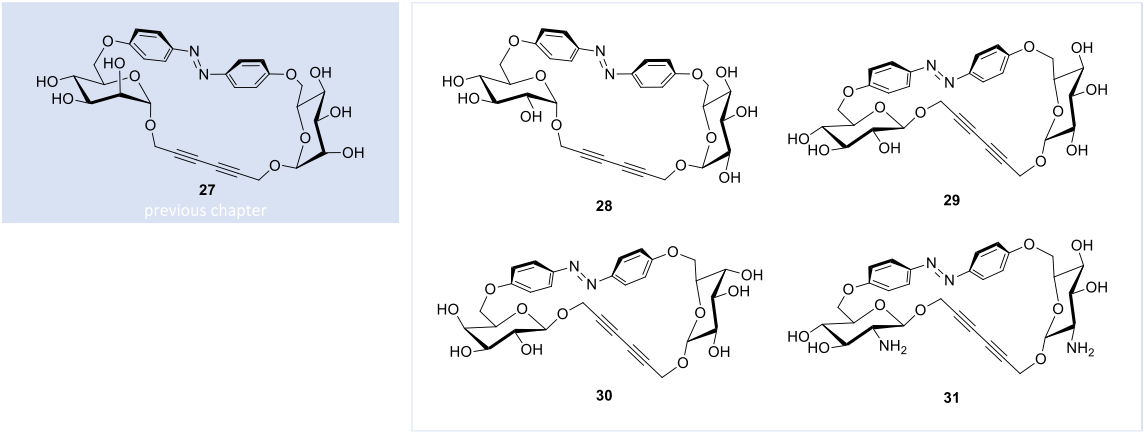

Figure 6.1: Library of the targeted photoswitchable macrocycles.

Following the route for the synthesis of the mannose-derived macrocycle **27**, the analogous preparations started with the synthesis of both the respective propargyl glycosides and their regioselective 6-*O*-tosylations, in order to test both the Mitsunobu reaction and Williamson etherification pathways. Propargyl β-glucoside **32** and -galactoside **33** were synthesized analogous to the α-mannoside **24**[153] in three steps starting from the free sugars (Scheme 6.2). In contrast, the thermodynamically stable α-glucoside **34** was synthesized via Fischer glycosylation with propargyl alcohol and sulfuric acid supported on silica gel as the catalyst.[154] A sequence of protection and deprotection with acetyl groups was needed to separate the anomeric mixture of α- and β-glucosides. The tosylation of the resulting propargyl glycosides was realized under typical conditions,[155] using an excess of tosyl chloride in pyridine to give **35**, **36** and **37**, respectively. Preparation of 2-propynyl 2-(2,2,2-trifluoroacetamido)-2-deoxy-β-D-glucopyranoside (**38**) was realized through the glycosylation of oxazoline **40**, which was obtained in three steps from D-glucosamine hydrochloride,[156] and subsequent deprotection in a very good yield of 93 % over two steps. Regioselective tosylation and acetylation in one pot gave the corresponding **39** in a 55 % yield.

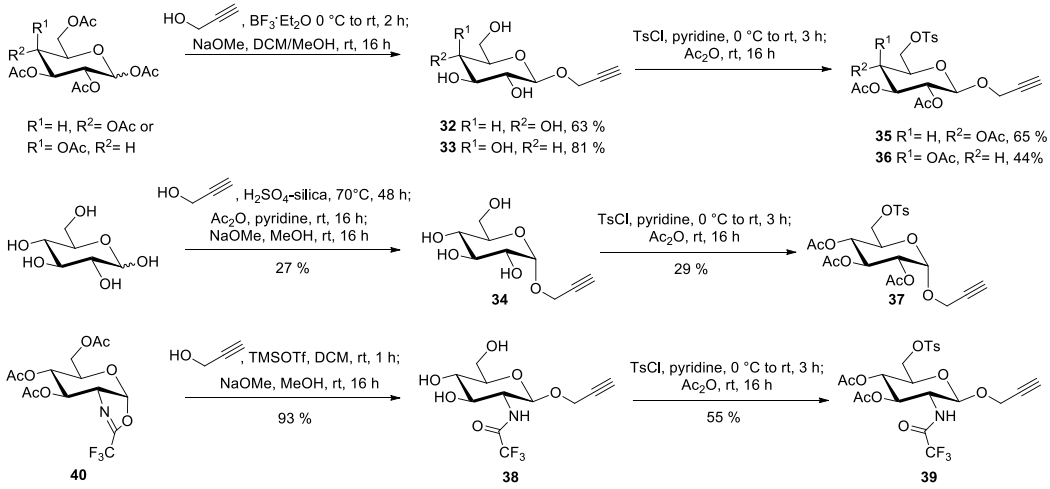

Scheme 6.2: Preparation of the propargyl glycosides **32**, **33**, **34** and **38** and the corresponding tosylates **35**, **36**, **37** and **39**.

The unprotected propargyl glycosides **32**, **33**, **34** and **38**, -analogues to **24**-, in hand, the bis-functionalization of azobenzene diol **5** was tested under Mitsunobu conditions. In parallel, the four 6-*O*-tosyl activated propargyl glycosides **35**, **36**, **37** and **39**, -analogues of the mannoside 25-, were reacted with **5** according to Williamson under cesium carbonate promotion (Table 6.2). The latter led to satisfying results for the glucosides **41** and **42** with yields of 70 % or higher. However, the reaction did not lead to the desired galactoside **43** and glucoside **44**.

Table 6.2: Bis-functionalization of azobenzene **5** via Mitsunobu reaction or Williamson etherification.

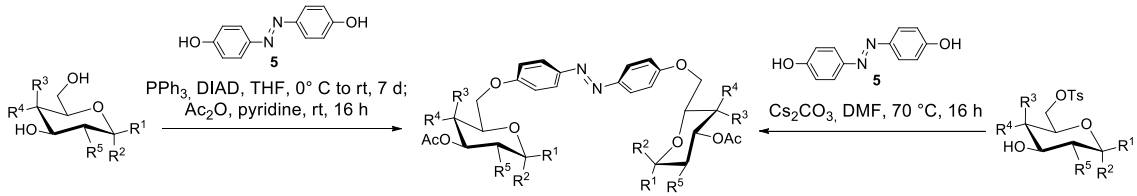

34 $R^{1/3}$= H, R^2= $OCH_2C{\equiv}CH$, $R^{4/5}$= OH
32 R^1= $OCH_2C{\equiv}CH$, $R^{2/3}$= H, $R^{4/5}$= OH
33 R^1= $OCH_2C{\equiv}CH$, $R^{2/4}$= H, $R^{3/5}$= OH
38 R^1= $OCH_2C{\equiv}CH$, $R^{2/3}$= H, R^4= OH, R^5= $NHCOCF_3$

41 $R^{1/3}$= H, R^2= $OCH_2C{\equiv}CH$, $R^{4/5}$= OH
42 R^1= $OCH_2C{\equiv}CH$, $R^{2/3}$= H, $R^{4/5}$= OH
43 R^1= $OCH_2C{\equiv}CH$, $R^{2/4}$= H, $R^{3/5}$= OH
44 R^1= $OCH_2C{\equiv}CH$, $R^{2/3}$= H, R^4= OH, R^5= $NHCOCF_3$

37 $R^{1/3}$= H, R^2= $OCH_2C{\equiv}CH$, $R^{4/5}$= OH
35 R^1= $OCH_2C{\equiv}CH$, $R^{2/3}$= H, $R^{4/5}$= OH
36 R^1= $OCH_2C{\equiv}CH$, $R^{2/4}$= H, $R^{3/5}$= OH
39 R^1= $OCH_2C{\equiv}CH$, $R^{2/3}$= H, R^4= OH, R^5= $NHCOCF_3$

Product	Mitsunobu Reaction with	Yield (%)	Williamson etherification with	Yield (%)
41	**34**	22	**37**	70
42	**32**	-	**35**	76
43	**33**	-	**36**	-
44	**38**	-	**39**	-

The successful utilization of the Mitsunobu reaction for the preparation of the 6-*O*-azobenezene-modified α-mannoside derivative **23**, was not possible for any of the other sugars, with only 22 % yield for α-glucoside **41** and no formation of the β-anomers **42**, **44** and **43**. This led to the assumption that the anomeric configuration of glycosides could be a determining factor for the success of the 6-*O*-arylation of glycosides under Mitsunobu conditions. While the glucoside precursors **41** and **42** could be obtained through Williamson etherification, a different approach towards the cyclic precursors **43** and **44** was necessary.

α-Configured diacetone galactose **45**[157] was reacted under Mitsunobu conditions to give the bis-functionalized azobenzene **46** in a good yield of 46 %, while the reaction with the corresponding tosylate **47**[158] lead to the desired product in poor yields of only 15 % (Scheme 6.3). However, this approach was discontinued, as the deprotection of the isopropylidene protecting groups was not possible without degradation of the compound. Galactosides **48** and **49** were synthesized following modified procedures for the synthesis of other 3,4-protected galactosides, starting from propargyl galactoside **33**.[159, 160] However, successful preparation of the desired bis-functionalized azobenzene **50** was not possible with either compound.

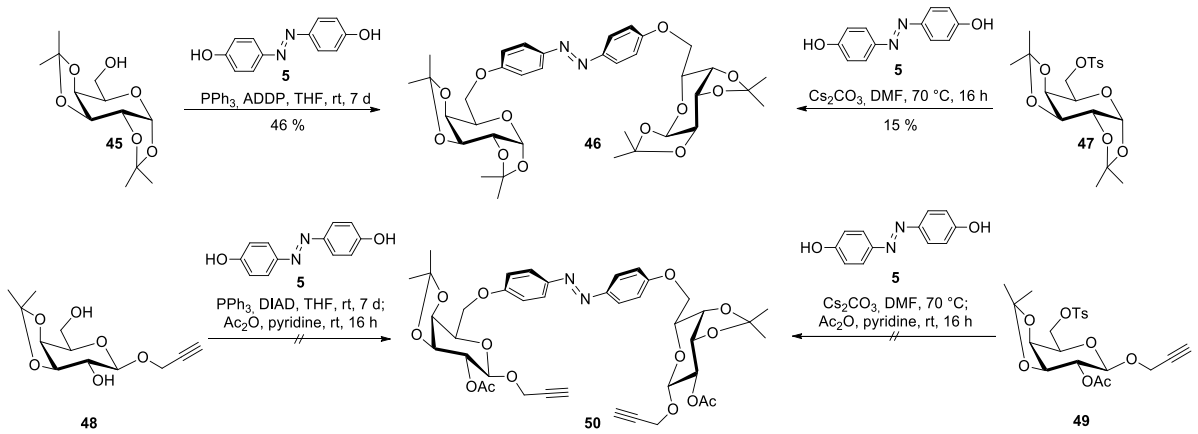

Scheme 6.3: Reactions for the synthesis of the bis-functionalized azobenzene compounds **46** and **50**. ADDP: azodicarbonyldipiperidine.

Test reactions with propargyl mannoside **24** under Mitsunobu conditions showed, that the 6-*O*-arylation with the more acidic *p*-nitrophenol (**51**) and with *N*-Boc-*p*-aminophenol (**52**) proceeded in higher yields compared to the bis-functionalization of 4,4-dihydroxyazobenzene (**5**), to give **53** and **54** respectively. This allows for the synthesis of the desired precursors for macrocyclization via reductive or oxidative azocoupling (Table 6.3).

Table 6.3: Different 6-O arylations with *p*-nitrophenol (**51**) and *N*-Boc-*p*-aminophenol (**52**).

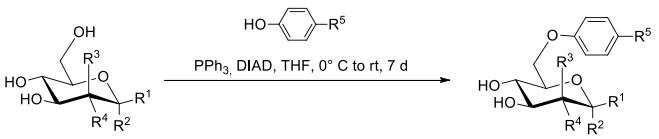

24 $R^{1/4}$ = H, R^2 = $OCH_2C{\equiv}CH$, R^3 = OH
32 R^1 = $OCH_2C{\equiv}CH$, $R^{2/3}$ = H, R^4 = OH
38 R^1 = $OCH_2C{\equiv}CH$, $R^{2/3}$ = H, R^4 = $NHCOCF_3$

53 $R^{1/4}$ = H, R^2 = $OCH_2C{\equiv}CH$, R^3 = OH, R^5 = NO_2
54 $R^{1/4}$ = H, R^2 = $OCH_2C{\equiv}CH$, R^3 = OH, R^5 = NHBoc
55 R^1 = $OCH_2C{\equiv}CH$, $R^{2/3}$ = H, R^4 = OH, R^5 = NHBoc
56 R^1 = $OCH_2C{\equiv}CH$, $R^{2/3}$ = H, R^4 = $NHCOCF_3$, R^5 = NHBoc

Product	Reagent	Yield (%)
53	**24**	88
54	**24**	77
55	**32**	15
56	**38**	-

As before, reactions with β-configured compounds, glucosides **32** and **38**, performed very poorly. **55** could only be obtained in a yield of 15 %, while **56** was not formed at all. Due to these results the preparation of the amino glucoside-based macrocycle **31** was not pursued further, in order to concentrate on the synthetic route for the galactoside-derived macrocycle **30**. Diacetone galactose **45**

was reused, to utilize the advantage of its α-configuration in the synthesis of **57** (Scheme 6.4). But the unsatisfying yields for the subsequent deprotection to **58** and glycosylation to **59** were not satisfactory.

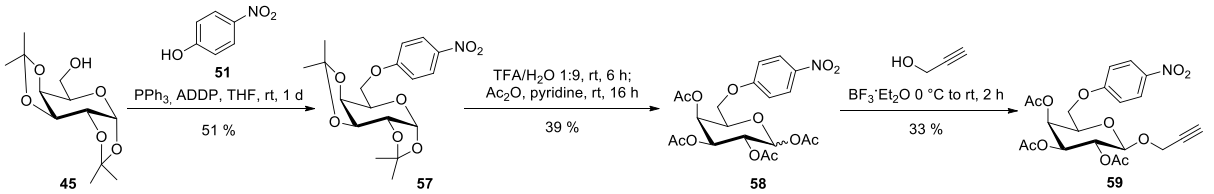

Scheme 6.4: Synthesis of galactoside **59** through a sequence of Mitsunobu reaction, reprotection and glycosylation.

Therefore, the Mitsunobu reaction of propargyl galactoside **33** with N-Boc protected aminophenol **52** to **60** was optimized. Exchange of the reaction solvent showed that the yield was reciprocally dependent on their ability to solvate the polar reactant **33**, with THF giving the best yield (30 %, Scheme 6.5). Here it is assumed that the slow provision of reactant available for substitution, combined with the slow rate of the reaction is responsible for the positive effect on the yield. Boc-deprotection gave the free aniline **61** in quantitative yields.

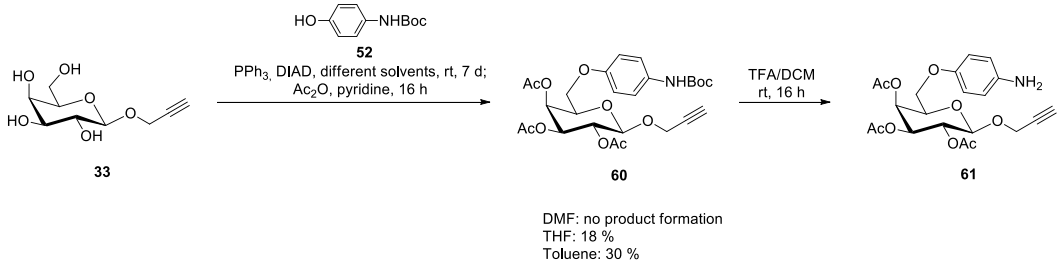

Scheme 6.5: The effect of different solvents on the synthesis of **60** via Mitsunobu reaction.

With both **59** and **61** in hand, both reductive and oxidative azocoupling could be utilized for the synthesis of the galactoside-based macrocyclic precursor **43**. However, repeated test reactions attempting to reduce the mannoside **53** to the macrocyclization precursor **62** with $LiAlH_4$[161] remained unsuccessful, so only the oxidative azocoupling was considered for the synthesis of **23**. Sodium dithionite[162] was used to reduce the remaining **59** to the respective aminophenyl derivative **61** for the forthcoming oxidation. However, this reduction was unsuccessful as well (Scheme 6.6).

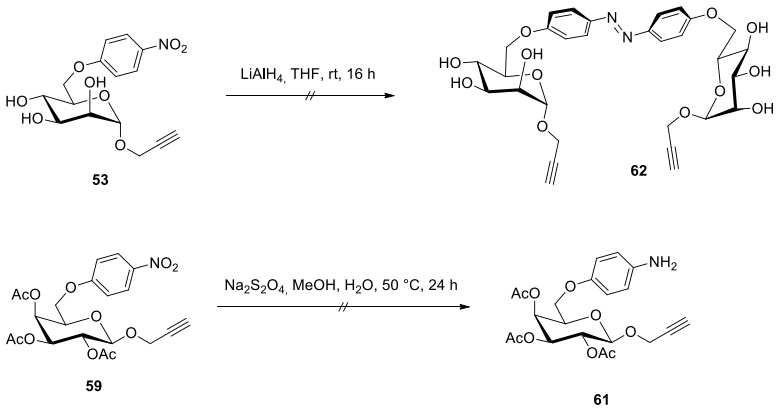

Scheme 6.6: Failed attempts at reduction of **53** and **59**.

Aminophenyl mannoside derivative **63** and galactoside **61** were tested under several oxidizing conditions (Table 6.4). In order to prevent an unwanted reaction on the terminal alkyne, oxidizing reactions using copper(I) reagents as catalyst have been omitted.[163, 164]

At first reactions with organic oxidants, such as hypervalent iodine species[165, 166] and NCS,[167] were tested as they have been reported as highly selective and proceeding under mild reaction conditions and tolerating the terminal alkyne functional group. Also, the use of sodium hypochlorite has been described with the same advantages.[168] However, these reactions all led to complete decomposition of the starting materials before any significant amount of product formation could be detected via TLC reaction control (Entries 1-4).

This led us to take a closer look at the classic oxidation reaction with manganese(IV) oxide, where a first attempt at room temperature, adapted from a procedure to generate *cis*-azobenzene derivatives from hydrazobenzene derivatives[169] lead to moderate yields (Entry 5). In order to improve the yield, various conditions from in the literature were tested. As most of the reported procedures emphasized the importance of anhydrous conditions, increasing measures were taken to ensure water-free reaction conditions. Surprisingly, this had a reverse effect and led to decreasing amounts of isolated product **23** or **43** (Entries 6 – 12). After further literature research, a procedure from 1964 was found in which it was stated that the yields for the synthesis of azobenzene from anilines improved with using less extensive measures of water separation than for other oxidation reactions.[170] Keeping this in mind, performing the reaction without anhydrous conditions and letting MnO_2 equilibrate with the atmospheric moisture as described in the procedure, led to a satisfying yield of 52 % for the synthesis of **43** (Entry 13).

Table 6.4: Different conditions for the oxidative azocoupling.

63 $R^{1/4/5}$ = H, R^2 = -$CH_2C{\equiv}CH$, $R^{3/6}$ = OAc
61 R^1 = -$CH_2C{\equiv}CH$, $R^{2/3/6}$ = H, $R^{4/5}$ = OAc

23 $R^{1/4/5}$ = H, R^2 = -$CH_2C{\equiv}CH$, $R^{3/6}$ = OAc
43 R^1 = -$CH_2C{\equiv}CH$, $R^{2/3/6}$ = H, $R^{4/5}$ = OAc

Entry	Reactant	Oxidizing Conditions	Yield (%)
1[165]	**63**	PIDA, DCM, rt, 5	-
2[166]	**63**	PIDA, EtOH, -20 °C to 65 °C, 30 min	-
3[168]	**63**	NaOCl, HCl, H_2O, EtOH, rt, 30 m	-
4[167]	**61**	NCS, DBU, DCM, -78 °C, 15 min	-
5[169]	**63**	MnO_2, $CHCl_3$, rt, 16 h	25
6	**63**	MnO_2, benzene, 110 °C 16 h [a], [b]	17
7	**63**	MnO_2, toluene, 150 °C, 5 h [a], [b], [c]	14
8	**61**	MnO_2, toluene, 100 °C, 3 h [a], [b], [d]	14
9	**63**	MnO_2, benzene, rt, 4 d [a], [d], [e]	9
10	**63**	MnO_2, toluene, 120 °C, 6 h [a], [b], [d]	traces
11	**63**	MnO_2, toluene, rt, 3 d [a], [b], [d]	traces
12	**63**	MnO_2, toluene, benzene, 50 °C, 4 d [a], [d], [e]	traces
13[170]	**61**	MnO_2, toluene, 110 °C, 16 h	52

[a] dry solvent, [b] drying tube, [c] Dean-Stark apparatus, [d] activated molecular sieves 3Å, [e] N_2 atmosphere

With all the precursors **41**, **42** and **43** in hand, the Glaser coupling for macrocyclization was performed under analogous conditions as those reported for the macrocyclization of the mannose derivative **23**. Again, pre-irradiation of the precursors **41**, **42** and **43** with a 365 nm LED before addition of the reagents CuBr and PMDETA was critical to allow for the intramolecular Glaser coupling to occur. Through isomerization of the azobenzene hinge from the *trans*- to the *cis*-form, the proximity of the terminal alkynes leads to the formation of the diyne bridge and therefore the macrocycles **64**, **65** and **66** respectively (Table 6.5).

The reactions were carried out at different concentrations to optimize the yield. Both β-configured macrocycles **65** and **66** could be obtained in higher yields by increasing the concentration of the reaction mixture to 10 mM. For α-configured **64**, the yield increased until a concentration of 7 mM, before decreasing again. Presumably, the obtained yields could be even higher, but the similarity in their polarity makes the unreacted precursor and the desired product difficult to separate. Further addition of copper(I) bromide and PMDETA did not lead to a full conversion of starting material. The formation of slower moving species could be observed by TLC, but the isolation of side products was not possible. Analysis of the crude material suggests the presence of multiple intermolecular reaction products. As the final step the acetyl groups were cleaved under Zemplén conditions[100] in quantitative yields to obtain the target macrocycles **28**, **29** and **30** (Scheme 6.7).

Table 6.5: Synthesis of **64**, **65** and **66**, with the yields corresponding to the different concentrations for the macrocyclization reactions.

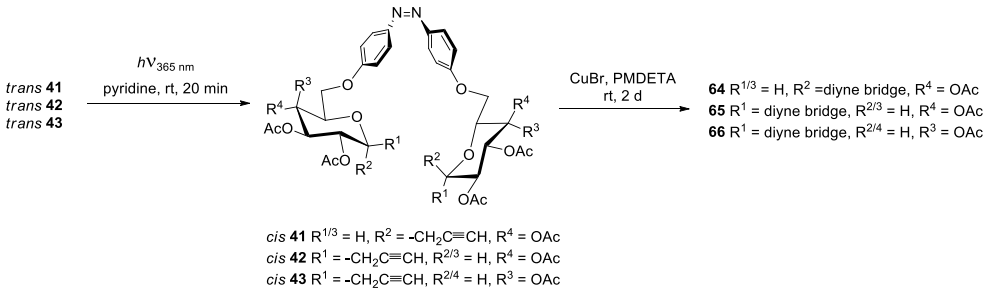

Product	1 mM	2 mM	5 mM	7 mM	10 mM
64	21 %	33 %	44 %	48 %	39 %
65	31 %	39 %	50 %	65 %	69 %
66	18 %	21 %	43 %	55 %	58 %

Scheme 6.7: Synthesis of the target macrocycles **28**, **29** and **30**.

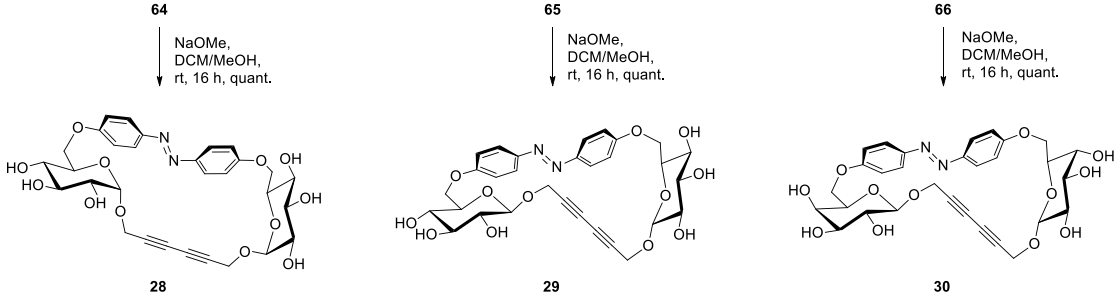

6.4 Photochromic properties of the macrocycles

After the successful synthesis of four glycoazobenzene macrocycles **28**, **29** and **30** differing in their carbohydrate moiety and anomeric configuration, their photochromic properties were assessed using UV/Vis, NMR and CD spectroscopy.

Irradiation of the fully relaxed samples (containing 100 % *trans*-isomer after relaxation for 16 h at 40 °C in the dark) with a 365 nm LED for 5 min led to isomerization to the corresponding *cis*-macrocycles with a minimum of 97 % *cis*-isomer in the photostationary state. The switching efficiency was quantified using ^{1}H NMR by integration of characteristic signals (see chapter 6.7 and Figure 6.56-6.58 in chapter 6.6 for spectra). Although the switching efficiency is nearly quantitative, slight overlap of the *trans* π → π* transition (λ_{max} = 360 nm) with the *cis* π → π* transition (λ_{max} = 315 nm) prevents complete *cis*-isomerization (Figure 6.3). Likewise, full back switching by irradiation, in contrast to thermal isomerization, is not possible due to an overlap of the forbidden n → π* transition for both isomers. Therefore, irradiation with a 520 nm LED lamp led to PSS with a maximum of 15 % remaining *cis*-isomer. Switching the samples back and forth with alternating irradiation wavelengths led to no signs of photobleaching in UV/Vis measurements after 20 cycles (Figure S20 in chapter 6.7 and Figure 6.60 in chapter 6.6).

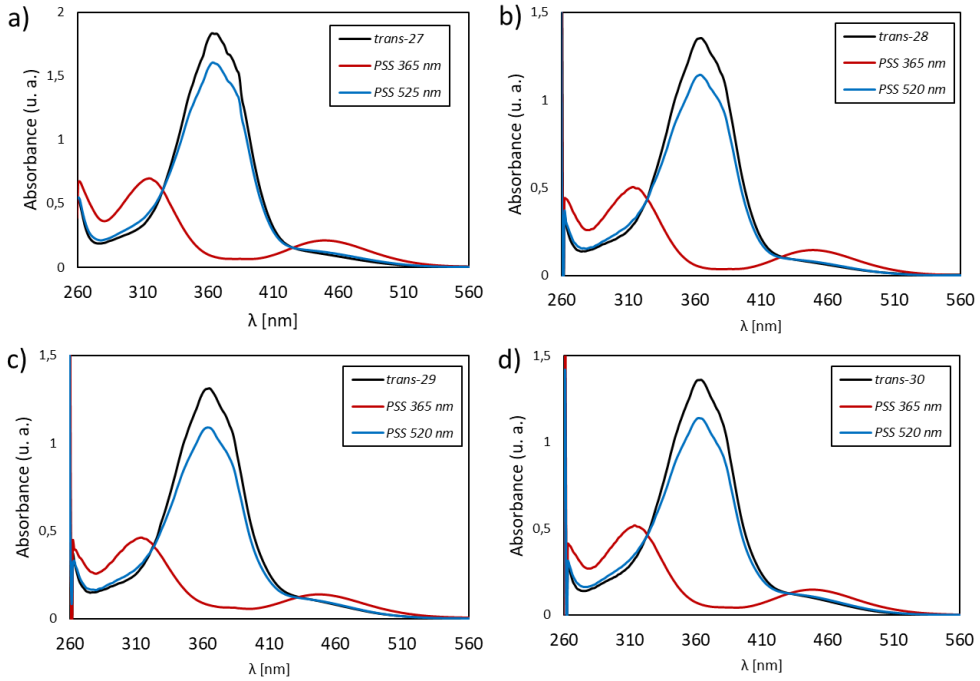

Figure 6.3: Absorption spectra of the synthesized macrocycles in DMSO at 298 K (a) **27** at 100 µM; (b) **28** at 50 µM; (c) **29** at 50 µM; (d) **30** at 50 µM; black line: *trans*-macrocycle, red line: PSS after irradiation with 365 nm for 5 min, blue line: PSS after irradiation with 520 nm for 5 min.

The effect of the anomeric configuration on the shape of the macrocycles cannot be observed by UV/Vis spectroscopy. However, molecular modelling together with NMR studies allow to make assumptions about the shape. Force field-minimized geometries (OPL3 in water)[101] reveal different trapezoid-like structures for the α- and β-configured *trans*-macrocycles. More notable is the difference in the shape of the *cis*-isomers: the α-configured *cis*-macrocycles **27** and **28** form a triangle shape, while

the β-configured *cis*-macrocycles **29** and **30** look similar to a pentagon (Figure 6.3). Both *trans*- and *cis*-macrocycles exhibit a C_2 symmetry with a perpendicular bisector as the axis.

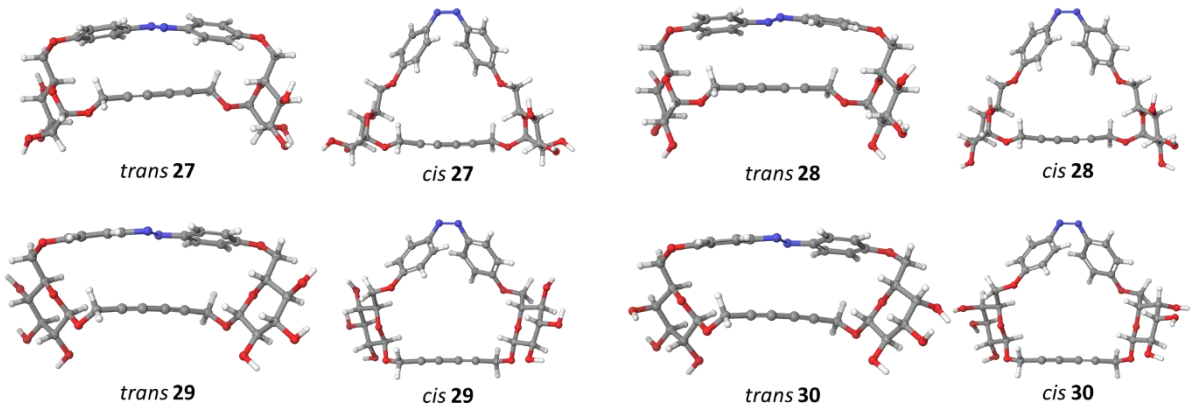

Figure 6.3: Force field-minimized structures (OPL3 in water) of the different *trans*- and *cis*-isomers.[101]

^{1}H NMR provided further insights towards the shape of the cycles. Upon switching to the *cis*-isomer, the signals of the anomeric protons and CH_2 protons of the dyine bridge are subject to a strong downfield shift. This indicates a deshielding effect due to an increased distance to the aromatic rings as a direct result of the shape change induced by the isomerization. To a lesser extent this can also be seen for the rest of the protons in the carbohydrate ring, while the H-6a and H-6b signals are shifted upfield, indicating greater shielding due to an closer proximity to the aromatic rings (Figure 6.4).

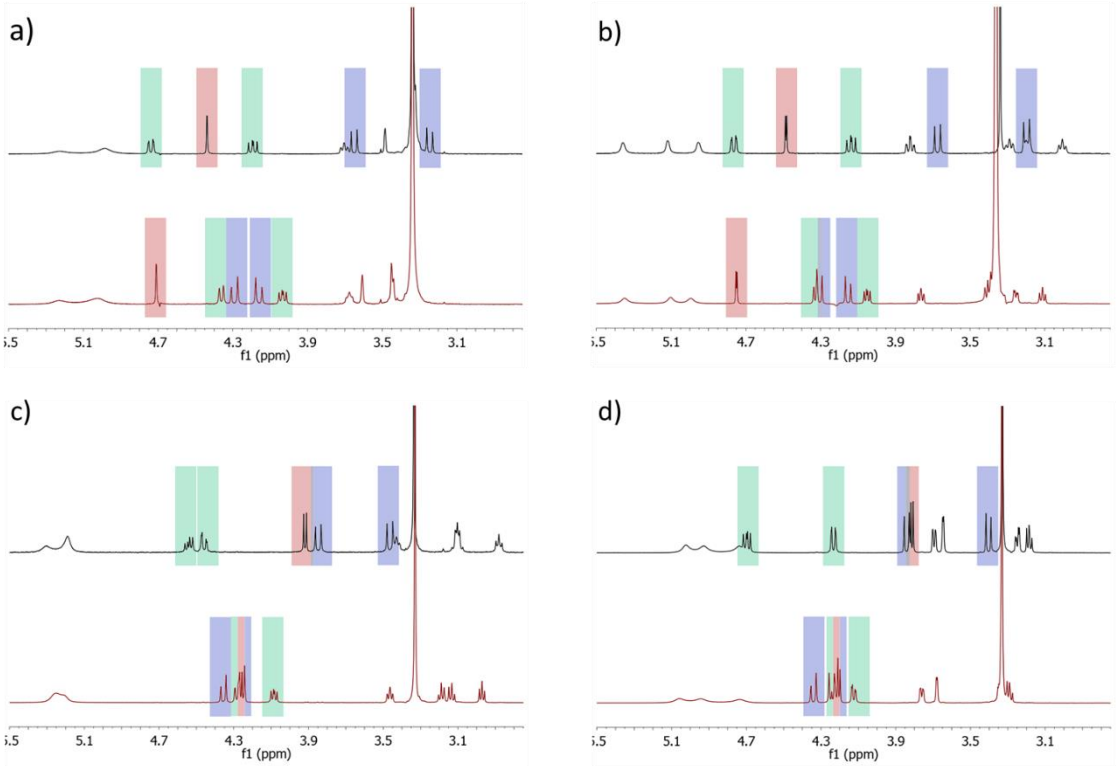

Figure 6.4: Excerpt of the ^{1}H NMR spectra of the different macrocycles (600 MHz, DMSO-d_6, 298 K): (a) **27**; (b) **28**; (c) **29**; (d) **30**; black line: *trans*-macrocycle, red line: PSS after irradiation with 365 nm for 5 min; red highlight: H-1, blue highlight: diyne CH_2a and CH_2b, green highlight: H-6a and H-6b.

Notably, there is a strong correlation between the CD spectra and the anomeric configuration of the macrocycles (Figure 6.5). The observed CD bands correspond to the π → π* and n → π* transitions of

the azobenzene units as seen in the UV/Vis spectra, showing a chirality transfer from the carbohydrate moieties to the photoswitch. The stark difference in the intensities of the CD bands show that this chiral transfer is more favorable for the β-configured macrocycles **29** and **30**, leading to a more twisted conjugated π-electron system.[102, 142] *Trans*-**27** and **28** show a weak negative Cotton effect at 440 nm and a stronger one at 360 nm. Isomerization to *cis*-**27** and **28** led to an increase of the negative Cotton effect corresponding to the n → π* transition at 440 nm and a conversion to a positive Cotton effect for the π → π* transition at 360 nm. For the β-configured *trans*-**29** and **30** the n → π* transition shows a strong positive Cotton effect. The π → π* transition is indiscernible for *trans*-**29** but shows a weak negative Cotton effect for *trans*-**30**. After isomerization to *cis*-**29** and **30**, the intensities of the transitions increase significantly while keeping their respective signs.

The strong Cotton effects in the range of 450 nm in all spectra indicate helical chirality (*P* or *M*), which is caused through the insertion of azobenzene moieties into a strained system.[86, 103, 140-142] It could be shown that due to the dominance of the n → π* transition at 450 nm, *(P)*-chirality shows a negative Cotton effect while *M* chirality shows a positive Cotton effect in that region of the CD spectrum.[82, 86, 104] These findings suggest that the α-configured macrocycles **27** and **28** generate a *(M)*-helical conformation in *trans* and *cis*, while the β-configured **29** and **30** generate a *(P)*-helical conformation for both isomers.

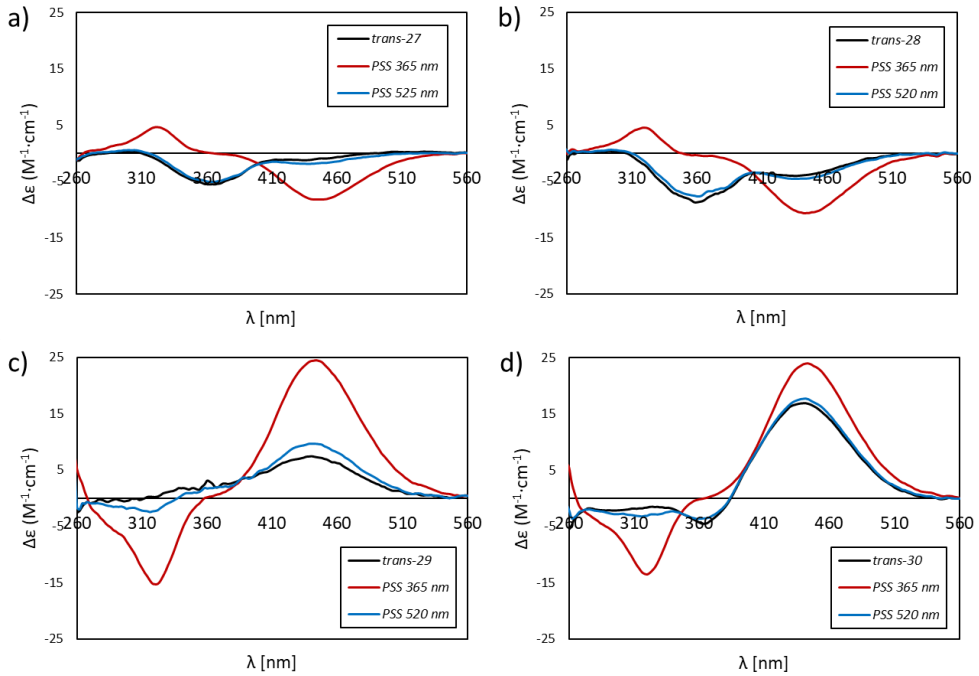

Figure 6.5: CD spectra of the different macrocycles in DMSO at 298 K (a) **27**; (b) **28**; (c) **29**; (d) **30**; black line: *trans*-macrocycle, red line: PSS after irradiation with 365 nm for 5 min, blue line: PSS after irradiation with 520 nm for 5 min.

Compared to the β-configured ones, the α-configured macrocycles show a reduced chiral transfer visible in the CD spectra, lower specific rotation values and a higher half-life of the *cis*-isomer upon thermal relaxation ($\tau_{1/2}$= 55 h and 59 h respectively for **27** and **28**, 18 h and 25 h respectively for **29** and **30**, at 25 °C in DMSO, see Figure 6.61 in chapter 6.6). This suggests that the ring strain of the α-configured macrocycles mannoside **27** and glucoside **28** is lower than for the β macrocycles, presumably leading to less distortion in the conjugated π-electron system and thus a less pronounced helicity.[102] The stability of the *cis*-isomer is increased compared to the β configured macrocycles, which leads to longer relaxation times.[171]

After deprotection, the mannoside macrocycle **27** displayed poor solubility in almost all solvents except DMSO. However, upon trying to measure photochromic properties it could be shown that the solubility in water could be reversibly switched upon isomerization. This is a known effect for azobenzene, as the bent structure of the *cis*-isomers prevents intermolecular interactions which leads to improved aqueous solubility.[120] To test if this was the case for all macrocycles, samples with 500 µg/mL of **27**, **28**, **29** and **30** were prepared in water and heated at 40 °C over night in the dark. Mannoside **27** and galactoside **30** were largely insoluble while the glucosides **28** and **29** were mostly soluble (Figure 6.6). Upon irradiation with 365 nm for 10 min, the suspension of mannoside **27** turned to a clear solution while galactoside **30** became more soluble but the sample remained turbid. Back isomerization with a 520 nm LED or by thermal relaxation again led to the precipitation of **27** and **30**. For the sample containing **28**, back switching with 520 nm led to the precipitation of fine needle-like crystals.

Figure 6.6: Reversible solubility switching of the different macrocycles in water at a concentration of 500 µg/mL: (a) *trans*-rich samples; (b) after irradiation with 365 nm for 10 min; (c) after irradiation with 520 nm for 10 min; from left to right: α-mannoside **27**, α-glucoside **28**, β-glucoside **29**, β-galactoside **30**.

With hopes to find that the solvatation and precipitation of the macrocycles in water led to the formation of defined aggregates, DLS measurements were carried out. However, the results were inconclusive, as the observed particle sizes were either too small or too large for accurate detection, or polydisperse.

In order to test if the solubility of the *trans*-macrocycles would change over time, samples of 15 µL of 10 M stock solutions in DMSO were diluted with 1985 µL water to give samples containing 0.5 % DMSO. As the previous measurements in DMSO showed that the absorbance for all macrocycles was in the same range, UV/Vis spectra were measured in order to quantify a change in solubilty (Table 6.6). The measurements showed that the solubility of the mannoside **27** was the lowest and decreased even more until 24 h after initial mixing, while the solubility of the glucosides remained constant until the experiment was stopped after 72 d. The solubility of galactoside **30**, although considerably higher than of the mannoside **27**, showed a slow but steady decrease over time. These findings suggest that the presence of all-equatorial secondary hydroxyls may be advantageous for solvation in water.

Table 6.6: UV/Vis absorbance at 360 nm of the different macrocycles in 50 µM in DMSO or water containing 0.5 % DMSO.

Macrocyle	Absorbance in DMSO	Absorbance in water after the time of initial mixing: 1 min	30 min	1 d	2 d	5 d	30 d	72 d
27	1,28	0,56	0,55	0,15	0,12	0,08	0,05	0,04
28	1,32	1,24	1,24	1,24	1,24	1,24	1,24	1,24
29	1,29	1,18	1,18	1,17	1,17	1,17	1,17	1,17
30	1,36	1,13	1,12	1,05	1,03	1,03	0,91	0,86

UV/Vis spectra still showed the same pattern in water with 0.5 % DMSO and in pure DMSO, albeit for **27** and **28** with decreased intensity and a higher baseline due to their inclomplete solvatation. This was also the case for the CD spectra of the β-configured **29** and **30** (see Figure 6.62 in chapter 6.6). However, the CD spectra for the α-configured macrocycles **27** and **28** showed a very different pattern for the *trans*-spectra in water with 0.5 % DMSO, with a higher intensity of the n → π* transition (Figure 6.7), in comparison to the measures in pure DMSO. Isomerization to the *cis*-macrocycle led to comparable patterns to the ones measured in DMSO, but with a strongly increased intensity, suggesting a stronger twist of the conjugated π-electron system. Suprisingly, upon back switching with 520 nm, the CD spectrum for **27** did not look similar to the fully relaxed *trans*-spectrum, but showed an altogether new pattern, suggesting that the original state of the fully relaxed sample was not restored yet. The differences in the CD pattern of **27** and **28** upon changing the solvent (DMSO or water with 0.5 % DMSO) showed that the shape and therefore chiroptical response of the α-configured macrocycles is solvent-dependent. Interestingly, this is not the case for their β-configured counterparts **29** and **30**.

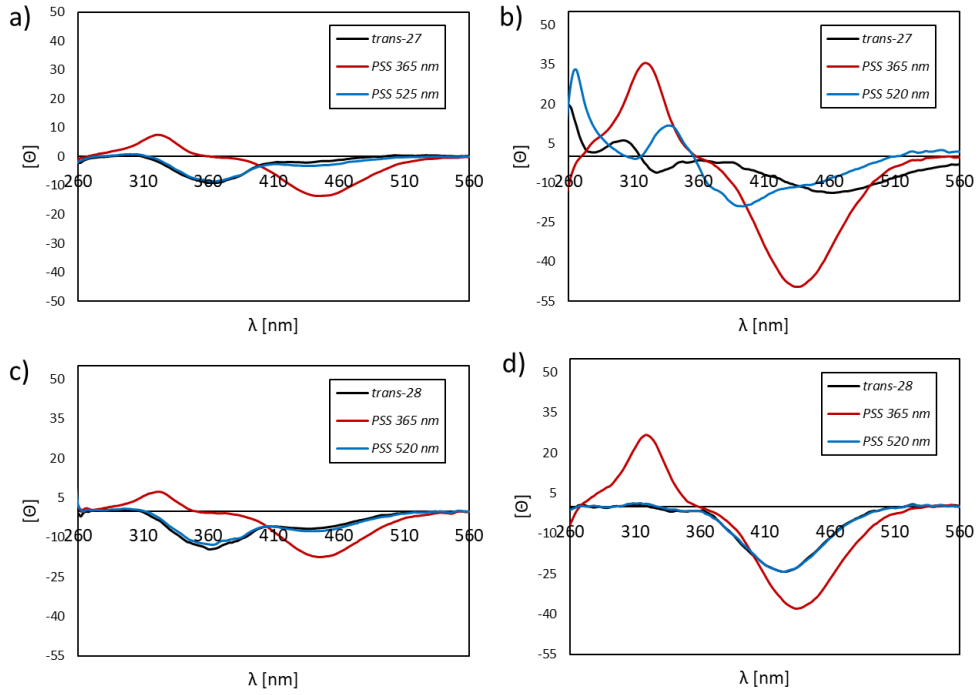

Figure 6.7: CD spectra of the α-configured macrocycles in a concentration of 50 µM in DMSO and water with 0.5 % DMSO at 298 K (a) **27** in DMSO; (b) **27** in water; (c) **28** in DMSO; (d) **28** in water; black line: *trans*-macrocycle, red line: PSS after irradiation with 365 nm for 5 min, blue line: PSS after irradiation with 520 nm for 5 min.

6.5 Conclusion

In summary, the four macrocycles **27**, **28**, **29** and **30** could be synthesized using the Glaser coupling in the key macrocyclization step in good yields of higher than 48 % (Figure 6.8). While the mannoside **27** was the easiest to synthesize in only two steps, the other macrocycles were more difficult to obtain, due to a presumed interference between the Mitsunobu reaction and the configuration of the utilized carbohydrate. Precursors of the glucosides **28** and **29** could be synthesized through Williamson etherification instead, while a synthesis optimization for the Mitsunobu reaction and subsequent oxidative azocoupling led to the precursor of the galactoside **30**.

The photochemical properties of all four macrocycles were tested and it could be shown that there is a strong correlation between the anomeric configuration and the shape, and thus the chirality of the macrocycles (Table 6.7). Additionally, the synthesized compounds show an interesting solvation behavior in water, which is unrelated to the anomeric configuration and shape of the molecule.

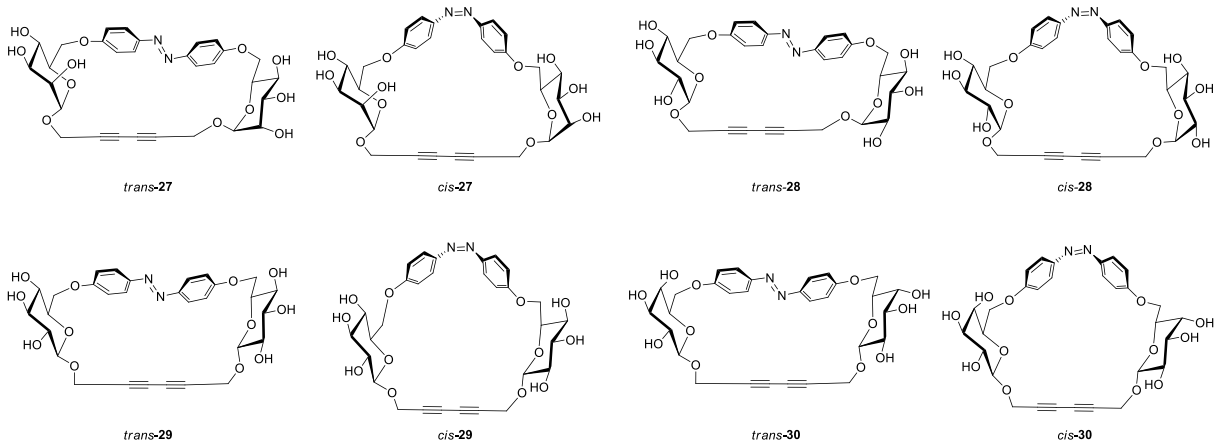

Figure 6.8: Depiction of the synthesized macrocycles in their *trans*- and *cis*-conformation.

Table 6.7: Selected properties of the different macrocycles.

Compound	$[\alpha]^{24}_D$ *trans*[a]	$[\alpha]^{24}_D$ PSS_{365nm}[a]	$\tau_{1/2}$[a,b] [h]	Δε *trans*[a,c] [$M^{-1}cm^{-1}$]	Δε PSS_{365nm}[a,c] [$M^{-1}cm^{-1}$]
27	-146	-576	55	-0.9	-8.1
28	-408	-684	59	-3.6	-11
29	+474	+1959	18	+6.9	+24
30	+893	+1693	25	+16	+23

[a] measured in DMSO, [b] at a concentration of 50 mM, [c] at 450 nm.

6.6 Experimental section

For general methods and instrumentation refer to **4.4**.

Synthesis

2-Propynyl 2-(2,2,2-trifluoroacetamido)-2-deoxy-β-D-glucopyranoside (**38**):

2-trifluoromethyl-(3,4,6-tri-*O*-acetyl-1,2-dideoxy-α-D-glucopyranose)-[1,2,*d*]-2-oxazoline (**40**)[156] (2.37 g, 6.18 mmol) and an equal volume of activated 3 Å molecular sieve were suspended in dry dichloromethane (63.0 mL) under nitrogen and propargyl alcohol (540 µL, 9.13 mmol) was added. The mixture was stirred for 15 min at room temperature before TMSOTf (110 µL, 608 µmol) was added dropwise and stirring was continued for 1 h. NEt_3 (400 µL) was added to quench the reaction mixture before filtration and concentration under reduced pressure. The crude mixture was purified by flash chromatography (cyclohexane/ethyl acetate 3:2). The acetylated product was dissolved in MeOH (20.0 mL), NaOMe (5.4 M, 100 µL) was added and stirred at room temperature for 16 h The mixture was neutralized with Amberlite® IR120 H^+, filtered and concentrated to dryness. The residue was purified by recrystallization from dichloromethane/methanol 9:1 to give **38** (1.37 g, 4.37 mmol, 71 % over two steps) as a white powder.

Mp: 213 °C; $[\alpha]^{20}_D$= -50.1 (c= 1.09 in MeOH); ^{1}H NMR (500 MHz, DMSO-d_6) δ = 9.23 (d, $^3J_{NH,2}$ = 8.3 Hz, 1 H, N*H*), 5.21 (d, $^3J_{OH,3}$ = 5.5 Hz, 1 H, O*H*-3), 5.16 – 5.09 (m, 1 H, O*H*-4), 4.59 (t, $^3J_{OH,6}$ = 6.1 Hz, 1 H, O*H*-6), 4.53 (d, $^3J_{1,2}$ = 8.1 Hz, 1 H, H-1), 4.34 (dd, $^2J_{CH2,CH2}$ = 15.9 Hz, $^4J_{CH2,CH}$ = 2.4 Hz, 1 H, CH_2C≡CHa), 4.25 (dd, $^2J_{CH2,CH2}$ = 15.9 Hz, $^4J_{CH2,CH}$ = 2.4 Hz, 1 H, CH_2C≡CHb), 3.69 (dd, $^2J_{6a,6b}$ = 11.6 Hz, $^3J_{6a,5}$ = 6.6 Hz, 1 H, H-6a), 3.54. – 3.45 (m, 3 H, H-2, H-3, H-6b), 3.44 (t, $^4J_{CH2,CH}$ = 2.4 Hz, 1 H, CH_2C≡C*H*), 3.14 – 3.05 (m, 2 H, H-4, H-5) ppm; ^{13}C NMR (126 MHz, DMSO-d_6) δ = 156.2 (q, ^2J = 35.9 Hz, CF_3*C*=O), 115.9 (q, ^1J = 289 Hz, *C*F_3C=O), 98.1 (C-1), 79.4 (CH_2*C*≡CH), 77.3 (CH_2C≡*C*H), 77.1 (C-5), 72.9 (C-3), 70.3 (C-4), 60.8 (C-6), 55.9 (C-2), 55.0 (*C*H_2C≡CH) ppm; IR (ATR): ũ = 3567, 3459, 3263, 1706, 1570, 1190, 1157, 1079, 1056, 887 cm^{-1}; ESI-MS m/z: calc. 336.06654 for $[C_{11}H_{14}O_6NF_3+Na]^+$; found 336.06613 for $[C_{11}H_{14}O_6NF_3+Na]^+$.

2-Propynyl 2-(2,2,2-trifluoroacetamido)-2-deoxy-3,4-di-*O*-acetyl-6-tosyl-β-D-glucopyranoside (**39**):

Glucopyranoside **38** (429 mg, 137 mmol) was dissolved in dry pyridine (4.00 mL) and cooled to 0 °C, tosyl chloride (522 mg, 2.74 mmol) was added portion wise and the mixture was stirred for 30 min at 0 °C before stirring at room temperature for 3 h. Ac_2O (1.25 mL) was added and stirred at room temperature for 16 h. 2 N HCl (15 mL) was added and the mixture was extracted with DCM (3 x 50 mL), dried over $MgSO_4$, filtered and evaporated under reduced pressure and repeatedly co-evaporated with toluene. The crude residue was purified by flash chromatography (cyclohexane/ethyl acetate 7:3) to give **39** (417 mg, 756 µmol, 55 %) as a white solid.

Mp: 146 °C; $[\alpha]^{20}_D$= -27.9 (c= 1.01 in CH_2Cl_2); ^{1}H NMR (600 MHz, $CDCl_3$) δ = 7.84 – 7.71 (m, 2 H, Ar-H_{ortho}), 7.46 – 7.31 (m, 2 H, Ar-H_{meta}), 6.69 (d, $^3J_{NH,2}$ = 9.1 Hz, 1 H, N*H*), 5.31 (dd, $^3J_{3,2}$ = 10.6 Hz, $^3J_{3,4}$ = 9.4 Hz, 1 H, H-3), 4.96 (dd~t, $^3J_{4,3}$ = $^3J_{4,5}$ = 9.6 Hz, 1 H, H-4), 4.82 (d, $^3J_{1,2}$ = 8.4 Hz, 1 H, H-1), 4.32 (dd, $^2J_{CH2,CH2}$ = 16.0 Hz, $^4J_{CH2,CH}$ = 2.4 Hz, 1 H, CH_2C≡CHa), 4.27 (dd, $^2J_{CH2,CH2}$ = 16.0 Hz, $^4J_{CH2,CH}$ = 2.3 Hz, 1 H, CH_2C≡CHb),

4.15 (dd, $^{2}J_{6a,6b}$ = 11.2 Hz, $^{3}J_{6a,5}$ = 2.9 Hz, 1 H, H-6a), 4.11 (dd, $^{2}J_{6b,6a}$ = 11.2 Hz, $^{3}J_{6a,5}$ = 5.7 Hz, 1 H, H-6b), 4.01 – 3.93 (m, 1 H, H-2), 3.83 (ddd, $^{3}J_{5,4}$ = 9.8 Hz, $^{3}J_{5,6b}$ = 5.7 Hz, $^{3}J_{5,6a}$ = 2.9 Hz, 1 H, H-5), 2.46 (s, 4 H, $CH_2C{\equiv}CH$, Ar-CH_3), 2.03 (s, 3 H, $CH_3C{=}O$), 2.02 (s, 3 H, $CH_3C{=}O$) ppm; ^{13}C NMR (151 MHz, $CDCl_3$) δ = 171.1 ($CH_3C{=}O$), 169.4 ($CH_3C{=}O$), 157.4 (q, ^{2}J = 37.6 Hz, $CF_3C{=}O$), 145.3 (Ar-C_{para}), 132.4 (Ar-C_{ipso}), 130.0 (Ar-C_{meta}), 128.1 (Ar-C_{ortho}), 115.5 (q, ^{1}J = 288 Hz, $CF_3C{=}O$), 97.5 (C-1), 77.9 ($CH_2C{\equiv}CH$), 75.8 ($CH_2C{\equiv}CH$), 71.9 (C-5), 71.5 (C-3), 68.4 (C-4), 67.6 (C-6), 56.1 ($CH_2C{\equiv}CH$), 54.3 (C-2), 21.7 (Ar-CH_3), 20.6 ($CH_3C{=}O$), 20.4 ($CH_3C{=}O$) ppm; IR (ATR): ũ = 3312, 3259, 1750, 1710, 1559, 1344, 1180, 1162, 969, 810, 697 cm^{-1}; ESI-MS m/z: calc. 574.09652 for $[C_{22}H_{24}O_{10}NF_3S+Na]^+$; found 574.09623 for $[C_{22}H_{24}O_{10}NF_3S+Na]^+$.

Williamson Etherification general procedure:

A suspension of the corresponding tosylated glycoside (1.00 g, 2.00 mmol), 4,4'-dihydroxyazobenzene[98] (**5**) (160 mg, 747 µmol) and Cs_2CO_3 (750 mg, 2.30 mmol) in dry DMF (80.0 mL) under nitrogen was stirred at 70 °C for 16 h then concentrated under reduced pressure and co-evaporated with toluene repeatedly. The crude mixture was dissolved in dry pyridine (20.0 mL) and acetic anhydride (10.0 mL, 106 mmol) was added. The mixture was stirred at room temperature for 16 h, then concentrated and co-evaporated with toluene under reduced pressure. The crude residue was dissolved in ethyl acetate (100 mL), washed with water three times (100 mL each) and dried over $MgSO_4$, filtered and concentrated to dryness before purification by flash chromatography (cyclohexane/ethyl acetate 3:2 -> 1:1) to give the precursors as an orange foam.

β-Glucoside precursor **42**:

Prepared from **35**[155] to give 485 mg (560 µmol, 75 %) of **42**.

$[\alpha]^{20}_{D}$= -43.0 (c= 1.02 in CH_2Cl_2); ^{1}H NMR (600 MHz, $CDCl_3$) δ = 7.90 – 7.82 (m, 4 H, Ar-H_{ortho}), 7.02 – 6.94 (m, 4 H, Ar-H_{meta}), 5.31 (dd~t, $^{3}J_{3,2}$ = $^{3}J_{3,4}$ = 9.5 Hz, 2 H, H-3), 5.20 (dd~t, $^{3}J_{4,2}$ = $^{3}J_{4,3}$ = 9.5 Hz, 2 H, H-4), 5.06 (dd, $^{3}J_{2,3}$ = 9.5 Hz, $^{3}J_{2,1}$ = 8.0 Hz, 2 H, H-2), 4.84 (d, $^{3}J_{1,2}$ = 8.0 Hz, 2 H, H-1), 4.37 (dd, $^{4}J_{CH2,\,CH}$ = 2.3 Hz, $^{2}J_{CH2,\,CH2}$ = 1.0 Hz, 4 H, $CH_2C{\equiv}C$), 4.19 – 4.11 (m, 4 H, H-6), 3.93 (ddd, $^{2}J_{5,4}$ = 9.8 Hz, $^{3}J_{5,6a}$ = 5.2 Hz, $^{3}J_{5,6b}$ = 3.3 Hz, 2 H, H-5), 2.47 (t, $^{4}J_{CH,CH2}$ = 2.4 Hz, 2 H, $CH_2C{\equiv}CH$), 2.08 (s, 6 H,2 $CH_3C{=}O$), 2.03 (s, 12 H, 4 $CH_3C{=}O$) ppm; ^{13}C NMR (151 MHz, $CDCl_3$) δ = 170.3 ($CH_3C{=}O$), 169.6 ($CH_3C{=}O$), 169.5 ($CH_3C{=}O$), 160.43(Ar-C_{para}), 147.4 (Ar-C_{ipso}), 124.4 (Ar-C_{ortho}), 114.9 (Ar-C_{meta}), 98.2 (C-1), 78.2 ($CH_2C{\equiv}CH$), 75.5 ($CH_2C{\equiv}CH$), 72.8 (C-3), 72.6 (C-5), 71.1 (C-2), 69.2 (C-4), 67.3 (C-6), 56.0 ($CH_2C{\equiv}CH$), 20.7 (6 C, $CH_3C{=}O$) ppm; IR (ATR): ũ = 3282, 2937, 1749, 1597, 1499, 1367, 1211, 1035, 841 cm^{-1}; ESI-MS m/z: calc. 867.28184 for $[C_{42}H_{46}O_{18}N_2+H]^+$; found 867.28033 for $[C_{42}H_{46}O_{18}N_2+H]^+$.

α-Glucoside precursor **41**:

Prepared from **37**[154, 155] to give 454 mg (523 µmol, 70 %) of **41**.

$[\alpha]^{20}_{D}$= +158 (c= 1.46 in CH_2Cl_2); ^{1}H NMR (500 MHz, $CDCl_3$) δ = 7.88 – 7.83 (m, 4 H, Ar-H_{ortho}), 7.02 – 6.97 (m, 4 H, Ar-H_{meta}), 5.59 – 5.53 (m, 2 H, H-3), 5.34 (d, $^{3}J_{1,2}$ = 3.8 Hz, 2 H, H-1), 5.26 – 5.20 (m, 2 H, H-4), 4.97 (dd, $^{3}J_{2,3}$ = 10.3, $^{3}J_{2,1}$ = 3.8 Hz, 2 H, H-2), 4.33 (d, $^{4}J_{CH2,CH}$ = 2.4 Hz, 4 H, $CH_2C{\equiv}CH$), 4.25 (ddd, $^{3}J_{5,4}$ = 10.3 Hz, $^{3}J_{5,6b}$ = 5.2 Hz, $^{3}J_{5,6a}$ = 2.8 Hz, 2 H, H-5), 4.14 (dd, $^{3}J_{6a,6b}$ = 10.5 Hz, $^{3}J_{6a,5}$ = 2.7 Hz, 2 H, H-6a), 4.10 (dd, $^{3}J_{6b,6a}$ = 10.6 Hz, $^{3}J_{6b,5}$ = 5.2 Hz, 2 H, H-6b), 2.45 (t, $^{4}J_{CH,CH2}$ = 2.4 Hz, 2 H, $CH_2C{\equiv}CH$), 2.10 (s, 6 H, 2 $CH_3C{=}O$), 2.04 (s, 6 H, 2 $CH_3C{=}O$), 2.03 (s, 6 H, 2 $CH_3C{=}O$) ppm; ^{13}C NMR (126 MHz, $CDCl_3$) δ = 170.2 ($CH_3C{=}O$), 170.1 ($CH_3C{=}O$), 169.7 ($CH_3C{=}O$), 160.3 (Ar-C_{para}), 147.4 (Ar-C_{ipso}), 124.4 (Ar-C_{ortho}), 114.9 (Ar-C_{meta}), 94.4 (C-1), 78.2 ($CH_2C{\equiv}CH$), 75.3 ($CH_2C{\equiv}CH$), 70.5 (C-2), 70.0 (C-3), 69.2 (C-4), 68.3 (C-5), 66.9 (C-6), 55.3 ($CH_2C{\equiv}CH$), 20.7 (6 C, $CH_3C{=}O$) ppm; IR (ATR): ũ = 3283, 2938, 1746, 1598, 1500, 1367, 1213,

1029, 841 cm^{-1}; ESI-MS m/z: calc. 867.28184 for $[C_{42}H_{46}O_{18}N_2+H]^+$; found 867.28101 for $[C_{42}H_{46}O_{18}N_2+H]^+$.

1,2:1',2':3,4:3',4'-Tetra-*O*-isopropylidene-6,6'-[(diazene-1,2-diylbis(4,1-phenylene))bis(oxy)]bis(α-D-galactopyranose) (**46**):

Mitsunobu Reaction:

A solution of 1,2:3,4-di-*O*-isopropylidene-α-D-galactopyranose (**45**) (500 mg, 1.92 mmol), 4,4'-dihydroxyazobenzene[98] (**5**) (225 mg, 1.05 mmol) and triphenylphosphine (1.36 g, 5.25 mmol) in dry tetrahydrofurane (13.0 mL) under nitrogen was cooled to 0 °C and azodicarbonyldipiperidine[172] (1.34 g, 5.22 mmol) was added portion wise. The mixture was allowed to warm to room temperature and stirred for 7 d then concentrated under reduced pressure after filtration. The crude residue was purified by flash chromatography (cyclohexane/ethyl acetate 7:3) to give **46** (308 mg, 442 µmol, 46 %) as an orange foam.

Williamson etherification:

A solution of 1,2:3,4-di-*O*-isopropylidene-6-*O*-tosyl-α-D-galactopyranose (**47**)[158] (161 mg, 388µmol), 4,4'-dihydroxyazobenzene[98] (**5**) (40.0 mg, 187 µmol) and Cs_2CO_3 (151 mg, 463 µmol) in dry DMF (15.0 mL) under nitrogen was stirred at 90 °C for 3 h then concentrated under reduced pressure and co-evaporated with toluene repeatedly. The crude mixture was purified by flash chromatography (cyclohexane/ethyl acetate 8:2) to give **46** (19.5 mg, 27.9 µmol, 15 %) as an orange foam.

^{1}H NMR (500 MHz, DMSO-d_6) δ = 7.91 – 7.73 (m, 4 H, Ar-H_{ortho}), 7.18 – 7.06 (m, 4 H, Ar-H_{meta}), 5.51 (d, $^3J_{1,2}$ = 5.0 Hz, 2 H, H-1), 4.66 (dd, $^3J_{3,2}$ = 7.9 Hz, $^3J_{3,4}$ = 2.4 Hz, 2 H, H-3), 4.46 – 4.36 (m, 4 H, H-2, H-4), 4.34 – 4.26 (m, 2 H, H-6a), 4.13 – 4.05 (m, 4 H, H-5, H-6b),), 1.39 (s, 12 H, 4 CH_3), 1.32 (s, 6 H, 2 CH_3), 1.29 (s, 6 H, 2 CH_3) ppm; ^{13}C NMR (126 MHz, DMSO-d_6) δ = 160.8 (Ar-C_{para}), 146.8 (Ar-C_{ipso}), 124.6 (Ar-C_{ortho}), 115.7 (Ar-C_{meta}), 109.1 ($(CH_3)_2C$), 108.4 ($(CH_3)_2C$), 96.1 (C-1), 70.8 (C-3 or C-4), 70.5 (C-3 or C-4), 70.2 (C-2), 67.6 (C-6), 66.3 (C-5), 26.4 (CH_3), 26.2 (CH_3), 25.3 (CH_3), 24.8 (CH_3) ppm; IR (ATR): ũ = 2986, 1598, 1499, 1381, 1251, 1210, 1067, 1000, 841 cm^{-1}; ESI-MS m/z: calc. 699.31235 for $[C_{36}H_{46}O_{12}N_2+H]^+$; found 699.31198 for $[C_{36}H_{46}O_{12}N_2+H]^+$.

2-Propynyl 3,4-*O*-isopropylidene-β- D-galactopyranoside (**48**):

2-Propynyl β-D-galactopyranoside (**33**) (218 mg, 1.00 mmol) was suspended in acetone dimethyl acetal (10.0 mL) under nitrogen and D(+)-camphor-10-sulfonic acid (10.0 mg, 43.0 µmol) was added. The mixture was stirred at room temperature for 2 d before triethylamine (60.0 µL) was added and stirred additionally for 15 min at room temperature. The mixture was concentrated and co-evaporated with toluene under reduced pressure before dissolving in methanol/water (11:1, 6.00 mL) and heating to reflux for 6 h. After concentration under reduced pressure and co-evaporated with toluene repeatedly the crude mixture was purified by flash chromatography (ethyl acetate) to give **48** (187 mg, 723 µmol, 72 %) as a white foam.

^{1}H NMR (500 MHz, DMSO-d_6) δ = 5.37 (d, $^3J_{OH,2}$ = 5.2 Hz, 1 H, OH-2), 4.81 (t, $^3J_{OH,6}$ = 5.8 Hz, 1 H, OH-6), 4.38 (dd, $^2J_{CH2,CH2}$ = 15.8 Hz, $^4J_{CH2,CH}$ = 2.5 Hz, 1 H, CH_2C≡CHa), 4.29 (dd, $^2J_{CH2,CH2}$ = 15.6 Hz, $^4J_{CH2,CH}$ = 2.6 Hz, 1 H, CH_2C≡CHb), 4.27 (d, $^3J_{1,2}$ = 8.0 Hz, 1 H, H-1), 4.11 (dd, $^3J_{4,3}$ = 5.6 Hz, $^3J_{4,5}$ = 2.0 Hz, 1 H, H-4), 3.95 (dd, $^3J_{3,2}$ = 6.9 Hz, $^3J_{3,4}$ = 5.6 Hz, 1 H, H-3), 3.74 (ddd~td, $^3J_{5,6a}$ = $^3J_{5,6b}$ = 6.3 Hz, $^3J_{5,4}$ = 2.0 Hz, 1 H, H-5) 3.58 – 3.54 (m, 2 H, H-6), 3.46 (t, $^4J_{CH2,CH}$ = 2.4 Hz, 1 H, CH_2C≡CH), 3.24 – 3.19 (m, 1 H, H-2), 1.38 (s, 3 H, CH_3), 1.25 (s, 3 H, CH_3) ppm; ^{13}C NMR (126 MHz, DMSO-d_6) δ = 108.5 ($(CH_3)_2C$), 100.2 (C-1), 79.7 (CH_2C≡CH),

79.2 (C-3), 77.3 ($CH_2C{\equiv}\mathit{C}H$), 73.28 (C-5), 73.1 (C-4), 72.1 (C-2), 60.4 (C-6), 54.6 ($\mathit{C}H_2C{\equiv}CH$), 28.0 ($\mathit{C}H_3$), 26.2 ($\mathit{C}H_3$) ppm; ESI-MS m/z: calc. 281.10011 for $[C_{12}H_{18}O_6+Na]^+$; found 281.09959 for $[C_{12}H_{18}O_6+Na]^+$.

2-Propynyl 2-*O*-acetyl-3,4-*O*-isopropylidene-6-*O*-tosyl-β-D-galactopyranoside (**49**):

Galactoside **48** (100 mg, 387 µmol) was dissolved in dry pyridine (1.00 mL) and cooled to 0 °C. Tosyl chloride (90.0 mg, 472 µmol) was added portion wise and the mixture was stirred at 0 °C for 10 min before continuing stirring at room temperature for 2 h. Acetic anhydride (500 µL) was added and the mixture was stirred at room temperature for 16 hours. After addition of dichloromethane and water the aqueous phase was extracted with dichloromethane and the combined organic phase was washed with sat. $NaHCO_3$ solution and brine (20 mL each) and dried over $MgSO_4$, filtered and concentrated to dryness before purification by flash chromatography (cyclohexane/ethyl acetate 7:3) to give **49** (117 mg, 259 µmol, 67 %) as a white foam.

^{1}H NMR (500 MHz, DMSO-d_6) δ = 7.84 – 7.80 (m, 2 H, Ar-H_{ortho}), 7.53 – 7.48 (m, 2 H, Ar-H_{meta}), 4.69 (dd, $^3J_{2,1}$ = 8.2 Hz, $^3J_{2,3}$ = 7.6 Hz, 1 H, H-2), 4.58 (d, $^3J_{1,2}$ = 8.3 Hz, 1 H, H-1), 4.31 (dd, $^2J_{6a,6b}$ = 10.5 Hz, $^3J_{6a,5}$ = 3.3 Hz, 1 H, H-6a), 4.27 (dd, $^2J_{CH2,CH2}$ = 13.8 Hz, $^4J_{CH2,CH}$ = 2.2 Hz, 1 H, CH_2C≡CHa), 4.25 – 4.23 (m, 1 H, H-3), 4.21 (ddd, $^3J_{5,6b}$ = 8.2 Hz, $^3J_{5,6a}$ = 3.2 Hz, $^3J_{5,4}$ = 2.3 Hz, 1 H, H-5), 4.17 (dd, $^3J_{4,3}$ = 5.0 Hz, $^3J_{4,5}$ = 1.7 Hz, 1 H, H-4), 4.15 (dd, $^2J_{CH2,CH2}$ = 16.0 Hz, $^4J_{CH2,CH}$ = 2.4 Hz, 1 H, CH_2C≡CHb), 4.06 (dd, $^2J_{6b,6a}$ = 10.4 Hz, $^3J_{6b,5}$ = 8.3 Hz, 1 H, H-6b), 3.52 (t, $^4J_{CH2,CH}$ = 2.4 Hz, 1 H, $CH_2C{\equiv}\mathit{C}H$), 2.44 (s, 3 H, Ar-CH_3), 2.04 (s, 3 H, CH_3C=O), 1.37 (s, 3 H, CH_3), 1.21 (s, 3 H, CH_3) ppm; ^{13}C NMR (126 MHz, DMSO-d_6) δ = 169.1 ($CH_3\mathit{C}$=O), 145.06 (Ar-C_{ipso}), 132.01 (Ar-C_{para}), 130.15 (Ar-C_{meta}), 127.54 (Ar-C_{ortho}), 109.59 ($(CH_3)_2\mathit{C}$), 97.15 (C-1), 79.08 ($CH_2\mathit{C}$≡CH), 77.66 ($CH_2C{\equiv}\mathit{C}H$), 75.93 (C-3), 72.82 (C-4), 71.92 (C-2), 69.74 (C-5), 69.01 (C-6), 55.10 ($\mathit{C}H_2C{\equiv}CH$), 27.36 ($\mathit{C}H_3$), 26.09 ($\mathit{C}H_3$), 21.02 (Ar-$\mathit{C}H_3$), 20.58 ($\mathit{C}H_3C$=O) ppm; IR (ATR): ũ = 3271, 2922, 1737, 1598, 1450, 1351, 1245, 1173, 1077, 978, 839 cm^{-1}; ESI-MS m/z: calc. 477.11897 for $[C_{21}H_{26}O_9S+Na]^+$; found 477.11864 for $[C_{21}H_{26}O_9S+Na]^+$.

2-Propynyl 6-*O*-(*p*-nitrophenyl)-α-D-manopyranoside (**53**):

A suspension of 2-propynyl α-D-mannopyranoside (**24**)[137] (50 mg, 229 µmol), 4-nitrophenol (**51**) (64.0 mg, 460 µmol) and triphenylphosphine (249 mg, 950 µmol) in dry tetrahydrofurane (2.30 mL) under nitrogen was cooled to 0 °C and diisopropyl azodicarboxylate (110 µL, 522 µmol) was added dropwise. The mixture was allowed to warm to room temperature and stirred for 8 d then concentrated under reduced pressure. The crude residue was purified by flash chromatography (dichloromethane/methanol 9:1) to give **53** (68.5 mg, 202 µmol, 88 %) as an off-white solid.

^{1}H NMR (500 MHz, MeOH-d_4) δ = 8.29 – 8.19 (m, 2 H, Ar-H_{meta}), 7.21 – 7.13 (m, 2 H, Ar-H_{ortho}), 5.01 (d, $^3J_{1,2}$ = 1.6 Hz, 1 H, H-1), 4.45 (dd, $^2J_{6a,6b}$ = 10.7 Hz, $^3J_{6a,5}$ = 1.8 Hz, 1 H, H-6a), 4.35 (dd, $^2J_{6b,6a}$ = 10.7 Hz, $^3J_{6b,5}$ = 5.9 Hz, 1 H, H-6b), 4.30 (dd, $^4J_{CH,CH2}$ = 2.4 Hz, $^2J_{CH2,CH2}$ = 1.5 Hz, 2 H, CH_2C≡CH), 3.89 (ddd, $^3J_{5,4}$ = 8.7 Hz, $^3J_{5,6b}$ = 6.6 Hz, $^3J_{5,6a}$ = 1.5 Hz, 1 H, H-5), 3.87 (dd, $^3J_{2,3}$ = 3.4 Hz, $^3J_{2,1}$ = 1.7 Hz, 1 H, H-2), 3.82 (dd~t, $^3J_{4,3}$ = $^3J_{4,5}$ = 9.6 Hz, 1 H, H-4), 3.75 (dd, $^3J_{3,4}$ = 9.2 Hz, $^3J_{3,2}$ = 3.4 Hz, 1 H, H-3), 2.89 (t, $^4J_{CH,CH2}$ = 2.4 Hz, 1 H, $CH_2C{\equiv}C\mathit{H}$) ppm; IR (ATR): ũ = 3536, 3478, 3370, 3262, 2922, 1591, 1337, 1052, 1002 cm^{-1}; ESI-MS m/z: calc. 362.08464 for $[C_{15}H_{17}O_8N+Na]^+$; found 362.08394 for $[C_{15}H_{17}O_8N+Na]^+$.

2-Propynyl 6-*O*-[*p*-((*tert*-butoxycarbonyl)amino)phenyl]-α-D-mannopyranoside (**54**):

A suspension of 2-propynyl α-D-mannopyranoside (**24**)[137] (438 mg, 2.01 mmol), 4-[(*tert*-butoxycarbonyl)amino]phenyl (**52**)[173] (844 mg, 4.03 mmol) and triphenylphosphine (2.18 g,

8.32 mmol) in dry tetrahydrofurane (20.0 mL) under nitrogen was cooled to 0 °C and diisopropyl azodicarboxylate (960 µL, 4.56 mmol) was added dropwise. The mixture was allowed to warm to room temperature and stirred for 7 d then concentrated under reduced pressure. The crude residue was purified by flash chromatography (dichloromethane/methanol 95:5) to give **54** (629 mg, 1.54 mmol, 77 %) as a white foam.

^{1}H NMR (500 MHz, DMSO-d_6) δ = 9.13 (s, 1 H, N*H*), 7.41 – 7.28 (m, 2 H, Ar-H_{ortho}), 6.96 – 6.73 (m, 2 H, Ar-H_{meta}), 5.00 (d, $^3J_{OH,4}$ = 5.6 Hz, 1 H, O*H*-4), 4.96 (d, $^3J_{OH,2}$ = 4.3 Hz, 1 H, O*H*-2), 4.81 (d, $^3J_{1,2}$ = 1.5 Hz, 1 H, H-1), 4.73 (d, $^3J_{OH,3}$ = 4.3 Hz, 1 H, O*H*-3), 4.25 (dd, $^4J_{CH2,CH}$ = 15.9 Hz, $^2J_{CH2,CH2}$ = 2.4 Hz, 1 H, CH_2C≡CHa), 4.18 – 4.15 (m, 1 H, H-6a), 4.15 (dd, $^4J_{CH2,CH}$ = 15.9 Hz, $^2J_{CH2,CH2}$ = 2.4 Hz, 1 H, CH_2C≡CHb), 4.00 (dd, $^2J_{6b,6a}$ = 10.6 Hz, $^3J_{6b,5}$ = 6.0 Hz, 1 H, H-6b), 3.66 – 3.62 (m, 1 H, H-2), 3.61 – 3.56 (m, 1 H, H-5), 3.56 – 3.51 (m, 1 H, H-4), 3.50 – 3.48 (m, 1 H, H-3), 3.47 (t, $^4J_{CH,CH2}$ = 2.4 Hz, 1 H, CH_2C≡C*H*), 1.47 (s, 9 H, COOC(CH_3)$_3$) ppm; ^{13}C NMR (126 MHz, $CDCl_3$) δ = 153.7 (Ar-C_{ipso}), 152.8 (Ar-C_{para}), 132.5 ((*C*OOC(*C*H_3)$_3$), 119.5 (Ar-C_{ortho}), 114.5 (Ar-C_{meta}), 98.2 (C-1), 79.5 (CH_2*C*≡CH), 78.5 ((COO*C*(CH_3)$_3$), 77.3 (CH_2C≡*C*H), 71.9 (C-5), 70.8 (C-3), 69.9 (C-2), 67.7 (C-6), 66.4 (C-4), 53.1 (*C*H_2C≡CH), 28.1 ((COOC(*C*H_3)$_3$) ppm; IR (ATR): ũ = 3290, 2931, 1693, 1514, 1228, 1157, 1041, 828 cm^{-1}; ESI-MS m/z: calc. 432.16289 for [$C_{20}H_{27}O_8N$+Na]$^+$; found 432.16300 for [$C_{20}H_{27}O_8N$+Na]$^+$.

2-Propynyl 2,3,4-tri-*O*-acetyl-6-*O*-(*p*-aminophenyl)-β-D-galactopyranoside (**63**):

Mannopyranoside **54** (625 mg, 1.53 mmol) was dissolved in dry pyridine (6.00 mL) and acetic anhydride (3.00 mL, 31.8 mmol) was added. The mixture was stirred at room temperature for 16 h, then concentrated under reduced pressure and co-evaporated with toluene repeatedly. The residue was dissolved in dichloromethane (5.00 mL) and trifluoroacetic acid (500 µL) was added dropwise and stirred at room temperature for 16 h. The mixture was diluted with dichloromethane, washed with sat. $NaHCO_3$ solution and brine (50 mL each) and dried over $MgSO_4$, filtered and concentrated to dryness to give **63** (658 mg, 1.52 mmol, 99 %) as a white foam.

^{1}H NMR (500 MHz, DMSO-d_6) δ = 6.69 – 6.60 (m, 2 H, Ar-H_{ortho}), 6.54 – 6.43 (m, 2 H, Ar-H_{meta}), 5.25 (t, $^3J_{4,3}$ = $^3J_{4,5}$ = 9.8 Hz, 1 H, H-4), 5.15 – 5.09 (m, 2 H, H-2, H-3), 5.04 – 5.00 (m, 1 H, H-1), 4.64 (s, 2 H, NH_2), 4.36 (dd, $^2J_{CH2,CH2}$ = 16.0 Hz, $^4J_{CH2,CH}$ = 2.4 Hz, 1 H, CH_2C≡CHa), 4.27 (dd, $^2J_{CH2,CH2}$ = 16.0 Hz, $^4J_{CH2,CH}$ = 2.4 Hz, 1 H, CH_2C≡CHb), 3.99 (ddd, $^3J_{5,4}$ = 9.9 Hz, $^3J_{5,6b}$ = 4.8 Hz, $^3J_{5,6a}$ = 3.0 Hz, 1 H, H-5), 3.94 (dd, $^2J_{6a,6b}$ = 10.8 Hz, $^3J_{6a,5}$ = 2.9 Hz, 1 H, H-6a), 3.88 (dd, $^2J_{6b,6a}$ = 10.8 Hz, $^3J_{6a,5}$ = 5.0 Hz, 1 H, H-6b), 3.56 (t, $^4J_{CH,CH2}$ = 2.4 Hz, 1 H, CH_2C≡C*H*), 2.13 (s, 3 H, CH_3C=O), 2.01 (s, 3 H, CH_3C=O), 1.95 (s, 3 H, CH_3C=O) ppm; ^{13}C NMR (151 MHz, DMSO-d_6) δ = 169.7 (2 CH_3*C*=O), 169.3 (CH_3*C*=O), 149.4 (Ar-C_{ipso}), 142.9 (Ar-C_{para}), 115.9 (Ar-C_{ortho}), 114.8 (Ar-C_{meta}), 95.3 (C-1), 78.8 (CH_2C≡*CH*), 78.2 (CH_2*C*≡CH), 68.9 (C-5), 68.8 (C-3), 68.6 (C-2), 67.5 (C-6), 65.7 (C-4), 54.3 (*C*H_2C≡CH), 20.6 (*C*H_3C=O), 20.5 (*C*H_3C=O), 20.4 (*C*H_3C=O) ppm; IR (ATR): ũ = 3370, 3274, 2925, 1742, 1510, 1215, 1073, 1043, 825 cm^{-1}; ESI-MS m/z: calc. 436.16021 for [$C_{21}H_{25}O_9N$+H]$^+$; found 436.16005 for [$C_{21}H_{25}O_9N$+H]$^+$.

2-Propynyl 6-*O*-[*p*-((*tert*-butoxycarbonyl)amino)phenyl]-β-D-glucopyranoside (**55**):

A suspension of 2-propynyl β-D-glucopyranoside (**32**)[137] (438 mg, 2.01 mmol), 4-[(*tert*-butoxycarbonyl)amino]phenyl (**52**)[173] (844 mg, 4.03 mmol) and triphenylphosphine (2.18 g, 8.32 mmol) in dry tetrahydrofurane (20.0 mL) under nitrogen was cooled to 0 °C and diisopropyl azodicarboxylate (960 µL, 4.56 mmol) was added dropwise. The mixture was allowed to warm to room temperature and stirred for 7 d then concentrated under reduced pressure. The crude residue was purified by flash chromatography (dichloromethane/methanol 19:1) to give **55** (123 mg, 300 µmol, 15 %) as a white foam.

^{1}H NMR (500 MHz, MeOH-d_4) δ = 7.38 – 7.22 (m, 2 H, Ar-H_{ortho}), 6.98 – 6.87 (m, 2 H, Ar-H_{meta}), 4.53 (d, $^3J_{1,2}$ = 7.8 Hz, 1 H, H-1), 4.42 (dd, $^4J_{CH2,CH}$ = 15.7 Hz, $^2J_{CH2,CH2}$ = 2.5 Hz, 1 H, CH_2C≡CHa), 4.38 (dd, $^4J_{CH2,CH}$ = 15.7 Hz, $^2J_{CH2,CH2}$ = 2.4 Hz, 1 H, CH_2C≡CHb), 4.30 (dd, $^2J_{6a,6b}$ = 10.7 Hz, $^3J_{6a,5}$ = 1.9 Hz, 1 H, H-6a), 4.15 (dd, $^2J_{6b,6a}$ = 10.8 Hz, $^3J_{6b,5}$ = 5.6 Hz, 1 H, H-6b), 3.59 (ddd, , $^3J_{5,4}$ = 9.3 Hz, $^3J_{5,6b}$ = 5.6 Hz, $^3J_{5,6a}$ = 1.9 Hz, 1 H, H-5), 3.47 (dd~t, $^3J_{4,5}$ = $^3J_{4,3}$ = 9.2 Hz, 1 H, H-4), 3.43 (dd~t, $^3J_{3,4}$ = $^3J_{3,2}$ = 8.8 Hz, 1 H, H-3), 3.27 (dd, $^3J_{2,3}$ = 8.8 Hz, $^3J_{2,1}$ = 7.9 Hz 1 H, H-2), 2.89 (t, $^4J_{CH,CH2}$ = 2.4 Hz, 1 H, CH_2C≡CH), 1.54 (s, 9 H, COOC(CH_3)$_3$) ppm; ESI-MS m/z: calc. 432.16289 for [$C_{20}H_{27}O_8N$+Na]$^+$; found 432.16281 for [$C_{20}H_{27}O_8N$+Na]$^+$.

1,2:3,4-Di-*O*-isopropylidene-6-*O*-(*p*-nitrophenyl)-α-D-galactopyranose (**57**):

A solution of 1,2:3,4-di-*O*-isopropylidene-α-D-galactopyranose (**45**) (2.00 g, 7.70 mmol), 4-nitrophenol (**51**) (2.14 g, 15.4 mmol) and triphenylphosphine (8.05 g, 31.1 mmol) in dry tetrahydrofurane (120 mL) under nitrogen was cooled to 0 °C and diisopropyl azodicarboxylate (6.00 mL, 28.5 mmol) was added dropwise. The mixture was allowed to warm to room temperature and stirred for 1 d then concentrated under reduced pressure. The crude residue was suspended in cyclohexane and warmed to 40 °C before filtering the phosphine oxide off. After concentration of the remaining solution under reduced pressure it was purified by flash chromatography (toluene/ethyl acetate 9:1) to give **57** (1.49 g, 3.90 mmol, 51 %) as a white foam. Analytical and spectroscopic data were found to be in agreement with reported literature.[174]

1,2,3,4-Tetra-*O*-acetyl-6-*O*-(*p*-nitrophenyl)-D-galactopyranose (**58**):

Galactopyranose **57** (690 mg, 1.81 mmol) was dissolved in water/TFA (9:1, 10.0 mL) and stirred at room temperature for 6 hours before concentrating under reduced pressure and repeated co-evaporation with toluene. The crude substance was dissolved in dry pyridine (6.00 mL), Ac_2O (3.00 mL) was added and stirred at room temperature for 16 hours before concentrating the mixture under reduced pressure and repeated co-evaporation with toluene. The crude residue was purified by flash chromatography (toluene/ethyl acetate 9:1) to give **58** (329 mg, 701 µmol, 39 %) as a white solid.

^{1}H NMR (600 MHz, $CDCl_3$) δ = 8.21 – 8.16 (m, 2 H, Ar-H_{meta}), 6.96 – 6.90 (m, 2 H, Ar-H_{ortho}), 6.42 (d, $^3J_{1,2}$ = 3.3 Hz, 1 H, H-1α), 5.76 (d, $^3J_{1,2}$ = 8.3 Hz, 1 H, H-1β), 5.71 – 5.67 (m, 1 H, H-4α), 5.62 (d, $^3J_{4,3}$ = 3.3 Hz, 1 H, H-4β), 5.44 – 5.35 (m, 3 H, H-2α, H-2β, H-3α), 5.15 (dd, $^3J_{3,2}$ = 10.4 Hz, $^3J_{3,4}$ = 3.4 Hz, 1 H, H-3β), 4.53 (dd~t, $^3J_{5,6a}$ = $^3J_{5,6b}$ = 6.4 Hz, 2 H, H-5α), 4.26 – 4.19 (m, 2 H, H-5β, H-6aβ), 4.15 (dd, $^2J_{6a,6b}$ = 9.4 Hz, $^3J_{6a,5}$ = 6.0 Hz, 1 H, H-6aα), 4.07 – 3.98 (m, 2 H, H-6bα, H-6bβ), 2.18 (s, 3 H, CH_3C=O), 2.14 (s, 6 H, CH_3C=O), 2.12 (s, 3 H, CH_3C=O), 2.07 (s, 3 H, CH_3C=O), 2.04 (s, 3 H, CH_3C=O), 2.03 (s, 3 H, CH_3C=O), 2.02 (s, 3 H, CH_3C=O) ppm; ^{13}C NMR (151 MHz, $CDCl_3$) δ = 170.2 (CH_3*C*=O), 170.0 (3 CH_3*C*=O), 169.9 (CH_3*C*=O), 169.4 (CH_3*C*=O), 169.0 (CH_3*C*=O), 168.9 (CH_3*C*=O), 162.7 (Ar-C_{ipso}), 142.2 (Ar-C_{para}), 126.0 (Ar-C_{meta}), 114.6 (Ar-C_{ortho}), 92.2 (C-1β), 89.7 (C-1α), 72.0 (C-5β), 70.8 (C-3β), 69.2 (C-5α), 67.7 (C-2β), 67.6 (C-4α), 67.3 (C-2α), 67.0 (C-4β), 66.4 (C-3α), 66.0 (C-6α), 65.7 (C-6β), 20.9 (s), 20.7 (3 *C*H_3C=O), 20.6 (4 *C*H_3C=O) ppm; IR (ATR): ũ = 1744, 1592, 1341, 1206, 1065, 1039, 1012, 847 cm^{-1}; ESI-MS m/z: calc. 492.11125 for [$C_{20}H_{23}O_{12}N$+Na]$^+$; found 492.11051 for [$C_{20}H_{23}O_{12}N$+Na]$^+$.

2-Propynyl 2,3,4-tri-*O*-acetyl-6-*O*-(*p*-nitrophenyl)-β-D-galactopyranoside (**59**):

Galactopyranose **59** (150 mg, 319 µmol) was dissolved in dry dichloromethane (2.50 mL) under nitrogen and cooled to 0 °C and propargyl alcohol (25.0 µL, 423 µmol) and BF_3·Et_2O (60.0 µL) were added. Stirred at room temperature for 2.5 h before adding K_2CO_3 (50.0 mg) and stirring for an additional 30 min. The crude mixture was filtered, diluted with ethyl acetate and washed three times

with water (25 mL each) before drying over $MgSO_4$ and concentrating under reduced pressure. The crude residue was purified by flash chromatography (toluene/ethyl acetate 9:1 and cyclohexane/ethyl acetate 7:3) to give 336 (48.3, 104 µmol, 33 %) as a white solid.

^{1}H NMR (600 MHz, $CDCl_3$) δ = 8.27 – 8.15 (m, 2 H, Ar-H_{meta}), 7.01 – 6.89 (m, 2 H, Ar-H_{ortho}), 5.58 (d, $^3J_{4,3}$ = 3.3 Hz, 1 H, H-4), 5.27 (dd, $^3J_{2,3}$ = 10.4 Hz, $^3J_{2,1}$ = 8.0 Hz, 1 H, H-2), 5.13 (dd, $^3J_{3,2}$ = 10.4 Hz, $^3J_{3,4}$ = 3.4 Hz, 1 H, H-3), 4.81 (d, $^3J_{1,2}$ = 8.0 Hz, 1 H, H-1), 4.39 (d, $^4J_{CH2,CH}$ = 2.2 Hz, 2 H, CH_2C≡CH), 4.22 (dd, $^2J_{6a,6b}$ = 9.2 Hz, $^3J_{6a,5}$ = 6.0 Hz, 1 H, H-6a), 4.13 (dd~t, $^3J_{5,6a}$ = $^3J_{5,6b}$ = 6.2 Hz, 1 H, H-5), 4.08 (dd, $^2J_{6b,6a}$ = 9.2 Hz, $^3J_{6a,5}$ = 6.5 Hz, 1 H, H-6b), 2.48 (t, $^4J_{CH,CH2}$ = 2.1 Hz, 1 H, CH_2C≡C*H*), 2.13 (s, 3 H, CH_3C=O), 2.09 (s, 3 H, CH_3C=O), 2.01 (s, 3 H, CH_3C=O) ppm; ^{13}C NMR (151 MHz, $CDCl_3$) δ = 170.16 (CH_3*C*=O), 170.13 (CH_3*C*=O), 169.60 (CH_3*C*=O), 162.92 (Ar-C_{ipso}), 142.13 (Ar-C_{para}), 125.98 (Ar-C_{meta}), 114.63 (Ar-C_{ortho}), 98.80 (C-1), 78.09 (CH_2C≡*C*H), 75.54 (CH_2*C*≡CH), 71.49 (C-5), 70.83 (C-3), 68.44 (C-2), 67.26 (C-4), 66.17 (C-6), 56.05 (*C*H_2C≡CH), 20.81 (*C*H_3C=O), 20.65 (*C*H_3C=O), 20.60 (*C*H_3C=O) ppm; IR (ATR): ũ = 3274, 2929, 1743, 1592, 1341, 1213, 1075, 1056, 846 cm^{-1}; ESI-MS m/z: calc. 488.11633 for [$C_{21}H_{23}O_{11}$N+Na]$^+$; found 488.11641 for [$C_{21}H_{23}O_{11}$N+Na]$^+$.

2-Propynyl 2,3,4-tri-*O*-acetyl-6-*O*-[*p*-((*tert*-butoxycarbonyl)amino)phenyl]-β-D-galactopyranoside (**60**):

A suspension of 2-propynyl β-D-galactopyranoside (**33**)[153] (500 mg, 2.29 mmol), 4-[(*tert*-butoxycarbonyl)amino]phenyl (**52**)[173] (963 mg, 4.60 mmol) and triphenylphosphine (2.49 g, 9.50 mmol) in dry tetrahydrofurane (30.0 mL) under nitrogen was cooled to 0 °C and diisopropyl azodicarboxylate (1.10 mL, 5.22 mmol) was added dropwise. The mixture was allowed to warm to room temperature and stirred for 7 d then concentrated under reduced pressure. The crude residue was purified by flash chromatography (dichloromethane/methanol 9:1) to give a mixture of the unprotected product and excess **33**. The crude mixture was dissolved in dry pyridine (2.00 mL) and acetic anhydride (1.00 mL, 10.6 mmol) was added. The mixture was stirred at room temperature for 16 h, then concentrated under reduced pressure and co-evaporated with toluene repeatedly. The crude residue was purified by flash chromatography (cyclohexane/ethyl acetate 4:1 -> 3:1) to give **60** (374 mg, 698 µmol, 30 % over two steps) as a white foam.

[α]$^{20}_D$= -16.3 (c= 0.02 in CH_2Cl_2); ^{1}H NMR (600 MHz, $CDCl_3$) δ = 7.26 – 7.23 (m, 2 H, Ar-H_{ortho}), 6.83 – 6.79 (m, 2 H, Ar-H_{meta}), 6.34 (s, 1 H, NH), 5.58 – 5.55 (m, 1 H, H-4), 5.25 (dd, $^3J_{2,3}$ = 10.4 Hz, $^3J_{2,1}$ = 8.0 Hz, 1 H, H-2), 5.11 (dd, $^3J_{3,2}$ = 10.4 Hz, $^3J_{3,4}$ = 3.4 Hz, 1 H, H-3), 4.78 (d, $^3J_{1,2}$ = 8.0 Hz, 1 H, H-1), 4.39 (dd~t, $^4J_{CH2,CH}$ = $^2J_{CH2,CH2}$ = 2.0 Hz, 2 H, CH_2C≡CH), 4.10 (dd, $^2J_{6a,6b}$ = 9.2 Hz, $^3J_{6a,5}$ = 5.9 Hz, 1 H, H-6a), 4.08 – 4.04 (m, 1 H, H-5), 3.95 (dd, $^2J_{6b,6a}$ = 9.2 Hz, $^3J_{6b,5}$ = 6.7 Hz, 1 H, H-6b), 2.47 (t, $^4J_{CH,CH2}$ = 2.4 Hz, 1 H, CH_2C≡C*H*), 2.10 (s, 3 H, CH_3C=O), 2.08 (s, 3 H, CH_3C=O), 2.00 (s, 3 H, CH_3C=O), 1.50 (s, 9 H, COOC(*C*H_3)$_3$) ppm; ^{13}C NMR (151 MHz, $CDCl_3$) δ = 170.2 (CH_3*C*=O), 170.1 (CH_3*C*=O), 169.7 (CH_3*C*=O), 154.1 (Ar-C_{ipso}), 153,1 (Ar-C_{para}), 132.2 ((*C*OOC(CH$_3$)$_3$), 120.4 (Ar-C_{ortho}), 115.3 (Ar-C_{meta}), 98.7 (C-1), 80.4 (COO*C*(CH$_3$)$_3$), 78.3 (CH_2C≡*C*H), 75.4 (CH_2*C*≡CH), 71.7 (C-5), 71.0 (C-3), 68.6 (C-2), 67.3 (C-4), 66.0 (C-6), 56.0 (*C*H_2C≡CH), 28.4 ((COOC(*C*H$_3$)$_3$), 20.8 (*C*H_3C=O), 20.7 (*C*H_3C=O), 20.6 (*C*H_3C=O) ppm; IR (ATR): ũ = 3287, 2980, 1747, 1514, 1367, 1215, 1157, 1051 cm^{-1}; ESI-MS m/z: calc. 536.21264 for [$C_{26}H_{33}O_{11}$N+H]$^+$; found 536.21212 for [$C_{26}H_{33}O_{11}$N+H]$^+$.

2-Propynyl 2,3,4-tri-*O*-acetyl-6-*O*-(*p*-aminophenyl)-β-D-galactopyranoside (**61**):

To a solution of 2-propynyl 2,3,4-tri-*O*-acetyl-6-*O*-[*p*-((*tert*-butoxycarbonyl)amino)phenyl]-β-D-galactopyranoside (**60**) (320 mg, 597 µmol) in dichloromethane (5.00 mL) trifluoroacetic acid (300 µL) was added dropwise and stirred at room temperature for 16 h. The mixture was diluted with ethyl acetate (100 mL), washed with sat. $NaHCO_3$ solution and brine (100 mL each) and dried over $MgSO_4$, filtered and concentrated to dryness to give **61** (257 mg, 589 µmol, 99 %) as a white foam.

$[\alpha]^{20}_D$= -57.5 (c= 1.10 in CH_2Cl_2); ^{1}H NMR (500 MHz, DMSO-d_6) δ = 6.68 – 6.58 (m, 2 H, Ar-H_{ortho}), 6.53 – 6.43 (m, 2 H, Ar-H_{meta}), 5.36 (dd, $^3J_{4,3}$ = 3.6 Hz, $^3J_{4,5}$ = 0.9 Hz, 1 H, H-4), 5.23 (dd, $^3J_{3,2}$ = 10.4 Hz, $^3J_{3,4}$ = 3.6 Hz, 1 H, H-3), 4.95 (dd, $^3J_{2,3}$ = 10.4 Hz, $^3J_{2,1}$ = 8.0 Hz, 1 H, H-2), 4.84 (d, $^3J_{1,2}$ = 8.0 Hz, 1 H, H-1), 4.64 (s, 2 H, NH_2), 4.36 (dd, $^2J_{CH2,CH2}$ = 16.0 Hz, $^4J_{CH2,CH}$ = 2.5 Hz, 1 H, CH_2C≡CHa), 4.32 – 4.24 (m, 2 H, H-5, CH_2C≡CHb), 3.92 (dd, $^2J_{6a,6b}$ = 10.0 Hz, $^3J_{6a,5}$ = 6.3 Hz, 1 H, H-6a), 3.81 (dd, $^2J_{6b,6a}$ = 10.0 Hz, $^3J_{6a,5}$ = 6.5 Hz, 1 H, H-6b), 3.53 (t, $^4J_{CH,CH2}$ = 2.4 Hz, 1 H, CH_2C≡C*H*), 2.09 (s, 3 H, CH_3C=O), 2.03 (s, 3 H, CH_3C=O), 1.92 (s, 3 H, CH_3C=O) ppm; ^{13}C NMR (126 MHz, DMSO-d_6) δ = 169.8 (CH_3*C*=O), 169.4 (CH_3*C*=O), 169.1 (CH_3*C*=O), 149.2 (Ar-C_{ipso}), 142.9 (Ar-C_{para}), 115.7 (Ar-C_{ortho}), 114.7 (Ar-C_{meta}), 98.2 (C-1), 79.2 (CH_2*C*≡CH), 77.7 (CH_2C≡*C*H), 70.5 (C-5), 70.3 (C-3), 68.5 (C-2), 67.3 (C-4), 66.3 (C-6), 55.6 (*C*H_2C≡CH), 20.5 (*C*H_3C=O), 20.3 (2 C, *C*H_3C=O) ppm; IR (ATR): ũ = 3272, 1741, 1511, 1214, 1043 827 cm^{-1}; ESI-MS m/z: calc. 436.16021 for $[C_{21}H_{25}O_9N+H]^+$; found 436.15956 for $[C_{21}H_{25}O_9N+H]^+$.

β-Galactoside precursor **43**:

To a solution of 2-propynyl 2,3,4-tri-*O*-acetyl-6-*O*-(*p*-aminophenyl)-β-D-galactopyranoside (**61**) (80.0 mg, 184 µmol) in toluene (1.80 mL) MnO_2 (128 mg, 1.48 mmol) was added and stirred at 110 °C for 16 h. The suspension was filtered over a Celite pad and concentrated under reduced pressure. The crude residue was purified by flash chromatography (cyclohexane/ethyl acetate 2:1) to give **43** (41.9 mg, 48.3 µmol, 52 %) as an orange foam.

$[\alpha]^{20}_D$= -94.5 (c= 0.87 in CH_2Cl_2); ^{1}H NMR (500 MHz, $CDCl_3$) δ = 7.87 – 7.83 (m, 4 H, Ar-H_{ortho}), 6.99 – 6.96 (m, 4 H, Ar-H_{meta}), 5.60 (dd, $^3J_{4,3}$ = 3.4, $^3J_{4,5}$ = 0.9 Hz, 2 H, H-4), 5.27 (dd, $^3J_{2,3}$ = 10.5, $^3J_{2,1}$ = 8.0 Hz, 2 H, H-2), 5.14 (dd, $^3J_{3,2}$ = 10.4, $^3J_{3,4}$ = 3.4 Hz, 2 H, H-3), 4.81 (d, $^3J_{1,2}$ = 8.0, 2 H, H-1), 4.41 (dd, $^4J_{CH2,CH}$ = 2.3 Hz, $^2J_{CH2,CH2}$ = 0.9 Hz, 4 H, CH_2C≡CH), 4.22 (dd, $^3J_{6a,6b}$ = 9.1 Hz, $^3J_{6a,5}$ = 5.8 Hz, 2 H, H-6a), 4.15 – 4.11 (m, 2 H, H-5), 4.07 (dd, $^3J_{6b,6a}$ = 9.1 Hz, $^3J_{6b,5}$ = 6.6 Hz, 2 H, H-6b), 2.48 (t, $^4J_{CH,CH2}$ = 2.4 Hz, 2 H, CH_2C≡C*H*), 2.12 (s, 6 H, 2 CH_3C=O), 2.09 (s, 6 H, 2 CH_3C=O), 2.01 (s, 6 H, 2 CH_3C=O) ppm; ^{13}C NMR (126 MHz, $CDCl_3$) δ = 170.2 (CH_3*C*=O), 170.1 (CH_3*C*=O), 169.6 (CH_3*C*=O), 160.1 (Ar-C_{para}), 147.5 (Ar-C_{ipso}), 124.4 (Ar-C_{ortho}), 114.9 (Ar-C_{meta}), 98.8 (C-1), 78.2 (CH_2*C*≡CH), 75.4 (CH_2C≡*C*H), 71.7 (C-5), 71.0 (C-3), 68.6 (C-2), 67.3 (C-4), 65.8 (C-6), 56.0 (*C*H_2C≡CH), 20.8 (*C*H_3C=O), 20.7 (*C*H_3C=O), 20.6 (*C*H_3C=O) ppm; IR (ATR): ũ = 3283, 1750, 1599, 1501 1369, 1223, 1079, 764 cm^{-1}; ESI-MS m/z: calc. 867.28184 for $[C_{42}H_{46}O_{18}N_2+H]^+$; found 867.28052 for $[C_{42}H_{46}O_{18}N_2+H]^+$.

Macrocyclyzation general procedure:

A solution of the precursor (25.0 mg, 28.8 µmol) in dry pyridine (1 – 10 mM) was stirred at room temperature and irradiated with a LED lamp emitting 365 nm light from a distance of 15 cm for 20 min. After irradiation, the solution was shielded from light and CuBr (62.0 mg, 432 µmol) and *N,N,N′,N″,N‴*-pentamethyldiethylenetriamine (90.0 µL, 432 µmol) were added. The mixture was stirred at room temperature for 2 d then concentrated to dryness and coevaporated with toluene. The crude residue was dissolved in ethyl acetate, washed four times with water (50 mL each) and dried over $MgSO_4$. After filtration and concentration under reduced pressure, the residue was purified by flash chromatography (cyclohexane/ethyl acetate 3:2) to give the corresponding macrocycles as an orange foam.

α-Glucoside macrocycle **64**:

Made from **41** to give 12.0 mg (13.8 µmol, 48 %) of **64**.

$[\alpha]^{20}_D$=-200 (c= 1.03 in CH_2Cl_2); ^{1}H NMR (500 MHz, $CDCl_3$) δ = 7.99 – 7.93 (m, 4 H, Ar-H_{ortho}), 7.10 – 7.06 (m, 4 H, Ar-H_{meta}), 5.38 (dd, $^3J_{3,2}$ = 10.1 Hz, $^3J_{3,4}$ = 9.4 Hz, 2 H, H-3), 4.92 – 4.84 (m, 4 H, H-1, H-4), 4.79 (dd, $^3J_{2,3}$ = 10.2 Hz, $^3J_{2,1}$ = 3.8 Hz, 2 H, H-2), 4.38 – 4.30 (m, 4 H, H-6), 4.25 – 4.19 (m, 2 H, H-5), 3.50 (d,

$^{2}J_{CH2,CH2}$ = 3.1 Hz, 4 H, C*H*$_2$C≡C), 2.13 (s, 6 H, 2 C*H*$_3$C=O), 2.01 (s, 6 H, 2 C*H*$_3$C=O), 2.00 (s, 6 H, 2 C*H*$_3$C=O); ^{13}C NMR (151 MHz, $CDCl_3$) δ = 170.2 (CH_3*C*=O), 170.1 (CH_3*C*=O), 169.9 (CH_3*C*=O), 158.1 (Ar-C_{para}), 147.6 (Ar-C_{ipso}), 124.5 (Ar-C_{ortho}), 117.3 (Ar-C_{meta}), 94.1 (C-1), 72.7 (CH_2*C*≡C), 70.2 (4 C, C-2, CH_2C≡*C*), 69.9 (C-4), 69.7 (C-3), 66.8 (C-6), 65.2 (C-5), 55.0 (*C*H_2C≡C), 20.8 (*C*H_3C=O), 20.7 (4 C, *C*H_3C=O); IR (ATR): ũ = 1744, 1207, 1019, 846 cm^{-1}; ESI-MS m/z: calc. 865.26619 for $[C_{42}H_{44}O_{18}N_2+H]^+$; found 865.26495 for $[C_{42}H_{46}O_{18}N_2+H]^+$.

β-Glucoside macrocycle **65**:

Prepared from **42** (20.0 mg, 23.1 µmol) to give 13.7 mg (15.8 µmol, 68 %) of **65**.

$[\alpha]^{20}_D$=+458 (c= 0.25 in CH_2Cl_2); ^{1}H NMR (600 MHz, $CDCl_3$) δ = 7.90 – 7.84 (m, 4 H, Ar-H_{meta}), 7.14 – 7.08 (m, 4 H, Ar-H_{ortho}), 5.16 (dd~t, $^{3}J_{3,2}$ = $^{3}J_{3,4}$ = 9.5 Hz, 2 H, H-3), 4.96 (dd~t, $^{3}J_{4,3}$ = $^{3}J_{4,5}$ = 9.7 Hz, 2 H, H-4), 4.86 (dd, $^{3}J_{2,3}$ = 9.6 Hz, $^{3}J_{2,1}$ = 8.1 Hz, 2 H, H-2), 4.46 (dd, $^{2}J_{6a,6b}$ = 13.3 Hz, $^{3}J_{6a,5}$ = 7.8 Hz, 2 H, H-6a), 4.29 – 4.23 (m, 4 H, H-1, H-6b), 3.83 – 3.74 (m, 4 H, H-5, C*H*$_2$C≡Ca), 3.57 (d, $^{2}J_{CH2,CH2}$ = 14.9 Hz, 2 H, C*H*$_2$C≡Cb), 2.10 (s, 6 H, 2 C*H*$_3$C=O), 2.00 (s, 6 H, 2 C*H*$_3$C=O), 1.99 (s, 6 H, 2 C*H*$_3$C=O); ^{13}C NMR (151 MHz, $CDCl_3$) δ = 170.2 (CH_3*C*=O), 169.7 (CH_3*C*=O), 169.3 (CH_3*C*=O), 160.6 (Ar-C_{para}), 147.8 (Ar-C_{ipso}), 124.2 (Ar-C_{ortho}), 117.3 (Ar-C_{meta}), 98.4 (C-1), 74.3 (C-5), 73.3 (CH_2*C*≡C), 72.7 (C-3), 70.8 (C-2), 70.3 (CH_2C≡*C*), 69.1 (C-4), 67.3 (C-6), 55.5 (*C*H_2C≡C), 20.7 (4 C, *C*H_3C=O), 20.6 (*C*H_3C=O); IR (ATR): ũ = 2944, 1749, 1596, 1497, 1367, 1212, 1036, 841 cm^{-1}; ESI-MS m/z: calc. 865.26619 for $[C_{42}H_{44}O_{18}N_2+H]^+$; found 865.26508 for $[C_{42}H_{46}O_{18}N_2+H]^+$.

β-Galactoside macrocycle **66**:

Prepared from **43** (26.6 mg, 30.7 µmol) to give 15.5 mg (17.9 µmol, 58 %) of **66**.

$[\alpha]^{20}_D$=.+697 (c= 0.90 in CH_2Cl_2); ^{1}H NMR (500 MHz, $CDCl_3$) δ = 7.88 – 7.83 (m, 4 H, Ar-H_{ortho}), 7.13 – 7.09 (m, 4 H, Ar-H_{para}), 5.40 (d, $^{3}J_{4,3}$ = 3.5 Hz, 2 H, H-4), 5.12 (dd, $^{3}J_{2,3}$ = 10.3 Hz, $^{3}J_{2,1}$ = 8.0 Hz, 2 H, H-2), 4.95 (dd, $^{3}J_{3,2}$ = 10.3 Hz, $^{3}J_{3,4}$ = 3.5 Hz, 2 H, H-3), 4.48 (dd, $^{2}J_{6a,6b}$ = 13.1 Hz, $^{3}J_{6a,5}$ = 8.5 Hz, 2 H, H-6a), 4.26 – 4.14 (m, 4 H, H-1, H-6b), 3.99 – 3.93 (m, 2 H, H-5), 3.86 (d, $^{2}J_{CH2,\ CH2}$ = 15.3 Hz, 2 H, C*H*$_2$C≡Ca), 3.65 (d, $^{2}J_{CH2,\ CH2}$ = 15.3 Hz, 2 H, C*H*$_2$C≡Cb), 2.20 (s, 6 H, 2 C*H*$_3$C=O), 2.01 (s, 6 H, 2 C*H*$_3$C=O), 1.98 (s, 6 H, 2 C*H*$_3$C=O); ^{13}C NMR (126 MHz, $CDCl_3$) δ = 170.4 (CH_3*C*=O), 170.1 (CH_3*C*=O), 169.4 (CH_3*C*=O), 160.2 (Ar-C_{para}), 148.1 (Ar-C_{ipso}), 124.2 (Ar-C_{ortho}), 117.7 (Ar-C_{meta}), 98.97 (C-1), 73.5 (C-5), 73.4 (CH_2*C*≡C), 71.0 (C-3), 70.5 (CH_2C≡*C*), 68.4 (C-2), 68.1 (C-4), 68.0 (C-6), 55.8 (*C*H_2C≡C), 20.8 (*C*H_3C=O), 20.7 (*C*H_3C=O), 20.6 (*C*H_3C=O); IR (ATR): ũ = 1746, 1596, 1496, 1368, 1212, 1149, 1055 cm^{-1}; ESI-MS m/z: calc. 865.26619 for $[C_{42}H_{44}O_{18}N_2+H]^+$; found 865.26532 for $[C_{42}H_{46}O_{18}N_2+H]^+$.

Deprotection general procedure:

To a solution of the protected macrocycle (43.0 – 64.0 mg) in a mixture of dichloromethane and methanol (1:1, 4.00 mL) NaOMe (5.4M in methanol, 50 µL) was added and stirred at room temperature for 16 h. If the product precipitated, the suspension was irradiated with a LED lamp emitting 365 nm light until everything was solubilized. The mixture was neutralized with Amberlite® IR120 H^+, filtered and concentrated to dryness to give the corresponding macrocycles as yellow amorphous solids in quantitative yields.

α-Glucoside macrocycle **28** from **64**:

trans-**28**:

$[\alpha]^{24}_{D}$= -408 (c= 0.08 in DMSO); ^{1}H NMR (500 MHz, DMSO-d_6) δ = 7.92 – 7.83 (m, 4 H, Ar-H_{ortho}), 7.17 – 7.11 (m, 4 H, Ar-H_{meta}), 5.36 (bs, 2 H, OH), 5.12 (bs, 2 H, OH), 4.96 (bs, 2 H, OH), 4.76 (dd, $^{2}J_{6a,6b}$ = 12.7 Hz, $^{3}J_{6a,5}$ = 2.1 Hz, 2 H, H-6a), 4.48 (d, $^{3}J_{1,2}$ = 3.7 Hz, 2 H, H-1), 4.14 (dd, $^{2}J_{6b,6a}$ = 12.9 Hz, $^{3}J_{6b,5}$ = 10.3 Hz, 2 H, H-6b), 3.82 (ddd~td, $^{3}J_{5,6b}$ = $^{3}J_{5,4}$ = 10.3 Hz, $^{3}J_{5,6a}$ = 2.3 Hz, 2 H, H-5), 3.67 (d, $^{2}J_{CH2,CH2}$ = 15.3 Hz, 2 H, CH_2C≡Ca), 3.29 (dd~t, $^{3}J_{3,4}$ = $^{3}J_{3,2}$ = 8.5 Hz, 2 H, H-3), 3.24 – 3.14 (m, 4 H, H-2, CH_2C≡Cb), 3.01 (dd~t, $^{3}J_{4,3}$ = $^{3}J_{4,5}$ = 9.0 Hz, 2 H, H-4) ppm; ^{13}C NMR (126 MHz, DMSO-d_6) δ = 158.4 (Ar-C_{para}), 146.4 (Ar-C_{ipso}), 123.8 (Ar-C_{ortho}), 117.5 (Ar-C_{meta}), 97.8 (C-1), 74.5 (CH$_2$*C*≡C), 73.1 (C-3), 71.6 (C-4), 71.3 (C-2), 68.5 (CH$_2$C≡*C*), 67.9 (C-6), 65.7 (C-5), 53.8 (*C*H$_2$C≡C) ppm; IR (ATR): ũ = 3366, 2920, 1594, 1495, 1145, 1032, 846 cm^{-1}; ESI-MS m/z: calc. 613.20280 for $[C_{30}H_{32}O_{12}N_2+H]^+$; found 613.20215 for $[C_{30}H_{32}O_{12}N_2+H]^+$.

cis-**28**:

$[\alpha]^{24}_{D}$= -684 (c= 0.08 in DMSO); ^{1}H NMR (600 MHz, DMSO-d_6) δ = 6.92 – 6.84 (m, 4 H, Ar-H_{meta}), 6.86 – 6.74 (m, 4 H, Ar-H_{ortho}), 5.35 (bs, 2 H, OH), 5.10 (bs, 2 H, OH), 4.99 (bs, 2 H, OH), 4.75 (d, $^{3}J_{1,2}$ = 3.6 Hz, 2 H, H-1), 4.39 – 4.27 (m, 4 H, H-6a, CH_2C≡Ca), 4.15 (d, $^{2}J_{CH2,CH2}$ = 16.7 Hz, 2 H, CH_2C≡Cb), 4.05 (dd, $^{2}J_{6b,6a}$ = 11.5 Hz, , $^{3}J_{6b,5}$ = 7.7 Hz, 2 H, H-6b), 3.76 (dd~t, $^{3}J_{5,6}$ = $^{3}J_{5,4}$ = 8.9 Hz, 2 H, H-5), 3.47 – 3.38 (m, 2 H, H-3), 3.25 (dd, $^{3}J_{2,3}$ = 9.6 Hz, $^{3}J_{2,1}$ = 3.5 Hz, 2 H, H-2), 3.11 (dd~t, $^{3}J_{4,5}$ = $^{3}J_{4,3}$ = 9.4 Hz, 2 H, H-4) ppm; ^{13}C NMR (151 MHz, DMSO-d_6) δ = 157.2 (Ar-C_{para}), 146.7 (Ar-C_{ipso}), 122.3 (Ar-C_{ortho}), 114.4 (Ar-C_{meta}), 99.3 (C-1), 76.5 (CH$_2$C≡*C*), 73.0 (C-3), 71.6 (C-2), 70.7 (2 C, C-4, C-5), 69.5 (CH$_2$*C*≡C), 67.6 (C-6), 55.4 (*C*H$_2$C≡C) ppm.

β-Glucoside macrocycle **29** made from **65**:

trans-**29**:

$[\alpha]^{24}_{D}$= +474 (c= 0.08 in DMSO); ^{1}H NMR (500 MHz, DMSO-d_6) δ = 7.81 – 7.70 (m, 4 H, Ar-H_{ortho}), 7.27 – 7.12 (m, 4 H, Ar-H_{meta}), 5.30 (bs, 2 H, OH), 5.19 (bs, 4 H, OH), 4.54 (dd, $^{2}J_{6a,6b}$ = 13.1 Hz, $^{3}J_{6a,5}$ = 7.8 Hz, 2 H, H-6a), 4.46 (dd, $^{2}J_{6b,6a}$ = 13.1 Hz, $^{3}J_{6b,5}$ = 2.2 Hz, 2 H, H-6b), 3.92 (d, $^{3}J_{1,2}$ = 7.8 Hz, 2 H, H-1), 3.85 (d, $^{2}J_{CH2,CH2}$ = 15.1 Hz, 2 H, CH_2C≡Ca), 3.46 (d, $^{2}J_{CH2,CH2}$ = 15.2 Hz, 2 H, CH_2C≡Cb), 3.44 – 3.40 (m, 2 H, H-5), 3.14 – 3.05 (m, 4 H, H-3, H-4), 3.49 (dd~t, $^{3}J_{2,3}$ = $^{3}J_{2,1}$ = 8.2 Hz, 2 H, H-2) ppm; ^{13}C NMR (126 MHz, DMSO-d_6) δ = 161.7 (Ar-C_{para}), 146.4 (Ar-C_{ipso}), 123.3 (Ar-C_{ortho}), 117.2 (Ar-C_{meta}), 100.9 (C-1), 76.6 (C-5), 76.4 (C-3), 75.0 (CH$_2$*C*≡C), 72.8 (C-2), 70.1 (C-4), 68.6 (CH$_2$C≡*C*), 67.8 (C-6), 54.2 (*C*H$_2$C≡C) ppm; IR (ATR): ũ = 3369, 1586, 1498, 1225, 1073, 1046, 1028, 841 cm^{-1}; ESI-MS m/z: calc. 613.20280 for $[C_{30}H_{32}O_{12}N_2+H]^+$; found 613.20209 for $[C_{30}H_{32}O_{12}N_2+H]^+$.

cis-**29**:

$[\alpha]^{24}_{D}$= +1959 (c= 0.08 in DMSO); ^{1}H NMR (600 MHz, DMSO-d_6) δ = 6.95 – 6.85 (m, 4 H, Ar-H_{meta}), 6.85 – 6.73 (m, 4 H, Ar-H_{ortho}), 5.35 – 5.13 (m, 6 H, OH), 4.36 (d, $^{2}J_{CH2,CH2}$ = 16.7 Hz, 2 H, CH_2C≡Ca), 4.31 – 4.23 (m, 6 H, H-1, H-6a, CH_2C≡Cb), 4.08 (dd, $^{2}J_{6b,6a}$ = 11.3 Hz, , $^{3}J_{6b,5}$ = 7.7 Hz, 2 H, H-6b), 3.53 – 3.41 (m, 2 H, H-5), 3.19 (dd~t, $^{3}J_{3,4}$ = $^{3}J_{3,2}$ = 8.8 Hz, 2 H, H-3), 3.13 (dd~t, $^{3}J_{4,5}$ = $^{3}J_{4,3}$ = 9.2 Hz, 2 H, H-4), 2.97 (dd~t, $^{3}J_{2,3}$ = $^{3}J_{2,1}$ = 8.3 Hz, 2 H, H-2) ppm; ^{13}C NMR (151 MHz, DMSO-d_6) δ = 157.7 (Ar-C_{para}), 147.0 (Ar-C_{ipso}), 121.8 (Ar-C_{ortho}), 114.8 (Ar-C_{meta}), 102.6 (C-1), 76.4 (C-3), 76.3 (CH$_2$C≡*C*), 75.2 (C-5), 73.2 (C-2), 70.2 (C-4), 69.4 (CH$_2$*C*≡C), 67.7 (C-6), 56.4 (*C*H$_2$C≡C) ppm.

β-Galactoside macrocycle **30** from **66**:

trans-**30**:

$[\alpha]^{24}_{D}$= +893 (c= 0.08 in DMSO); ^{1}H NMR (600 MHz, DMSO-*d*$_6$) δ = 7.80 – 7.74 (m, 4 H, Ar-H$_{ortho}$), 7.19 – 7.13 (m, 4 H, Ar-H$_{meta}$), 5.02 (bs, 2 H, OH), 4.93 (bs, 2 H, OH), 4.74 (bs, 2 H, OH), 4.70 (dd, $^{2}J_{6a,6b}$ = 13.0 Hz, $^{3}J_{6a,5}$ = 9.5 Hz, 2 H, H-6a), 4.23 (dd, $^{2}J_{6b,6a}$ = 12.9 Hz, $^{3}J_{6b,5}$ = 1.8 Hz, 2 H, H-6b), 3.84 (d, $^{2}J_{CH2,CH2}$ = 15.4 Hz, 2 H, C*H*$_2$C≡Ca), 3.81 (d, $^{3}J_{1,2}$ = 7.6 Hz, 2 H, H-1), 3.69 (d, $^{3}J_{5,6a}$ = 8.8 Hz, 2 H, H-5), 3.65 (d, $^{3}J_{4,3}$ = 3.0 Hz, 2 H, H-4), 3.40 (d, $^{2}J_{CH2,CH2}$ = 15.4 Hz, H-2, C*H*$_2$C≡Cb), 3.25 (dd, $^{3}J_{3,2}$ = 9.4 Hz, $^{3}J_{3,4}$ = 3.2 Hz, 2 H, H-3) 3.21 – 3.15 (m, 2 H, H-2) ppm; ^{13}C NMR (151 MHz, DMSO-*d*$_6$) δ = 161.6 (Ar-C$_{para}$), 146.6 (Ar-C$_{ipso}$), 123.5 (Ar-C$_{ortho}$), 117.5 (Ar-C$_{meta}$), 101.5 (C-1), 75.4 (C-5), 75.1 (CH$_2$*C*≡C), 73.1 (C-3), 70.0 (C-2), 68.8 (2 C, C-6, CH$_2$C≡*C*), 68.7 (C-4), 54.3 (*C*H$_2$C≡C) ppm; IR (ATR): ũ = 3389, 1598, 1496, 1209, 1080, 1034, 843 cm^{-1}; ESI-MS m/z: calc. 613.20280 for $[C_{30}H_{32}O_{12}N_2+H]^+$; found 613.20215 for $[C_{30}H_{32}O_{12}N_2+H]^+$.

cis-**30**:

$[\alpha]^{24}_{D}$= +1693 (c= 0.08 in DMSO); ^{1}H NMR (600 MHz, DMSO-*d*$_6$) δ = 6.91 – 6.85 (m, 4 H, Ar-H$_{meta}$), 6.84 – 6.73 (m, 4 H, Ar-H$_{ortho}$), 5.06 (bs, 2 H, OH), 4.94 (bs, 2 H, OH), 4.74 (bs, 2 H, OH), 4.34 (d, $^{2}J_{CH2,CH2}$ = 16.6 Hz, 2 H, C*H*$_2$C≡Ca), 4.28 – 4.16 (m, 6 H, H-1, H-6a, C*H*$_2$C≡Cb), 4.12 (dd, $^{2}J_{6b,6a}$ = 11.3 Hz, , $^{3}J_{6b,5}$ = 2.6 Hz, 2 H, H-6b), 3.76 (dd, $^{3}J_{5,6a}$ = 8.7 Hz, $^{3}J_{5,6b}$ = 2.1 Hz, 2 H, H-5), 3.68 (dd, $^{3}J_{4,3}$ = 2.8 Hz, 2 H, H-4), 3.36 – 3.34 (m, 2 H, H-3), 3.31 – 3.22 (m, 2 H, H-2) ppm; ^{13}C NMR (151 MHz, DMSO-*d*$_6$) δ = 157.7 (Ar-C$_{para}$), 146.8 (Ar-C$_{ipso}$), 122.0 (Ar-C$_{ortho}$), 114.8 (Ar-C$_{meta}$), 102.8 (C-1), 76.3 (CH$_2$*C*≡C), 73.9 (C-5), 73.0 (C-3), 70.3 (C-2), 69.5 (CH$_2$C≡*C*), 68.8 (C-4), 68.0 (C-6), 56.1 (*C*H$_2$C≡C) ppm.

NMR spectra of synthesized compounds

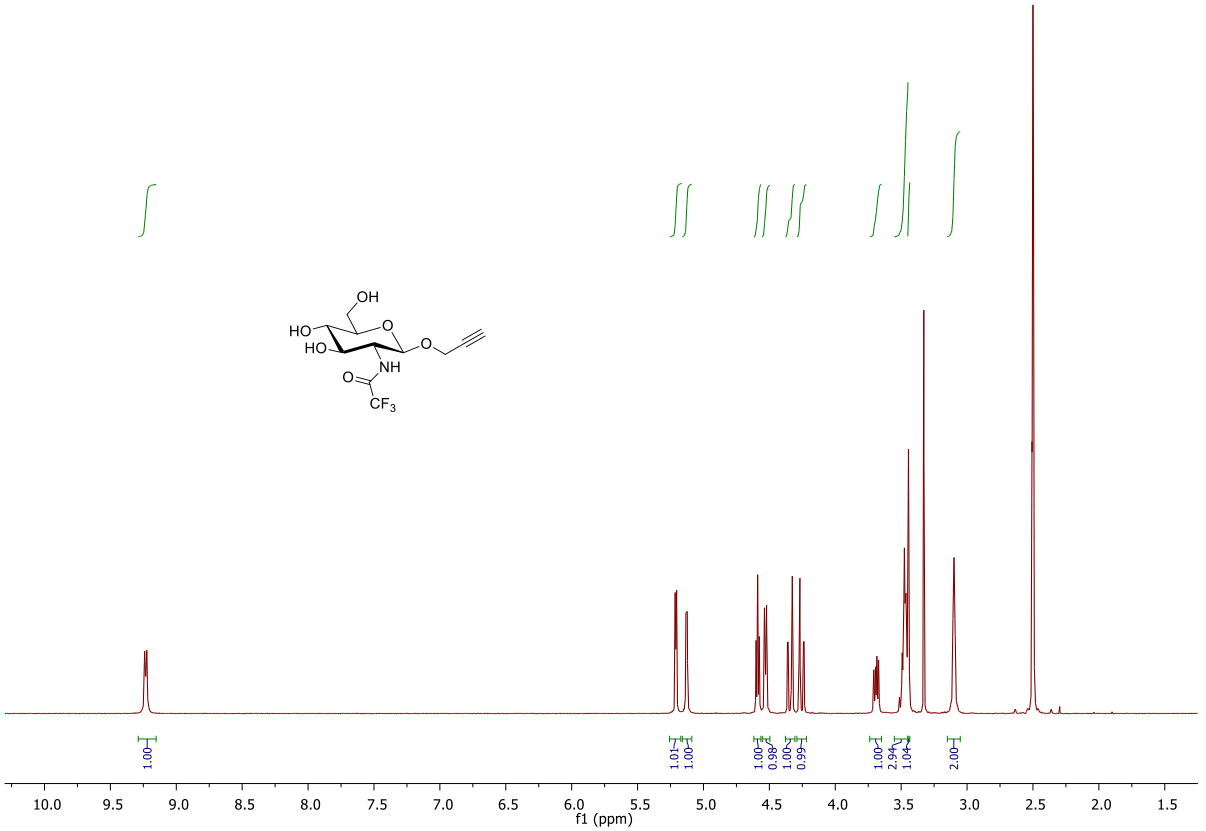

Figure 6.9: ^{1}H NMR spectrum of **38** (500 MHz, DMSO-d_6, 298 K).

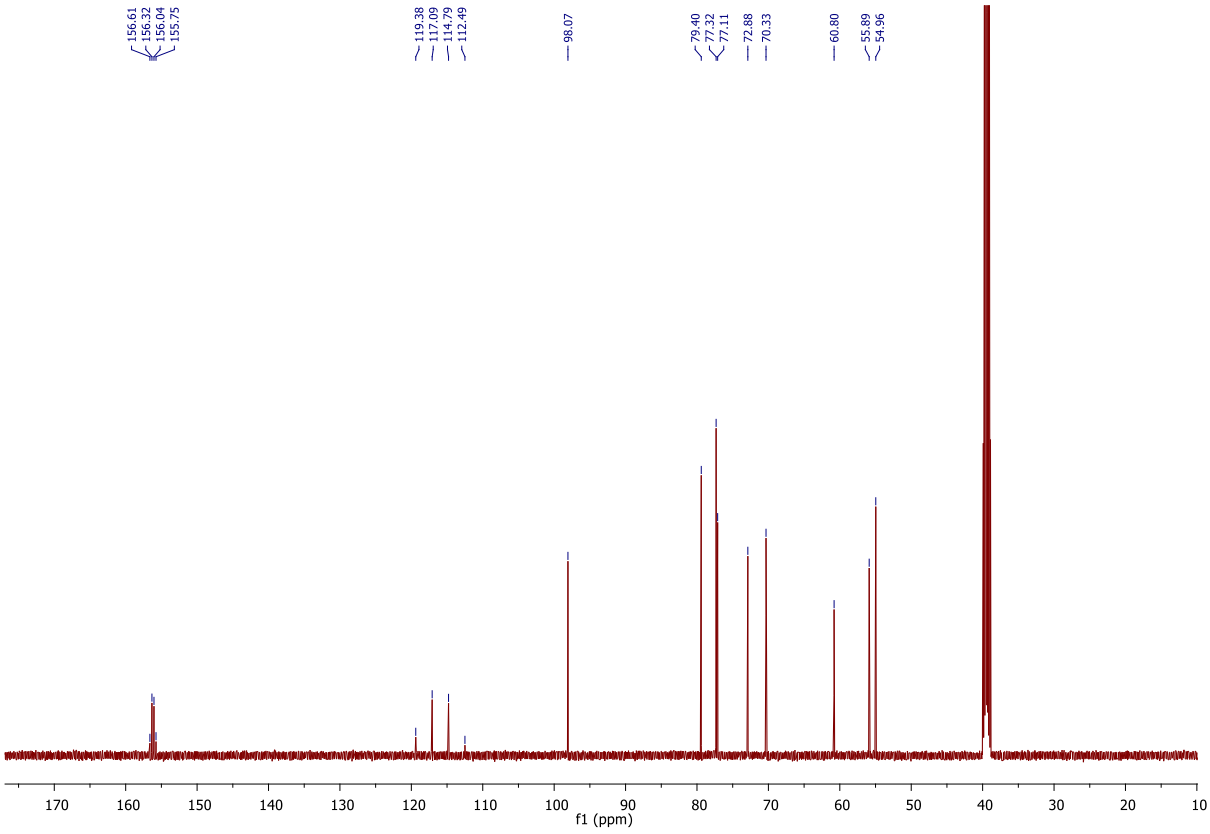

Figure 6.10: ^{13}C NMR spectrum of **38** (126 MHz, DMSO-d_6, 298 K).

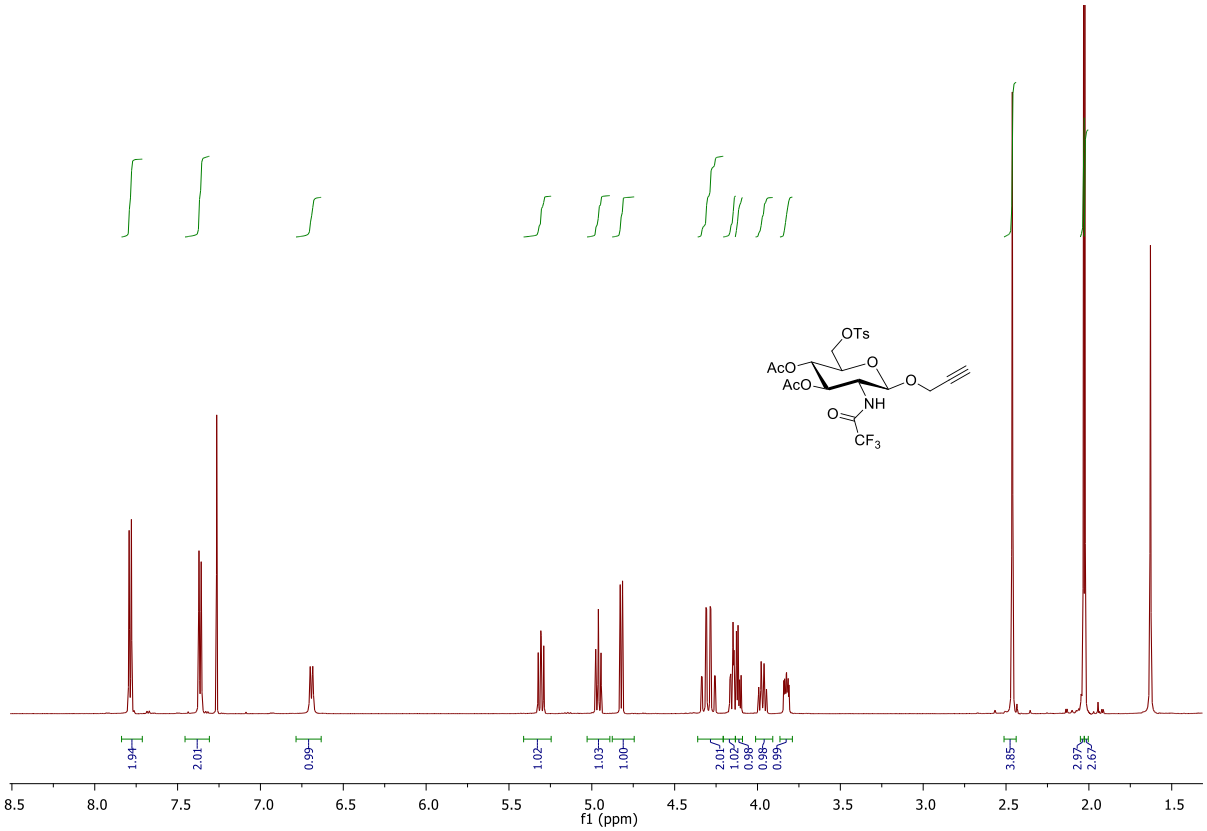

Figure 6.11: ^{1}H NMR spectrum of **39** (600 MHz, $CDCl_3$, 298 K).

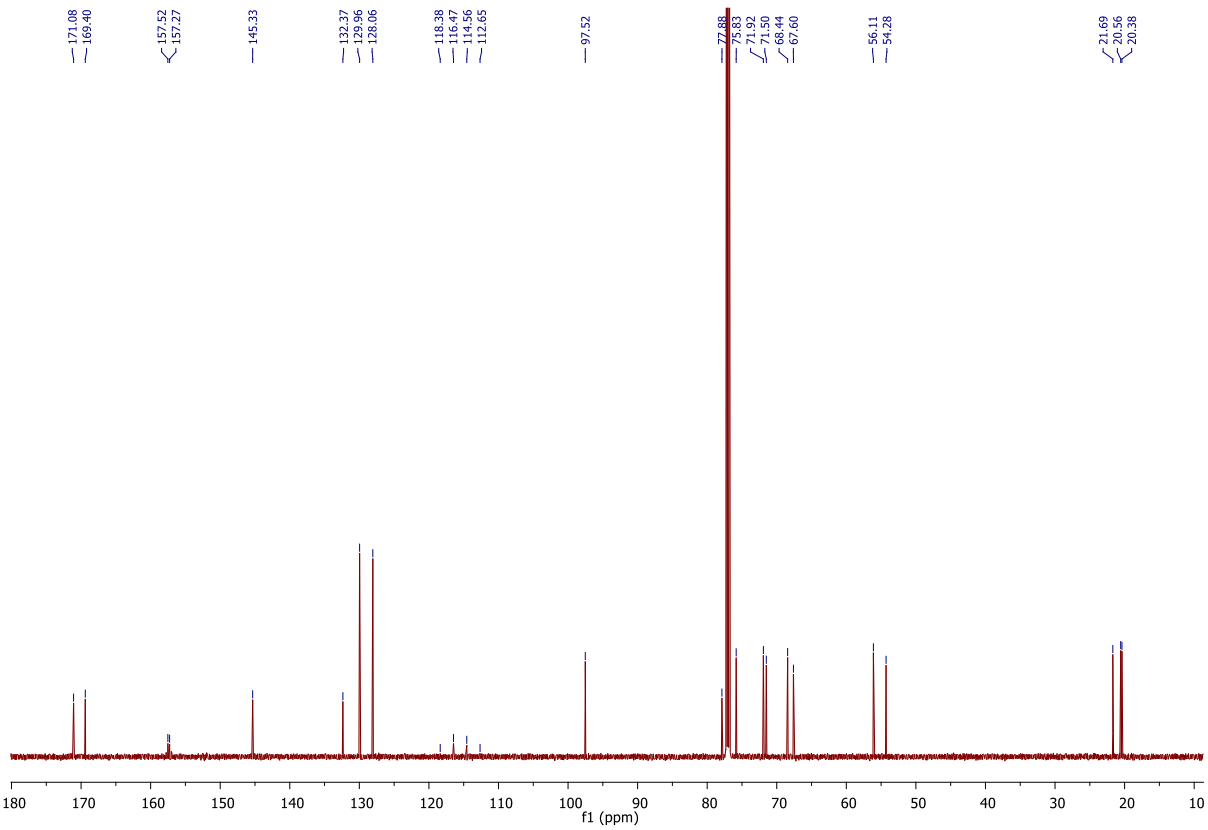

Figure 6.12: ^{13}C NMR spectrum of **39** (151 MHz, $CDCl_3$, 298 K).

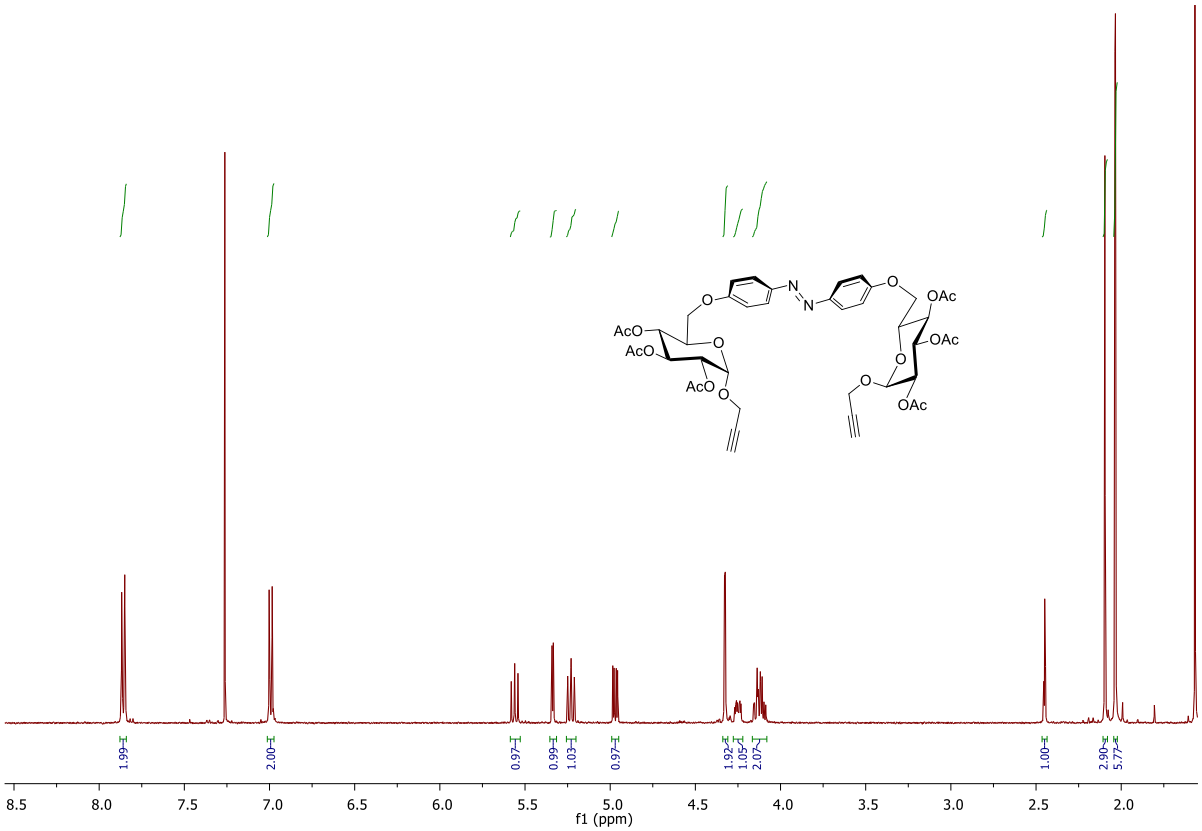

Figure 6.13: ^{1}H NMR spectrum of *trans*-**41** (500 MHz, $CDCl_3$, 298 K).

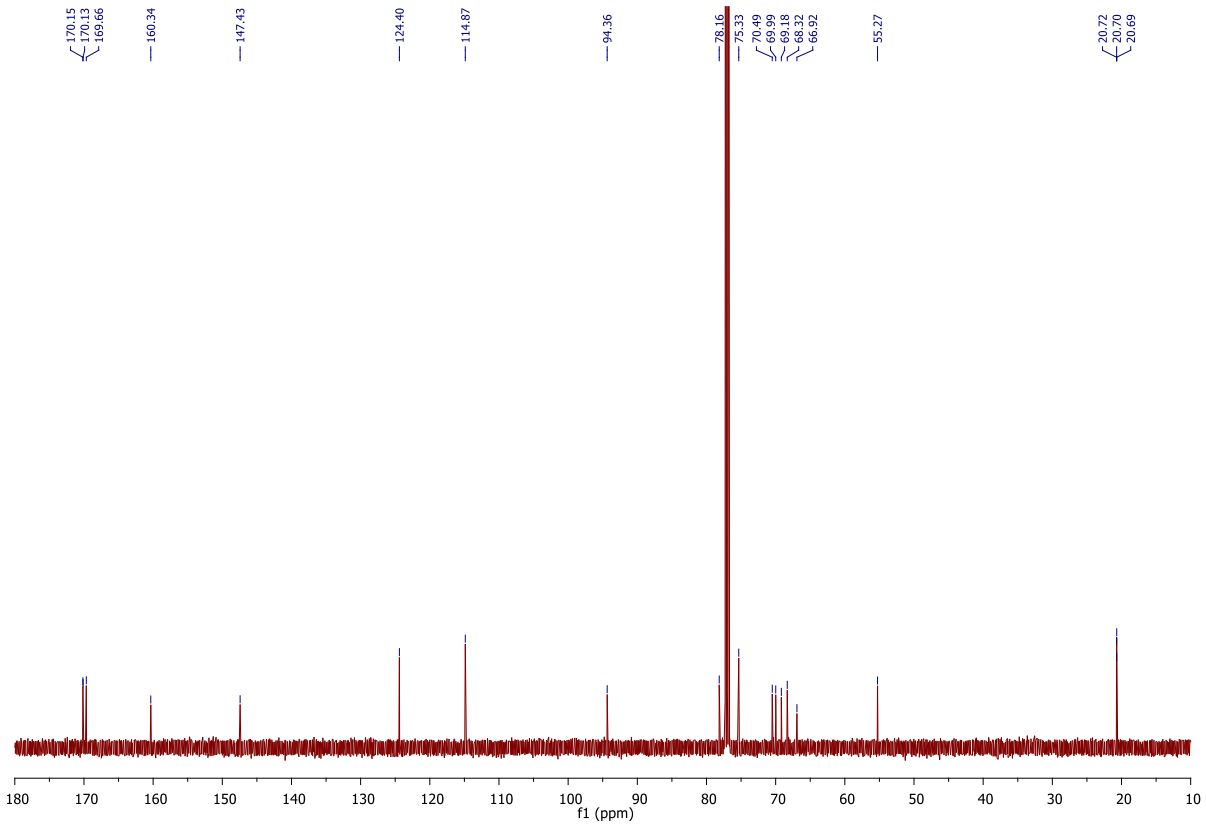

Figure 6.14: ^{13}C NMR spectrum of *trans*-**41** (126 MHz, $CDCl_3$, 298 K).

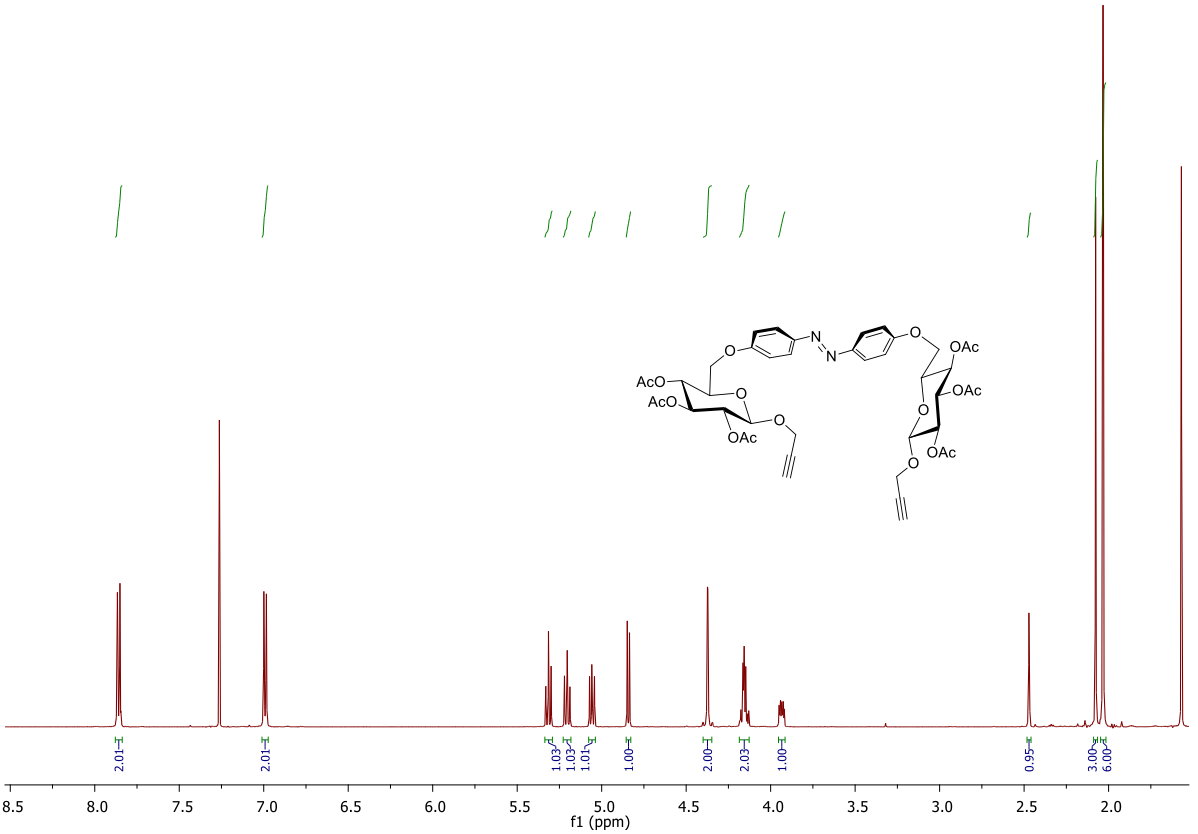

Figure 6.15: ^{1}H NMR spectrum of *trans*-**42** (600 MHz, $CDCl_3$, 298 K).

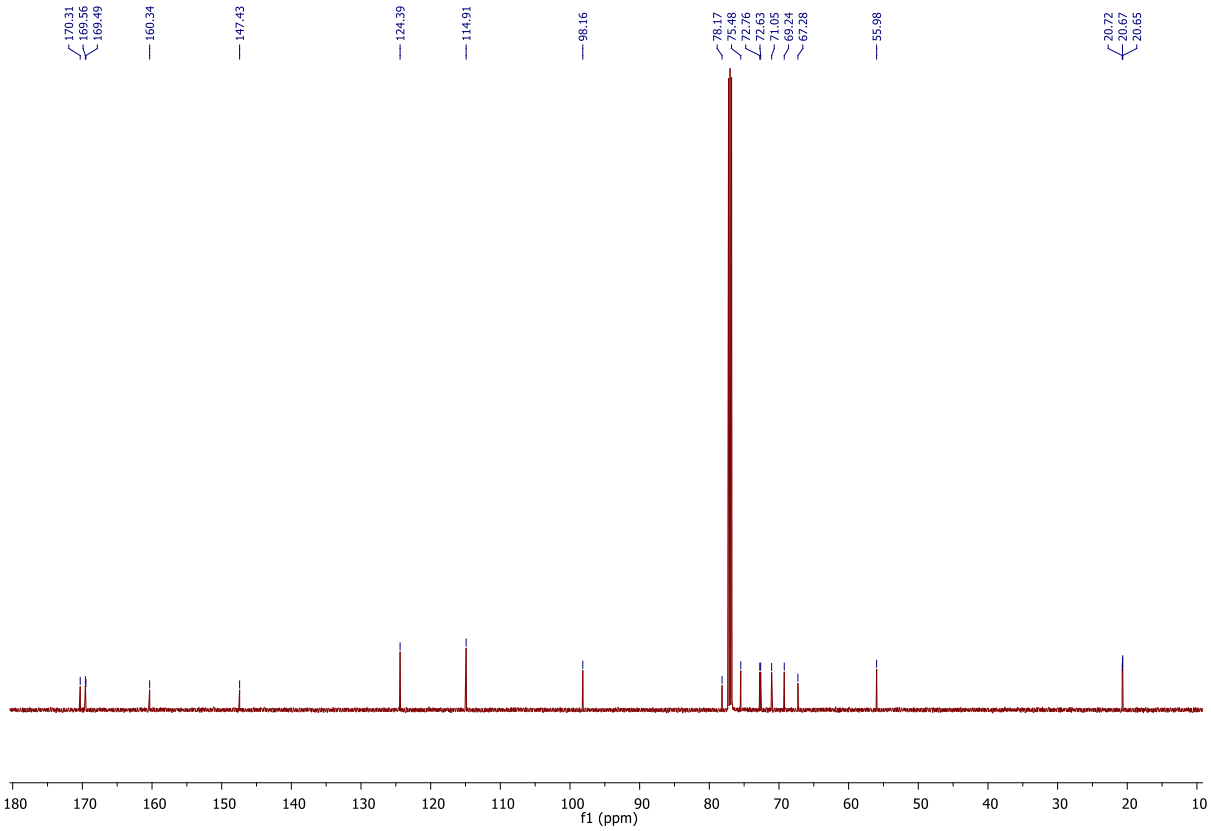

Figure 6.16: ^{13}C NMR spectrum of *trans*-**42** (151 MHz, $CDCl_3$, 298 K).

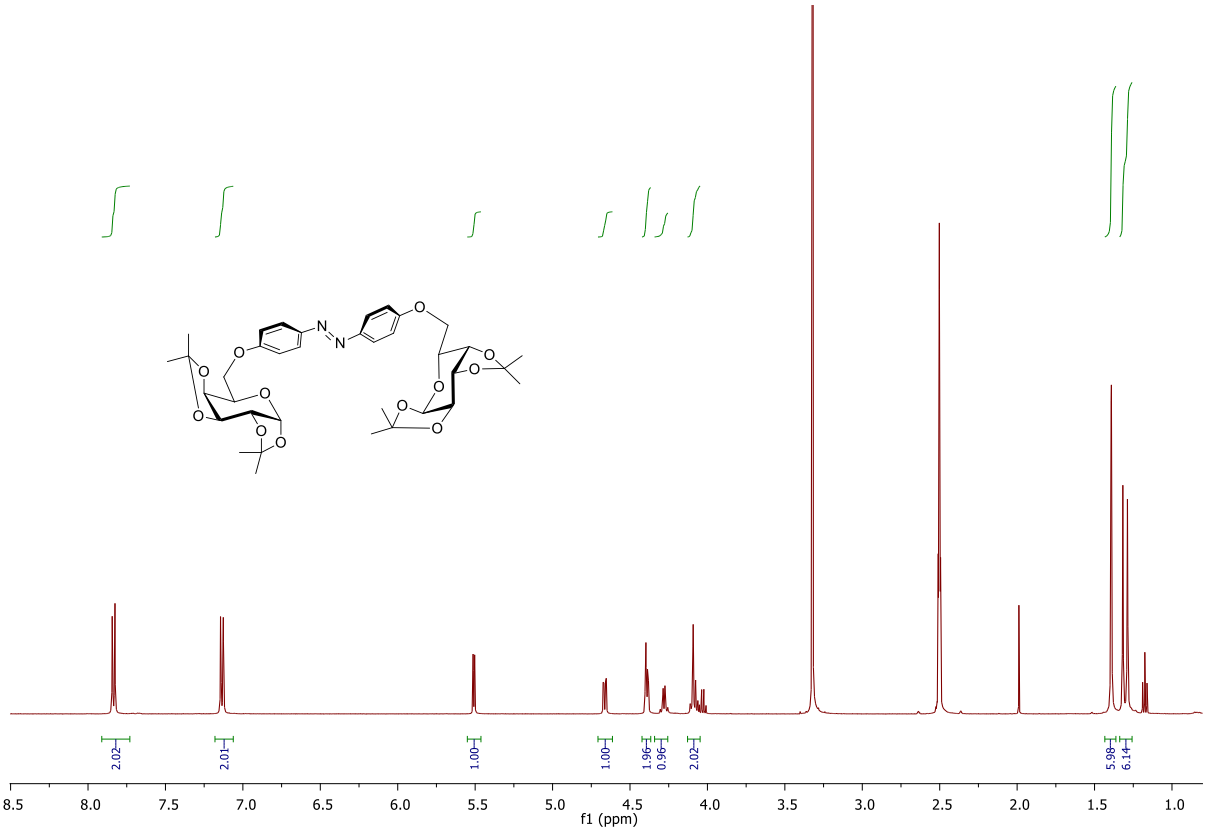

Figure 6.17: ^{1}H NMR spectrum of *trans*-**46** (500 MHz, DMSO-d_6, 298 K).

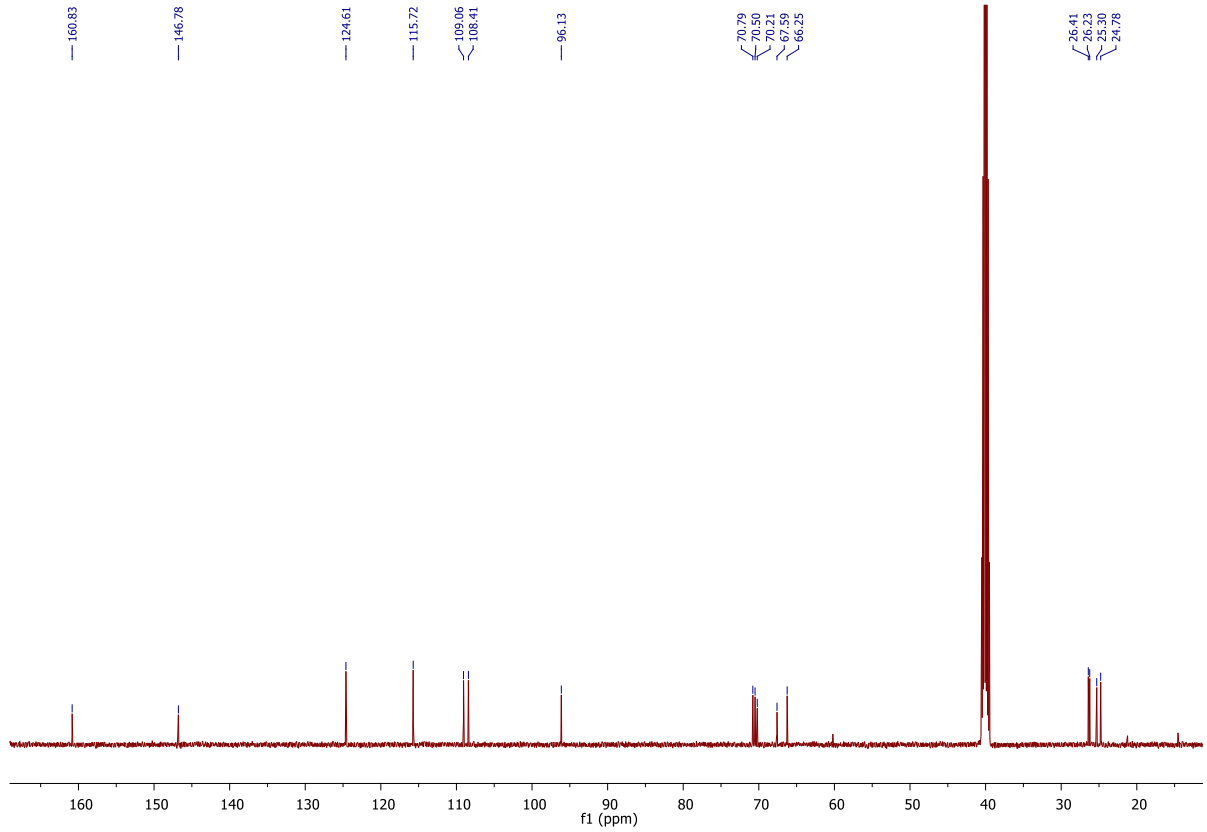

Figure 6.18: ^{13}C NMR spectrum of *trans*-**46** (126 MHz, DMSO-d_6, 298 K).

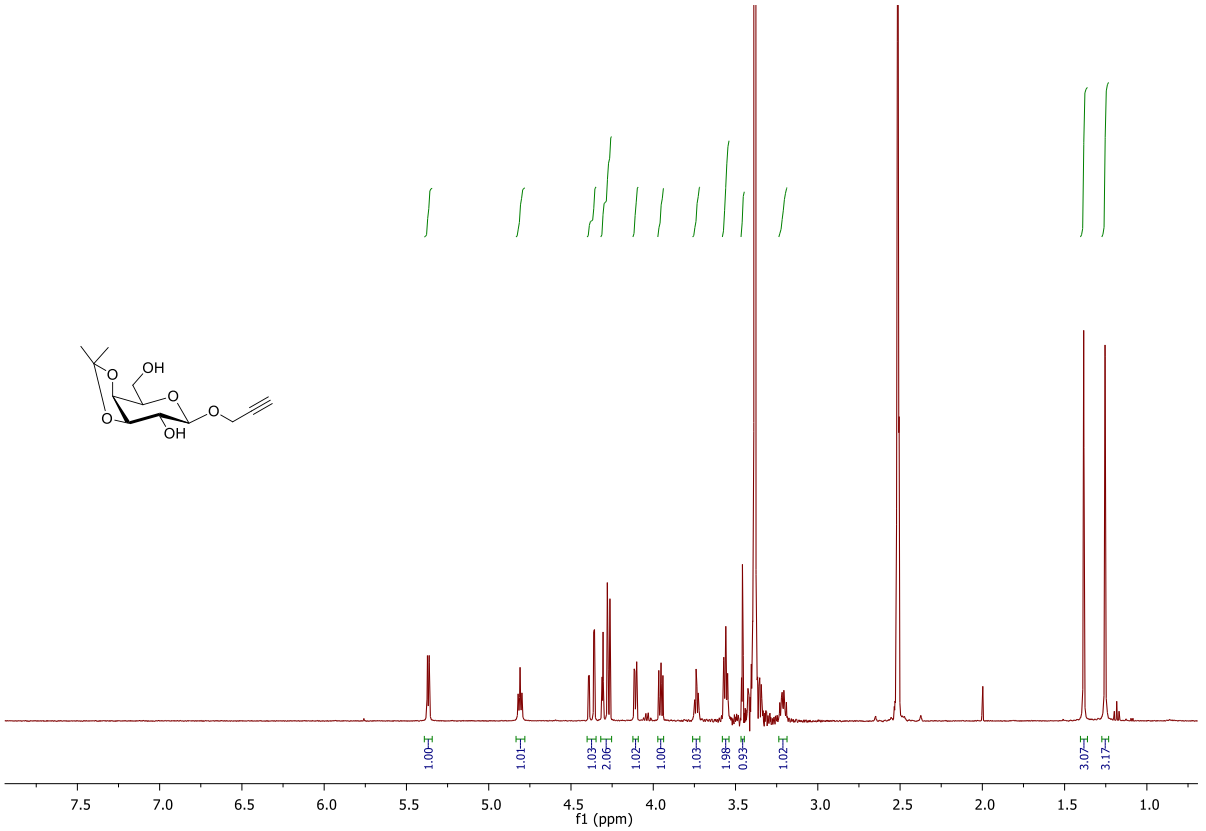

Figure 6.19: ^{1}H NMR spectrum of **48** (500 MHz, DMSO-d_6, 298 K).

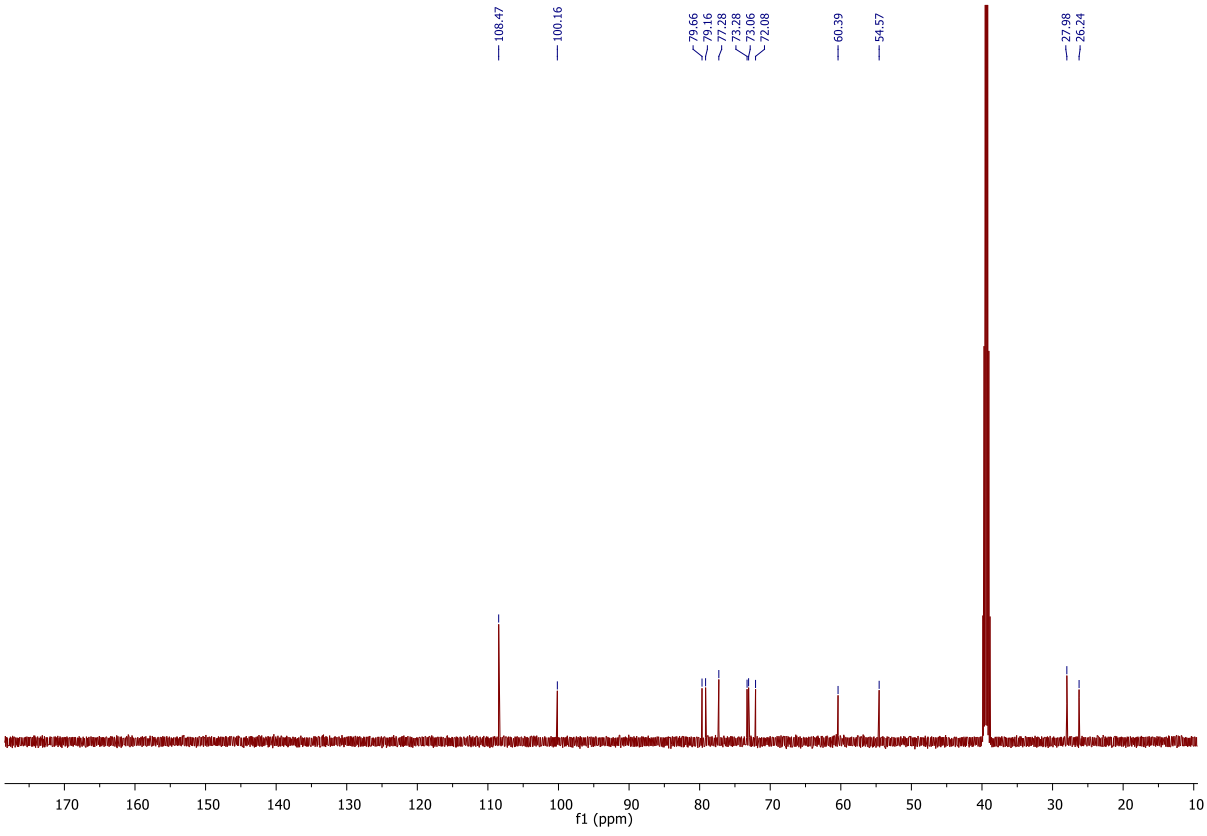

Figure 6.20: ^{13}C NMR spectrum of **48** (126 MHz, DMSO-d_6, 298 K).

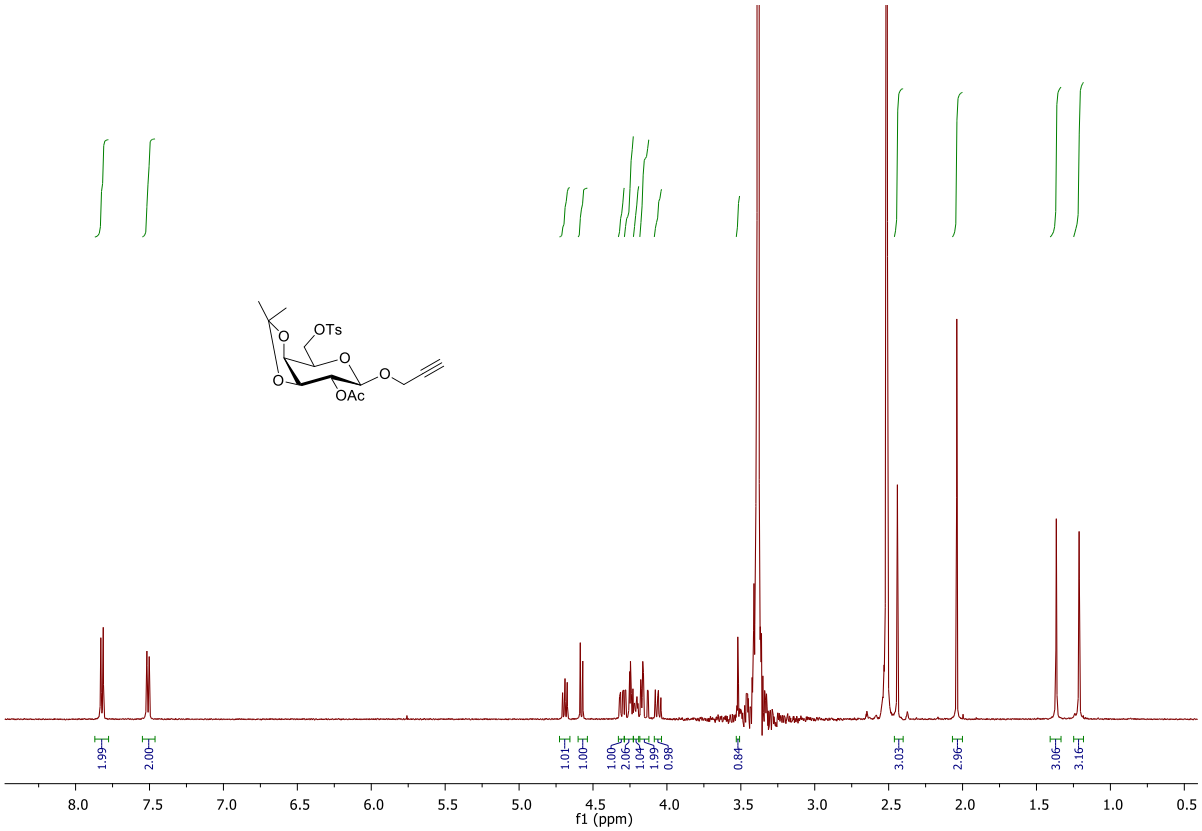

Figure 6.21: ^{1}H NMR spectrum of **49** (500 MHz, DMSO-d_6, 298 K).

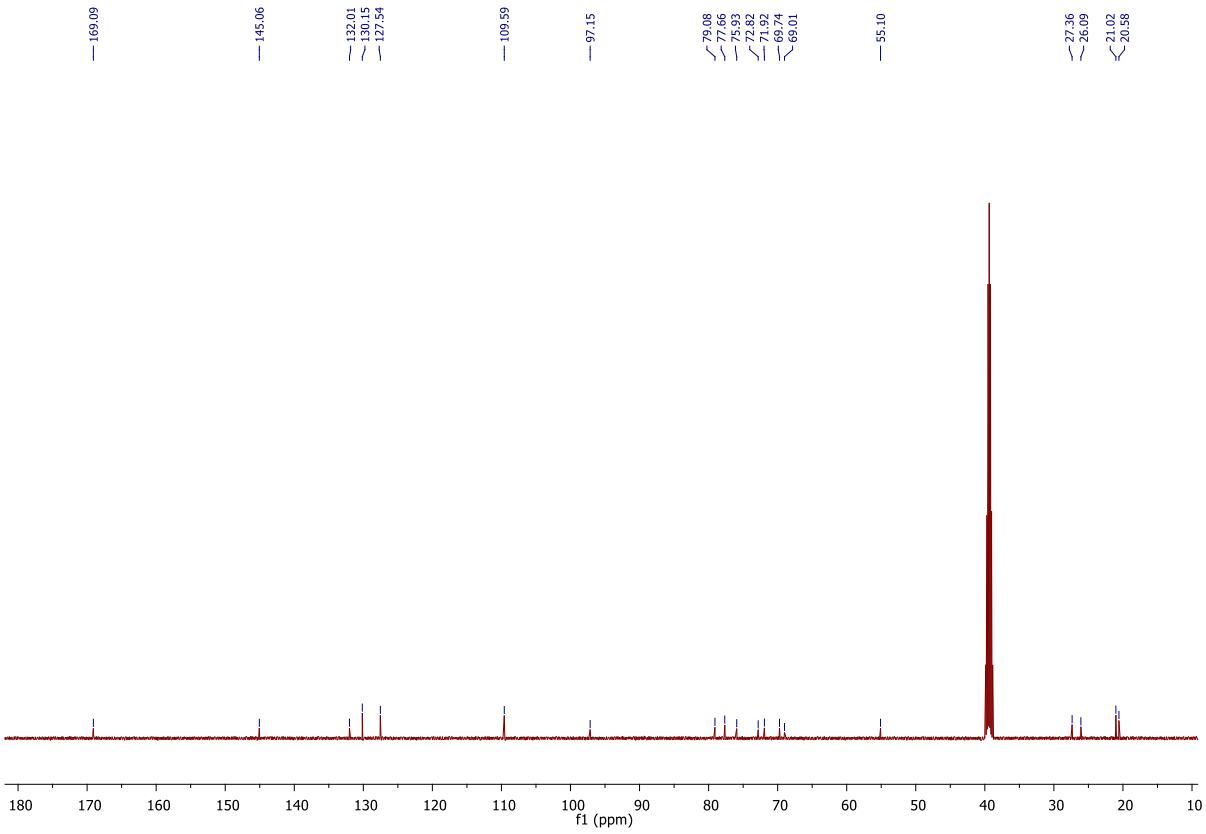

Figure 6.22: ^{13}C NMR spectrum of **49** (126 MHz, DMSO-d_6, 298 K).

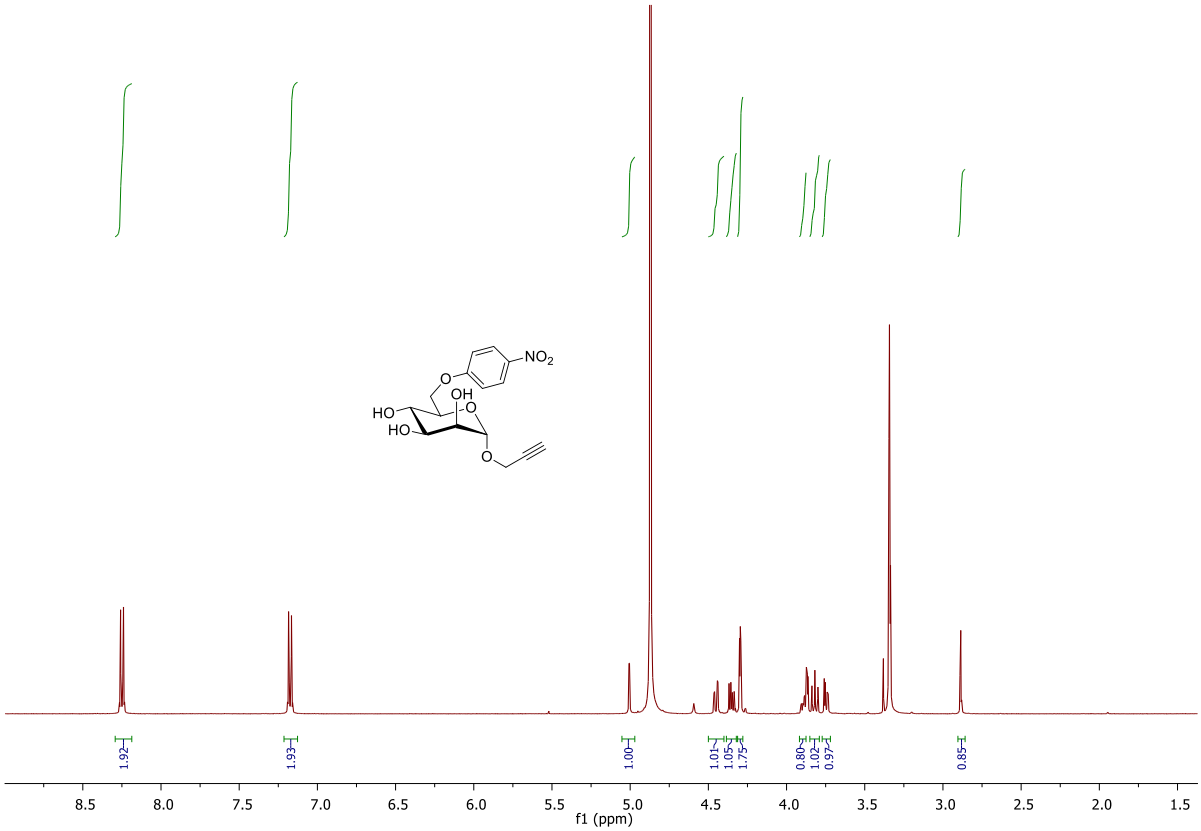

Figure 6.23: ^{1}H NMR spectrum of **53** (500 MHz, MeOH-d_4, 298 K).

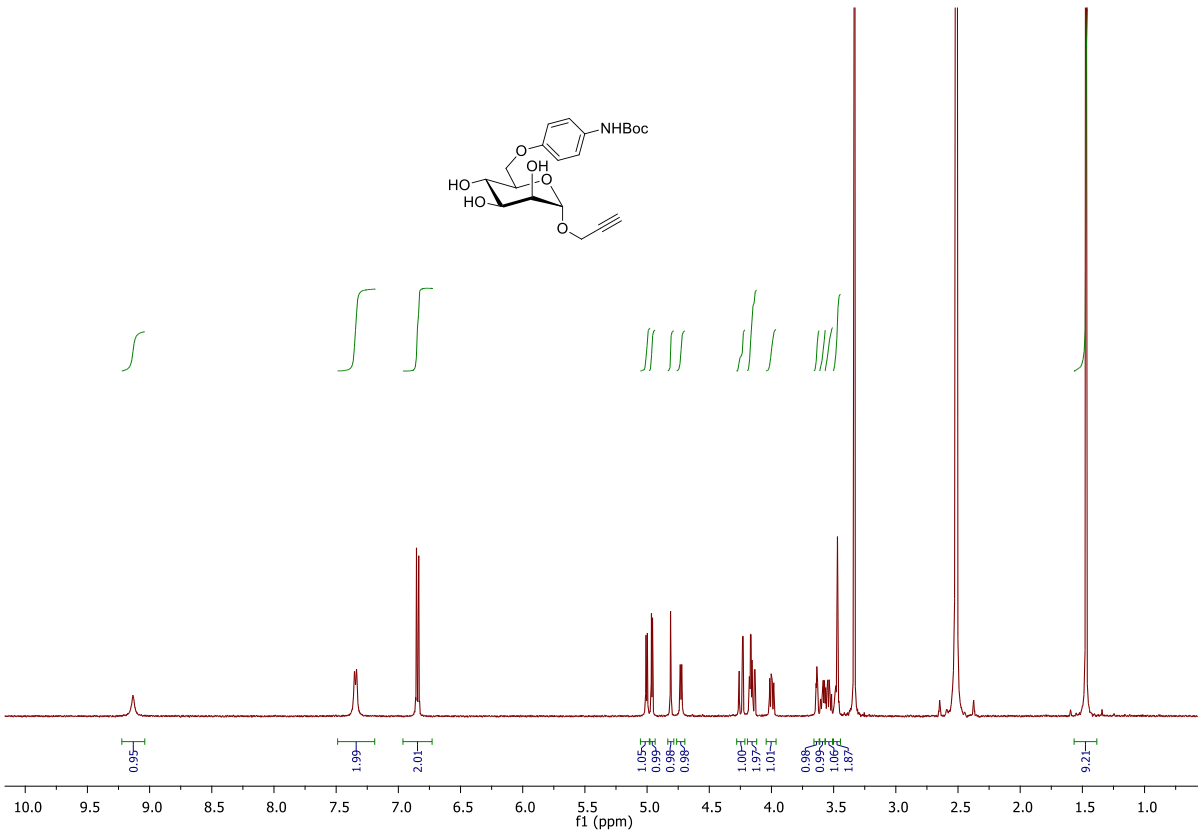

Figure 6.24: ^{1}H NMR spectrum of **54** (500 MHz, DMSO-d_6, 298 K).

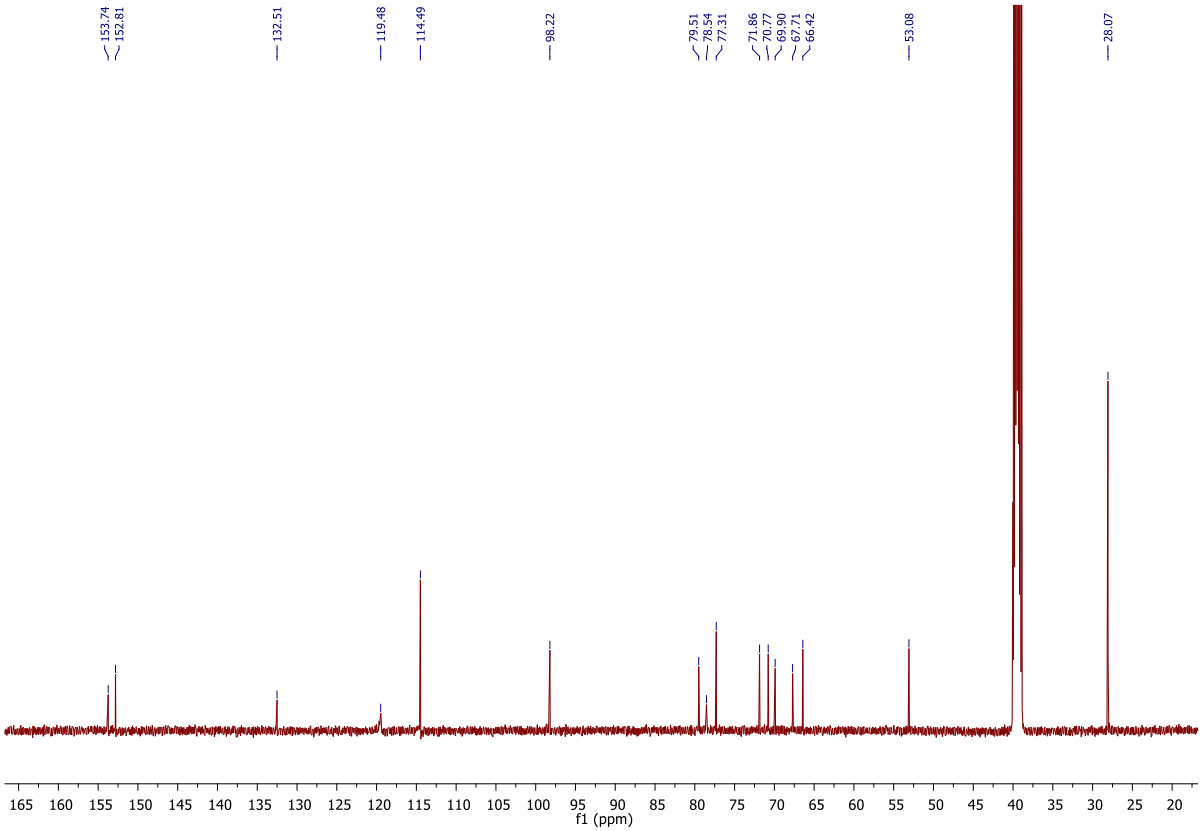

Figure 6.25: ^{13}C NMR spectrum of **54** (126 MHz, DMSO-d_6, 298 K).

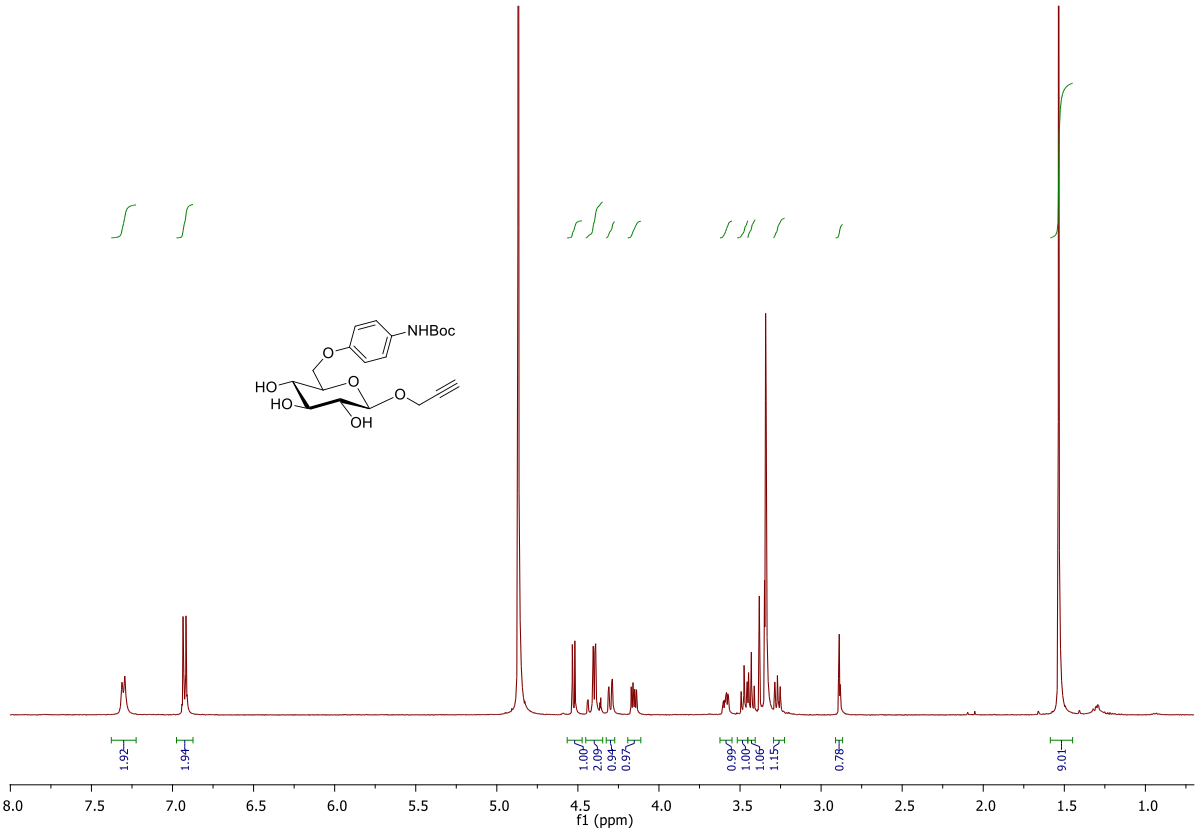

Figure 6.26: ^{1}H NMR spectrum of **55** (500 MHz, MeOH-d_4, 298 K).

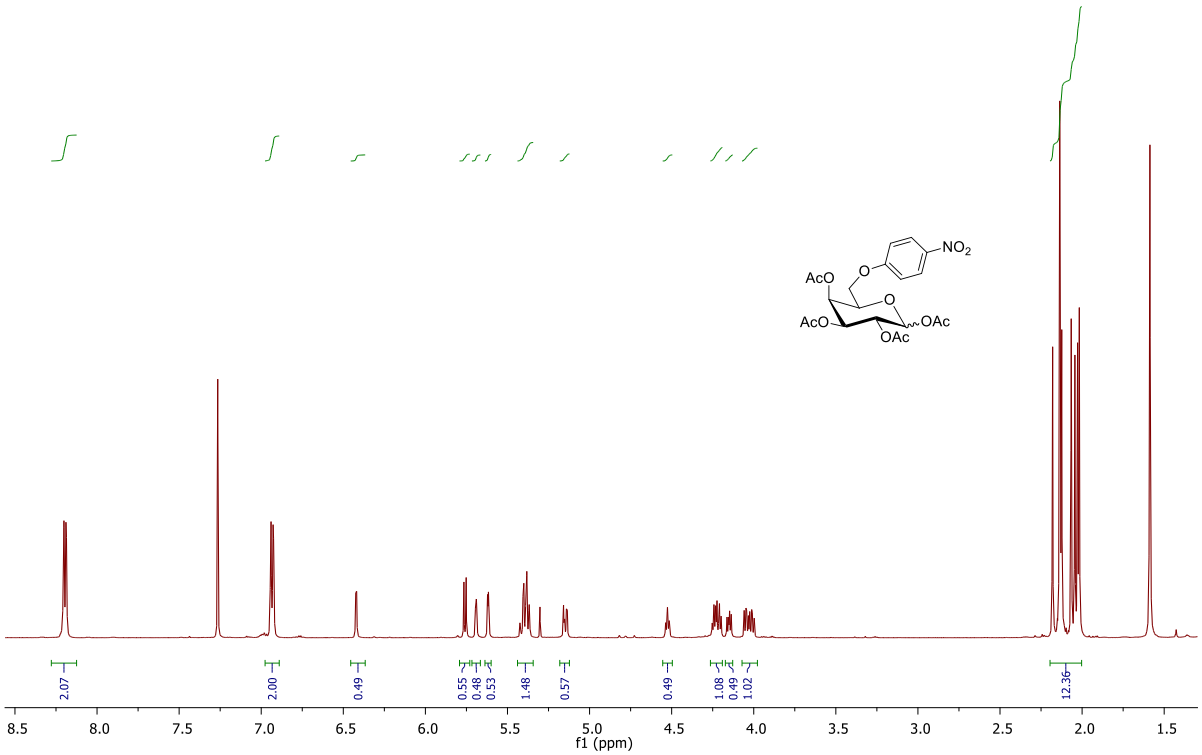

Figure 6.27: ^{1}H NMR spectrum of **58** (600 MHz, $CDCl_3$, 298 K).

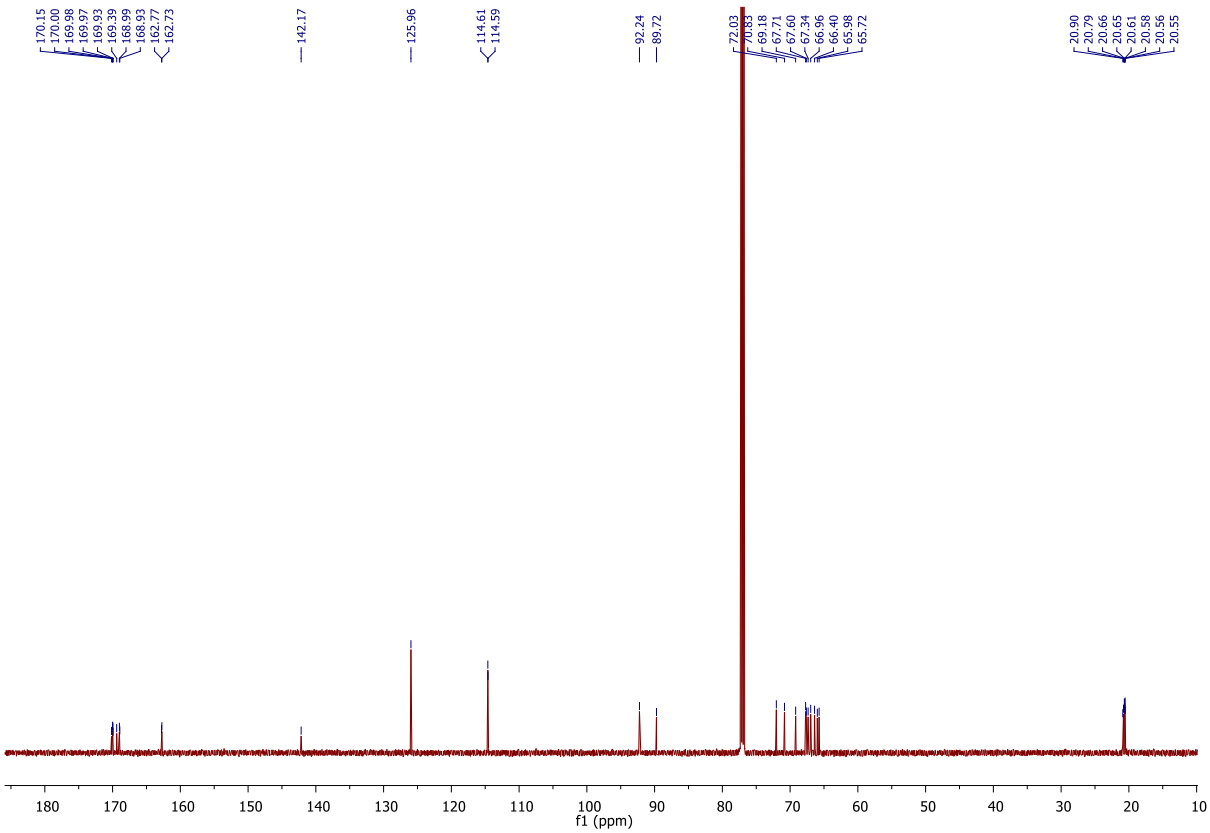

Figure 6.28: ^{13}C NMR spectrum of **58** (151 MHz, $CDCl_3$, 298 K).

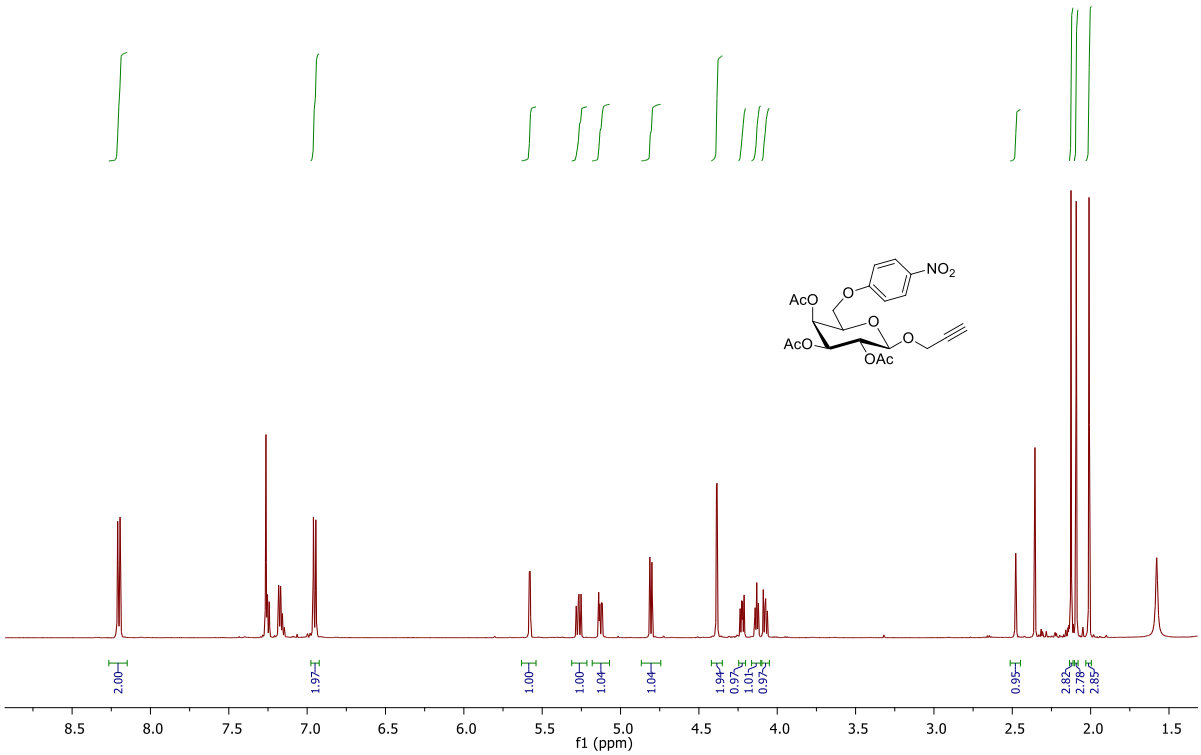

Figure 6.29: ^{1}H NMR spectrum of **59** (600 MHz, $CDCl_3$, 298 K).

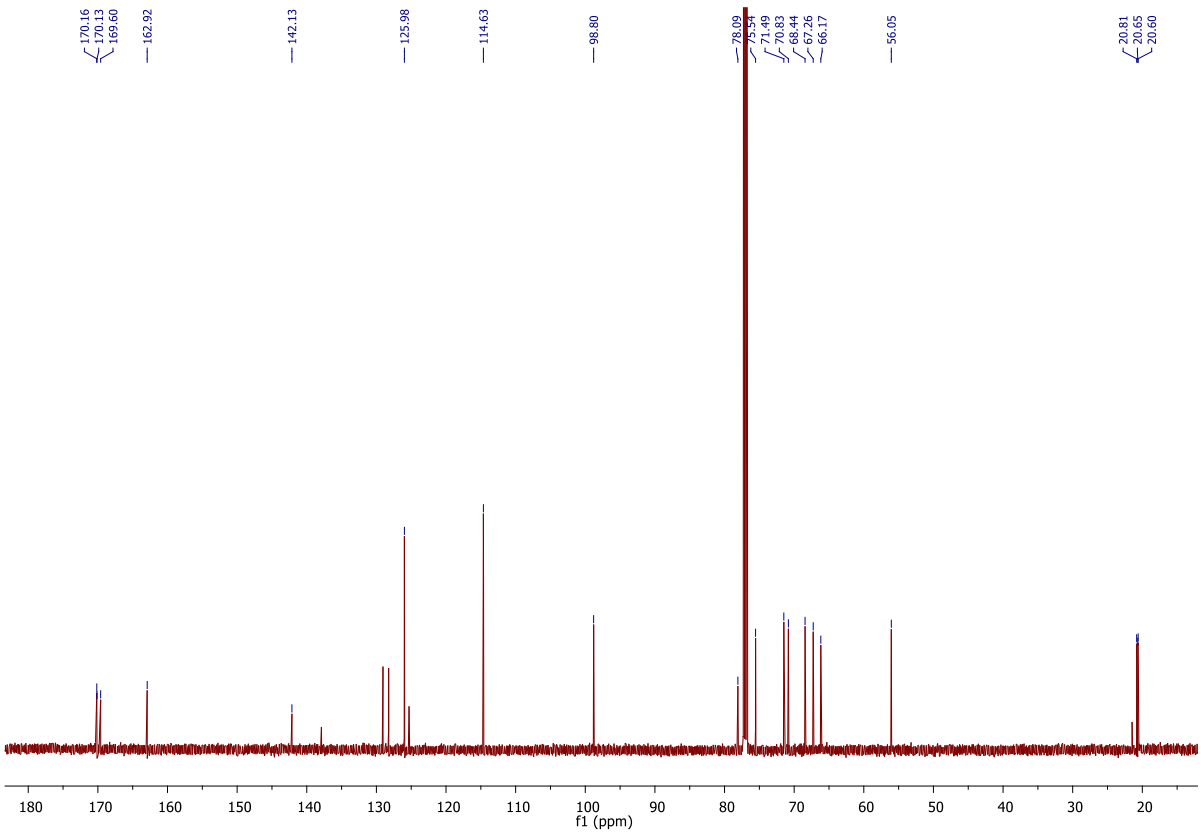

Figure 6.30: ^{13}C NMR spectrum of **59** (151 MHz, $CDCl_3$, 298 K).

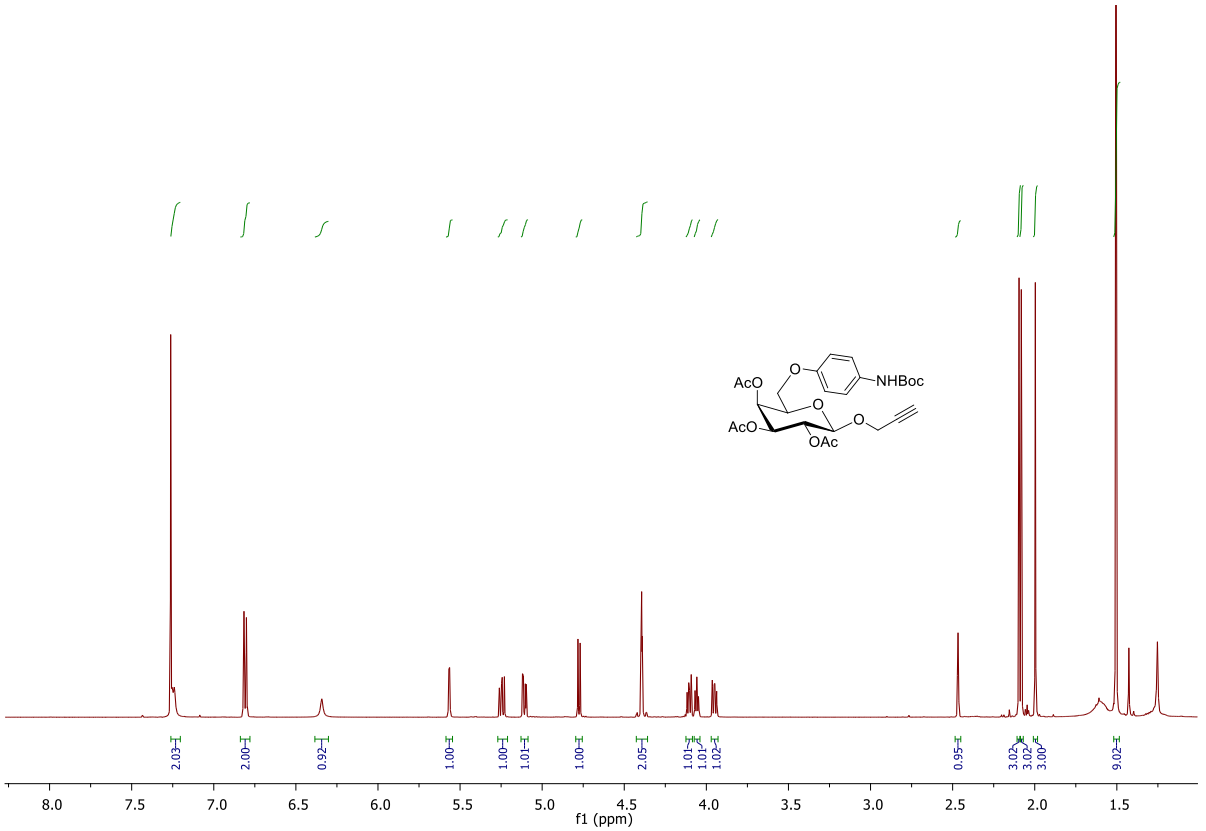

Figure 6.31: ^{1}H NMR spectrum of **60** (600 MHz, $CDCl_3$, 298 K).

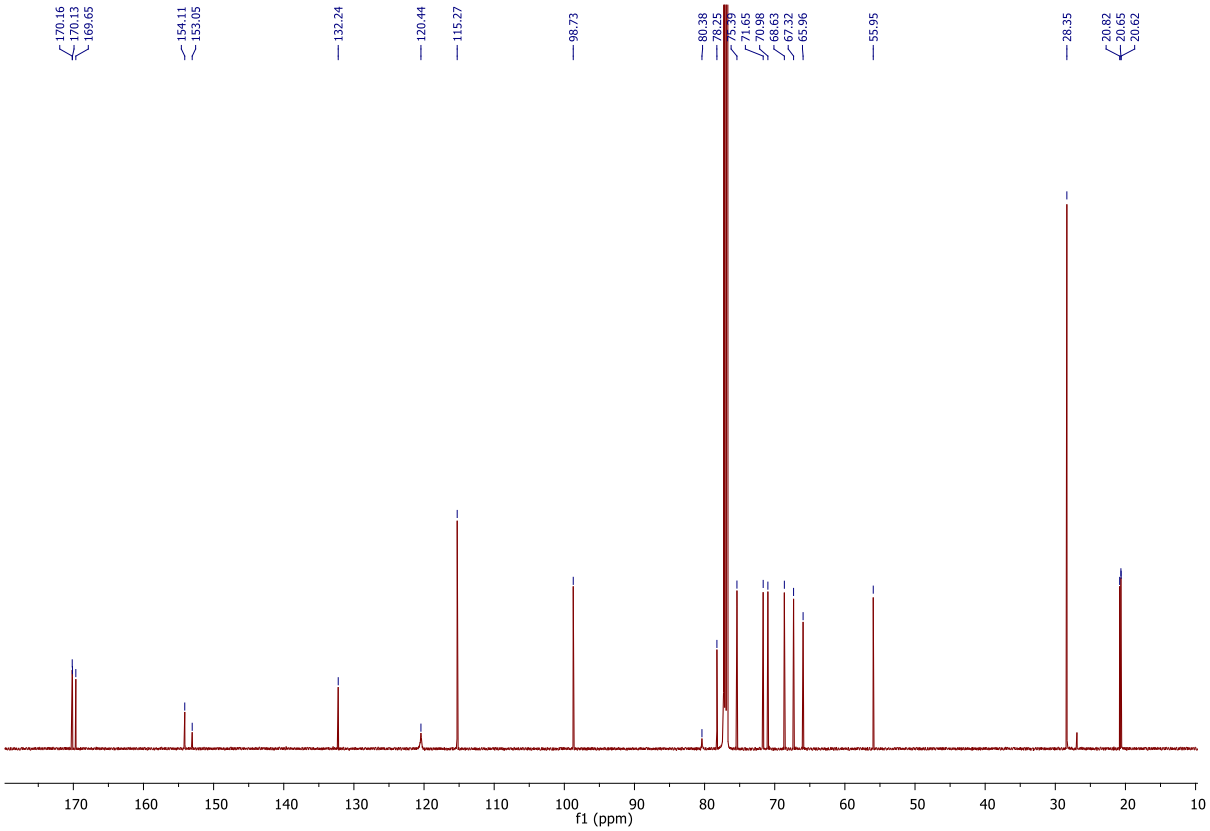

Figure 6.32: ^{13}C NMR spectrum of **60** (151 MHz, $CDCl_3$, 298 K).

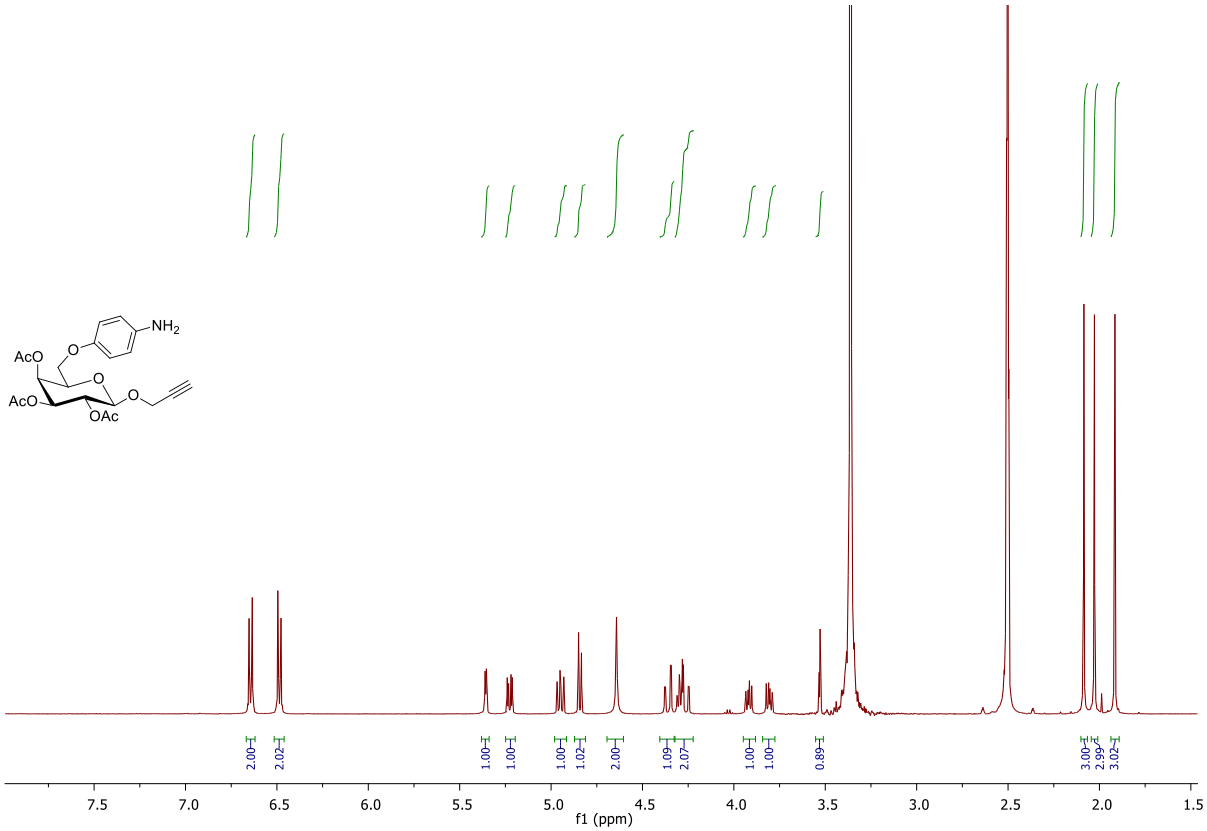

Figure 6.33: ^{1}H NMR spectrum of **61** (500 MHz, DMSO-d_6, 298 K).

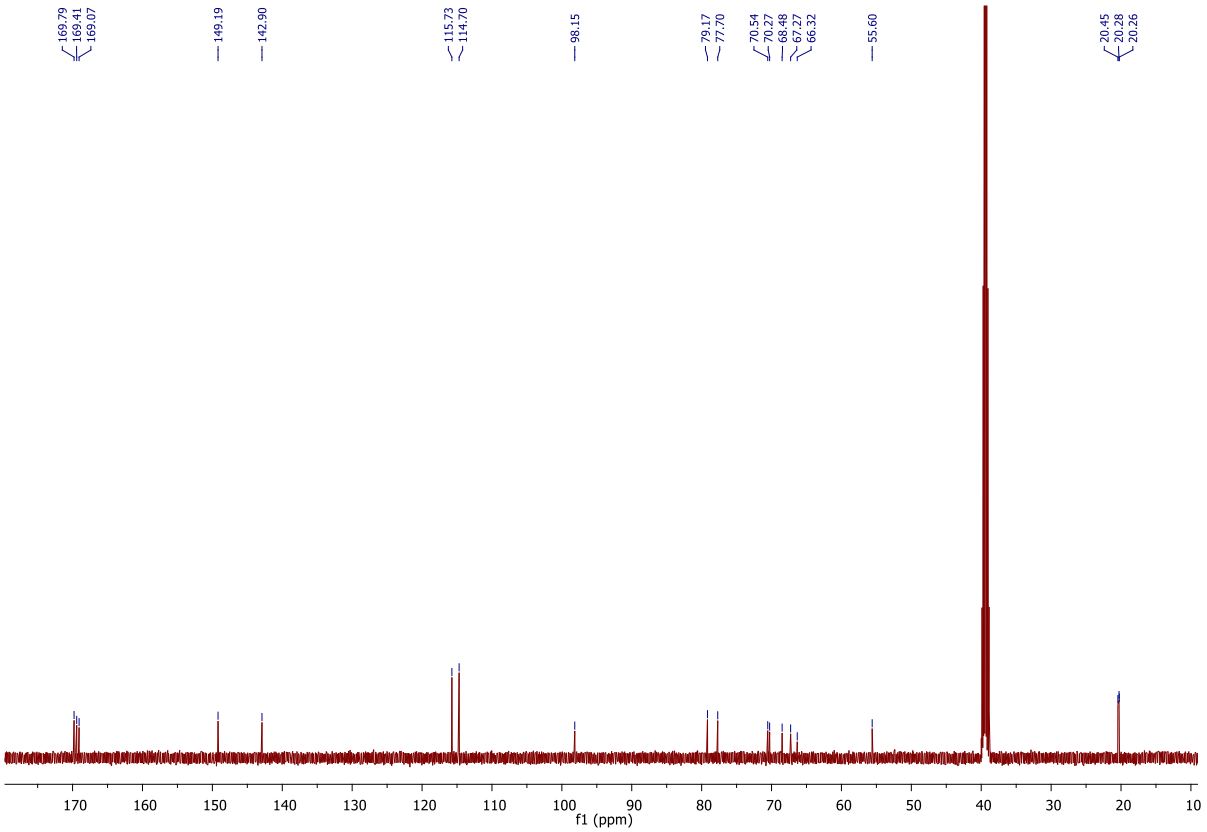

Figure 6.34: ^{13}C NMR spectrum of **61** (126 MHz, DMSO-d_6, 298 K).

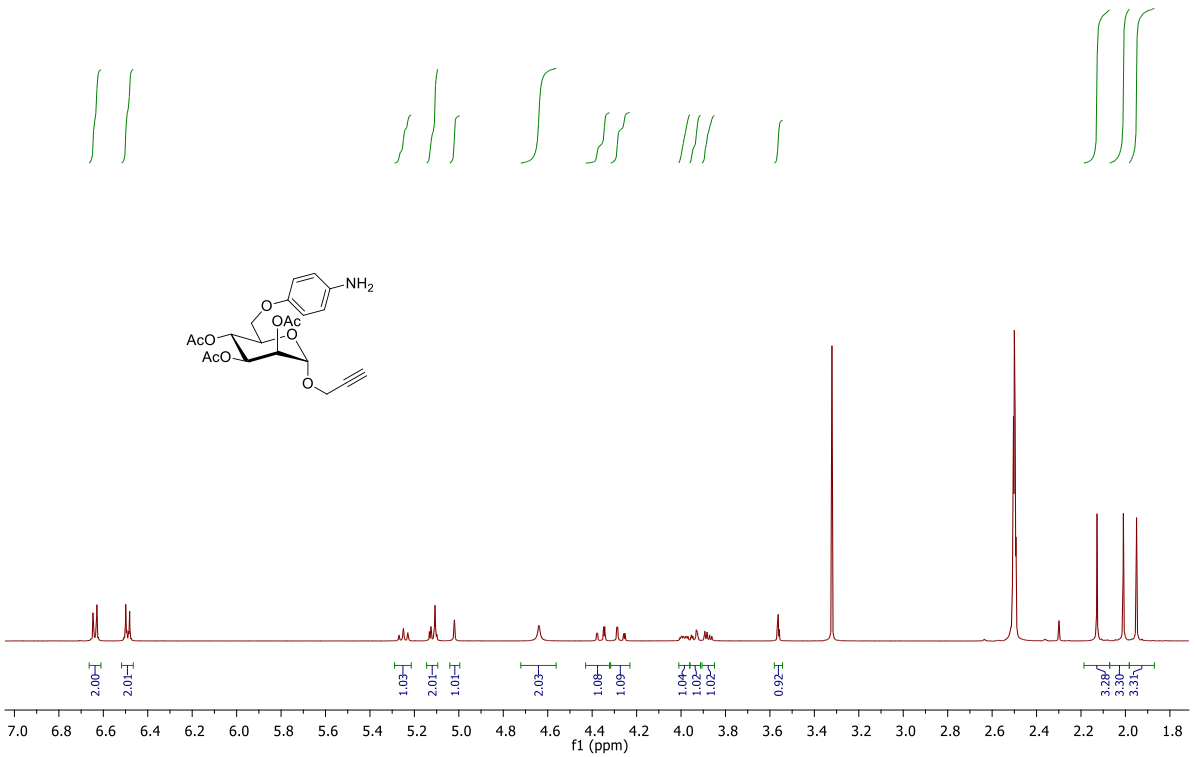

Figure 6.35: ^{1}H NMR spectrum of **63** (500 MHz, DMSO-d_6, 298 K).

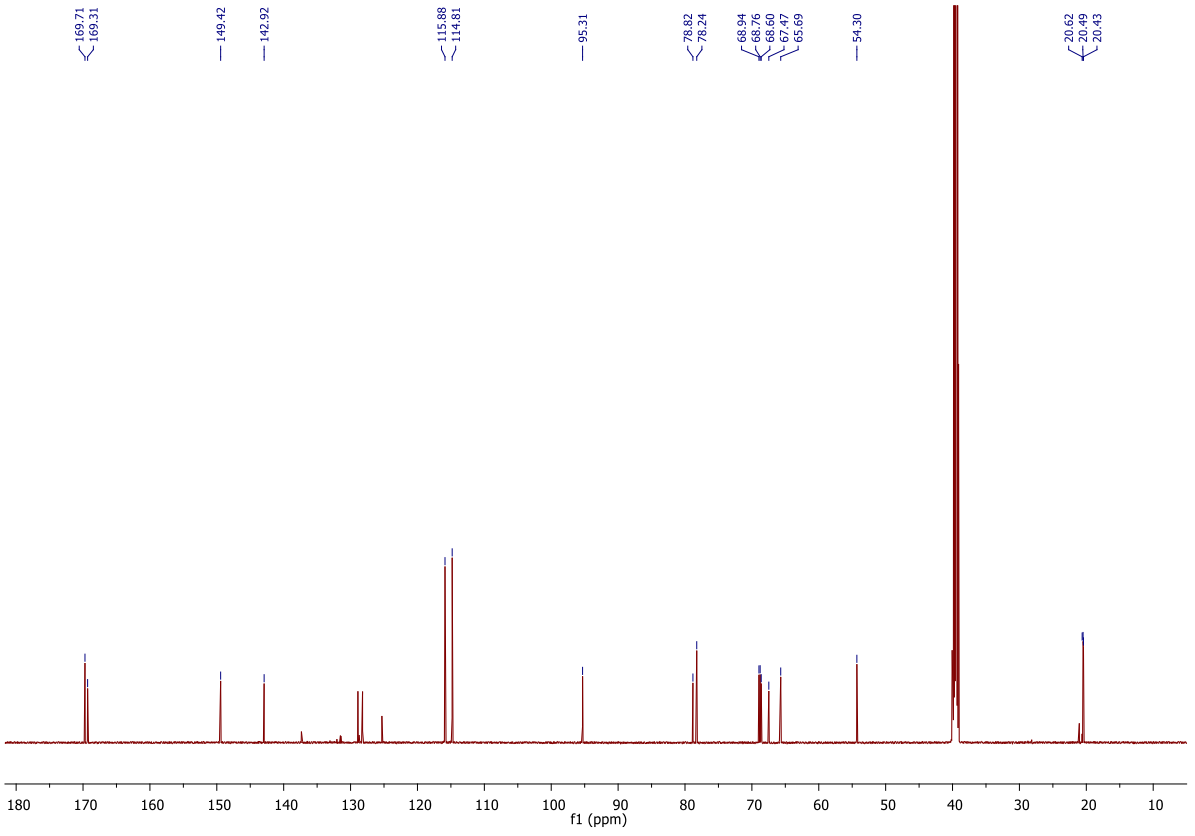

Figure 6.36: ^{13}C NMR spectrum of **63** (126 MHz, DMSO-d_6, 298 K).

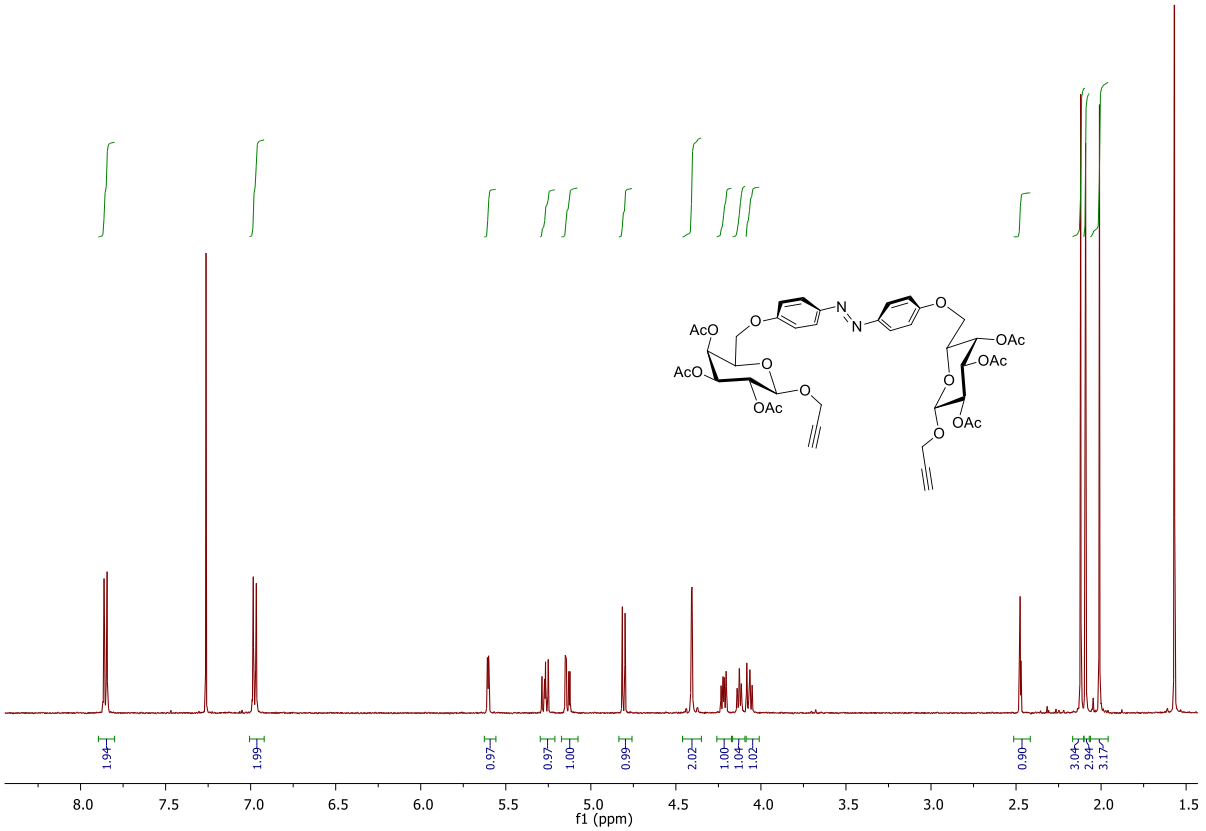

Figure 6.37: ^{1}H NMR spectrum of *trans*-**43** (500 MHz, $CDCl_3$, 298 K).

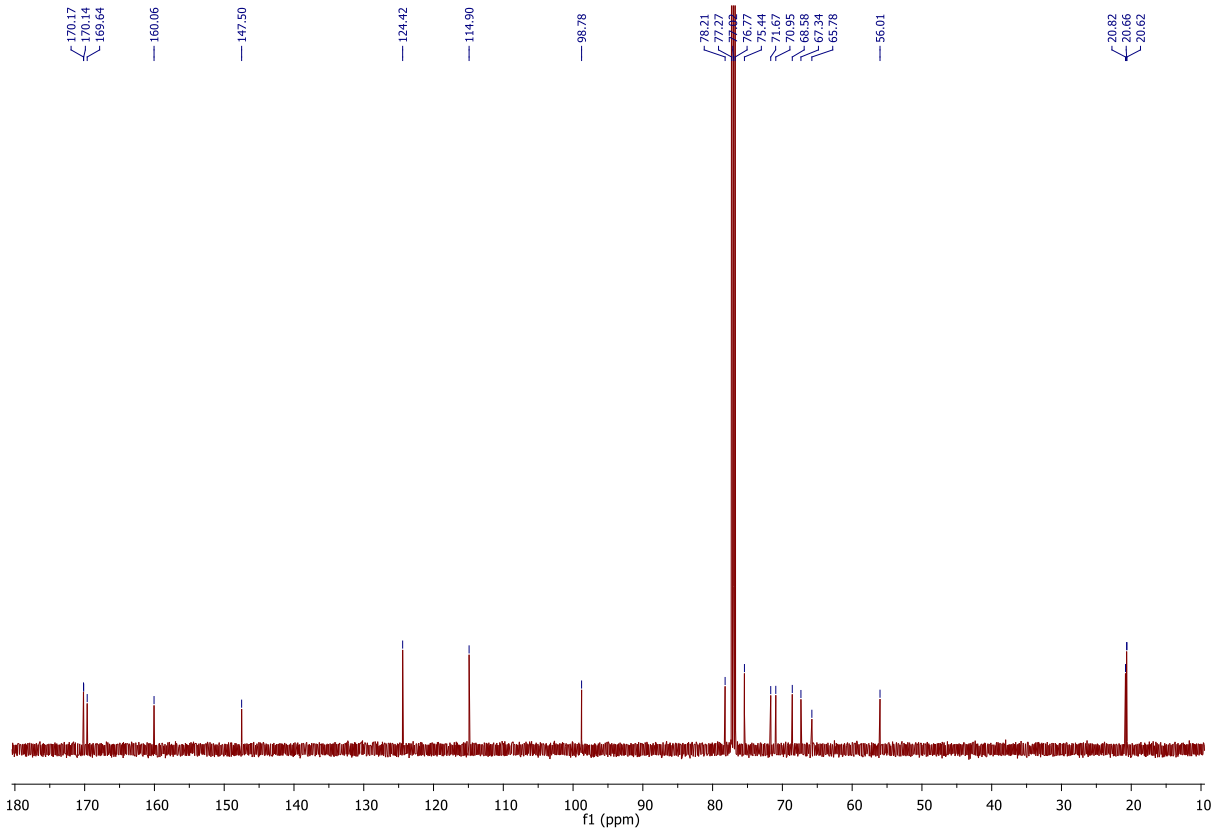

Figure 6.38: ^{13}C NMR spectrum of *trans*-**43** (126 MHz, $CDCl_3$, 298 K).

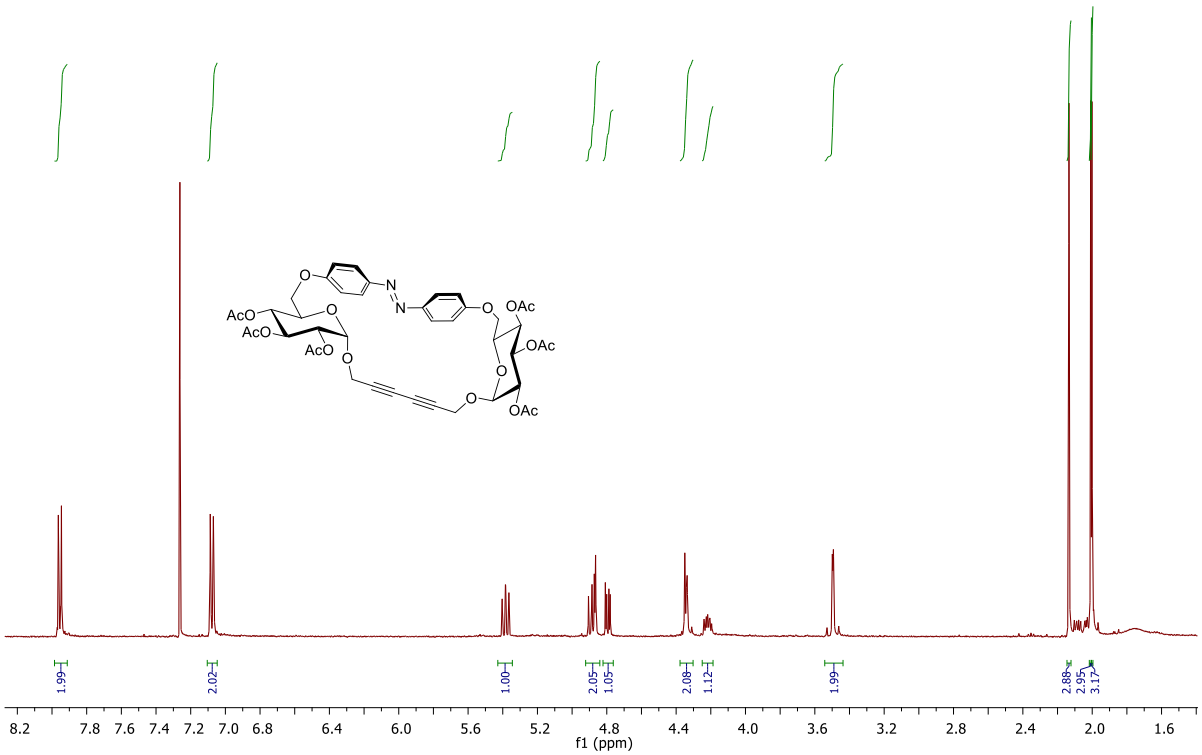

Figure 6.39: ^{1}H NMR spectrum of *trans*-**64** (500 MHz, $CDCl_3$, 298 K).

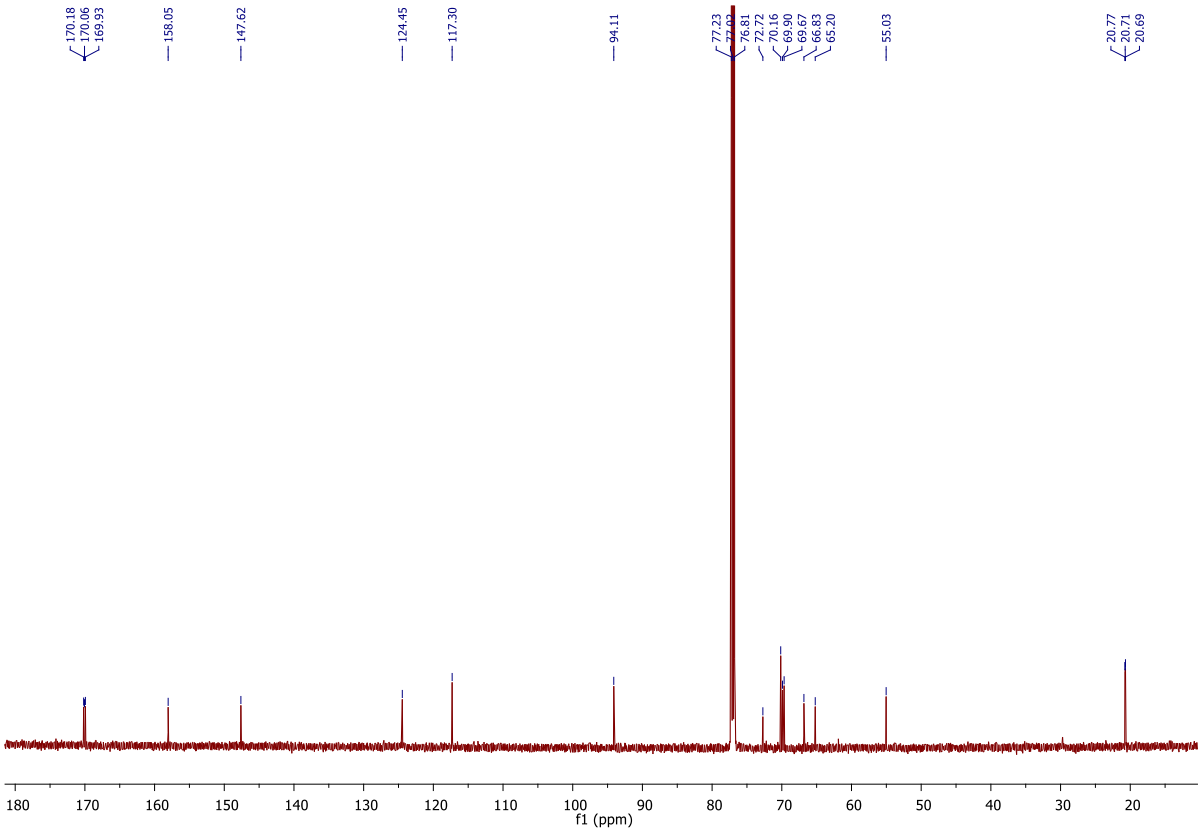

Figure 6.40: ^{13}C NMR spectrum of *trans*-**64** (151 MHz, $CDCl_3$, 298 K).

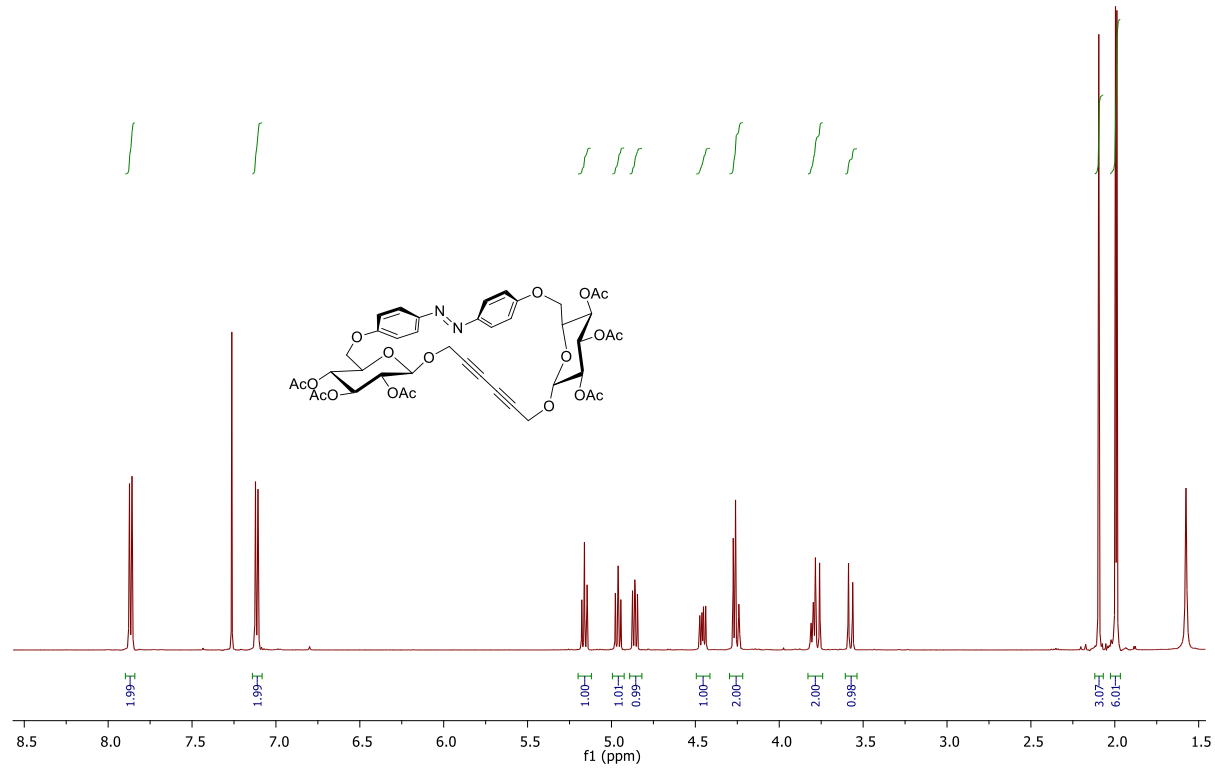

Figure 6.41: ^{1}H NMR spectrum of *trans*-**65** (600 MHz, $CDCl_3$, 298 K).

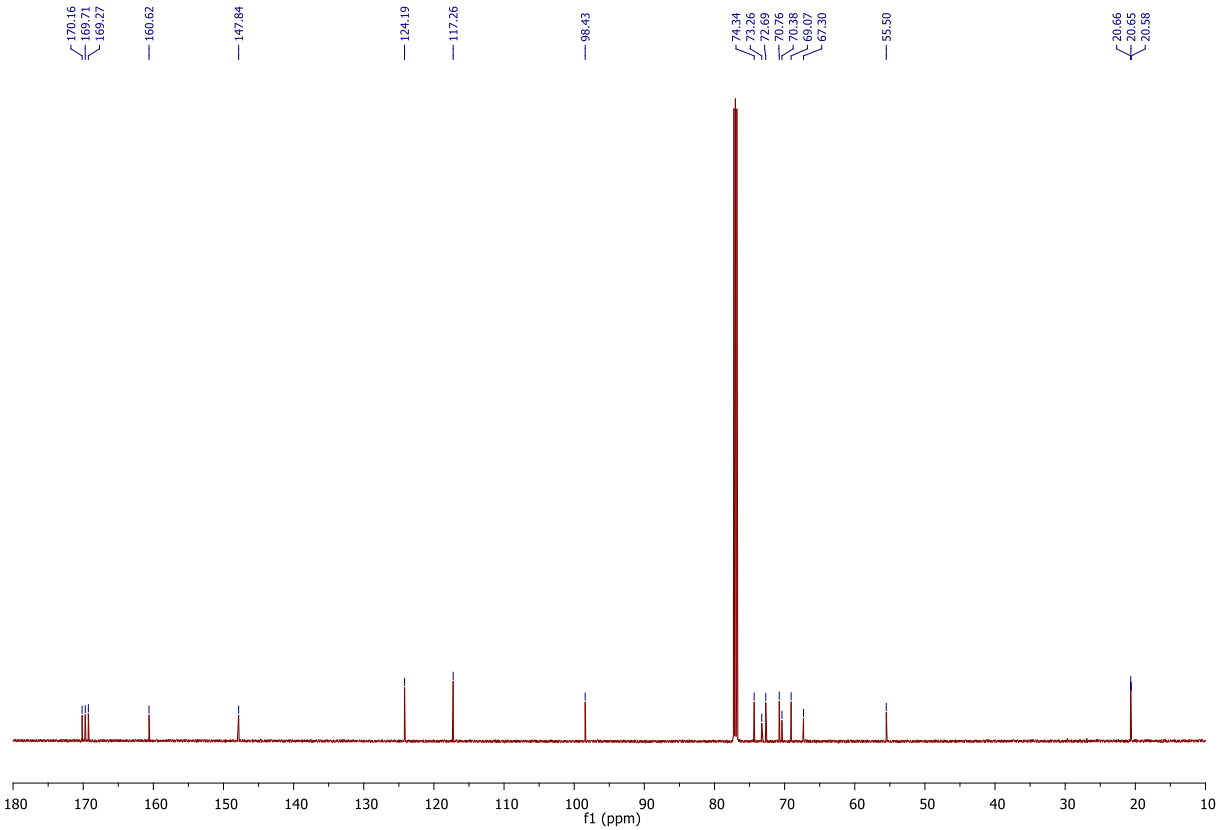

Figure 6.42: ^{13}C NMR spectrum of *trans*-**65** (151 MHz, $CDCl_3$, 298 K).

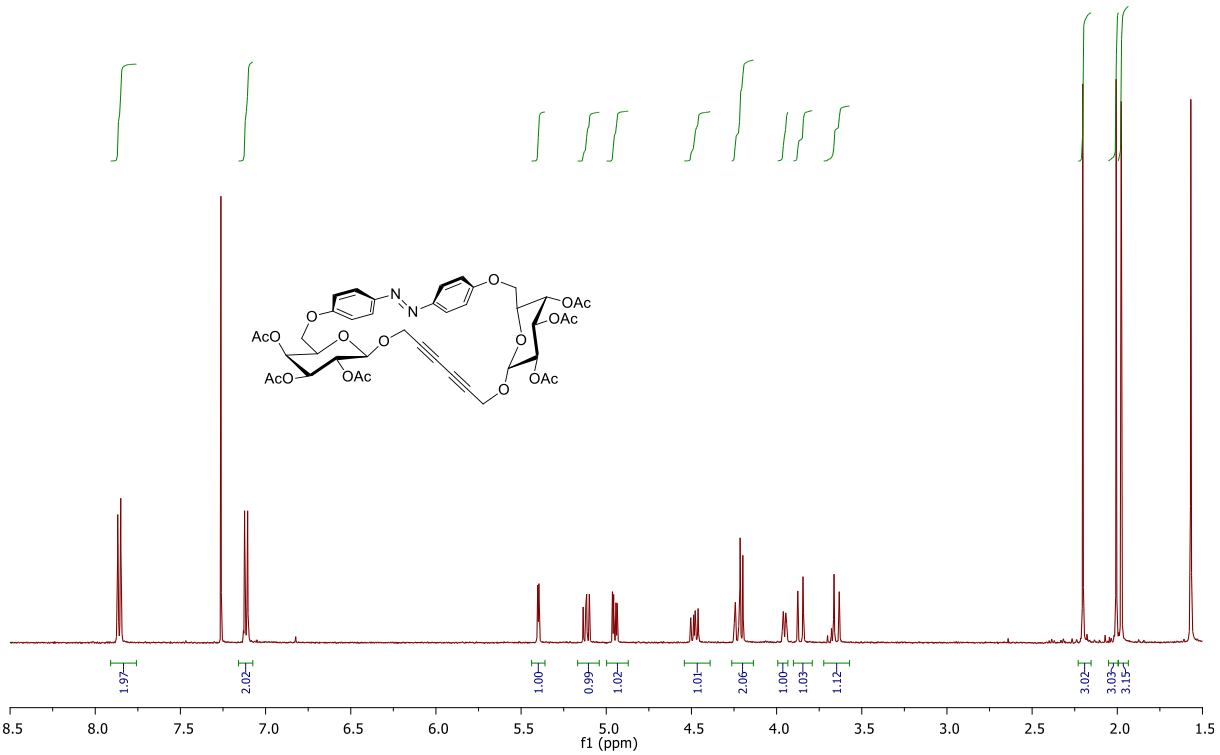

Figure 6.43: ^{1}H NMR spectrum of *trans*-**66** (500 MHz, $CDCl_3$, 298 K).

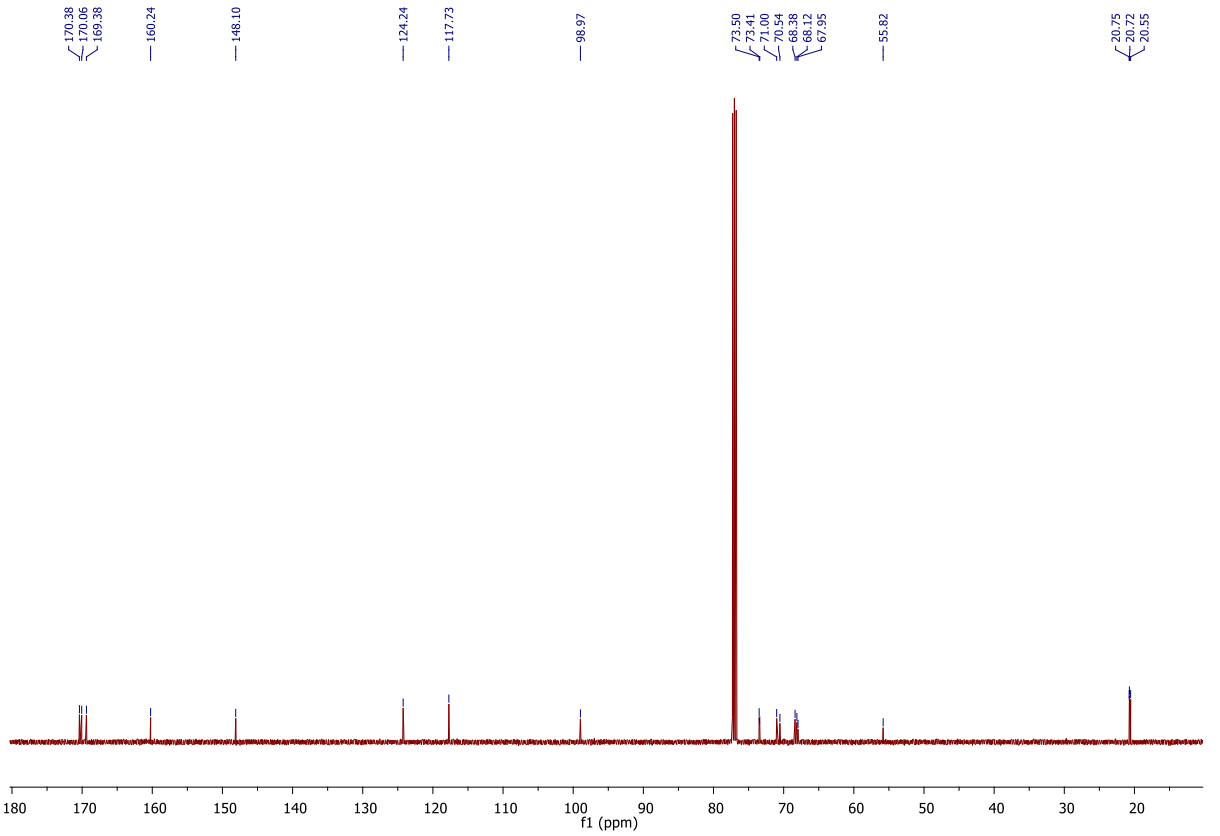

Figure 6.44: ^{13}C NMR spectrum of *trans*-**66** (126 MHz, $CDCl_3$, 298 K).

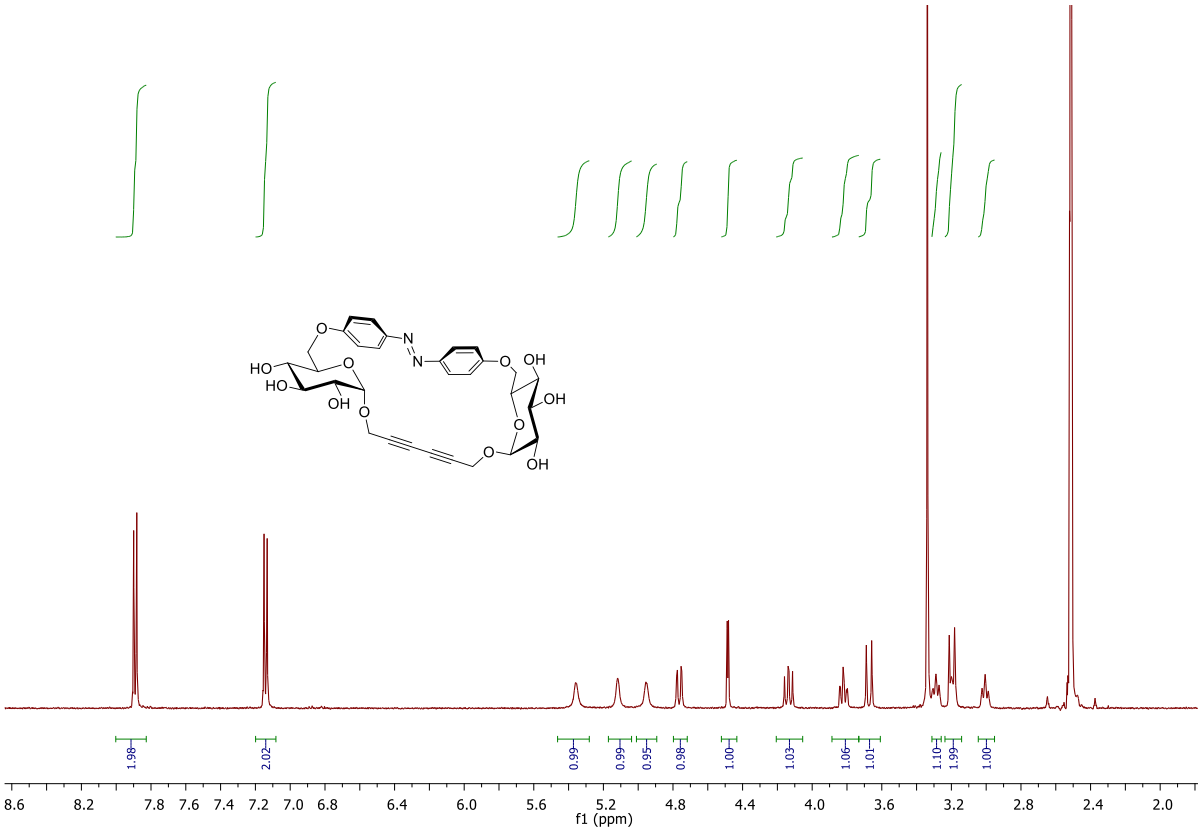

Figure 6.45: ^{1}H NMR spectrum of *trans*-**28** (500 MHz, DMSO-d_6, 298 K).

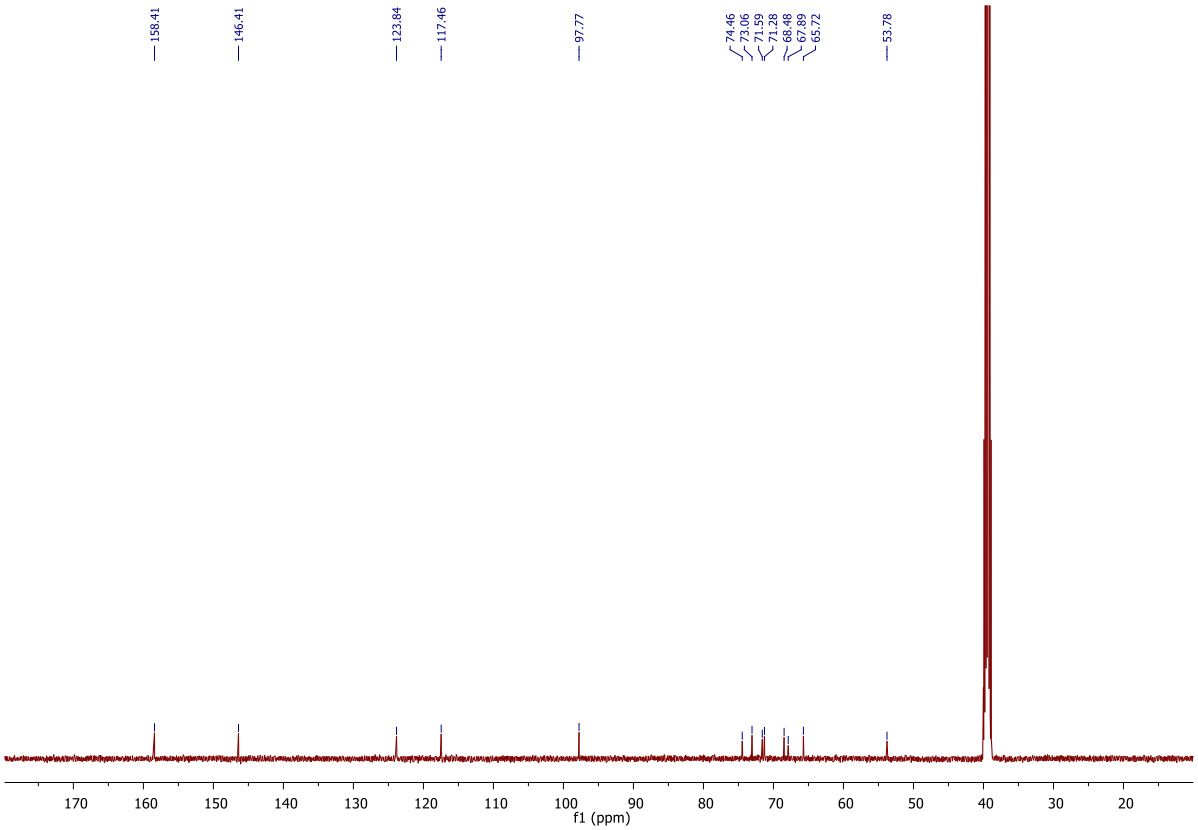

Figure 6.46: ^{13}C NMR spectrum of *trans*-**28** (126 MHz, DMSO-d_6, 298 K).

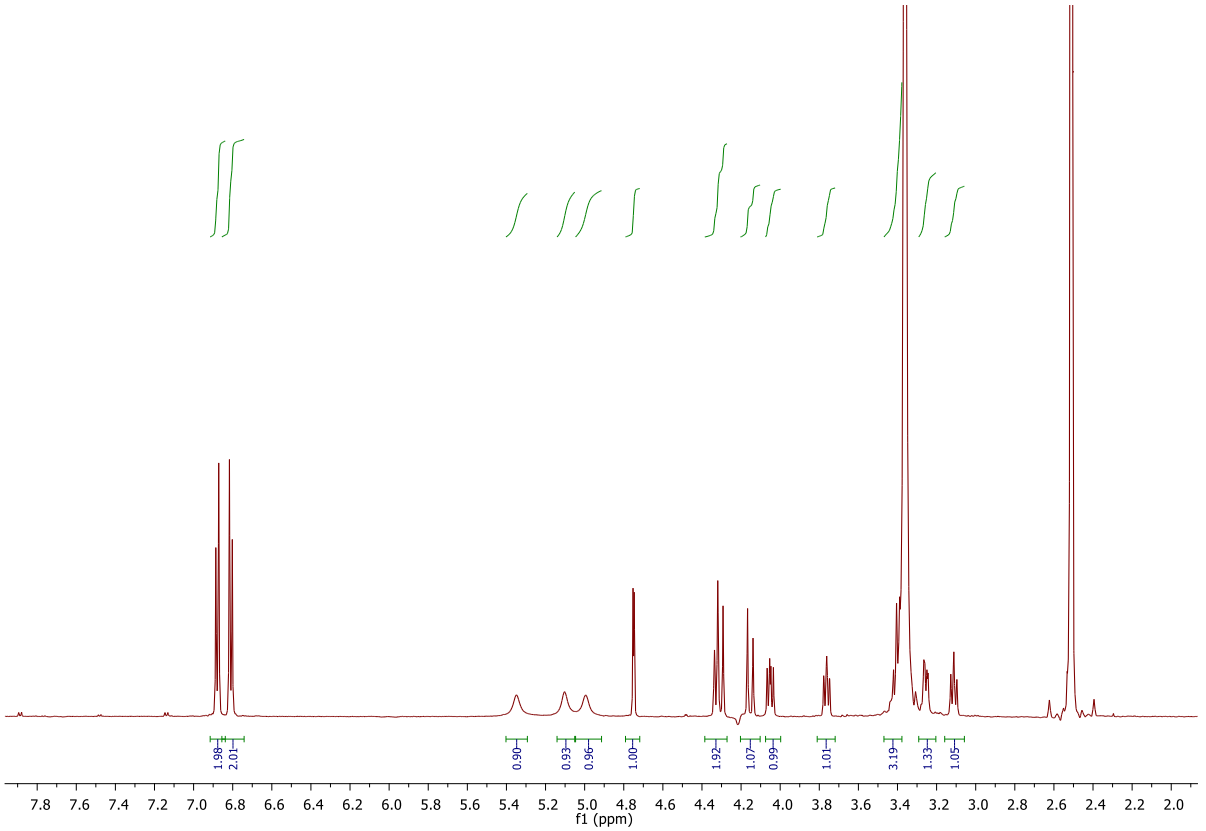

Figure 6.47: ^{1}H NMR spectrum of *cis*-**28** (600 MHz, DMSO-d_6, 298 K).

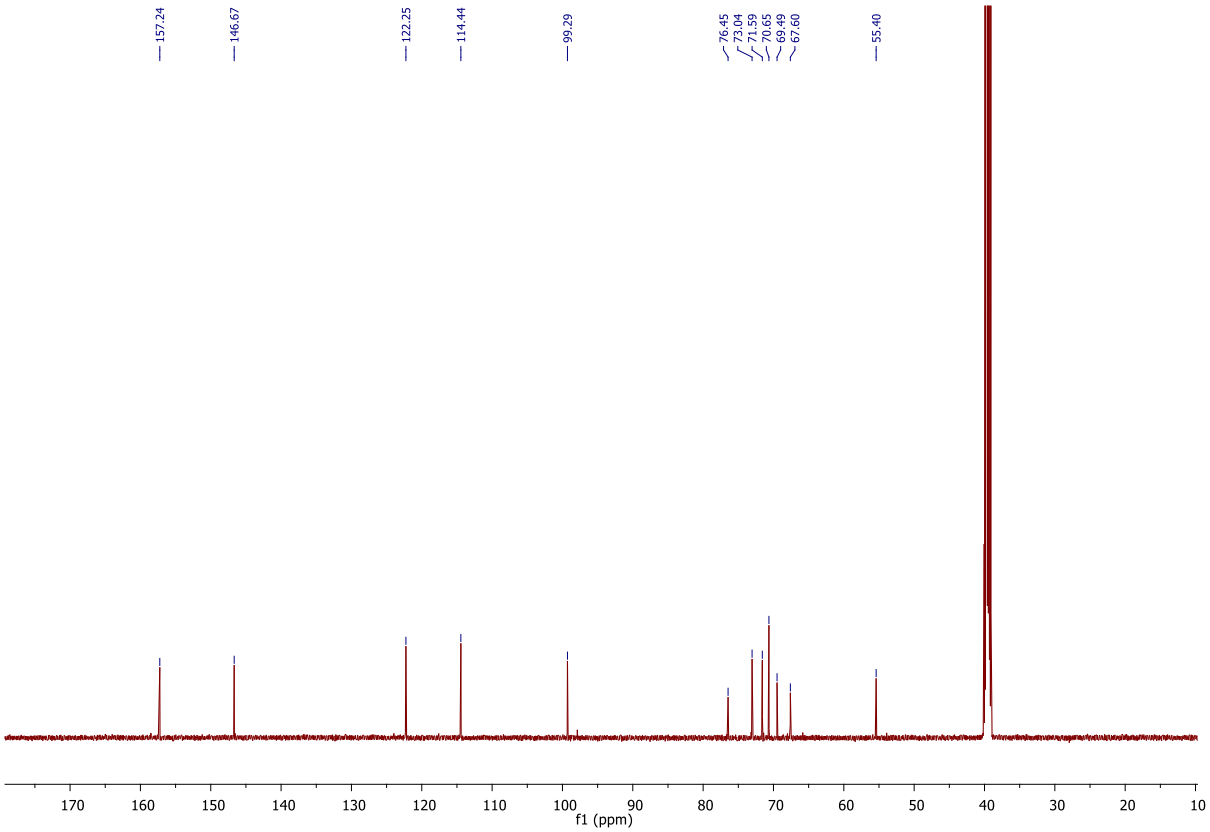

Figure 6.48: ^{13}C NMR spectrum of *cis*-**28** (151 MHz, DMSO-d_6, 298 K).

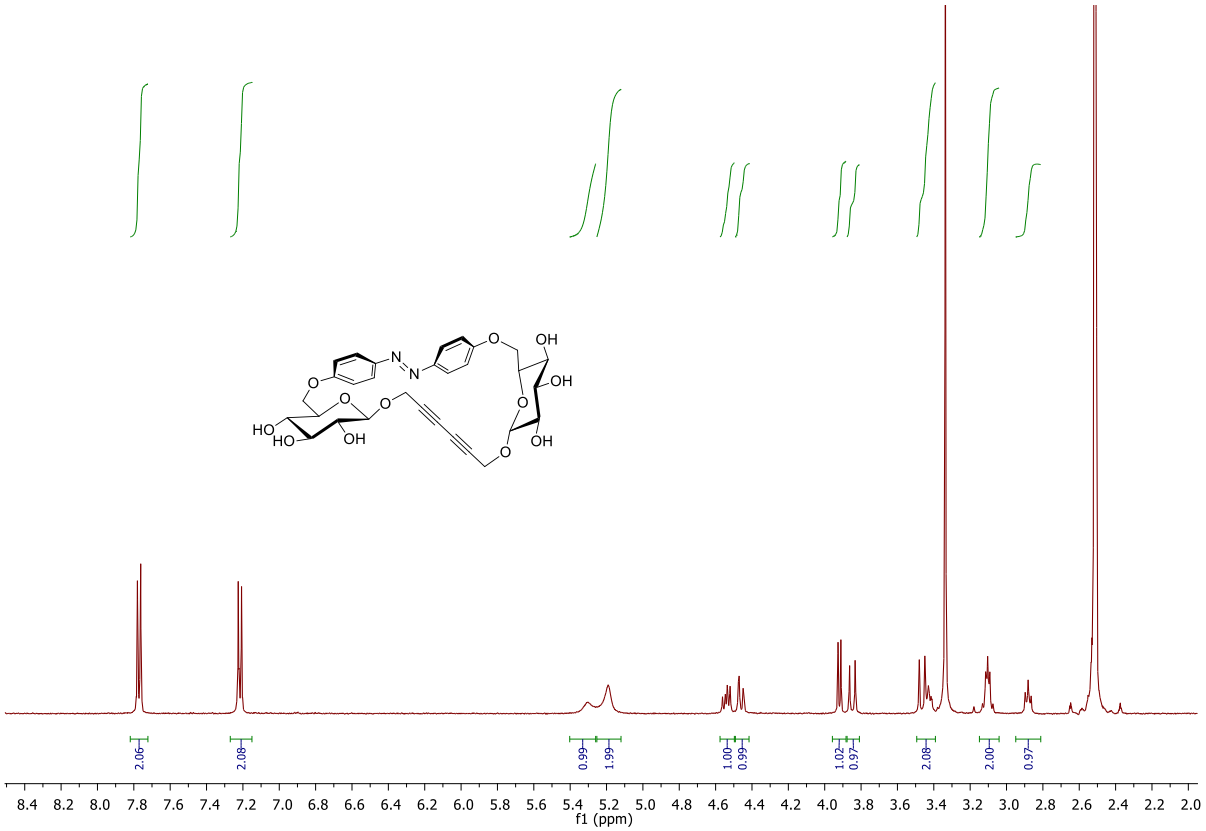

Figure 6.49: ^{1}H NMR spectrum of *trans*-**29** (500 MHz, DMSO-d_6, 298 K).

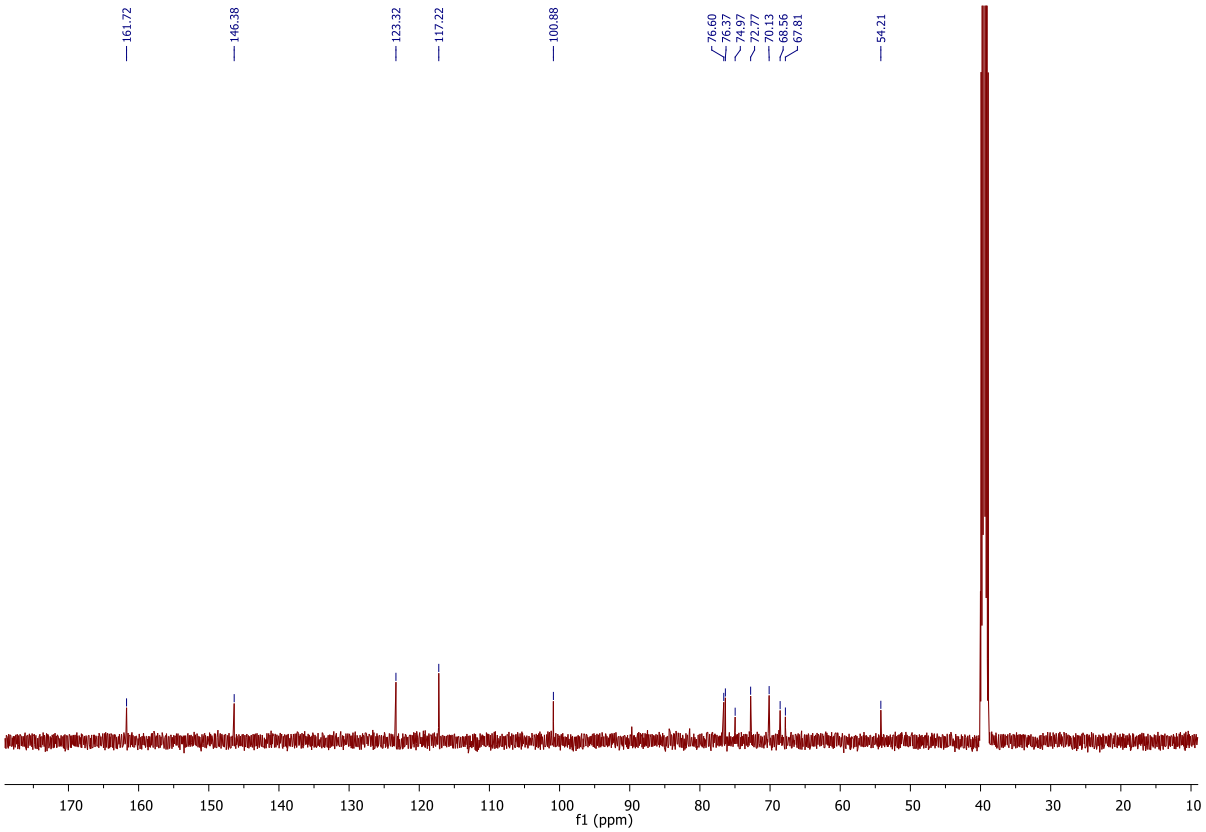

Figure 6.50: ^{13}C NMR spectrum of *trans*-**29** (126 MHz, DMSO-d_6, 298 K).

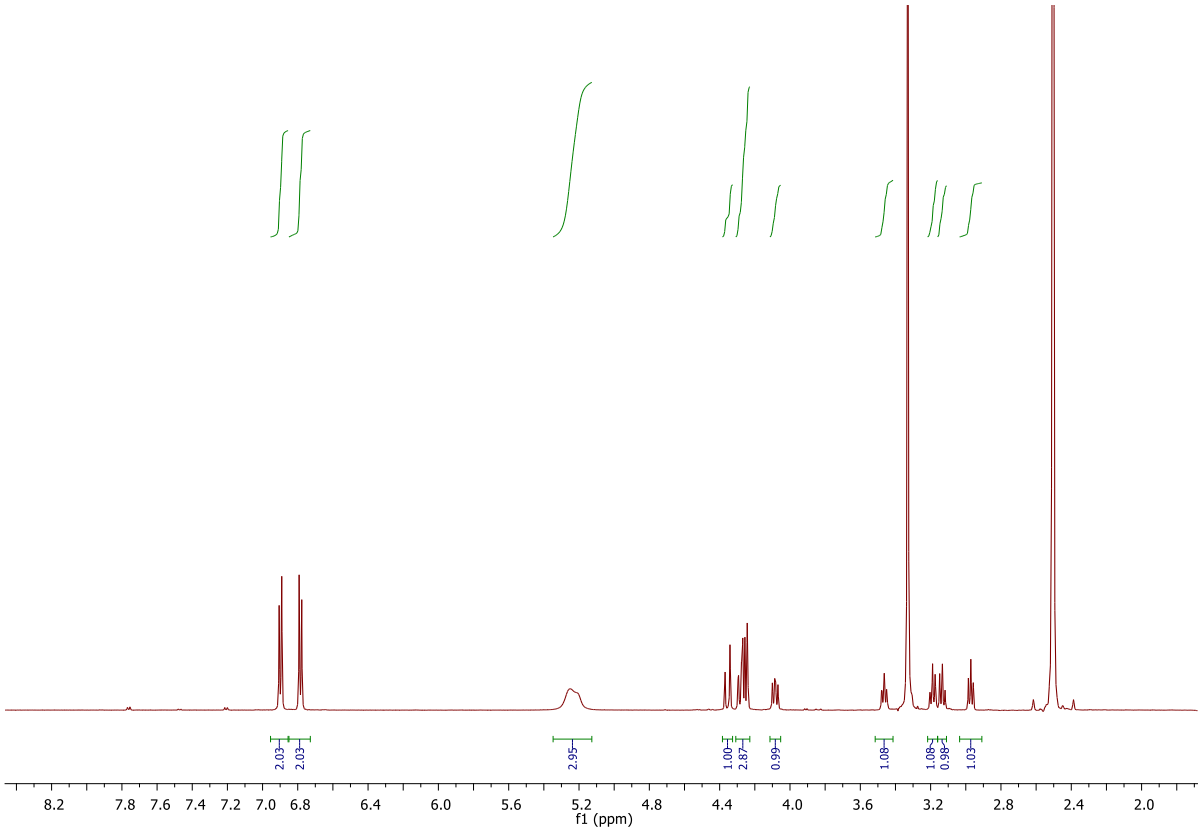

Figure 6.51: ^{1}H NMR spectrum of *cis*-**29** (600 MHz, DMSO-d_6, 298 K).

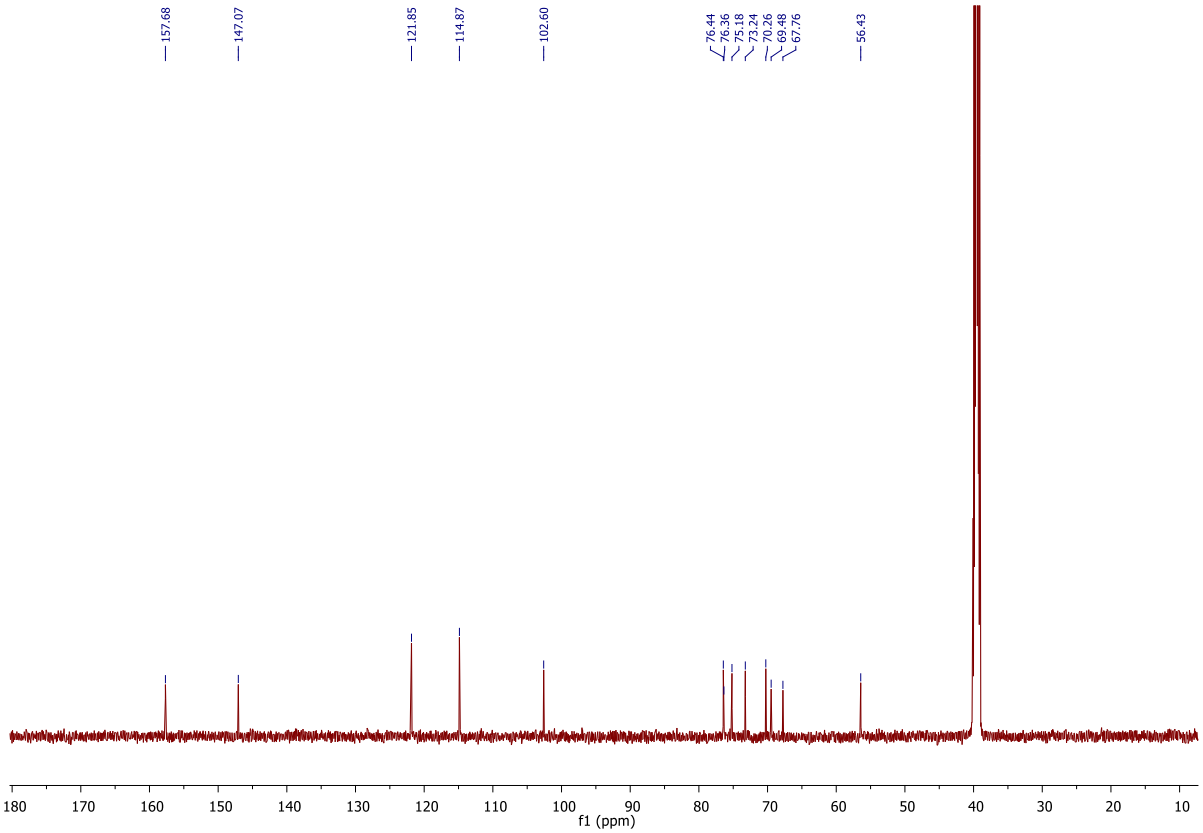

Figure 6.52: ^{13}C NMR spectrum of *cis*-**29** (151 MHz, DMSO-d_6, 298 K).

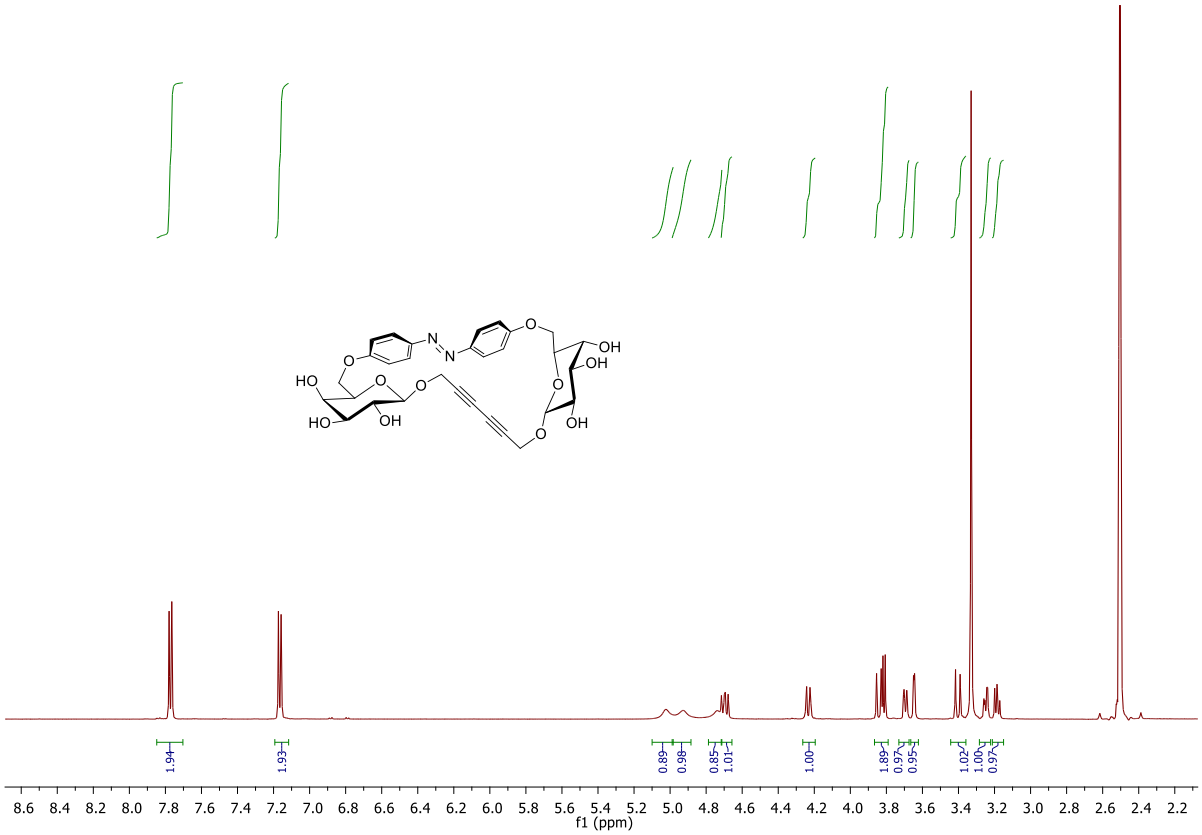

Figure 6.53: ^{1}H NMR spectrum of *trans*-**30** (600 MHz, DMSO-d_6, 298 K).

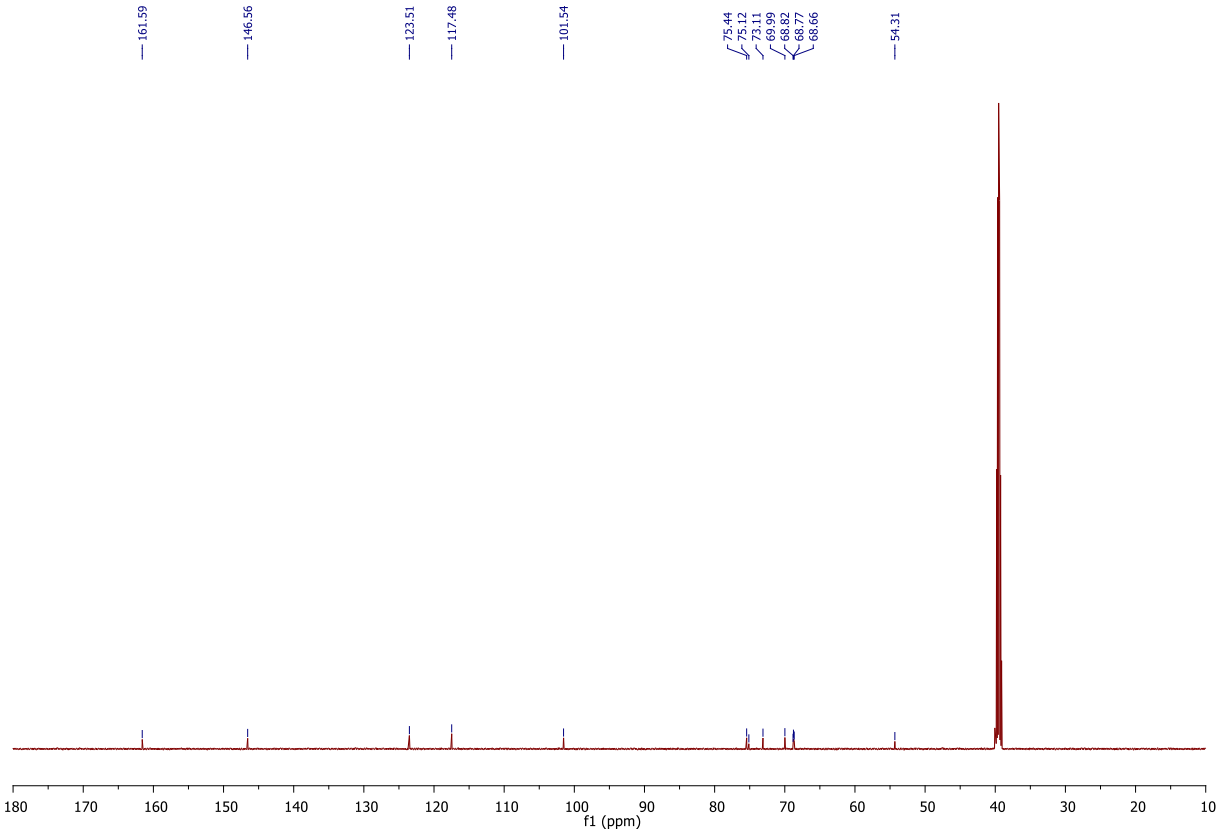

Figure 6.54: ^{13}C NMR spectrum of *trans*-**30** (151 MHz, DMSO-d_6, 298 K).

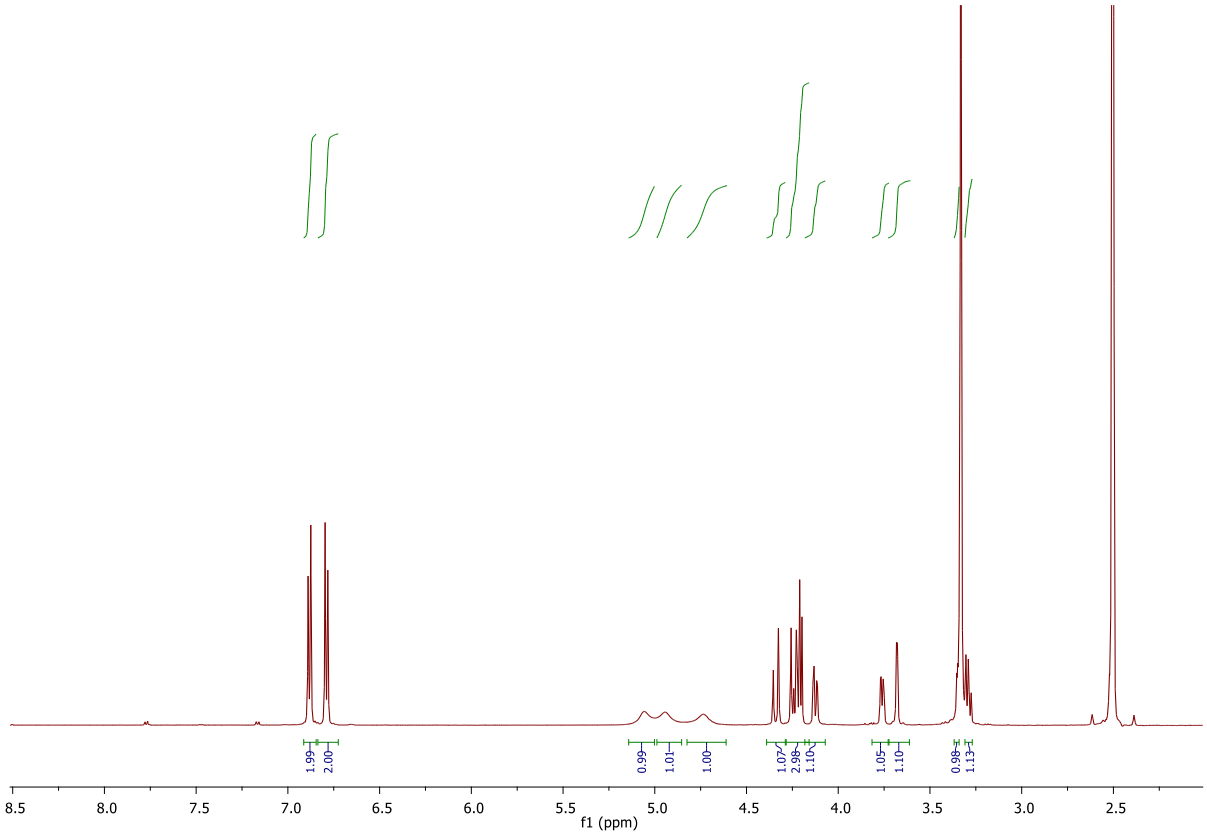

Figure 6.55: ^{1}H NMR spectrum of *cis*-**30** (600 MHz, DMSO-d_6, 298 K).

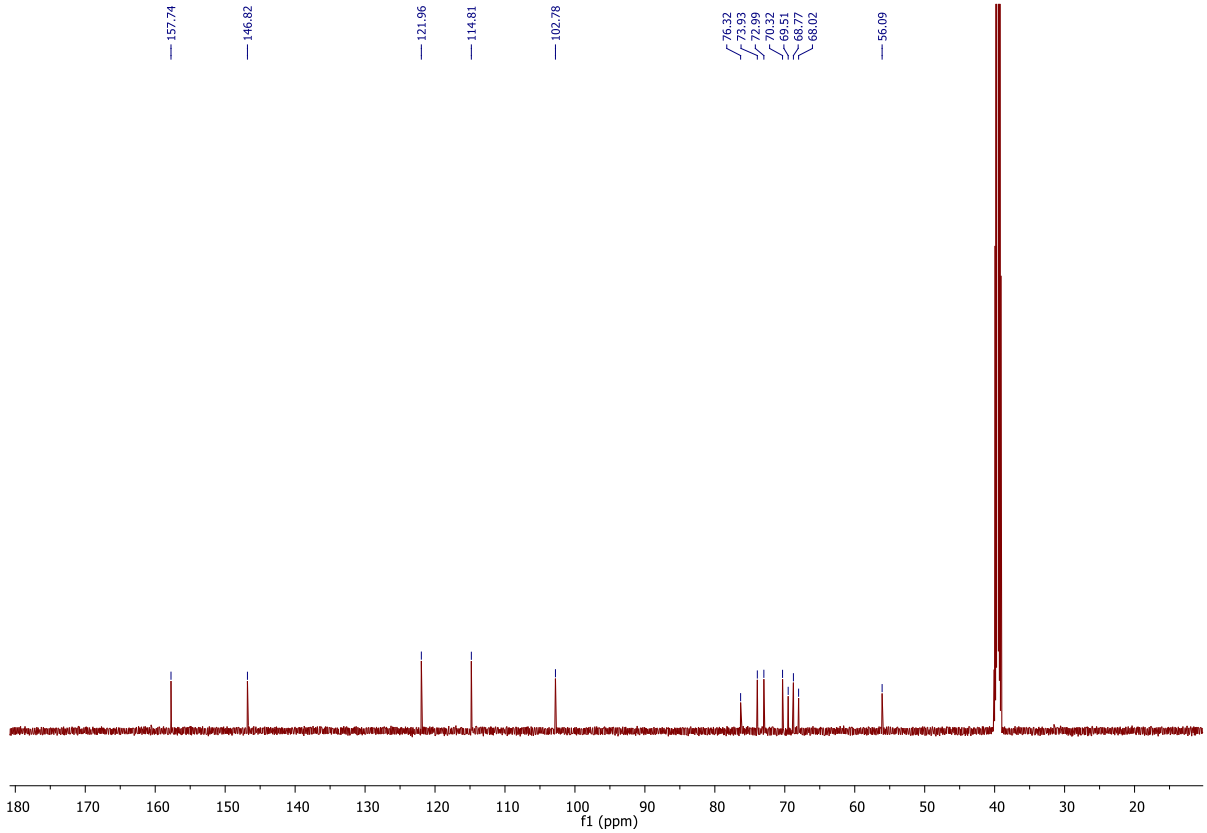

Figure 6.56: ^{13}C NMR spectrum of *cis*-**30** (151 MHz, DMSO-d_6, 298 K).

Irradiation experiments

PSS was reached after irradiating the respective sample for 5 min with 365 nm or 5 min with 520 nm and the respective *trans:cis* ratios of are shown in Figure 6.56, 6.57 and 6.58.

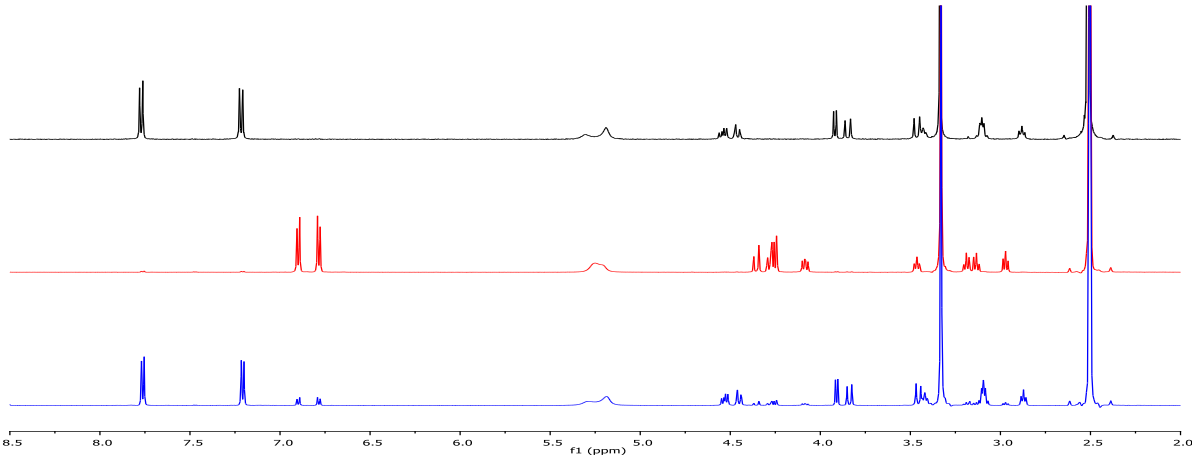

Figure 6.56: NMR spectra of *trans*-**29** after heating at 45 °C in the dark for 20 h (black), after irradiation with 365 nm for 5 min with a PSS of *trans:cis* 3:97 (red)and after irradiation with 520 nm (blue) for 5 min with a PSS of *trans*:*cis* 85:15.

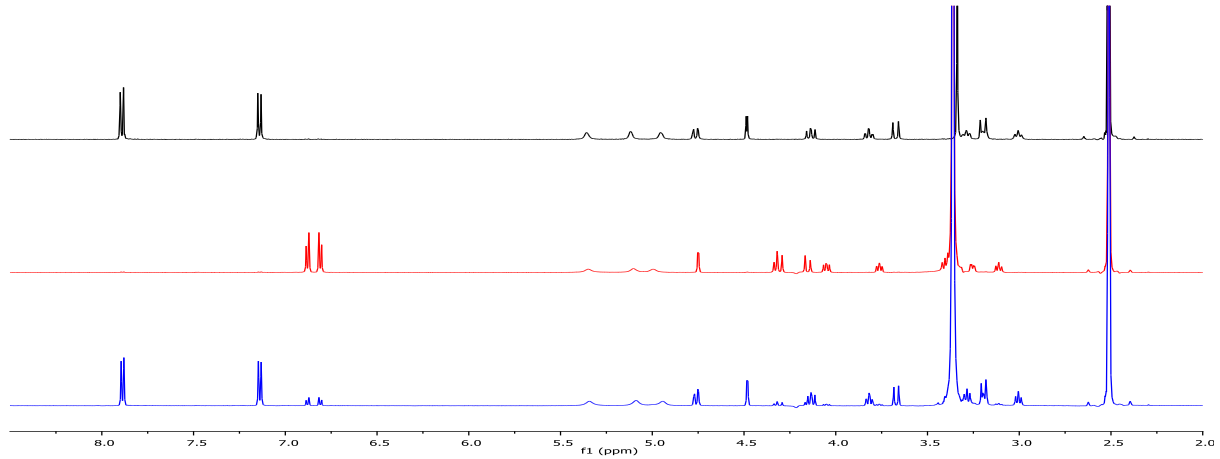

Figure 6.57: NMR spectra of *trans*-**28** after heating at 45 °C in the dark for 20 h (black), after irradiation with 365 nm for 5 min (red) with a PSS of *trans:cis* 3:97 and after irradiation with 520 nm (blue) for 5 min with a PSS of *trans:cis* 87:13.

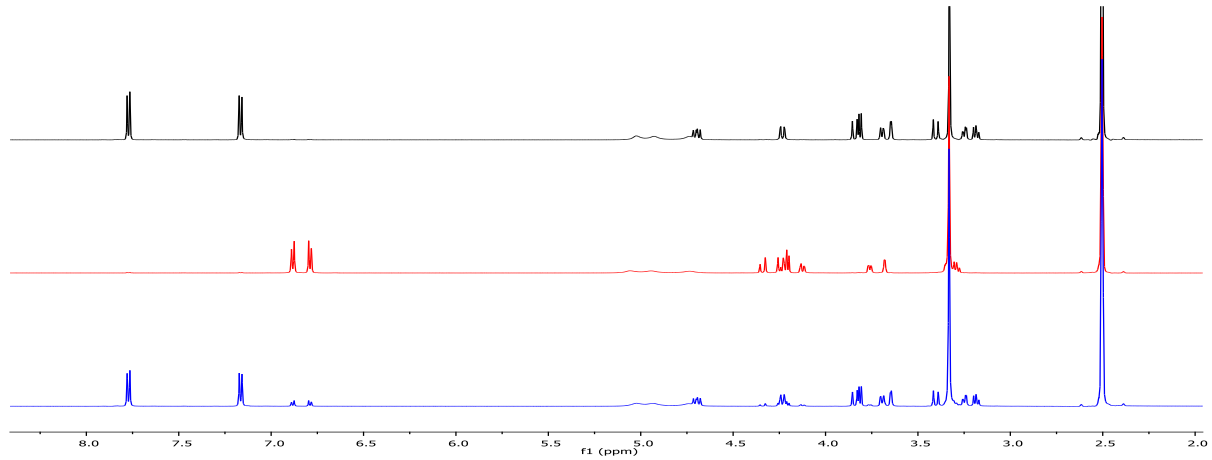

Figure 6.58: NMR spectra of *trans*-**30** after heating at 45 °C in the dark for 20 h (black), after irradiation with 365 nm for 4 min (red) with a PSS of *trans:cis* 3:97 and after irradiation with 520 nm (blue) for 8 min with a PSS of *trans:cis* 87:13.

The extinction coefficient ε and the coefficient of determination of the linear fitting for *trans*- and *cis*-**28**, -**29** and -**30** are shown along the plot of the absorbance against the concentration in Figure 6.59.

The switching cycle experiments for **28, 29** and **30** are shown in Figure 6.60 with the plot of the value of the absorbance at $\lambda_{max(E)}$ against the number of times the sample was irradiated.

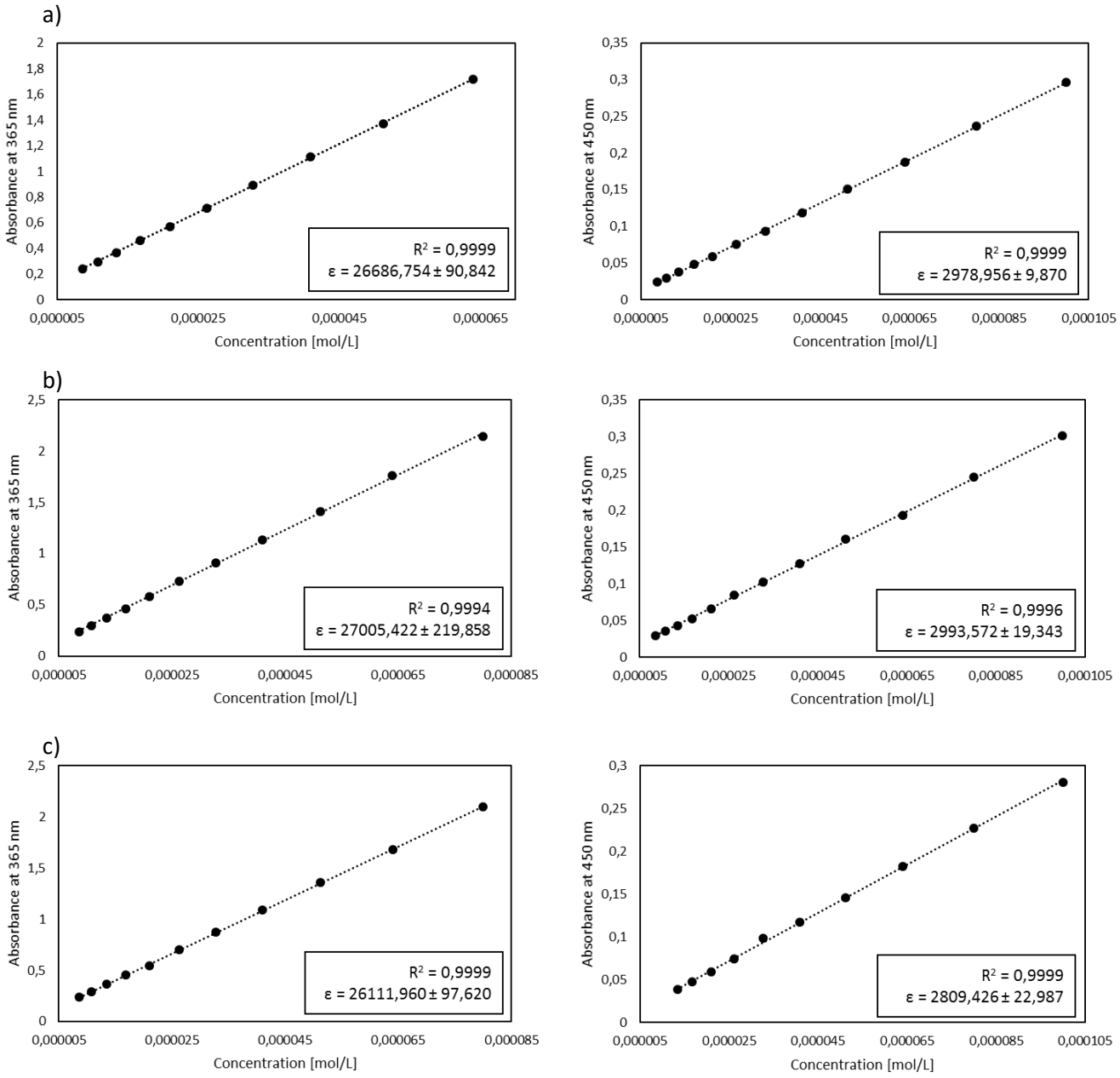

Figure 6.59: Plot of the absorbance at the λ_{max} versus the concentration; the slope of the linear curve gives the value of the molar extinction coefficient ε. Measured at 298 K in DMSO in concentrations from $8 \cdot 10^{-6}$ to 10^{-4} mol·L^{-1}. (a) *trans*-**29** at 365 nm and PSS 365 nm at 450 nm; (b) *trans*-**28** at 365 nm and PSS 365 nm at 450 nm; (c) *trans*-**30** at 365 nm and PSS 365 nm at 450 nm.

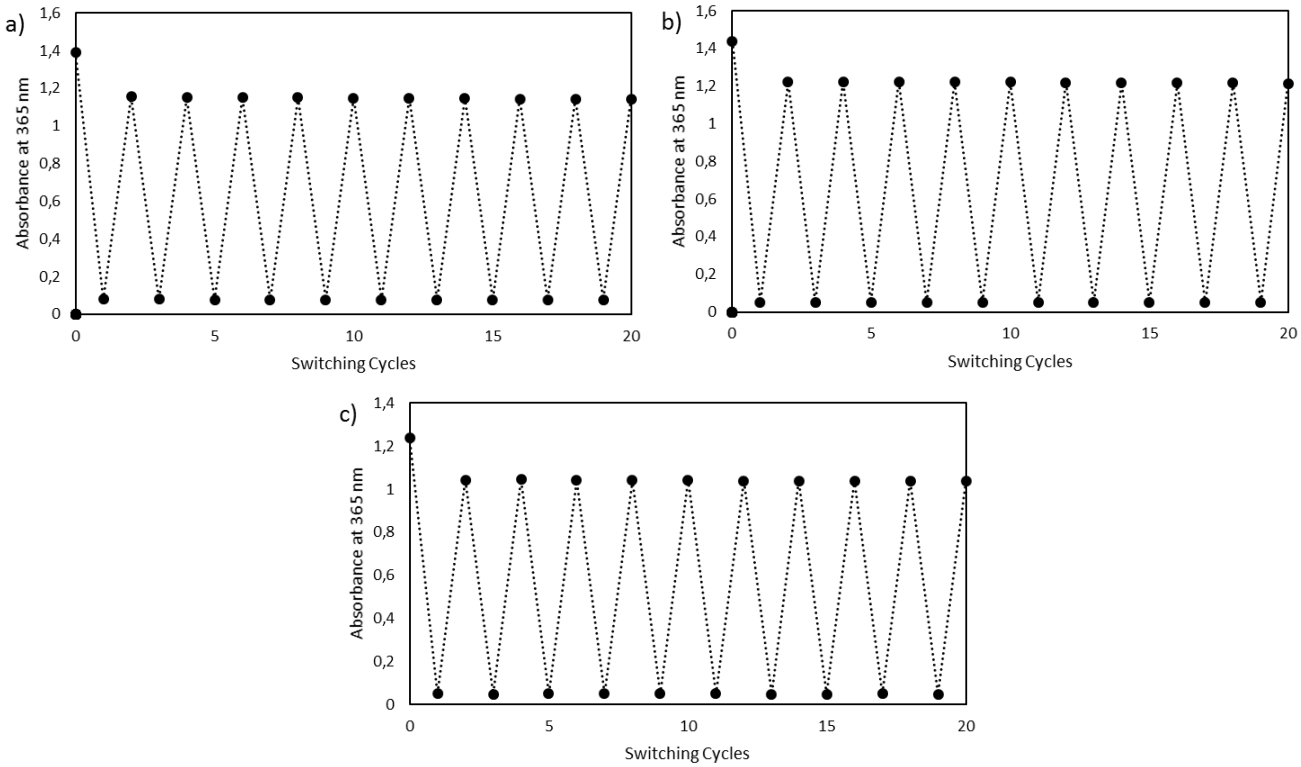

Figure 6.60: Measured absorbance after alternating photoirradiation with 365 nm and 520 nm. Measured at 298 K in DMSO in a concentration of 50 µM. (a) **29**; (b) **28**; (c) **30**.

The decay of the absorbance of the n-π* band λ_{max} of cis-**27**, **28**, **29** and **30** are shown alongside the coefficient of determination of the exponential fitting and the absorbance at infinite time in Figure 6.61. The linearization of the absorbance is shown with the coefficient of determination of the linear fitting, the rate constant and the ensuing half-life time

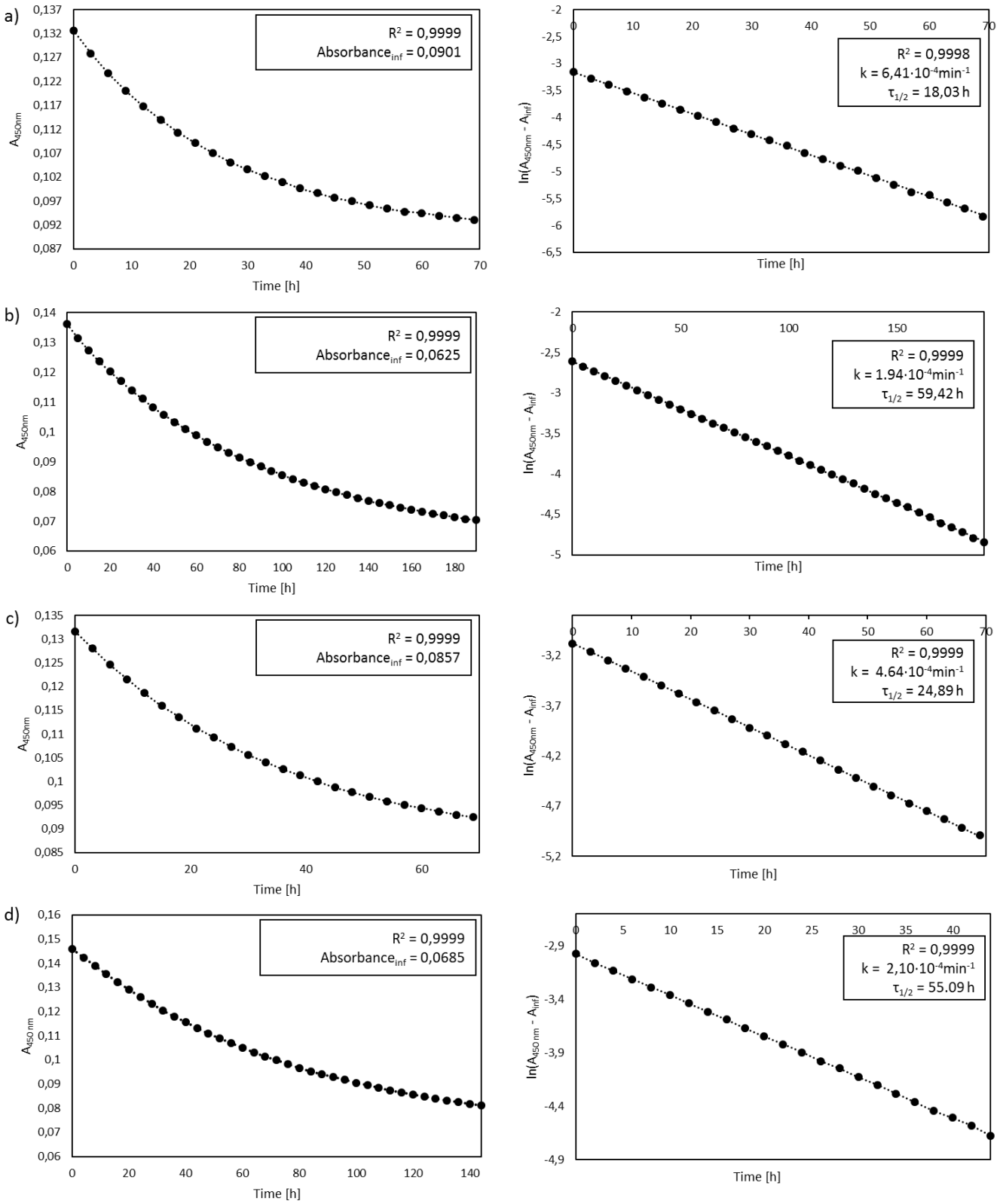

Figure 6.61: Kinetics of the *cis*→*trans* thermal relaxation process, measured at 298 K in DMSO at a concentration of 50 µM, showing the exponential decay of the absorbance at 450 nm and the linearization with the corresponding coefficient of determination and the half-life time for the *cis*-form of the respective compounds. (a) **29**; (b) **28**; (c) **30**; (d) **27**.

CD measurements in water

To measure the CD spectra of the partially soluble macrocycles **27**, **28**, **29** and **30** in water, 10 µL of a 10 mM stock solution in DMSO of the respective compound was added to 1990 µL water and mixed vigorously right before measuring the first spectrum.

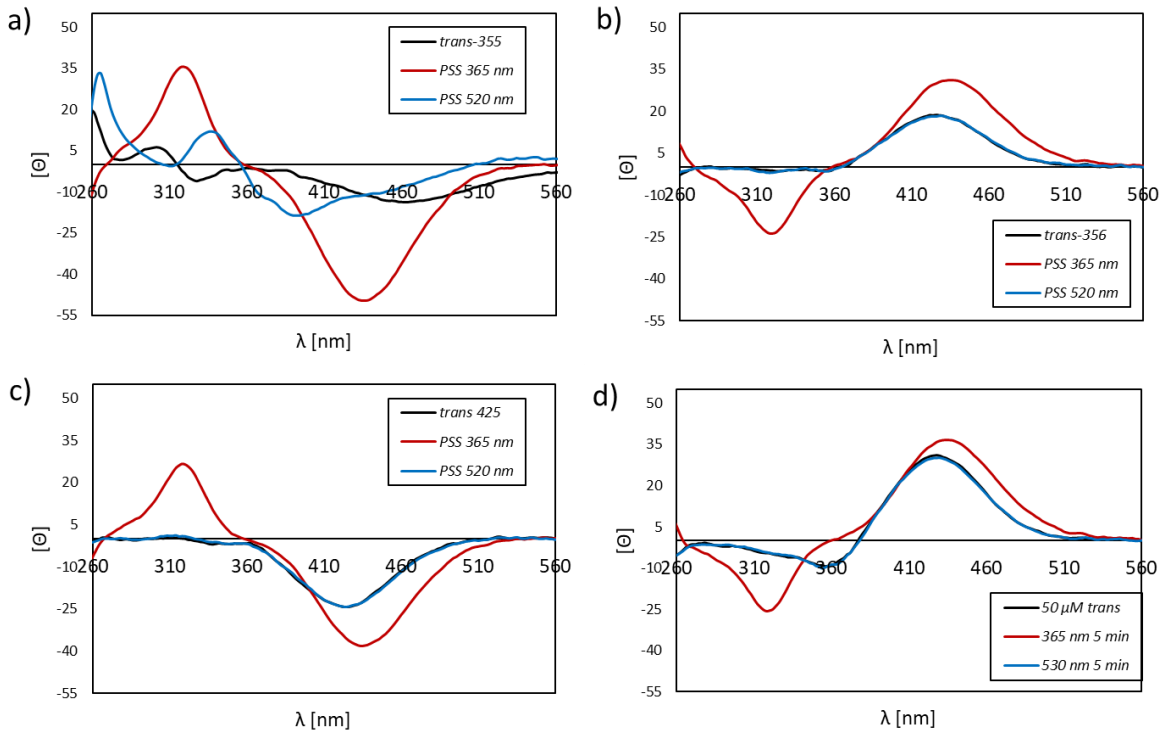

Figure 6.62: CD spectra of the macrocycles in water with 0.5 % DMSO at 298 K (a) **27**; (b) **29**; (c) **28**; (d) **30**; black line: *trans*-macrocycle, red line: PSS after irradiation with 365 nm for 5 min, blue line: PSS after irradiation with 520 nm for 5 min.

6.7 Publication: A two-step approach to a glycoazobenzene macrocycle with remarkable photoswitchable features

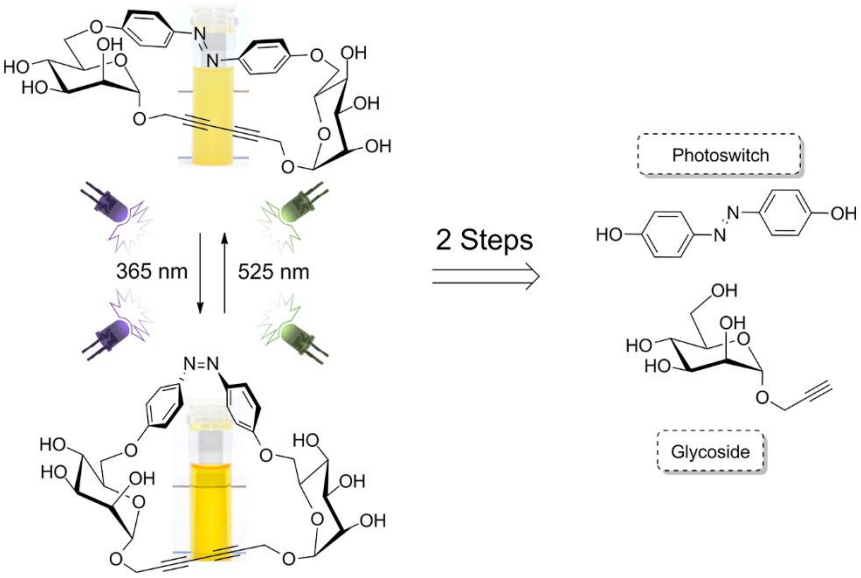

J. Hain, G. Despras, *Chemm. Commun.* **2018**, *54*, 8563-8566.

DOI: 10.1039/c8cc03724h

Volume 54 | Number 62 | 11 August 2018 | Pages 8537–8656

ChemComm

Chemical Communications
rsc.li/chemcomm

ISSN 1359-7345

ROYAL SOCIETY OF CHEMISTRY

COMMUNICATION
Julia Hain and Guillaume Despras
A two-step approach to a glycoazobenzene macrocycle with remarkable photoswitchable features

ChemComm

COMMUNICATION

View Article Online
View Journal | View Issue

Cite this: *Chem. Commun.*, 2018, 54, 8563

Received 8th May 2018,
Accepted 31st May 2018

DOI: 10.1039/c8cc03724h

rsc.li/chemcomm

A two-step approach to a glycoazobenzene macrocycle with remarkable photoswitchable features†

Julia Hain and Guillaume Despras *

A combination of the Mitsunobu reaction and Glaser coupling was used to achieve a new glycoazobenzene macrocycle. This photosensitive macrocycle can be efficiently and reversibly switched between two stable conformational isomers, which are characterized with photoswitchable shape, chiroptical and solubility behaviour.

Macrocycles are an interesting class of molecules with unique properties and a broad scope of applications, both for their natural representatives and synthetic counterparts.[1–3] Carbohydrates are especially suitable as components for macrocycles, due to their natural abundance and biocompatibility on one hand, and their synthetic potential, based on their defined stereochemistry, multifunctionality and structural diversity, on the other hand.[4–8] In recent years, azobenzenes have been increasingly implemented in macrocycles in order to allow for temporal and spatial control of the physicochemical properties through irradiation with light.[9–15] Azobenzenes are indeed an ideal class of photoswitches, as they undergo fast, efficient and reversible *trans–cis* isomerisation with high quantum yields and robustness against photobleaching, while undergoing a significant change in molecular size, geometry and polarity upon switching.[16–18] Although azobenzene glycoconjugates are already known for their excellent properties and applications in bioorganic chemistry,[19–23] carbohydrate-based macrocycles containing azobenzene units have only recently become a subject of interest.[24,25] We showed that the combination of azobenzenes with rigid pyranoside units leads to macrocycles that are able to change remarkably in form and function by switching between two defined structural shapes.[24] Importantly, a transfer of chirality proceeds from the carbohydrate(s) to the azobenzene unit, resulting in a remarkable chiroptical behaviour and a unidirectional photoisomerization of the azo bond.[26–30]

To broaden the collection of photoswitchable glycomacrocycles and thereby modulate further molecular properties upon shape switching, in this communication we report on an alternative design based on the straightforward connection of the azobenzene moiety at the 6-position of a α-propargyl mannoside and a subsequent cyclisation *via* intramolecular Glaser coupling (compound **1**, Fig. 1).[31–33] In fact, we chose this method for its high efficiency and because it requires simple reaction conditions and stable alkyne-based reactants. Also, we reasoned that the stiff 1,3-diyne linkage may provide rigidity to the target macrocycle as well as hydrophobicity, in balance with the hydrophilicity of the carbohydrate units.

We started our synthesis with the known α-D-propargyl mannoside **2**, which can be obtained in three steps from D-mannose.[34] From earlier studies carried out by Lindhorst's group on the preparation of azobenzene glycoconjugates, we knew of the advantages of the Mitsunobu reaction for the regioselective protecting group-free substitution at the primary alcohol of sugars.[35] Here, with successfully applied this methodology to the synthesis of the macrocycle precursor **4** (Scheme 1). In a first step, 4,4′-dihydroxyazobenzene **3**[36] was reacted at both ends with **2**, and activated in the presence of triphenylphosphine and

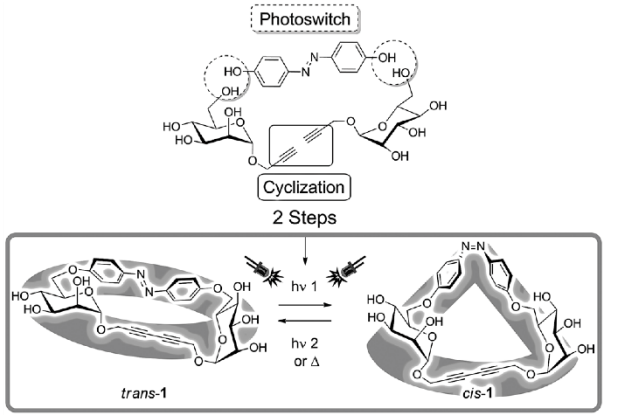

Fig. 1 Reversible *trans*/*cis* isomerisation of the azobenzene unit leads to shape-switching of the macrocycle **1**.

Otto Diels Institute of Organic Chemistry Christiana Albertina University of Kiel Otto-Hahn-Platz 3/4, 24118 Kiel, Germany. E-mail: gdespras@oc.uni-kiel.de

† Electronic supplementary information (ESI) available: Experimental procedures, characterization data and copies of ^{1}H and ^{13}C-NMR spectra of new compounds, details on photoswitching experiments. See DOI: 10.1039/c8cc03724h

View Article Online
Communication ChemComm

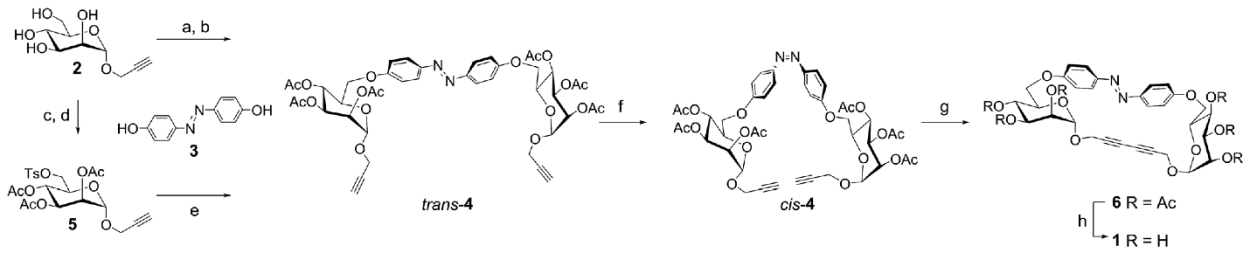

Scheme 1 Synthesis of macrocycle **1**. *Reagents and conditions*: (a) **3**, PPh_3, DIAD, THF, 0 °C to RT; (b) Ac_2O, pyridine, RT, 50% over two steps; (c) TsCl, pyridine, 0 °C to RT; (d) Ac_2O, pyridine, RT, 61% over two steps; (e) **3**, Cs_2CO_3, DMF, 70 °C, 70%; (f) irr. with 365 nm in pyridine; (g) CuBr, PMDETA, RT (see Table 1 for yields); (h) NaOMe, MeOH/DCM, RT, quant. PMDETA: *N*,*N*,*N*′,*N*′′,*N*′′′-pentamethyldiethylenetriamine.

diisopropyl azodicarboxylate (DIAD). After separation of the Mitsunobu reagents, the crude product was acetylated in order to remove the excess of unreacted **2**, hence affording the linear azobenzene bis-glycosyl conjugate **4** in 50% yield over two steps. Alternatively **2** was converted into **5** *via* tosylation and subsequent acetylation[34] in a yield of 61%, in order to test if a Williamson etherification would be more effective for the synthesis of **4**.[21] Although **4** was isolated in 70% yield, the pathway involving the Mitsunobu reaction is preferable as it requires one step less and leads to a higher overall yield.

The cyclisation was performed in pyridine under high dilution, using copper(I) bromide and the ligand *N*,*N*,*N*′,*N*′′,*N*′′′-pentamethyldiethylenetriamine (PMDETA) for catalysing the intramolecular Glaser coupling (Scheme 1 and Table 1). Conveniently, the photoswitching properties of the azobenzene moiety were used in this step to our advantage: the solution of the linear precursor **4** was irradiated at 365 nm for 20 min prior to the addition of the catalyst, transforming *trans*-**4** to *cis*-**4** and thus enabling a closer proximity for the propargyl groups.[24] As a result, the target macrocycle **6** was isolated in a satisfying yield of 42% (Table 1, entry 1). The significance of the preliminary geometrical arrangement of the open substrate was confirmed by running a test reaction omitting the irradiation step, which produced the desired cycle only in traces (Table 1, entry 2). With a view to improve the reaction, the cyclisation was carried out at different concentrations (Table 1, entries 3–5) but it was not possible to raise the yield higher than 50%. Cleavage of the acetyl groups was performed using sodium methoxide in methanol to yield the target compound **1** in quantitative yield. The macrocyclisation was confirmed using mass spectrometry and NMR spectroscopy (see the ESI†). Indeed, the ^{1}H NMR spectrum of *trans*-**1** shows a single set of signals for both sugars and benzene rings, as expected for a symmetrical molecule, and the absence of the acetylene proton. Moreover, in comparison with the open precursor **4**, the high difference in the chemical shifts of the CH_2 protons at the sugar primary position and the propargyl moiety supports an increase in conformational restriction, as a result of the cyclisation (see the ESI†).

Table 1 Conditions and resulting yields for the macrocyclisation of **4**

Entry	Pre-irradiation (nm)	Concentration (mM)	Yield (%)
1	365	5	42
2	—	5	5[a]
3	365	2	50
4	365	1	26
5	365	7	39

[a] Yield determined by NMR.

The photoswitching ability was investigated using UV/visible absorption and NMR spectroscopy. *trans*-**1** shows a strong $\pi \rightarrow \pi^*$ transition (λ_{max} = 360 nm) and a very weak forbidden $n \rightarrow \pi^*$ transition (λ_{max} = 450 nm) (Fig. 2a). After irradiation with a 365 nm LED for 5 min, the macrocycle switched readily to its corresponding *cis* isomer with a photostationary state (PSS) of *cis*/*trans* 98 : 2 (measured by ^{1}H-NMR, see Fig. S23, ESI†), leading to a decrease in the hypsochromic shift of the $\pi \rightarrow \pi^*$ band to 315 nm and an increase of the $n \rightarrow \pi^*$ band at 450 nm. According to the previous reports on glycoazobenzene macrocycles, complete back switching to *trans*-**1** is not possible by irradiation with visible light, due to the overlap of the $n \rightarrow \pi^*$ bands of both isomers, leading to a simultaneous *trans* → *cis* isomerisation.[24,25] However, a close look to the UV/vis spectrum of *cis*-**1** reveals that the two transitions are almost resolved in the green range and it is therefore possible to reach a good PSS of *cis*/*trans* 12 : 88 by irradiation at 525 nm (Fig. S23, ESI†). Full relaxation to *trans*-**1** was realized by heating a solution of the *cis* isomer in the dark (40 °C for 16 h), whereas the half-life of the metastable *cis*-**1** at 27 °C was measured to be 114 h (see the ESI†). Finally, **1** showed excellent resistance to switching fatigue after alternating irradiation with 365 nm and 525 nm light within 19 cycles (see Fig. S22, ESI†). To verify whether a chirality transfer operates from the carbohydrate blocks to the azobenzene unit, we measured circular dichroism (CD) spectra in DMSO (Fig. 2b).

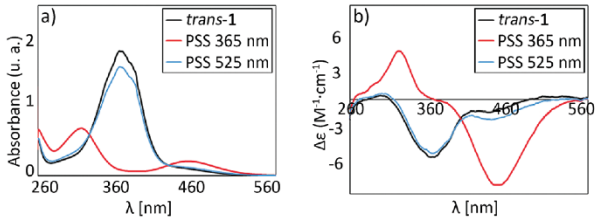

Fig. 2 (a) Absorption spectra of **1** (100 μM in DMSO) at 298 K; (b) CD spectra of **1** (50 μM in DMSO) at 293 K; black line: *trans*-**1**, red line: PSS after irradiation with 365 nm for 5 min, and blue line: PSS after irradiation with 525 nm for 15 min.

trans-**1** shows a negative Cotton effect at 360 nm and a weaker one at 440 nm corresponding to the respective $\pi \rightarrow \pi^*$ and $n \rightarrow \pi^*$ transitions of the UV/visible spectrum. After irradiation with 365 nm light, the spectrum changes significantly to show a positive Cotton effect at 320 nm and a strong negative band at 440 nm, indicating a major change in chirality upon irradiation, as previously observed with photoswitchable glycomacrocycles.[24,25] In accordance with the UV/vis measurements, addressing *cis*-**1** with green light leads to a PSS in which the CD pattern corresponding to the pure *trans*-**1** is nearly recovered. It has been demonstrated that azobenzenes embedded in chiral frames can selectively generate either a *P* or an *M* helical conformation, corresponding to a *trans*/*cis* isomerisation in a single direction.[26–30] Our results suggest a similar behaviour for the macrocycle **1**.

The fact that the isomerisation from *trans*-**1** to *cis*-**1** leads to a change in the shape of the molecule is visible *via* NMR. The H-6a and H-6b signals are shifted upfield, while the H-1 and the propargyl–CH_2 proton signals are shifted downfield, suggesting a shielding and a deshielding effect respectively due to a closer proximity or an increased distance to the aromatic rings. In the case of the propargylic protons, this is supported by the significant decrease in intensity of the NOE cross-peaks with the aromatic protons upon photoisomerization (Fig. 3a, b and Fig. S15, S20, ESI†). Additionally, energy-minimized structures were calculated to give an approximation of the shapes for **1** in *trans* and *cis* configurations (Fig. 3c and d).[37]

While attempting to record spectra in water despite the poor solubility of *trans*-**1** in any solvent besides DMSO, we noticed that after irradiation with UV light, the aqueous suspension turns to a clear solution. If *trans*-**1** is added to water from a concentrated stock solution in DMSO, the prepared suspension (0.5% DMSO in water) shows a Tyndall effect, which disappears with triggering solvation upon irradiation at 365 nm. This phenomenon, also visible with the naked eye at higher concentrations, is reversible

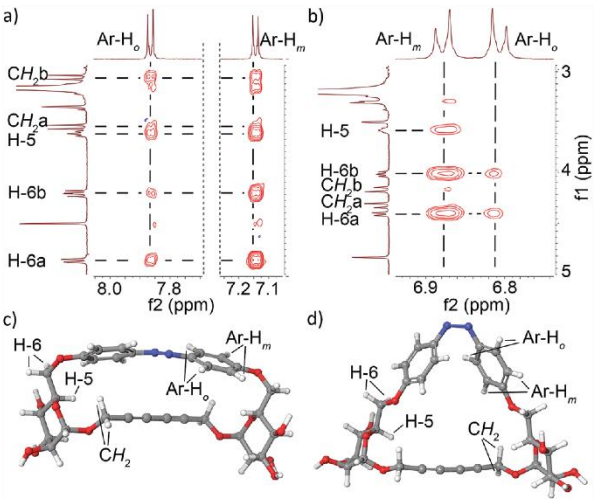

Fig. 3 (a) Expansion of the NOESY spectrum for *trans*-**1** and (b) PSS at 365 nm in DMSO at 300 K; (c) force field-minimized structures of *trans*-**1** and (d) *cis*-**1**.[37]

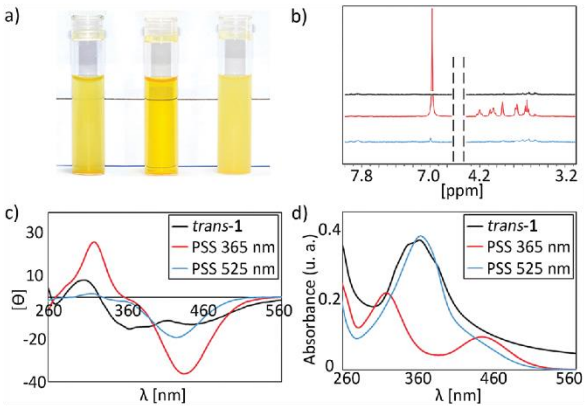

Fig. 4 Reversible switching of the solubility: (a) *trans*-**1** in water (1.0 mg mL^{-1}) and after irradiation with 365 nm for 3 min and 525 nm for 10 min; (b) ^{1}H-NMR spectra of **1** (2.5 mg mL^{-1} in D_2O); (c) CD spectra of **1** (0.3 mg mL^{-1} in H_2O with 0.5% DMSO) at 293 K; (d) absorption spectra of **1** (0.3 mg mL^{-1} in H_2O with 0.5% DMSO) at 298 K; black line: *trans*-**1**, red line: PSS after irradiation with 365 nm for 5 min, and blue line: PSS after irradiation with 525 nm for 5 min.

by switching back with 525 nm light, leading to a sudden precipitation of the macrocycle, and is repeatable for at least 10 cycles (Fig. 4a). Moreover, heating the solution obtained after UV irradiation, and thus relaxing the *cis* isomer, also leads to the formation of a suspension. These observations led us to the following hypothesis: in water, *trans*-**1** is largely insoluble, while *cis*-**1** is soluble, making the irradiation with different wavelengths a solubility switch for the macrocycle.[38]

To support our assumption and get more insight into the solubility switching, we measured ^{1}H-NMR, CD and UV/vis spectra in aqueous suspensions before and after irradiation with UV and green light (Fig. 4b–d). Hence, the ^{1}H-NMR spectrum of *trans*-**1** shows very weak signals that can barely be distinguished from the background noise, while the spectrum after switching at 365 nm reveals strong resonances in the regions corresponding to the sugars and the azobenzene (Fig. 4b). Switching back to the *trans* isomer with 525 nm light provides a spectrum similar to the one observed before irradiation with UV light. Regarding the CD spectra, the pattern of *trans*-**1** (Fig. 4c) is more complex than observed in pure DMSO, while the signal corresponding to the PSS at 365 nm rather fits to the one shown in Fig. 2b. Remarkably, the back photoisomerization with 525 nm light leads to a pattern that does not fit any longer to the one of the pure *trans*-**1**, in sharp contrast with the same experiment carried out in DMSO. UV/vis measurements before and after irradiation showed the same trend (Fig. 4d). Indeed, the spectrum of *trans*-**1** exhibits a broad band for the $\pi \rightarrow \pi^*$ transition, along with a raised-up baseline, whereas the spectrum recorded in the UV PSS looks very similar to the one measured in a DMSO solution (Fig. 2a). Taken together, these spectroscopic data provide the qualitative evidence that the solubility behaviour of *trans*- and *cis*-**1** sharply differs in water. In particular, the CD and UV/vis spectra hint for a possible aggregation process of the *trans* isomer. Moreover, two distinct aggregation states may occur whether the *trans* macrocycle is directly suspended in

water or formed by irradiation of the solution containing the *cis* isomer, as suggested by the two different patterns observed in CD (Fig. 4c) and also by the different appearance of the suspension in the vial (Fig. 4a).

In summary, we have described a short synthesis process of a new photoswitchable glycoazobenzene macrocycle using a combination of the Mitsunobu reaction, for forming the linear precursor, and a photo-assisted intramolecular Glaser coupling, for the cyclisation. It could be shown using NMR, UV/visible and CD spectroscopy that the cycle exhibits excellent photochromic properties, leading to a significant change in shape and chirality. Intriguingly, it was found that irradiation of **1** in water with light of two different wavelengths acts as a solubility switch, which will be investigated further.

We kindly thank Prof. Dr T. K. Lindhorst for fundamental support and Prof. Dr J. Grötzinger for the CD measurements. Verband der Chemischen Industrie (VCI) and SFB 677 are also acknowledged for financial support.

Conflicts of interest

There are no conflicts to declare.

Notes and references

1 A. K. Yudin, *Chem. Sci.*, 2015, **6**, 30–49.
2 E. M. Driggers, S. P. Hale, J. Lee and N. K. Terrett, *Nat. Rev. Drug Discovery*, 2008, 7, 608–624.
3 E. Marsault and M. L. Peterson, *J. Med. Chem.*, 2011, **54**, 1961–2004.
4 J. Xie and N. Bogliotti, *Chem. Rev.*, 2014, **114**, 7678–7739.
5 N. Pietrzik, D. Schmollinger and T. Ziegler, *Beilstein J. Org. Chem.*, 2008, **4**, 30.
6 J. F. Billing and U. J. Nilsson, *J. Org. Chem.*, 2005, **70**, 4847–4850.
7 T. Haag, R. A. Hughes, G. Ritter and R. R. Schmidt, *Eur. J. Org. Chem.*, 2007, 6016–6033.
8 C.-Y. Tsai, X. Huang and C.-H. Wong, *Tetrahedron Lett.*, 2000, **41**, 9499–9503.
9 F. Vögtle, W. M. Müller, U. Müller, M. Bauer and K. Rissanen, *Angew. Chem., Int. Ed.*, 1993, **32**, 1295–1297.
10 T. Muraoka, K. Kinbara and T. Aida, *Nature*, 2006, **440**, 512–515.
11 E. Wagner-Wysiecka, N. Łukasik, J. F. Biernat and E. Luboch, *J. Inclusion Phenom. Macrocyclic Chem.*, 2018, **90**, 189–257.
12 M. C. Basheer, Y. Oka, M. Mathews and N. Tamaoki, *Chem. – Eur. J.*, 2010, **16**, 3489–3496.
13 M. Kawamoto, T. Aoki and T. Wada, *Chem. Commun.*, 2007, 930–932.
14 Y. Norikane, Y. Hirai and M. Yoshida, *Chem. Commun.*, 2011, **47**, 1770–1772.
15 R. Reuter and H. A. Wegner, *Org. Lett.*, 2011, **13**, 5908–5911.
16 H. M. D. Bandara and S. C. Burdette, *Chem. Soc. Rev.*, 2012, **41**, 1809–1825.
17 M. Baroncini, G. Ragazzon, S. Silvi, M. Venturi and A. Credi, *Pure Appl. Chem.*, 2015, **87**, 537–545.
18 A. A. Beharry and G. A. Woolley, *Chem. Soc. Rev.*, 2011, **40**, 4422–4437.
19 F. Hamon, F. Djedaini-Pilard, F. Barbot and C. Len, *Tetrahedron*, 2009, **65**, 10105–10123.
20 V. Chandrasekaran, E. Johannes, H. Kobarg, F. D. Sönnichsen and T. K. Lindhorst, *ChemistryOpen*, 2014, **3**, 99–108.
21 V. Chandrasekaran and T. K. Lindhorst, *Chem. Commun.*, 2012, **48**, 7519–7521.
22 A. Müller, H. Kobarg, V. Chandrasekaran, J. Gronow, F. D. Sönnichsen and T. K. Lindhorst, *Chem. – Eur. J.*, 2015, **21**, 13723–13731.
23 A. Müller and T. K. Lindhorst, *Eur. J. Org. Chem.*, 2016, 1669–1672.
24 G. Despras, J. Hain and S. O. Jaeschke, *Chem. – Eur. J.*, 2017, **23**, 10838–10847.
25 C. Lin, S. Maisonneuve, R. Métivier and J. Xie, *Chem. – Eur. J.*, 2017, **23**, 14996–15001.
26 G. Haberhauer and C. Kallweit, *Angew. Chem., Int. Ed.*, 2010, **49**, 2418–2421.
27 G. Haberhauer, C. Kallweit, C. Wölper and D. Bläser, *Angew. Chem., Int. Ed.*, 2013, **52**, 7879–7882.
28 K. Takaishi, M. Kawamoto, K. Tsubaki and T. Wada, *J. Org. Chem.*, 2009, **74**, 5723–5726.
29 K. Takaishi, A. Muranaka, M. Kawamoto and M. Uchiyama, *J. Org. Chem.*, 2011, **76**, 7623–7628.
30 K. Takaishi, M. Kawamoto, K. Tsubaki, T. Furuyama, A. Muranaka and M. Uchiyama, *Chem. – Eur. J.*, 2011, **17**, 1778–1782.
31 J. Lu, A. Xia, N. Zhou, W. Zhang, Z. Zhang, X. Pan, Y. Yang, Y. Wang and X. Zhu, *Chem. – Eur. J.*, 2015, **21**, 2324–2329.
32 P. Siemsen, R. C. Livingston and F. Diederich, *Angew. Chem., Int. Ed.*, 2000, **39**, 2632–2657.
33 W. Shi and A. Lei, *Tetrahedron Lett.*, 2014, **55**, 2763–2772.
34 M. Poláková, M. Beláňová, K. Mikušová, E. Lattová and H. Perreault, *Bioconjugate Chem.*, 2011, **22**, 289–298.
35 J. Hain, V. Chandrasekaran and T. K. Lindhorst, *Isr. J. Chem.*, 2015, **55**, 383–386.
36 H. J. Jung, H. Min, H. Yu, T. G. Lee and T. D. Chung, *Chem. Commun.*, 2010, **46**, 3863–3865.
37 Schrödinger Release 2018-1: MacroModel, Schrödinger, LLC, New York, NY, 2018.
38 M. Ishikawa, T. Ohzono, T. Yamaguchi and Y. Norikane, *Sci. Rep.*, 2017, 7, 6909.

Electronic Supplementary Material (ESI) for ChemComm.

Supporting Information

A Two-Step Approach to a Glycoazobenzene Macrocycle with Remarkable Photoswitchable Features

Julia Hain and Guillaume Despras*

Table of Contents

General Information

Methods:
Moisture-sensitive reactions were carried out in flame-dried glassware and under a positive pressure of nitrogen. Analytical thin layer chromatography (TLC) was performed on silica gel plates (GF 254, Merck). Visualization was achieved by UV light and/or with 10% sulfuric acid in ethanol or vanillin (3.0g vanillin and 0.5 mL H2SO4 in 100 mL EtOH), followed by heat treatment at ca. 200 °C. The products were purified by flash chromatography on silica gel columns (Merck, 230–400 mesh, particle size 0.040–0.063 mm). Pyridine was dried over KOH, tetrahydrofuran and *N,N*-dimethylformamide were stored over 3Å molecular sieves under a nitrogen atmosphere.

Instrumentation:

Optical rotations were measured with a PerkinElmer 241 polarimeter with a sodium D-line (589 nm) and a cuvette of 10 cm path length, in the solvents indicated.Circular dichroism spectroscopy was performed on a Jasco J-720 CD spectrometer (Jasco, Tokyo, Japan) with a bandwidth of 1 nm and a cuvette of 10 mm path length. Proton (^{1}H) nuclear magnetic resonance spectra and carbon (^{13}C) nuclear magnetic resonance spectra were recorded on a Bruker DRX-500 and AV-600 spectrometer. Chemical shifts are referenced to internal tetramethylsilane (TMS) or 4,4-dimethyl-4-silapentane-1-sulfonic acid (DSS), or to the residual proton of the NMR solvent. Data are presented as follows: chemical shift, multiplicity (s=singlet, d=doublet, t=triplet, q=quartet, m=multiplet, and br=broad signal), coupling constant in hertz (Hz) and, integration. Full assignment of the signals was achieved by using 2D NMR techniques (^{1}H - ^{1}H COSY and ^{1}H - ^{13}C HSQC and HMBC. Infrared (IR) spectra were measured with a PerkinElmer FTIR Paragon 1000 (ATR) spectrometer and were reported in cm^{-1}. ESI mass spectra were recorded on a Thermo Scientific™ Q Exactive™. *Trans* → *cis* photoisomerization experiments were performed using a LED emitting a 365 nm light from Nichia Corporation with a FWHM of 10 nm and intensity of 25 mW/cm^{2}. *Cis* → *trans* photoisomerization experiments were

performed using a LED emitting a 525 nm light from Nichia Corporation with a FWHM of 45 nm and intensity of 1 mW/cm^2. UV/Vis absorption spectra were measured on PerkinElmer Lambda-241.

Synthesis

Trans-Precursor **4**:

From 2-propynyl α-D-mannopyranoside **2**[1]:

A suspension of **2** (500 mg, 2.29 mmol), 4,4'-dihydroxyazobenzene[2] (**3**) (225 mg, 1.05 mmol) and triphenylphosphine (1.37 g, 5.22 mmol) in dry tetrahydrofurane (11.0 mL) under nitrogen was cooled to 0 °C and diisopropyl azodicarboxylate (1.00 mL, 5.22 mmol) was added dropwise. The mixture was allowed to warm to room temperature and stirred for 4 d then concentrated under reduced pressure. The crude residue was purified by flash chromatography (dichloromethane/methanol 9:1) to give a mixture of the unprotected product and excess **2**. The crude mixture was dissolved in dry pyridine (2.00 mL) and acetic anhydride (1.00 mL, 10.6 mmol) was added. The mixture was stirred at room temperature for 16 h, then concentrated under reduced pressure and co-evaporated with toluene repeatedly. The crude residue was purified by flash chromatography (cyclohexane/ethyl acetate 3:2) to give **4** (450 mg, 519 µmol, 50% over two steps) as an orange foam.

From 2-propynyl 2,3,4-tri-*O*-acetyl-6-*O*-tosyl-α-D-mannopyranoside **5**[1]:

A suspension of **5** (100 mg, 200 µmol), 4,4'-dihydroxyazobenzene[2] (**3**) (16.0 mg, 75.0 µmol) and Cs_2CO_3 (75.0 mg, 231 µmol) in dry DMF (8.00 mL) under nitrogen was stirred at 70 °C for 16 h then diluted with ethyl acetate (50 mL), washed with 2N HCl, brine and water (50 mL each) and dried over $MgSO_4$, filtered and concentrated to dryness. The crude residue was purified by flash chromatography (cyclohexane/ethyl acetate 3:2) to give **4** (46 mg, 53 µmol, 70%) as an orange foam.

$[\alpha]^{20}_D$= +112 (c= 0.41 in $CHCl_2$); ^{1}H NMR (500 MHz, $CDCl_3$) δ = 7.90 – 7.84 (m, 4 H, Ar-H_{ortho}), 7.05 – 6.96 (m, 4 H, Ar-H_{meta}), 5.45 – 5.37 (m, 4 H, H-3, H-4), 5.32 (dd, $^3J_{2,3}$ = 2.9 Hz, $^3J_{2,1}$ = 1.8 Hz, 2 H, H-2), 5.08 (d, $^3J_{1,2}$ = 1.6 Hz, 2 H, H-1), 4.33 (d, $^4J_{CH2,CH}$ = 2.4 Hz, 4 H, CH_2C≡CH), 4.25 – 4.13 (m, 6 H, H-5, H-6a, H-6b), 2.47 (t, $^4J_{CH,CH2}$ = 2.4 Hz, 2 H, CH_2C≡C*H*), 2.18 (s, 6 H, 2 CH_3C=O), 2.05 (s, 6 H, 2 CH_3C=O), 2.02 (s, 6 H, 2 CH_3C=O); ^{13}C NMR (126 MHz, $CDCl_3$) δ = 170.0 (CH_3*C*=O), 169.9 (2 C, CH_3*C*=O), 160.4 (Ar-C_{para}), 147.3 (Ar-C_{ipso}), 124.4 (Ar-C_{ortho}), 114.9 (Ar-C_{meta}), 96.0 (C-1), 77.9 (CH_2*C*≡CH), 75.6 (CH_2C≡*C*H), 69.5 (C-5), 69.4 (C-2), 68.9 (C-3), 67.5 (C-6), 66.8 (C-4), 54.8 (*C*H_2C≡CH), 20.9 (*C*H_3C=O), 20.8 (*C*H_3C=O), 20.7 (*C*H_3C=O); IR (ATR): ũ = 2363, 1746, 1369, 1215, 1135, 1043, 973, 841, 492 cm^{-1}; ESI-HRMS m/z: calc. 867.28184 for $[C_{42}H_{46}O_{18}N_2+H]^+$; found 867.28077 for $[C_{42}H_{46}O_{18}N_2+H]^+$.

Trans-Macrocycle **6**:

A solution of the precursor **4** (25.0 mg, 28.8 µmol) in dry pyridine (15.0 mL) was stirred at room temperature and irradiated with a LED lamp emitting 365 nm light from a distance of 15 cm for 20 min. After irradiation, the solution was shielded from light and CuBr (62.0 mg, 432 mmol) and N,N,N',N'',N''-pentamethyldiethylenetriamine (90.0 µL, 432 µmol) were added. The mixture was stirred at room temperature for 2 d then concentrated to dryness and coevaporated with toluene. The crude residue was dissolved in ethyl acetate, washed four times with water (50 mL each) and dried over $MgSO_4$. After filtration and concentration under reduced pressure, the residue was

purified by flash chromatography (cyclohexane/ethyl acetate 3:2) to give **6** (12.4 mg, 14.3 µmol, 50%) as an orange foam.

$[\alpha]^{20}_D$=-182 (c= 0.12 in $CHCl_2$); ^{1}H NMR (500 MHz, $CDCl_3$) δ = 7.90 – 7.84 (m, 4 H, Ar-H_{ortho}), 7.05 – 6.99 (m, 4 H, Ar-H_{meta}), 5.18 (dd, $^3J_{3,2}$ = 10.0 Hz, $^3J_{3,4}$ = 3.4 Hz, 2 H, H-3), 5.09 – 5.02 (m, 4 H, H-2, H-4), 4.53 (s, 2 H, H-1), 4.36 (dd, $^2J_{6a,6b}$ = 13.0 Hz, $^3J_{6a,5}$ = 9.1 Hz, 2 H, H-6a), 4.28 (dd, $^2J_{6b,6a}$ = 13.1 Hz, $^3J_{6b,5}$ = 2.3 Hz, 2 H, H-6b), 4.13 – 4.06 (m, 2 H, H-5), 3.47 (d, $^2J_{CH2,\ CH2}$ = 15.4 Hz, 2 H, CH_2C≡Ca), 3.43 (d, $^2J_{CH2,\ CH2}$ = 15.5 Hz, 2 H, CH_2C≡Cb), 2.07 (s, 6 H, 2 CH_3C=O), 2.06 (s, 6 H, 2 CH_3C=O), 1.91 (s, 6 H, 2 CH_3C=O); ^{13}C NMR (126 MHz, $CDCl_3$) δ = 170.0 (CH_3*C*=O), 169.7 (CH_3*C*=O), 169.6 (CH_3*C*=O), 158.4 (Ar-C_{para}), 147.7 (Ar-C_{ipso}), 124.4 (Ar-C_{ortho}), 117.5 (Ar-C_{meta}), 96.0 (C-1), 72.8 (CH_2*C*≡C), 70.3 (CH_2C≡*C*), 69.2 (C-2), 68.6 (C-3), 67.3 (C-6), 67.2 (2 C, C-4, C-5), 54.8 (*C*H_2C≡C), 20.8 (2 C, *C*H_3C=O), 20.6 (*C*H_3C=O), IR (ATR): ũ = 2923, 2360, 1747, 1209, 1068, 1040, 967, 847, 492 cm^{-1}; ESI-HRMS m/z: calc. 865.26619 for $[C_{42}H_{44}O_{18}N_2+H]^+$; found 865.26543 for $[C_{42}H_{46}O_{18}N_2+H]^+$.

Trans-Macrocycle **1**:

To a solution of the protected macrocycle **6** (55.0 mg, 63.6 µmol) in a mixture of dichloromethane and methanol (1:1, 4.00 mL), NaOMe (5.4 M in methanol, 30 µL) was added and the solution was stirred at room temperature for 16 h. The mixture was neutralized with Amberlite® IR120 H^+ and concentrated to dryness to give the macrocycle **1** (38.8 mg, 63.3 µmol, quantitative) as a yellow amorphous solid.

$[\alpha]^{24}_D$=-146 (c= 0.08 in DMSO); ^{1}H NMR (500 MHz, DMSO-*d6*) δ = 7.90 – 7.83 (m, 4 H, Ar-H_{ortho}), 7.19 – 7.11 (m, 4 H, Ar-H_{meta}), 5.23 (bs, 2 H, 2 OH), 4.99 (bs, 4 H, 4 OH), 4.74 (dd, $^2J_{6a,6b}$ = 12.8 Hz, $^3J_{6a,5}$ = 2.0 Hz, 2 H, H-6a), 4.44 (d, $^3J_{1,2}$ = 1.3 Hz, 2 H, H-1), 4.19 (dd, $^2J_{6b,6a}$ = 12.8 Hz, $^3J_{6b,5}$ = 10.0 Hz, 2 H, H-6b), 3.70 (ddd, $^3J_{5,6a}$ = $^3J_{5,6b}$ = 9.5 Hz, $^3J_{5,4}$ = 1.6 Hz, 2 H, H-5), 3.65 (d, $^2J_{CH2,CH2}$ = 15.3 Hz, 2 H, CH_2C≡Ca), 3.49 (d, $^3J_{1,2}$ = 0.9 Hz, 2 H, H-2), 3.32 – 3.28 (m, 4 H, H-3, H-4), 3.25 (d, $^2J_{CH2,CH2}$ = 15.4 Hz, 2 H, CH_2C≡Cb); ^{13}C NMR (126 MHz, DMSO-*d6*) δ = 158.7 (Ar-C_{para}), 146.4 (Ar-C_{ipso}), 123.8 (Ar-C_{ortho}), 117.6 (Ar-C_{meta}), 99.0 (C-1), 74.4 (CH_2*C*≡C), 70.6 (C-3), 69.6 (C-2), 68.5 (CH_2C≡*C*), 67.9 (C-6), 67.7 (C-4), 67.6 (C-5), 53.2 (*C*H_2C≡C), IR (ATR): ũ = 3371, 2916, 2363, 1595, 1210, 1065, 1040, 851, 556, 485 cm^{-1}; ESI-HRMS m/z: calc. 613.20280 for $[C_{30}H_{32}O_{12}N_2+H]^+$; found 613.20237 for $[C_{30}H_{32}O_{12}N_2+H]^+$.

Cis-Macrocycle **1**:

$[\alpha]^{24}_D$=-576 (c= 0.08 in DMSO); ^{1}H NMR (500 MHz, DMSO-*d6*) δ = 6.90 – 6.85 (m, 4 H, Ar-H_{meta}), 6.84 – 6.78 (m, 4 H, Ar-H_{ortho}), 5.22 (bs, 2 H, 2 OH), 4.99 (bs, 4 H, 4 OH), 4.71 (s, 2 H, H-1), 4.36 (d, $^2J_{6a,6b}$ = 10.8 Hz, 2 H, H-6a), 4.29 (d, $^2J_{CH2,CH2}$ = 16.5 Hz, 2 H, CH_2C≡Ca), 4.16 (d, $^2J_{CH2,CH2}$ = 16.6 Hz, 2 H, CH_2C≡Cb), 4.03 (dd, $^2J_{6b,6a}$ = 11.3 Hz, $^3J_{6b,5}$ = 8.0 Hz, 2 H, H-6b), 3.68 (dd, $^3J_{5,6a}$ = $^3J_{5,6b}$ = 8.0 Hz, 2 H, H-5), 3.61 (s, 2 H, H-2), 3.46 - 3.43 (m, 2 H, H-3, H-4); ^{13}C NMR (126 MHz, DMSO-*d6*) δ = 157.2 (Ar-C_{para}), 146.5 (Ar-C_{ipso}), 122.1 (Ar-C_{ortho}), 114.3 (Ar-C_{meta}), 100.2 (C-1), 76.2 (CH_2*C*≡C), 71.8 (C-5), 70.6 (C-3), 69.7 (C-2), 69.6 (CH_2C≡*C*), 67.6 (C-6), 66.8 (C-4), 54.7 (*C*H_2C≡C).

NMR spectra of the synthesized compounds

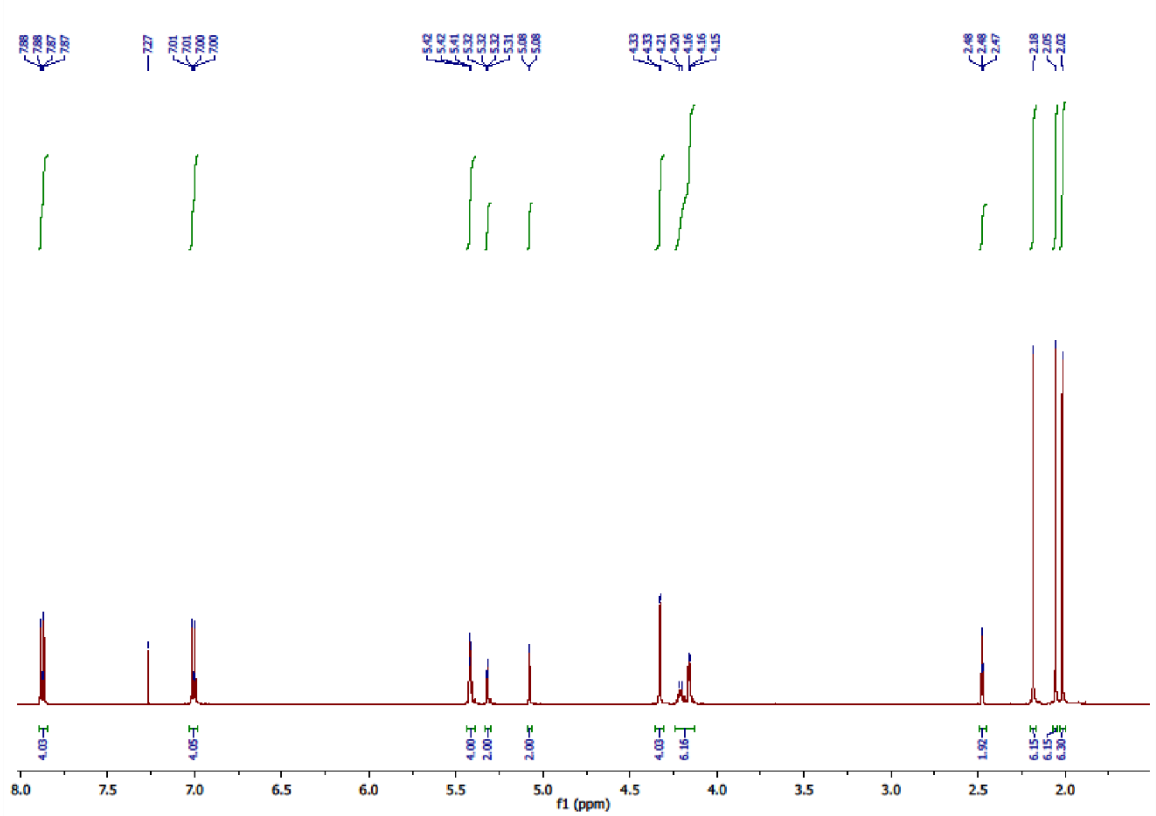

Figure S1: ^{1}H NMR spectrum of *trans*- **4** (500 MHz, $CDCl_3$, 300 K).

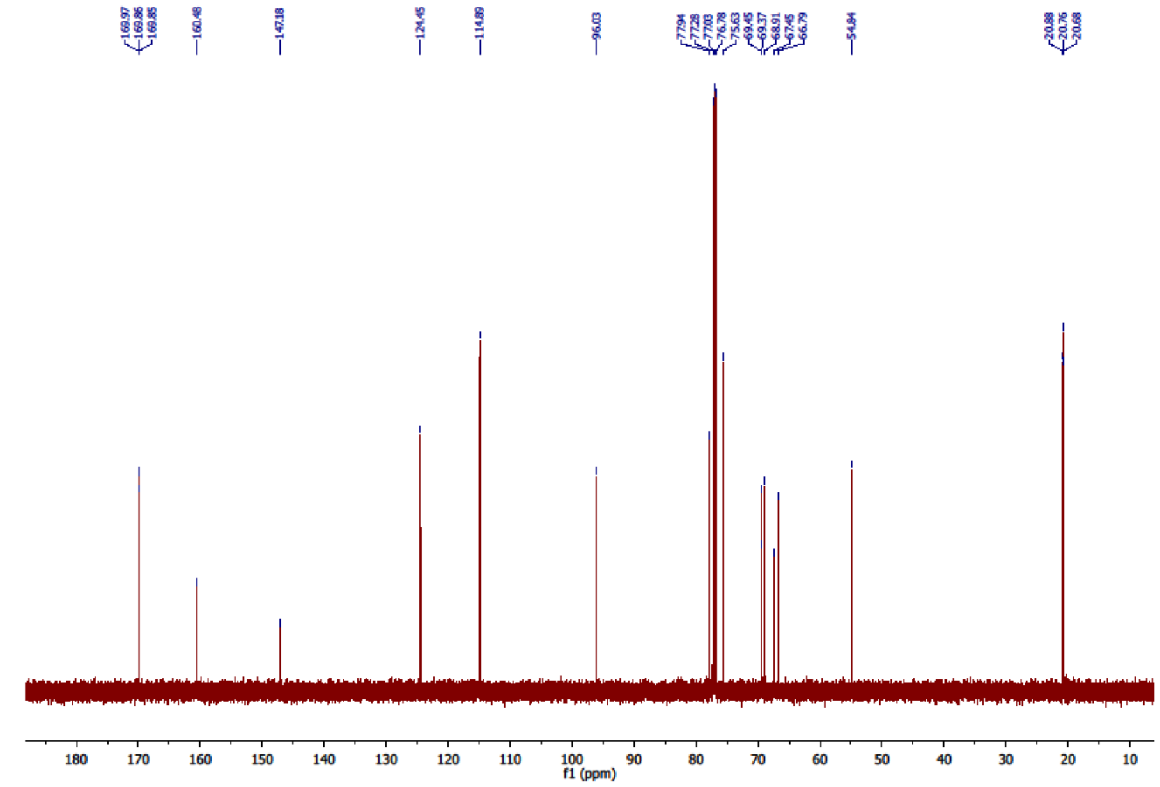

Figure S2: ^{13}C NMR spectrum of *trans*- **4** (126 MHz, $CDCl_3$, 300 K).

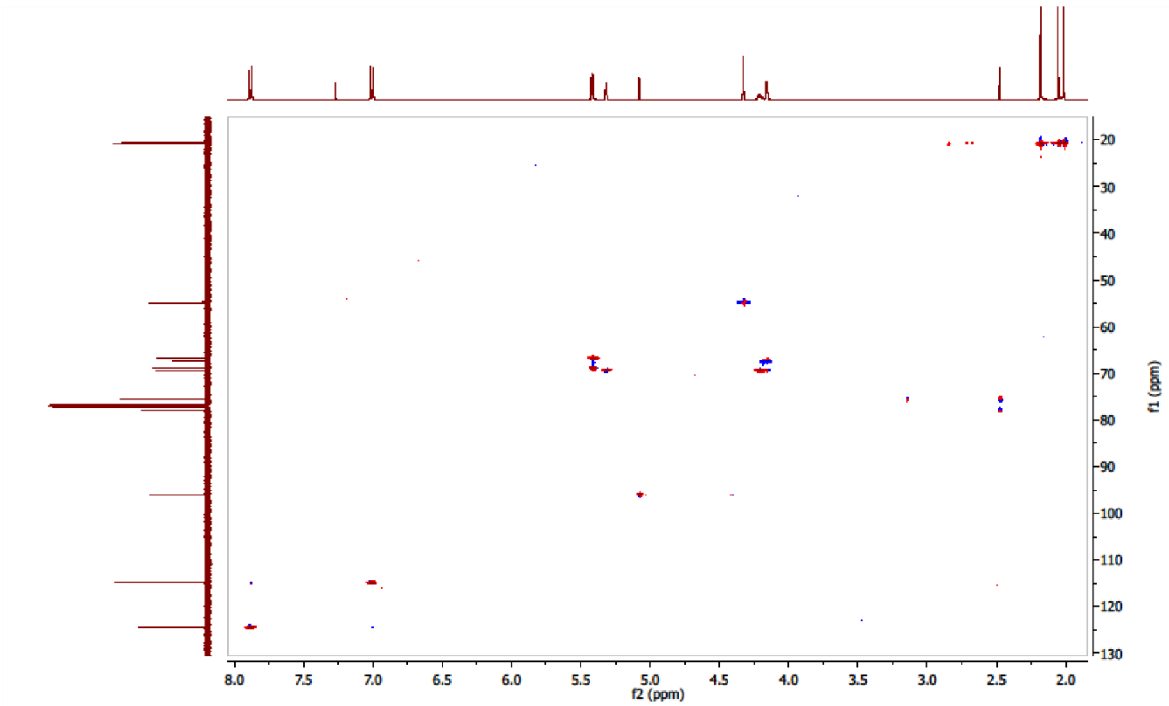

Figure S3: HSQC spectrum of *trans*- **4** ($CDCl_3$, 300 K).

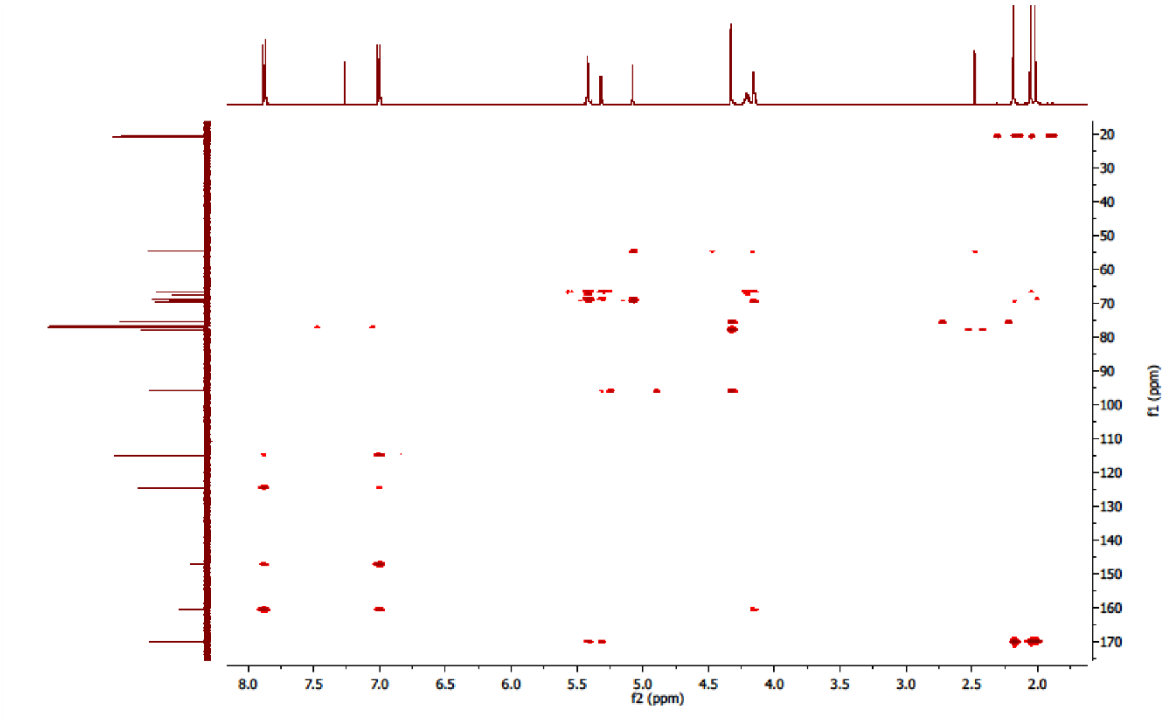

Figure S4: HMBC spectrum of *trans*- **4** ($CDCl_3$, 300 K).

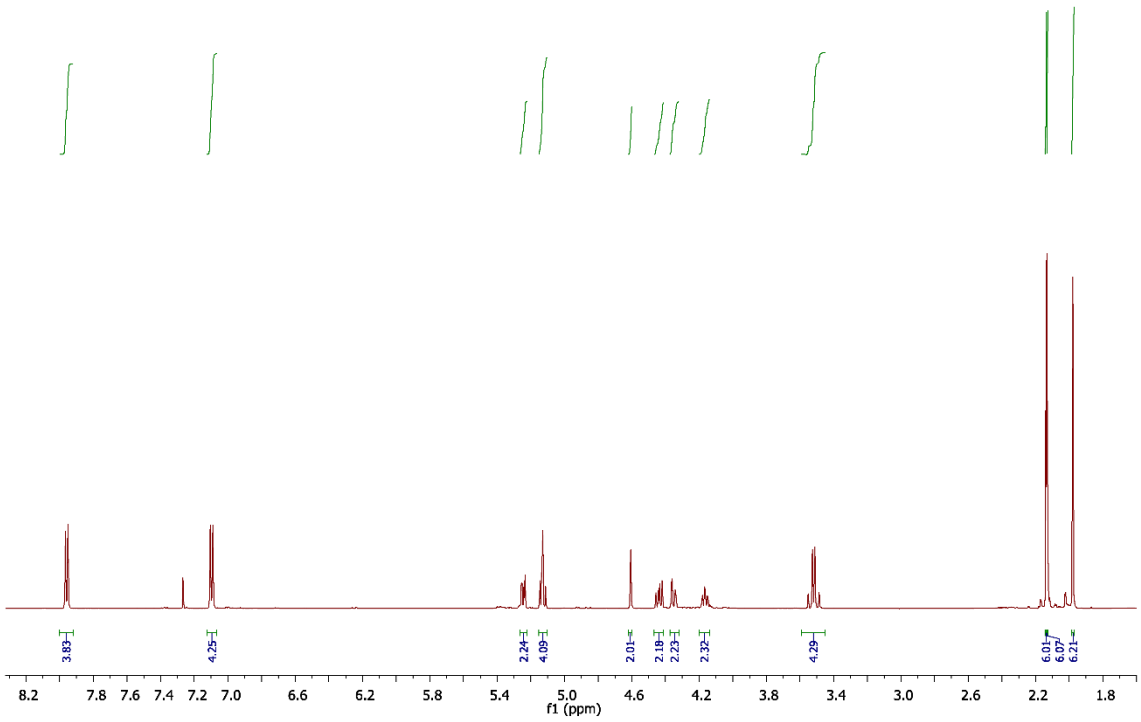

Figure S5: ^{1}H NMR spectrum of *trans*-macrocycle **6** (600 MHz, $CDCl_3$, 300 K).

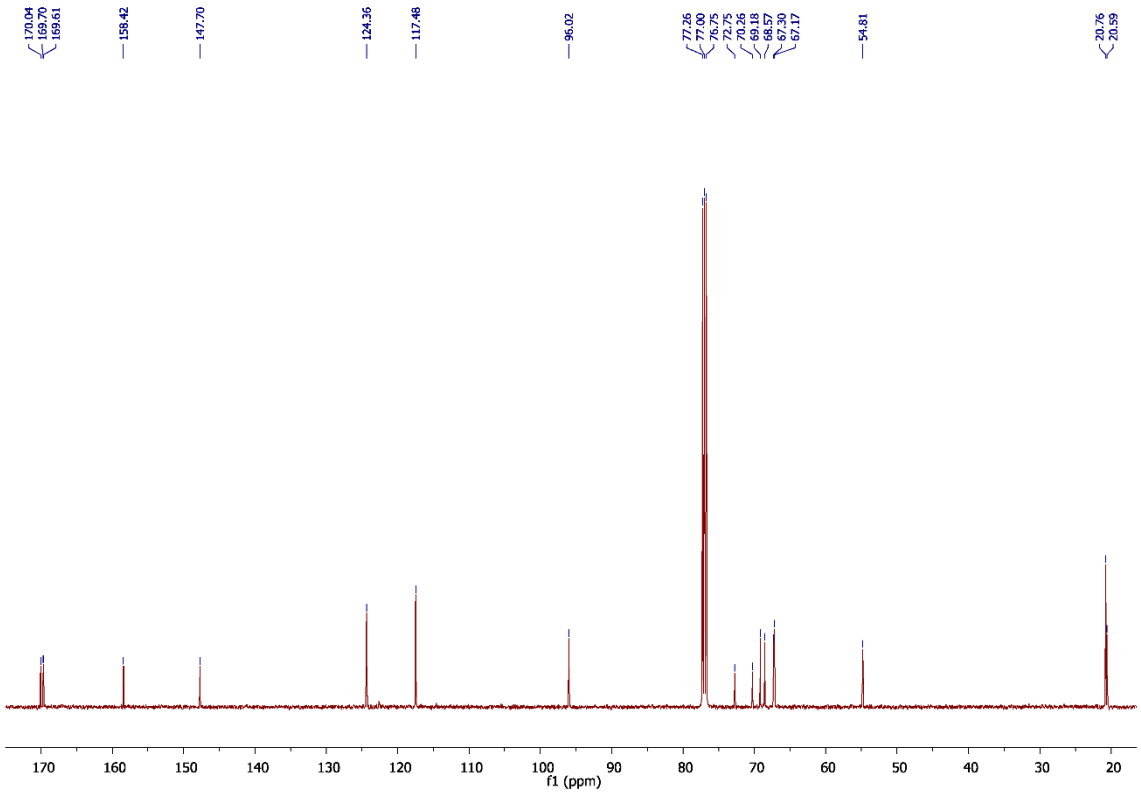

Figure S6: ^{13}C NMR spectrum of *trans*-macrocycle **6** (125 MHz, $CDCl_3$, 300 K).

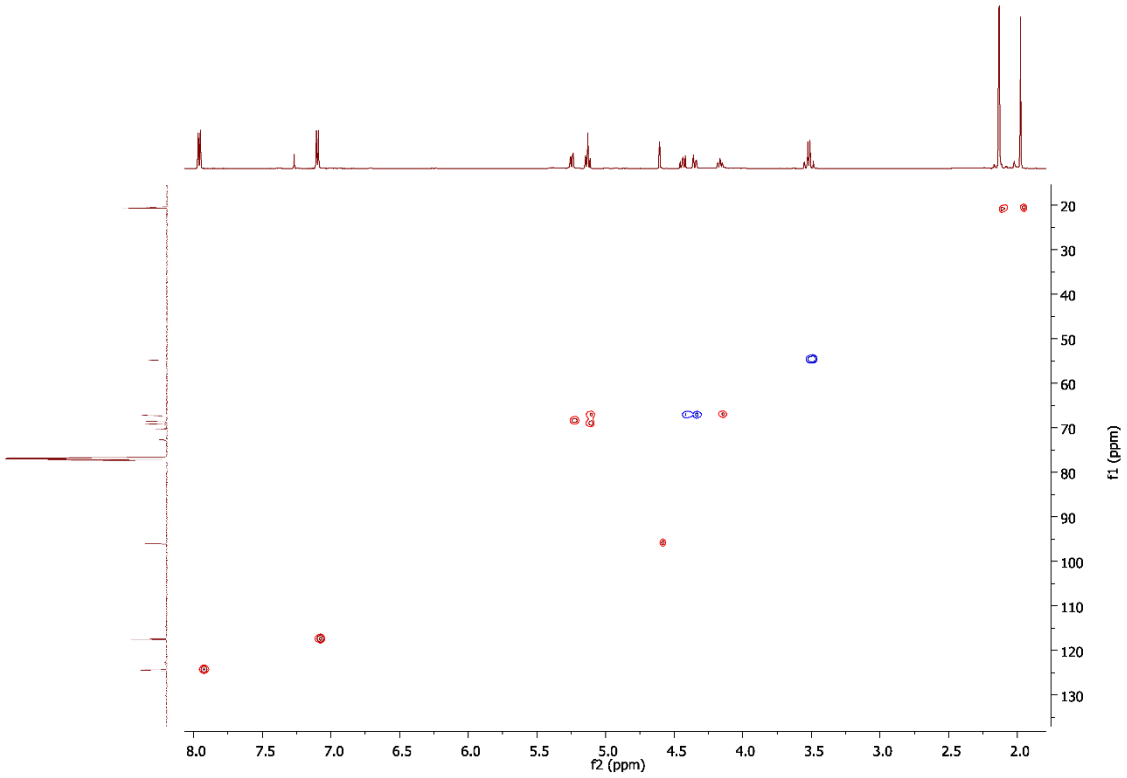

Figure S7: HSQC spectrum of *trans*-macrocycle **6** ($CDCl_3$, 300 K).

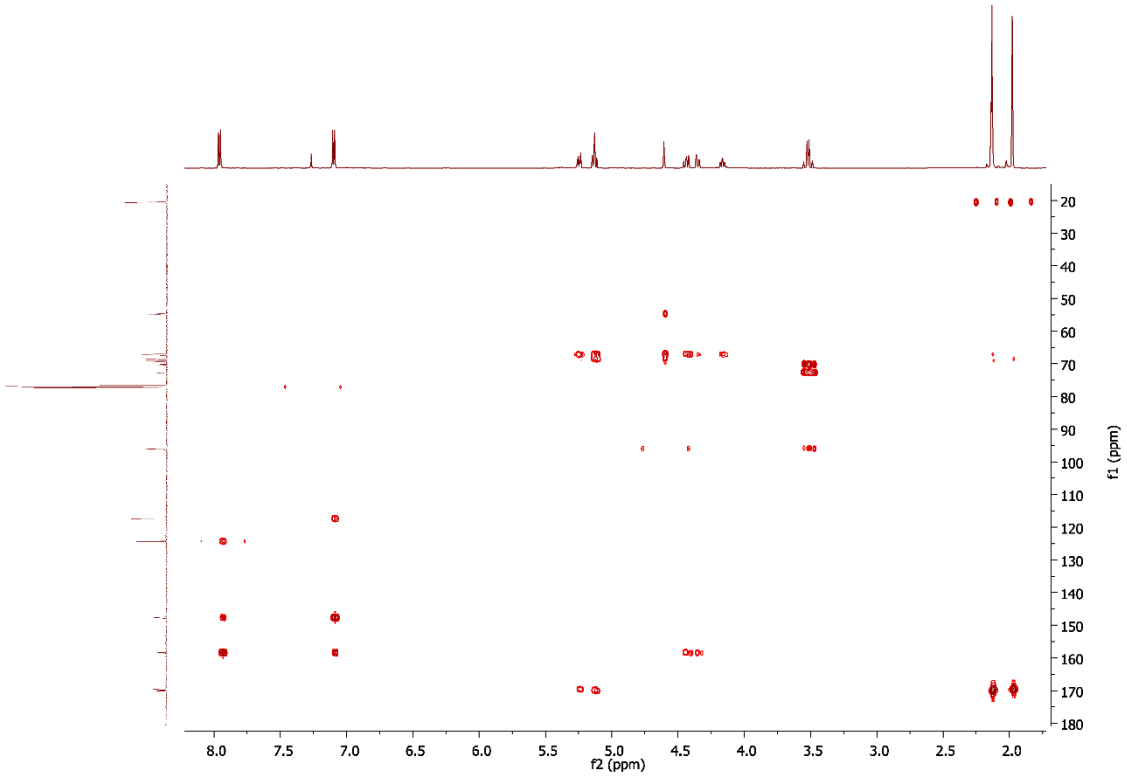

Figure S8: HMBC spectrum of *trans*-macrocycle **6** ($CDCl_3$, 300 K).

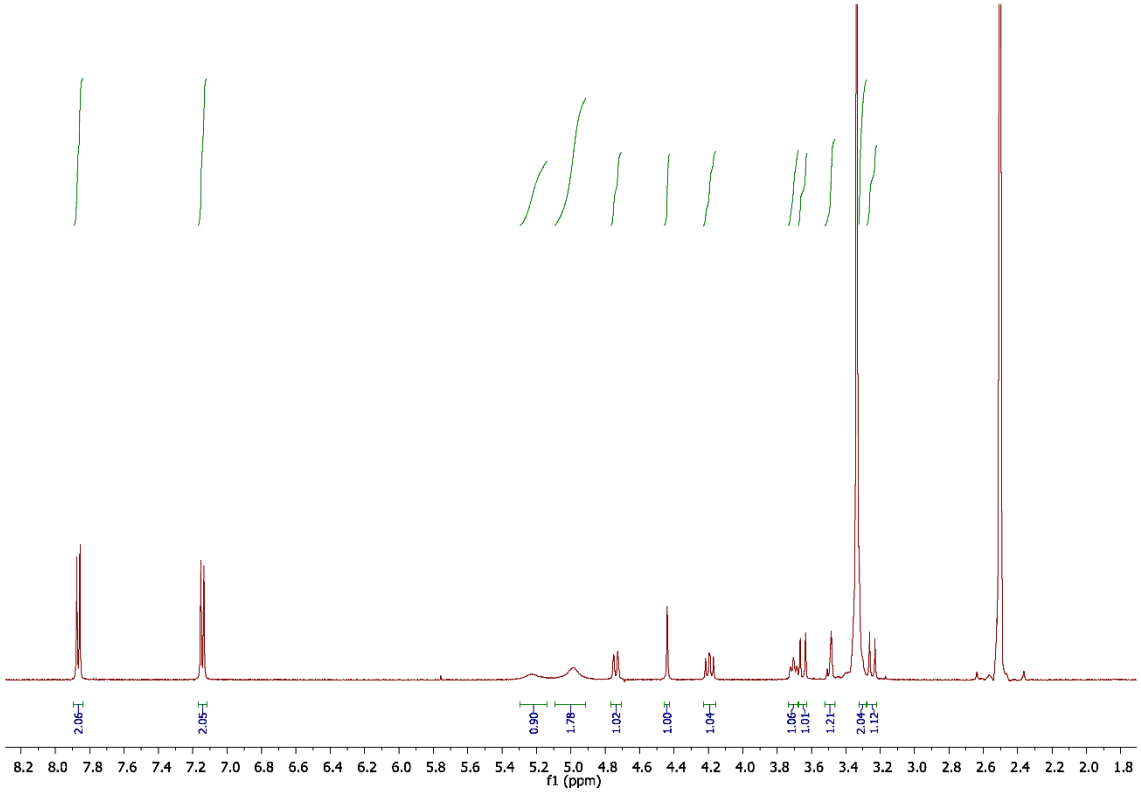

Figure S9: ^{1}H NMR spectrum of *trans*-macrocycle **1** (500 MHz, DMSO-d_6, 300 K).

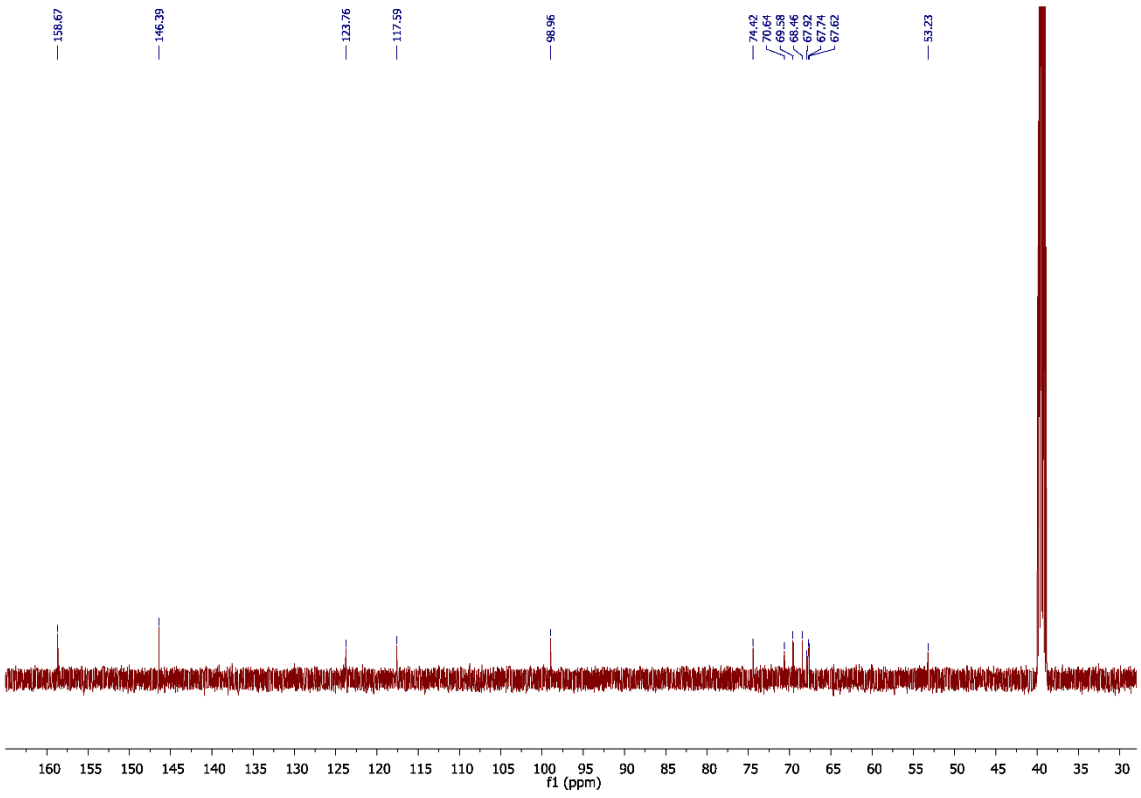

Figure S10: ^{13}C NMR spectrum of *trans*-macrocycle **1** (126 MHz, DMSO-d_6, 300 K).

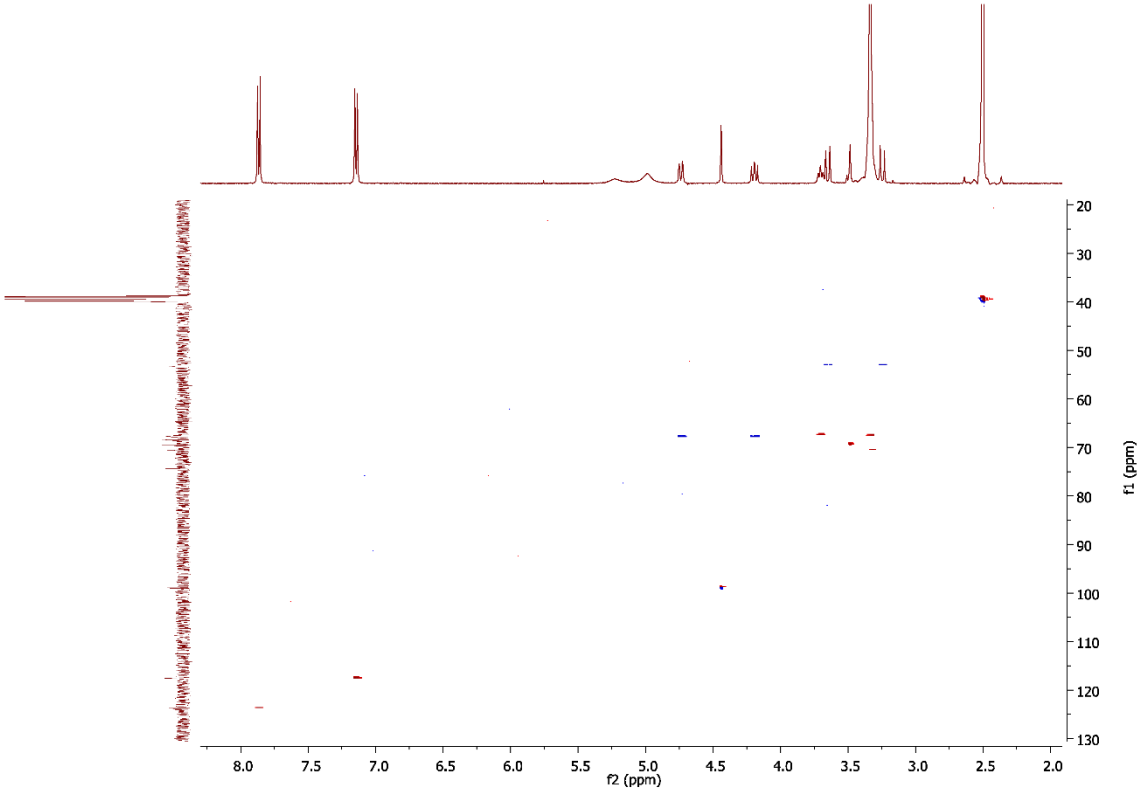

Figure S11: HSQC spectrum of *trans*-macrocycle **1** (DMSO-d_6, 300 K).

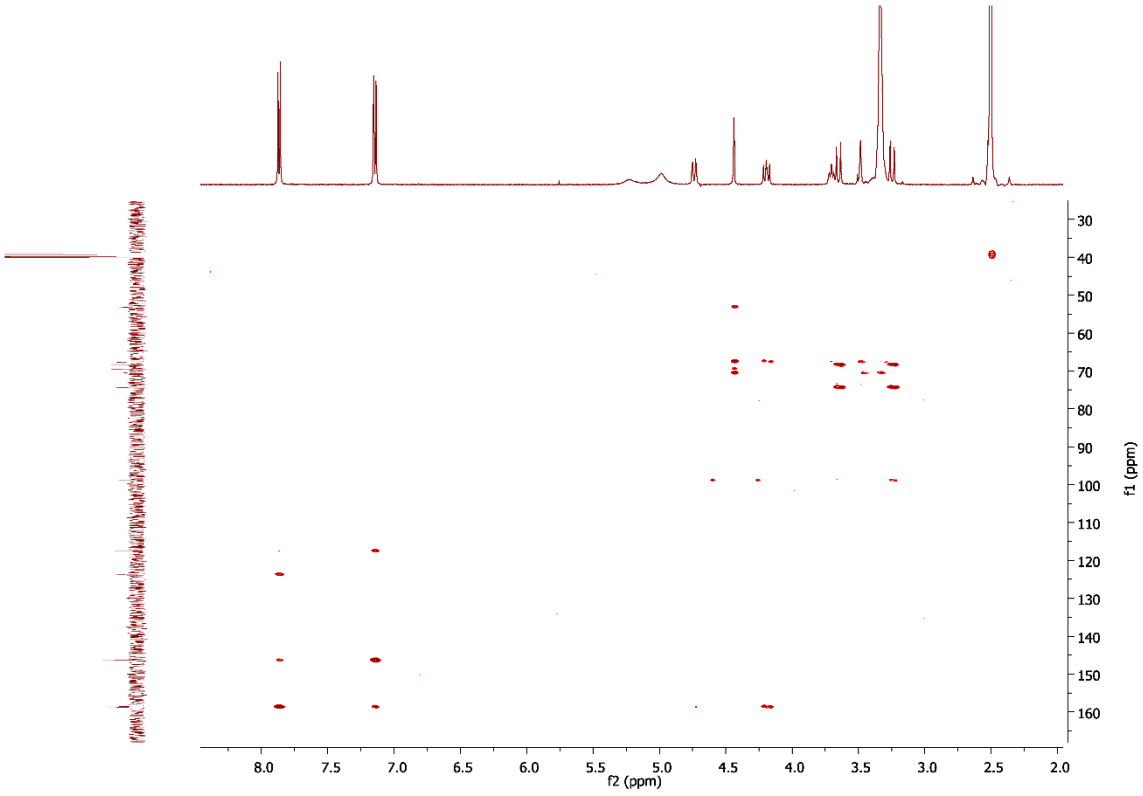

Figure S12: HMBC spectrum of *trans*-macrocycle **1** (DMSO-d_6, 300 K).

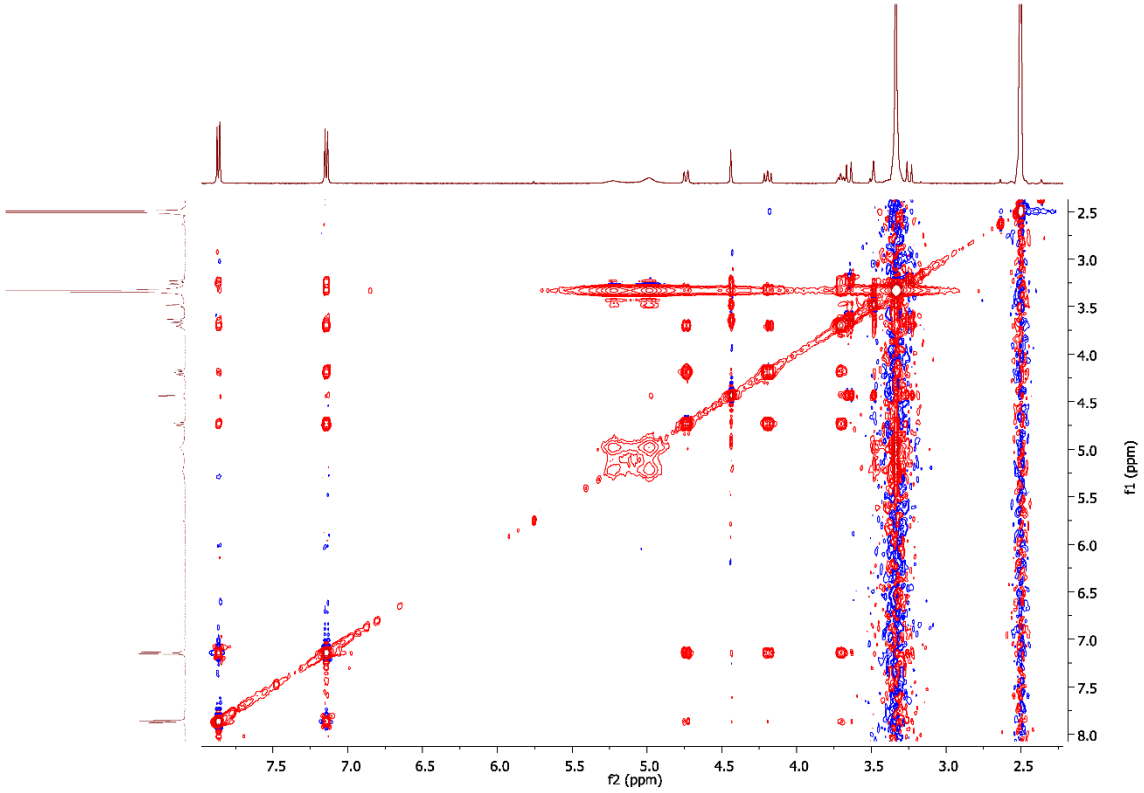

Figure S13: NOESY spectrum of *trans*-macrocycle **1** (DMSO-d_6, 300 K).

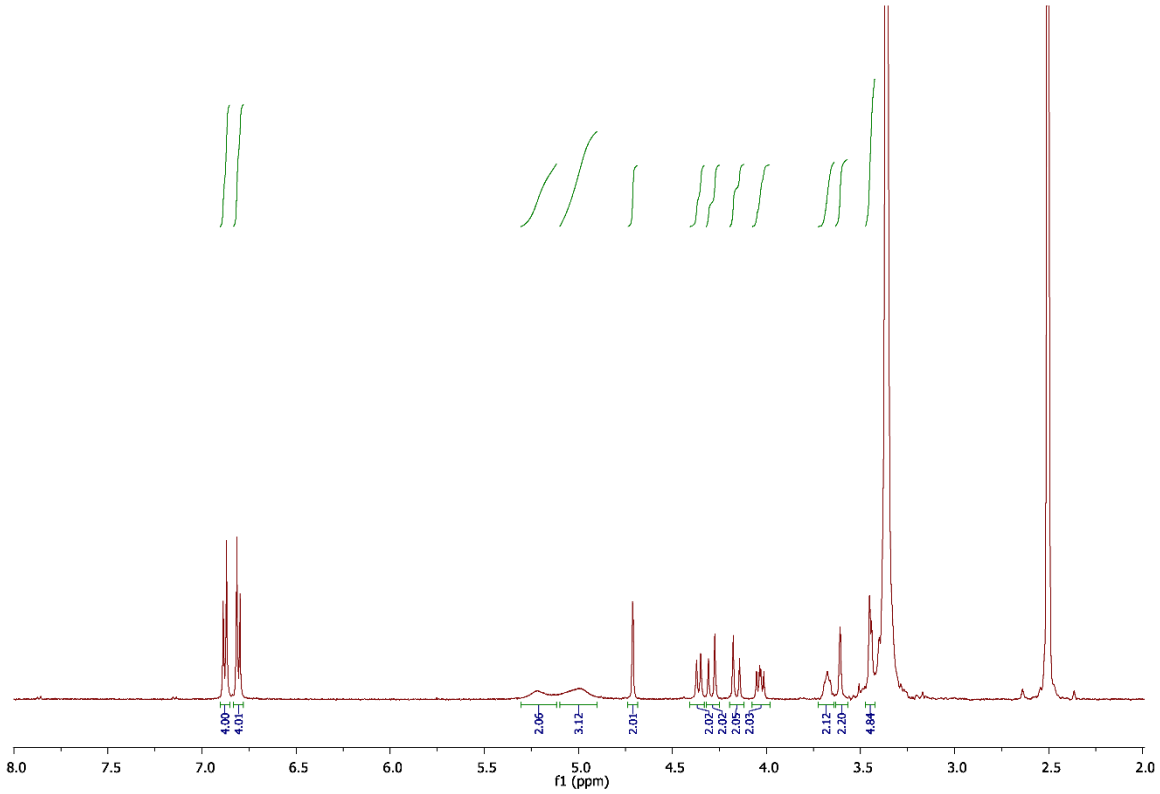

Figure S14: ^{1}H NMR spectrum of *cis*-macrocycle **1** (500 MHz, DMSO-d_6, 300 K).

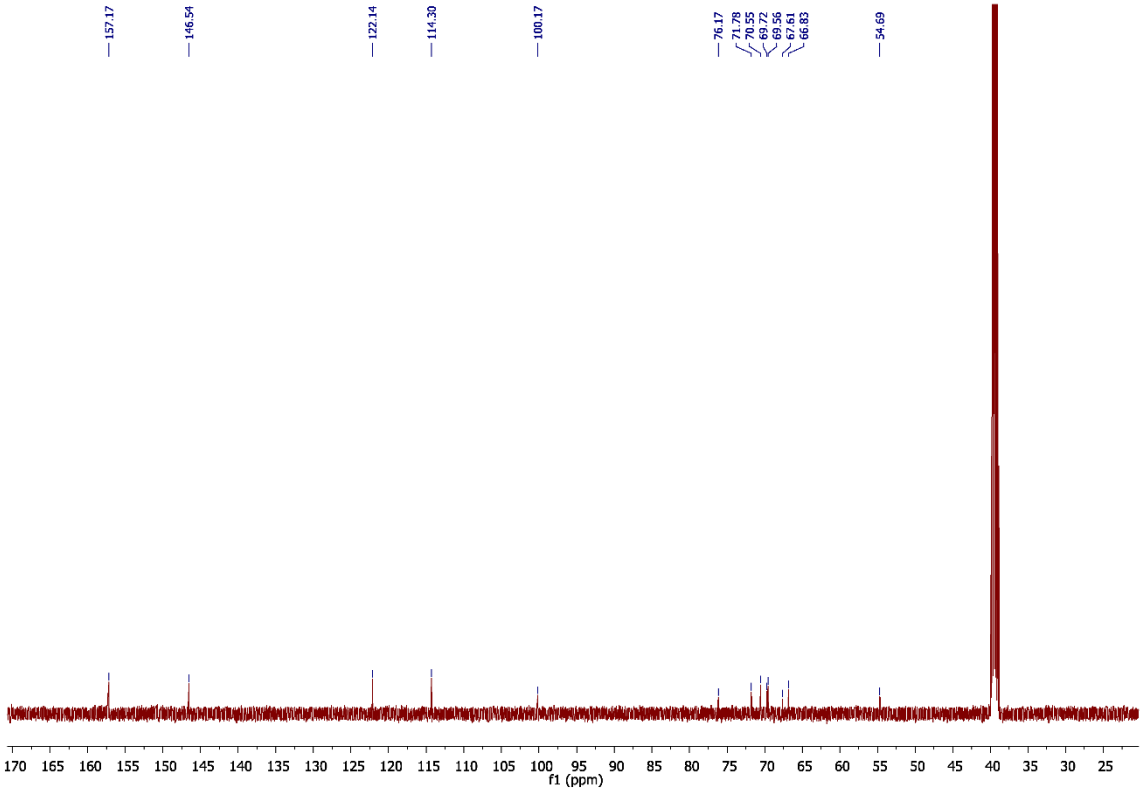

Figure S15: ^{13}C NMR spectrum of *cis*-macrocycle **1** (125 MHz, DMSO-d_6, 300 K).

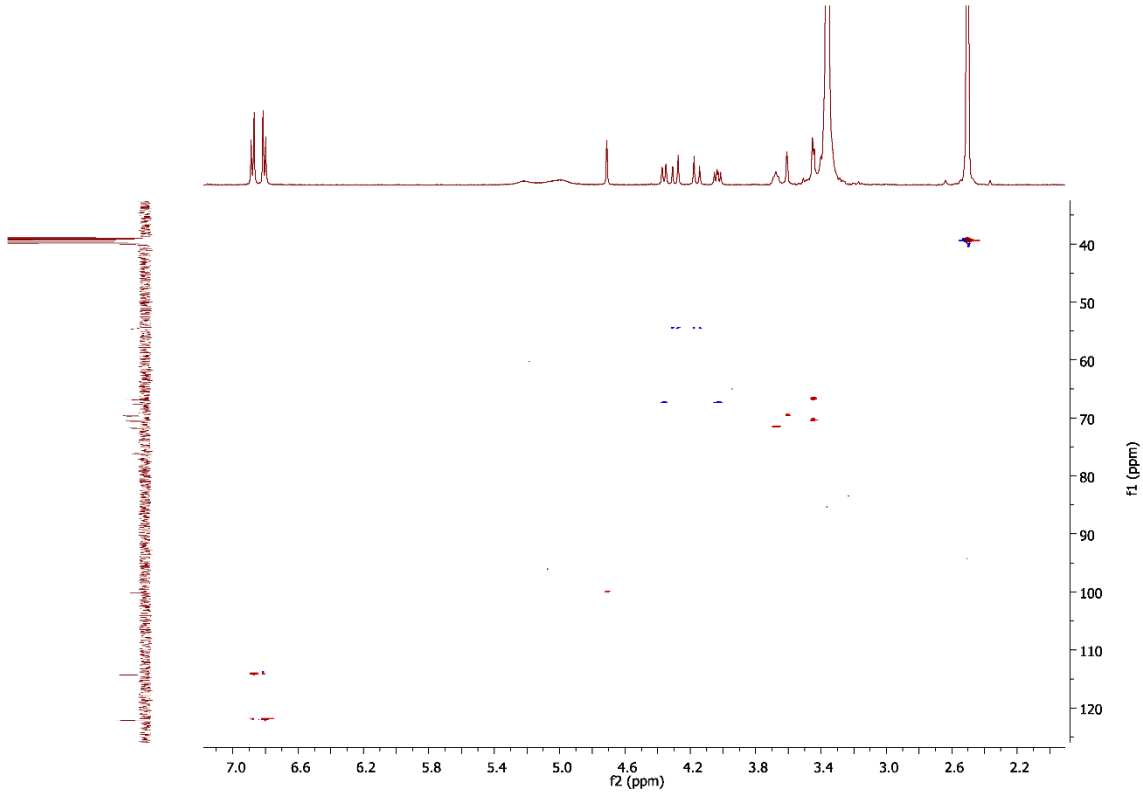

Figure S16: HSQC spectrum of *cis*-macrocycle **1** (DMSO-d_6, 300 K).

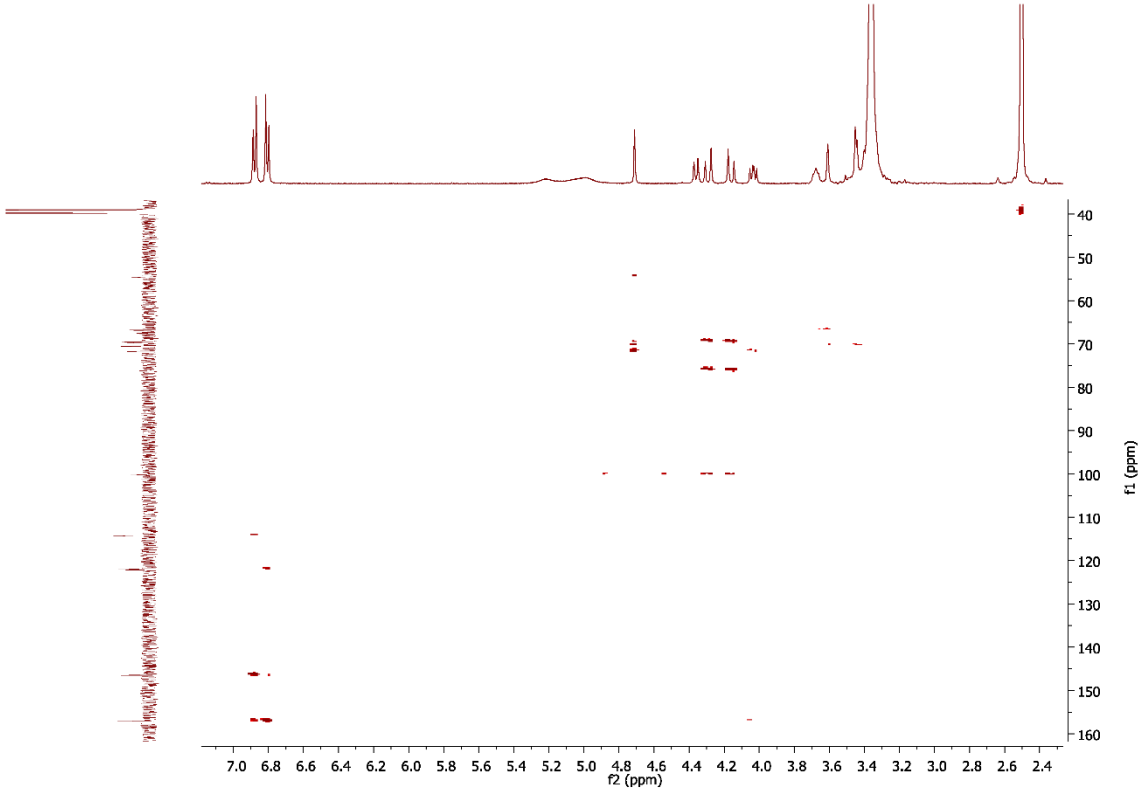

Figure S17: HMBC spectrum of *cis*-macrocycle **1** (DMSO-d_6, 300 K).

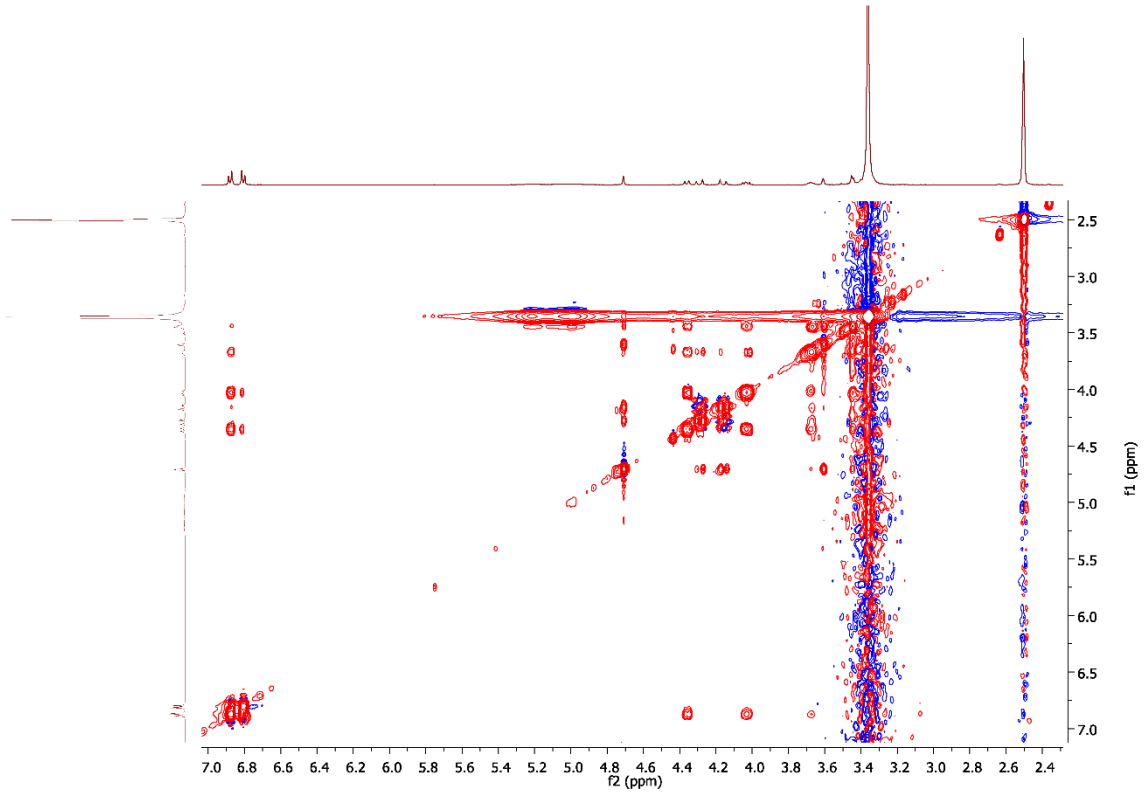

Figure S18: NOESY spectrum of *cis*-macrocycle **1** (DMSO-d_6, 300 K).

Irradiation Experiments

Each sample was heated at 45 °C in the dark for 20 h prior to the beginning of each experiment in order to fully relax the azobenzene to its *trans* form. The respective sample was irradiated in the dark, the distance between the lamp and the sample being about 5 cm, then the respective measurement was performed immediately afterwards.

Absorption spectroscopy

Photostationary states (PSS) were reached after irradiating the respective sample for 3 min at 365 nm or 14 min at 525 nm. Extinction coefficients (ε) were calculated using the Beer-Lambert law (see equation below), plotting the absorbance at the respective λ_{max} versus the concentration (6 - 8 different concentrations in a range of 2.10^{-5} to 10^{-4} mol·L^{-1}). In the case of PSS 365 nm, the λ_{max} of the n-π* band was used. A linear fitting gave the value of ε as the slope of the linear plot.

$$A = \varepsilon \cdot c \cdot l$$

A = absorbance
ε = extinction coefficient = slope of the plot
c = molar concentration in mol·L^{-1}
l = optical path length in cm

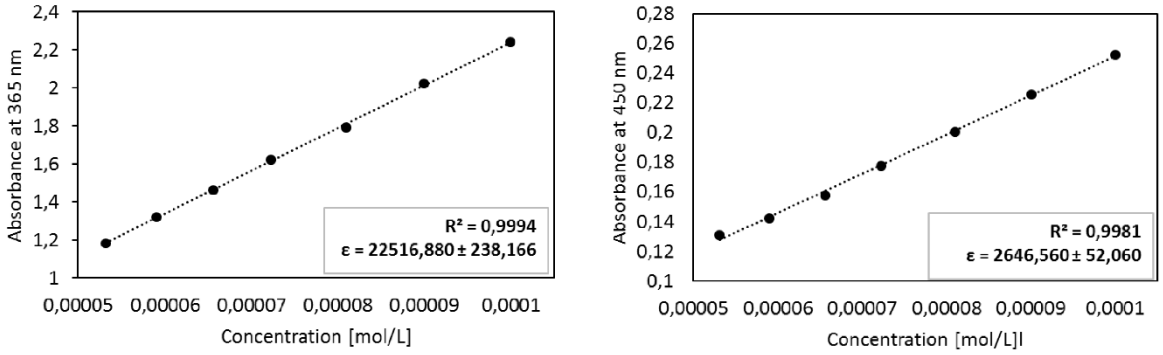

Figure S19: Plot of the absorbance at the λ_{max} versus the concentration; the slope of the linear curve gives the value of the molar extinction coefficient ε. Measured at 298 K in DMSO in concentrations from 5.10^{-5} to 10^{-4} mol·L^{-1} (a) *trans*-**1**, absorbance at 365 nm; (b) PSS after irradiation at 365 nm, absorbance at 450 nm.

Switching cycle experiments were performed by irradiating the sample alternatively for 3 min at 365 nm and 14 min at 525 nm, within 19 cycles. The value of the absorbance at $\lambda_{max(trans)}$ was plotted against the number of times the sample was irradiated.

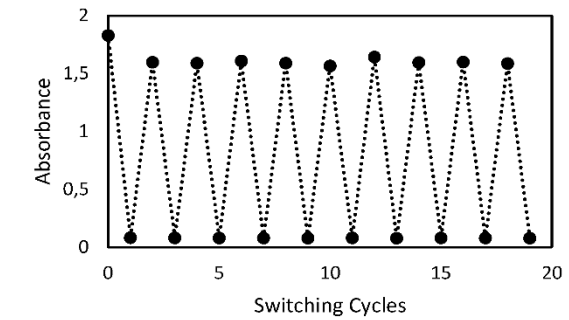

Figure S20: Measured absorbance after alternating photoirradiation with 365 nm and 525 nm. Measured at 298 K in DMSO at a concentration of 100 µM.

NMR spectroscopy

PSS was reached after irradiating the respective sample for 3 min with 365 nm or 17 min with 525 nm and the *cis*:*trans* ratios were measured by ^{1}H NMR spectroscopy. The PSS were determined by integration of one aromatic signal of each isomer.

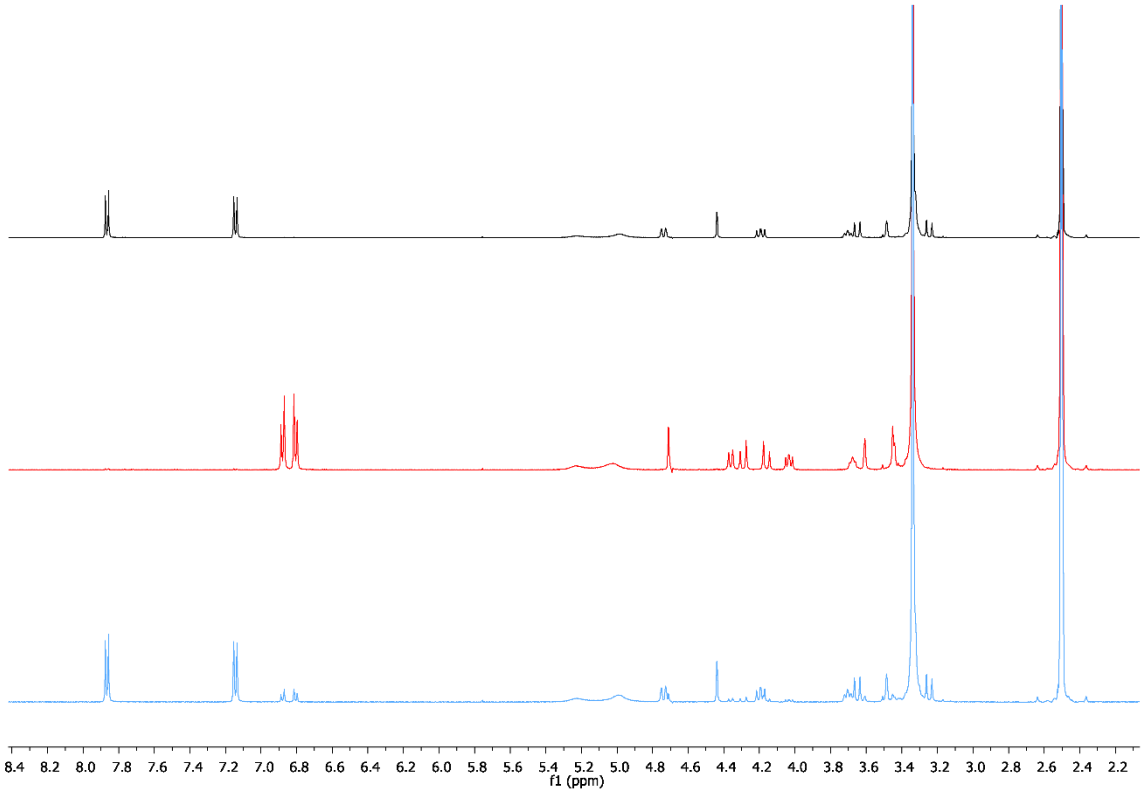

Figure S21: NMR spectra of trans-1 after heating at 45 °C in the dark for 20h (black), after irradiation with 365 nm for 3 min (red) and after irradiation with 525 nm (blue).

Thermal *cis*→*trans* relaxation

The kinetics of thermal *cis*→*trans* relaxation process was determined by ^{1}H NMR. After irradiation, the spectra of the samples were recorded in regular intervals, keeping the sample inside the probe at a constant temperature of 300 K, over a period of 7 days. The decay of the integral of the *cis* form was plotted versus the time, and an exponential decay of first order fitted to the data, according to the following equation:

$$I = I_{inf} + A \cdot \exp^{-k \cdot t}$$

I = integral of the *cis* isomer
I_{inf} = integral of the *cis* isomer at infinite time
A = pre-exponential factor proportional to the initial integral of the *cis* isomer
k = rate of thermal isomerization
t = time

A linear fitting gave the value of *k* as the slope of the following plot:

$$\ln(I - I_{inf}) = \ln(A) - kt$$

The half-life of the *cis* isomer ($\tau_{1/2}$) was determined as $\tau_{1/2} = \ln 2/k$.

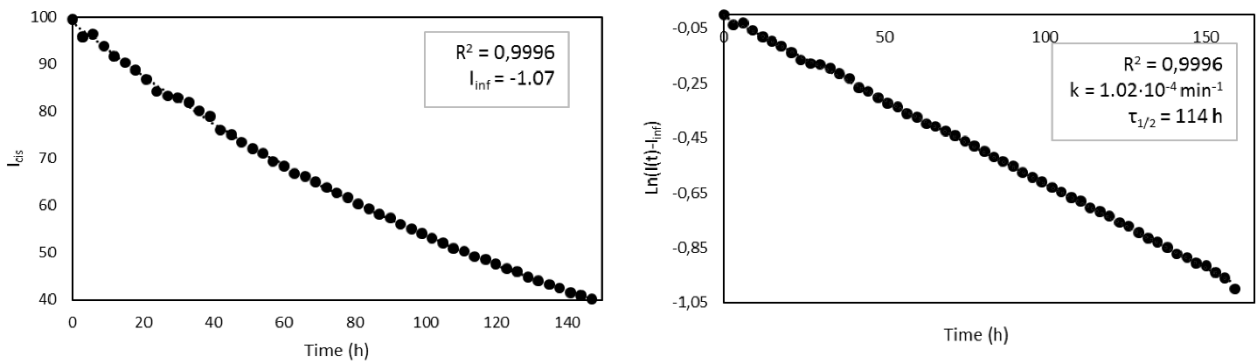

Figure S22: Kinetics of the *cis*→*trans* thermal relaxation process at 300 K investigated by 1H NMR spectroscopy. (a) Exponential decay of the integral of an aromatic signal of *cis*-**1** (300 MHz, DMSO-d6); (b) Linearization of the exponential decay of *cis*-**1**.

Specific rotation and circular dichroism

The optical rotation and the circular dichroism spectra were measured at 293 K after irradiating the respective sample at 365 nm for 10 min. The CD signal was recorded as ellipticity (θ), expressed in units of millidegrees (mdeg). The ellipticity was converted into difference in molar absorption coefficient (Δε), expressed in $M^{-1} \cdot cm^{-1}$, by using the following equation:

$\Delta\varepsilon = \theta / (32980 \cdot c \cdot l)$
Δε = difference in molar absorption coefficient
θ = ellipticity
c = molar concentration in $mol \cdot L^{-1}$
l = optical path length in cm

Literature References

[1] M. Poláková, M. Beláňová, K. Mikušová, E. Lattová and H. Perreault, *Bioconjugate Chemistry* **2011**, *22*, 289-298.
[2] H. J. Jung, H. Min, H. Yu, T. G. Lee and T. D. Chung, *Chem. Comm.* **2010**, *46*, 3863-3865.

7. Summary

Eight novel shape-switchable glycoazobenzene macrocycles (Figure 7.1), comprising carbohydrates and azobenzene moieties were prepared, using different chemistries for macrocyclization, thiourea bridging, CuAAC-click reaction, Sonogashira coupling and Glaser coupling.

The macrocycles prepared via the first three reactions were all synthesized using intermolecular cyclizations of two building blocks, while the Glaser coupling macrocyclizations were performed in an intramolecularly. For both the intermolecular thiourea bridging with piperazine, and the intramolecular Glaser coupling, isomerization from *trans*- to *cis*-isomer of the precursor molecules was crucial to facilitate the cyclization by decreasing the distance between the reactive sites. In the cyclizations enabled by click reaction and Sonogashira coupling, the interatomic distances between the functional groups of both reaction partners were similar enough to allow for the reaction to take place.

Starting from readily available building blocks, the longest reaction sequence to achieve the desired macrocycle consisted of only five steps. However, a specific approach employing a particular ligation chemistry was not necessarily suited for a wide range of macrocycles with varied carbohydrate moieties and hence the modularity of our approaches was found somewhat limited.

Whereas the Sonogashira coupling led to **17** and **18** under the same reaction conditions, variation of the carbohydrate unit led to complications in the synthesis towards the precursors of the Glaser coupled macrocycles. The 6-*O* arylation of different carbohydrates with dihydroxy azobenzene proceeded with varying success, hence reaction conditions had to be adapted for each reaction

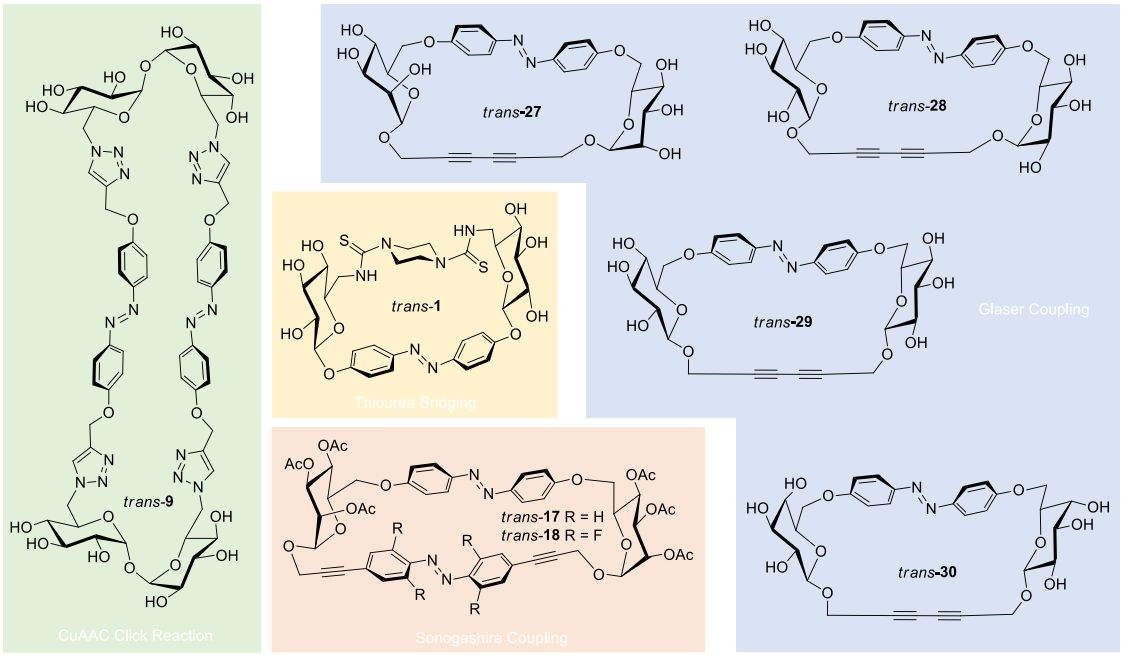

Figure 7.1: Collection of the new synthesized glycoazobenzene macrocycles and their macrocyclization chemistry.

The photochromic properties of all synthesized macrocycles were investigated. UV/Vis and CD spectra were measured in DMSO and in water for unprotected macrocycles. The UV/Vis spectra all presented the typical pattern for azobenzene-containing compounds, while measurements in water with 0.5 % DMSO revealed that most cycles were not fully solubilized in this solvent mixture. The diyne bridged macrocycles with non-all-equatorial hydroxyl groups **27** and **30** showed especially poor solubility in the *trans*-state. Isomerization to the *cis*-isomer remarkably improved the solubilization in water for every macrocycle.

Strong bands in the CD spectra corresponding to the absorption in the UV/Vis attest that all macrocycles transfer chirality onto the azobenzene moiety with a defined preferential conformation. The macrocycles **9**, **17** and **18** which contain two azobenzene moieties present an exciton coupling in their *trans*-form but not in *cis*, indicating that the π-π coupling between the two azobenzene moieties does not occur any longer upon switching into the more bent structure. The oftentimes large difference between the CD spectra measured in DMSO and water show that the shape of the macrocyclic structures is not only dependent on the *trans*- and *cis*-isomerization, but also on the solvent through a possible conformational change.

8. Other Publications

8.1 Introduction

During this dissertation the following projects were realized in different collaborations.

In chapter 8.2, in collaboration with P. Rollin (Université d'Orléans) and W. Klaffke (Haus der Technik e. V.), we reviewed the Mitsunobu reaction for the modification of sugar hemiacetals. While the Mitsunobu reaction finds widespread applications in the substitution of the carbohydrate hydroxy groups, the reaction at the anomeric position is less known. Additionally, collection of the available reactions showed that the modification at the anomeric position often takes place regioselectively, making the use of protecting groups redundant.

In chapters 8.3 – 8.5, together with K. Ruppersberg (Leibniz-Institut für die Pädagogik der Naturwissenschaften und Mathematik an der Universität Kiel), the Wöhlk reaction was evaluated. A classical detection reaction for lactose in urine, this experiment is still taught in schools and pharmaceutical classes. In the experiment aqueous solutions containing lactose turn a brightly red color after addition of ammonia and potassium hydroxide and subsequent heating. However, the cause for this red color was unknown and assertions found in old schoolbooks that claim the color to be pyrrole red could be refuted. Still, while experiments have been performed with different substrates to shed light on this unusual reaction that was almost forgotten, the elucidation of the structure of the chromophore was not yet possible.

8.2 J. Hain, P. Rollin, W. Klaffke, Th. K. Lindhorst, Anomeric modification of carbohydrates using the Mitsunobu reaction, *Beilstein J. Org. Chem.* **2018**, *14*, 1619-1636.

BEILSTEIN JOURNAL OF ORGANIC CHEMISTRY

OPEN ACCESS PLATINUM

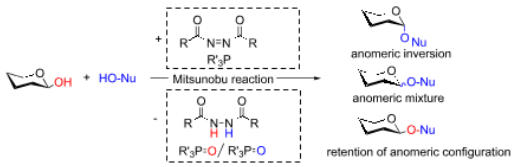

Anomeric modification of carbohydrates using the Mitsunobu reaction

Julia Hain, Patrick Rollin, Werner Klaffke et al.

Beilstein J. Org. Chem. **2018,** *14,* 1619–1636.

doi:10.3762/bjoc.14.138

BEILSTEIN JOURNAL OF ORGANIC CHEMISTRY

Anomeric modification of carbohydrates using the Mitsunobu reaction

Julia Hain[1], Patrick Rollin[*2], Werner Klaffke[3] and Thisbe K. Lindhorst[*1]

Review

Open Access

Address:
[1]Christiana Albertina University of Kiel, Otto Diels Institute of Organic Chemistry, Otto-Hahn-Platz 3–4, D-24118 Kiel, Germany, Fax: +49 431 8807410, [2]Université d'Orléans et CNRS, ICOA, UMR 7311, BP 6759, 45067 Orléans, France, Fax: +33 238 417281 and [3]Haus der Technik e.V., Hollestr. 1, 45127 Essen, Germany, Fax: +49 201 1803269

Email:
Patrick Rollin[*] - Patrick.Rollin@univ-orleans.fr; Thisbe K. Lindhorst[*] - tklind@oc.uni-kiel.de

* Corresponding author

Keywords:
anomeric stereoselectivity; carbohydrates; glycoside synthesis; Mitsunobu reaction

Beilstein J. Org. Chem. **2018,** *14,* 1619–1636.
doi:10.3762/bjoc.14.138

Received: 21 March 2018
Accepted: 06 June 2018
Published: 29 June 2018

This article is part of the Thematic Series "The glycosciences". Dedicated to Professor Joachim Thiem in recognition of his constant inspiration and support as a teacher, colleague and friend.

Associate Editor: S. Flitsch

Abstract

The Mitsunobu reaction basically consists in the conversion of an alcohol into an ester under inversion of configuration, employing a carboxylic acid and a pair of two auxiliary reagents, mostly triphenylphosphine and a dialkyl azodicarboxylate. This reaction has been frequently used in carbohydrate chemistry for the modification of sugar hydroxy groups. Modification at the anomeric position, leading mainly to anomeric esters or glycosides, is of particular importance in the glycosciences. Therefore, this review focuses on the use of the Mitsunobu reaction for modifications of sugar hemiacetals. Strikingly, unprotected sugars can often be converted regioselectively at the anomeric center, whereas in other cases, the other hydroxy groups in reducing sugars have to be protected to achieve good results in the Mitsunobu procedure. We have reviewed on the one hand the literature on anomeric esterification, including glycosyl phosphates, and on the other hand glycoside synthesis, including S- and N-glycosides. The mechanistic details of the Mitsunobu reaction are discussed as well as this is important to explain and predict the stereoselectivity of anomeric modifications under Mitsunobu conditions. Though the Mitsunobu reaction is often not the first choice for the anomeric modification of carbohydrates, this review shows the high value of the reaction in many different circumstances.

Introduction

Fifty years ago, Oyo Mitsunobu reported a preparation of esters from alcohols and carboxylic acids supported by two auxiliary reagents, diethyl azodicarboxylate (DEAD) and triphenylphosphine [1]. This reaction has ever since become known as the "Mitsunobu reaction", being a frequently utilized tool in organic synthesis. In 1981, Mitsunobu published a first review about this reaction, entitled "The Use of Diethyl Azodicarboxylate and Triphenylphosphine in Synthesis and Transformation

Beilstein J. Org. Chem. **2018,** *14,* 1619–1636.

of Natural Products" [2]. Thereafter, several further general reviews have appeared [3-6], owing to the spectacular development of diversified synthetic applications of the Mitsunobu reaction, whilst the long term debate about the mechanism of this reaction was still ongoing [7-12].

The standard Mitsunobu reaction involves coupling of an alcohol and a nucleophile in a dehydrative S_N2 process activated by a reactive combination of a triaryl- or trialkylphosphine as reducing agent and a dialkyl azodicarboxylate as oxidant. In a redox process, the phosphine species is oxidized to the respective phosphine oxide and the azo reagent is reduced to the corresponding 1,2-hydrazinodicarboxylate (Scheme 1). As we have frequently utilized this valuable reaction in carbohydrate chemistry, in this account we have compiled literature, where the Mitsunobu reaction was used for the anomeric modification of carbohydrates.

The reaction proceeds under mild, neutral conditions that are compatible with a wide range of functional groups. In the case where a stereogenic center is involved, the reaction takes place with stereochemical inversion [6]. The reaction partners are mostly primary or secondary alcohols, while the nucleophilic species needs to be acidic [13] with a $pK_a < 11$. Otherwise the azo reagent would compete with the acidic nucleophile and participate in the substitution reaction [14]. Various compounds comply with that condition: carboxylic acids, phenols, hydrazoic acid, some other NH acids, and thiols. The standard azo reagents used are diethyl- (DEAD) or diisopropyl- (DIAD) azodicarboxylate. However, alternative reagents such as azodicarboxamides [15,16] or stabilized phosphoranes were also developed to allow reaction with nucleophiles of weaker acidity. The typical phosphine reagents are triphenyl- (Ph_3P) or tributylphosphine (n-Bu_3P). In recent years, advances have been made using solid supported reagents, thus facilitating work-up conditions [17,18]. The polarity of the commonly aprotic solvents used in the Mitsunobu reaction, including toluene, tetrahydrofuran or dimethylformamide, has been shown to be influential in terms of efficacy and stereoselectivity [19].

Since its infancy, the Mitsunobu reaction has found applications in carbohydrate chemistry, as its broad scope and mild conditions are ideal for the formation of conjugates with sensitive natural products. Standard applications of the Mitsunobu reaction in glycochemistry have mostly dealt with the functionalization of the primary hydroxy group of sugars and, to a lesser extent, with modifications of the secondary alcohol array in carbohydrate rings [2-6], for example for halogenation [20]. However, the Mitsunobu reaction can also be profitably utilized for the anomeric modification of carbohydrates. Hence, we have focused this review on the utilization of the Mitsunobu reaction for manipulations of the carbohydrate hemiacetal, where reducing (anomerically unprotected) sugars react as the alcohol component to be either converted into glycosides or into other anomerically modified carbohydrate derivatives. We intend to provide a critical survey as well as a source of inspiration, even more so as glycosylation remains a challenge in carbohydrate chemistry.

Review

Mechanistic considerations

Since Mitsunobu's postulate of a three-reaction-step mechanism in 1981 [2] many further mechanistic investigations have been performed and reported [3,7,8,19]. To rationalize the outcome of the Mitsunobu reaction with reducing sugars, special mechanistic considerations have to be taken into account. On the one hand, the equilibrium between the azodicarboxylate, the phosphine, and the acidic component, Nu-OH, is important (cf. Scheme 2, left dashed box). On the other hand, mutarotation of the sugar hemiacetal has to be discussed to predict the stereochemical outcome of the reaction. Mutarotation results in an equilibrium of both, α- and β-anomers (Scheme 2, right dashed box). However, full anomerization is often not observed as the rate and the extent of

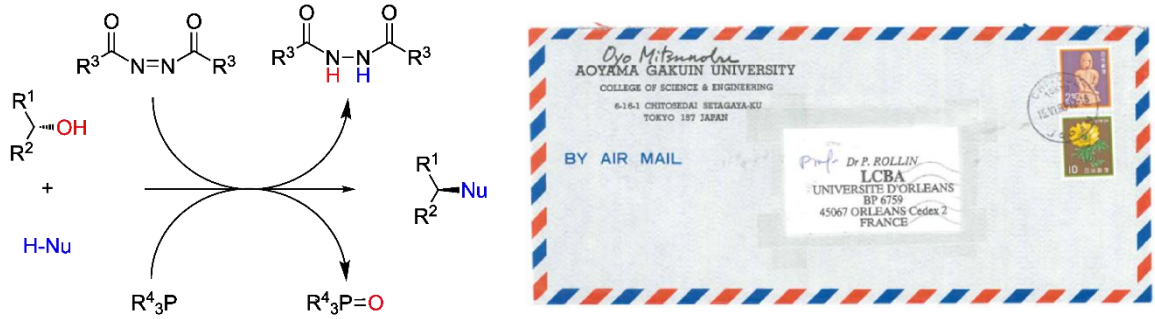

Scheme 1: Left: The Mitsunobu reaction is essentially a nucleophilic substitution of alcohols occurring with inversion of configuration at the alcohol stereocenter. The auxiliary reagents are involved in a redox process. Right: Original correspondence with Professor Oyo Mitsunobu (letter to P.R. in 1993).

Beilstein J. Org. Chem. **2018,** *14,* 1619–1636.

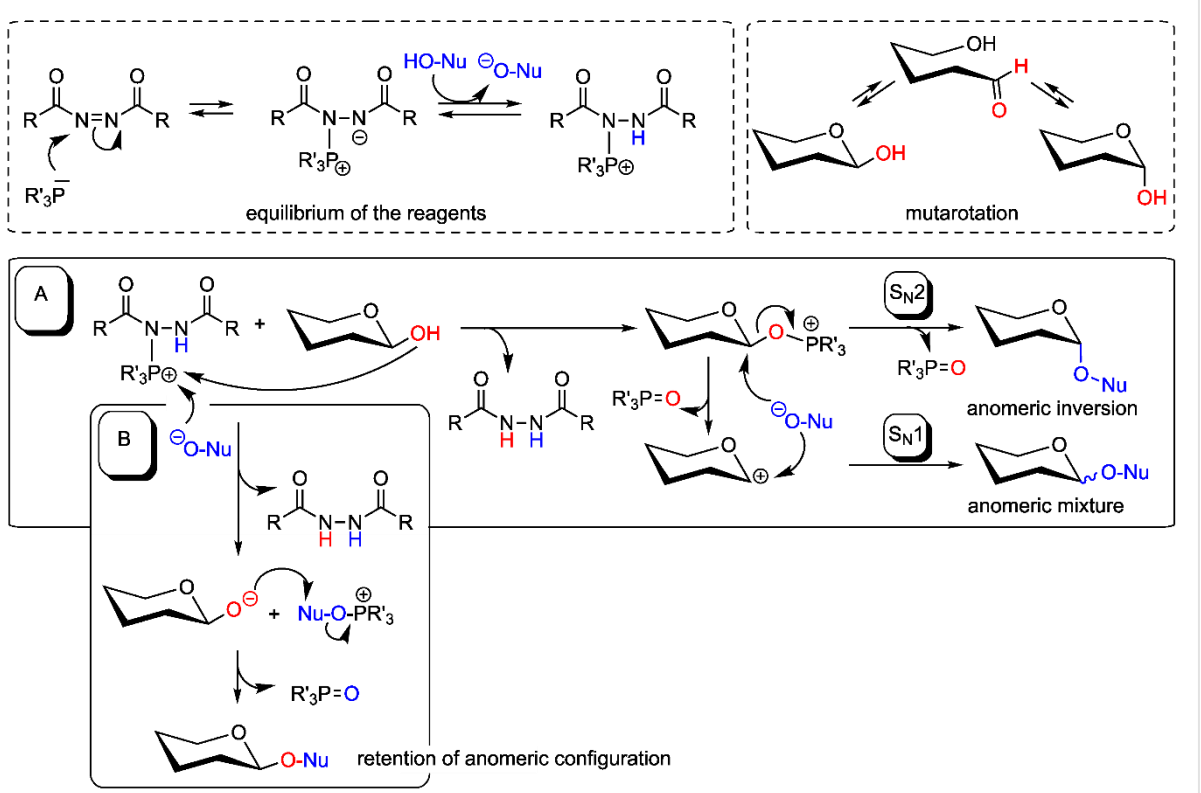

Scheme 2: Mechanistic considerations on the Mitsunobu reaction with carbohydrate hemiacetals (depicted in simplified form). Two equilibria are relevant for this reaction (top dashed boxes), (i) the formation of the "Mitsunobu reagent" from the employed azodicarboxylate, phosphine and the acidic nucleophile, and (ii) the mutarotation equilibrium of the reducing sugar in solution. These can give rise to at least two different reaction pathways, A and B, as explained in the main text. Depending on various parameters, the anomerically modified sugar, a glycoside or an anomeric ester, respectively, is obtained with full inversion of anomeric configuration or as anomeric mixture (A), or with retention of the anomeric configuration via *O*-alkylation (B). For clarity both reaction pathways are exemplified with only one sugar anomer.

mutarotation depends on various parameters such as anchimeric effects of neighboring groups and the reaction conditions. Hence it has been frequently observed in Mitsunobu reactions with carbohydrate hemiacetals, that sugar anomerization is either absent or slower than the formation of the *O*-glycosyloxyphosphonium salt, which can play the intermediate during the reaction (Scheme 2, pathway A) [21]. Another possible explanation for limited anomerization lies in the different stability of anomeric glycosyloxyphosphonium salts, where one anomer can be sterically favored over the other, thereby pushing the equilibrium to a product with the respective anomeric configuration. Regardless of the rate of mutarotation, the Mitsunobu reaction can proceed through a mechanistic pathway A or B as depicted in Scheme 2. Especially when the sugar alcohol is not sterically hindered, phosphorus transfer occurs to yield a phosphine-activated anomeric alcohol (a glycosyloxyphosphonium ion, pathway A). This in turn can be attacked by the deprotonated nucleophile resulting in an anomerically modified carbohydrate with inversion of configuration at the anomeric center, according to a S_N2 mechanism. Pathway A can also proceed through a S_N1 mechanism when the intermediate glycosyloxyphosphonium ion is less stable. Then, it can decompose into the corresponding anomeric oxocarbenium ion and phosphine oxide. The oxocarbenium ion would then react with the NuO^- anion in a S_N1 mechanism. While this would lead to racemization under normal circumstances, in most carbohydrates, participation effects of neighboring groups in the vicinity (typically at the 2-position of the sugar ring) affect the reaction outcome, favoring nucleophilic attack from a preferred face of the sugar ring [22,23]. Grynkiewicz and colleagues have discussed anchimeric assistance even when no protecting group is present at C-2, assuming a Brigl's anhydride type intermediate [24]. In the absence of a substituent at C-2, however, typically poor stereoselectivity is observed in Mitsunobu reactions with carbohydrate hemiacetals, indicating a S_N1-type pathway A of the reaction [25].

The Mitsunobu reaction can also follow a different pathway B (Scheme 2), as first suggested by Hughes [13] and later by Ahn et al. [26]. Assuming that the alcohol is sterically hindered

Beilstein J. Org. Chem. **2018,** *14,* 1619–1636.

and thus represents a relatively weak nucleophile, the deprotonated acidic partner, NuO^-, can react with the phosphonium intermediate first to afford an intermediate Nu-O-PR'$_3$. In the case where a carboxylic acid is used, Nu-O-PR'$_3$ represents an acyloxyphosphonium ion. This in turn reacts with the anomeric oxyanion to furnish the anomerically modified sugar with retention of configuration via anomeric *O*-alkylation. This mechanistic proposal is in agreement with observations by Lubineau et al., who could correlate the acidity of the employed nucleophile with the anomeric outcome of the Mitsunobu reaction [27].

Both reaction pathways, A and B, have a "raison d'être" in addressing different outcomes of the Mitsunobu reaction, which vary depending on the substrates used. While these variables make the already complex Mitsunobu reaction even more demanding, they can also be manipulated to one's advantage, for example for the stereoselective formation of β-mannosides [28].

Reactions with protic acids to achieve anomeric esters

The first application of the Mitsunobu reaction involved esterification of a secondary alcohol. Although an anomeric OH group cannot be regarded as a classical secondary alcohol group but as a hemiacetal OH, it can be successfully involved in Mitsunobu reactions to achieve 1-*O*-acyl glycoses. Thus, searching for an efficient protocol for the preparation of complex, multifunctional glycosyl esters in the context of the total synthesis of phyllanthostatin antitumor agents, A. B. Smith and colleagues soundly investigated the suitability of the Mitsunobu reaction [29]. They concluded already back in 1986 that "the anomeric hydroxyl group of various pyranose hemiacetals can be esterified with inversion of configuration, conveniently, mildly and on large-scale using Ph_3P, with either DIAD or DEAD and a carboxylic acid in THF at either –50 °C or at room temperature". Hence, several protected mono- and disaccharides, such as **1**–**4** (Scheme 3) were selectively esterified with simple benzoic acid to give **5**–**7** and **9**, respectively. In addition, **4** was also converted with the phyllanthostatin aglycone **8** to give **10** with inversion of anomeric configuration. Extension of this work to other more complex antineoplastic glycosyl esters was successfully investigated by the same group [30-34].

De Mesmaeker et al. reported the stereoselective coupling of an allyl glucuronide, in which all hydroxy groups except the anomeric OH were *O*-acyl-protected, with carboxylic acids by a Mitsunobu reaction [35]. The reaction was successful even when a free phenolic function was present in the employed acid and the desired β-anomer of the 1-*O*-acyl-β-D-glucuronide products could be isolated in up to 50% yield. Similarly, regioselective esterification of unprotected allyl glucuronide **11** was

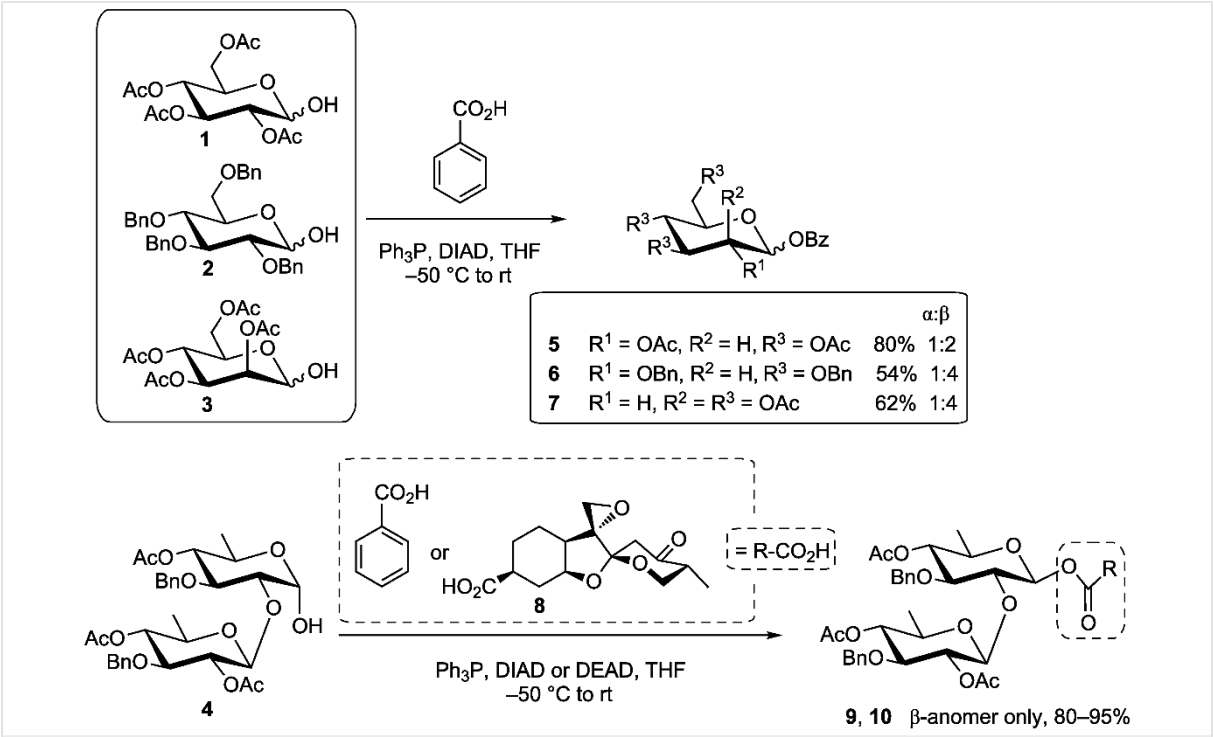

Scheme 3: Anomeric esterification using the Mitsunobu procedure [29].

Beilstein J. Org. Chem. **2018,** *14,* 1619–1636.

performed by Juteau et al. with the acids **12**–**16** yielding anomeric mixtures of the respective 1-*O*-acyl-β-D-glucuronides **18**–**22** in quite acceptable yields even with complex acids like **16** (Scheme 4) [36]. The same approach was chosen in the Stachulski group for the anomeric modification of glucuronides with the anti-inflammatory drug diclofenac (**17**) to give the respective product **23** (Scheme 4) [37].

Bourhim et al. reported that the Mitsunobu reaction with native D-glucose, D-GlcNAc or D-maltose resulted in regioselective esterification of the primary OH group, leaving all other hydroxy groups including the anomeric OH unmodified [38]. On the other hand, other authors have reported that the anomeric position can be selectively modified in a Mitsunobu reaction without concomitant modification of the primary 6-OH (vide infra). Apparently, fine-tuning of reaction conditions can alter the selectivity of the Mitsunobu reaction and in addition, different regioselectivities might origin in the structure of the sugar substrate.

In the course of a synthesis of carbocyclic lignan variants related to podophyllotoxin, a pseudo-anomeric stereospecific inversion of a carbasugar was achieved in good yield in Nishimura's group [39]. More recently, the Mitsunobu procedure was applied in the context of gold-catalyzed glycosylation in order to install a reactive anomeric ester function in a series of *O*-benzylated glycoses (**2**, **24**, **25**) employing the branched carboxylic acid **26** (Scheme 5) [40]. The produced esters **27**–**29** were obtained as anomeric mixtures.

Lubineau et al. [27] investigated the stereoselectivity of the anomeric Mitsunobu coupling of 2,3,4,6-tetra-*O*-chloroacetyl-D-glucose (**30**) as well as its *galacto*-configured analogue with the carboxylic acids **31**–**34** to obtain products **35**–**38** which are related to various pesticide agents (Scheme 6). Their results supported the theory that, along with an effect of the reaction temperature, an increase of the pK_a of the employed acidic reaction partner can lead to predominant formation of the β-configured product, whereas stronger acidic reagents can favor the

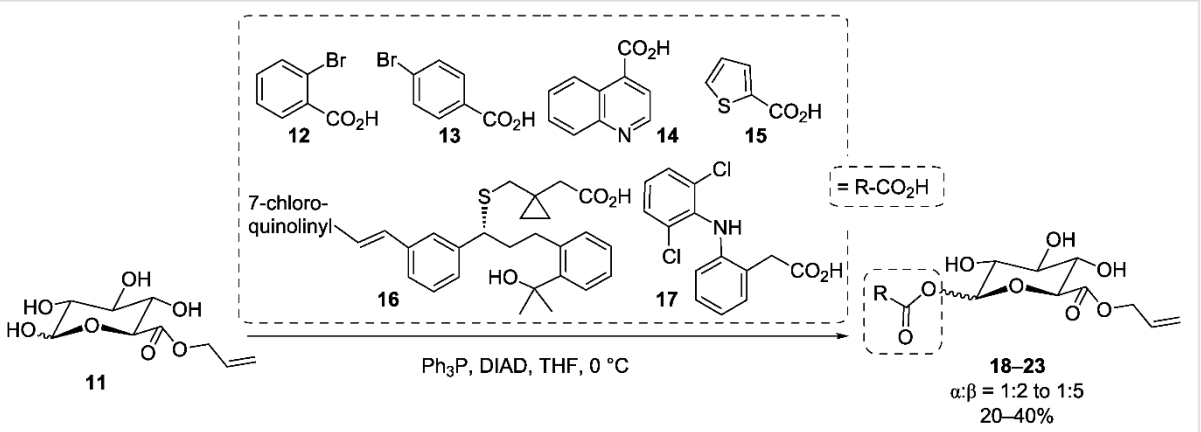

Scheme 4: Conversion of allyl glucuronate into various 1-O-esterified allyl glucuronates using anomeric Mitsunobu esterification [36,37].

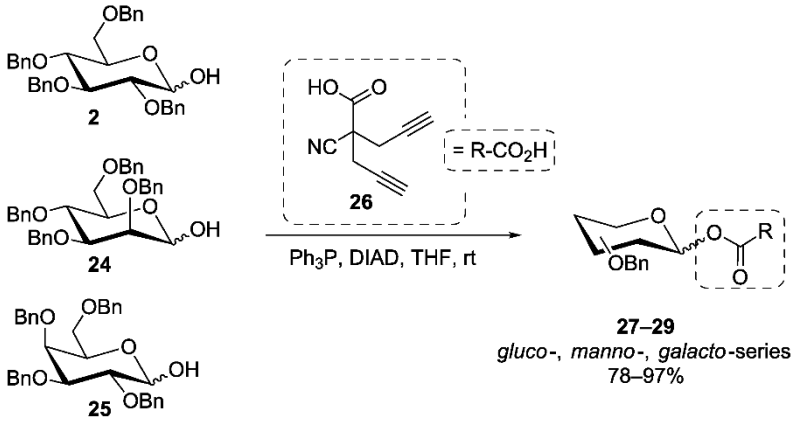

Scheme 5: Synthesis of anomeric glycosyl esters as substrates for Au-catalyzed glycosylation [40].

Beilstein J. Org. Chem. **2018,** *14,* 1619–1636.

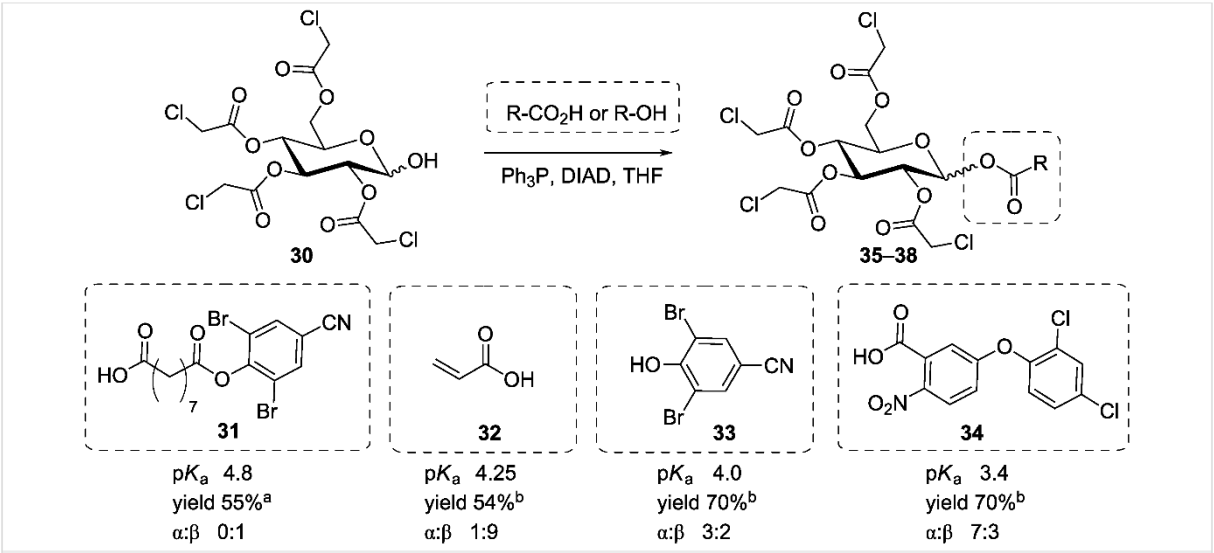

Scheme 6: Correlation between pK_a value of the employed acids (or alcohol) and the favoured anomeric configuration of the respective product. [a]Carried out at 0 °C; [b]carried out at rt [27].

formation of the respective α-anomers. These findings can be explained by considering the two different reaction pathways A and B as shown above in Scheme 2. The authors state that the observed pK_a effect is either due to the influence of the acidity of the employed acid on the reaction mechanism or results from the proton-catalyzed change of the anomeric ratio of the starting material **30** in solution.

Very recently, anomeric phosphorylation via a Mitsunobu approach was concomitantly undertaken by groups from Japan and Austria, respectively [41,42], aiming at the synthesis of the bacterial metabolite and potent innate immune modulator D-*glycero*-β-D-*manno*-heptose-1,7-bisphosphate (**43**, HBP, Scheme 7). The group around Zamyatina employed 2,3,4,6-tetra-*O*-acetyl-mannopyranose (**3**) as a 9:1 α,β-mixture in order

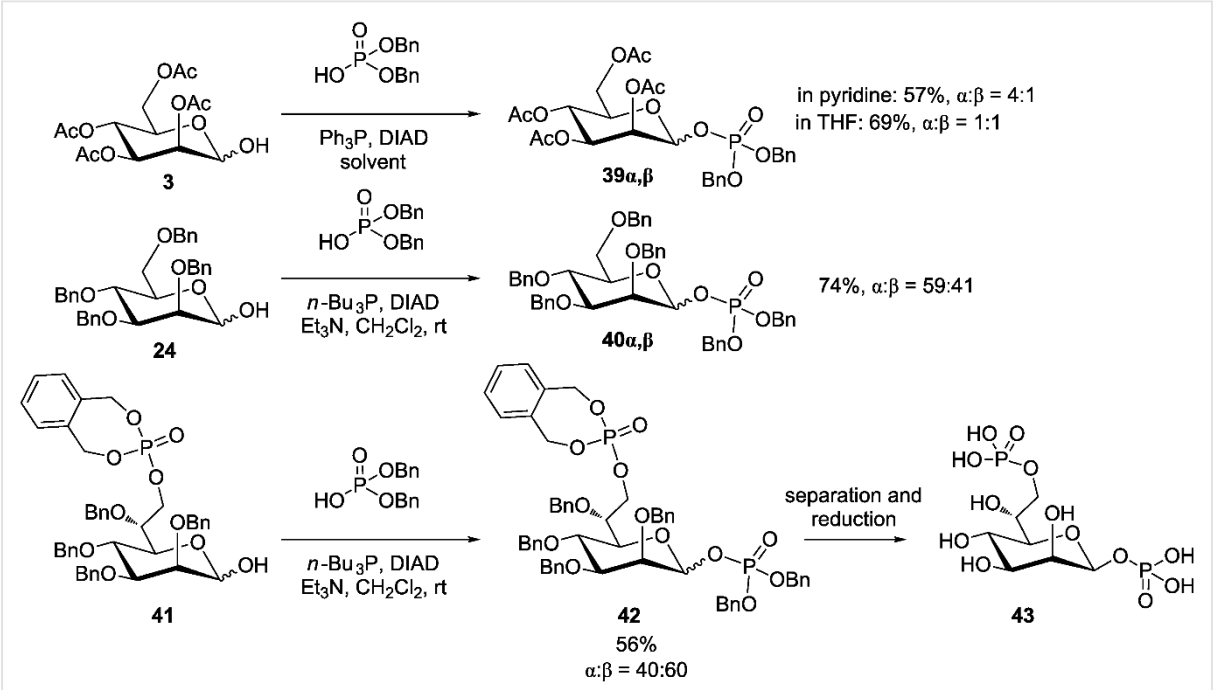

Scheme 7: Synthesis of the β-mannosyl phosphates for the synthesis of HBP **43** by anomeric phosphorylation according to Mitsunobu [41,42].

Beilstein J. Org. Chem. **2018,** *14,* 1619–1636.

to optimize the reaction conditions for the Mitsunobu reaction with phosphoric acid dibenzyl ester. The anomeric mannosyl phosphate derivatives **39α** and **39β** were obtained in 57% total yield when pyridine was used as the solvent, as depicted in Scheme 7. In THF, the same reaction furnished a 1:1-anomeric mixture in 69% yield. The authors thus considered the Mitsunobu reaction as unsatisfactory for the synthesis of IIBP. On the other hand, Inuki et al. optimized the Mitsunobu conditions with 2,3,4,6-tetra-*O*-benzyl-mannopyranose (**24**) and found that the addition of trimethylamine in dichloromethane improved the Mitsunobu process, leading to **40α** and **40β** in more than 70% yield. When such optimized conditions were applied to the mannose-6-phosphate derivative **41**, the desired bisphosphate **42** was obtained in 56% yield as a 40:60 α,β-anomeric mixture before work-up, and in a 53:47 ratio after work-up due to slight anomerization. As **42** can be easily converted into the target molecule, the authors concluded, that in spite of the poor stereoselectivity, the Mitsunobu reaction constitutes a key step in a successful access to β-mannosyl phosphates such as **43**.

Reactions with phenols to achieve aryl glycosides

Not only anomeric esters, but also glycosides can be obtained through the Mitsunobu reaction. Dehydrative glycosylation approaches with reducing sugars were previously reviewed [43,44]. As phenols are weak acids, they are suitable reaction partners in the Mitsunobu reaction, leading to aryl glycosides with reducing sugars as the alcohol components. Grynkiewicz can be called the pioneer of Mitsunobu glycosylation, as having explored the Mitsunobu reaction for the synthesis of various aryl glycosides [24,45]. Thus, native sugars such as D-glucose and D-mannose (Scheme 8) were converted into the respective unprotected phenyl glycosides **44** and **45** with phenol in just one step in moderate to good yields.

Recently, the scope of this synthetic approach was expanded by the Lindhorst group employing D-mannose and hydroxyazobenzene **46** for the synthesis of the photoswitchable azobenzene α-D-mannoside **47** (Scheme 9) [46]. Notably, in this reaction, traces of an anomeric mixture of the respective furanoside **48** were detected.

The Mitsunobu synthesis of aryl glycosides was also applied to *p*-nitrophenol [47], naphthols [48,49], or multifunctional phenols [27,50]. Such arylglycosylation was also extended for the synthesis of aureolic acid antibiotics [21,51,52]. In search of convenient methods for the synthesis of aryl sialosides, Gao et al. explored the scope of the Mitsunobu reaction with the sialic acid derivative **49**, employing a range of phenols **50**–**58** in acetonitrile to achieve sialosides **59**–**67**, albeit with modest anomeric selectivity (Scheme 10) [25].

Interestingly, no correlation between the pK_a of the employed acids and the stereoselectivity of the reaction could be established in this case, since similar anomeric mixtures were obtained throughout all experiments. In this case, the absence of a neighboring group in position 3 of the sugar ring could account

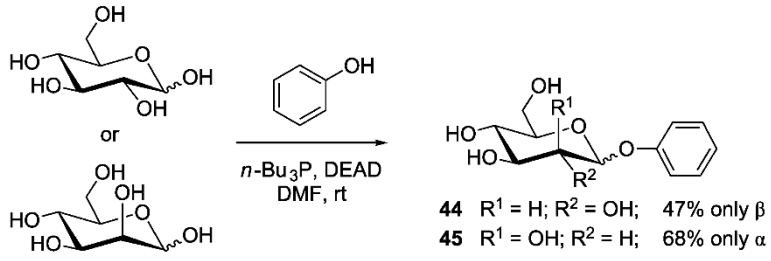

Scheme 8: Synthesis of phenyl glycosides **44** and **45** from unprotected sugars [24].

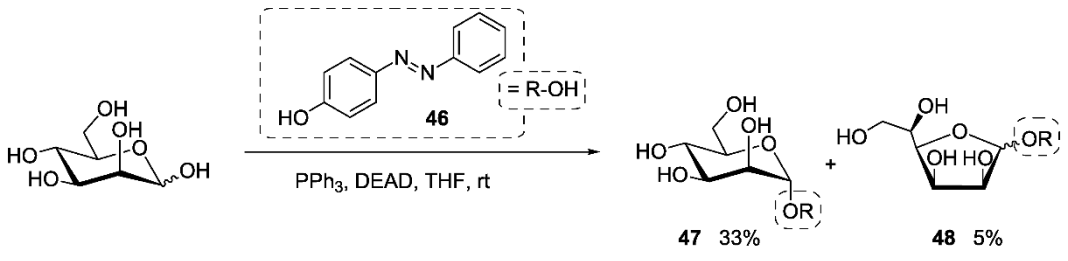

Scheme 9: Synthesis of azobenzene mannosides **47** and **48** without protecting group chemistry [46].

Beilstein J. Org. Chem. **2018,** *14,* 1619–1636.

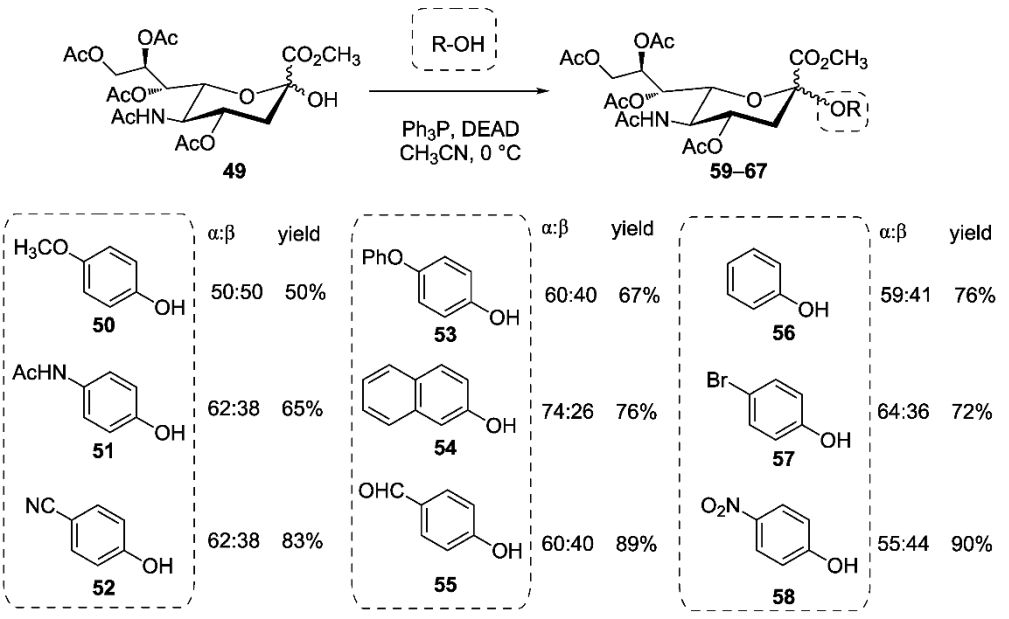

Scheme 10: Synthesis of various aryl sialosides using Mitsunobu glycosylation [25].

for low stereoselectivity. To explain the lack of stereoselectivity, the authors considered a S_N1 reaction mechanism, involving the respective oxocarbenium ion or, alternatively, the formation of both α- and β-configured glycosyloxyphosphonium ions, which are in turn displaced by the nucleophile in the expected S_N2 fashion, resulting in a respective anomeric mixture of products (cf. Scheme 2).

In contrast to this, the yields of the obtained aryl sialosides strongly correlated with the pK_a of the utilized phenols, with stronger acids leading to higher yields. This yield-to-pK_a correlation is in accordance with earlier findings in the synthesis of aryl glucuronides where the yields were equally affected by the pK_a of the chosen phenols, while the neighboring group effect was found to govern the stereochemical outcome of the reaction towards β-configured products [53]. In this case, phenolic chromium tricarbonyl complexes of weaker acids such as *p*-cresol were employed to improve the yield.

The challenge of glycoside synthesis using sugars devoid of a C-2 participating group is also highlighted by a total synthesis of various jadomycins [54]. Whereas the Mitsunobu glycosidation of **68** with the phenolic aglycon **70** yields the pure 1,2-*trans*-glycoside **71**, the 2-deoxy sugar **69** yields the glycoside **72** as a 6:1 α,β-anomeric mixture (Scheme 11). In contrast to this, the jadomycin B carbasugar analogue **75** was formed stereoselectively from the 2-deoxy-carbasugar **73** in a Mitsunobu reaction with the aglycon **74** [55].

Benzyl protection, which does not exert neighboring group effects in classical glycosylations, resulted in the predominant formation of 1,2-*trans* glycosides in the Mitsunobu reaction with catechol. In fact, benzyl-protected reducing glucose derivative **2** gave the β-glucoside **76** with good stereoselectivity, and the respective mannose derivative **24** resulted in the pure α-mannoside **77** in good yield (Scheme 12) [56].

In a general approach to coumarin-derived inhibitors of gyrase B, a group working at Hoechst Marion Roussel developed a Mitsunobu process to connect noviose with a broad range of 7-hydroxycoumarins [57]. Similarly, Imamura and colleagues used 4-methylumbelliferone (**79**) as acidic reaction partner in a Mitsunobu glycosylation with a reducing galabioside **78** (Scheme 13) [22]. Advantage was taken of the bulky DTBS protecting group to enforce α-stereoselection despite of the anchimeric effect of the vicinal *N*-Troc protecting group to achieve the α-glycoside **80** in high yield. Nevertheless, this reaction needed optimization, such as an unusually high reaction temperature.

Also weakly acidic phenols were used by Vaccaro et al. [58] for Mitsunobu glycosylation in the D-glucuronic series, employing the reagent pair *n*-Bu_3P-ADDP (1,1'-(azodicarbonyl)dipiperidine) developed by Tsunoda et al. [59]. Interestingly, Davis and co-workers could employ 2,3:4,6-di-*O*-isopropylidene mannopyranose **81** in a Mitsunobu reaction with phenol to stereoselectively achieve the respective β-mannoside **82** in good yield (Scheme 14) [60].

Beilstein J. Org. Chem. **2018,** *14,* 1619–1636.

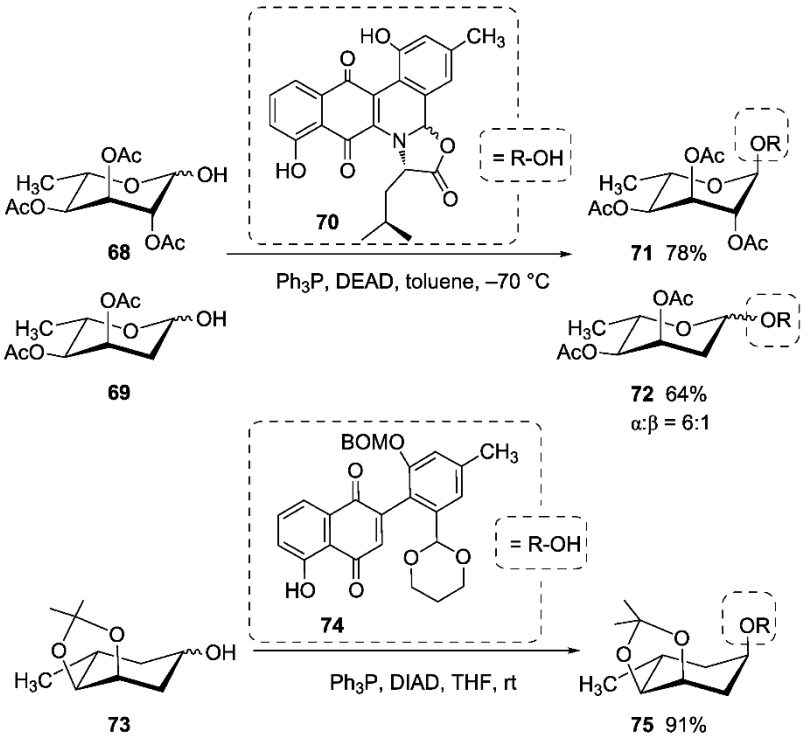

Scheme 11: Mitsunobu synthesis of different jadomycins [54,55]. BOM: benzyloxymethyl.

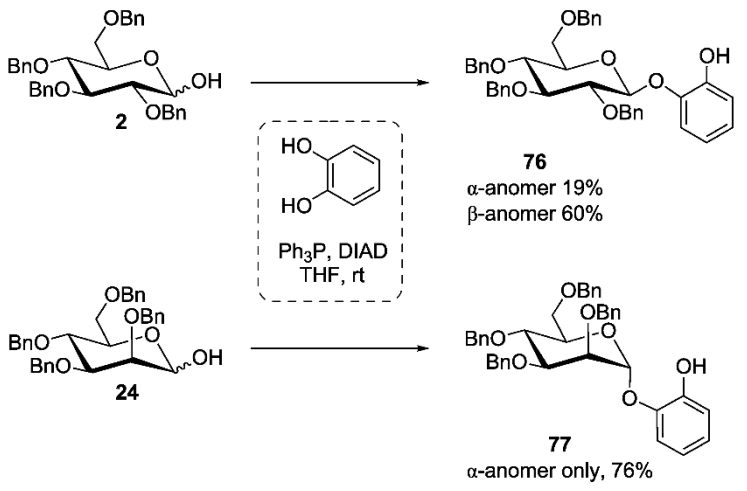

Scheme 12: Stereoselectivity in the Mitsunobu synthesis of catechol glycosides in the *gluco*- and *manno*-series [56].

This stereo-differentiating effect of isopropylidene protecting groups was also observed in other cases with D-mannopyranose [46,61]. It might be used as a key to a reliable approach to otherwise difficult to synthesize β-mannosides using the Mitsunobu procedure. This approach to 1,2-*cis*-mannosides is equally effective when cyclohexylidene protecting groups are used [28,47,62].

Mitsunobu glycosylation was also a successful method in total synthesis. In the course of a 17-step synthesis of hygromycin A, Donohoe et al. used a Mitsunobu glycosylation of **84** with the arabinose derivative **83**. This reaction could be tuned to deliver the required β-arabinofuranoside building block **85** with high stereoselectivity and under the assistance of triisopropylsilyl (TIPS) protecting groups (Scheme 15) [63].

Beilstein J. Org. Chem. **2018,** *14,* 1619–1636.

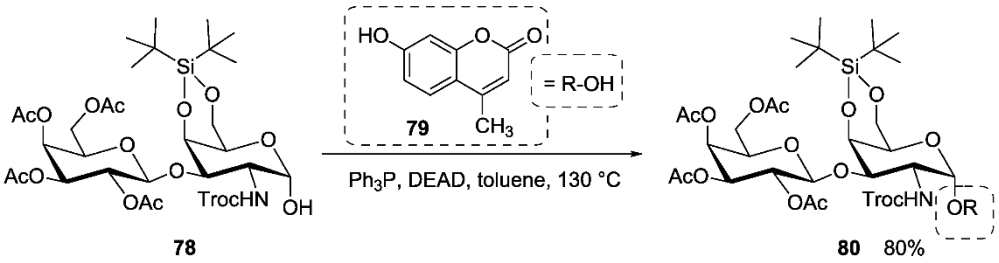

Scheme 13: Formation of a 1,2-*cis* glycoside **80** assisted by steric hindrance of the β-face of the disaccharide through the DTBS protection. DTBS: di-*tert*-butylsilylene; Troc: 2,2,2-trichloroethoxycarbonyl [22].

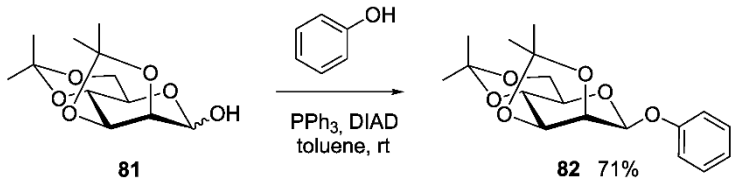

Scheme 14: Stereoselective β-D-mannoside synthesis [60].

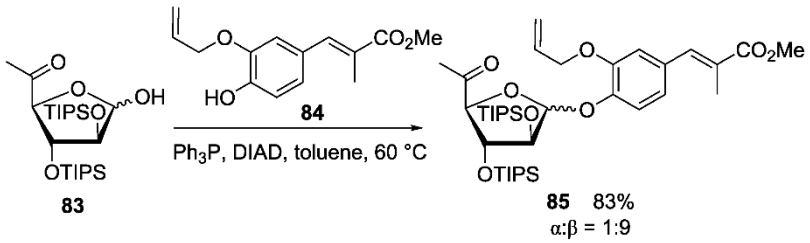

Scheme 15: TIPS-assisted synthesis of 1,2-*cis* arabinofuranosides [63]. TIPS: triisopropylsilyl.

Similar reaction conditions were applied by Nie et al. in the total synthesis of the nucleoside antibiotic A201A [64]. Notably, the *n*-Bu_3P-ADDP reagent system led here to the formation of the pure α-glycoside. Likewise, a Mitsunobu glycosylation of complex phenols was successfully implemented in the preparation of novobiocin analogues [65], and formed a key step in the synthesis of new glycosidic PDE4 (phosphodiesterase type 4) inhibitors [66]. Also calix[4]arenes could be selectively mono- or diglycosylated by means of the Mitsunobu methodology [67,68].

The Mitsunobu reaction was also employed with glycals like **86** and **87** reacting with *p*-methoxyphenol as an alternative to the Ferrier rearrangement in the synthesis of 2-*C*-methylene glycosides and other rearrangement products **88**–**92**, some of which cannot be obtained in a classical Ferrier reaction (Scheme 16) [69-72]. The results outlined in Scheme 16 are consistent with early findings of Guthrie et al. exploring the Mitsunobu benzoylation of 4,6-*O*-benzylidene-D-allal [73].

Reactions with alcohols to yield alkyl glycosides

In contrast to aryl ethers, the formation of alkyl ethers is not observed under Mitsunobu conditions. Likewise, standard alcohols are typically poor reaction partners in Mitsunobu glycosylations. Due to their high pK_a values, the formation of the transient phosphonium betaine is hampered [43]. In an effort to overcome this drawback, several decades ago, Szarek et al. tested mercuric halides to assist the betaine formation in such cases, and indeed cyclohexyl glycosides could be formed in various sugar series with decent yields [74]. Consequently, this approach was explored in a Mitsunobu-type disaccharide synthesis reacting **93** with the alcohol components **94**–**96** to give **97**–**99**, albeit with moderate success (Scheme 17) [75].

Contradictory results were reported on the Mitsunobu glycosylation of 1,3,4,6-tetra-*O*-protected fructofuranosides. In contrast to Guthrie et al. [76], Bouali and colleagues claimed an effective synthesis of alkyl fructofuranoside **101**–**103** from **100** using

Beilstein J. Org. Chem. 2018, 14, 1619–1636.

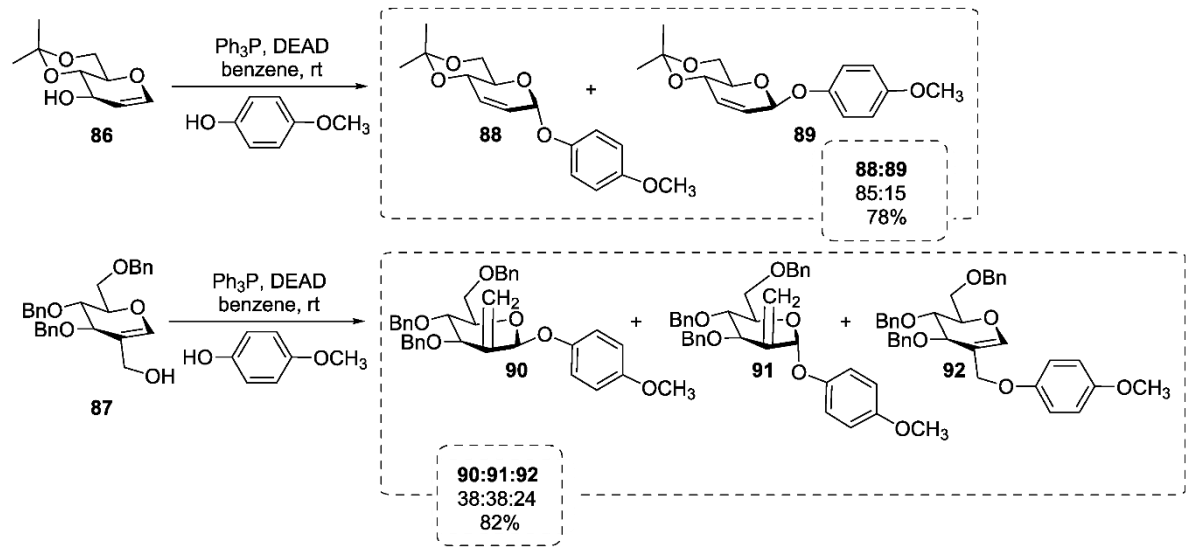

Scheme 16: The Mitsunobu reaction with glycals leads to interesting rearrangement products [69].

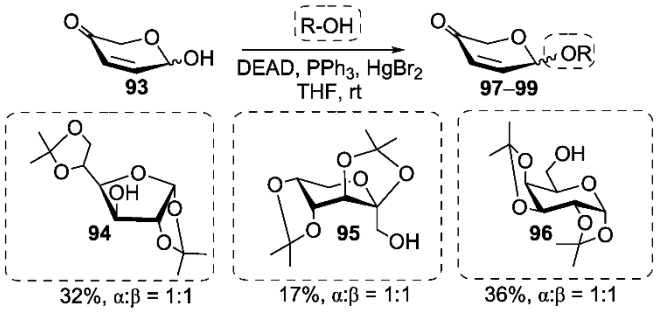

Scheme 17: Synthesis of disaccharides using mercury(II) bromide as co-activator in the Mitsunobu reaction [75].

simple alcohols (Scheme 18) [23]. The reaction was rationalized by participation of the C-3 neighboring group (structure **104**) with intermediate formation of a dioxolanium derivative **105** [23].

On the other hand, the Mitsunobu reaction was advantageous for the acetalization of the antimalarial drug dihydroartemisinin **106** to give **107** with trifluoroethanol, having a pK_a of 12.4 (Scheme 19) [77]. The efficiency of the Mitsunobu glycosylation with fluorinated alcohols with pK_a values between 9 and 12 was demonstrated with several other examples [78].

Also thiols, according to their pK_a value range between 10 and 11 should be qualified appropriate reagents for a Mitsunobu thioglycosylation. However, a competitive redox reaction with the PR_3-azodicarboxylate reagent system precludes this application [79,80]. In spite of that, thioglycosides **111**–**113** could be prepared via a Mitsunobu-type condensation of thioglycosides such as **108** and **109** with simple alcohols (Scheme 20) [81,82]. In this case, of course, the sugar thioglycoside takes the role of the nucleophile rather than of the alcohol component in the Mitsunobu reaction.

Reactions with NH acids to achieve N-glycosides

Early on, phthalimide was regarded as a good Mitsunobu reagent, owing to its NH acidity with a pK_a of 8.3, thus offering the opportunity for the synthesis of N-glycosides of the *N*-glycosylimide type [83]. However, along with the formation of *N*-glycosylphthalimides, a side-reaction takes place, producing both glycosyl carbonates and *N*-glycosyl-1,2-dialkoxycarbonylhydrazines [84]. This anomeric *N*-phthalimidation was

Beilstein J. Org. Chem. **2018,** *14,* 1619–1636.

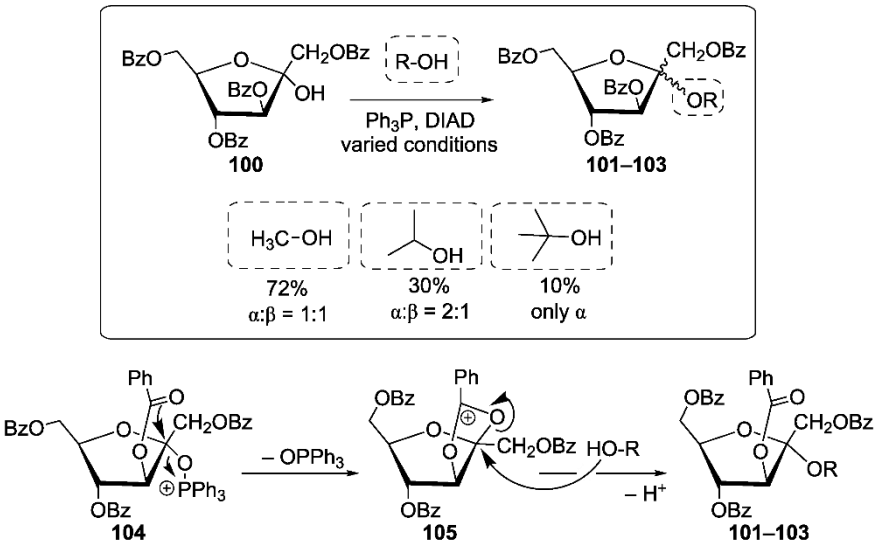

Scheme 18: Synthesis of various fructofuranosides according to Mitsunobu and proposed neighbouring group participation [23].

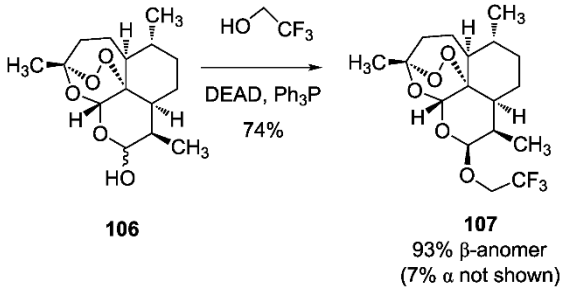

Scheme 19: The Mitsunobu reaction allows stereoselective acetalization of dihydroartemisinin [77].

later implemented by Nishimura et al. for the iminosugar **114** with phthalimide to give **115** in a high yield, en route to a new family of α-L-fucosidase inhibitors (Scheme 21) [85].

More generally, the preparation of modified glycosylamines under Mitsunobu conditions requires a sufficiently acidic NH nucleophile. A particularly illustrative procedure was disclosed by van Boom's group, who used *N*-nosyl-activated amino-acid esters for anomeric modification of sugars in order to produce substrates for a novel route to Amadori rearrangement products [86]. The same approach was recently adopted in a total synthesis of aurantoside G, involving the Mitsunobu ligation of a D-xylopyranose derivative **116** and *N*-nosylated methyl asparaginate **117** to give **118** (Scheme 22) [87].

Compared to *N*-sulfonylation, *N*-carbamoylation can also prove effective to enhance the acidity of a NH group. Hence, the trichloroethoxycarbonyl (Troc) protection/activation of the amino group of questiomycin **119** allowed Igarashi et al. to access the *N*-glucosylated derivative **120** in good yield and complete β-stereoselectivity from hemiacetal **1** (Scheme 23) [88].

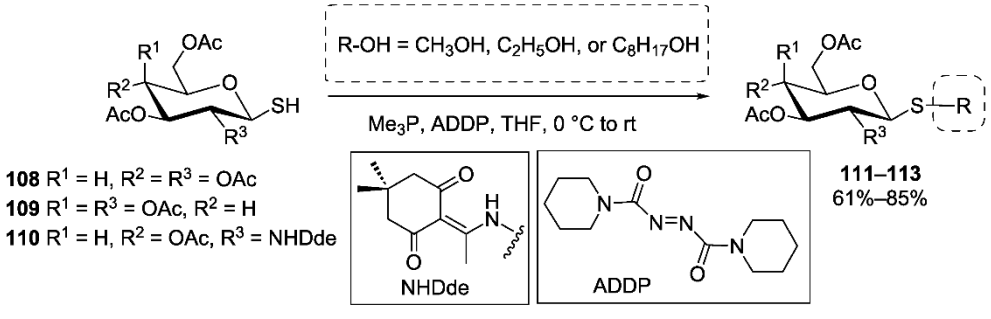

Scheme 20: Synthesis of alkyl thioglycosides by Mitsunobu reaction [81].

Beilstein J. Org. Chem. **2018,** *14,* 1619–1636.

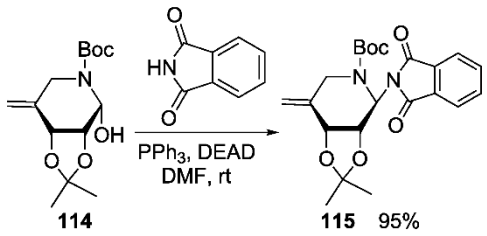

Scheme 21: Preparation of iminoglycosylphthalimide **115** from **114** [85].

Also some aza-heterocycles bearing a free NH group possess a low enough pK_a to allow Mitsunobu coupling. In the course of the synthesis of the hexasaccharidic fragment of landomycin A, the L-rhodinose derivative **121** underwent glycosylation with 1*H*-tetrazole to give **122**, which has a pK_a that compares to carboxylic acids (Scheme 24) [89].

In spite of the fact that parent indole is too weak an acid to undergo Mitsunobu conversions, a model maleimide–indole hybrid was investigated by Ohkubo and colleagues to pave the way for the synthesis of indolo[2,3-*a*]pyrrolo[3,4-*c*]carbazole compounds with anticancer activity [90,91]. N-Glycosides of indole derivatives were also approached by Zembower et al. employing 2,3,4,6-tetra-*O*-benzyl glucopyranose in a Mitsunobu reaction [92]. In the same period, Prudhomme's group followed closely related approaches for the *N*-glycosylation of indolic structures. Various rebeccamycin analogues were efficiently synthesized from indolo[2,3-*c*]carbazole frameworks using the methodology previously developed by Voldoire et al. [93]. Further applications to 7-aza-indolic analogues of rebeccamycin [94-96], granulatimide and isogranulatimide [97-100] were also reported. In addition, using the same Mitsunobu methodology, the rebeccamycin analogue **124** was synthesized in high yield and complete β-stereoselectivity by Wang et al. from the glucose derivative **2** and **123** (Scheme 25) [101].

Application of the anomeric Mitsunobu coupling in nucleoside synthesis was pioneered by Szarek et al. [102], who reacted 6-chloropurine with various reducing sugars using methyldiphenylphosphine as activator. Extension to the D-*ribo* series with 6-chloro- and 2,6-dichloropurines was later reported by Hertel and co-workers [103]. In the course of an exploration of modified L-nucleosides, 6-chloropurin-9-yl derivatives were obtained in moderate yields [104]. Aiming at an improved procedure to synthesize nucleosides with glycosylation of the nucleobase, De Napoli et al. used the Bu_3P-ADDP system to connect inosine and uridine derivatives with D-ribofurano and D-glucopyrano moieties [105]. Hocek's group in 2015 published a direct one-pot synthesis of exclusively β-configured nucleosides from unprotected or 5-*O*-monoprotected

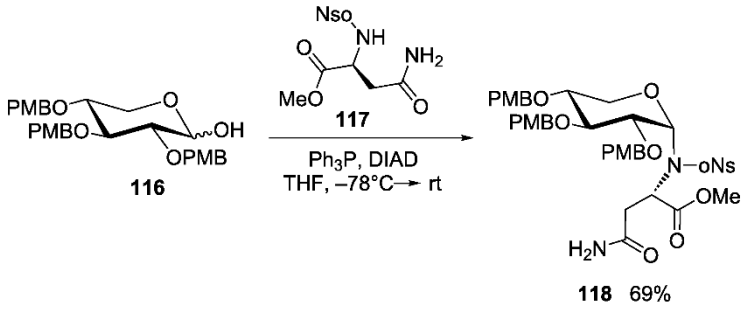

Scheme 22: Mitsunobu reaction as a key step in the total synthesis of aurantoside G [87].

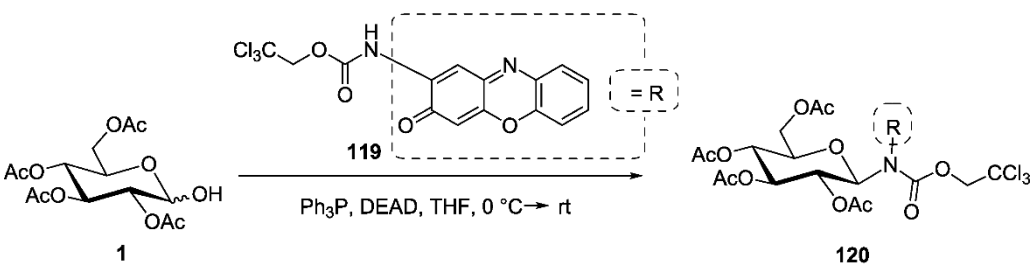

Scheme 23: Utilization of an N–H acid in the Mitsunobu reaction [88].

Beilstein J. Org. Chem. **2018,** *14,* 1619–1636.

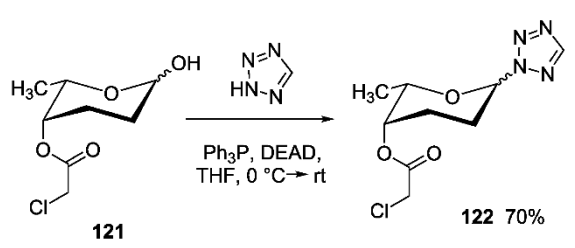

Scheme 24: Mitsunobu reaction with 1*H*-tetrazole [89].

D-ribose using optimized Mitsunobu conditions with various purine- and pyrimidine-based heterocycles. Here, DBU was applied first, followed by DIAD and P(*n*-Bu)$_3$ [106]. Two years later Seio and colleagues set out to systematically study the effect of phosphine, azodicarbonyl reagent, and solvent on the yield and α/β ratio in the synthesis of 2'-deoxynucleosides [107]. They reported that the highest yield and β-selectivity were obtained using (*n*-Bu)$_3$P and 1,1′-(azodicarbonyl)dipiperidine in DMF. In a model study directed towards the synthesis of guanofosfocin, Sugimura et al. used the Mitsunobu *N*-glycosylation to attach a glucopyranosyl donor on either 6-*N*-trityl-8-oxoadenosine or 6-*O*-benzyl-8-oxoinosine [108].

Reactions with N–OH acids to yield NO-glycosides

Because of its well-suited pK_a (6.3), *N*-hydroxyphthalimide was early considered in Mitsunobu reactions, for example by Grochowski and Jurczak to form an anomeric phthalimide–oxy bond as shown in several sugar series [109-111]. This gives access to new *O*-glycosylhydroxylamines, namely for the construction of glycosidic N–O linkages in calicheamycin oligosaccharides [112,113]. This option was applied in the synthesis of trichostatin D involving glucose derivative **2** and *N*-hydroxyhexahydrophthalimide as the glycosyl acceptor to give **125** (Scheme 26) [114].

By using diverse *N*-hydroxylated azaheterocycles in the Mitsunobu glycosylation, Grochowski explored the synthesis of new nucleoside analogues. 1-Hydroxy-benzotriazole, 1-hydroxy-2-cyanobenzimidazole, 1-hydroxyuracil, and

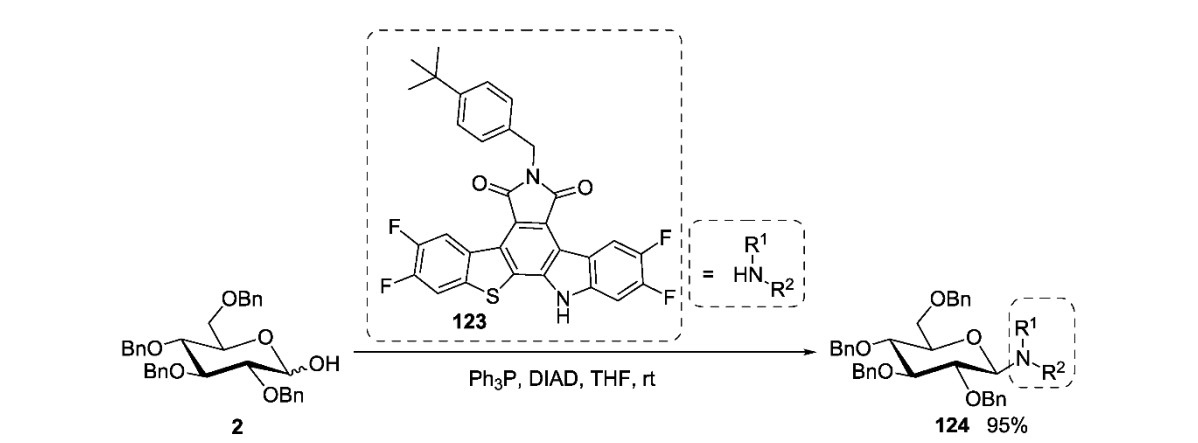

Scheme 25: Formation of a rebeccamycin analogue using the Mitsunobu reaction [101].

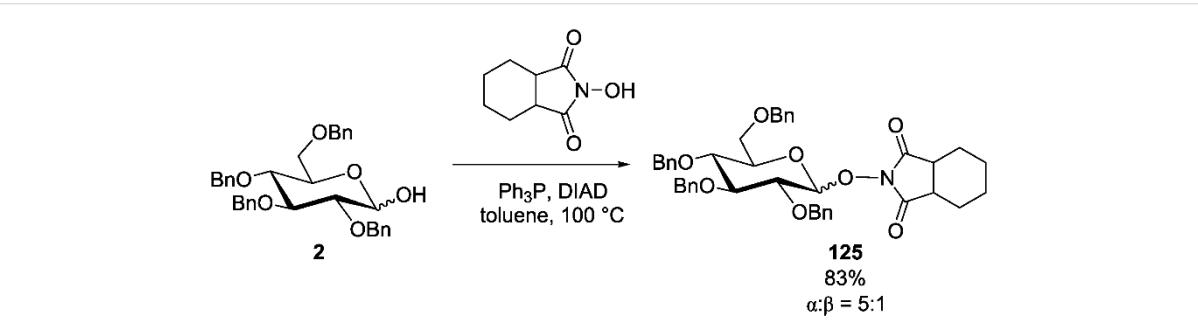

Scheme 26: Synthesis of carbohydrates with an alkoxyamine bond [114].

Beilstein J. Org. Chem. **2018,** *14,* 1619–1636.

1-hydroxythymine were used to prepare the respective NO-furanosides in the *manno*- and *ribo*-series [115-117].

Miscellaneous

The Mitsunobu reaction was also applied for other anomeric modifications, such as fluorination, reported by Kunz et al. for the synthesis of the α-D-mannofuranosyl fluoride **126**, however, in moderate yield (Scheme 27) [118]. The advantage of this approach lies in the mild fluorine source, triethyloxonium tetrafluoroborate, which, in combination with the Ph_3P-DEAD system, leaves the acid-labile protecting groups of **127** intact, other than when HF is used. Zbiral's group on the other hand, developed the synthesis of glycosyl azides such as **128** in a Mitsunobu procedure with **127**, using hydrazoic acid as the azide source (Scheme 27) [119].

This approach was extended by Besset et al. to D-fructose and a range of unprotected mono- and disaccharides, again showing a preference of the reaction for the anomeric position instead of the primary [120]. Anomeric azidation was also investigated on diverse unprotected hexopyranoses by Larabi et al. using a modified Appel-type procedure [121].

A striking oxidation reaction of alcohols to carbonyl compounds was disclosed by Mitsunobu and colleagues, involving the sterically hindered nitrophenol **130** [122]. With sugars like **129**, the Mitsunobu glycosylation is hampered, and instead an anomeric aci-nitroester **131** is formed, which is converted into the corresponding gluconolactone **133** under elimination of a quinone monoxime **132** (Scheme 28).

Conclusion

In this account, 15 years after Professor Mitsunobu has passed away, we have surveyed the literature on the Mitsunobu reaction for anomeric modifications of carbohydrates. As in classical glycosylation reactions, not all mechanistic details of the anomeric conversion of sugars in a Mitsunobu process are known and well understood. Hence until today, surprising results and unexpected side reactions are being observed in Mitsunobu type conversions of hemiacetals. In addition, the reaction conditions of a Mitsunobu process often require particular optimization efforts. Thus, the Mitsunobu reaction has not become a standard procedure in glycoside synthesis nor in anomeric esterification, but on the other hand, it was demonstrated to serve as a key step in many cases of carbohydrate modification including total synthesis of sensitive natural products. This is also due to the mild and neutral conditions under which the Mitsunobu reaction occurs. Additionally, it has a rather broad scope as many building blocks are acidic enough to react with reducing sugars representing the alcohol component of the reaction. The stereochemical outcome of a Mitsunobu glycosylation is often advantageous such as in the synthesis of β-D-mannosides, which are otherwise difficult to prepare. However, often, the stereoselectivity of the reaction is less definite than our text books claim. Unfortunately, the Mitsunobu reaction is uneasy to scale up and this is probably one of the biggest

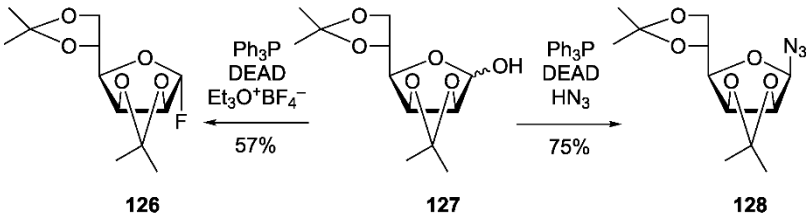

Scheme 27: Synthesis of glycosyl fluorides and glycosyl azides according to Mitsunobu [118,119].

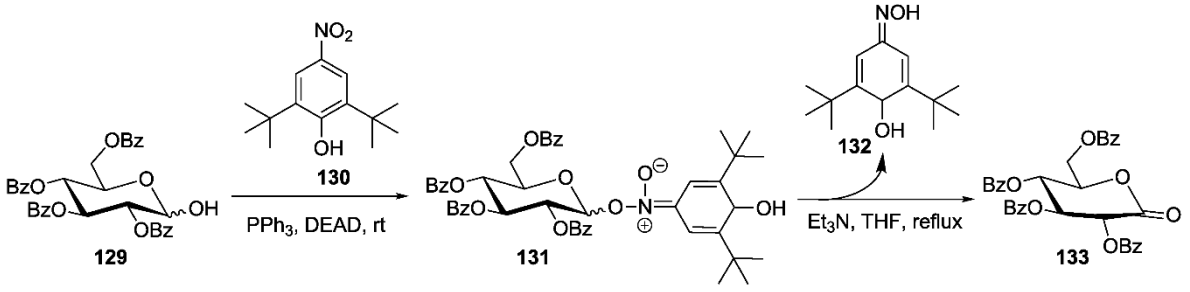

Scheme 28: Anomeric oxidation under Mitsunobu conditions [122].

Beilstein J. Org. Chem. **2018,** *14,* 1619–1636.

obstacles for a broad and also technical use of this reaction. Nevertheless, this review proves that in the glycosciences, the Mitsunobu reaction must not be overlooked as it is an important method in the synthetic toolbox for anomeric modification of sugars and glycoconjugate preparation.

ORCID® iDs

Julia Hain - https://orcid.org/0000-0001-6701-283X
Patrick Rollin - https://orcid.org/0000-0001-5951-9614
Thisbe K. Lindhorst - https://orcid.org/0000-0001-6788-4224

References

1. Mitsunobu, O.; Yamada, M.; Mukaiyama, T. *Bull. Chem. Soc. Jpn.* **1967,** *40,* 935–939. doi:10.1246/bcsj.40.935
2. Mitsunobu, O. *Synthesis* **1981,** 1–28. doi:10.1055/s-1981-29317
3. Hughes, D. L. *Org. React.* **1992,** *42,* 335–656. doi:10.1002/0471264180.or042.02
4. Hughes, D. L. *Org. Prep. Proced. Int.* **1996,** *28,* 127–164. doi:10.1080/00304949609356516
5. But, T. Y. S.; Toy, P. H. *Chem. – Asian J.* **2007,** *2,* 1340–1355. doi:10.1002/asia.200700182
6. Swamy, K. C. K.; Kumar, N. N. B.; Balaraman, E.; Kumar, K. V. P. P. *Chem. Rev.* **2009,** *109,* 2551–2651. doi:10.1021/cr800278z
7. Varasi, M.; Walker, K. A. M.; Maddox, M. L. *J. Org. Chem.* **1987,** *52,* 4235–4238. doi:10.1021/jo00228a016
8. Hughes, D. L.; Reamer, R. A.; Bergan, J. J.; Grabowski, E. J. J. *J. Am. Chem. Soc.* **1988,** *110,* 6487–6491. doi:10.1021/ja00227a032
9. Camp, D.; Jenkins, I. D. *J. Org. Chem.* **1989,** *54,* 3045–3054. doi:10.1021/jo00274a016
10. Elson, K. E.; Jenkins, I. D.; Loughlin, W. A. *Org. Biomol. Chem.* **2003,** *1,* 2958–2965. doi:10.1039/B305375J
11. Schenk, S.; Weston, J.; Anders, E. *J. Am. Chem. Soc.* **2005,** *127,* 12566–12576. doi:10.1021/ja052362i
12. Camp, D.; von Itzstein, M.; Jenkins, I. D. *Tetrahedron* **2015,** *71,* 4946–4948. doi:10.1016/j.tet.2015.05.099
13. Hughes, D. L.; Reamer, R. A. *J. Org. Chem.* **1996,** *61,* 2967–2971. doi:10.1021/jo952180e
14. Lindhorst, T. K.; Thiem, J. *Liebigs Ann. Chem.* **1990,** 1237–1242. doi:10.1002/jlac.1990199001222
15. Tsunoda, T.; Otsuka, J.; Yamamiya, Y.; Itô, S. *Chem. Lett.* **1994,** *23,* 539–542. doi:10.1246/cl.1994.539
16. Itô, S.; Tsunoda, T. *Pure Appl. Chem.* **1999,** *71,* 1053–1057. doi:10.1351/pac199971061053
17. Guinó, M.; Hii, K. K. M. *Chem. Soc. Rev.* **2007,** *36,* 608–617. doi:10.1039/B603851B
18. Ma, X.; Shi, R.; Zhang, B.; Yan, B. *J. Comb. Chem.* **2009,** *11,* 438–445. doi:10.1021/cc900004m
19. Camp, D.; Harvey, P. J.; Jenkins, I. D. *Tetrahedron* **2015,** *71,* 3932–3938. doi:10.1016/j.tet.2015.04.035
20. Dar, A. R.; Aga, M. A.; Kumar, B.; Yousuf, S. K.; Taneja, S. C. *Org. Biomol. Chem.* **2013,** *11,* 6195–6207. doi:10.1039/c3ob40853a
21. Roush, W. R.; Lin, X.-F. *J. Am. Chem. Soc.* **1995,** *117,* 2236–2250. doi:10.1021/ja00113a013
22. Imamura, A.; Ando, H.; Ishida, H.; Kiso, M. *Org. Lett.* **2005,** *7,* 4415–4418. doi:10.1021/ol051592z
23. Bouali, A.; Descotes, G.; Ewing, D. F.; Grouiller, A.; Lefkidou, J.; Lespinasse, A.-D.; Mackenzie, G. *J. Carbohydr. Chem.* **1992,** *11,* 159–169. doi:10.1080/07328309208017797
24. Grynkiewicz, G. *Pol. J. Chem.* **1979,** *53,* 1571–1579.
25. Gao, G.; Schwardt, O.; Ernst, B. *Carbohydr. Res.* **2004,** *339,* 2835–2840. doi:10.1016/j.carres.2004.10.003
26. Ahn, C.; Correia, R.; DeShong, P. *J. Org. Chem.* **2002,** *67,* 1751–1753. doi:10.1021/jo001590m
27. Lubineau, A.; Meyer, E.; Place, P. *Carbohydr. Res.* **1992,** *228,* 191–203. doi:10.1016/S0008-6215(00)90559-7
28. Åkerfeldt, K.; Garegg, P. J.; Iversen, T. *Acta Chem. Scand.* **1979,** *B33,* 467–468. doi:10.3891/acta.chem.scand.33b-0467
29. Smith, A. B., III; Hale, K. J.; Rivero, R. A. *Tetrahedron Lett.* **1986,** *27,* 5813–5816. doi:10.1016/S0040-4039(00)85334-4
30. Smith, A. B., III; Rivero, R. A. *J. Am. Chem. Soc.* **1987,** *109,* 1272–1274. doi:10.1021/ja00238a061
31. Smith, A. B., III; Hale, K. J.; Vaccaro, H. A. *Tetrahedron Lett.* **1987,** *28,* 5591–5594. doi:10.1016/S0040-4039(00)96788-1
32. Vaccaro, H. A.; Rivero, R. A.; Smith, A. B., III. *Tetrahedron Lett.* **1989,** *30,* 1465–1466. doi:10.1016/S0040-4039(00)99491-7
33. Smith, A. B., III; Rivero, R. A.; Hale, K. J.; Vaccaro, H. A. *J. Am. Chem. Soc.* **1991,** *113,* 2092–2112. doi:10.1021/ja00006a030
34. Smith, A. B., III; Hale, K. J.; Vaccaro, H. A.; Rivero, R. A. *J. Am. Chem. Soc.* **1991,** *113,* 2112–2122. doi:10.1021/ja00006a031
35. De Mesmaeker, A.; Hoffmann, P.; Ernst, B. *Tetrahedron Lett.* **1989,** *30,* 3773–3776. doi:10.1016/S0040-4039(01)80651-1
36. Juteau, H.; Gareau, Y.; Labelle, M. *Tetrahedron Lett.* **1997,** *38,* 1481–1484. doi:10.1016/S0040-4039(97)00135-4
37. Kenny, J. R.; Maggs, J. L.; Meng, X.; Sinnott, D.; Clarke, S. E.; Park, B. K.; Stachulski, A. V. *J. Med. Chem.* **2004,** *47,* 2816–2825. doi:10.1021/jm030891w
38. Bourhim, A.; Czernecki, S.; Krausz, P. *J. Carbohydr. Chem.* **1993,** *12,* 853–863. doi:10.1080/07328309308020100
39. Saito, H.; Nishimura, Y.; Kondo, S.; Takeuchi, T. *Chem. Lett.* **1988,** *17,* 1235–1238. doi:10.1246/cl.1988.1235
40. Rao Koppolu, S.; Niddana, R.; Balamurugan, R. *Org. Biomol. Chem.* **2015,** *13,* 5094–5097. doi:10.1039/C5OB00248F
41. Inuki, S.; Aiba, T.; Kawakami, S.; Akiyama, T.; Inoue, J.-i.; Fujimoto, Y. *Org. Lett.* **2017,** *19,* 3079–3082. doi:10.1021/acs.orglett.7b01158
42. Borio, A.; Hofinger, A.; Kosma, P.; Zamyatina, A. *Tetrahedron Lett.* **2017,** *58,* 2826–2829. doi:10.1016/j.tetlet.2017.06.014
43. Gin, D. *J. Carbohydr. Chem.* **2002,** *21,* 645–665. doi:10.1081/CAR-120016485
44. Yang, Y.; Zhang, X.; Yu, B. *Nat. Prod. Rep.* **2015,** *32,* 1331–1355. doi:10.1039/C5NP00033E
45. Grynkiewicz, G. *Carbohydr. Res.* **1977,** *53,* C11–C12. doi:10.1016/S0008-6215(00)85467-1
46. Hain, J.; Chandrasekaran, V.; Lindhorst, T. K. *Isr. J. Chem.* **2015,** *35,* 383–386. doi:10.1002/ijch.201400211
47. Garegg, P. J.; Iversen, T.; Norberg, T. *Carbohydr. Res.* **1979,** *73,* 313–314. doi:10.1016/S0008-6215(00)85506-8
48. Kometani, T.; Kondo, H.; Fujimori, Y. *Synthesis* **1988,** 1005–1007. doi:10.1055/s-1988-27788
49. Roush, W. R.; Lin, X. F. *J. Org. Chem.* **1991,** *56,* 5740–5742. doi:10.1021/jo00020a003
50. Chida, N.; Ohtsuka, M.; Nakazawa, K.; Ogawa, S. *J. Org. Chem.* **1991,** *56,* 2976–2983. doi:10.1021/jo00009a009
51. Roush, W. R.; Lin, X.-F. *Tetrahedron Lett.* **1993,** *34,* 6829–6832. doi:10.1016/S0040-4039(00)91806-9
52. Roush, W. R.; Hartz, R. A.; Gustin, D. J. *J. Am. Chem. Soc.* **1999,** *121,* 1990–1991. doi:10.1021/ja984229e

Beilstein J. Org. Chem. **2018,** *14,* 1619–1636.

53. Badman, G. T.; Green, D. V. S.; Voyle, M. *J. Organomet. Chem.* **1990,** *388,* 117–121. doi:10.1016/0022-328X(90)85353-Z
54. Yang, X.; Yu, B. *Chem. – Eur. J.* **2013,** *19,* 8431–8434. doi:10.1002/chem.201301297
55. Shan, M.; Sharif, E. U.; O'Doherty, G. A. *Angew. Chem.* **2010,** *122,* 9682–9685. doi:10.1002/ange.201005329
56. Luo, S.-Y.; Jang, Y.-J.; Liu, J.-Y.; Chu, C.-S.; Liao, C.-C.; Hung, S.-C. *Angew. Chem.* **2008,** *120,* 8202–8205. doi:10.1002/ange.200802693
57. Ferroud, D.; Collard, J.; Klich, M.; Dupuis-Hamelin, C.; Mauvais, P.; Lassaigne, P.; Bonnefoy, A.; Musicki, B. *Bioorg. Med. Chem. Lett.* **1999,** *9,* 2881–2886. doi:10.1016/S0960-894X(99)00493-X
58. Vaccaro, W. D.; Davis, H. R., Jr. *Bioorg. Med. Chem. Lett.* **1998,** *8,* 313–318. doi:10.1016/S0960-894X(98)00008-0
59. Tsunoda, T.; Yamamiya, Y.; Itô, S. *Tetrahedron Lett.* **1993,** *34,* 1639–1642. doi:10.1016/0040-4039(93)85029-V
60. Cocinero, E. J.; Stanca-Kaposta, E. C.; Scanlan, E. M.; Gamblin, D. P.; Davis, B. G.; Simons, J. P. *Chem. – Eur. J.* **2008,** *14,* 8947–8955. doi:10.1002/chem.200800474
61. Deng, L.; Tsybina, P.; Gregg, K. J.; Mosi, R.; Zandberg, W. F.; Boraston, A. B.; Vocadlo, D. J. *Bioorg. Med. Chem.* **2013,** *21,* 4839–4845. doi:10.1016/j.bmc.2013.05.062
62. Otani, T.; Tsubogo, T.; Furukawa, N.; Saito, T.; Uchida, K.; Iwama, K.; Kanai, Y.; Yajima, H. *Bioorg. Med. Chem. Lett.* **2008,** *18,* 3582–3584. doi:10.1016/j.bmcl.2008.05.006
63. Donohoe, T. J.; Flores, A.; Bataille, C. J. R.; Churruca, F. *Angew. Chem.* **2009,** *121,* 6629–6632. doi:10.1002/ange.200902840
64. Nie, S.; Li, W.; Yu, B. *J. Am. Chem. Soc.* **2014,** *136,* 4157–4160. doi:10.1021/ja501460j
65. Audisio, D.; Methy-Gonnot, D.; Radanyi, C.; Renoir, J.-M.; Denis, S.; Sauvage, F.; Vergnaud-Gauduchon, J.; Brion, J.-D.; Messaoudi, S.; Alami, M. *Eur. J. Med. Chem.* **2014,** *83,* 498–507. doi:10.1016/j.ejmech.2014.06.067
66. Kawasaki, M.; Fusano, A.; Nigo, T.; Nakamura, S.; Ito, M. N.; Teranishi, Y.; Matsumoto, S.; Toda, H.; Nomura, N.; Sumiyoshi, T. *Bioorg. Med. Chem. Lett.* **2014,** *24,* 2689–2692. doi:10.1016/j.bmcl.2014.04.052
67. Marra, A.; Scherrmann, M.-C.; Dondoni, A.; Casnati, A.; Minari, P.; Ungaro, R. *Angew. Chem.* **1994,** *106,* 2533–2535. doi:10.1002/ange.19941062317
68. Dondoni, A.; Marra, A.; Scherrmann, M.-C.; Casnati, A.; Sansone, F.; Ungaro, R. *Chem. – Eur. J.* **1997,** *3,* 1774–1782. doi:10.1002/chem.19970031108
69. Ramesh, N. G.; Balasubramanian, K. K. *Tetrahedron* **1995,** *51,* 255–272. doi:10.1016/0040-4020(94)00939-R
70. Sobti, A.; Sulikowski, G. A. *Tetrahedron Lett.* **1994,** *35,* 3661–3664. doi:10.1016/S0040-4039(00)73065-6
71. Booma, C.; Balasubramanian, K. K. *Tetrahedron Lett.* **1993,** *34,* 6757–6760. doi:10.1016/S0040-4039(00)61694-5
72. Michigami, K.; Hayashi, M. *Tetrahedron* **2012,** *68,* 1092–1096. doi:10.1016/j.tet.2011.11.084
73. Guthrie, R. D.; Irvine, R. W.; Davison, B. E.; Henrick, K.; Trotter, J. *J. Chem. Soc., Perkin Trans. 2* **1981,** 468–472. doi:10.1039/P29810000468
74. Szarek, W. A.; Jarrell, H. C.; Jones, J. K. N. *Carbohydr. Res.* **1977,** *57,* C13–C16. doi:10.1016/S0008-6215(00)81946-1
75. Grynkiewicz, G.; Zamojski, A. *Synth. Commun.* **1978,** *8,* 491–496. doi:10.1080/00397917808063578
76. Guthrie, R. D.; Jenkins, I. D.; Yamasaki, R. *Aust. J. Chem.* **1982,** *35,* 1003–1018. doi:10.1071/CH9821003
77. Thanh Nga, T. T.; Ménage, C.; Bégué, J.-P.; Bonnet-Delpon, D.; Gantier, J. C.; Pradines, B.; Doury, J.-C.; Dinh Thac, T. *J. Med. Chem.* **1998,** *41,* 4101–4108. doi:10.1021/jm9810147
78. Gueyrard, D.; Rollin, P.; Thanh Nga, T. T.; Ourévitch, M.; Bégué, J.-P.; Bonnet-Delpon, D. *Carbohydr. Res.* **1999,** *318,* 171–179. doi:10.1016/S0008-6215(99)00089-0
79. Kato, K.; Mitsunobu, O. *J. Org. Chem.* **1970,** *35,* 4227–4229. doi:10.1021/jo00837a617
80. Camp, D.; Jenkins, I. D. *Aust. J. Chem.* **1990,** *43,* 161–168. doi:10.1071/CH9900161
81. Falconer, R. A.; Jablonkai, I.; Toth, I. *Tetrahedron Lett.* **1999,** *40,* 8663–8666. doi:10.1016/S0040-4039(99)01834-1
82. Ohnishi, Y.; Ichikawa, M.; Ichikawa, Y. *Bioorg. Med. Chem. Lett.* **2000,** *10,* 1289–1291. doi:10.1016/S0960-894X(00)00223-7
83. Jurczak, J.; Grynkiewicz, G.; Zamojski, A. *Carbohydr. Res.* **1975,** *39,* 147–150. doi:10.1016/S0008-6215(00)82648-8
84. Grynkiewicz, G.; Jurczak, J. *Carbohydr. Res.* **1975,** *43,* 188–191. doi:10.1016/S0008-6215(00)83985-3
85. Nishimura, Y.; Shitara, E.; Takeuchi, T. *Tetrahedron Lett.* **1999,** *40,* 2351–2354. doi:10.1016/S0040-4039(99)00184-7
86. Turner, J. J.; Wilschut, N.; Overkleeft, H. S.; Klaffke, W.; van der Marel, G. A.; van Boom, J. H. *Tetrahedron Lett.* **1999,** *40,* 7039–7042. doi:10.1016/S0040-4039(99)01452-5
87. Petermichl, M.; Loscher, S.; Schobert, R. *Angew. Chem.* **2016,** *128,* 10276–10279. doi:10.1002/ange.201604912
88. Igarashi, Y.; Takagi, K.; Kajiura, T.; Furumai, T.; Oki, T. *J. Antibiot.* **1998,** *51,* 915–920. doi:10.7164/antibiotics.51.915
89. Guo, Y.; Sulikowski, G. A. *J. Am. Chem. Soc.* **1998,** *120,* 1392–1397. doi:10.1021/ja973348b
90. Ohkubo, M.; Nishimura, T.; Jona, H.; Honma, T.; Ito, S.; Morishima, H. *Tetrahedron* **1997,** *53,* 5937–5950. doi:10.1016/S0040-4020(97)00286-X
91. Ohkubo, M.; Nishimura, T.; Honma, T.; Nishimura, I.; Ito, S.; Yoshinari, T.; Arakawa, H.; Suda, H.; Morishima, H.; Nishimura, S. *Bioorg. Med. Chem. Lett.* **1999,** *9,* 3307–3312. doi:10.1016/S0960-894X(99)00595-8
92. Zembower, D. E.; Zhang, H.; Lineswala, J. P.; Kuffel, M. J.; Aytes, S. A.; Ames, M. M. *Bioorg. Med. Chem. Lett.* **1999,** *9,* 145–150. doi:10.1016/S0960-894X(98)00710-0
93. Voldoire, A.; Sancelme, M.; Prudhomme, M.; Colson, P.; Houssier, C.; Bailly, C.; Léonce, S.; Lambel, S. *Bioorg. Med. Chem.* **2001,** *9,* 357–365. doi:10.1016/S0968-0896(00)00251-0
94. Marminon, C.; Pierré, A.; Pfeiffer, B.; Pérez, V.; Léonce, S.; Renard, P.; Prudhomme, M. *Bioorg. Med. Chem.* **2003,** *11,* 679–687. doi:10.1016/S0968-0896(02)00532-1
95. Messaoudi, S.; Anizon, F.; Pfeiffer, B.; Prudhomme, M. *Tetrahedron* **2005,** *61,* 7304–7316. doi:10.1016/j.tet.2005.04.043
96. Messaoudi, S.; Anizon, F.; Peixoto, P.; David-Cordonnier, M.-H.; Golsteyn, R. M.; Léonce, S.; Pfeiffer, B.; Prudhomme, M. *Bioorg. Med. Chem.* **2006,** *14,* 7551–7562. doi:10.1016/j.bmc.2006.07.013
97. Hugon, B.; Pfeiffer, B.; Renard, P.; Prudhomme, M. *Tetrahedron Lett.* **2003,** *44,* 4607–4611. doi:10.1016/S0040-4039(03)00924-9
98. Hénon, H.; Messaoudi, S.; Hugon, B.; Anizon, F.; Pfeiffer, B.; Prudhomme, M. *Tetrahedron* **2005,** *61,* 5599–5614. doi:10.1016/j.tet.2005.03.101
99. Hénon, H.; Anizon, F.; Pfeiffer, B.; Prudhomme, M. *Tetrahedron* **2006,** *62,* 1116–1123. doi:10.1016/j.tet.2005.10.077

Beilstein J. Org. Chem. **2018,** *14,* 1619–1636.

100. Hugon, B.; Anizon, F.; Bailly, C.; Golsteyn, R. M.; Pierré, A.; Léonce, S.; Hickman, J.; Pfeiffer, B.; Prudhomme, M. *Bioorg. Med. Chem.* **2007,** *15,* 5965–5980. doi:10.1016/j.bmc.2007.05.073
101. Wang, J.; Soundarajan, N.; Liu, N.; Zimmermann, K.; Naidu, B. N. *Tetrahedron Lett.* **2005,** *46,* 907–910. doi:10.1016/j.tetlet.2004.12.068
102. Szarek, W. A.; Depew, C.; Jarrell, H. C.; Jones, J. K. N. *J. Chem. Soc., Chem. Commun.* **1975,** 648–649. doi:10.1039/c39750000648
103. Hertel, L. W.; Grossmana, C. S.; Kroina, J. S.; Mineishi, S.; Chubb, S.; Novak, B.; Plunkett, W. *Nucleosides Nucleotides* **1989,** *8,* 951–955. doi:10.1080/07328318908054252
104. Kotra, L. P.; Xiang, Y.; Newton, M. G.; Schinazi, R. F.; Cheng, Y.-C.; Chu, K. C. *J. Med. Chem.* **1997,** *40,* 3635–3644. doi:10.1021/jm970275y
105. De Napoli, L.; Di Fabio, G.; Messere, A.; Montesarchio, D.; Piccialli, G.; Varra, M. *J. Chem. Soc., Perkin Trans. 1* **1999,** 3489–3493. doi:10.1039/a906195i
106. Downey, A. M.; Richter, C.; Pohl, R.; Mahrwald, R.; Hocek, M. *Org. Lett.* **2015,** *17,* 4604–4607. doi:10.1021/acs.orglett.5b02332
107. Seio, K.; Tokugawa, M.; Kaneko, K.; Shiozawa, T.; Masaki, Y. *Synlett* **2017,** *28,* 2014–2017. doi:10.1055/s-0036-1588445
108. Sugimura, H.; Koizumi, A.; Kiyohara, W. *Nucleosides, Nucleotides Nucleic Acids* **2003,** *22,* 727–729. doi:10.1081/NCN-120022620
109. Grochowski, E.; Jurczak, J. *Carbohydr. Res.* **1976,** *50,* C15–C16. doi:10.1016/S0008-6215(00)83868-9
110. Jurczak, J. *Carbohydr. Res.* **1982,** *104,* C18–C19. doi:10.1016/S0008-6215(00)82601-4
111. Nashed, E. M.; Grochowski, E.; Czyzewska, E. *Carbohydr. Res.* **1990,** *196,* 184–190. doi:10.1016/0008-6215(90)84118-E
112. Nicolaou, K. C.; Groneberg, R. D. *J. Am. Chem. Soc.* **1990,** *112,* 4085–4086. doi:10.1021/ja00166a082
113. Yang, D.; Kim, S. H.; Kahne, D. *J. Am. Chem. Soc.* **1991,** *113,* 4715–4716. doi:10.1021/ja00012a069
114. Hosokawa, S.; Ogura, T.; Togashi, H.; Tatsuta, K. *Tetrahedron Lett.* **2005,** *46,* 333–337. doi:10.1016/j.tetlet.2004.11.004
115. Grochowski, E.; Falent-Kwastowa, E. *J. Chem. Res., Synop.* **1978,** 300–301.
116. Grochowski, E.; Falent-Kwastowa, E. *Pol. J. Chem.* **1980,** *54,* 2229–2232.
117. Grochowski, E.; Stepowska, H. *Synthesis* **1988,** 795–797. doi:10.1055/s-1988-27710
118. Kunz, H.; Sager, W. *Helv. Chim. Acta* **1985,** *68,* 283–287. doi:10.1002/hlca.19850680134
119. Schörkhuber, W.; Zbiral, E. *Liebigs Ann. Chem.* **1980,** 1455–1469. doi:10.1002/jlac.198019800915
120. Besset, C.; Chambert, S.; Fenet, B.; Queneau, Y. *Tetrahedron Lett.* **2009,** *50,* 7043–7047. doi:10.1016/j.tetlet.2009.09.173
121. Larabi, M.-L.; Fréchou, C.; Demailly, G. *Tetrahedron Lett.* **1994,** *35,* 2175–2178. doi:10.1016/S0040-4039(00)76789-X
122. Kimura, J.; Kawashima, A.; Sugizaki, M.; Nemoto, N.; Mitsunobu, O. *J. Chem. Soc., Chem. Commun.* **1979,** 303–304. doi:10.1039/c39790000303

License and Terms

8.3 K. Ruppersberg, J. Hain, Wie kann der Lactosegehalt von Milchprodukten im Schulexperiment sichtbar gemacht werden? *CHEMKON* **2016**, *23*, 90-92.

DOI: 10.1002/ckon.201610272

DAS EXPERIMENT CHEMKON

DOI: 10.1002/ckon.201610272

Wie kann der Lactosegehalt von Milchprodukten im Schulexperiment sichtbar gemacht werden?

Die Wiederentdeckung der Wöhlk-Probe für den Chemieunterricht

*Klaus Ruppersberg**[a] *und Julia Hain**[b]

Stichworte: Lactose-Nachweis · Milchprodukte · Wöhlk-Probe

1. Einleitung

Viele Menschen meiden Milchprodukte, weil sie aus verschiedenen Gründen keine Lactose (Milchzucker) vertragen [1, 2]. Mit einem historischen Experiment von Alfred Wöhlk aus dem Jahr 1904 lässt sich herausfinden, wieviel Lactose in unterschiedlichen Milchprodukten enthalten ist [3].

Lactose ist ein Disaccharid, das sich von Saccharose durch einen anderen molekularen Aufbau unterscheidet (Abb. 1). Während Saccharose leicht in verdünnter Salzsäure hydrolysiert werden kann, ist dies bei Lactose nicht möglich. Der Grund dafür liegt in der Stabilität der β-1,4-glycosidischen Bindung, die nur enzymatisch oder in großer Hitze und mit starken Säuren gespalten werden kann [4].

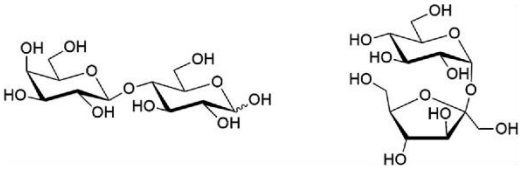

Abb. 1: Die Abbildung zeigt links die Sessel-Konformation von Lactose und rechts die von Saccharose. Die beiden Disaccharide sind aus unterschiedlichen Monomeren zusammengesetzt: Lactose ist nach IUPAC-Nomenklatur eine 4-*O*-(β-D-Galactopyranosyl)-D-glucopyranose, Saccharose ist ein α-D-Glucopyranosyl-(1-2)-β-D-fructofuranosid.

2. Experimentelles

Versuch 1: Nachweis von Lactose mit Ammoniak (Wöhlk-Probe)

Geräte und Chemikalien: Ammoniak-Lösung („Salmiakgeist"), $w(NH_3) = 10\,\%$, (Abzug) (GHS05, GHS07), Kalilauge, $c(KOH) = 1\ mol\,L^{-1}$ (GHS05, GHS07) [5], Heizplatte, 1000 mL-Becherglas, Thermometer (0 bis 100 °C), Wasser, wasserfester Stift zum Beschriften, Einmalpipetten, 12 Reagenzgläser mit passenden Stopfen, Reagenzglasständer, Smartphone oder eine Kamera für die Fotodokumentation, verschiedene, möglichst naturbelassene Milchprodukte, zum Vergleich folgende Reinstoffe (je 50 mg) Lactose, Fructose, Glucose, Galactose, Saccharose (Abb. 2).

Zeitbedarf: ca. 45 Minuten

Abb. 2: Milchprodukte, mit denen die Wöhlk-Probe durchgeführt wurde

Hinweis: Mit der (Smartphone-) Kamera werden zu Dokumentationszwecken Aufnahmen von allen wichtigen Schritten und Veränderungen erstellt.

Durchführung: In einem 1000 mL-Becherglas werden 300 mL Wasser auf 60 °C erhitzt.

Von unterschiedlichen Milchprodukten aus einem Supermarkt werden je 2 mL mit Einmalpipetten in nummerierte Reagenzgläser pipettiert. Je nach Viskosität der Milchprodukte müssen die Spitzen der Einwegpipetten etwas gekürzt werden. Damit der Nachweis nicht gestört wird, dürfen die Milchprodukte keine roten Farbstoffe oder Glucose oder Fructose enthalten. Wir verwendeten : 1) Vollmilch, 2) lactosefreie Milch, 3) Buttermilch, 4) Kefir, 5) Naturjoghurt, 6) Kaffeesahne, 7) Saure Sahne (Abb. 3)

In fünf weitere Reagenzgläser werden die oben genannten Zucker gegeben und jeweils in 2 mL Wasser gelöst. Anschließend werden jeweils 2 mL Ammoniak-Lösung sowie 3 Tropfen Kalilauge hinzu pipettiert. Vorsichtig, aber gründlich schütteln, damit sich alles gut durchmischt! Dann werden die

[a] K. Ruppersberg
IPN an der Universität zu Kiel
Abt. Chemiedidaktik
Olshausenstr. 62
24118 Kiel
* E-Mail: ruppersberg@ipn.uni-kiel.de

[b] J. Hain
Christian-Albrechts Universität zu Kiel
Otto-Diels Institut für Organische Chemie
Otto-Hahn-Platz 4
24118 Kiel
* E-Mail: jhain@oc.uni-kiel.de

Abb. 3: Reagenzgläser vor der Wöhlk-Probe
1–7: Milchprodukte (links), 8–12: Zucker-Lösungen (rechts)

Reagenzgläser in das heiße Wasserbad gestellt und für mindestens 15 Minuten dort belassen, bis sich die Farben der Proben gut entwickelt haben. Nach jeweils 5 Minuten erfolgt eine Sichtkontrolle mit Fotodokumentation.
Während der Wartezeit können begründete Hypothesen für den erwarteten Ausgang des Experiments angefertigt werden. Nach spätestens 30 Minuten werden alle Reagenzgläser aus dem Wasserbad geholt.
Beobachtung: Je nach Lactosegehalt des untersuchten Milchprodukts ergibt sich eine unterschiedlich starke rote Färbung. Lösungen von Fructose, Glucose und Galactose ergeben in Nuancen unterschiedliche Gelbfärbungen, die Saccharose-Lösung bleibt klar und farblos (Abb. 4).

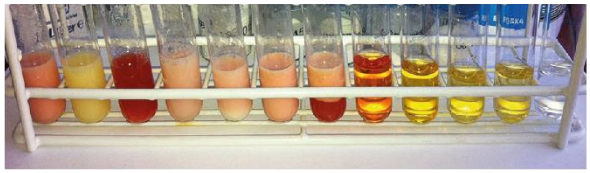

Abb. 4: Reagenzgläser nach der Wöhlk-Probe
Von links nach rechts befanden sich in den Reagenzgläsern 1) Vollmilch, 2) lactosefreie Milch, 3) Buttermilch, 4) Kefir, 5) Naturjoghurt, 6) Kaffeesahne, 7) Saure Sahne, 8) Lactose, 9) Fructose, 10) Glucose, 11) Galactose, 12) Saccharose

Auswertung: Mit reiner Lactose ergibt sich die typisch lachsrote Färbung, die schon von Alfred Wöhlk im Jahre 1904 beobachtet wurde und die er damals „krapprot" nannte [3]. Monosaccharide wie Fructose, Glucose und Galactose ergeben gelbliche Färbungen. Mit ihnen findet zwar eine Reaktion statt, aber es kommt nicht zur Entstehung des lachsroten Farbstoffs, weil keine Verknüpfung mit einem zweiten Monosaccharid vorhanden ist. Mit Saccharose ergibt sich keine Reaktion, da diese kein anomeres C-Atom enthält. Dadurch ist die Entstehung einer offenkettigen Form mit einem reduzierenden Ende ausgeschlossen. In den Milchprodukten erscheint eine dunkelrosa bis rote Färbung, wenn viel Lactose vorhanden ist (Vollmilch, Buttermilch, Kaffeesahne). Bei einem geringeren Lactosegehalt wird die Färbung schwächer. In lactosefreier Milch wurde Lactose enzymatisch in Galactose und in Glucose gespalten, daher ergibt sich eine gelbe Färbung, die auch bei einem Lösungsgemisch von Glucose und Galactose zu beobachten ist.

Schwierige Hydrolyse und widersprüchliche Angaben

Während man das Disaccharid Saccharose mit verdünnter Salzsäure problemlos hydrolysieren kann, ist dies bei Lactose nur mit besonderem Aufwand möglich, denn die β-1,4-Bindung zwischen Galactose und Glucose ist stabiler als die 1,2-Bindung zwischen Glucose und Fructose [4]. Allerdings lässt sich das Vollacetal mit dem Enzym Lactase (richtiger Name: β-Galactosidase) spalten. Dieses Enzym wird bei der Herstellung lactosefreier Milch eingesetzt und ist darüber hinaus in der Apotheke in Tablettenform erhältlich.
Es ist anzumerken, dass es einige Internet-Fundstellen gibt, bei denen eine angebliche Hydrolyse von Lactose im Reagenzglas beschrieben wird. Dieser Irrtum ist bereits in der Original-Veröffentlichung von Alfred Wöhlk [3] enthalten; dort ist in einer Tabelle „hydrolysierter Milchzucker" mit dem Ergebnis „hellgelb" aufgeführt. Dieses (falsche) Ergebnis erhielt auch der Autor, als er versuchte, Lactose ähnlich wie Saccharose mit Salzsäure zu hydrolysieren: man erhält aber kein Hydrolysat, sondern lediglich eine Lösung mit einem für die Wöhlk-Reaktion zu niedrigen pH-Wert. Neutralisiert man das vermeintliche Hydrolysat und führt dann die Wöhlk-Reaktion nach o. a. Versuchsanleitung durch, dann ergibt sich wieder die lachsrote Färbung. Wie Alfred Töpel [4] ausführlich darlegt, lässt sich Lactose nämlich gerade nicht „mit schwacher Salzsäure" hydrolysieren. Wäre dies der Fall, hätten Millionen von Menschen keine Lactoseunverträglichkeit mehr, denn dann würde die Lactose bereits im Magen hydrolysiert. Axel Schunk [6] führt in seinem Experiment des Monats November 2012, fußend auf P. Grob [7], eine falsche Erklärung an: *„Im stark basischen Milieu wird Lactose zu Glucose und Galactose hydrolysiert. Galactose wird durch Luftsauerstoff zu Schleimsäure (eine Dicarbonsäure) oxidiert und diese reagiert weiter mit Ammoniak zu einem roten Farbstoff („Pyrrolrot-Reaktion")"* [6].
Ein Kontrollexperiment mit Schleimsäure erbrachte keine Färbung. In einem weiteren Kontrollexperiment ließ sich die Wöhlk-Probe auch bei Sauerstoffabschluss (unter Stickstoffatmosphäre) erfolgreich durchführen. Nach allem, was die Autoren bisher dargelegt haben, müssen die Erklärungen aus [6] und [7] falsch sein. Wahrscheinlich liegt eine Verwechslung mit einer Anleitung zur Pyrrol-Herstellung aus dem wohl bekannten Lehrbuch von Gattermann und Wieland vor [8], wo Pyrrol aus Ammoniummucat hergestellt und anschließend mit einem salzsauren Fichtenspan nachgewiesen wird. Diese Reaktion setzt jedoch ganz andere Versuchsbedingungen voraus, nämlich Temperaturen von 170–300 °C. Weiterhin ist in [7] die Verwendung von 25 %iger Ammoniak-Lösung und 32 %iger Natronlauge aufgeführt. Solch hohe Konzentrationen sind unnötig und können dazu führen, dass die Reaktion mit einer unansehnlichen schwarz-braunen Farbe endet.
Eine weitere Unkorrektheit ist bei Ch. Fleiss in „Kohlenhydrate im Unterricht" [9] zu finden: *„Da Vollmilch eine Rotfärbung aufweist, ist der Test auf Lactose (oder Galactose) positiv. Die Farbreaktion der laktosefreien Milch zeigt eine leichte Orangefärbung. Daraus ist zu schließen, dass in dieser Galactose enthalten ist."* Wie oben bereits mehrfach dargelegt und wie sogar auch die Abbildung in [9] zeigt, ist bei lactosefreier Milch oder bei Galactose oder bei Glucose oder bei einer Mischung von beiden lediglich eine Gelbfärbung zu erkennen, die je nach Konzentration unterschiedlich intensiv ist. Galactose führt, wie auch schon von A. Wöhlk im Jahre 1904 festgestellt, zu keiner lachsroten Färbung; sogar eine Mischung von Galactose und Glucose ergibt keine „Wöhlk-Färbung". Das bedeutet, dass für die Bildung des lachsroten Farbstoffes unbedingt das Disaccharid Lactose (oder Maltose) vorhanden sein muss.

DAS EXPERIMENT

Ruppersberg, Hain

Etwas unbefriedigend und Gegenstand weiterer Untersuchungen ist die fehlende Antwort auf die berechtigte Frage, „… *worauf aber die Bildung der roten Farbe beruht… da sich nämlich der Farbstoff nicht ausschütteln lässt und durch Zusatz von Säuren zersetzt wird*“ [3]. An der Lösung dieses Problems arbeiten die Autoren derzeit. Ein möglicher Mechanismus beginnt sicherlich mit einer Öffnung der Lactose am anomeren C-Atom (Abb. 5).

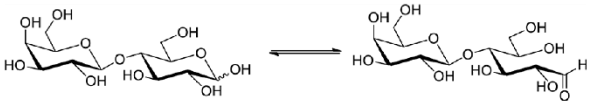

Abb. 5: Gleichgewicht zwischen ringförmiger und offenkettiger Form bei Lactose nach [10]

Anschließend ist durch den erheblichen Ammoniak-Überschuss die Bildung einer Schiffschen Base oder eines Enamins möglich [11]. Wegen des stark alkalischen pH-Werts muss aber auch an eine Lobry-de-Bruyn-van-Ekenstein-Umlagerung gedacht werden [12]. Die Autoren untersuchen derzeit verschiedene Mechanismen und hoffen auf ein baldiges Ergebnis.

Literatur

[1] Curry, A. (2013). Die Milch-Revolution. http://www.spektrum.de/news/die-milch-revolution/1203870 (letzter Aufruf 25.11.2015)
[2] Höffeler, F. (2009). Geschichte und Evolution der Lactose(in)toleranz. Biologie in unserer Zeit 39, S. 378–387.
[3] Wöhlk, A. (1904). Über eine neue Reaktion auf Milchzucker (und Maltose). Fresenius' Journal of Analytical Chemistry 43/11, 670–679.
[4] Töpel, A. (2004). Chemie und Physik der Milch. Behr's Verlag Hamburg, S. 98.
[5] https://www.experimentas.de/experiments/view/1429 (letzter Aufruf 25.11.2015).
[6] http://www.axel-schunk.de/experiment/edm1211.html (letzter Aufruf 25.11.2015).
[7] Grob, P. (2000). Einfache Schulversuche zur Lebensmittelchemie, Aulis-Verlag Köln, S. 65–66).
[8] Gattermann, L., Wieland, T. (1982). Die Praxis des organischen Chemikers. Walter de Gruyter Verlag New York, Berlin, S. 644.
[9] Fleiss, Ch.(2013). Kohlenhydrate im Unterricht. Plus Lucis 1-2/2013, S. 40–41; siehe auch: http://pluslucis.univie.ac.at/PlusLucis/131/s40.pdf (letzter Aufruf am 25.11.2015).
[10] Bukatsch, F., Glöckner, W. (1975). Experimentelle Schulchemie Band 6.1. Aulis Verlag Köln, S. 124.
[11] https://de.wikipedia.org/wiki/Imine (letzter Aufruf am 25.11.2015).
[12] https://de.wikipedia.org/wiki/Lobry-de-Bruyn-Alberda-van-Ekenstein-Umlagerung (letzter Aufruf am 25.11.2015).

Eingegangen am 21. August 2015
Angenommen am 26. November 2015
Online veröffentlicht am 21. März 2016

8.4 K. Ruppersberg, J. Hain, Die Wiederentdeckung der Wöhlk-Probe, *Chem. Unserer Zeit* **2017**, *51*, 106-111.

DOI: 10.1002/ciuz.201600744

CHEMIE IN UNSERER ZEIT
www.chiuz.de
DOI: 10.1002/ciuz.201600744

Abb. 1 *Die Wöhlk-Probe funktioniert mit Lactose und Maltose, nicht aber mit Schleimsäure (ganz links) oder mit den Monomeren Glucose (mitte-rechts) und Galactose (ganz rechts).*

Der geheimnisvolle lachsrote Farbstoff

Die Wiederentdeckung der Wöhlk-Probe

KLAUS RUPPERSBERG | JULIA HAIN

Wie kann man im Chemieunterricht den Lactosegehalt von Milchprodukten anschaulich, überzeugend und mit einfachen Mitteln sichtbar machen? Hierzu eignet sich hervorragend die fast in Vergessenheit geratene Wöhlk-Probe, die im Jahr 1904 von ihrem Entdecker Alfred Wöhlk an der Pharmazeutischen Lehranstalt Kopenhagen beschrieben wurde. Allerdings hüllt sich damals wie heute der lachsrote Farbstoff in ein scheinbar unlösbares Geheimnis, denn er lässt sich nicht mit organischen Lösungsmitteln ausschütteln und konnte bislang noch nicht sicher identifiziert werden.

Die Wöhlk-Reaktion ist eine Nachweisreaktion auf Lactose und Maltose [1]. Sie fand zunächst Anwendung in klinischen und ärztlichen Laboratorien, nämlich um eine gefährliche Schwangerschaftsdiabetes von einem vergleichsweise harmlosen Milchstau zu unterscheiden. Da die in Frage kommenden Zucker Glucose und Lactose beide auf Fehling- oder Benedict-Reagenz positiv reagieren, war man froh, die Lactose durch eine leuchtende lachsrote Färbung (damals „Krapp-Farbe“ genannt) nachweisen zu können [2].

Bis in die 1960er Jahre hinein, teilweise darüber hinaus, wurden in Arztlaboren hierzu 5 mL Urin mit Ammoniaklösung und einigen Tropfen Kalilauge im Wasserbad erhitzt. Eine Rotfärbung zeigte Lactose (aber auch Maltose) an. [3, 4, 5]. In vielen Kliniklaboratorien wurde diese Methode schon ab 1950 wieder abgeschafft, da sie durch andere reduzierende Zucker gestört wird und zuverlässigere spektroskopische Methoden zur Verfügung standen [6].

Im Schulexperiment ist die Wöhlk-Probe hingegen hervorragend einsetzbar, sehr anschaulich, kostengünstig und nicht zuletzt durch die ästhetischen Farben hochmotivierend. Es gibt verschiedene Varianten der Durchführung; die

CHEMIE IN UNSERER ZEIT
www.chiuz.de

ursprüngliche von Alfred Wöhlk selbst beschriebene funktioniert mit „0,7–0,5 g Milchzucker in einem schmalen Reagensglas (sic!) in 10 cc 10-prozentigem Ammoniak“ bzw. 20%iger Ammoniaklösung, sofern dasselbe Volumen flüssiger Milch zugegeben wird [1].

Eine Verbesserung von Zeitablauf und Genauigkeit brachte ab 1905 eine Variante von Hans Malfatti (1864–1945, Rovereto und Innsbruck): „Zu zirka 5 cm^3 (1/4 Eprouvette voll) des zu untersuchenden Harns fügt man etwa die Hälfte seines Volumens starke Ammoniakflüssigkeit und etwa fünf Tropfen Kalilauge, worauf man das Ganze in ein heißes, aber nicht siedendes Wasserbad einstellt und die oft schon nach fünf Minuten auftretende, allmählich sich verstärkende Rotfärbung beobachtet“ [7].

Es gibt auch noch Varianten mit Temperaturangaben bis von 80 °C [4] oder mit 25%iger Ammoniaklösung und 20%iger Kalilauge [2]; je höher die Temperatur ist und je konzentrierter die Laugen sind, desto größer ist die Gefahr, dass die Reaktion in eine unkontrollierte Maillard-Reaktion oder wässrige Karamellisierung läuft, was an einer unschönen Braunfärbung erkennbar wird. Im Schulunterricht sind aus Sicherheitsgründen immer möglichst niedrige Konzentrationen von Laugen zu bevorzugen, um unnötige Risiken zu vermeiden.

Wie bei vielen alten Nachweisreaktionen der medizinischen Laborchemie ist der genaue Mechanismus der Wöhlk-Malfatti-Reaktion, wie sie eigentlich heißen müsste, nicht bekannt und wie sich zeigt, auch nicht einfach zu klären; es ist aber einen Versuch wert, ein wenig Licht in das Dunkel zu bringen.

Eine sehr verwandte Nachweisreaktion ist der Fearon-Test aus dem Jahr 1942 (benannt nach William Robert Fearon, 1882–1959, Universität Dublin), der sich in Irland, Großbritannien und USA großer Beliebtheit erfreute [8]; hier wird allerdings Methylamin-hydrochlorid (anstelle von Ammoniak) verwendet und über der Brennerflamme für 30 Sekunden aufgekocht, wobei die Gefahr des Siedeverzuges besteht.

Alfred Wöhlk war nicht der einzige, der Ammoniaklösung mit Milchzucker erhitzte

Beim Recherchieren fiel auf, dass es noch weitere Namen gibt, die sich mit der Reaktion von Lactose und Ammoniaklösungen in Verbindung bringen lassen, sogar noch früher als Alfred Wöhlk. Er war zwar der erste, der die Reaktion von reinen Zuckerlösungen mit Ammoniaklösung beschrieben hat, aber schon 1896 wurde die Reaktion von Milch mit Ammoniak durch Nersess Umikoff und 1900 durch N. Sieber alias Nadina Ziber-Shumova, beide in St. Petersburg, sowie 1896 durch Marchetti in Florenz untersucht und publiziert [9, 10, 11].

Umikoff und Sieber untersuchten vor allem Muttermilch, die Ammen für das kaiserliche Findelhaus in St. Petersburg ablieferten. Bei Umikoff stand 1896 sicherlich der Aspekt der Qualitätskontrolle im Vordergrund, während Sieber vier Jahre später systematische Untersuchungen des als „violett“ bezeichneten Farbstoffes publizierte.

Muttermilch enthält außer Lactose über 130 verschiedene Oligosaccharide [12], zudem nimmt der Lactosegehalt nach dem Beginn der Milchabgabe (Laktation) zu und steigert sich bis zum 5. Laktationsmonat, von Umikoff und Sieber missverständlich als „Alter der Milch“ bezeichnet. Aus dem „Alter der Milch“ und dem damit korrelierenden Lactosegehalt, ggf. aber auch anderer Saccharide, erklärt sich die zunehmend tiefere Farbgebung bei Muttermilch, welche die Autoren aber eher als brombeerrot denn als violett bezeichnen würden.

Die Natur des lachsroten Farbstoffs bleibt geheimnisvoll

Bei der Suche nach weiteren Details für einen Reaktionsmechanismus der Wöhlk-Reaktion ließen sich in Deutschland und Österreich mehrere Publikationen [13, 14, 15, 16] finden, die den lachsroten Farbstoff einer „Pyrrolrot-Reaktion“ zusprechen. Bei der genaueren Recherche ließ sich aber kein Hinweis auf das Vorhandensein von Pyrrol finden. Eventuell sollte die Bezeichnung Pyrrolrot auf einen bekannten Farbstoff hinweisen, der ähnlich aussieht, ohne eine direkte chemische Klassifizierung vorzunehmen.

Vielleicht liegt auch eine Verwechslung mit einer Versuchsanleitung aus dem Lehrbuch von Gattermann und Wieland [17] vor, bei der Pyrrol aus Ammoniummucat hergestellt wird. Durch Abspaltung von Kohlenstoffdioxid entsteht aus der 1,6-Dicarbonsäure eine 1,4-Dicarbonsäure, aus der sich wie in Abbildung 3 dargestellt das farblose Pyrrol bildet.

Die Reaktion setzt allerdings Temperaturen zwischen 170 und 300 °C voraus, während die Wöhlk-Probe bei nur 60 °C stattfindet und keine Kohlenstoffdioxidentwicklung zu beobachten ist.

Abb. 2 *Wöhlk-Reaktionen verschiedener Milchprodukte und Referenzsubstanzen: Von links nach rechts befanden sich in den Reagenzgläsern jeweils 2 mL 1) Vollmilch, 2) lactosefreie Milch, 3) Buttermilch, 4) Kefir, 5) Naturjoghurt, 6) Kaffeesahne, 7) Saure Sahne; sowie als Referenz 2,5%ige Lösungen von 8) Lactose, 9) Fructose, 10) Glucose, 11) Galactose, 12) Saccharose.*

CHEMIE IN UNSERER ZEIT
www.chiuz.de

Schleimsäure (Mucinsäure) oder deren Salz Ammoniummucat lässt sich zwar aus Lactose herstellen, ansonsten gibt es aber keinen weiteren Zusammenhang zur Wöhlk-Probe. Schleimsäure kann auch deshalb kein Zwischenprodukt bei der Wöhlk-Reaktion sein, da sie mit Ammoniaklösung im Wasserbad nicht die geringste Farbänderung zeigte (siehe Abbildung 1).

ABB. 3 | PYRROLSYNTHESE AUS AMMONIUMMUCAT NACH [17]

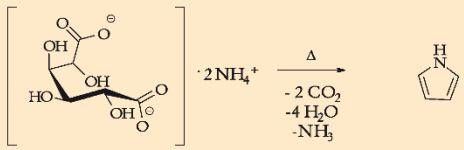

ABB. 4 | OFFENKETTIGE FORM DER LACTOSE NACH [18]

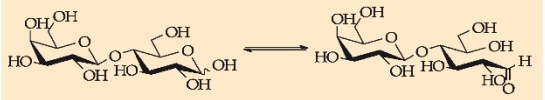

Beim Nachforschen fanden sich leider weitere Fehler: „Das Disaccharid Lactose … wird durch verdünnte Säuren zu Glucose und Galactose hydrolysiert" [18]. Lactose lässt sich – im Gegensatz zu Saccharose – aber gerade nicht durch Zugabe von schwachen Säuren hydrolysieren. Wäre dies der Fall, dürfte es beim Menschen keine Milchzuckerunverträglichkeit [19, 20] geben, weil dann die Lactose bereits durch die im Magen befindliche Salzsäure hydrolysiert würde. Sie wird aber erst im Dünndarm enzymatisch hydrolysiert, sofern dort das Enzym vorhanden ist [21]. Der Grund liegt darin, dass die β-1,4-Bindung bei Lactose viel stärker ist als die α,β-1,2-Bindung bei Saccharose. Lactose lässt sich daher entweder mit dem Enzym β-Galactosidase (oft lapidar „Lactase" genannt) oder durch einstündiges Erhitzen bei 90 °C mit 1,5 molarer Salzsäure hydrolysieren [21].

Weiterhin heißt es in Bezug auf die Wöhlk-Reaktion: „Galaktose wird durch Luftsauerstoff zu Schleimsäure (eine Dicarbonsäure) oxidiert (…)" [13]. Auch dies konnten wir widerlegen: Führt man die Wöhlk-Probe unter inerter Atmosphäre mit entgasten Komponenten durch, ist kein Unterschied in der Farbgebung zu erkennen, Sauerstoff ist somit für die Reaktion nicht essenziell.

Führt man die Reaktion jedoch im wasserfreien Milieu durch (die wässrige Ammoniaklösung wird dabei durch methanolisches Ammoniak ersetzt), ist nach anfänglicher Schwerlöslichkeit der Lactose lediglich eine Gelbfärbung

ABB. 5 | LOBRY-DE-BRUYN-VAN-EKENSTEIN-UMLAGERUNG VON LACTOSE IM ALKALISCHEN MILIEU

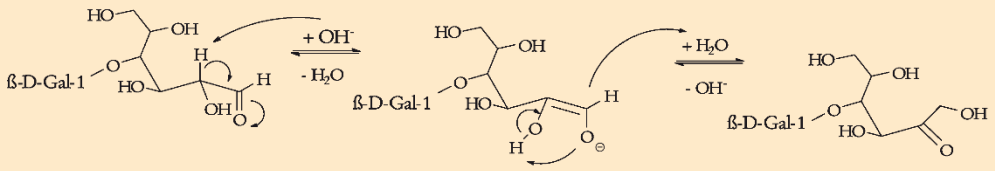

ABB. 6 | MÖGLICHE ENTSTEHUNG EINES CHROMOPHORS AUS LACTOSE

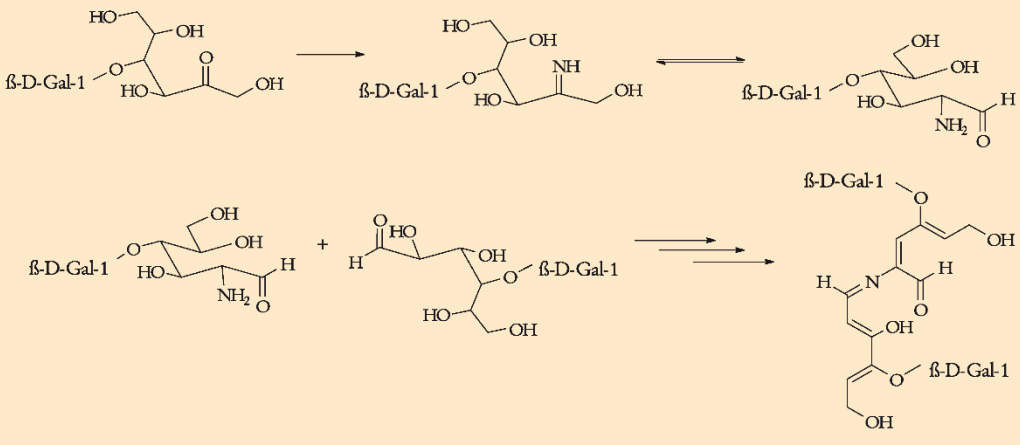

CHEMIE IN UNSERER ZEIT
www.chiuz.de

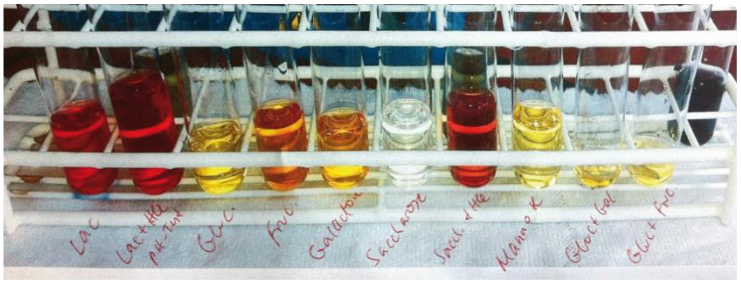

Abb. 7 ***Wöhlk-Probe mit Lösungen von verschiedenen reinen Zuckern und Zucker-Gemischen, von links nach rechts: 1. Lactose, 2. Lactose mit HCl-Zugabe, nach 20 Min. neutralisiert, 3. Glucose, 4. Fructose, 5. Galactose, 6. Saccharose, 7. Saccharose mit HCl, nach 20 Min. neutralisiert, 8. Mannose, 9. Glucose und Galactose, 10. Glucose und Fructose.***

zu beobachten. Selbst nach einer längeren Reaktionszeit bleibt die markante rote Farbe aus. Wasser ist also anscheinend wichtig für die Reaktion.

ALFRED WÖHLK (1868–1949)

Alfred Wöhlk (Schreibweise auch englisch: Woehlk oder dänisch: Wøhlk) war ein dänischer Chemiker, Apotheker und Pharmazeut. Er wurde am 25.7.1868 in Frederikshavn als achtes von 11 Kindern der Eheleute Carl Andreas Nicolai Wöhlk und Clara Wilhelmine Knutzen geboren. Nach seinem Studium und anschließender Arbeit an der Pharmazeutischen Lehranstalt Kopenhagen war er von 1910 bis zu seinem Tod am 2.3.1949 Leiter der Trianglen-Apotheke, die auch heute noch in der Nordre Frihavnsgade 3, 2100 Kopenhagen besteht.

Abb. K1 ***Alfred Wöhlk (links) und Mitarbeiter vor der Trianglen-Apotheke.***

Abb. K2 ***Magnyl = ASS+MgO.***

Abb. K3 ***Historisches Rezept-Kuvert aus der Trianglen-Apotheke.***

Bevor er ab seinem 43. Lebensjahr die Trianglen-Apotheke leitete, arbeitete Alfred Wöhlk an der Pharmazeutischen Lehranstalt Kopenhagen, wo er in deutscher Sprache publizierte und zum Beispiel ein Herstellungsverfahren für Acrylsäure aus Glycerin erfand oder ein Nachweisverfahren für Lactose und Maltose beschrieb, das vielen Pharmaziestudenten als Wöhlk-Probe bekannt ist. Im Krankenhauslabor haben spektrometrische Methoden die Wöhlk-Probe ersetzt, aber sie eignet sich hervorragend, um im Schulexperiment den Gehalt von Lactose in Milchprodukten sichtbar zu machen (siehe Abb. K4).

Abb. K4 ***Die Wöhlk-Probe als anschauliches und kostengünstiges Schulexperiment.***

Alfred Wöhlk wurde auch bekannt durch „Magnyl", einem dänischen Konkurrenzprodukt zu Aspirin®, bei dem die Acetylsalicylsäure durch Magnesiumoxid neutralisiert wurde (siehe Abb. K2). Weiterhin war er aktiv bei der Dänischen Pharmazeutischen Gesellschaft (Danmarks Farmaceutiske Selskab), wo er regelmäßig Vorträge hielt. Er wurde 80 Jahre alt und würde am 25.7.2018 seinen 150. Geburtstag feiern.

(zusammengefasst aus persönlichen Unterlagen von Poul Nissen durch Klaus Ruppersberg, IPN Kiel)

Für die Überlassung der Fotos und die biografischen Angaben bedanken wir uns ganz herzlich bei Herrn Apotheker Poul Nissen, dem gegenwärtigen Leiter der Trianglen-Apotheke in Kopenhagen!

CHEMIE IN UNSERER ZEIT
www.chiuz.de

ABB. 8 | **FARBREAKTION DIVERSER KOHLENHYDRATE MIT AMMONIAKLÖSUNG**

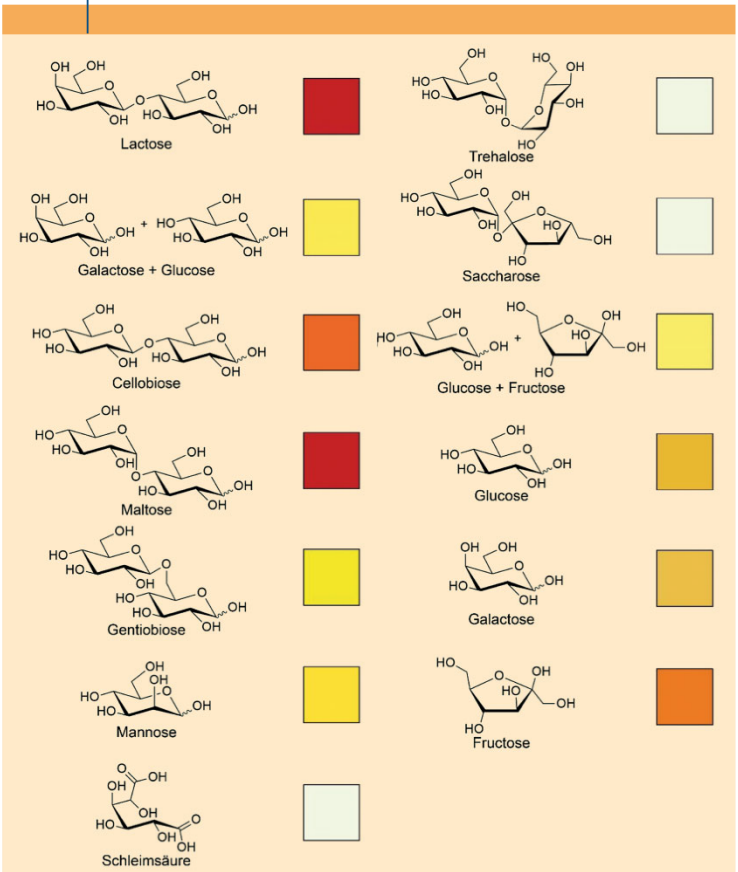

ABB. 9 | **FARBREAKTION STICKSTOFFHALTIGER VERBINDUNGEN MIT LACTOSE**

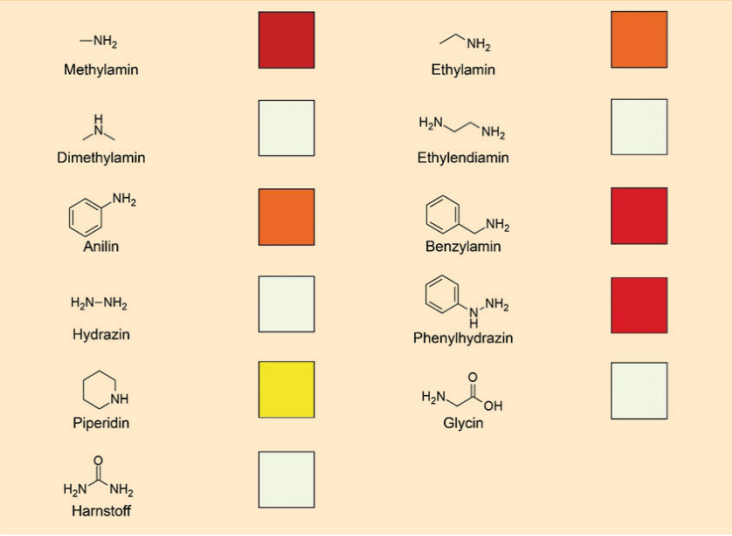

Auf welchem Wege könnte aus Lactose ein Chromophor entstehen?

Bei der Suche nach dem Mechanismus für die Wöhlk-Reaktion vermuten die Autoren, dass die Lactose (chemisch korrekt: 4-*O*-(β-D-Galactopyranosyl)-D-glucopyranose) nicht hydrolysiert, sondern als Vollacetal vorliegt, bei dem der Ring des reduzierenden Zuckers im Gleichgewichtszustand zwischen zwei anomeren Formen temporär geöffnet ist (Abbildung 4).

Durch eine Keto-Enol-Umlagerung am offenen Aldehyd-Ende des Disaccharids, auch Lobry-de-Bruyn-van-Ekenstein-Umlagerung genannt [22], entsteht eine Keto-Gruppe an C_2 (Abbildung 5).

Was nun folgt, ist hypothetisch und muss noch überprüft werden: Durch den Überschuss an NH_3 kommt es zur Bildung eines Imins an der Keto-Gruppe des umgelagerten Zuckers. Dieses kann zu einem Aldehyd und einem sekundären Amin tautomerisieren, welches mit einer Aldehydgruppe eines weiteren Lactosemoleküls zu einem Imin kondensieren könnte. Durch Wasserabspaltung entstehen konjugierte Doppelbindungen, die durch ihr konjugiertes π-System ein Chromophor bilden (Abbildung 6).

Was passiert, wenn man Lactose durch andere Zucker austauscht?

Durch weitere Untersuchungen haben wir versucht, das Problem einzukreisen: Da der lachsrote Farbstoff mit reiner Galactose oder mit reiner Glucose oder mit einer 1:1-Mischung von Galactose und Glucose *nicht* entsteht (Abbildung 7), ist die Unversehrtheit der 1,4-glykosidischen Bindung im Lactosemolekül offenkundig essentiell.

Sowohl die Wöhlk-Probe als auch der Fearon-Test ergeben mit Maltose ebenfalls den schönen lachsroten Farbstoff. Es ist also gleichgültig, ob 4-*O*-(β-D-Galactopyranosyl)-D-glucopyranose oder 4-*O*-(β-D-Glucopyranosyl)-D-glucopyranose zur Reaktion kommt.

Interessant ist nun das Verhalten der Cellobiose, die wie Maltose aus zwei Molekülen Glucose zusammengesetzt ist, aber eine andere Verknüpfung aufweist. Sie heißt korrekt 4-*O*-(β-D-Glucopyranosyl)-β-(1→4)-D-glucopyranose und zeigt in der Wöhlk-Probe eine dunkelgelbe bis orange Färbung. Eventuell konkurriert hier die Wöhlk-Reaktion mit der alkalischen Hydrolyse von Cellobiose, die bei derselben Temperatur, nämlich 60 °C durchgeführt werden kann [23].

Nicht-reduzierende Disaccharide wie Saccharose und Trehalose zeigen in der Wöhlk-Probe keine Reaktion: Die Lösungen bleiben klar und farblos, ebenso wie bei der mitgetesteten Alkoholvariante Isomalt. Gentiobiose, obwohl reduzierendes Disaccharid, führt lediglich zu einer gelben Färbung. Reduzierende Monosaccharide zeigen in Nuancen unterschiedliche Gelbfärbungen. Erhöht man die Konzentration der eingesetzten Lactoselösungen im Bereich von 0,1 bis 5 %, tritt wie erwartet eine Farbvertiefung ein. Bei Zuckerkonzentrationen über 5 % gibt es jedoch keine weitere Farbvertiefung (Abbildung 8).

CHEMIE IN UNSERER ZEIT
www.chiuz.de
WÖHLK-PROBE | DAS EXPERIMENT

Was passiert, wenn man Ammoniak durch verschiedene Amine ersetzt?

Der Austausch von Ammoniak durch andere stickstoffhaltige Verbindungen führt bei der Wöhlk-Probe zu interessanten Varianten, die ebenfalls Hinweise auf den Reaktionsmechanismus liefern können (Abbildung 9). Auf den ersten Blick ist ein offensichtlicher Zusammenhang zwischen der Art des Amins und einer positiven Wöhlk-Probe nicht zu finden, es ist aber auffällig, dass immer ein Stickstoffatom mit mindestens zwei Wasserstoffatomen und mit gegebenenfalls elektronenschiebenden Substituenten vorhanden sein müssen, so dass ein gutes Nucleophil entsteht. Eine Ausnahme von dieser Regel ist Piperidin.

Mit Benzylamin ergibt sich ein blutroter Farbstoff, der sich mit Diethylether oder Chloroform ausschütteln lässt. Mit Glycin ergab sich im Kontrollexperiment keine Färbung, Fearon hingegen beschreibt lachsrot, führt es aber auf eine Decarboxylierung der Aminosäure zurück. Weiterhin beschreibt Fearon eine lachsrote Farbe bei der Reaktion mit 2-Hydroxyethylamin [8].

Wöhlk selbst war auch schon über die Natur des Farbstoffes ratlos: „Worauf die Bildung der roten Farbe beruht, ist eine Frage, die schwierig zu beantworten ist, da sich der Farbstoff … nicht ausschütteln lässt und beim Zusatz von Säuren zersetzt wird“ [1].

Bei chromatografischen Untersuchungen an der Universität Bristol wurde ein außerordentlich komplexes Gemisch („an exceedingly complex mixture“) aus der Reaktion von Lactose und Ammoniaklösung gefunden [24]. Dies könnte einem nun fast den Mut nehmen, weiter zu forschen. Dennoch glauben die Autoren, dass die Struktur des lachsroten Farbstoffes aufgeklärt werden wird.

Dank

Für freundliche Beratung, Unterstützung und hilfreiche Diskussion bedanken wir uns ganz herzlich bei Dr. Oksana Sereda, Prof. Dr. Thisbe K. Lindhorst, beide CAU Kiel, bei Prof. Dr. Petra Mischnick, TU Braunschweig und Prof. Dr. Lothar Jaenicke, Köln.

Zusammenfassung

Die Wöhlk-Probe ist eine Nachweisreaktion für Lactose und Maltose aus dem Jahre 1904. Sie wurde zunächst klinisch für die Analyse von zuckerhaltigem Urin verwendet. Im Schulunterricht kann sie auf einfache Weise den Lactosegehalt von Milchprodukten zeigen; dies ist insofern interessant, da viele Menschen mit einer Unverträglichkeit auf Milchzucker reagieren. Der genaue Reaktionsmechanismus der Wöhlk-Reaktion (ähnlich: Umikoff-Reaktion, Wöhlk-Malfatti-Nachweis, Fearon's Test) ist trotz vieler Bemühungen noch unbekannt.

Summary

Woehlk's test is a detection reaction for lactose and maltose from 1904. It was first used clinically for the analysis of sugars in urine. In science education the test can show in a simple way the lactose content of dairy products. This is interesting because many people react intolerant to lactose. The exact reaction mechanism of Woehlk reaction (similarly: Umikoff reaction, Woehlk-Malfatti-proof, Fearon's test) is still unknown despite many efforts.

Schlagwörter

Wöhlk-Probe, Wöhlk-Malfatti-Nachweis, Umikoff-Reaktion, Fearon-Test, Lactosenachweis, Chemiegeschichte

Literatur

[1] A. Wöhlk, *Fresenius' J. Anal. Chem.*, **1904**, *43*, 670–679.
[2] W. Proske, F. Walter, Reagenzglasversuche zur Chemie der Kohlenhydrate, MNU-Tagung Bremerhaven 2013, siehe auch http://www.fachreferent-chemie.de/wp-content/uploads/Kohlenhydrate-Reagenzglasversuche2_FW141113_CvD2.pdf, zuletzt abgerufen am 12.7.2016.
[3] Siegfried GmbH, *Das Labor des Arztes*, Säckingen, **1962**, S. 30.
[4] G. Ahrens, *Die Urinanalyse*, Johann Ambrosius Barth Verlag, Leipzig, **1966**, S.35f.
[5] W. Teichmann, *Untersuchungen von Harn und Konkrementen*, VEB Verlag Volk und Gesundheit, Berlin, **1980**, S.41.
[6] *D-Glucose und verwandte Verbindungen in Medizin und Biologie*, (Hrsg.: H. Bartelheimer, W. Heyde und W. Thorn), Ferdinand Enke Verlag, Stuttgart, **1966**, S.690–691.
[7] H. Malfatti, *Centralblatt für die Krankheiten der Harn- und Sexualorgane*, Thieme, Leipzig, **1905**, 68–71, siehe auch: https://archive.org/details/centralblattfrd03unkngoog, zuletzt abgerufen am 12.7.2016.
[8] W.R. Fearon, *Analyst*, **1942**, *67*, 130–132.
[9] N. Umikoff, *Jahrb. Kinderheilk.*, **1896**, 356–359.
[10] N. Sieber, *Hoppe-Seyler's Zeitschrift fuer physiologische Chemie*, **1900**, *30*, 101–106.
[11] Marchetti, *Richard Maly's Jahresbericht über die Fortschritte der Thier-Chemie*, **1897**, 266, zit. [10].
[12] P. McVeagh und J. Brand Miller, *J. Paediatr. Child Health*, **1997**, *33*, 281–286.
[13] www.axel-schunk.de/experiment/edm1211.html, zuletzt abgerufen am 12.7.2016.
[14] www.boeck.chemie.uni-rostock.de/fileadmin/MathNat_Chemie_Boeck/Vorlesungsfolien/Praktikum/Folien/2014_P_7_folie.pdf, S.10, zuletzt abgerufen am 13.7.2015.
[15] http://pluslucis.univie.ac.at/PlusLucis/131/s40.pdf, zuletzt abgerufen am 12.7.2016.
[16] P. Grob, *Einfache Schulversuche zur Lebensmittelchemie*, Aulis Verlag Deubner und Co KG, Köln, **2000**, S.65–66.
[17] L. Gattermann und T. Wieland, *Die Praxis des organischen Chemikers*, Berlin, **1982**, S. 644.
[18] F. Bukatsch und W. Glöckner, *Experimentelle Schulchemie Band 6.1*, Aulis Deubner Köln, **1975**, S.124.
[19] http://www.spektrum.de/news/die-milch-revolution/1203870, zuletzt abgerufen am 12.7.2016.
[20] F. Höffeler, Biol. Unserer Zeit, **2009**, *39*, 378–387.
[21] A. Töpel, *Chemie und Physik der Milch*, Behr's Verlag Hamburg, **2004**, S.98.
[22] https://de.wikipedia.org/wiki/Lobry-de-Bruyn-Alberda-van-Ekenstein-Umlagerung, zuletzt abgerufen am 12.7.2016.
[23] https://de.wikipedia.org/wiki/Cellobiose, zuletzt abgerufen am 12.7.2016.
[24] L. Hough, J. Jones und E. Richards, *J. Chem. Soc.*, **1953**, 2005–2009.

Die Autoren

Klaus Ruppersberg, Jahrgang 1959, hat sein Studium der Chemie und Biologie an der Albertus Magnus-Universität Köln 1986 mit dem 1. Staatsexamen abgeschlossen. Nach dem 2. Staatsexamen in Bensheim an der Bergstraße war er über 20 Jahre Lehrer an verschiedenen Schulformen, zuletzt als Fachbereichsleiter Chemie an der Domschule in Schleswig. Seit August 2014 ist er an das Leibniz-Institut für die Pädagogik der Naturwissenschaften und Mathematik (Abt. Chemiedidaktik – Prof. Dr. Ilka Parchmann) in Kiel abgeordnet.

Julia Hain, Jahrgang 1990, hat ihr Studium der Chemie 2014 mit dem Master of Science abgeschlossen und arbeitet als wissenschaftliche Mitarbeiterin unter Leitung von Prof. Dr. Thisbe K. Lindhorst am Otto-Diels-Institut für Organische Chemie an der Christian-Albrechts-Universität zu Kiel.

Korrespondenzadresse:
Leibniz-Institut für die Pädagogik der Naturwissenschaften und Mathematik, Abt. Chemiedidaktik, Olshausenstr. 62, 24118 Kiel
E-Mail: ruppersberg@ipn.uni-kiel.de

8.5 K. Ruppersberg, J. Hain, P. Mischnick, Auf der Spur der roten Farbe: Ein historischer Lactose-Nachweis wiederentdeckt, *CHEMKON* **2017**, *24*, 302-324.

DOI: 10.1002/ckon.201790012

ARTIKEL Forschung trifft Schule CHEMKON

DOI: 10.1002/ckon.201790012

Auf der Spur der roten Farbe: Ein historischer Lactose-Nachweis wiederentdeckt

Klaus Ruppersberg,[a] Julia Hain[b] und Petra Mischnick[c]*

Zusammenfassung: Chemiegeschichte(n), Medizin und Grundlagenforschung – diese drei Zugänge für ganz unterschiedliche Interessen- und Motivationslagen bei Schülerinnen und Schülern lassen sich über einen gemeinsamen Kontext zusammenführen, in dessen Mittelpunkt ein roter Farbstoff steht. Schwangerschaftsdiabetes und Lactoseunverträglichkeit erfordern geeignete Nachweise, deren Entdeckung, Nutzung und Aufklärung der zugrundeliegenden Mechanismen spannende Fragen für den Chemieunterricht im Themenfeld Kohlenhydrate bereithalten, verbunden mit einem Blick zurück in europäische Forschungsgeschichte(n) und mit einem Blick nach vorn auf heute noch offene Forschungsfragen.

Stichworte: Lactose- und Maltosenachweis · Chemieunterricht · Kohlenhydrat-Ammoniak-Reaktion · Wöhlk-Malfatti-Probe

Abstract: Chemistry history, medicine and basic research - these three approaches can be combined using a common context focused on a red dye when dealing with students' different interests and motivation levels. Diabetes during pregnancy and lactose intolerance require appropriate methods, the discovery, application and elucidation of which provide exciting questions for chemistry lessons in the field of carbohydrates, when keeping in mind European research history and today's open research questions.

Keywords: Lactose and maltose detection · Chemistry Education · Carbohydrate ammonia reaction · Woehlk-Malfatti-Test

1. Eine europäische Detektivgeschichte: Warum ist die Wöhlk-Malfatti-Probe interessant für den Unterricht?

Einen kontextbasierten, alltagsrelevanten Zugang zur Chemie der Kohlenhydrate zu finden ist heute leicht möglich: Vor dem Hintergrund einer zunehmenden Sensibilität gegenüber Nahrungsmittelunverträglichkeiten, bspw. der Lactoseunverträglichkeit, lässt sich eine ganze Reihe von motivierenden Fragen aufwerfen:

- Wie unterscheiden sich verschiedene Zucker, in welchen Lebensmitteln kommen welche Kohlenhydrate vor?
- Wie weist man heute Diabetes oder Lactosurie nach, wie wurde dies früher gemacht?
- Weshalb tritt Lactoseunverträglichkeit in verschiedenen Gebieten gehäuft (nicht) auf?

Im Rahmen des hier zugrundeliegenden Projekts war es eigentlich das Ziel, einen einfachen und für Schülerinnen und Schüler selbst durchführbaren Lactosenachweis für einen Schulversuch aufzubereiten – herausgekommen sind neben diesem Experiment eine interessante Reise durch die europäische Chemiegeschichte, grundlegende Fragestellungen zur Aufklärung des tatsächlichen Mechanismus der Farbreaktion und ein Projekt in einem Schülerlabor. Wie so oft in der Forschung sind Resultate und Entwicklungen nicht immer geplant, führen aber oftmals zu interessanten und unerwarteten Kooperationsmöglichkeiten und Folgefragen, die mit Hilfe der Arbeitsblätter im Anhang dieses Artikels auch von Schülerinnen und Schülern weiterverfolgt werden können.

Ausgangspunkt war die so genannte „Wöhlk-Malfatti-Probe", die einst für Krankenhaus- und Arztlabore von großer Bedeutung war [1]. Es handelt sich dabei um einen optisch ansprechenden, von Schülerinnen und Schülern gut durchführbaren nasschemischen Nachweis für den Zucker Lactose (aber auch andere 1,4-verknüpfte Disaccharide, wie Maltose und Cellobiose), der mehr als 100 Jahre nach seiner Einführung auch für die Forschung noch offene Fragen bereithält [2–4]. In einer Zusammenarbeit zwischen Chemiedidaktik, Organischer Chemie, Lebensmittelchemie und einem Schülerlabor wurde dieses historische Experiment genauer unter die Lupe genommen und mit Hilfe von FachdidaktikerInnen, FachwissenschaftlerInnen und am Ende sogar SchülerInnen für den Chemieunterricht bearbeitet.

2. Dem Mechanismus der Wöhlk-Probe auf der Spur – was steckt dahinter?

Ein Nachweis für Milchzucker, die Lactose, ließ sich in der Literatur finden: die so genannte Wöhlk-Probe [5]. Dieser funktionierte gut und schien auch für Schülerversuche geeignet – bis der Versuch unternommen wurde, das Ergebnis mit einer einfachen mechanistischen Deutung zu verbinden!

Eine zunächst vorgenommene vertiefte Literaturrecherche ergab, dass sich auch andere Forscher am Wöhlk-Mechanismus die Zähne ausgebissen haben, da der Farbstoff instabil ist

[a] K. Ruppersberg
Leibniz-Institut für die Pädagogik der Naturwissenschaften und Mathematik an der Christian-Albrechts-Universität zu Kiel (Abt. Chemiedidaktik), Olshausenstr. 62, 24118 Kiel
* E-Mail: ruppersberg@ipn.uni-kiel.de

[b] J. Hain
Otto-Diels-Institut für Organische Chemie an der Christian-Albrechts-Universität zu Kiel, Arbeitsgruppe Lindhorst, Otto-Hahn-Platz 4, 24118 Kiel
* E-Mail: jhain@oc.uni-kiel.de

[c] Prof. Dr. P. Mischnick
Technische Universität Braunschweig, Institut für Lebensmittelchemie, Schleinitzstr. 20, 38106 Braunschweig
* E-Mail: p.mischnick@tu-braunschweig.de

und sich bisher nicht isolieren ließ [6]. Dennoch führte gerade diese Recherche zu interessanten Quellen und Informationen über die Nutzung der Reaktion, auch ohne die Struktur des Farbstoffs und den Mechanismus seiner Bildung genauer zu kennen. Eine anschauliche und alltagsrelevante Aufbereitung des historischen Experiments aus der Pharmazeutischen Lehranstalt Kopenhagen, das in ähnlicher Form auch in St. Petersburg (Umikoff 1896 [7], Sieber 1900 [8]) und später in Dublin (Fearon, 1942 [9]) durchgeführt worden war, kann problemlos auch mit Schulexperimenten realisiert werden [2]. Ergänzend genutzt werden können Quellen aus Amsterdam, denn auch dort war die rote Farbe schon aufgefallen, aber nicht weiterverfolgt worden (van Leent 1894, publiziert in Basel, [10]).

Angestoßen durch diese mehrfache Entdeckung bei gleichzeitig fehlender klarer Deutung des Mechanismus wurden die Autorinnen und Autoren selbst noch einmal forschend tätig, und zwar in einem Team aus einem Lehrer und Chemikerinnen aus den Bereichen der Organik und Lebensmittelchemie. Über einen Zeitraum von mehreren Wochen wurden viele gemeinsame Experimente durchgeführt, die eine Annäherung an den Mechanismus bringen sollten und überraschende Fehler in Publikationen zu diesem Thema aufzeigten. Durch die Diskussionen wurde die Komplexität des Themas mehr und mehr offensichtlich und es stellte sich die Frage, ob es überhaupt „einen Wöhlk-Farbstoff“ gibt oder ob es sich nicht letztlich um ein Gemisch handelt. Die nachfolgenden Ausführungen bieten einen kurzen Einblick in diesen Ausflug in die Grundlagenforschung.

Von der Überprüfung historischer Befunde …

Bei der Suche nach einem Mechanismus für die Wöhlk-Malfatti-Reaktion gab es zunächst einige Unstimmigkeiten zu klären. So sollte der prachtvolle rote Farbstoff „Pyrrolrot“ heißen und durch Oxidation von Galactose zu Schleimsäure (auch: Galactarsäure, Mucinsäure) gebildet werden [11–13]. Welche Anhaltspunkte können zur Aufklärung des tatsächlichen Reaktionsmechanismus herangezogen, welche ausgeschlossen werden?

Beim Nachforschen fand sich eine grundlegende Fehlannahme: „Durch das Kochen im Wasserbad mit NaOH und NH_3 erfolgt eine hydrolytische Spaltung von Lactose in D-Glucose und D-Galactose.“ [13]. Unter alkalischen Bedingungen ist aber keine Hydrolyse zu erwarten, sondern hier finden Umlagerungen statt, wie sie schon 1885 von Cornelis Adriaan Lobry van Troostenburg de Bruyn und Willem Alberda van Ekenstein beschrieben wurden [14]. Hydrolysieren lässt sich Lactose entweder mit dem Enzym β-Galactosidase („Lactase“) oder z. B. durch einstündiges Erhitzen auf 90 °C mit 1,5 M Salzsäure, also unter viel heftigeren Bedingungen als bei der Hydrolyse von Saccharose [15]. Anstelle einer hydrolytischen Spaltung in die Endprodukte Glucose und Galactose kann es aber im Reaktionsverlauf zu Umlagerungen und Eliminierungen kommen, wie wir noch sehen werden.

An anderer Stelle heißt es in Bezug auf die Wöhlk-Reaktion: „Galaktose wird durch Luftsauerstoff zu Schleimsäure (eine Dicarbonsäure) oxidiert (…)“ [12]. Auch dies konnten die Autoren widerlegen: Führt man die Wöhlk-Probe unter inerter Atmosphäre mit entgasten Komponenten durch, ist kein Unterschied in der Farbentwicklung zu erkennen, Sauerstoff ist somit für die Reaktion nicht essenziell.

Wird die Reaktion jedoch im wasserfreien Milieu durchgeführt (die wässrige Ammoniaklösung wird dabei durch methanolisches Ammoniak ersetzt, 60 °C, Rückflusskühlung), ist nach anfänglicher Schwerlöslichkeit der Lactose lediglich eine Gelbfärbung zu beobachten (siehe Abb. 1). Selbst nach einer Stunde Reaktionszeit bleibt die markante rote Farbe aus. Das Vorhandensein von Wasser ist also offensichtlich wichtig für die Reaktion [16].

Die Pyrrolbildung aus Schleimsäure, wie sie im bekannten Lehrbuch von Gattermann beschrieben wird, setzt Temperaturen zwischen 170 °C und 300 °C voraus und findet unter Kohlenstoffdioxidabspaltung statt, während die Wöhlk-Probe bei nur 60 °C–80 °C stattfindet und keine Kohlenstoffdioxidentwicklung zu beobachten ist [17].

Schleimsäure (Mucinsäure) und deren Salz Ammoniummucat lassen sich zwar aus Lactose herstellen, ansonsten gibt es aber keinen weiteren Zusammenhang zur Wöhlk-Probe.

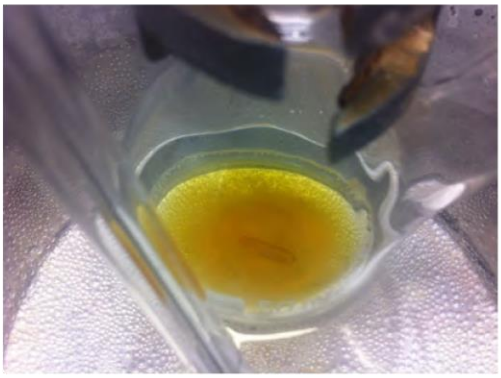

Abb. 1: Reaktionsprodukt von Lactose und wasserfreiem Ammoniak, 60 °C, Rückflusskühlung.

Wie lässt sich die Reaktion genauer aufklären? Dazu wurden weitere systematische Reihenuntersuchungen mit verschiedenen Kohlenhydraten durchgeführt.

… zu systematischen Analysen der Wirksamkeit …

Die bisher getesteten Zucker (s. Abb. 2), die im Wöhlk-Test die charakteristische rote Farbe ergaben, haben eines gemeinsam: Es sind reduzierende Disaccharide, die über die OH-Gruppe in Position 4 verknüpft sind.

Die Stereochemie der Glycosidbindung (α, wie in Maltose oder β, wie in Lactose und Cellobiose) scheint hingegen keine Rolle zu spielen. Die Stereochemie am nicht reduzierenden Ende (Galactose in Lactose versus Glucose in Maltose und Cellobiose) wirkt sich nicht erkennbar auf die Farbstoffbildung aus. Es stellt sich folglich die Frage, ob die Blockierung der OH-Gruppe am C-4 den Reaktionsverlauf so „kanalisiert“, dass letztlich ein lachsroter Farbstoff entsteht, der von Wöhlk als „Krapprot“ bezeichnet wurde. Daher wurden weitere verfügbare Zucker getestet, darunter Lactulose (Gal-β-1,4-Fru), Maltulose (Glc-α-1,4-Fru), Gentiobiose (Glc-β-1,6-Glc) und Maltotriose (Glc-α-1,4-Glc-α-1,4-Glc) (s. Abb. 2). Auch ein geschütztes Monosaccharid, die 4,6-*O*-Benzyliden-D-glucopyranose, stand zur Verfügung. Das positive Ergebnis für Lactulose und Maltulose bestätigte noch einmal, dass die im Alkalischen zu erwartende Isomerisierung der Glucoseeinheit zur Fructose ohnehin im Rahmen der Reaktion abläuft, zumindest aber, zumal reversibel, die Reaktion nicht erkennbar verändert. Auch Maltotriose reagierte positiv, was anzeigt, dass es egal ist, ob die Kette um eine weitere Glucoseeinheit verlängert wird. Die 1,6-verknüpfte Gentiobiose zeigt hingegen keine rote Farbe, obwohl sie auch ein reduzierendes Disaccharid ist.

Das 4,6-überbrückte und so an zwei Positionen geschützte Glucosederivat ergab eine orange Färbung. Eine fotometrische Überprüfung ergab keine Absorption, die auf den typischen roten Farbstoff schließen ließe. Da die Benzylidenbrücke den Zucker in seiner Flexibilität einschränkt und nicht nur die 4-Position, sondern auch die 6-Position schützt, kann dieser Befund die Frage, ob 4-OH lediglich blockiert sein

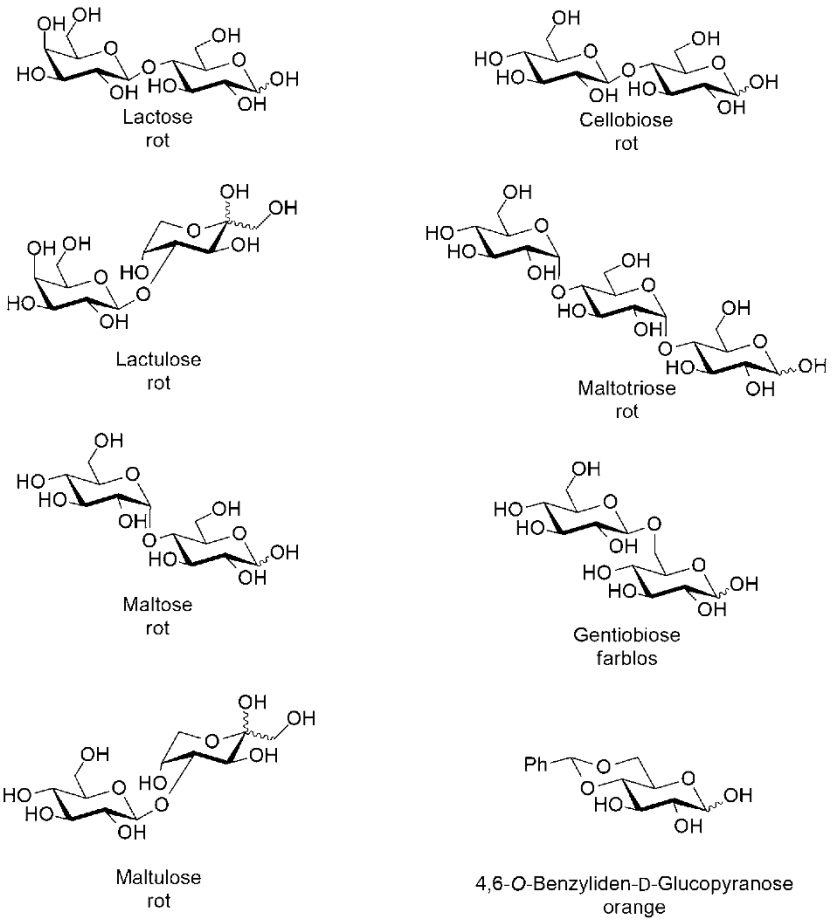

Abb. 2: Übersicht über die Formeln der hier erwähnten Moleküle sowie deren farbliches Ergebnis im Wöhlk-Test.

muss, egal ob mit einem weiteren Zucker oder einer Schutzgruppe, leider nicht abschließend beantworten.

Wenngleich der visuelle Eindruck bei den rot gefärbten Proben unabhängig vom Substrat gleich war, sollte ein Vergleich der UV/Vis-Spektren zeigen, ob sie auch dasselbe Absorptionsverhalten zeigen. Alle rot gefärbten Lösungen zeigten sehr intensive Absorptionen bei 306 und 362 nm sowie das für den roten Farbeindruck verantwortliche Maximum bei 527 nm (siehe Abb. 3a).

Die Absorptionsbande bei 527 nm ist so symmetrisch und für alle drei Zucker identisch (Abb. 3b), dass man eine einheitliche Komponente vermuten kann. Auch die positiv reagierenden Zucker Cellobiose, Maltulose und Maltotriose zeigen dieses Absorptionsspektrum.

… und mechanistischen Überlegungen

Wie kommt man nun von den Beobachtungen zu mechanistischen Überlegungen? Auf Basis der bis dahin gesammelten Beobachtungen konnten die im Folgenden ausgeführten Erkenntnisse festgehalten werden und diese dienten im Anschluss als Ausgangspunkt für weitere Überlegungen zum Mechanismus der Wöhlk-Probe. Die Autoren gehen davon aus, dass die Lactose (chemisch korrekt: 4-*O*-β-D-Galactopyranosyl-D-glucopyranose) unter den Versuchsbedingungen nicht hydrolysiert wird. Damit in Einklang steht, dass eine Mischung von Glucose und Galactose im Experiment lediglich eine Gelbfärbung zeigt (siehe Abb. A2.7). Weiterhin kann die Galactose auch durch Glucose ersetzt sein. Dies wird dadurch bewiesen, dass die „prachtvolle rote Farbe" auch bei Cellobiose und Maltose entsteht. Die positiven Reaktionen von Maltose und Maltotriose zeigen, dass auch die Stereochemie der 1,4-Glycosidbindung keine Rolle spielt.

In wässriger Lösung öffnet und schließt sich das Halbacetal am reduzierenden Ende, sodass im Gleichgewichtszustand neben den anomeren Pyranosen und ggf. auch Furanoseformen auch eine offenkettige Form mit reaktionsfreudiger Aldehydgruppe vorliegt (Mutarotation, Abb. 4).

Im alkalischen Milieu kann es nun zu einer Vielzahl von Reaktionen und Reaktionsprodukten kommen:

a) Durch eine Keto-Enol-Umlagerung des Aldehyds, auch Lobry-de-Bruyn-van-Ekenstein-Umlagerung genannt [14], entsteht eine Keto-Gruppe an C-2 (Abb. 5). Die Rückreaktion zur Aldose kann sowohl zur *gluco*- als auch zur *manno*-Konfiguration führen.

b) Bei der Wöhlk-Reaktion wird aus Aldehyd (bzw. ggf. aus der Keto-Form, s. a.), was hier nicht weiter betrachtet werden soll) und Ammoniak ein Aminal gebildet, das nach Wasserabspaltung in die Schiff'sche Base (Imin) übergeht. Durch Amadori-Umlagerung – analog der Maillard-Reaktion zwischen Zucker und Aminosäuren [18,19] – entsteht daraus die 1-Amino-1-desoxy-ketose, im Fall von Ammoniak ein primäres Amin, das dann weitere Folgereaktionen eingehen kann. Bei Einsatz von Methylamin (in Form von Methylammoniumchlorid) gemäß Fearon's Test [9], ebenso bei Sieber [8], bildet sich analog ein sekundäres Amin (Abb. 6).

Aber nicht nur Methylamin liefert eine Reaktion, die der Wöhlk-Probe ähnlich ist: Zur Bildung des roten Farbstoffs tragen ganz allgemein primäre Amine bei, die einen elektronenliefernden Rest besitzen (Methylgruppe, Ethylgruppe, Benzylgruppe, …). Darüber berichteten auch schon Sieber und Fearon [siehe 1, im Original: 8,9].

c) Auch Cellobiose, Maltulose, Maltose und Maltotriose liefern das lachsrote „Wöhlk-Produkt". Diese Beobachtung legt

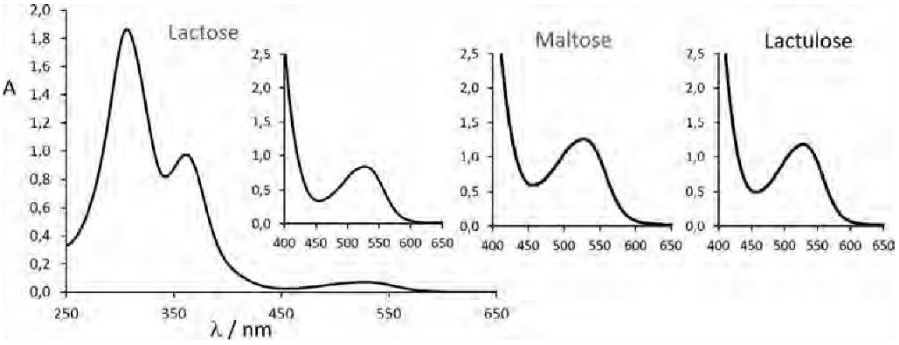

Abb. 3a: UV/Vis-Spektren der „Wöhlk-Produkte" von Lactose (volles Spektrum mit vergrößertem Ausschnitt im für die rote Farbe verantwortlichen Bereich), Maltose und Lactulose (nur Ausschnitt).

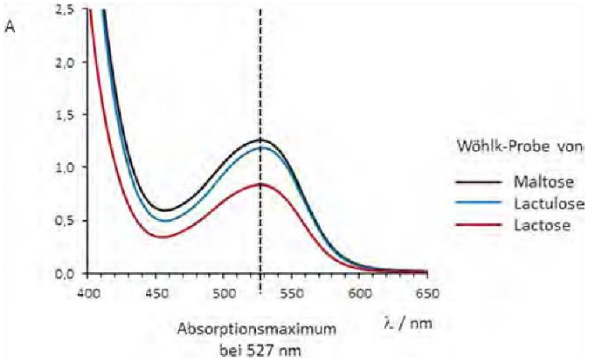

Abb. 3b: Überlagerte Ausschnitte der UV/Vis-Spektren der „Wöhlk-Produkte" von Lactose, Maltose und Lactulose, Vergrößerung der Absorption des roten Farbstoffs bei 527 nm.

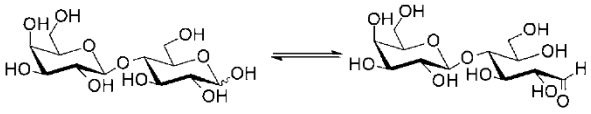

Abb. 4: α,β-Lactose (links) im Gleichgewicht mit der offenkettigen Form der Lactose (rechts).

nahe, dass der Schutz an C-4 der reduzierenden Glucoseeinheit durch einen offensichtlich austauschbaren Zucker die Reaktion in eine bestimmte Bahn lenkt. Hier setzte eine gezielte Literaturrecherche an, deren Ergebnis diese Vermutung stützt. Hollnagel und Kroh berichteten 2002 über die Umsetzung von Glucose, Maltose und Maltotriose in Abwesenheit und in Gegenwart der einfachsten Aminosäure Glycin [20]. Nur bei Maltose und Maltotriose, nicht aber bei Glucose und verstärkt in Gegenwart der Aminokomponente wird die Bildung von 3-Deoxypentosulose (3-DP) beobachtet. Der Zucker an O-4 fungiert dabei als Abgangsgruppe, die die Reaktion in Richtung des 1-Amino-1,4-dideoxyhexosons (1,4-DDH) lenkt (s. Abb. 7). Durch Angriff von OH^- kann die tautomere Iminform unter C-C-Spaltung 3-DP liefern. Bereits 2000 beschrieben Hollnagel und Kroh die ausgeprägte Bildung des Vorläufers 1,4-DDH als Eliminierungsprodukt von Maltose [21]. Henle et al. beschreiben in verschiedenen Arbeiten ebenfalls besondere Reaktionswege von 1,4-Disacchariden mit Aminosäuren [22–24]. Dabei weisen sie auch eine 3,4-Dideoxypentosulose (3,4-DDP) nach, deren Entstehung man sich, alternativ zur Oxidation zur 3-DP, durch β-Eliminierung von Wasser aus der Vorstufe der 3-Desoxypentulose in Abb. 8 vorstellen kann. Solche α-Dicarbonylverbindungen können mit oder auch ohne Einbau von Stickstoff zu Heteroaromaten wie z. B. Furanen, Pyrrolen oder Oxopyridinderivaten führen, die als Vorstufen höhermolekularer farbiger Verbindungen denkbar sind. Für weitere Forschungen wäre es daher interessant, diese bekannten Intermediate herzustellen und für die Wöhlk-Reaktion einzusetzen. Es sollte erwähnt werden, dass die genannten Modellstudien bei neutralem pH durchgeführt wurden. Bei dem für die Wöhlk-Reaktion notwendigen alkalischen pH mag der Reaktionsweg anders verlaufen. Aber diese Literaturbeispiele unterstützen sehr stark die Hypothese, dass eine Abgangsgruppe an Position 4 die entscheidende Weichenstellung für die gleiche Reaktion der 1,4-verknüpften Disaccharide darstellt.

3. Von wissenschaftlichen Untersuchungen zu Schülerforschungsprojekten

Exemplarische Darstellung der Bearbeitung des Themas in einer ForscherInnen-AG

Ein Ausgangspunkt für die weitere Erarbeitung des Nachweises bietet der Befund, dass es bei Menschen unterschiedlich ausgeprägte Lactoseunverträglichkeiten gibt: Bis zu 240 mL Milch, entsprechend etwa 12 g Lactose, werden von Men-

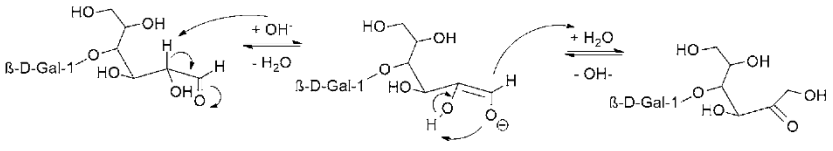

Abb. 5: Lobry-de-Bruyn-van-Ekenstein-Umlagerung von Lactose zu Lactulose im alkalischen Milieu.

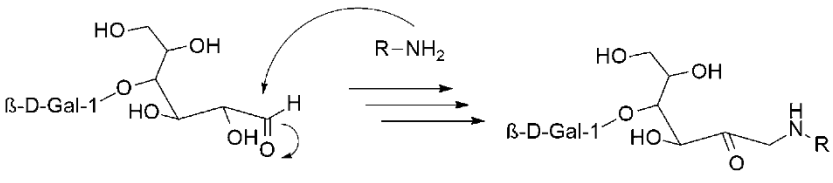

Abb. 6: Reaktion von Lactose mit Ammoniak (R = H) bzw. Methylamin ($R = CH_3$).

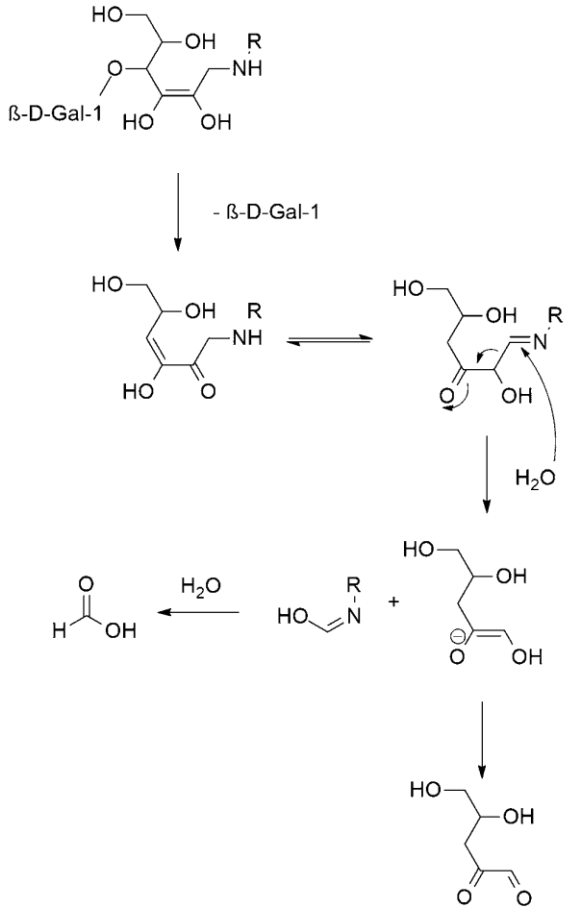

Abb. 7: Bildung von 1-Amino-1,4-didesoxyhexoson (1,4-DDH) und Weiterreaktion zu 3-Deoxypentosulose (3-DP) nach Hollnagel und Kroh 2002 [20]).

schen, die über Lactoseintoleranz klagen, verteilt über den Tag oftmals vertragen, ohne dass Beschwerden auftreten [25]. Für eine quantitative Bestimmung sollte daher die Konzentrationsabhängigkeit der Farbstoffbildung fotometrisch untersucht werden. Dieses Projekt wurde von einem Schüler der ForscherInnen-AG am Agnes-Pockels-SchülerInnen-Labor an der TU Braunschweig durchgeführt. Die Schülerinnen und Schüler dieser AG kommen seit der 4. Grundschulklasse wöchentlich an diesen außerschulischen Lernort, wo sie nach Anfänger- und Fortgeschrittenen-AG schließlich in die gemischte ForscherInnen-AG münden und dort ihren eigenen kleinen Projekten nachgehen können. Die AGs wurden vor 10 Jahren mit Unterstützung des FCI (Fonds der Chemischen Industrie) ins Leben gerufen und haben sich als ein Projekt mit langem Atem bewährt, in dem die Kinder und dann Jugendlichen im Labor heimisch werden, experimentelles Geschick erwerben und die wissenschaftliche Arbeitsweise lernen sollen. Nachdem das Interesse von Paul Gardlos (14), Schüler der 8. Klasse, geweckt war, widmete er sich Woche für Woche der Aufnahme einer Kalibrationskurve mit definierten Lactoselösungen, die dann unter den von Ruppersberg und Hain angegebenen Bedingungen [2] umgesetzt wurden. Es ergab sich ein linearer Absorptionsbereich im Bereich von 0,1–1,0%igen Lösungen mit Absorptionen im Bereich 0–1. Abb. 9 zeigt Paul beim Messen an dem kleinen Fotometer des Agnes-Pockels-SchülerInnen-Labors, Abb. 10 die von ihm erstellte Kalibrationsgerade.

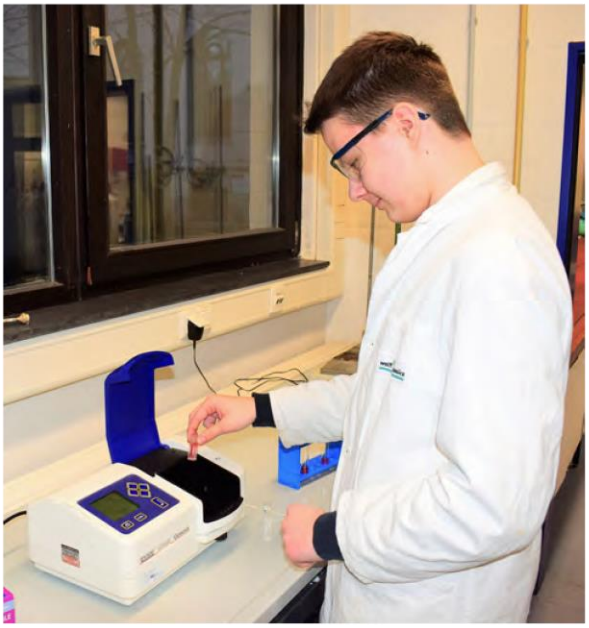

Abb. 9: Schüler im Agnes-Pockels-SchülerInnen-Labor bei der Messung am Fotometer zur Erstellung der Kalibrationsgeraden.

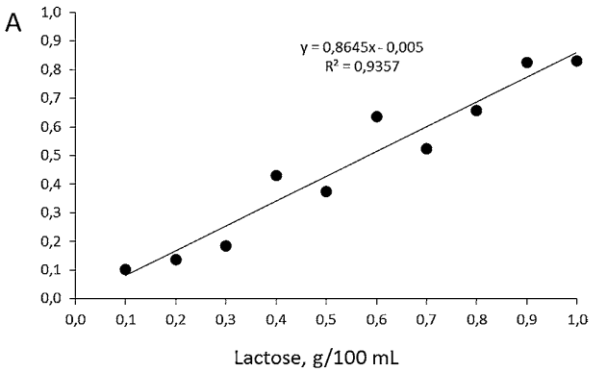

Abb. 10: Kalibrationsgerade für den aus Lactose gebildeten roten Farbstoff der Wöhlk-Probe; 2 mL Lösung. der angegebenen Lactosekonzentration wurden mit 2 mL 10%igem Ammoniak und 3 Tropfen 1-molarer KOH-Lösung umgesetzt und 15 Min. im Wasserbad bei 70 °C erwärmt. Die Absorption wurde dann bei Wellenlängen zwischen 523 oder 527 nm gemessen. Die einzelnen Punkte sind die Ergebnisse von Messungen an verschiedenen AG-Tagen im Agnes-Pockels-SchülerInnen-Labor.

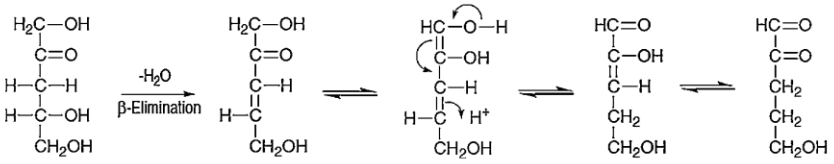

Abb. 8: β-Elimination und Reaktionsweg zur 3,4-Dideoxypentosulose (nach Mavrik/Henle [22]).

Dass man bei einer solchen empirischen Methode, wie sie für die Lebensmittelchemie bis zur Entwicklung moderner instrumenteller Analytik typisch war, die Bedingungen strikt einhalten muss, konnte auch der Schüler feststellen, wenn er bei verschiedenen AG-Terminen einzelne Lactose-Lösungen umsetzte, deren Ergebnisse nicht immer ganz zusammenpassten (Abb. 9). So spielen der pH-Wert und die Temperatur eine wichtige Rolle für die Geschwindigkeit der Farbstoffbildung, die nach einer exakt einzuhaltenden Reaktionszeit gemessen werden muss. Immer exakt 70 °C in einem einfachen Wasserbad ohne Thermostat zu halten, ist nicht so einfach.

Eine ähnliche Kalibrationsgerade, allerdings nach Umsetzung mit Methylamin anstelle von Ammoniak, hatten 1949 Malpress und Morrison veröffentlicht [16]. Angeregt durch diese Arbeit untersucht der Schüler jetzt die Abhängigkeit der Farbstoffbildung von verschiedenen Parametern.

Die bisherigen Ergebnisse geben Anregungen für weitere kleine Projekte, die von Schülerinnen und Schülern in einer AG wie am Agnes-Pockels-SchülerInnen-Labor oder in Facharbeiten bearbeitet werden können. Eine quantitative Untersuchung der Maltooligosaccharide könnte aufzeigen, ob derselbe molare Umsatz wie bei Maltose erfolgt oder ob die Ausbeute an Farbstoff höher ausfällt, weil z. B. im Zuge der Farbstoffbildung Maltose freigesetzt wird und ebenfalls nach Wöhlk reagieren kann.

Natürlich kann die Methode auch zur Bestimmung des Lactosegehalts in Produkten angewandt werden.

Hinsichtlich der Struktur des roten Farbstoffs und der Bedeutung der verknüpften 4-Position sind ebenfalls weitere Untersuchungen möglich, die den Forschergeist von Schülerinnen und Schülern inspirieren könnten. Auf jeden Fall bietet sich hier ein ästhetisch ansprechendes, von Schülerinnen und Schülern mit einfachen Mitteln durchführbares Experiment, das zu weiteren Expeditionen in die Forschung einlädt (siehe hierzu auch Arbeitsblätter 1–6 im Anhang dieses Artikels).

4. Zusammenfassung und Mehrwert für die Schule

Stand der Überlegungen:

Obwohl das eigentliche Ziel, das Reaktionsprodukt und den Reaktionsmechanismus der Wöhlk-Reaktion zu finden, noch nicht erreicht werden konnte, ergab sich eine ganze Reihe von Ergebnissen, welche den kontextorientierten Experimentalunterricht erheblich bereichern: Durch die Auswahl von verschiedenen Milchprodukten, die wegen der Gefahr einer Verfälschung des Ergebnisses oder Störung der Reaktion möglichst keine Farbstoffe oder Zuckerzusätze beinhalten sollen, kann nun anschaulich deren unterschiedlicher Lactosegehalt gezeigt werden. Darüber hinaus wird Chemiegeschichte mit umfangreichem Arbeitsmaterial, teilweise als Faksimile-Abdruck, als spannende Detektivarbeit herausgehoben. Weiterhin wird wissenschaftliches Arbeiten durch die Kooperationsbeispiele für Schülerinnen und Schüler transparent und nachvollziehbar gemacht.

Mehrwert für die Schule:

Der Tatsache, dass Interessen von Schülerinnen und Schülern sehr unterschiedlich ausgeprägt und aktiviert werden können, kann in diesem Thema in vielfacher Weise Rechnung getragen werden. Für geschichtlich und an Personen Interessierte bieten die historischen Entwicklungen, die das häufig auftretende Phänomen paralleler wissenschaftlicher Erkenntnisse in Abhängigkeit von den jeweiligen gesellschaftlichen Bedarfen zeigen, einen Zugang – in diesem Fall etwa die Diagnose der Schwangerschaftsdiabetes und der Lactosurie, die theoretischen und methodischen Zugänge sowie die Rollen verschiedener Wissenschaftler und (seltener) Wissenschaftlerinnen (Arbeitsblatt 2). An chemischen Grundlagen Interessierte können mechanistische und analytische Fragen weiter untersuchen, wie nachfolgend am Beispiel einer ForscherInnen-AG skizziert wird (Arbeitsblätter 1, 3, 4, 5). Die Ausgangsfrage der Lactoseunverträglichkeit führt schließlich auch in den Kontext von Medizin, Gesundheit und Gesellschaft und bietet damit interessante fächerverbindende Zugänge – nicht nur zur Biologie, sondern auch in die Geschichte und Geografie über die Rolle von Milchviehwirtschaft und dem Vorkommen der Verträglichkeit für Milchzucker (Arbeitsblatt 6).

Als besonderes Highlight ergeben sich aus den bisherigen Schlussfolgerungen weitere Forschungsfragen, die von Schülerinnen und Schülern selbsttätig oder mit Hilfe gefunden werden können und z. B. im Rahmen einer extracurricularen Förderung bei der Arbeit in einem Schülerlabor erforscht werden können. Das heißt mit anderen Worten: Genetisches Lernen wird durch forschendes Lernen ersetzt.

Es bleiben folgende Aufgaben offen, zu dessen Klärung die Autoren gerne ermuntern wollen:

a) Es sollte der Hypothese nachgegangen werden, dass auch Glucose mit einer anderen Abgangsgruppe als einem zweiten Monosaccharid an Position 4 unter Wöhlk-Bedingugngen zur Rotfärbung führt.

b) Offen ist weiterhin, ob die Stereochemie der reduzierenden Zuckerkomponentes des 1,4-verknüpften Disaccharids eine Rolle spielt.

Die zu erwartenden Ergebnisse sind kleine Puzzlesteine, die Mut zur Weiterarbeit an der Aufklärung des „Wöhlk-Reaktionsmechanismus“ machen sollen.

Literatur

[1] Ruppersberg, K. (2016). Dem Milchzucker auf der Spur – eine europäische Detektivgeschichte. PdN-ChiS, **65**/8, 30–33.

[2] Ruppersberg, K., Hain, J. (2016). Das Experiment: Wie kann der Lactosegehalt von Milchprodukten im Schulexperiment sichtbar gemacht werden? CHEMKON **23**/2, 90–92.

[3] Ruppersberg, K., Hain, J. (2016), Die Wiederentdeckung der Wöhlk-Probe. Der geheimnisvolle lachsrote Farbstoff. ChiuZ **51**/2, 106–111.

[4] Ruppersberg, K. (2016). Stärkeverdauung durch Speichel - was kommt eigentlich dabei heraus? Ein einfacher Maltose-Nachweise am Ende der enzymatischen Hydrolyse von Amylose und die überraschende Anwesenheit von Glucose, MNU **69**/5, 325–328.

[5] Wöhlk, A. (1904). Über eine neue Reaktion auf Milchzucker (und Maltose). Fresenius J Anal Chem. **43**/11, 670–679.

[6] Hough, L., Jones, J., Richards, E. (1953). The reaction of aminocompounds with sugars. Part II. The action of ammonia on glucose, maltose, and lactose, J. Chem. Soc. **27**/1, 2005–2009.

[7] Umikoff, N. (1896). Zur differentiellen Reaction der Frauen- und Kuhmilch und über die Bestimmung der Lactationsdauer in der Frauenbrust. Aus dem chemischen Laboratorium des kaiserlichen Findelhauses in St. Petersburg, Leipzig, Jahrbuch für Kinderheilkunde, 356–359.

[8] Sieber, N. (1900). Ueber die Umikoff'sche Reaction in der Frauenmilch. Hoppe-Seyler's Zeitschrift für physiologische Chemie, Berlin, **30**/1 & 2, 101–106.

[9] Fearon, W. R. (1942). The detection of lactose and maltose by means of methylamine, The Analyst, **67**, 130–132.

[10] Van Leent, F. H. (1894). Einige Untersuchungen über Milchzucker, Galactose und Maltose und ihre Ammoniakverbindungen. Dissertation. Universität Basel, Verlag Mouton & Co., Haag.

[11] Grob, P. (2000). Einfache Schulversuche zur Lebensmittelchemie, Aulis Verlag Deubner und Co KG, Köln, 65–66.

[12] Schunk, A. (2012). Experiment des Monats, November 2012: Wöhlksche Probe. http://www.axel-schunk.de/experiment/edm1211.html (letzter Zugriff: 01.06.2017).

[13] Fleiss, Ch. (2013). Kohlenhydrate im Chemieunterricht. Plus Lucis 1–2/2013, 40–41.

[14] Wikipedia (Hrsg.). „Lobry-de-Bruyn-Alberda-van-Ekenstein-Umlagerung. https://de.wikipedia.org/wiki/Lobry-de-Bruyn-Alberda-van-Ekenstein-Umlagerung (letzter Zugriff: 01.06.2017).

[15] Töpel, A. (2004). Chemie und Physik der Milch, Behr's Verlag, Hamburg.
[16] Malpress, F. H., Morrison, A. B. (1949). The semi-micro estimation of lactose alone and in the presence of other sugars. Biochem. J., **45**/4, 455–459.
[17] Gattermann, L., Wieland, T. (1982). Die Praxis des organischen Chemikers, de Gruyter, Berlin, 644.
[18] Angrick, M., Rewicki, D. (1980). Die Maillard-Reaktion. ChiuZ **14**/5, 149–157.
[19] Hellwig, M., Henle, T. (2014). Backen, Altern, Diabetes: eine kurze Geschichte der Maillard-Reaktion. Angew. Chem. **126**/39, 10482–10496.
[20] Hollnagel, A., Kroh, L. (2002). 3-Deoxypentosulose: An α-Dicarbonyl Compound Predominating in Nonenzymatic Browning of Oligosaccharides in Aqueous Solution. J. Agric. Food Chem. **50**/6, 1659–1664.
[21] Hollnagel, A., Kroh, L. (2000). Degradation of Oligosaccharides in Nonenzymatic Browning by Formation of α-Dicarbonyl Compounds via a "Peeling Off" Mechanism. J. Agric. Food Chem. **48**/12, 6219–6226.
[22] Mavric, E., Henle, T. (2006). Isolation and identification of 3,4-dideoxypentosulose as specific degradation product of oligosaccharides with 1,4-glycosidic linkages. Eur. Food Res. Technol. **223**/6, 803–810.
[23] Hellwig, M., Henle, T. (2010). Formyline, a new glycation compound from the reaction of lysine and 3-deoxypentosone. Eur. Food Res. Technol. **230**/6, 903–914.
[24] Hellwig, M., Kiessling, M., Rother, S., Henle, T. (2016). Quantification of the glycation compound 6-(3-hydroxy-4-oxo-2-methyl-4(1H)-pyridin-1-yl)-l-norleucine (maltosine) in model systems and food samples. Eur. Food Res. Technol. **242**/4, 547–557.
[25] Lomer, M. C. E., Parkes, G. C., Sanderson, J. D. (2008). Review article: lactose intolerance in clinical practice – myths and realities. Aliment. Pharmacol. Ther. **27**/2, 93–103.

9. References

[1] A. Villiers, Sur la transformation de la fécule en dextrine par le ferment butyrique, *Compt. Rend. Acad. Sci.* **1891**, *112*, 536–538.

[2] D. French, in *Advances in Carbohydrate Chemistry, Vol. 12* (Eds.: M. L. Wolfrom and R. S. Tipson), Academic Press, New York, **1957**, pp. 189-260.

[3] J. Szejtli, Introduction and General Overview of Cyclodextrin Chemistry, *Chem. Rev.* **1998**, *98*, 1743-1754.

[4] E. M. M. Del Valle, Cyclodextrins and their uses: a review, *Process Biochem.* **2004**, *39*, 1033-1046.

[5] L. Ruzicka, Zur Kenntnis des Kohlenstoffringes I. Über die Konstitution des Zibetons, *Helv. Chim. Acta* **1926**, *9*, 230-248.

[6] L. Ruzicka, Zur Kenntnis des Kohlenstoffringes VII. Über die Konstitution des Muscons, *Helv. Chim. Acta* **1926**, *9*, 715-729.

[7] L. Ruzicka, M. Stoll, H. Schinz, Zur Kenntnis des Kohlenstoffringes II. Synthese der carbocyclischen Ketone vom Zehner- bis zum Achtzehnerring, *Helv. Chim. Acta* **1926**, *9*, 249-264.

[8] L. Ruzicka, in *Nobel Lectures, Chemistry 1922-1941*, Elsevier, Amsterdam, **1966**.

[9] C. J. Pedersen, Cyclic polyethers and their complexes with metal salts, *J. Am. Chem. Soc.* **1967**, *89*, 2495-2496.

[10] C. J. Pedersen, Cyclic polyethers and their complexes with metal salts, *J. Am. Chem. Soc.* **1967**, *89*, 7017-7036.

[11] D. J. Cram, Von molekularen Wirten und Gästen sowie ihren Komplexen (Nobel-Vortrag), *Angew. Chem.* **1988**, *27*, 1041-1052; The Design of Molecular Hosts, Guests, and Their Complexes (Nobel Lecture), *Angew. Chem. Int. Ed.* **1988**, *27*, 1009-1020.

[12] J.-M. Lehn, Supramolekulare Chemie – Moleküle, Übermoleküle und molekulare Funktionseinheiten (Nobel-Vortrag), *Angew. Chem.* **1988**, *27*, 91-116; Supramolecular Chemistry—Scope and Perspectives Molecules, Supermolecules, and Molecular Devices (Nobel Lecture), *Angew. Chem. Int. Ed.* **1988**, *27*, 89-112.

[13] C. J. Pedersen, Die Entdeckung der Kronenether (Nobel-Vortrag), *Angew. Chem.* **1988**, *27*, 1053-1059; The Discovery of Crown Ethers (Noble Lecture), *Angew. Chem. Int. Ed.* **1988**, *27*, 1021-1027.

[14] L. A. Wessjohann, E. Ruijter, D. Garcia-Rivera, W. Brandt, What can a chemist learn from nature's macrocycles? – A brief, conceptual view, *Molecular Diversity* **2005**, *9*, 171-186.

[15] E. Marsault, M. L. Peterson, Macrocycles Are Great Cycles: Applications, Opportunities, and Challenges of Synthetic Macrocycles in Drug Discovery, *J. Med. Chem.* **2011**, *54*, 1961-2004.

[16] D. J. Newman, G. M. Cragg, in *Macrocycles in Drug Discovery* (Ed.: J. Levin), The Royal Society of Chemistry, **2015**, pp. 1-36.

[17] L. A. Wessjohann, R. Bartelt, W. Brandt, in *Practical Medicinal Chemistry with Macrocycles* (Eds.: E. Marsault and M. L. Peterson), John Wiley & Sons, Inc., Hoboken, **2017**, pp. 77-100.

[18] S. Kartikey, T. Rama Pati, An Overview on Glyco-Macrocycles: Potential New Lead and their Future in Medicinal Chemistry, *Current Medicinal Chemistry* **2019**, *26*, 1-23.

[19] E. M. Driggers, S. P. Hale, J. Lee, N. K. Terrett, The exploration of macrocycles for drug discovery — an underexploited structural class, *Nature Reviews Drug Discovery* **2008**, *7*, 608-624.

[20] C. M. Madsen, M. H. Clausen, Biologically Active Macrocyclic Compounds – from Natural Products to Diversity-Oriented Synthesis, *Eur. J. Org. Chem.* **2011**, *2011*, 3107-3115.

[21] P. Ermert, Design, Properties and Recent Application of Macrocycles in Medicinal Chemistry, *CHIMIA International Journal for Chemistry* **2017**, *71*, 678-702.

[22] E. A. Villar, D. Beglov, S. Chennamadhavuni, J. A. Porco, D. Kozakov, S. Vajda, A. Whitty, How proteins bind macrocycles, *Nature Chemical Biology* **2014**, *10*, 723-731.

[23] A. A. Beharry, G. A. Woolley, Azobenzene photoswitches for biomolecules, *Chem. Soc. Rev.* **2011**, *40*, 4422-4437.
[24] M. Bauer, W. M. Müller, U. Müller, K. Rissanen, F. Vögtle, Azobenzene-Based Photoswitchable Catenanes, *Liebigs Ann.* **1995**, *1995*, 649-656.
[25] R. Reuter, H. A. Wegner, Oligoazobenzenophanes-synthesis, photochemistry and properties, *Chem. Commun.* **2011**, *47*, 12267-12276.
[26] J. Griffiths, II. Photochemistry of azobenzene and its derivatives, *Chem. Soc. Rev.* **1972**, *1*, 481-493.
[27] G. S. Hartley, The Cis-form of Azobenzene, *Nature* **1937**, *140*, 281-281.
[28] P. Cattaneo, M. Persico, An abinitio study of the photochemistry of azobenzene, *PCCP* **1999**, *1*, 4739-4743.
[29] C. R. Crecca, A. E. Roitberg, Theoretical Study of the Isomerization Mechanism of Azobenzene and Disubstituted Azobenzene Derivatives, *J. Phys. Chem. A* **2006**, *110*, 8188-8203.
[30] H. M. D. Bandara, S. C. Burdette, Photoisomerization in different classes of azobenzene, *Chem. Soc. Rev.* **2012**, *41*, 1809-1825.
[31] H. A. Wegner, Azobenzenes in a New Light—Switching In Vivo, *Angew. Chem.* **2012**, *51*, 4787-4788; *Angew. Chem. Int. Ed.* **2012**, *51*, 4787-4788.
[32] M. J. Hansen, M. M. Lerch, W. Szymanski, B. L. Feringa, Direct and Versatile Synthesis of Red-Shifted Azobenzenes, *Angew. Chem.* **2016**, *55*, 13712-13716; *Angew. Chem. Int. Ed.* **2016**, *55*, 13514-13518.
[33] S. Samanta, A. A. Beharry, O. Sadovski, T. M. McCormick, A. Babalhavaeji, V. Tropepe, G. A. Woolley, Photoswitching Azo Compounds in Vivo with Red Light, *J. Am. Chem. Soc.* **2013**, *135*, 9777-9784.
[34] O. Sadovski, A. A. Beharry, F. Zhang, G. A. Woolley, Spectral Tuning of Azobenzene Photoswitches for Biological Applications, *Angew. Chem.* **2009**, *48*, 1512-1514; *Angew. Chem. Int. Ed.* **2009**, *48*, 1484-1486.
[35] L. F. Kadem, K. G. Suana, M. Holz, W. Wang, H. Westerhaus, R. Herges, C. Selhuber-Unkel, High-Frequency Mechanostimulation of Cell Adhesion, *Angew. Chem.* **2017**, *56*, 231-235; *Angew. Chem. Int. Ed.* **2017**, *56*, 225-229.
[36] R. Siewertsen, H. Neumann, B. Buchheim-Stehn, R. Herges, C. Näther, F. Renth, F. Temps, Highly Efficient Reversible Z−E Photoisomerization of a Bridged Azobenzene with Visible Light through Resolved S1(nπ*) Absorption Bands, *J. Am. Chem. Soc.* **2009**, *131*, 15594-15595.
[37] E. Merino, M. Ribagorda, Control over molecular motion using the cis–trans photoisomerization of the azo group, *Beilstein J. Org. Chem.* **2012**, *8*, 1071-1090.
[38] E. R. Kay, D. A. Leigh, F. Zerbetto, Synthetische molekulare Motoren und mechanische Maschinen, *Angew. Chem.* **2007**, *46*, 72-196; Synthetic Molecular Motors and Mechanical Machines, *Angew. Chem. Int. Ed.* **2007**, *46*, 72-191.
[39] J.-P. Sauvage, Von der chemischen Topologie zu molekularen Maschinen (Nobel-Aufsatz), *Angew. Chem.* **2017**, *56*, 11228-11242; From Chemical Topology to Molecular Machines (Nobel Lecture), *Angew. Chem. Int. Ed.* **2017**, *56*, 11080-11093.
[40] J. F. Stoddart, Mechanisch verzahnte Moleküle (MIMs) – molekulare Shuttle, Schalter und Maschinen (Nobel-Aufsatz), *Angew. Chem.* **2017**, *56*, 11244-11277; Mechanically Interlocked Molecules (MIMs)—Molecular Shuttles, Switches, and Machines (Nobel Lecture), *Angew. Chem. Int. Ed.* **2017**, *56*, 11094-11125.
[41] B. L. Feringa, The Art of Building Small: From Molecular Switches to Motors (Nobel Lecture), *Angew. Chem.* **2017**, *56*, 11206-11226; Die Kunst, klein zu bauen: von molekularen Schaltern bis zu Motoren (Nobel-Aufsatz), *Angew. Chem. Int. Ed.* **2017**, *56*, 11060-11078.
[42] D. Trauner, Der Chemiker und der Architekt, *Angew. Chem.* **2018**, *57*, 4249-4264; The Chemist and the Architect, *Angew. Chem. Int. Ed.* **2018**, *57*, 4177-4191; D. Trauner, in *Unendliche Weiten: Kreuz und quer durchs Chemie-Universum,* (Eds.: T. K. Lindhorst and H.-J. Quadbeck-Seeger), **2018**, Wiley-VCH, Weinheim, pp. 191-203.
[43] E. Wagner-Wysiecka, N. Łukasik, J. F. Biernat, E. Luboch, Azo group(s) in selected macrocyclic compounds, *J. Incl. Phenom. Macro.* **2018**.

[44] E. Luboch, Z. Poleska-Muchlado, M. Jamrógiewicz, J. F. Biernat, in *Macrocyclic Chemistry: Current Trends and Future Perspectives* (Ed.: K. Gloe), Springer Netherlands, Dordrecht, **2005**, pp. 203-218.
[45] A. Harada, Y. Takashima, M. Nakahata, Supramolecular Polymeric Materials via Cyclodextrin–Guest Interactions, *Acc. Chem. Res.* **2014**, *47*, 2128-2140.
[46] D. Wang, S. Gao, Sonogashira coupling in natural product synthesis, *Org. Chem. Front.* **2014**, *1*, 556-566.
[47] S. A. Nepogodiev, J. F. Stoddart, Cyclodextrin-Based Catenanes and Rotaxanes, *Chem. Rev.* **1998**, *98*, 1959-1976.
[48] A. Harada, Cyclodextrin-Based Molecular Machines, *Acc. Chem. Res.* **2001**, *34*, 456-464.
[49] H. Murakami, A. Kawabuchi, K. Kotoo, M. Kunitake, N. Nakashima, A Light-Driven Molecular Shuttle Based on a Rotaxane, *J. Am. Chem. Soc.* **1997**, *119*, 7605-7606.
[50] A. Samanta, M. C. A. Stuart, B. J. Ravoo, Photoresponsive Capture and Release of Lectins in Multilamellar Complexes, *J. Am. Chem. Soc.* **2012**, *134*, 19909-19914.
[51] T. Fujimoto, A. Nakamura, Y. Inoue, Y. Sakata, T. Kaneda, Photoswitching of the association of a permethylated α-cyclodextrin-azobenzene dyad forming a Janus [2]pseudorotaxane, *Tetrahedron Lett.* **2001**, *42*, 7987-7989.
[52] P. V. Jog, M. S. Gin, A Light-Gated Synthetic Ion Channel, *Org. Lett.* **2008**, *10*, 3693-3696.
[53] S. Seiji, O. Toshiyuki, K. Yumiko, M. Osamu, SELECTIVE EXTRACTION OF ALKALI METAL CATIONS BY A PHOTORESPONSIVE BIS(CROWN ETHER), *Chem. Lett.* **1980**, *9*, 283-286.
[54] S. Shinkai, O. Manabe in *Photocontrol of ion extraction and ion transport by photofunctional crown ethers*, *Vol.* Springer Berlin Heidelberg, Berlin, Heidelberg, **1984**, pp. 67-104.
[55] S. Shinkai, T. Nakaji, T. Ogawa, K. Shigematsu, O. Manabe, Photoresponsive crown ethers. 2. Photocontrol of ion extraction and ion transport by a bis(crown ether) with a butterfly-like motion, *J. Am. Chem. Soc.* **1981**, *103*, 111-115.
[56] S. Shinkai, T. Minami, Y. Kusano, O. Manabe, Photoresponsive crown ethers. 8. Azobenzenophane-type switched-on crown ethers which exhibit an all-or-nothing change in ion-binding ability, *J. Am. Chem. Soc.* **1983**, *105*, 1851-1856.
[57] N. Hosono, T. Kajitani, T. Fukushima, K. Ito, S. Sasaki, M. Takata, T. Aida, Large-Area Three-Dimensional Molecular Ordering of a Polymer Brush by One-Step Processing, *Science* **2010**, *330*, 808-811.
[58] H. Wen, W. Zhang, Y. Weng, Z. Hu, Photomechanical bending of linear azobenzene polymer, *RSC Adv.* **2014**, *4*, 11776-11781.
[59] W. Szymański, J. M. Beierle, H. A. V. Kistemaker, W. A. Velema, B. L. Feringa, Reversible Photocontrol of Biological Systems by the Incorporation of Molecular Photoswitches, *Chem. Rev.* **2013**, *113*, 6114-6178.
[60] W. A. Velema, W. Szymanski, B. L. Feringa, Photopharmacology: Beyond Proof of Principle, *J. Am. Chem. Soc.* **2014**, *136*, 2178-2191.
[61] R. J. Mart, R. K. Allemann, Azobenzene photocontrol of peptides and proteins, *Chem. Commun.* **2016**, *52*, 12262-12277.
[62] M. Zhu, H. Zhou, Azobenzene-based small molecular photoswitches for protein modulation, *Org. Biomol. Chem.* **2018**, *16*, 8434-8445.
[63] M. Banghart, K. Borges, E. Isacoff, D. Trauner, R. H. Kramer, Light-activated ion channels for remote control of neuronal firing, *Nature Neuroscience* **2004**, *7*, 1381-1386.
[64] G. A. Woolley, Photocontrolling Peptide α Helices, *Acc. Chem. Res.* **2005**, *38*, 486-493.
[65] G. M. Bennett, The mechanism and kinetics of ring-closure, *Transactions of the Faraday Society* **1941**, *37*, 794-803.
[66] J. Blankenstein, J. Zhu, Conformation-Directed Macrocyclization Reactions, *Eur. J. Org. Chem.* **2005**, *2005*, 1949-1964.
[67] V. Martí-Centelles, M. D. Pandey, M. I. Burguete, S. V. Luis, Macrocyclization Reactions: The Importance of Conformational, Configurational, and Template-Induced Preorganization, *Chem. Rev.* **2015**, *115*, 8736-8834.

[68] C. J. White, A. K. Yudin, Contemporary strategies for peptide macrocyclization, *Nat. Chem.* **2011**, *3*, 509-524.

[69] S. Porwanski, A. Marsura, Tandem Staudinger–Aza-Wittig Templated Reaction: De Novo Synthesis of Sugar–Ureido Cryptands, *Eur. J. Org. Chem.* **2009**, *2009*, 2047-2050.

[70] R. Hoss, F. Vögtle, Templatsynthesen, *Angew. Chem.* **1994**, *33*, 389-398; Template Syntheses, *Angew. Chem. Int. Ed.* **1994**, *33*, 375-384.

[71] D. G. Rivera, O. E. Vercillo, L. A. Wessjohann, Rapid generation of macrocycles with natural-product-like side chains by multiple multicomponent macrocyclizations (MiBs), *Org. Biomol. Chem.* **2008**, *6*, 1787-1795.

[72] L. A. Wessjohann, B. Voigt, D. G. Rivera, Diversity Oriented One-Pot Synthesis of Complex Macrocycles: Very Large Steroid–Peptoid Hybrids from Multiple Multicomponent Reactions Including Bifunctional Building Blocks, *Angew. Chem.* **2005**, *44*, 4863-4868; *Angew. Chem. Int. Ed.* **2005**, *44*, 4785-4790.

[73] L. A. Wessjohann, D. G. Rivera, O. E. Vercillo, Multiple Multicomponent Macrocyclizations (MiBs): A Strategic Development Toward Macrocycle Diversity, *Chem. Rev.* **2009**, *109*, 796-814.

[74] K. L. Bailey, T. F. Molinski, Entropically Favorable Macrolactamization. Synthesis of Isodityrosine Peptide Analogues by Tandem Erlenmeyer Condensation−Macrolactamization, *J. Org. Chem.* **1999**, *64*, 2500-2504.

[75] L. Yang, L. Zhong, K. Yamato, X. Zhang, W. Feng, P. Deng, L. Yuan, X. C. Zeng, B. Gong, Aromatic oligoamide macrocycles from the bimolecular coupling of folded oligomeric precursors, *New J. Chem.* **2009**, *33*, 729-733.

[76] V. A. Azov, J. Cordes, D. Schlüter, T. Dülcks, M. Böckmann, N. L. Doltsinis, Light-Controlled Macrocyclization of Tetrathiafulvalene with Azobenzene: Designing an Optoelectronic Molecular Switch, *J. Org. Chem.* **2014**, *79*, 11714-11721.

[77] J. Xie, N. Bogliotti, Synthesis and Applications of Carbohydrate-Derived Macrocyclic Compounds, *Chem. Rev.* **2014**, *114*, 7678-7739.

[78] V. Dimakos, M. S. Taylor, Site-Selective Functionalization of Hydroxyl Groups in Carbohydrate Derivatives, *Chem. Rev.* **2018**, *118*, 11457-11517.

[79] F. Hamon, F. Djedaini-Pilard, F. Barbot, C. Len, Azobenzenes—synthesis and carbohydrate applications, *Tetrahedron* **2009**, *65*, 10105-10123.

[80] Y. Hu, R. F. Tabor, B. L. Wilkinson, Sweetness and light: design and applications of photo-responsive glycoconjugates, *Org. Biomol. Chem.* **2015**, *13*, 2216-2225.

[81] C. Lin, S. Maisonneuve, R. Métivier, J. Xie, Photoswitchable Carbohydrate-Based Macrocyclic Azobenzene: Synthesis, Chiroptical Switching, and Multistimuli-Responsive Self-Assembly, *Chem. Eur. J.* **2017**, *23*, 14996-15001.

[82] C. Lin, S. Maisonneuve, C. Theulier, J. Xie, Synthesis and Photochromic Properties of Azobenzene-Derived Glycomacrolactones, *Eur. J. Org. Chem.* **2019**, *2019*, 1770-1777.

[83] M. Kawamoto, T. Aoki, T. Wada, Light-driven twisting behaviour of chiral cyclic compounds, *Chem. Commun.* **2007**, 930-932.

[84] G. Haberhauer, C. Kallweit, Ein verbrücktes Azobenzol-Derivat als reversibler lichtinduzierter Chiralitätsschalter, *Angew. Chem.* **2010**, *49*, 2468-2471; A Bridged Azobenzene Derivative as a Reversible, Light-Induced Chirality Switch, *Angew. Chem. Int. Ed.* **2010**, *49*, 2418-2421.

[85] R. Reuter, H. A. Wegner, A Chiral Cyclotrisazobiphenyl: Synthesis and Photochemical Properties, *Org. Lett.* **2011**, *13*, 5908-5911.

[86] K. Takaishi, M. Kawamoto, K. Tsubaki, T. Furuyama, A. Muranaka, M. Uchiyama, Helical Chirality of Azobenzenes Induced by an Intramolecular Chiral Axis and Potential as Chiroptical Switches, *Chem. Eur. J.* **2011**, *17*, 1778-1782.

[87] A. Ossian Aschan, Ueber die Einwirkung von Phenylsenföl auf Amidofettsäuren, *O. Ber.* **1883**, 1544 -1545.

[88] P. Edman, Preparation of Phenyl Thiohydantoins from Some Natural Amino Acids, *Acta Chem. Scand.* **1950**, *4*, 277 - 282.

[89] P. Edman, Preparation of Phenyl Thiohydantoins from Some Natural Amino Acids, *Acta Chem. Scand.* **1950**, *4*, 283 - 293.

[90] H. C. Kolb, M. G. Finn, K. B. Sharpless, Click-Chemie: diverse chemische Funktionalität mit einer Handvoll guter Reaktionen, *Angew. Chem.* **2001**, *40*, 2056-2075; Click Chemistry: Diverse Chemical Function from a Few Good Reactions, *Angew. Chem. Int. Ed.* **2001**, *40*, 2004-2021.

[91] A. J. Sindt, M. D. Smith, P. J. Pellechia, L. S. Shimizu, Thioureas and Squaramides: Comparison with Ureas as Assembly Directing Motifs for m-Xylene Macrocycles, *Cryst. Growth Des.* **2018**, *18*, 1605-1612.

[92] Y. Touati-Jallabe, E. Bojnik, B. Legrand, E. Mauchauffée, N. N. Chung, P. W. Schiller, S. Benyhe, M.-C. Averlant-Petit, J. Martinez, J.-F. Hernandez, Cyclic Enkephalins with a Diversely Substituted Guanidine Bridge or a Thiourea Bridge: Synthesis, Biological and Structural Evaluations, *J. Med. Chem.* **2013**, *56*, 5964-5973.

[93] J. M. Benito, J. L. Jiménez Blanco, C. Ortiz Mellet, J. M. García Fernández, Cyclotrehalins: Cyclooligosaccharide Receptors Featuring a Hydrophobic Cavity, *Angew. Chem.* **2002**, *41*, 3826-3828; *Angew. Chem. Int. Ed.* **2002**, *41*, 4370-4370.

[94] D. Rodríguez-Lucena, J. M. Benito, E. Álvarez, C. Jaime, J. Perez-Miron, C. Ortiz Mellet, J. M. García Fernández, Synthesis, Structure, and Inclusion Capabilities of Trehalose-Based Cyclodextrin Analogues (Cyclotrehalans), *J. Org. Chem.* **2008**, *73*, 2967-2979.

[95] J. L. Jiménez Blanco, F. Ortega-Caballero, L. Blanco-Fernández, T. Carmona, G. Marcelo, M. Martínez-Negro, E. Aicart, E. Junquera, F. Mendicuti, C. Tros de Ilarduya, C. Ortiz Mellet, J. M. García Fernández, Trehalose-based Janus cyclooligosaccharides: the "Click" synthesis and DNA-directed assembly into pH-sensitive transfectious nanoparticles, *Chem. Commun.* **2016**, *52*, 10117-10120.

[96] Y. S. Lee, J. Nyberg, S. Moye, R. S. Agnes, P. Davis, S.-w. Ma, J. Lai, F. Porreca, R. Vardanyan, V. J. Hruby, Understanding the structural requirements of 4-anilidopiperidine analogues for biological activities at μ and δ opioid receptors, *Bioorg. Med. Chem. Lett.* **2007**, *17*, 2161-2165.

[97] A. Müller, T. K. Lindhorst, Synthesis of Hetero-bifunctional Azobenzene Glycoconjugates for Bioorthogonal Cross-Linking of Proteins, *Eur. J. Org. Chem.* **2016**, *2016*, 1669-1672.

[98] H. J. Jung, H. Min, H. Yu, T. G. Lee, T. D. Chung, Electrochemical cleavage of azo linkage for site-selective immobilization and cell patterning, *Chem. Comm.* **2010**, *46*, 3863-3865.

[99] M. I. García-Moreno, P. Díaz-Pérez, J. M. Benito, C. Ortiz Mellet, J. Defaye, J. M. García Fernández, One-step synthesis of non-anomeric sugar isothiocyanates from sugar azides, *Carbohydr. Res.* **2002**, *337*, 2329-2334.

[100] G. Zemplén, E. Pacsu, Über die Verseifung acetylierter Zucker und verwandter Substanzen, *Ber. Dtsch. Chem. Ges. (A and B)* **1929**, *62*, 1613-1614.

[101] Schrödinger Release 2018-1: MacroModel, Schrödinger, LLC, New York, NY, **2018**.

[102] N. Harada, in *Circular Dichroism: Principles and Applications, Vol. 1* (Eds.: K. Nakanishi, N. Berova and R. W. Woody), VCH Publishers, New York, **1994**, pp. 335 - 360.

[103] G. Haberhauer, C. Kallweit, C. Wölper, D. Bläser, Eine in ein Cyclopeptid eingebettete Azobenzol-Einheit als Schalter mit vorgegebener Richtung und Art der Bewegung, *Angew. Chem.* **2013**, *52*, 8033-8036; An Azobenzene Unit Embedded in a Cyclopeptide as a Type-Specific and Spatially Directed Switch, *Angew. Chem. Int. Ed.* **2013**, *52*, 7879-7882.

[104] A. Adam, G. Haberhauer, Switching Process Consisting of Three Isomeric States of an Azobenzene Unit, *J. Am. Chem. Soc.* **2017**, *139*, 9708-9713.

[105] A. Adam, S. Mehrparvar, G. Haberhauer, An azobenzene container showing a definite folding – synthesis and structural investigation, *Beilstein J. Org. Chem.* **2019**, *15*, 1534-1544.

[106] T. Raeker, Full-Dimensional Photodynamics Simulations: From Photoisomerizations to Excited-State Proton Transfer Reactions, *dissertation thesis*, Christian-Albrechts-Universität (Kiel), **2018**.

[107] A. Michael, Ueber die Einwirkung von Diazobenzolimid auf Acetylendicarbonsäuremethylester, *J. Prakt. Chem.* **1893**, *48*, 94-95.

[108] R. Huisgen, 1.3-Dipolare Cycloadditionen Rückschau und Ausblick, *Angew. Chem.* **1963**, *2*, 604-637; 1,3-Dipolar Cycloadditions. Past and Future, *Angew. Chem. Int. Ed.* **1963**, *2*, 565-598.

[109] C. W. Tornøe, C. Christensen, M. Meldal, Peptidotriazoles on Solid Phase: [1,2,3]-Triazoles by Regiospecific Copper(I)-Catalyzed 1,3-Dipolar Cycloadditions of Terminal Alkynes to Azides, *J. Org. Chem.* **2002**, *67*, 3057-3064.

[110] V. V. Rostovtsev, L. G. Green, V. V. Fokin, K. B. Sharpless, A Stepwise Huisgen Cycloaddition Process: Copper(I)-Catalyzed Regioselective "Ligation" of Azides and Terminal Alkynes, *Angew. Chem.* **2002**, *41*, 2708-2711; *Angew. Chem. Int. Ed.* **2002**, *41*, 2596-2599.

[111] H. Ben El Ayouchia, L. Bahsis, H. Anane, L. R. Domingo, S.-E. Stiriba, Understanding the mechanism and regioselectivity of the copper(i) catalyzed [3 + 2] cycloaddition reaction between azide and alkyne: a systematic DFT study, *RSC Adv.* **2018**, *8*, 7670-7678.

[112] L. Zhang, X. Chen, P. Xue, H. H. Y. Sun, I. D. Williams, K. B. Sharpless, V. V. Fokin, G. Jia, Ruthenium-Catalyzed Cycloaddition of Alkynes and Organic Azides, *J. Am. Chem. Soc.* **2005**, *127*, 15998-15999.

[113] G. Wittig, A. Krebs, Zur Existenz niedergliedriger Cycloalkine, I, *Chem. Ber.* **1961**, *94*, 3260-3275.

[114] N. J. Agard, J. A. Prescher, C. R. Bertozzi, A Strain-Promoted [3 + 2] Azide−Alkyne Cycloaddition for Covalent Modification of Biomolecules in Living Systems, *J. Am. Chem. Soc.* **2004**, *126*, 15046-15047.

[115] J. E. Hein, V. V. Fokin, Copper-catalyzed azide–alkyne cycloaddition (CuAAC) and beyond: new reactivity of copper(i) acetylides, *Chem. Soc. Rev.* **2010**, *39*, 1302-1315.

[116] D. Pasini, The Click Reaction as an Efficient Tool for the Construction of Macrocyclic Structures, *Molecules* **2013**, *18*, 9512-9530.

[117] F. M. Menger, B. N. A. Mbadugha, Gemini Surfactants with a Disaccharide Spacer, *J. Am. Chem. Soc.* **2001**, *123*, 875-885.

[118] V. Chandrasekaran, T. K. Lindhorst, Sweet switches: azobenzene glycoconjugates synthesized by click chemistry, *Chem. Commun.* **2012**, *48*, 7519-7521.

[119] F. Reise, J. E. Warias, K. Chatterjee, N. R. Krekiehn, O. Magnussen, B. M. Murphy, T. K. Lindhorst, Photoswitchable Glycolipid Mimetics: Synthesis and Photochromic Properties of Glycoazobenzene Amphiphiles, *Chem. Eur. J.* **2018**, *24*, 17497-17505.

[120] M. Ishikawa, T. Ohzono, T. Yamaguchi, Y. Norikane, Photo-enhanced Aqueous Solubilization of an Azo-compound, *Sci. Rep.* **2017**, *7*, 6909.

[121] K. Nakanishi, N. Berova, in *Circular Dichroism: Principles and Applications, Vol. 1* (Eds.: K. Nakanishi, N. Berova and R. W. Woody), VCH Publishers, New York, **1994**, pp. 361 - 398.

[122] R. D. Stephens, C. E. Castro, The Substitution of Aryl Iodides with Cuprous Acetylides. A Synthesis of Tolanes and Heterocyclics1, *J. Org. Chem.* **1963**, *28*, 3313-3315.

[123] F. Cataldo, C. S. Casari, Synthesis, Structure and Thermal Properties of Copper and Silver Polyynides and Acetylides, *J. Inorg. Organomet. Polym.* **2007**, *17*, 641-651.

[124] K. Sonogashira, Y. Tohda, N. Hagihara, A convenient synthesis of acetylenes: catalytic substitutions of acetylenic hydrogen with bromoalkenes, iodoarenes and bromopyridines, *Tetrahedron Lett.* **1975**, *16*, 4467-4470.

[125] L. Cassar, Synthesis of aryl- and vinyl-substituted acetylene derivatives by the use of nickel and palladium complexes, *J. Organomet. Chem.* **1975**, *93*, 253-257.

[126] H. A. Dieck, F. R. Heck, Palladium catalyzed synthesis of aryl, heterocyclic and vinylic acetylene derivatives, *J. Organomet. Chem.* **1975**, *93*, 259-263.

[127] R. Chinchilla, C. Nájera, The Sonogashira Reaction: A Booming Methodology in Synthetic Organic Chemistry, *Chem. Rev.* **2007**, *107*, 874-922.

[128] R. Chinchilla, C. Nájera, Recent advances in Sonogashira reactions, *Chem. Soc. Rev.* **2011**, *40*, 5084-5121.

[129] M. Gazvoda, M. Virant, B. Pinter, J. Košmrlj, Mechanism of copper-free Sonogashira reaction operates through palladium-palladium transmetallation, *Nat. Commun.* **2018**, *9*, 4814.

[130] C. S. Jones, M. J. O'Connor, M. M. Haley, in *Acetylene Chemistry* (Eds.: F. Diederich, P. J. Stang and R. R. Tykwinski), Wiley-VCH, Weinheim, **2005**, pp. 303-385.

[131] T. O. Ronson, W. P. Unsworth, I. J. S. Fairlamb, in *Practical Medicinal Chemistry with Macrocycles* (Eds.: E. Marsault and M. L. Peterson), John Wiley & Sons, Inc., Hoboken, **2017**, pp. 281-305.

[132] D. Zhao, J. S. Moore, Shape-persistent arylene ethynylene macrocycles: syntheses and supramolecular chemistry, *Chem. Commun.* **2003**, 807-818.
[133] W. Zhang, J. S. Moore, Formtreue Makrocyclen: Strukturen und Synthesen aus Arylen- und Ethinylen-Bausteinen, *Angew. Chem.* **2006**, *45*, 4524-4548; Shape-Persistent Macrocycles: Structures and Synthetic Approaches from Arylene and Ethynylene Building Blocks, *Angew. Chem. Int. Ed.* **2006**, *45*, 4416-4439.
[134] U. Kusebauch, S. A. Cadamuro, H.-J. Musiol, M. O. Lenz, J. Wachtveitl, L. Moroder, C. Renner, Lichtgesteuerte Faltung und Entfaltung einer Collagen-Tripelhelix, *Angew. Chem.* **2006**, *45*, 7170-7173; Photocontrolled Folding and Unfolding of a Collagen Triple Helix, *Angew. Chem. Int. Ed.* **2006**, *45*, 7015-7018.
[135] Y. Takeda, S. Okumura, S. Minakata, A Practical Synthesis of Azobenzenes through Oxidative Dimerization of Aromatic Amines Using tert-Butyl Hypoiodite, *Synthesis* **2013**, *45*, 1029-1033.
[136] D. Bléger, J. Schwarz, A. M. Brouwer, S. Hecht, o-Fluoroazobenzenes as Readily Synthesized Photoswitches Offering Nearly Quantitative Two-Way Isomerization with Visible Light, *J. Am. Chem. Soc.* **2012**, *134*, 20597-20600.
[137] M. Poláková, M. Beláňová, K. Mikušová, E. Lattová, H. Perreault, Synthesis of 1,2,3-Triazolo-Linked Octyl (1→6)-α-d-Oligomannosides and Their Evaluation in Mycobacterial Mannosyltransferase Assay, *Bioconjugate Chem.* **2011**, *22*, 289-298.
[138] M. Bergeron-Brlek, T. C. Shiao, M. C. Trono, R. Roy, Synthesis of a small library of bivalent α-d-mannopyranosides for lectin cross-linking, *Carbohydr. Res.* **2011**, *346*, 1479-1489.
[139] R. Roy, S. K. Das, R. Dominique, M. C. Trono, F. Hernández-Mateo, F. Santoyo-González in *Transition metal catalyzed neoglycoconjugate syntheses*, *Vol. 71* **1999**, p. 565.
[140] G. Haberhauer, C. Kallweit, A Bridged Azobenzene Derivative as a Reversible, Light-Induced Chirality Switch, *Angew. Chem. Int. Ed.* **2010**, *49*, 2418-2421.
[141] K. Takaishi, M. Kawamoto, K. Tsubaki, T. Wada, Photoswitching of Dextro/Levo Rotation with Axially Chiral Binaphthyls Linked to an Azobenzene, *J. Org. Chem.* **2009**, *74*, 5723-5726.
[142] K. Takaishi, A. Muranaka, M. Kawamoto, M. Uchiyama, Planar Chirality of Twisted trans-Azobenzene Structure Induced by Chiral Transfer from Binaphthyls, *J. Org. Chem.* **2011**, *76*, 7623-7628.
[143] C. Glaser, Beiträge zur Kenntniss des Acetenylbenzols, *Ber. Dtsch. Chem. Ges.* **1869**, *2*, 422-424.
[144] G. Eglinton, A. R. Galbraith, Cyclic Diynes, *Chem. Ind.* **1956**, 737 - 738.
[145] G. Eglinton, A. R. Galbraith, 182. Macrocyclic acetylenic compounds. Part I. Cyclotetradeca-1 :3-diyne and related compounds, *J. Chem. Soc.* **1959**, 889-896.
[146] A. S. Hay, Oxidative Coupling of Acetylenes. II1, *J. Org. Chem.* **1962**, *27*, 3320-3321.
[147] F. Bohlmann, H. Schönowsky, E. Inhoffen, G. Grau, Polyacetylenverbindungen, LII. Über den Mechanismus der oxydativen Dimerisierung von Acetylenverbindungen, *Chem. Ber.* **1964**, *97*, 794-800.
[148] J. Jover, P. Spuhler, L. Zhao, C. McArdle, F. Maseras, Toward a mechanistic understanding of oxidative homocoupling: the Glaser–Hay reaction, *Catal. Sci. Technol.* **2014**, *4*, 4200-4209.
[149] S. Höger, Shape-Persistent Macrocycles: From Molecules to Materials, *Chem. Eur. J.* **2004**, *10*, 1320-1329.
[150] W. Chodkiewicz, P. Cadiot, New synthesis of symmetrical and asymmetrical conjugated polyacetylenes, *C. R. Hebd. Seances Acad. Sci.* **1955**, *241*, 1055-1057.
[151] W. Chodkiewicz, Synthesis of acetylenic compounds, *Ann. Chim.* **1957**, *2*, 819-869.
[152] J. Hain, V. Chandrasekaran, T. K. Lindhorst, Joining Hydroxyazobenzene and Mannose under Mitsunobu Conditions, *Isr. J. Chem.* **2015**, *55*, 383-386.
[153] J. Zhao, Y. Liu, H.-J. Park, J. M. Boggs, A. Basu, Carbohydrate-Coated Fluorescent Silica Nanoparticles as Probes for the Galactose/3-Sulfogalactose Carbohydrate–Carbohydrate Interaction Using Model Systems and Cellular Binding Studies, *Bioconjugate Chem.* **2012**, *23*, 1166-1173.
[154] K. K. Yeoh, T. D. Butters, B. L. Wilkinson, A. J. Fairbanks, Probing replacement of pyrophosphate via click chemistry; synthesis of UDP-sugar analogues as potential glycosyl transferase inhibitors, *Carbohydr. Res.* **2009**, *344*, 586-591.

[155] N. Pietrzik, D. Schmollinger, T. Ziegler, Dimerization of propargyl and homopropargyl 6-azido-6-deoxy-glycosides upon 1,3-dipolar cycloaddition, *Beilstein J. Org. Chem.* **2008**, *4*, 30.

[156] J. Brekalo, G. Despras, T. K. Lindhorst, Pseudoenantiomeric glycoclusters: synthesis and testing of heterobivalency in carbohydrate–protein interactions, *Org. Biomol. Chem.* **2019**, *17*, 5929-5942.

[157] A. Gille, M. Hiersemann, (−)-Lytophilippine A: Synthesis of a C1−C18 Building Block, *Org. Lett.* **2010**, *12*, 5258-5261.

[158] J. Yang, X. Fu, Q. Jia, J. Shen, J. B. Biggins, J. Jiang, J. Zhao, J. J. Schmidt, P. G. Wang, J. S. Thorson, Studies on the Substrate Specificity of Escherichia coli Galactokinase, *Org. Lett.* **2003**, *5*, 2223-2226.

[159] G. Catelani, F. Colonna, A. Marra, An improved preparation of 3,4-O-isopropylidene derivatives of α- and β-d-galactopyranosides, *Carbohydr. Res.* **1988**, *182*, 297-300.

[160] S. A. S. Al Janabi, J. G. Buchanan, A. R. Edgar, Base-catalysed equilibration and conformational analysis of some methyl 2,3- and 3,4-anhydro-6-deoxy-β-D-hexopyranosides, *Carbohydr. Res.* **1974**, *35*, 151-164.

[161] A. Müller, H. Kobarg, V. Chandrasekaran, J. Gronow, F. D. Sönnichsen, T. K. Lindhorst, Synthesis of Bifunctional Azobenzene Glycoconjugates for Cysteine-Based Photosensitive Cross-Linking with Bioactive Peptides, *Chem. Eur. J.* **2015**, *21*, 13723-13731.

[162] S. Aichhorn, M. Himmelsbach, W. Schöfberger, Synthesis of quinoxalines or quinolin-8-amines from N-propargyl aniline derivatives employing tin and indium chlorides, *Org. Biomol. Chem.* **2015**, *13*, 9373-9380.

[163] M. Hammerich, R. Herges, Laterally Mounted Azobenzenes on Platforms, *J. Org. Chem.* **2015**, *80*, 11233-11236.

[164] C. B. R. Reddy, S. R. Reddy, S. Naidu, Cu(I) catalyzed dehydrogenative homo coupling of aromatic amines under simple and mild reaction conditions, *Catal. Commun.* **2014**, *56*, 50-54.

[165] H. Ma, W. Li, J. Wang, G. Xiao, Y. Gong, C. Qi, Y. Feng, X. Li, Z. Bao, W. Cao, Q. Sun, C. Veaceslav, F. Wang, Z. Lei, Organocatalytic oxidative dehydrogenation of aromatic amines for the preparation of azobenzenes under mild conditions, *Tetrahedron* **2012**, *68*, 8358-8366.

[166] K. Monir, M. Ghosh, S. Mishra, A. Majee, A. Hajra, Phenyliodine(III) Diacetate (PIDA) Mediated Synthesis of Aromatic Azo Compounds through Oxidative Dehydrogenative Coupling of Anilines: Scope and Mechanism, *Eur. J. Org. Chem.* **2014**, *2014*, 1096-1102.

[167] A. Antoine John, Q. Lin, Synthesis of Azobenzenes Using N-Chlorosuccinimide and 1,8-Diazabicyclo[5.4.0]undec-7-ene (DBU), *J. Org. Chem.* **2017**, *82*, 9873-9876.

[168] G. F. P. de Souza, T. W. von Zuben, A. G. Salles, A metal-catalyst-free oxidative coupling of anilines to aromatic azo compounds in water using bleach, *Tetrahedron Lett.* **2018**, *59*, 3753-3755.

[169] J. A. Hyatt, Stereospecific synthesis of cis-azobenzenes, *Tetrahedron Lett.* **1977**, *18*, 141-142.

[170] E. F. Pratt, T. P. McGovern, Oxidation by Solids. III. Benzalanilines from N-Benzylanilines and Related Oxidations by Manganese Dioxide, *J. Org. Chem.* **1964**, *29*, 1540-1543.

[171] A. H. Heindl, J. Becker, H. A. Wegner, Selective switching of multiple azobenzenes, *Chem. Sci.* **2019**, *10*, 7418-7425.

[172] E. E. Smissman, A. Makriyannis, Azodicarboxylic acid esters as dealkylating agents, *J. Org. Chem.* **1973**, *38*, 1652-1657.

[173] N. Kawatsuki, H. Matsushita, T. Washio, J. Kozuki, M. Kondo, T. Sasaki, H. Ono, Photoinduced Orientation of Photoresponsive Polymers with N-Benzylideneaniline Derivative Side Groups, *Macromolecules* **2014**, *47*, 324-332.

[174] G. L. Tolnai, U. J. Nilsson, B. Olofsson, Efficient O-Functionalization of Carbohydrates with Electrophilic Reagents, *Angew. Chem.* **2016**, *55*, 11392-11396; *Angew. Chem. Int. Ed.* **2016**, *55*, 11226-11230.

Danksagung

Mein besonderer Dank gilt Frau Prof. Dr. Thisbe K. Lindhorst für die Betreuung dieser Arbeit, vor allem für das entgegengebrachte Vertrauen und die gewährten Freiräume bei der Ausgestaltung dieses neuen Projekts. Danke auch für die stets konstruktive Kritik, sowohl bei wissenschaftlichen als auch künstlerischen Dingen.

Ebenfalls möchte ich mich bei Dr. Guillaume Despras bedanken, der dies hier sicherlich lesen kann, für die Betreuung und Zusammenarbeit bei der Entstehung dieses Projekts.

Weiterhin danke ich Frau Prof. Dr. Anna McConnell für die Betreuung dieser Arbeit als Zweitgutachterin.

Meinen Kooperationspartnern Prof. Dr. Patrick Rollin und Klaus Ruppersberg danke ich für die erfolgreiche Zusammenarbeit.

Dank gebührt ebenfalls den Mitarbeitern der analytischen Abteilungen, Holger Franzen, Marion Höftmann, Gitta Kohlmeyer-Yilmaz, Dirk Meyer, Silke Rühl und Rolf Schmied für die Vielzahl an aufgenommenen NMR- und Massenspektren. Insbesondere Dank an Prof. Dr. Grötzinger für die Bereitstellung des CD-Messgeräts.

Ein großes Dankeschön geht an die allerbeste Laborpartnerin Elwira Klima-Bartczak und an Christine Haug, die beide stets mit großer Hilfsbereitschaft und Engagement für alle großen und kleinen Probleme zur Stelle waren.

Dem aktuellen Arbeitskreis Lindhorst sowie den ehemaligen Mitgliedern danke ich für die tolle Arbeits- und Kaffeeraumatmosphäre, den Zusammenhalt und die Unterstützung bei wirklich allen möglichen und unmöglichen Dingen.

Weiterhin möchte ich auch meinem allerbesten Bachelorstudenten Clemens Lütjohann und meinen großartigen F3 Praktikanten Janine Pahlke und Leon Merten Friedrich bedanken.

Zum Schluss gilt mein ganz besonderer Dank meinen Eltern und meinem Ehemann, die mich stets unterstützt und nie an meinen Fähigkeiten gezweifelt haben.